frontiers | Research Topics

Improving crop nutritional security for sustainable agriculture in the era of climate change

Edited by
M. Iqbal R. Khan, Mohammad Irfan and Ravi Gupta

Published in
Frontiers in Plant Science

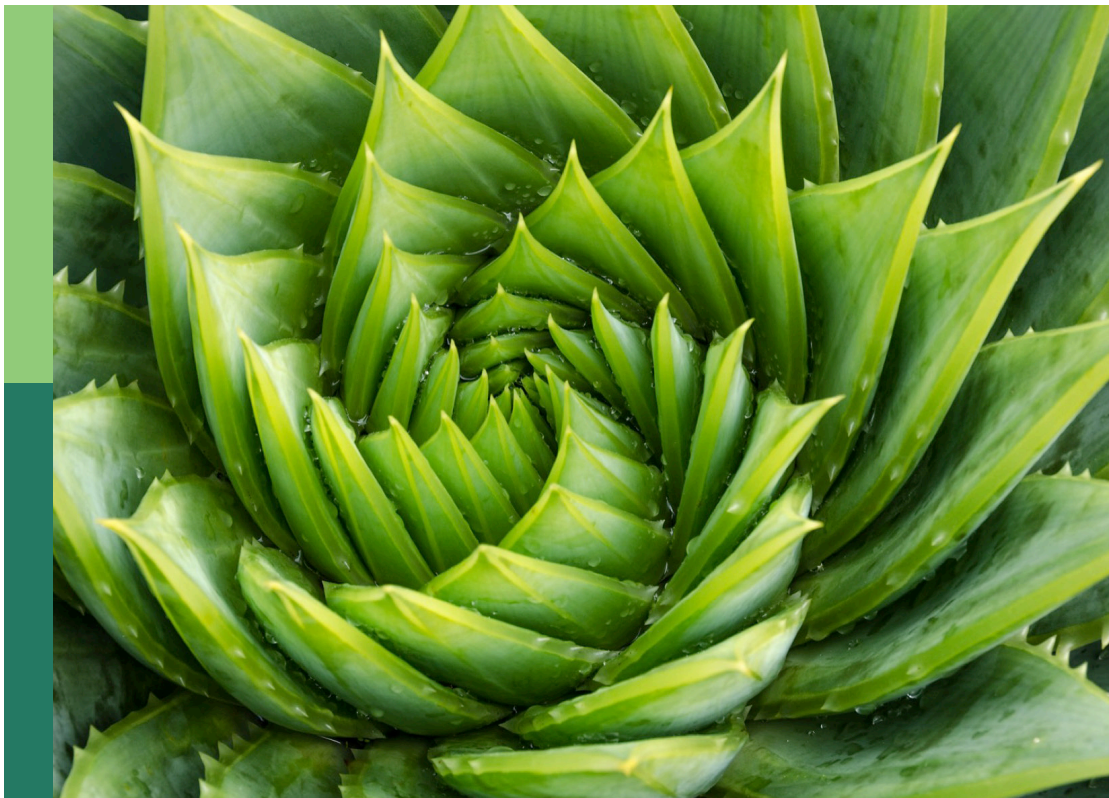

ISSN 1664-8714
ISBN 978-2-8325-3661-2
DOI 10.3389/978-2-8325-3661-2

About Frontiers

Frontiers is more than just an open access publisher of scholarly articles: it is a pioneering approach to the world of academia, radically improving the way scholarly research is managed. The grand vision of Frontiers is a world where all people have an equal opportunity to seek, share and generate knowledge. Frontiers provides immediate and permanent online open access to all its publications, but this alone is not enough to realize our grand goals.

Frontiers journal series

The Frontiers journal series is a multi-tier and interdisciplinary set of open-access, online journals, promising a paradigm shift from the current review, selection and dissemination processes in academic publishing. All Frontiers journals are driven by researchers for researchers; therefore, they constitute a service to the scholarly community. At the same time, the *Frontiers journal series* operates on a revolutionary invention, the tiered publishing system, initially addressing specific communities of scholars, and gradually climbing up to broader public understanding, thus serving the interests of the lay society, too.

Dedication to quality

Each Frontiers article is a landmark of the highest quality, thanks to genuinely collaborative interactions between authors and review editors, who include some of the world's best academicians. Research must be certified by peers before entering a stream of knowledge that may eventually reach the public - and shape society; therefore, Frontiers only applies the most rigorous and unbiased reviews. Frontiers revolutionizes research publishing by freely delivering the most outstanding research, evaluated with no bias from both the academic and social point of view. By applying the most advanced information technologies, Frontiers is catapulting scholarly publishing into a new generation.

What are Frontiers Research Topics?

Frontiers Research Topics are very popular trademarks of the *Frontiers journals series*: they are collections of at least ten articles, all centered on a particular subject. With their unique mix of varied contributions from Original Research to Review Articles, Frontiers Research Topics unify the most influential researchers, the latest key findings and historical advances in a hot research area.

Find out more on how to host your own Frontiers Research Topic or contribute to one as an author by contacting the Frontiers editorial office: frontiersin.org/about/contact

Improving crop nutritional security for sustainable agriculture in the era of climate change

Topic editors

M. Iqbal R. Khan — Jamia Hamdard University, India
Mohammad Irfan — Cornell University, United States
Ravi Gupta — Kookmin University, Republic of Korea

Citation

Khan, M. I. R., Irfan, M., Gupta, R., eds. (2023). *Improving crop nutritional security for sustainable agriculture in the era of climate change*. Lausanne: Frontiers Media SA. doi: 10.3389/978-2-8325-3661-2

Table of contents

frontiers | Frontiers in Plant Science

TYPE Editorial
PUBLISHED 25 September 2023
DOI 10.3389/fpls.2023.1292264

OPEN ACCESS

EDITED AND REVIEWED BY
Leo Marcelis,
Wageningen University and Research, Netherlands

*CORRESPONDENCE
M. Iqbal R. Khan
iqbal.khan@jamiahamdard.ac.in

RECEIVED 11 September 2023
ACCEPTED 13 September 2023
PUBLISHED 25 September 2023

CITATION
Khan MIR, Irfan M and Gupta R (2023) Editorial: Improving crop nutritional security for sustainable agriculture in the era of climate change.
Front. Plant Sci. 14:1292264.
doi: 10.3389/fpls.2023.1292264

Editorial: Improving crop nutritional security for sustainable agriculture in the era of climate change

M. Iqbal R. Khan[1]*, Mohammad Irfan[2] and Ravi Gupta[3]

[1]Department of Botany, Jamia Hamdard, New Delhi, India, [2]School of Integrative Plant Science, College of Agriculture and Life Sciences, Cornell University, Ithaca, NY, United States, [3]College of General Education, Kookmin University, Seoul, Republic of Korea

KEYWORDS

environment, climate change, nutritional security, food security, plant

Editorial on the Research Topic
Improving crop nutritional security for sustainable agriculture in the era of climate change

Global nutritional security is indispensable to boost agricultural productivity to feed the growing population, and amid the challenges posed by climate change. Thus, securing our future food supply remains a critical concern. Several factors including population size, climatic fluctuations, and the environmental degradation causing declination in the quality of natural resources (land, water and air). These factors contribute and lead to the nutritional instabilities, consequently hampering the sustainable production of agricultural goods. Hence, food security has become a major issue in the recent decade and is going to be intensified further in the coming years. Despite signature achievements in the agricultural industry, reports suggest that there are approximately 820 million people who are suffering from chronic hunger, and 2 billion lack a sufficient supply of nutrition in their daily intake of food (Bhardwaj et al., 2022). This duplex burden of malnutrition has been emerging as the 'new normal' in the present circumstances. Thus, nutritional security is a subject of major concern from the perspective of human health as well as livestock, while sustaining the agricultural inputs for the burgeoning population size. Researchers have been establishing numerous ways to alleviate nutritional insecurity through conventional and biotechnological interventions, few of these have been discussed here.

Strategic interventions to improve sustainable nutritional security under environmental stresses

Plant growth, physiology, and metabolic profile management

In the pursuit of future food security, a critical challenge lies in deciphering how climate variables interact with plant growth, fitness, and yield parameters. Such interactions can

trigger unique shifts in various aspects of plants, including morphology, physiology, and metabolite accumulation, ultimately leading to adaptive responses tailored to specific climate scenarios (Nazir et al., 2023). Večeřová et al. deciphered the intricate interactions between climate variables and plant responses. By subjecting spring wheat cultivar Cadenza to simulated climate conditions projected for the year 2100, they uncovered a mitigating effect of elevated carbon dioxide (CO_2) on the adverse impacts of dynamic changes in the temperature range. Metabolite profiling revealed the accumulation of key compounds linked to cellular energy, biosynthesis, and oxidative balance. This pioneering research demonstrates the potential for developing climate-resilient wheat cultivars by leveraging these identified metabolites as breeding targets, ultimately bolstering food and nutritional security in the face of changing climates. Considering the potential role of metabolites, plant secondary metabolites (SMs) were also found pivotal in modulating the growth and developmental processes, along with exhibiting a variety of therapeutic effects in response to environmental stressors. For instance, in order to understand the medicinal properties of Euphorbia latex, Benjamaa et al. reviewed the therapeutic potential of latex obtained from various Euphorbia species. Although Euphorbia latex is considered poisonous and exhibits toxicity if consumed raw in larger amounts, it has been used in traditional medicines for ages. Euphorbia latex is known to contain various SMs such as phenolic compounds, alkaloids, saponins, and flavonoids, among others that potentially account for its antioxidant, antimicrobial, and a variety of therapeutic effects. In the past, Euphorbia latex has been used for the treatment of various diseases including some of the most serious diseases such as dropsy, paralysis, and deafness, along with some of the common diseases like wounds, skin warts, and amaurosis, among others. In addition, based on recent research, the anti-carcinogenic potential of Euphorbia latex was also highlighted.

Fertilizer management and its systemic utilization

Over the last few years, research has delved into multifaceted strategies that hold promise for sustainable agriculture under changing climatic conditions. One such approach under the attention is effective fertilizer management, which plays a pivotal role in ensuring crop productivity and nutritional security. Sustainable utilization and management of fertilizers critically determine the agricultural productivity under diverse climatic fluctuations. In this approach, Reduced Basal and Increased Topdressing (RBIT) fertilizer rate has been found as an efficient approach to avoid yield penalties of rice (*Oryza sativa*) and wheat (*Triticum aestivum*) in response to environmental stressors. Zhang et al. explored the potential of RBIT fertilizer rates to address the challenges posed by climate change. Conducted over a span of nine years in the lower Yangtze River rice-wheat system region of China, the study revealed significant enhancements in rice yields. RBIT, when combined with straw incorporation, led to substantial increases in both average and annual rice yields. Notably, this approach displayed a remarkable potential to elevate the Sustainable Yield Index (SYI) of wheat and rice by 7.6% and 12.8%, respectively, compared to conventional fertilization. The implications extend beyond mere yield improvements; RBIT emerged as a potent driver of carbon (C) sequestration, with the combination of RBIT and straw incorporation showing the highest rates of sequestration. This study highlights the positive effects of these practices on soil health, emphasizing their role in fortifying rice production sustainability and soil organic carbon (SOC) sequestration. Accurately assessing the C footprint of rice cultivation is pivotal in curbing greenhouse gas emissions from global food production. To enhance the credibility and efficiency of this evaluation, Xu et al. conducted sensitivity and uncertainty analyses on a C footprint model integrated with a typical East Asian rice production system employing different fertilization approaches. The outcomes of sensitivity and uncertainty analyses shed light on crucial parameters, with methane (CH_4) emission estimation taking center stage. Notably, organic rice production exhibited a C footprint significantly surpassing that of conventional rice production, mainly attributed to increased CH_4 emissions impact. This comprehensive framework offers valuable insights for shaping future strategies aimed at mitigating the greenhouse gas effects of rice production.

Mutagens-mediated approaches to achieve high-yield crop varieties

The development of high-yielding cultivars is another important aspect that must be taken into consideration for achieving food security. Therefore, researchers around the globe are making continuous attempts to generate high-yielding cultivars by a variety of breeding approaches. Raina and Khan utilized γ-rays and sodium azide-based induced mutagenesis to develop high-yielding cowpea (*Vigna unguiculata* L. Walp.) cultivars (Raina and Khan, 2023). The authors showed that mutants developed using low and intermediate doses of these mutagens exhibit improved agronomic traits as compared to their parental lines Gomati VU-89 and Pusa-578. In particular, the number of seeds per pod was highly increased among other agronomic traits; however, these mutations led to a decline in the overall plant height, the contents of chlorophyll and carotenoids, and the activity of nitrate reductase (NR) enzymes. These results indicate that plant growth parameters and agronomic traits are negatively correlated and targeting one may compromise the other characteristics in cowpea.

Transcriptional regulations-mediated strategies

Amidst the changing landscape of nutritional security and climate change, the exploration of plant defence mechanisms gains prominence (Iqbal et al., 2021). The enigmatic role of WRKY transcription factors (TFs) emerges as a pivotal aspect of ensuring both crop productivity and food security in the

countenance of evolving climate patterns. In a bid to decipher the intricate interplay between genetic factors, climate variations, and disease resistance, Yan et al. delve into *WRKY* family TFs functions in peanuts (*Arachis hypogaea*). The study unveils 174 *WRKY* genes (*AhWRKY*) within the peanut genome, offering a deeper understanding of their genetic composition and potential functions. Moreover, this study also investigates how these *WRKY* genes respond to *Ralstonia solanacearum* infection, a prominent disease affecting peanuts. Ankit et al. utilized an integrated morpho-physiological and transcriptome analysis to understand the effects of potassium (K^+) deficiency on the chickpea cultivars {Formatting Citation}. The authors compared PUSA362 (K^+ deficiency-sensitive) and PUSA372 (K^+ deficiency-tolerant) cultivars of chickpea of which PUSA362 showed stunted plant growth along with reduced root development under K^+ deficiency while PUSA372 was less affected. RNA-seq-based transcriptome analysis identified 820 K^+ deficiency-responsive genes that were majorly associated with metabolism, signal transduction, TFs, ion transport, phytohormones, and root development. In particular, the sensitive cultivar showed suppression of genes associated with sucrose transport from shoot to root, indicating a lower energy production and thus contributing to the reduced root growth in PUSA362. Based on these results, authors concluded that the interplay of these genes, particularly those related to phytohormones, signal transduction, ion transport, and TFs, contributes to the differential response to K^+ deficiency in chickpea.

The interplay between plant signaling regulators

A review by Son and Park highlighted the effects of varying climatic factors such as temperature, humidity, and high CO_2 on plant immune responses. In addition, the authors also reviewed the effects of endogenous calcium (Ca^{2+}) ions and hydrogen peroxide (H_2O_2) concentrations on plant defence against invading pathogens. Plant immunity consists of two major components, pathogen-associated molecular pattern (PAMP)-triggered immunity (PTI) and effector-triggered immunity (ETI; Meng et al., 2019). Of these, PTI acts as a first line of defence and is activated upon recognition of conserved pathogen-derived molecular signatures that triggers a rapid oxidative burst, callose deposition, and closure of stomata to inhibit the entry of invading pathogens inside the plant cells (Gupta et al., 2015). On the other hand, ETI is comparatively more robust signaling that may lead to a hypertensive response to kill the pathogen-infected cells. Phytohormone, salicylic acid (SA), has been shown to play key roles in the activation of plant immune responses and the effects of temperature and other environmental and endogenous factors on the SA-dependent and -independent immune responses was reviewed. In conclusion, these changing environmental factors are shown to repress the plant immune responses and affect global food security negatively.

In summary, these studies collectively highlight innovative approaches and insights that are integral to addressing the intertwined challenges of climate change and nutritional security. From sustainable nutritional management and their footprint assessment to deciphering plant responses and disease resistance mechanisms, these findings offer promising pathways for ensuring a resilient and secure global food supply.

Green technologies-based sustainable agricultural practices to ensure the nutritional security in environmentally-challenged crops

Green technologies have been emerging as the potential tool to manage the nutritional security to sustain the agricultural productivity in the epoch of unexpected climatic conditions. Considering the present situation, several researchers explored the methodologies to incorporate and align the concept of green technologies with nutritional security. For instance, Li and Lin investigated the effects of green technology application on sustainable grain production and developed threshold models to improve agricultural production in China. In particular, the authors analyzed the impact of green technologies on Green Total Factor Productivity Growth (GTFPG) in the context of agricultural mechanized production. They especially focused on the green technologies related to plowing, sowing, fertilization, and irrigation to construct the threshold models. The authors showed that the correlation between GTFPG and green technologies varies across regions, with distinct preferences for specific technologies in major and non-major grain-producing areas. Based on their results, the authors concluded the importance of tailored agricultural strategies considering regional disparities and technology-specific effects to promote sustainable productivity growth in the agricultural sector in China. Altogether, green nanoscience and nanotechnology has been regarded as the 'roadmap' to explore the different facets to achieve the nutritional homeostasis for agricultural sustainability (Rasheed et al., 2022).

Conclusively, this article contributes and comprehends with the present knowledge of nutritional security as a regulatory action to avail the sustainable practices of agriculture. Herein, the food nutritional value serves as the mediator in harmonizing the relationship between the plant and human health, as well as the livestock fidelity. The article has discussed the recent progression and strategic approaches for achieving the underlying aim, however, future studies focusing on these disciplines will help to unravel environmental stress-responsive networks and cascade signaling pathways and elucidate how they act together to determine which pathways may have induced first in the environmental stress, will further aid to create strategies for boosting the current status of food nutrition, which are becoming more widespread and frequent due to the persistent but abrupt climate changes.

Author contributions

MK: Conceptualization, Writing – original draft. MI: Writing – review & editing. RG: Writing – review & editing.

Conflict of interest

The authors declare that the research was conducted in the absence of any commercial or financial relationships that could be construed as a potential conflict of interest.

The author(s) declared that they were an editorial board member of Frontiers, at the time of submission. This had no impact on the peer review process and the final decision.

Publisher's note

References

Bhardwaj, A. K., Chejara, S., Malik, K., Kumar, R., Kumar, A., and Yadav, R. K. (2022). Agronomic biofortification of food crops: An emerging opportunity for global food and nutritional security. *Front. Plant Sci.* 13, 1055278. doi: 10.3389/fpls.2022.1055278

Gupta, R., Lee, S. E., Agrawal, G. K., Rakwal, R., Park, S., Wang, Y., et al. (2015). Understanding the plant-pathogen interactions in the context of proteomics-generated apoplastic proteins inventory. *Front. Plant Sci.* 6, 352. doi: 10.3389/fpls.2015.00352

Iqbal, Z., Iqbal, M. S., Khan, M. I. R., and Ansari, M. I. (2021). Toward integrated multi-omics intervention: rice trait improvement and stress management. *Front. Plant Sci.* 12, 741419. doi: 10.3389/fpls.2021.741419

Meng, Q., Gupta, R., Min, C. W., Kwon, S. W., Wang, Y., Je, B. I., et al. (2019). Proteomics of Rice—*Magnaporthe oryzae* interaction: what have we learned so far? *Front. Plant Sci.* 10, 1383. doi: 10.3389/fpls.2019.01383

Nazir, F., Mahajan, M., Khatoon, S., Albaqami, M., Ashfaque, F., Chhillar, H., et al. (2023). Sustaining nitrogen dynamics: a critical aspect for improving salt tolerance in plants. *Front. Plant Sci.* 14, 1087946. doi: 10.3389/fpls.2023.1087946

Rasheed, A., Li, H., Tahir, M. M., Mahmood, A., Nawaz, M., Shah, A. N., et al. (2022). The role of nanoparticles in plant biochemical, physiological, and molecular responses under drought stress: A review. *Front. Plant Sci.* 13, 976179. doi: 10.3389/fpls.2022.976179

frontiers | Frontiers in Plant Science

TYPE Original Research
PUBLISHED 26 August 2022
DOI 10.3389/fpls.2022.964957

OPEN ACCESS

EDITED BY
Mohammad Irfan,
Cornell University, United States

REVIEWED BY
Baizhao Ren,
Shandong Agricultural University, China
Silvia Pampana,
University of Pisa, Italy

*CORRESPONDENCE
Ganghua Li
lgh@njau.edu.cn

SPECIALTY SECTION
This article was submitted to Crop and Product Physiology, a section of the journal Frontiers in Plant Science

RECEIVED 09 June 2022
ACCEPTED 08 August 2022
PUBLISHED 26 August 2022

CITATION
Zhang J, Wang J, Zhou Y, Xu L, Chen Y, Ding Y, Ning Y, Liang D, Zhang Y and Li G (2022) Reduced basal and increased topdressing fertilizer rate combined with straw incorporation improves rice yield stability and soil organic carbon sequestration in a rice–wheat system. *Front. Plant Sci.* 13:964957. doi: 10.3389/fpls.2022.964957

Reduced basal and increased topdressing fertilizer rate combined with straw incorporation improves rice yield stability and soil organic carbon sequestration in a rice–wheat system

Jianwei Zhang[1,2], Jidong Wang[1,3], Yan Zhou[2], Lei Xu[2], Yinglong Chen[4], Yanfeng Ding[2], Yunwang Ning[1], Dong Liang[1], Yongchun Zhang[1] and Ganghua Li[2]*

[1]Scientific Observing and Experimental Station of Arable Land, Ministry of Agriculture and Rural/National Agricultural Experimental Station for Agricultural Environment/Institute of Agricultural Resources and Environment, Jiangsu Academy of Agricultural Sciences, Nanjing, China, [2]National Engineering and Technology Center for Information Agriculture/Key Laboratory of Crop Physiology and Ecology in Southern China/Jiangsu Collaborative Innovation Center for Modern Crop Production, Nanjing Agricultural University, Nanjing, Jiangsu, China, [3]School of Agricultural Equipment Engineering, Jiangsu University, Zhenjiang, China, [4]The UWA Institute of Agriculture and School of Agriculture and Environment, The University of Western Australia, Perth, WA, Australia

Fertilizer management is vital for sustainable agriculture under climate change. Reduced basal and increased topdressing fertilizer rate (RBIT) has been reported to improve the yield of in–season rice or wheat. However, the effect of RBIT on rice and wheat yield stability and soil organic carbon (SOC) sequestration potential is unknown, especially when combined with straw incorporation. Here, we report the effect of RBIT with/without straw incorporation on crop yields, yield stability, SOC stock, and SOC fractions in the lower Yangtze River rice–wheat system region over nine years. RBIT with/without straw incorporation significantly increased nine–year average and annual rice yields but not wheat yields. Compared with conventional fertilization (*CF*), RBIT did not significantly affect wheat or rice yield stability, but combined with straw incorporation, it increased the sustainable yield index (SYI) of wheat and rice by 7.6 and 12.8%, respectively. RBIT produced a higher C sequestration rate (0.20Mg C ha^{-1} $year^{-1}$) than *CF* (0.06Mg ha^{-1} $year^{-1}$) in the 0–20cm layer due to higher root C input and lower C mineralization rate, and RBIT in combination with straw incorporation produced the highest C sequestration rate (0.47Mg ha^{-1} $year^{-1}$). Long–term RBIT had a greater positive effect on silt+clay (0.053mm)–associated C, microbial biomass C (MBC), dissolved organic C, and hot water organic C in the surface layer (0–10cm) than in the subsurface layer (10–20cm). In particular, the increases in SOC pools and mean weight diameter (MWD) of soil aggregates were greater when RBIT was combined with straw incorporation. Correlation analysis indicated that topsoil SOC fractions and MWD were positively correlated with the SYI of

wheat and rice. Our findings suggest that the long–term application of RBIT combined with straw incorporation contributed to improving the sustainability of rice production and SOC sequestration in a rice–wheat system.

KEYWORDS

long–term experiment, fertilizer management, grain yield stability, soil organic carbon sequestration, rice–wheat system

Introduction

The rice–wheat system is the most important cropping system in southeastern Asia, with an area of 24 million hectares (Ladha et al., 2003). However, according to Ladha et al. (2003), rice and wheat yields have stagnated in 72 and 85% of Asia's rice–wheat systems. Ray et al. (2015) reported that year–to–year climate variability explained ~32% and ~36% of rice and wheat yield variability globally, respectively (Ray et al., 2015), suggesting that inter–annual climate variations greatly affect crop yield stability (Wang et al., 2017; Fatima et al., 2022). Some experiments indicated that poor management reduced the sustainable production of crops due to soil degradation (i.e., soil organic carbon (SOC) decline, soil compaction, and soil acidification) (Ladha et al., 2003; Zhang et al., 2015; Rubio et al., 2021). Moreover, data from 49 field experiments revealed that surface soil horizons would lose 30–203 petagrams of C under a 1°C warming scenario (Crowther et al., 2016), implying that climate change increases the risk of SOC loss. Therefore, optimal agricultural management improving crop yield stability and SOC content in the rice–wheat system will be very important under climate change (Ladha et al., 2003; Han et al., 2020; Bhatt et al., 2021; Fatima et al., 2022).

Fertilization management plays a vital role in the rice–wheat system (Ladha et al., 2003; Han et al., 2020; Bhatt et al., 2021). Reduced basal and increased topdressing fertilizer rate (RBIT) is an effective way and has been recommended in some rice and wheat planting countries, including China (Shi et al., 2012; Sui et al., 2013; Chen et al., 2015; Wang et al., 2019; Zhang et al., 2021; Ye et al., 2022), Japan (Myint et al., 2009; Kamiji et al., 2011; Moe et al., 2014), India (Khurana et al., 2008; Jat et al., 2012), Australia (Wood et al., 2020), Italy (Ercoli et al., 2013), Spain (Garrido-Lestache et al., 2005) and Argentina (Melaj et al., 2003). Short-term (2–3 years) field experiments showed that RBIT could generally increase in-season rice or wheat yield (Melaj et al., 2003; Kamiji et al., 2011; Jat et al., 2012; Shi et al., 2012; Ercoli et al., 2013; Chen et al., 2015; Wang et al., 2019; Wood et al., 2020; Zhang et al., 2021; Ye et al., 2022). This due to that RBIT provided better synchronization of rice and wheat nitrogen (N) demand with N supply, improving crop N uptake and promoting spikelet differentiation and carbohydrate synthesis, compared with conventional fertilization (*CF*) (Shi et al., 2012; Ercoli et al., 2013; Sui et al., 2013; Xu et al., 2015; Zhang et al., 2021). However, some studies found that N fertilizer timing and splitting had no effect on wheat yields, due to excessive rainfall and low temperature in the autumn-winter period and impeding the establishment and tillering of crop (Garrido-Lestache et al., 2005; Pampana and Mariotti, 2021). High N concentration in plant under frequent cloudy and rain may increase the risk of lodging and late maturity, leading to yield loss, implying that RBIT may increase the fluctuation of year–to–year crop yield under climate change. Especially the intensity and frequency of extreme temperature and precipitation are expected to increase due to climate change (IPCC, 2014, 2021). Therefore, it is necessary to effectively evaluate the effect of RBIT on crop yield stability in the rice–wheat system.

Long–term experiments offer important advantages relative to short–term studies in providing valuable information on the effect of fertilization management on the sustainability of crop production (Manna et al., 2005; Qaswar et al., 2019; Han et al., 2020). Studies have reported that the sustainable yield index (SYI) of rice and wheat has a positive relationship with SOC content (Wanjari et al., 2004; Qaswar et al., 2019). These findings suggest that SOC plays an important role in improving crop yield stability under climate change (Manna et al., 2005; Han et al., 2020; Shi et al., 2022). However, ^{15}N tracer tests found that the residual soil N derived from basal fertilizer was higher in the paddy (Wang et al., 2018) and upland soil (Shi et al., 2012) at harvest than from topdressing fertilizer. RBIT with low residual soil N from fertilizer N and high crop nutrient removal (Khurana et al., 2008; Sui et al., 2013; Xu et al., 2015) may cause a decrease in soil nutrient content, which in turn stimulates the mineralization of soil organic matter and releases more soil available nutrients for crop growth. Thus, we speculate that the continuous application of this practice may reduce SOC content, which in turn is not conducive to the sustainability of crop production in the rice–wheat system.

Straw incorporation is a common practice to improve the sustainability of crop production in the rice–wheat system (Sharma and Prasad, 2008; Huang et al., 2013; Zhu et al., 2015; Li et al., 2018; Han et al., 2020; Jin et al., 2020; Mohamed et al., 2021). The global meta-analysis showed that straw incorporation increased the SOC by 12.0%, easily oxidizable C (EOC) by 24.4%, microbial biomass C (MBC) by 26.7%, and dissolved organic C (DOC) by 24.2% (Liu et al., 2014). Some studies showed that straw incorporation could increase and stabilize crop yield in wheat–maize rotation (Shi et al., 2022) and rice-bases cropping system

(Qaswar et al., 2019) due to improving SOC. Some studies indicated that under straw incorporation conditions, N fertilizer rate should be increased in the early stage of growth to mitigate microbial competition for N with crops (Cao et al., 2018; Li et al., 2018; Wei et al., 2019; Zheng et al., 2019). However, there is a lack of effective information on whether straw incorporation with RBIT impacts the sustainability of crop production in rice–wheat systems. We therefore performed a 9–year field experiment to assess the effect of continuous application of RBIT with or without straw incorporation on crop yield, yield stability, and SOC sequestration potential in rice-wheat systems.

Materials and methods

Experiment site

The field experiment was conducted at the Danyang Experimental Station in Zhenjiang, Jiangsu province, eastern China (119°10′, 34°36′). This area has a subtropical humid monsoon climate with an average air temperature of 14–15°C and annual precipitation of 800–1,100 mm. The soil type was classified as waterloggogenic paddy soil (Chinese Soil Taxonomy). Before starting the experiment in 2009, the main properties of the soil (0–20 cm) were: SOC, 10.07 g kg^{-1}; total N, 0.97 g kg^{-1}; NH_4OAc K, 93.50 mg kg^{-1}; and Olsen P, 13.60 mg kg^{-1}.

Experimental design

The experiment was conducted in a rice–wheat rotation system from 2009 to 2018. The three treatments were as follows: *CF* as a control, RBIT only, and RBIT combined with straw incorporation (RBITS). Total N, P and K fertilizer rates for all treatments were the same with 300 kg N ha^{-1}, 150 kg P_2O_5 ha^{-1}, and 240 kg K_2O in the rice season, respectively, and 225 kg N ha^{-1}, 105 kg P_2O_5 ha^{-1} and 105 kg K_2O ha^{-1} in the wheat season, respectively. N rates of the basal fertilizer, tillering fertilizer, spikelets–promoting fertilizer, and spikelets–protecting fertilizer for *CF* and RBIT were 150–75–75–0 kg N ha^{-1} and 120–60–60–60 kg N ha^{-1} in the rice season, respectively, 125–0–100–0 kg N ha^{-1} and 90–45–45–45 kg N ha^{-1} in the wheat season, respectively. P fertilizer rates of the basal fertilizer and jointing fertilizer for *CF* and RBIT were 150–0 kg P_2O_5 ha^{-1} and 75–75 kg P_2O_5 ha^{-1} in the rice season, respectively, 105–0 kg P_2O_5 ha^{-1} and 60–45 kg P_2O_5 ha^{-1} in the wheat season, respectively. K fertilizer rates of the basal fertilizer and jointing fertilizer for *CF* and RBIT were 240–0 kg K_2O ha^{-1} and 120–120 kg K_2O ha^{-1} in the rice season, respectively, 105–0 kg K_2O ha^{-1} and 60–45 kg K_2O ha^{-1} in the wheat season, respectively. Basel fertilizers were applied one day before plowing at the time of rice transplanting and wheat sowing. Tiller fertilizers were applied seven days after rice transplanting and wheat three-leaf stage, respectively. Spikelets–promoting fertilizers were applied in the rice and wheat jointing stage, and then spikelets–protecting fertilizers were applied at the appearance of the inverse 2nd leaf. For RBITS, all rice and wheat straw were returned to the subsequent crop. N, P, and K fertilizer were in the form of urea, triple superphosphate, and potassium chloride, respectively. All treatments were arranged in a randomized block design with three replications, and each plot was 31.5 m^2. The rice planting density was 13.3 × 30.0 cm, and wheat was sown by broadcasting 225 kg of seed ha^{-1}. In each year, the rice variety Wuyunjing 23# (*Oryza sativa* L.) was transplanted by hand in mid–June with a rice planting density of 13.3 × 30.0 cm, and the wheat variety Yangmai 16# (2010–2013) and Yangmai 20 (2014–2018) (*Triticum aestivum* L.) was sown in mid–November at the seed rate of 225 kg ha^{-1}. Other agricultural management was carried out following the farmer's practices. The daily average temperature and precipitation during the rice and wheat seasons from 2010 to 2018 are shown in Figure 1.

Soil sampling and analyses

Collection of soil samples

Due to the small short-term response of total SOC content to fertilizer management, so we measured the total SOC content in the 0–20 cm soil layer annually after the rice harvest beginning in 2014 and continuing for five years through 2018. To clarify the effect of long–term fertilizer management on the SOC pools of different soil layers, we collected soil samples at depths of 0–10 cm and 10–20 cm after the 2018 rice harvest and divided them into two parts. One part was air–dried at room temperature, then ground and sieved to 0.15 mm for analyses of soil bulk SOC and EOC. The other part was sieved to 2 mm and analyzed for MBC, DOC, and HWOC. At the same time, undisturbed soil samples were collected at depths of 0–10 cm and 10–20 cm to measure soil aggregate fractions and their associated C contents.

Soil aggregate stability and SOC content in bulk soil and soil aggregate fractions

Soil aggregate fractions were separated using the wet–sieving method (Elliott, 1986). In brief, the following three aggregate size fractions were obtained using a series of sieves: 2–0.25 mm (macro–aggregates), 0.25–0.053 mm (micro–aggregates), and <0.053 mm (silt+clay). Pre-wetted dry soil samples (50 g) were automatically moved 3 cm up and down 30 times per min for 30 min using a soil aggregate analyzer (Model SAA 8052, Shanghai, China). The aggregates that remained on each sieve were then dried at 40°C for 72 h and weighed.

The formula for calculating mass percentage in each particle size aggregate fraction was as follows:

$$m_a = \frac{w_a}{M} \times 100\% \quad (1)$$

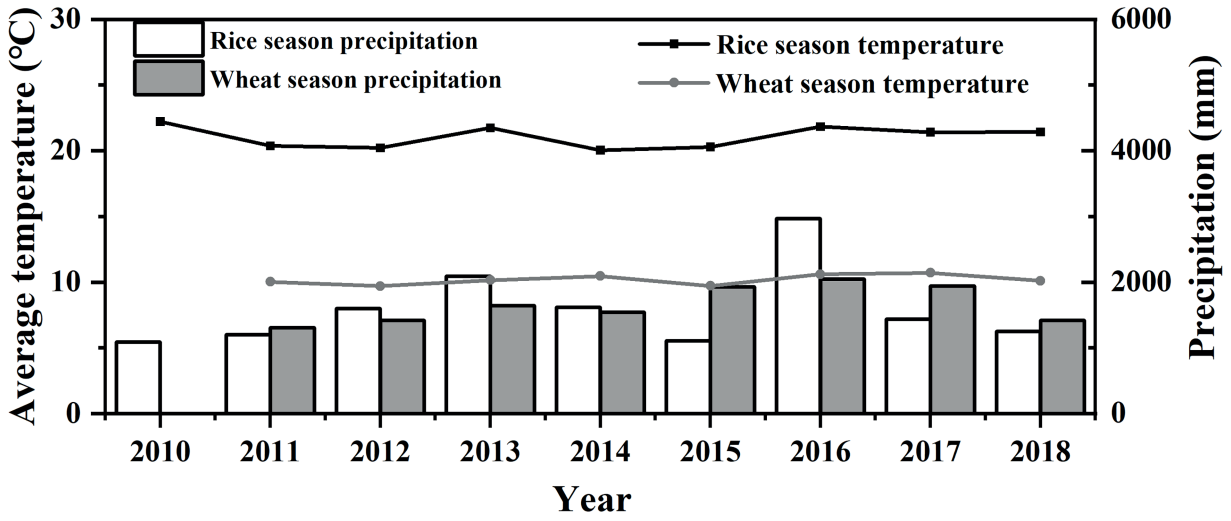

FIGURE 1
Average temperature and precipitation for the rice and wheat season from 2010–2018. Line: average temperature; Columnar: precipitation.

where m_a represents the mass percentage (%) of the a–size aggregate fraction, w_a represents the weight (g) of the a–size aggregate fraction, and M is the total weight of all aggregates (g).

The mean weight diameter (MWD) of soil aggregates is a common index used to represent soil aggregate stability and is calculated according to equation 2:

$$\mathrm{MWD} = \sum_{a=1}^{n} \left(D_a \times w_a \right) \tag{2}$$

where D_a represents the mean diameter (mean of two adjacent sieve diameters) of the a–size aggregate fraction.

Bulk soil and soil aggregates were finely ground (<0.15 mm) to determine SOC content (about 100 mg) with a Flash HT Plus elemental analyzer (Thermo Fisher Scientific, Bremen, Germany).

Contents of LOC fractions

MBC was extracted from fresh soil samples (<2 mm, 50 g) by chloroform fumigation and 0.5 M K_2SO_4 extraction (Vance et al., 1987) and analyzed using an automated TOC analyzer (Analytik Jena, Germany). The ratio of water and soil was 5:1. The MBC content was calculated using an extraction efficiency coefficient of 0.45 (Jenkinson et al., 2004).

DOC and HWOC were determined from fresh field samples (<2 mm, 10 g) following the procedure of Ghani et al. (2003). The ratio of water and soil was 5:1. The extractions were performed at 25°C for 30 min (DOC) and 80°C for 16 h (HWOC). The DOC and HWOC contents were then analyzed using the automated total organic C (TOC) analyzer (Analytik Jena, Germany).

EOC was determined from dry soil samples (<0.15 mm) following Blair et al. (1995). A soil sample containing about 15 mg C was oxidized with 25 ml 333 mM $KMnO_4$ while shaking for 6 h, followed by centrifugation for 10 min at 1000 *g*. The absorbances of the supernatant and standards were read at 565 nm. The change in $KMnO_4$ concentration was estimated to calculate the EOC content, assuming that 1 mM $KMnO_4$ was consumed in the oxidation of 9 mg of C (Table 1).

TABLE 1 Estimated 9–year cumulative carbon input for each treatment.

Treatment	Root C		Straw C		Total C input
	Wheat	Rice	Wheat	Rice	
CF	11.9 b	26.8 c	–	–	38.7 c
RBIT	12.7 a	27.9 b	–	–	40.6 b
RBITS	11.7 b	28.8 a	28.3	37.0	105.7 a

CF: conventional fertilization; RBIT: reduced basal and increased topdressing fertilizer rate; RBITS: RBIT combined with straw incorporation. Different lowercase letters represent significant differences among treatments ($p \leq 0.05$). –: no data.

C pool management index

The CMPI evaluates the relative potential of agricultural management measures to influence the SOC pool and C sequestration (Zhu et al., 2015). In the present study, the CMPI was used to monitor differences in SOC dynamics between treatments. A higher CMPI value indicated a more sustainable system. The CMPI was calculated using equations 3–6:

$$\mathrm{CMPI} = \mathrm{CPI} \times \mathrm{LI} \times 100\% \tag{3}$$

where CPI is the C pool index, and LI is the lability index.

$$\mathrm{CPI} = \frac{\mathrm{SOC_{BS}\ in\ PF\ or\ PFS}}{\mathrm{SOC_{BS}\ in\ CF}} \times 100\% \tag{4}$$

$$LI = \frac{E_{EOC} \text{ in PF or PFS}}{E_{EOC} \text{ in CF}} \quad (5)$$

$$E_{EOC} = \frac{\text{Content of EOC}}{SOC} \quad (6)$$

where SOC_{BS} is the SOC content in the bulk soil, and EOC refers to SOC oxidized by $KMnO_4$.

Yield measurements and estimates of cumulative C input

At the mature stage, grain yields and yield formations were determined by hand–harvesting in each plot; an area of 2.5 m^2 per plot was harvested in the rice season and 2 m^2 per plot in the wheat season. The rice and wheat yields were calculated at standard moisture contents of 13.5 and 12.5%, respectively. In the 2016 wheat season, low temperature during the seedling germination stage and poor management caused large–scale weed growth in spring, resulting in an average yield of only 2 t ha^{-1} in 2016. Therefore, to avoid interfering with the research results, the wheat yield and yield formation in 2016 were not counted.

Yield stability was evaluated by comparing the sustainable yield index (SYI) among treatments, which was calculated using equation 7 (Wanjari et al., 2004; Han et al., 2020):

$$SYI = \frac{Y_{mean} - Y_{sd}}{Y_{max}} \times 100\% \quad (7)$$

where Y_{mean} is the mean of combined rice and wheat (annual), rice, and wheat yields during 2010–2018, Y_{sd} is the standard deviation of yield, and Y_{max} is the maximum yield over 2010–2018 for each treatment.

$$CV = \frac{I_{mean}}{I_{sd}} \times 100\% \quad (8)$$

Where CV is the coefficient of variation of year–to–year rice and wheat yield formation parameters. I_{mean} and I_{sd} are the mean and standard deviation of rice and wheat yield formation parameters during 2010–2018.

The 9–year cumulative root–C and straw–C input were estimated (Table 1) using equations 9–11:

$$T_{root\ or\ straw} = \sum W_{root\ or\ straw} + \sum R_{root\ or\ straw} \quad (9)$$

$$\sum W_{root\ or\ straw} = \frac{\sum WB_{shoot} \times WC_{shoot}}{WR_{shoot}} \times WR_{root\ or\ straw} \quad (10)$$

$$\sum R_{root\ or\ straw} = \frac{\sum RB_{shoot} \times RC_{shoot}}{RR_{shoot}} \times RR_{root\ or\ straw} \quad (11)$$

TABLE 2 C content of shoots and relative allocation coefficients of crop C to different parts of wheat and rice.

Crop type	C_{shoot} (%)	Relative crop C allocation coefficients			
		R_{grain}	R_{straw}	R_{shoot}	R_{root}
Wheat	52	0.32#	0.48#	0.80#	0.20#
Rice	40	0.36##	0.36##	0.72###	0.28###

The data marked with # and ### were obtained from the reviews by Bolinder et al. (2007) and Liu et al. (2019). The data marked with ## was calculated based on a rice harvest index of 0.5.

where $T_{root\ or\ straw}$ is the total cumulative root–C or straw–C input (t C ha^{-1}); $\sum W_{root/straw}$ refers to the cumulative root–C or straw–C input (t C ha^{-1}) for wheat; $\sum R_{root\ or\ straw}$ refers to the cumulative root–C or straw–C input (t C ha^{-1}) for rice; $\sum WB_{shoot}$ and WC_{shoot} represent wheat shoot biomass (t ha^{-1}) and shoot C content (%), respectively; WR_{shoot} and $WR_{root\ or\ straw}$ represent the plant C allocation coefficients of the wheat shoots (grain+straw), roots (including all root–derived material not usually recovered with the roots), and straw, respectively (Table 2); RR_{shoot}, RR_{root}, and RR_{straw} represent the plant C allocation coefficients for the rice shoots, roots, and straw, respectively. The C content, RR_{grain}, and RR_{straw} were estimated according to the analytical data from 2017 and 2018.

SOC sequestration

The SOC stock at a depth of 0–20 cm was calculated using equation 11 (Brar et al., 2015).

$$SC = SOC \times BD \times h \times 10000 \times 0.1 \quad (12)$$

where SC is the SOC stock at a depth of 0–20 cm (Mg ha^{-1}), SOC is the SOC content (g kg^{-1}) of the plowed layer (0–20 cm), BD is the soil bulk density (kg m^{-3}), and h refers to the depth of the plowed layer (0.2 m).

The SOC sequestration (CS) of treatments compared with the initial SOC stock was calculated using equation 13. The sequestrated C rate and C mineralization rate were calculated using equations 14–15.

$$CS = SC_T - SC_{initial} \quad (13)$$

$$CSR = \frac{CS}{9} \quad (14)$$

$$CMR = \frac{CI}{9} - CSR \quad (15)$$

where SC_T refers to SOC stock after 9 years (Mg ha^{-1}), CSR is the C sequestration rate (Mg ha^{-1} $year^{-1}$), CMR is the C mineralization rate (Mg ha^{-1} $year^{-1}$), and CI is an estimate of the total C input over nine years (Mg ha^{-1} $year^{-1}$).

TABLE 3 Effect of fertilization management on yield components(No. of panicles, No.of spikelets per panicle, grain weight, seed setting rate), dry matter accumulation and harvest index and their coefficients of variation.

Treatments	No. of panicles (m^{-2})		No. of spikelets per panicle		Grain weight (mg)		Seed setting rate (%)		Total dry matter ($t\,ha^{-1}$)		Harvest index (%)	
	Average	CV	Average	CV	Average	CV	Average	CV	Average	CV	Average	CV
Wheat												
CF	391.1 ± 34.2 a	24.8	37.0 ± 2.3 a	17.8	41.9 ± 1.6 a	10.5	–	–	10.9 ± 0.5 a	23.5	52.6 ± 1.6 a	14.9
RBIT	405.9 ± 26.1 a	18.2	37.1 ± 2.3 a	17.3	42.4 ± 1.9 a	12.8	–	–	11.7 ± 0.4 a	15.5	53.6 ± 1.8 a	15.2
RBITS	386.8 ± 21.7 a	15.9	38.4 ± 2.1 a	15.4	42.0 ± 1.6 a	10.5	–	–	11.0 ± 0.3 a	12.5	51.3 ± 1.8 a	15.8
Rice												
CF	327.1 ± 7.9 A	12.2	123.4 ± 2.3 C	9.5	30.4 ± 0.2 A	3.9	89.9 ± 1.0 A	5.7	19.1 ± 0.3 B	8.1	49.4 ± 0.9 A	8.5
RBIT	344.5 ± 6.6 A	10.0	130.3 ± 1.5 B	6.1	30.3 ± 0.3 A	5.5	85.4 ± 1.3 B	8.0	19.9 ± 0.3 A	6.5	50.1 ± 0.8 A	8.3
RBITS	337.5 ± 7.4 A	11.5	138.7 ± 1.1 A	4.1	30.3 ± 0.3 A	5.2	84.2 ± 1.5 B	9.1	20.6 ± 0.2 A	5.8	49.4 ± 0.7 A	6.7

CF: conventional fertilization; RBIT: reduced basal and increased topdressing fertilizer rate; RBITS: RBIT combined with straw incorporation. MWD: mean weight diameter. Different lowercase and uppercase letters represent significant differences in yield components of wheat and rice, respectively ($P \leq 0.05$). Data: mean ± standard error (SE); –: no data.

Data analysis

Statistical analyses of the data were performed using SPSS 26.0 software (IBM Corp., Armonk, NY, USA). All analyses were carried out on the three replicates. A one-way analysis of variance (ANOVA) was performed to analyze the effect of different fertilization management on average yield, SYI, yield compounds, dry matter accumulation, harvest index, different SOC pools, soil aggregate mass distribution, MWD and pH. The least significant difference (LSD) was used to compare mean values between fertilization management. Differences between treatments were significant at $p \leq 0.05$. Pearson's correlations were determined among SYI, C input, SOC pool fractions, MWD, and pH, to clarify the relationship between yield stability and soil properties. SOC is usually protected by soil aggregate physically and chemically. Therefore, to determine the main factors affecting SOC, we used redundancy analysis (RDA) to quantify the relationships between the C content of soil aggregate fractions and other parameters (MBC, DOC, HWOC, EOC, C input, MWD, and pH).

Results

Yield and yield formation

Grain yield

Over the nine years, wheat yield, rice yield, and annual yield ranged from 4.6–7.6 $t\,ha^{-1}$, 9.4–13.0 $t\,ha^{-1}$, and 15.4–20.5 $t\,ha^{-1}$, respectively (Figure 2A). ANOVA results showed that fertilization management did not affect wheat yield but had a significant effect on the 9–year average rice yield and annual yield (Figure 2B). Compared with the *CF* treatment, the RBIT and RBITS treatments significantly increased the 9–year average rice yield by 4.6 and 6.8% and the annual yield by 4.9 and 5.1%, respectively. However, there was no statistical difference between the RBIT and RBITS treatments.

The wheat, rice, and annual SYIs were 66.0–74.2%, 74.9–84.9%, and 79.4–84.9%, respectively, and they were significantly affected by fertilization management (Figure 2C). Compared with the *CF* treatment, the RBIT treatment did not affect wheat, rice, or annual SYIs, but combined with straw incorporation (RBITS) significantly increased the SYI of rice by 13.4%.

Yield components

Fertilization management had no effect on the wheat yield components, and the average No. of panicles and grain weight for rice, but it significantly affected the average No. of spikelets per panicle and seed setting rate for rice (Table 3). Compared with the *CF* treatment, the RBIT and RBITS treatments significantly increased the average No. of spikelets per panicle for rice by 5.5 and 12.3%, respectively, but decreased the seed setting rate by 5.1 and 6.4%, respectively. Among them, the No. of rice spikelets per panicle of the RBITS was higher than that of RBIT.

In terms of CVs, wheat yield components were higher than rice, and they were ranked No. of panicles (15.9–24.8%) > No. of spikelets per panicle (15.4–17.8%) > grain weight (10.5–12.8%) for wheat and No. of panicles (10.0–12.2%) > seed setting rate (5.7–9.1%), No. of spikelets per panicle (4.1–9.5%) > grain weight (3.9–5.5%) for rice (Table 3). Compared with the *CF* treatment, the RBIT and RBITS treatments reduced the CVs of No. of panicles and No. of spikelets per panicle but increased the CVs of grain weight and seed setting rate; similar trends were observed in rice and wheat.

Dry matter accumulation and harvest index

Fertilization management significantly affected the average dry matter accumulation for rice, showing RBITS (20.6 $t\,ha^{-1}$) > RBIT (19.9 $t\,ha^{-1}$) > *CF* (19.1 $t\,ha^{-1}$), but it had no effect on the average dry matter accumulation for wheat and harvest index for rice and wheat (Table 3).

In terms of CVs, dry matter accumulation (12.5–23.5%) and harvest index (16.3–18.8%) for wheat were higher than for rice

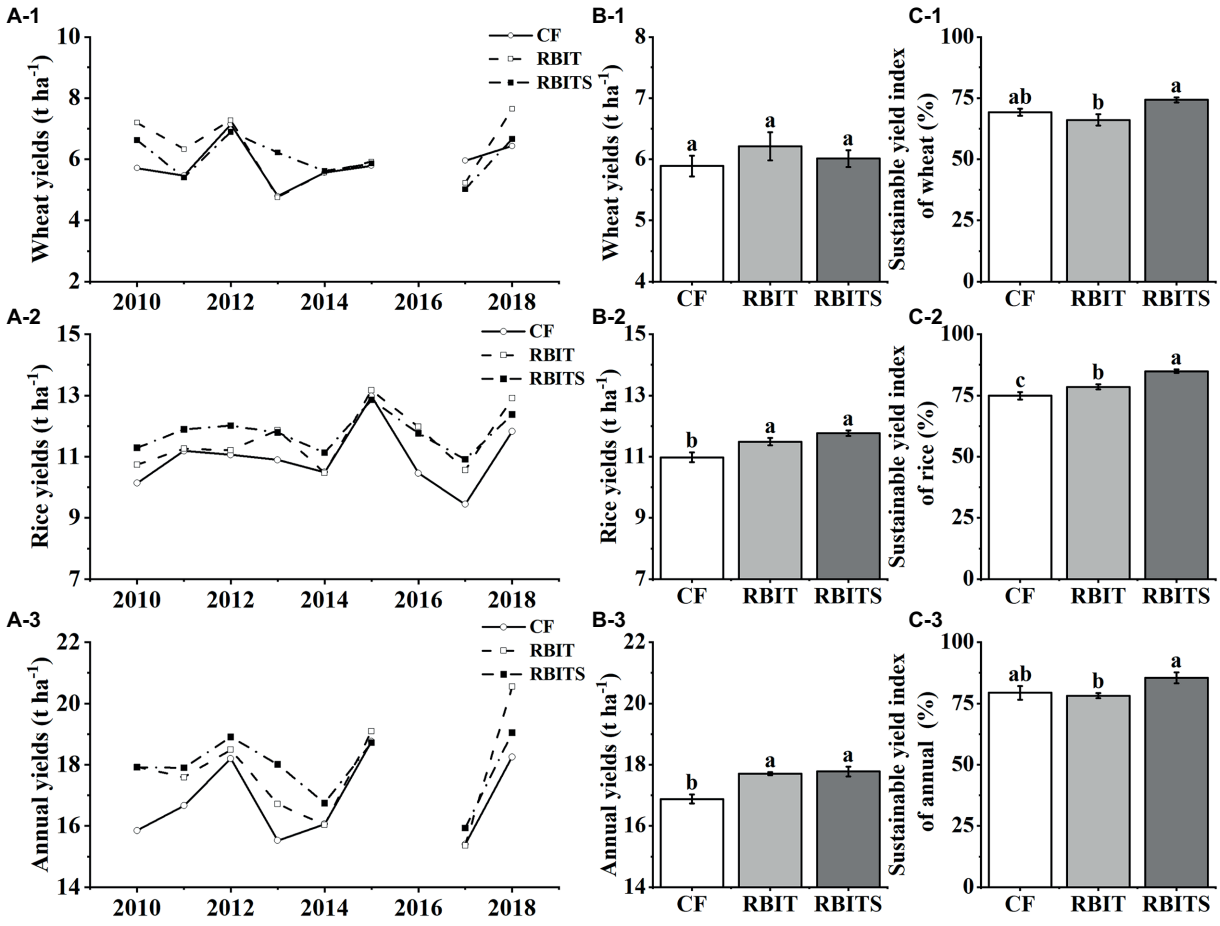

FIGURE 2
Effects of fertilization management on wheat, rice, and annual yield and their sustainable yield indexes. *CF*: conventional fertilization; RBIT: reduced basal and increased topdressing fertilizer rate; RBITS: RBIT combined with straw incorporation. **(A-C)** Show each year's yield, the 9–year average yield, and the sustainable yield index, respectively. **(1-3)** Show wheat, rice, and annual data, respectively. Different lowercase letters represent significant differences ($p \leq 0.05$) among treatments for the same crop type. Error bars are standard error (SE) of the mean.

(5.8–8.1%, 6.7–8.5%). The CVs of dry matter accumulation and harvest index among the treatments, except for the harvest index for wheat, showed a consistent trend, RBITS > RBIT > *CF* (Table 3).

SOC sequestration

Among the treatments, only bulk soil SOC (0–20 cm) ($R^2 = 0.77$, $p < 0.05$) in the RBITS treatment showed a significant trend of increasing over time (Figure 3A). After nine years, the content and stock of SOC in the 0–20 cm layer of the *CF* (10.3 g kg^{-1}, 26.2 Mg ha^{-1}), RBIT (11.0 g kg^{-1}, 27.5 Mg ha^{-1}), and RBITS (12.1 g kg^{-1}, 29.8 Mg ha^{-1}) treatments were higher than their initial values (10.1 g kg^{-1}, 25.6 Mg ha^{-1}) (Figures 3B,C). Statistical differences were observed between the *CF* treatment and the RBIT treatment with and without straw incorporation.

The estimated values of C input, C sequestration rate, and C mineralization rate in the 0–20 cm layer were 0.43–1.18 Mg ha^{-1} year^{-1}, 0.06–0.47 Mg ha^{-1} year^{-1}, and 0.25–0.71 Mg ha^{-1} year^{-1}, respectively (Figures 3D–F). Compared with the *CF* treatment, the RBIT and RBITS treatments significantly increased C input and C sequestration rate by 4.8, 173.1, 216.5, and 627.6%, respectively. In terms of the C mineralization rate, the RBIT treatment significantly decreased by 32.6%, but when combined with straw incorporation (RBITS), it increased by 92.8%.

SOC pools

Aggregate–associated C

Figure 4 shows that fertilization management significantly affected the SOC content of bulk soil and aggregate fractions in the 0–10 cm layer but had no effect in the 10–20 cm layer. In the 0–10 cm layer, compared with the *CF* treatment, the RBIT treatment significantly increased the SOC content of bulk soil and silt+clay by 8.35 and 25.0% but did not markedly

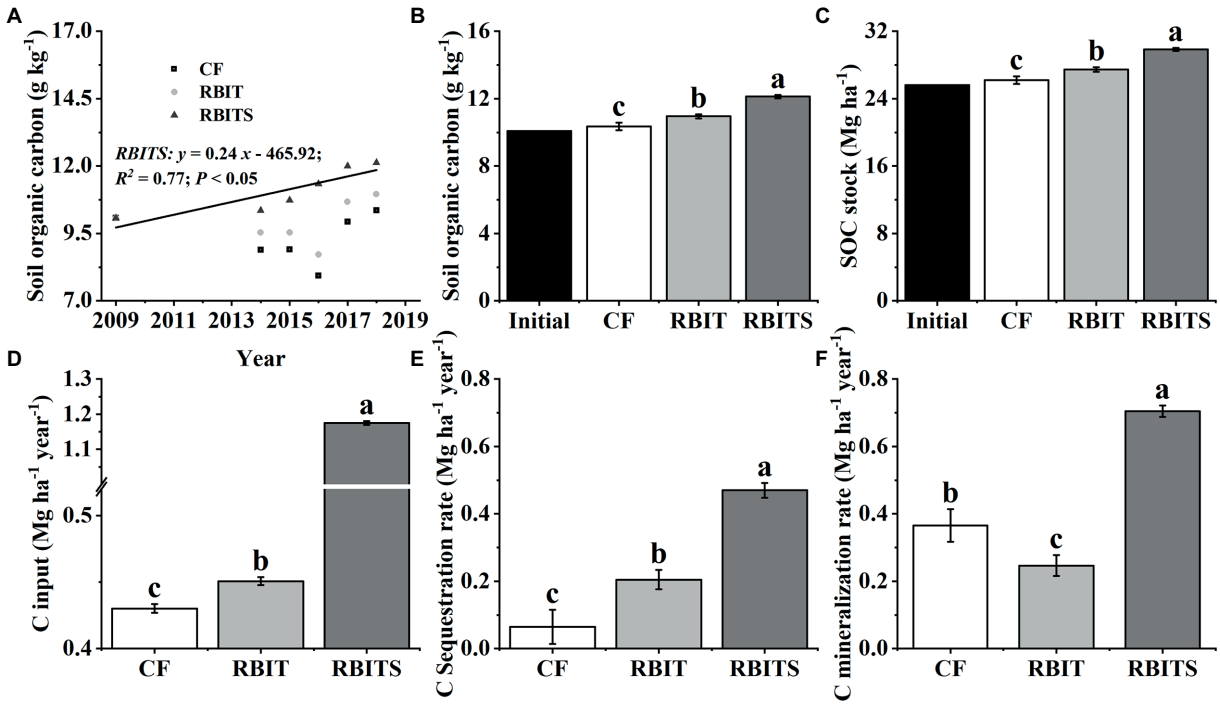

FIGURE 3
Effect of fertilization management on SOC dynamics **(A)**, SOC in 2018 **(B)**, SOC stock **(C)**, C input **(D)**, C sequestration rate **(E)**, and C mineralization rate **(F)** in the bulk soil (0–20cm). *CF*: conventional fertilization; RBIT: reduced basal and increased topdressing fertilizer rate; RBITS: RBIT combined with straw incorporation. Different lowercase letters represent significant differences ($p \leq 0.05$) among treatments for the same crop type. Error bars are standard error (SE) of the mean.

affect the macro– and micro–aggregate fractions; when RBIT combined with straw incorporation (RBITS), it significantly increased SOC levels in the bulk soil and macro–aggregate, micro–aggregate, and silt+clay fractions by 22.5, 24.4, 37.8, and 50.1%, respectively.

LOC fractions

LOC pool fractions in the two soil depths responded differently to fertilization management (Figure 5). In the 0–10 cm layer, the contents of MBC (446.5, 515.7 mg kg^{-1}), HWOC (378.5, 454.8 mg kg^{-1}), and DOC (26.6, 31.72 mg kg^{-1}) in the RBIT alone or in combination with straw incorporation (RBITS) were higher than in the *CF* treatment (334.1 mg kg^{-1}, 322.3 mg kg^{-1}, and 20.3 mg kg^{-1}). The RBITS treatment had the highest content of EOC among the treatments. In the 10–20 cm layer, fertilization management significantly affected the contents of MBC and EOC only. The RBIT and RBITS treatments increased MBC by 86.7 and 73.8%, and EOC by 31.6 and 29.4%, respectively, compared with the *CF* treatment. Furthermore, application of RBIT alone or in combination with straw incorporation (RBITS) produced a higher CMPI at both soil depths compared with the *CF* treatment, with increases of 4.3–31.1% and 29.2–31.4% at depths of 0–10 cm and 10–20 cm, respectively (Figure 6).

Soil aggregate stability and pH

The mass proportions of soil aggregate fractions were ranked macro–aggregates > micro–aggregates > silt+clay (Table 4). Compared with the *CF* treatment, the RBIT treatment produced no change in soil aggregate mass proportions at the two soil depths, but when combined with straw incorporation (RBITS), it had a significant effect on the mass proportions of macro–aggregate and micro–aggregate fractions in the 0–10 cm layer, increasing the macro–aggregate fraction by 13.9% and decreasing the micro–aggregate fraction by 36.7%. In terms of MWD, only the 0–10 cm layer showed significant differences among treatments, which were ranked RBITS (89.5 mm) > *CF* (80.3 mm) and RBIT (77.0 mm). However, there were no differences in pH among treatments at either soil depth (Table 4).

Relationships between yield stability and soil properties

Correlation analysis showed that the SYI of wheat and rice had a positive correlation with SOC fraction content, CMPI, and MWD in the 0–10 cm layer, and these relationships were stronger for rice (Figure 7). Significant positive correlations between different SOC pools were observed only

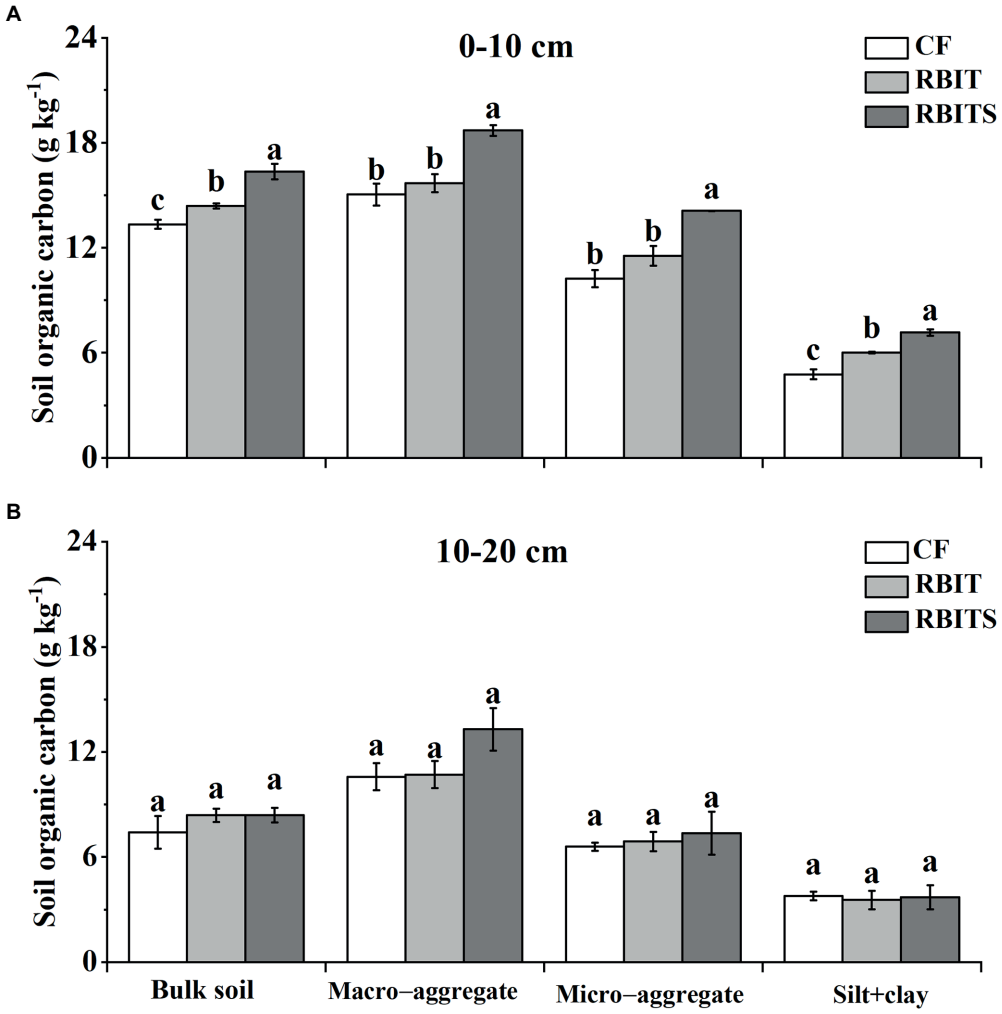

FIGURE 4
Effect of fertilization management on the SOC content in the bulk soil and aggregate fractions at depths of 0–10cm **(A)** and 10–20cm **(B)** after nine years. *CF*: conventional fertilization; RBIT: reduced basal and increased topdressing fertilizer rate; RBITS: RBIT combined with straw incorporation. Different lowercase letters represent significant differences ($p \leq 0.05$) among treatments in each graph and for each fraction. Error bars are standard error (SE) of the mean.

in the 0–10 cm layer. Furthermore, MWD was significantly correlated with SOC in the bulk soil and macro–aggregate and micro–aggregate fractions, and with EOC and C input in the 0–10 cm layer, but no significant relationships were observed in the 10–20 cm layer.

For the soil aggregate–associated C in the 0–10 cm layer, the first axis accounted for 94.7% of the overall variance, and the second axis accounted for 3.5% (Figure 8A); MBC ($F = 28.6$, $p = 0.002$) and C input ($F = 9.7$, $p = 0.012$) were the main parameters that affected soil aggregate–associated C, accounting for 80.3 and 12.1% of the total variance, respectively. In the 10–20 cm layer, the first and second axes accounted for 74.4 and 8.8% of the variance (Figure 8B). HWOC ($F = 10.0$, $p = 0.008$) was the main parameter that affected the soil aggregate–associated C content, explaining 58.9% of the total variance.

Discussion

RBIT with straw incorporation and increased crop yields in the rice–wheat system

With population growth and urbanization, increasing the grain yield per unit area is important for meeting future high food demands (Zhang et al., 2015; Hemathilake and Gunathilake, 2022). In our study, 9–year average rice yields of RBIT with/without straw incorporation in a rice–wheat system are consistent with previous studies (Khurana et al., 2008; Fan et al., 2009; Kamiji et al., 2011; Ercoli et al., 2013; Sui et al., 2013; Moe et al., 2014; Chen et al., 2015; Xu et al., 2015; Wang et al., 2019; Wood et al., 2020; Ye et al., 2022), in which found that higher grain yield and N use efficiency were obtained with reduced N application before

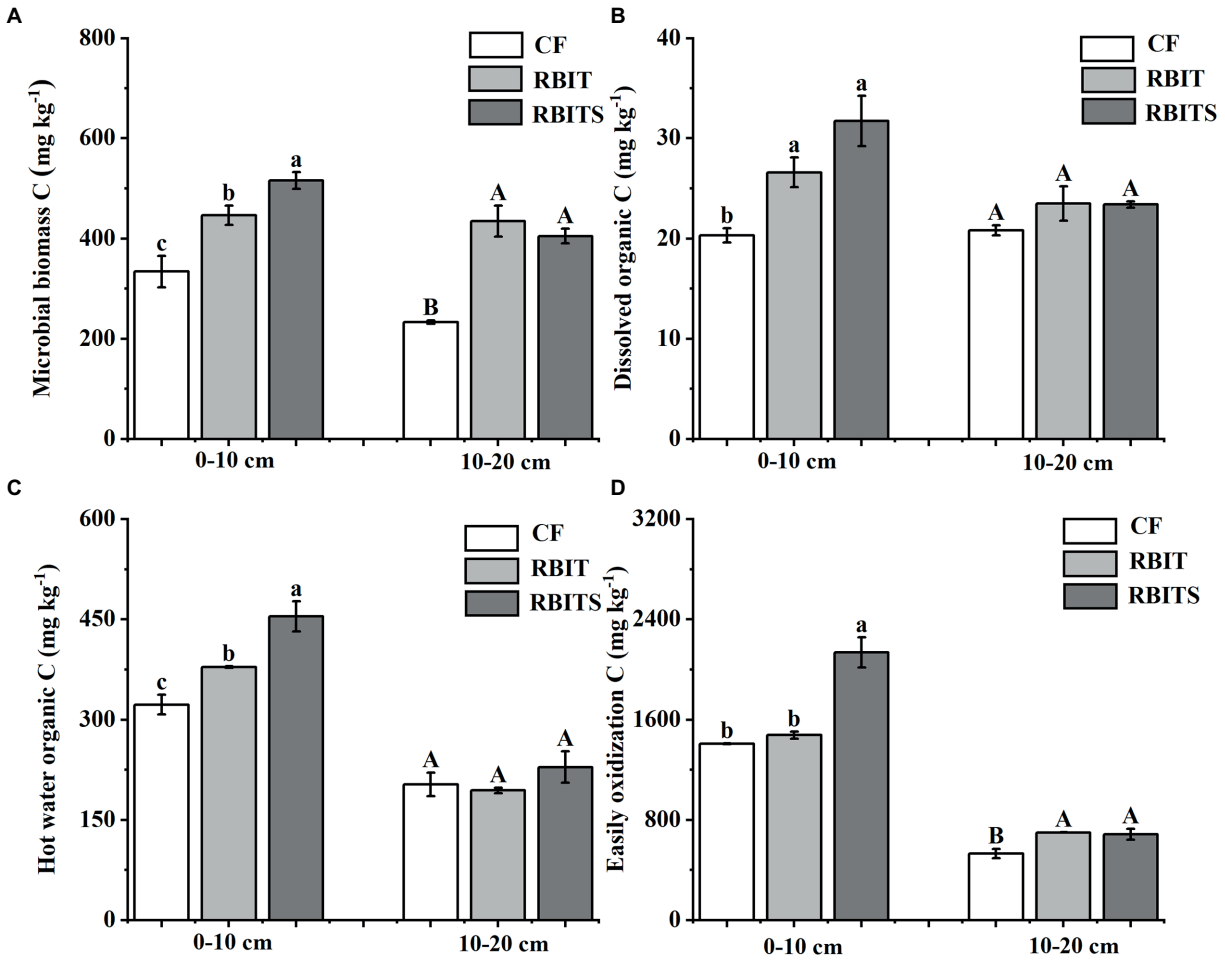

FIGURE 5
Effect of fertilization management on the content of microbial biomass C **(A)**, dissolved organic C **(B)**, hot water organic C **(C)**, and easily oxidizable C **(D)** at depths of 0–10cm and 10–20cm after nine years. *CF*: conventional fertilization; RBIT: reduced basal and increased topdressing fertilizer rate; RBITS: RBIT combined with straw incorporation. MBC: microbial biomass carbon; DOC: dissolved organic C; HWOC: hot water organic C; EOC: easily oxidizable C. The different lowercase and uppercase letters represent significant differences ($p \leq 0.05$) among treatments at depths of 0–10cm and 10–20cm, respectively. Error bars are standard error (SE) of the mean.

seeding. On the one hand, spikelets formation begins at the beginning of tillering and the number of spikelets is determined at the beginning of stem elongation (Mohapatra and Sahu, 2022). The yield advantage was related to a higher number of kernels per spike, resulting from a higher number of fertile spikelets per spike (Kamiji et al., 2011; Ercoli et al., 2013; Sui et al., 2013; Chen et al., 2015; Wang et al., 2019; Ye et al., 2022). Reducing N fertilizer rate in the early growth stage could limit the production of ineffective tillers, forming a healthy population (Myint et al., 2009; Zhang et al., 2011; Moe et al., 2014; Ye et al., 2022). Providing sufficient nutrients at the stem elongation stage could promote the differentiation of spikelets and reduce their degradation, thereby obtaining high No. of spikelets per panicle (Kamiji et al., 2011; Zhang et al., 2011; Sui et al., 2013). Similar results were observed in our 9-year field experiment. On the other hand, N is important for leaf chlorophyll, and fertilizer N application could improve leaf chlorophyll content and the photosynthetic capacity of crops (Zhang et al., 2021). Field experiments reported that the high yield of the crop was mainly attributable to the higher total and post-anthesis dry matter accumulation (Zhang et al., 2011, 2021; Ye et al., 2022). This study observed that RBIT had a high SPAD valve of 1st–4th leaf from the top (Supplementary Table S1) and photosynthetic rate of sword leaf (Supplementary Table S2) at the rice heading stage, thereby promoting the synthesis of photosynthetic products.

Abundant mineral elements in returned straw provide nutrients for crop growth and spikelet differentiation (Huang et al., 2013; Li et al., 2018). Previous studies observed that straw incorporation could immobilize fertilizer–derived N from previous and current seasons by improving soil quality and through the straw itself (Cao et al., 2018; Zheng et al., 2019). This immobilized N is released at the high nutrient demand stage (after the jointing stage) (Cao et al., 2018; Zheng et al., 2019), making obtain more No. of spikelets per panicle (Huang et al., 2013). In

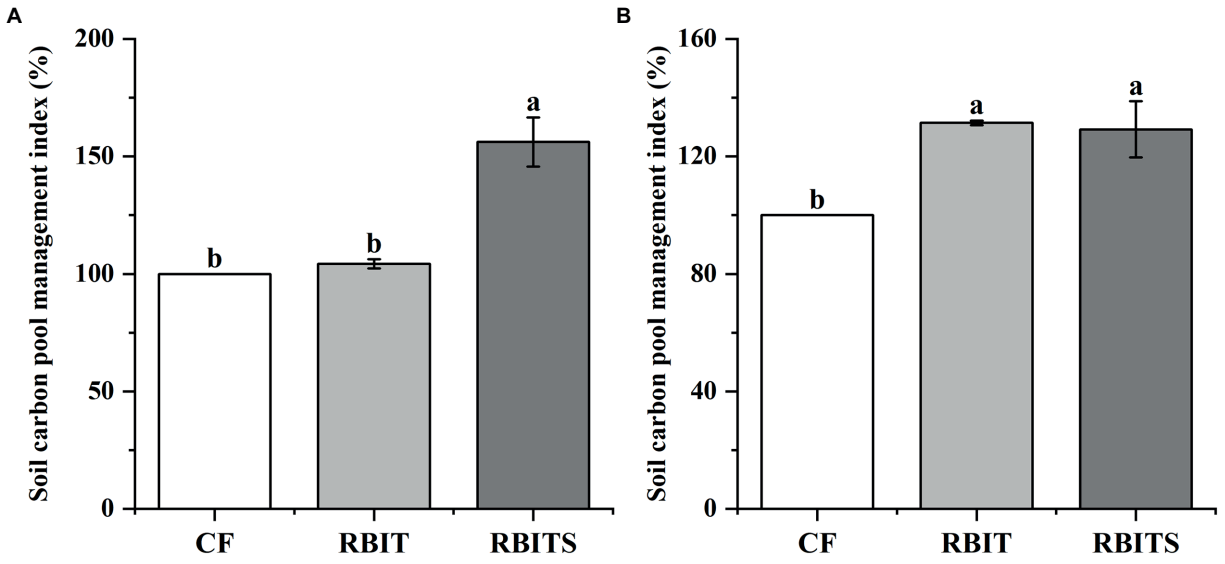

FIGURE 6
Effect of fertilization management on CMPI at depths of 0–10cm **(A)** and 10–20cm **(B)** after nine years. *CF*: conventional fertilization; RBIT: reduced basal and increased topdressing fertilizer rate; RBITS: RBIT combined with straw incorporation. The different lowercase letters represent significant differences ($p \leq 0.05$) among treatments in each soil depth. Error bars are standard error (SE) of the mean.

TABLE 4 Effect of fertilization management on soil aggregate mass distribution, mean weight diameter and pH at depths of 0–10cm (A) and 10–20cm (B) after nine years.

Treatments	Aggregate mass proportion (%)			MWD (mm)	pH (soil/water: 1/2.5)
	2–0.25 mm	0.25–0.053 mm	<0.053 mm		
0–10 cm					
CF	67.8 ± 1.6 b	24.7 ± 0.9 a	7.4 ± 0.7 a	80.3 ± 1.6 b	5.5 ± 0.2 a
RBIT	64.6 ± 2.6 b	27.2 ± 2.5 a	8.2 ± 0.4 a	77.0 ± 2.6 b	5.3 ± 0.0 a
RBITS	77.3 ± 1.7 a	15.6 ± 1.7 b	7.1 ± 0.5 a	89.5 ± 1.7 a	5.5 ± 0.0 a
10–20 cm					
CF	55.0 ± 9.2 A	34.9 ± 6.0 A	10.1 ± 3.5 A	67.5 ± 5.1 A	6.4 ± 0.1 A
RBIT	54.2 ± 7.2 A	35.2 ± 4.7 A	10.6 ± 2.9 A	66.6 ± 6.0 A	6.1 ± 0.1 A
RBITS	51.8 ± 4.9 A	39.4 ± 3.9 A	8.8 ± 1.6 A	64.4 ± 5.2 A	6.2 ± 0.1 A

CF: conventional fertilization; RBIT: reduced basal and increased topdressing fertilizer rate; RBITS: RBIT combined with straw incorporation. MWD: mean weight diameter. Different lowercase and uppercase letters represent significant differences ($P \leq 0.05$) among treatments in the 0–10 cm and 10–20 cm layers, respectively. Data: mean ± standard error (SE).

our study, straw incorporation had a high No. of spikelets per panicle but had a slightly negative effect on No. of panicles. This result was because the initial decomposition of straw could release phytotoxic substances (e.g., organic acids) and decrease soil available N content with high microbial N immobilization, thereby inhibiting rice tillering (Sharma and Prasad, 2008; Olk et al., 2009; Wei et al., 2019). Thus, the positive effects of straw incorporation on rice were possibly offset by its negative effects, leading to an ineffective yield increase.

However, negative effects of RBIT with/without straw incorporation on the seed setting rate for rice was possibly due to intensified competition for resources (e.g., space, nutrients, carbohydrates) between spikelets. Previous studies found a negative feedback effect between the number of spikelets and grain filling (Kamiji et al., 2011; Sui et al., 2013). Therefore, high yield strategies should pay greater attention to the intense source and smooth translocation for enlarging effective sink–filling ability in rice–wheat systems.

It is worth noting that RBIT with/without straw incorporation had no effect on wheat yield, which was in agreement with previous studies (Garrido-Lestache et al., 2005; Pampana and Mariotti, 2021). Mariana et al. (2003) found that N applications at tillering permit the highest wheat yields. Some studies demonstrated that the early season N environment had a large influence on N partitioning at maturity, whereas N applied at anthesis had little effect on N partitioning and was allocated more efficiently to wheat grain (Melaj et al., 2003; Wang et al., 2018). However, Shi et al. (2012) found that topdressing could obtain a high wheat yield due to giving better root growth and increasing plant N uptake. Zhang et al. (2021) found that increasing topdressing N fertilizer under

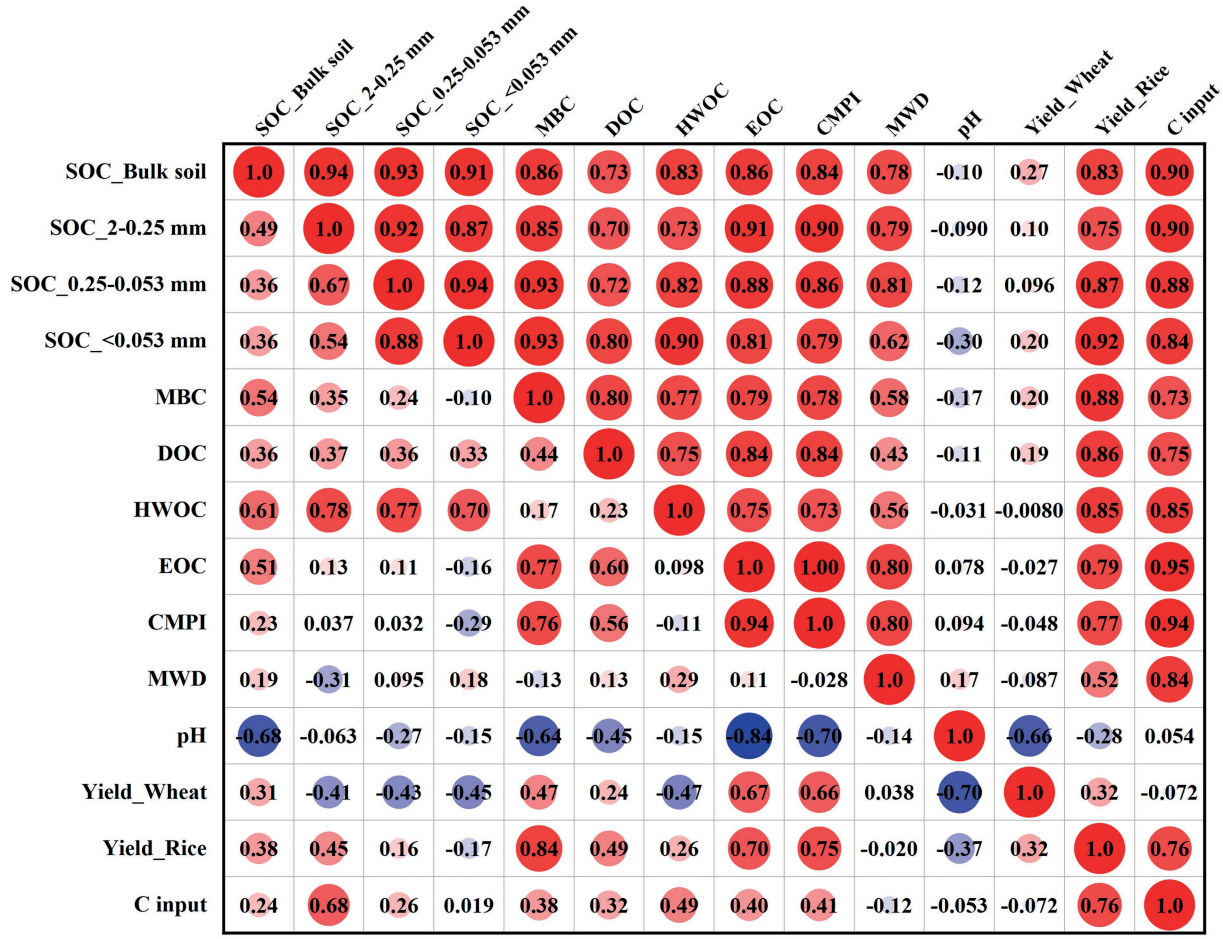

FIGURE 7
Correlation analysis between the SYI of wheat and rice and soil parameters at depths of 0–10cm (upper triangular matrix) and 10–20cm (lower triangular matrix). MBC: microbial biomass carbon; DOC: dissolved organic C; HWOC: hot water organic C; EOC: easily oxidized C; CMPI: C pool management index; MWD: mean weight diameter. SYI: sustainable yield index.

water-saving irrigation conditions could promote antioxidant enzyme activity and the remobilization of photosynthate after anthesis to increase wheat grain yield. In conclusion, this discrepancy may be attributed partly to variations in climatic conditions (i.g., rainfall and temperature), and soil residual N content prior to sowing (Melaj et al., 2003; Garrido-Lestache et al., 2005; Myint et al., 2009; Pampana and Mariotti, 2021).

RBIT with straw incorporation and crop yield stability in the rice–wheat system

SYI has been used to evaluate the sustainability and stability of crop production under climate change, and a lower value of SYI indicates a more unstable system (Wanjari et al., 2004; Han et al., 2020; Shi et al., 2022). In our study, the SYI of rice (74.9–84.9%) was higher than that of wheat (66.0–74.2%), in agreement with Han et al. (2020), who reported that the SYI of wheat and rice were 50–69% and 39–53%, respectively. Those results suggested that wheat growth was more vulnerable to year–to–year weather change (Fatima et al., 2022). Under the effects of climate change, the microclimate of the rice root growth environment can be protected by the water layer, whereas that of wheat is not. For upland rainfed wheat, mineralization of fertilizers and soil N depends on rainfall (namely soil water content) and temperature, affecting the establishment of tillers, the differentiation and formation of spikelets, and the synthesis of photosynthate (Garrido-Lestache et al., 2005; Homyak et al., 2017; Pampana and Mariotti, 2021). Indeed, in our study, the CVs of wheat panicle number (15.9–24.8%), spikelets per panicle (15.4–17.8%), dry matter accumulation (12.5–23.5%) were higher than that of grain weight (10.5–12.8%) and harvest index (14.9–15.8%).

Our experiment found that the application of RBIT did not affect crop yield stability in the rice–wheat system, but RBIT combined with straw incorporation helped stabilize rice and wheat yield, especially rice, which was in agreement with previous studies (Qaswar et al., 2019; Shi et al., 2022). These results might be attributed to alleviating the negative effect of climate change on

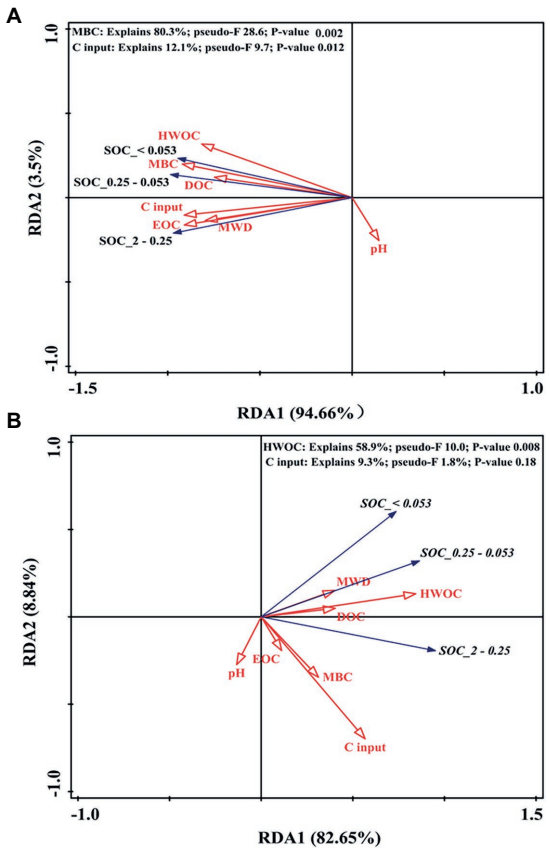

FIGURE 8
RDA plot showing the associations between the SOC content in soil aggregate fractions and different pools of organic C (MBC, DOC, HWOC, and EOC), C input, pH, and MWD at depths of 0–10cm **(A)** and 10–20cm **(B)**. MBC: microbial biomass carbon; DOC: dissolved organic C; HWOC: hot water organic C; EOC: easily oxidized C; MWD: mean weight diameter.

No. of panicles, No of spikelets per panicle and dry matter accumulation. Tillering, panicle differentiation and material synthesis depend on the nutrient status of crops (Melaj et al., 2003; Chen et al., 2015; Wang et al., 2018; Ye et al., 2022). Our results showed that the year–to–year fluctuation of the SPAD value of the 1st–4th leaf from the top at heading in the RBITS treatment was lower than that of the RBIT and *CF* treatments (Supplementary Figure S1). This finding implied that RBITS could stabilize the N status of crops, which might improve crop resistance to climate change. Strong root system and nutrient (i.e., N, K, Si) supply under straw incorporation (Li et al., 2018; Yan et al., 2018; Wei et al., 2019) might provide a favorable condition for stabilizing the nutrient status of crops and resisting abiotic stress (i.e., climate change). Indeed, Pan et al. (2016) showed that N fertilizer application could compensate for the negative effects of shading on photosynthesis and root morphologies of rice. A review summarized Si–mediated abiotic and biotic stress tolerance mechanisms by scavenging the reactive oxygen species and regulating different metabolic pathways (Ranjan et al., 2021). K application also had similar effects to Si application in alleviating abiotic stresses, contributing to the accumulation of photosynthetic products and N uptake (Sustr et al., 2019; Wang et al., 2020). These results suggested that RBITS might improve the physiological and biochemical mechanism of crop stress resistance for alleviating the negative effect of climate change and stabilizing crop yield. However, the effects of RBITS practice on the physiological/biochemical mechanisms underlying crop stability warrant further research.

Effect of RBIT and straw incorporation on SOC sequestration

The magnitude and direction of SOC sequestration are highly dependent on the quantity and quality of exogenous organic matter (Xu et al., 2020; Angst et al., 2021; Mohamed et al., 2021). In our experiment, root residues and root exudates were the main sources of soil organic matter input in the *CF* and RBIT treatments. RBIT application had a high SOC stock owing to vigorous crop growth and low SOC mineralization rate. A meta-analysis reported that increasing the splitting frequency of fertilizer N application and decreasing basal N fertilizer could reduce soil reactive N losses (Xia et al., 2018). ^{15}N tracer showed that RBIT application could increase the residual amount of panicle fertilizer N in the soil and decrease fertilizer N loss (Xu et al., 2015; Wang et al., 2018; Zheng et al., 2019; Ye et al., 2022). In this study, total N, P, and K contents after nine years of RBIT application were higher than the initial value and the value in the *CF* treatment (data not shown), indicating that this practice promotes the soil retention of fertilizer–derived nutrients and reduces the mineralization of soil organic matter.

It is widely acknowledged that there are two pathways by which microbes promote soil C turnover: one is catabolism, releasing CO_2 to the atmosphere from the mineralization of organic matter; the other is anabolism, sequestering C (such as the formation of stabilized C, humic acid) by the microbial "C pump" that processes fresh C inputs. In previous work, the relative strength of the two processes was closely related to C utilization efficiency (CUE) (Chen et al., 2020). When straw was removed, DOC input from rhizodeposition was the primary C source for microbial growth (Zhu et al., 2017). Root–derived C was regarded as a more efficient C source for the formation of stable SOC than aboveground residues (Kätterer et al., 2011). Indeed, in our study, DOC, MBC, and humic acid in the surface layer (data not shown) in the RBIT treatment were higher than that of the CT treatment. This result suggested that the microbial anabolism pathway was stronger than the catabolism pathway in the RBIT treatment, thus promoting humification. Christopher and Lal (2007) reported similar results in which optimized N fertilizer management could foster humus formation. Some studies have indicated that microbial necromass was associated with clay minerals, forming bio–recalcitrant organic compounds (Kätterer et al., 2011; Angst et al., 2021; Sokol et al., 2022). Our results showed that nine years of RBIT application positively affected silt+clay associated–C in the surface layer, and surface silt+clay associated–C was the most

closely related to MBC, suggesting that RBIT helped to increase the stable organic C pool. Therefore, the long–term application of RBIT contributes to stabilizing SOC pools, decreasing C emissions under climate change, and slowing the rate of global warming.

Straw incorporation as a globally protective tillage practice can improve the quantity and quality of SOC (Liu et al., 2014; Xia et al., 2018; Xu et al., 2020; Mohamed et al., 2021; Shi et al., 2022), as seen in the results of this study. This effect was due to residual plant input (Angst et al., 2021). In contrast to the C sequestration of RBIT, aboveground residues rich in easily decomposed organic matter (such as glucose and cellulose) were added to the soil, triggering the metabolism of microorganisms in the catabolism pathway and producing more CO_2 (Liu et al., 2014; Chen et al., 2020; Angst et al., 2021). In our study, the mineralization rate in the RBITS treatment was 0.9–fold and 1.3–fold that of *CF* and RBIT, implying that straw incorporation enhanced soil C emission (Liu et al., 2014; Xia et al., 2018). If this is true, how do we reduce soil C emissions when the straw is returned to the field? In this study, the negative effect of RBIT on the mineralization rate of SOC suggests that adjusting fertilization patterns under conditions of straw incorporation can reduce soil C emissions and synergize the effective use of nutrients, thereby reducing the risks of climate warming and environmental pollution.

Effect of RBIT and straw incorporation on soil physical properties

In our study, continuous application of RBIT caused no change in soil aggregate structure, but combined with straw incorporation could increase macro–aggregate mass percentage and MWD in the surface layer. Previous studies have shown similar results in which the positive effect of straw incorporation on soil structure was greater than that of inorganic fertilizer (Liu et al., 2014; Jin et al., 2020). This result may be attributable to the cementing effect of plant–derived compounds (such as carbohydrates), roots, and hyphae to fine particles. Some studies have reported that straw incorporation promoted strong root systems and high microbial biomass (Liu et al., 2014; Xia et al., 2018; Yan et al., 2018; Chen et al., 2020). In our study, positive correlations between MWD and SOC pool fractions and C input in the surface layer implied that stabilized soil structure in the RBITS treatment might limit organic matter decomposition and increase SOC storage.

Furthermore, no significant reduction in soil pH after nine years of RBIT application implies that long–term application may prevent soil acidification, which may be occurred through the substantial removal of base cations under conventional high–yield management (Zeng et al., 2017). Previous studies reported that straw incorporation could help to reduce soil acidification by returning base cations in crop straw to the soil (Zeng et al., 2017; Li et al., 2018). Similar results were also observed in this study. Therefore, long–term straw incorporation as a soil amendment can reduce soil acidification caused by the excessive application of inorganic N fertilizer.

Yield stability and soil properties

In our study, the SYIs of rice had positive relationships with SOC fractions and MWD in the surface layer, which was consistent with previous research (Wanjari et al., 2004; Han et al., 2020). This finding implied that improved soil quality could benefit the stability and sustainability of rice production (Wanjari et al., 2004; Qaswar et al., 2019; Han et al., 2020; Rubio et al., 2021; Shi et al., 2022). However, a weaker positive relationship between wheat yield stability and soil parameters suggested that improved wheat adaptability to climate change might require the selection and breeding of varieties with high tolerance to low temperatures and waterlogging injury based on appropriate cultivation practices.

Conclusion

A 9–year field experiment showed that RBIT positively affected rice yield and annual yield in rice–wheat systems but did not significantly affect yield stability. RBIT combined with straw incorporation stabilized rice yield owing to low year–to–year fluctuations in the No. of panicles, No. of spikelets per panicle, and dry matter accumulation. Long–term application of RBIT contributed to SOC sequestration due to high root C input and low C mineralization rate. When combined with straw incorporation, RBIT further improved SOC stock. Long–term RBIT application significantly increased silt+clay–associated C, MBC, DOC, and HWOC in the surface soil but not in the subsurface soil, and RBIT with straw incorporation resulted in the greatest SOC pool fractions and the most stable soil structure. Correlation analysis indicated that wheat and rice yields were more stable with the improvement in SOC, its fractions, and soil structure in the surface layer. Our findings suggest that the long–term application of RBIT with straw incorporation can improve sustainable rice production and SOC sequestration in rice–wheat systems.

Data availability statement

The original contributions presented in the study are included in the article/Supplementary material, further inquiries can be directed to the corresponding author.

Author contributions

JZ and JW contributed to the conception and design of the study. JZ, YZ, and LX organized the database. JZ performed the statistical analysis and wrote the first draft of the manuscript. All authors contributed to the article and approved the submitted version.

Funding

The research was supported by the National Key Research and Development Program of China (2017YFD0301203, 2017YFD0300100, and 2018YFD0300803) and the Jiangsu Agriculture Science and Technology Innovation Fund [JASTIF; CX(21)1009].

Conflict of interest

The authors declare that the research was conducted in the absence of any commercial or financial relationships that could be construed as a potential conflict of interest.

Publisher's note

Supplementary material

The Supplementary material for this article can be found online at: https://www.frontiersin.org/articles/10.3389/fpls.2022.964957/full#supplementary-material

References

Angst, G., Mueller, K. E., Nierop, K. G. J., and Simpson, M. J. (2021). Plant-or microbial-derived? A review on the molecular composition of stabilized soil organic matter. *Soil Biol. Biochem.* 156, 108189–108183. doi: 10.1016/j.soilbio.2021.108189

Bhatt, R., Singh, P., Hossain, A., and Timsina, J. (2021). Rice-wheat system in the northwest indo-Gangetic plains of South Asia: Issues and technological interventions for increasing productivity and sustainability. *Paddy Water Environ.* 19, 345–365. doi: 10.1007/s10333-021-00846-7

Blair, G., Lefroy, R., and Lisle, L. (1995). Soil carbon fractions based on their degree of oxidation, and the development of a carbon management index for agricultural systems. *Aust. J. Agr. Res.* 46, 393–406. doi: 10.1071/ar9951459

Bolinder, M. A., Janzen, H. H., Gregorich, E. G., Angers, D. A., and VandenBygaart, A. J. (2007). An approach for estimating net primary productivity and annual carbon inputs to soil for common agricultural crops in Canada. *Agric. Ecosyst. Environ.* 118, 29–42. doi: 10.1016/j.agee.2006.05.013

Brar, B. S., Singh, J., Singh, G., and Kaur, G. (2015). Effects of long term application of inorganic and organic fertilizers on soil organic carbon and physical properties in maize-wheat rotation. *Agron.-Basel* 5, 220–238. doi: 10.3390/agronomy5020220

Cao, Y. S., Sun, H. F., Zhang, J. N., Chen, G. F., Zhu, H. T., Zhou, S., et al. (2018). Effects of wheat straw addition on dynamics and fate of nitrogen applied to paddy soils. *Soil Tillage Res.* 178, 92–98. doi: 10.1016/j.still.2017.12.023

Chen, Y., Peng, J., Wang, J., Fu, P., Hou, Y., Zhang, C., et al. (2015). Crop management based on multi-split topdressing enhances grain yield and nitrogen use efficiency in irrigated rice in China. *Field Crop Res.* 184, 50–57. doi: 10.1016/j.fcr.2015.09.006

Chen, X., Xia, Y., Rui, Y., Ning, Z., Hu, Y., Tang, H., et al. (2020). Microbial carbon use efficiency, biomass turnover, and necromass accumulation in paddy soil depending on fertilization. *Agric. Ecosyst. Environ.* 292:106816. doi: 10.1016/j.agee.2020.106816

Christopher, S. F., and Lal, R. (2007). Nitrogen management affects carbon sequestration in north American cropland soils. *Crit. Rev. Plant Sci.* 26, 45–64. doi: 10.1080/07352680601174830

Crowther, T. W., Todd-Brown, K. E., Rowe, C. W., Wieder, W. R., Carey, J. C., Machmuller, M. B., et al. (2016). Quantifying global soil carbon losses in response to warming. *Nature* 540, 104–108. doi: 10.1038/nature20150

Elliott, E. T. (1986). Aggregate structure and carbon, nitrogen, and phosphorus in native and cultivated soils1. *Soil Sci. Soc. Am. J.* 50, 627–627. doi: 10.2136/sssaj1986.03615995005000030017x

Ercoli, L., Masoni, A., Pampana, S., Mariotti, M., and Arduini, I. (2013). As durum wheat productivity is affected by nitrogen fertilisation management in Central Italy. *Eur. J. Agron.* 44, 38–45. doi: 10.1016/j.eja.2012.08.005

Fan, M., Lu, S., Jiang, R., Liu, X., and Zhang, F. (2009). Triangular transplanting pattern and Split nitrogen fertilizer application increase rice yield and nitrogen fertilizer recovery. *Agron. J.* 101, 1421–1425. doi: 10.2134/agronj2009.0009

Fatima, Z., Naz, S., Iqbal, P., Khan, A., Ullah, H., Abbas, G., et al. (2022). "Field crops and climate change," in *Building Climate Resilience in Agriculture: Theory, Practice and Future Perspective*. eds. W. N. Jatoi, M. Mubeen, A. Ahmad, M. A. Cheema, Z. Lin and M. Z. Hashmi (Cham: Springer International Publishing), 83–94.

Garrido-Lestache, E., López-Bellido, R. J., and López-Bellido, L. (2005). Durum wheat quality under mediterranean conditions as affected by N rate, timing and splitting, N form and S fertilization. *Eur. J. Agron.* 23, 265–278. doi: 10.1016/j.eja.2004.12.001

Ghani, A., Dexter, M., and Perrott, K. W. (2003). Hot-water extractable carbon in soils: a sensitive measurement for determining impacts of fertilisation, grazing and cultivation. *Soil Biol. Biochem.* 35, 1231–1243. doi: 10.1016/S0038-0717(03)00186-X

Han, X., Hu, C., Chen, Y., Qiao, Y., Liu, D., Fan, J., et al. (2020). Crop yield stability and sustainability in a rice-wheat cropping system based on 34-year field experiment. *Eur. J. Agron.* 113:125695, 125965. doi: 10.1016/j.eja.2019.125965

Hemathilake, D. M. K. S., and Gunathilake, D. M. C. C. (2022). "Chapter 31-agricultural productivity and food supply to meet increased demands," in *Future Foods*. ed. R. Bhat (Cambridge: Academic Press), 539–553.

Homyak, P. M., Allison, S. D., Huxman, T. E., Goulden, M. L., and Treseder, K. K. (2017). Effects of drought manipulation on soil nitrogen cycling: A meta-analysis. *J. Geophys. Res. Biogeo.* 122, 3260–3272. doi: 10.1002/2017jg004146

Huang, S., Zeng, Y., Wu, J., Shi, Q., and Pan, X. (2013). Effect of crop residue retention on rice yield in China: A meta-analysis. *Field Crop Res.* 154, 188–194. doi: 10.1016/j.fcr.2013.08.013

IPCC (2014). "Synthesis Report," in *Pachauri Intergovernmental Panel on Climate Change*. ed. R. K. Pachauri (Geneva, Switzerland).

IPCC (2021). *Climate Change 2021: The Physical Science Basis. Contribution of Working Group I to the Sixth Assessment Report of the Intergovernmental Panel on Climate Change,* Cambridge University Press.

Jat, R. A., Wani, S. P., Sahrawat, K. L., Singh, P., Dhaka, S. R., and Dhaka, B. L. (2012). Recent approaches in nitrogen management for sustainable agricultural production and eco-safety. *Arch. Agron. Soil Sci.* 58, 1033–1060. doi: 10.1080/03650340.2011.557368

Jenkinson, D. S., Brookes, P. C., and Powlson, D. S. (2004). Measuring soil microbial biomass. *Soil Biol. Biochem.* 36, 5–7. doi: 10.1016/j.soilbio.2003.10.002

Jin, Z., Shah, T., Zhang, L., Liu, H., Peng, S., and Nie, L. (2020). Effect of straw returning on soil organic carbon in rice–wheat rotation system: A review. *Food Energy Secur.* 9:e200. doi: 10.1002/fes3.200

Kamiji, Y., Yoshida, H., Palta, J. A., Sakuratani, T., and Shiraiwa, T. (2011). N applications that increase plant N during panicle development are highly effective in increasing spikelet number in rice. *Field Crop Res.* 122, 242–247. doi: 10.1016/j.fcr.2011.03.016

Kätterer, T., Bolinder, M. A., Andrén, O., Kirchmann, H., and Menichetti, L. (2011). Roots contribute more to refractory soil organic matter than above-ground crop residues, as revealed by a long-term field experiment. *Agric. Ecosyst. Environ.* 141, 184–192. doi: 10.1016/j.agee.2011.02.029

Khurana, H. S., Phillips, S. B., Bijay, S., Alley, M. M., Dobermann, A., Sidhu, A. S., et al. (2008). Agronomic and economic evaluation of site-specific nutrient management for irrigated wheat in Northwest India. *Nutr. Cycl. Agroecosyst.* 82, 15–31. doi: 10.1007/s10705-008-9166-2

Ladha, J. K., Dawea, D., Pathakb, H., Padrea, A. T., Yadavc, R. L., Singhd, B., et al. (2003). How extensive are yield declines in long-term rice-wheat experiments in Asia? *Field Crop Res.* 81, 159–180. doi: 10.1016/S0378-4290(02)00219-8

Li, H., Dai, M., Dai, S., and Dong, X. (2018). Current status and environment impact of direct straw return in China's cropland – A review. *Ecotoxicol. Environ. Saf.* 159, 293–300. doi: 10.1016/j.ecoenv.2018.05.014

Liu, Y., Ge, T., Zhu, Z., Liu, S., Luo, Y., Li, Y., et al. (2019). Carbon input and allocation by rice into paddy soils: A review. *Soil Biol. Biochem.* 133, 97–107. doi: 10.1016/j.soilbio.2019.02.019

Liu, C., Lu, M., Cui, J., Li, B., and Fang, C. (2014). Effects of straw carbon input on carbon dynamics in agricultural soils: A meta-analysis. *Glob. Chang. Biol.* 20, 1366–1381. doi: 10.1111/gcb.12517

Manna, M. C., Swarup, A., Wanjari, R. H., Ravankar, H. N., Mishra, B., Saha, M. N., et al. (2005). Long-term effect of fertilizer and manure application on soil organic carbon storage, soil quality and yield sustainability under sub-humid and semi-arid tropical India. *Field Crop Res.* 93, 264–280. doi: 10.1016/j.fcr.2004.10.006

Mariana, A. M., Hernan, E. E., Silvia, C. L., Guillermo, S., Fernando, A., and Nestor, O. B. (2003). Timing of nitrogen fertilization in wheat under conventional and no-tillage system. *Agron. J.* 9, 1525–1531. doi: 10.2134/agronj2003.1525

Melaj, M. A., Echeverrıa, H. N. E., Pez, S. C. L., Studdert, G., Andrade, F., and Barbaro, N. S. O. (2003). Timing of nitrogen fertilization in wheat under conventional and no-tillage system. *Agron. J.* 95, 1525–1531. doi: 10.2134/agronj2003.1525

Moe, K., Yamakawa, T., Thu, T. T. P., and Kajihara, Y. (2014). Effects of pretransplant basal and Split applications of nitrogen on the growth and yield of Manawthukha rice. *Commun. Soil Sci. Plant Anal.* 45, 2833–2851. doi: 10.1080/00103624.2014.954717

Mohamed, I., Bassouny, M. A., Abbas, M. H. H., Ming, Z., Cougui, C., Fahad, S., et al. (2021). Rice straw application with different water regimes stimulate enzymes activity and improve aggregates and their organic carbon contents in a paddy soil. *Chemosphere* 274:129971. doi: 10.1016/j.chemosphere.2021.129971

Mohapatra, P. K., and Sahu, B. B. (2022). "Ontogeny of organ development in rice plant," in *Panicle Architecture of Rice and its Relationship with Grain Filling*. eds. P. K. Mohapatra and B. B. Sahu (Cham: Springer International Publishing), 49–61.

Myint, A. K., Yamakawa, T., and Zenmyo, T. (2009). Plant growth, seed yield and apparent nutrient recovery of rice by the application of manure and fertilizer as different nitrogen sources in paddy soils. *J. Fac. Agric. Kyushu Univ.* 54, 329–337. doi: 10.5109/16111

Olk, D. C., Jimenez, R. R., Moscoso, E., and Gapas, P. (2009). Phenol accumulation in a young humic fraction following anaerobic decomposition of rice crop residues. *Soil Soil Sci. Soc.Am. J.* 73, 943–951. doi: 10.2136/sssaj2007.0438

Pampana, S., and Mariotti, M. (2021). Durum wheat yield and N uptake as affected by N source, timing, and rate in two mediterranean environments. *Agron.-Basel* 11:1299. doi: 10.3390/agronomy11071299

Pan, S., Liu, H., Mo, Z., Patterson, B., Duan, M., Tian, H., et al. (2016). Effects of nitrogen and shading on root morphologies, nutrient accumulation, and photosynthetic parameters in different rice genotypes. *Sci. Rep.* 6:32148. doi: 10.1038/srep32148

Qaswar, M., Huang, J., Ahmed, W., Li, D., Liu, S., Ali, S., et al. (2019). Long-term green manure rotations improve soil biochemical properties, yield sustainability and nutrient balances in acidic paddy soil under a rice-based cropping system. *Agronomy* 9:780. doi: 10.3390/agronomy9120780

Ranjan, A., Sinha, R., Bala, M., Pareek, A., Singla-Pareek, S. L., and Singh, A. K. (2021). Silicon-mediated abiotic and biotic stress mitigation in plants: underlying mechanisms and potential for stress resilient agriculture. *Plant Physiol. Biochem.* 163, 15–25. doi: 10.1016/j.plaphy.2021.03.044

Ray, D. K., Gerber, J. S., MacDonald, G. K., and West, P. C. (2015). Climate variation explains a third of global crop yield variability. *Nat. Commun.* 6:5989. doi: 10.1038/ncomms6989

Rubio, V., Diaz-Rossello, R., Quincke, J. A., and van Es, H. M. (2021). Quantifying soil organic carbon's critical role in cereal productivity losses under annualized crop rotations. *Agric. Ecosyst. Environ.* 321:107607. doi: 10.1016/j.agee.2021.107607

Sharma, S. N., and Prasad, R. (2008). Effect of crop-residue management on the production and agronomic nitrogen efficiency in a rice–wheat cropping system. *J. Plant Nutr. Soil Sci.* 171, 295–302. doi: 10.1002/jpln.200700144

Shi, Z., Jing, Q., Cai, J., Jiang, D., Cao, W., and Dai, T. (2012). The fates of 15N fertilizer in relation to root distributions of winter wheat under different N splits. *Eur. J. Agron.* 40, 86–93. doi: 10.1016/j.eja.2012.01.006

Shi, J., Wang, S., Li, S., Tian, X., and Tian, X. (2022). Increasing soil organic carbon sequestration and yield stability by no-tillage and straw-returning in wheat–maize rotation. *Agron. J.* 114, 1534–1545. doi: 10.1002/agj2.21016

Sokol, N. W., Slessarev, E., Marschmann, G. L., Nicolas, A., Blazewicz, S. J., Brodie, E. L., et al. (2022). Life and death in the soil microbiome: How ecological processes influence biogeochemistry. *Nat. Rev. Microbiol.* 20, 415–430. doi: 10.1038/s41579-022-00695-z

Sui, B., Feng, X., Tian, G., Hu, X., Shen, Q., and Guo, S. (2013). Optimizing nitrogen supply increases rice yield and nitrogen use efficiency by regulating yield formation factors. *Field Crop Res.* 150, 99–107. doi: 10.1016/j.fcr.2013.06.012

Sustr, M., Soukup, A., and Tylova, E. (2019). Potassium in root growth and development. *Plants (Basel)* 8:435. doi: 10.3390/plants8100435

Vance, E. D., Brookes, P. C., and Jenkinson, D. S. (1987). An extraction method for measuring soil microbial biomass C. *Soil Biol. Biochem.* 19, 703–707. doi: 10.1016/0038-0717(87)90052-6

Wang, J., Fu, P., Wang, F., Fahad, S., Mohapatra, P. K., Chen, Y., et al. (2019). Optimizing nitrogen management to balance rice yield and environmental risk in the Yangtze River's middle reaches. *Environ. Sci. Pollut. Res.* 26, 4901–4912. doi: 10.1007/s11356-018-3943-5

Wang, Z., Shi, P., Zhang, Z., Meng, Y., Luan, Y., and Wang, J. (2017). Separating out the influence of climatic trend, fluctuations, and extreme events on crop yield: A case study in Hunan Province, China. *Clim. Dyn.* 51, 4469–4487. doi: 10.1007/s00382-017-3831-6

Wang, D., Xu, C., Ye, C., Chen, S., Chu, G., and Zhang, X. (2018). Low recovery efficiency of basal fertilizer-N in plants does not indicate high basal fertilizer-N loss from split-applied N in transplanted rice. *Field Crop Res.* 229, 8–16. doi: 10.1016/j.fcr.2018.09.008

Wang, Y., Zhang, Z., Liang, Y., Han, Y., Han, Y., and Tan, J. (2020). High potassium application rate increased grain yield of shading-stressed winter wheat by improving photosynthesis and photosynthate translocation. *Front. Plant Sci.* 11:134. doi: 10.3389/fpls.2020.00134

Wanjari, R. H., Singh, M. V., and Ghosh, P. K. (2004). Sustainable yield index: An approach to evaluate the sustainability of long-term intensive cropping systems in India. *J. Sustain. Agric.* 24, 39–56. doi: 10.1300/J064v24n04_05

Wei, Q., Xu, J., Sun, L., Wang, H., Lv, Y., Li, Y., et al. (2019). Effects of straw returning on rice growth and yield under water-saving irrigation. *Chilean J. Agricultural Res.* 79, 66–74. doi: 10.4067/s0718-58392019000100066

Wood, R. M., Dunn, B. W., Balindong, J. L., Waters, D. L. E., Blanchard, C. L., Mawson, A. J., et al. (2020). Effect of agronomic management on rice grain quality part II: Nitrogen rate and timing. *Cereal Chem.* 98, 234–248. doi: 10.1002/cche.10372

Xia, L., Lam, S. K., Wolf, B., Kiese, R., Chen, D., and Butterbach-Bahl, K. (2018). Trade-offs between soil carbon sequestration and reactive nitrogen losses under straw return in global agroecosystems. *Glob. Chang. Biol.* 24, 5919–5932. doi: 10.1111/gcb.14466

Xu, X., Schaeffer, S., Sun, Z., Zhang, J., An, T., and Wang, J. (2020). Carbon stabilization in aggregate fractions responds to straw input levels under varied soil fertility levels. *Soil Tillage Res.* 199:104593. doi: 10.1016/j.still.2020.104593

Xu, H. G., Zhong, G. R., Lin, J. J., Ding, Y. F., Li, G. H., Wang, S. H., et al. (2015). Effect of nitrogen management during the panicle stage in rice on the nitrogen utilization of rice and succeeding wheat crops. *Eur. J. Agron.* 70, 41–47. doi: 10.1016/j.eja.2015.06.008

Yan, F. J., Sun, Y. J., Xu, H., Yin, Y. Z., Wang, H. Y., Wang, C. Y., et al. (2018). Effects of wheat straw mulch application and nitrogen management on rice root growth, dry matter accumulation and rice quality in soils of different fertility. *Paddy Water Environ.* 16, 507–518. doi: 10.1007/s10333-018-0643-1

Ye, C., Ma, H., Huang, X., Xu, C., Chen, S., Chu, G., et al. (2022). Effects of increasing panicle-stage N on yield and N use efficiency of indica rice and its relationship with soil fertility. *Crop J.* [In Press]. doi: 10.1016/j.cj.2022.02.003

Zeng, D., Tian, Z., Rao, Y., Dong, G., Yang, Y., Huang, L., et al. (2017). Rational design of high-yield and superior-quality rice. *Nat. Plants* 3:17031. doi: 10.1038/nplants.2017.31

Zhang, X., Davidson, E. A., Mauzerall, D. L., Searchinger, T. D., Dumas, P., and Shen, Y. (2015). Managing nitrogen for sustainable development. *Nature* 528, 51–59. doi: 10.1038/nature15743

Zhang, H.-C., Wu, G.-C., Dai, Q.-G., Huo, Z.-Y., Xu, K., Gao, H., et al. (2011). Precise postponing nitrogen application and its mechanism in rice. *Acta Agron. Sin.* 37, 1837–1851. doi: 10.3724/sp.J.1006.2011.01837

Zhang, Z., Yu, Z., Zhang, Y., and Shi, Y. (2021). Split nitrogen fertilizer application improved grain yield in winter wheat (Triticum aestivum L.) via modulating antioxidant capacity and 13C photosynthate mobilization under water-saving irrigation conditions. *Ecol. Process.* 10, 1–13. doi: 10.1186/s13717-021-00290-9

Zheng, J., Zhang, G., Wang, D., Cao, Z., Wang, C., and Yan, D. (2019). Effects of straw incorporation on nitrogen absorption of split fertilizer applications and on rice growth. *Emirates J. Food Agriculture* 31, 59–68. doi: 10.9755/ejfa.2019.v31.i1.1902

Zhu, Z., Ge, T., Hu, Y., Zhou, P., Wang, T., Shibistova, O., et al. (2017). Fate of rice shoot and root residues, rhizodeposits, and microbial assimilated carbon in paddy soil-part 2: Turnover and microbial utilization. *Plant Soil* 416, 243–257. doi: 10.1007/s11104-017-3210-4

Zhu, L., Hu, N., Zhang, Z., Xu, J., Tao, B., and Meng, Y. (2015). Short-term responses of soil organic carbon and carbon pool management index to different annual straw return rates in a rice–wheat cropping system. *Catena* 135, 283–289. doi: 10.1016/j.catena.2015.08.008

frontiers | Frontiers in Plant Science

TYPE Original Research
PUBLISHED 20 September 2022
DOI 10.3389/fpls.2022.986673

OPEN ACCESS

EDITED BY
Mohammad Irfan,
Cornell University, United States

REVIEWED BY
Vinay Kumar,
The Ohio State University, United States
Engin Yol,
Akdeniz University, Turkey

*CORRESPONDENCE
Xiaoyun Zou
jxauzxy@163.com
Deping Gu
gudp1999@sina.com

SPECIALTY SECTION
This article was submitted to Crop and Product Physiology, a section of the journal Frontiers in Plant Science

RECEIVED 05 July 2022
ACCEPTED 16 August 2022
PUBLISHED 20 September 2022

CITATION
Yan L, Jin H, Raza A, Huang Y, Gu D and Zou X (2022) WRKY genes provide novel insights into their role against *Ralstonia solanacearum* infection in cultivated peanut (*Arachis hypogaea* L.). *Front. Plant Sci.* 13:986673. doi: 10.3389/fpls.2022.986673

WRKY genes provide novel insights into their role against *Ralstonia solanacearum* infection in cultivated peanut (*Arachis hypogaea* L.)

Lei Yan [1], Haotian Jin[1], Ali Raza [2], Yang Huang[1], Deping Gu[1]* and Xiaoyun Zou[1]*

[1]Institute of Crops, Jiangxi Academy of Agricultural Sciences, Nanchang, China, [2]College of Agriculture, Oil Crops Research Institute, Fujian Agriculture and Forestry University, Fuzhou, China

As one of the most important and largest transcription factors, WRKY plays a critical role in plant disease resistance. However, little is known regarding the functions of the WRKY family in cultivated peanuts (*Arachis hypogaea* L.). In this study, a total of 174 WRKY genes (*AhWRKY*) were identified from the genome of cultivated peanuts. Phylogenetic analysis revealed that AhWRKY proteins could be divided into four groups, including 35 (20.12%) in group I, 107 (61.49%) in group II, 31 (17.82%) in group III, and 1 (0.57%) in group IV. This division is further supported by the conserved motif compositions and intron/exon structures. All *AhWRKY* genes were unevenly located on all 20 chromosomes, among which 132 pairs of fragment duplication and seven pairs of tandem duplications existed. Eighteen miRNAs were found to be targeting 50 *AhWRKY* genes. Most *AhWRKY* genes from some groups showed tissue-specific expression. *AhWRKY46*, *AhWRKY94*, *AhWRKY156*, *AhWRKY68*, *AhWRKY41*, *AhWRKY128*, *AhWRKY104*, *AhWRKY19*, *AhWRKY62*, *AhWRKY155*, *AhWRKY170*, *AhWRKY78*, *AhWRKY34*, *AhWRKY12*, *AhWRKY95*, and *AhWRKY76* were upregulated in ganhua18 and kainong313 genotypes after *Ralstonia solanacearum* infection. Ten *AhWRKY* genes (*AhWRKY34*, *AhWRKY76*, *AhWRKY78*, *AhWRKY120*, *AhWRKY153*, *AhWRKY155*, *AhWRKY159*, *AhWRKY160*, *AhWRKY161*, and *AhWRKY162*) from group III displayed different expression patterns in *R. solanacearum* sensitive and resistant peanut genotypes infected with the *R. solanacearum*. Two AhWRKY genes (*AhWRKY76* and *AhWRKY77*) from group III obtained the LRR domain. *AhWRKY77* downregulated in both genotypes; *AhWRKY76* showed lower-higher expression in ganhua18 and higher expression in kainong313. Both *AhWRKY76* and *AhWRKY77* are targeted by ahy-miR3512, which may have an important function in peanut disease resistance. This study identified candidate *WRKY* genes with possible roles in peanut resistance against *R. solanacearum* infection. These findings not only contribute to our understanding of the novel role of *WRKY* family genes but also provide valuable information for disease resistance in *A. hypogaea*.

KEYWORDS

biotic stress, gene structure, oilseed crop, phylogenetic analysis, expression analysis, bacterial wilt

Introduction

Transcription factors (TFs) activate diverse signal transduction cascades and regulate the transcriptional mode of targeted genes, which helps crop plants to adapt to diverse environmental stresses (Javed et al., 2020, 2022; Zhu et al., 2021; Haider et al., 2022). Among various TFs, WRKY TFs are one of the largest TF families in plants and regulate various biological processes, including growth, development, stress, and disease resistance (Rushton et al., 2010; Zhu et al., 2021; Javed et al., 2022). WRKY proteins contain a highly conserved WRKYGQK motif at N-terminus and a zinc finger motif (C_2H_2: $CX_4CX_{22-23}HX_1H$, C_2HC: $CX_7CX_{23}HX_1C$) at C-terminus (Rushton et al., 2010). WRKY proteins can be classified into four groups (I, II, III, and IV). Group I members have two WRKY domains and the C_2H_2 type zinc finger. Group II and Group III members have one WRKY domain; Group II members have a C_2H_2 type zinc finger and Group III members have a C_2HC-type. Group I can be classified into two subgroups Ia and Ib based on two WRKY domains at the N and C terminus (Chen et al., 2019a; Li Z et al., 2020). Group II WRKY can be further classified into five subgroups (IIa, IIb, IIc, IId, and IIe) based on the sequence of the DNA-binding domain (Zhang and Wang, 2005). Group III is separated into subgroups IIIa and IIIb based on the zinc-finger motif structure (Eulgem et al., 2000; Chen et al., 2019a). Group IV has an incomplete or partial WRKY domain and lacks a zinc-finger motif, suggesting that members of this group may have lost their function as WRKY TFs (Li Z et al., 2020; Javed et al., 2022).

Ralstonia solanacearum is a soil-borne bacterium; it usually infects plants through roots and then spreads through the vascular system to the whole plant, eventually causing mechanical blockage of the water transport system. In response to bacterial wilt (BW) disease, plants become wilt and die when the leaves are still green (Hikichi et al., 2017). A previous study indicated that *AtWRKY52* (group III member) in *Arabidopsis thaliana* confers resistance to the bacterial soil-borne pathogen *R. solanacearum* (Deslandes et al., 1998, 2002). *CaWRKY28, CaWRKY30* (group III member), *CaWRKY40, CaWRKY41* (group III member), and *CaWRKY58* in pepper regulated the defense response to *R. solanacearum* in plants (Wang et al., 2012; Muhammad et al., 2018; Dang et al., 2019; Hussain et al., 2021; Liu et al., 2021; Yang et al., 2021). Overexpression of sugarcane class III *WRKY5* increased bacterial wilt resistance (Wang et al., 2020). Group III *SiWRKY53* is a source of resistance to BW in *Solanum incanum* L. (Mishra et al., 2021). WRKY, especially group III members, play a vital part in the BW resistance of plants.

So far, WRKY TF families have been identified in many plants. For instance, there are 74 *WRKY* genes in *Arabidopsis* (*Arabidopsis thaliana* L.) (Dong et al., 2003), 153 *WRKY* genes in rapeseed (*Brassica napus* L.) (He et al., 2016), 287 *WRKY* genes in banana (*Musa acuminata* L.) (Kaliyappan et al., 2016), 88 *WRKY* genes in common bean (*Phaseolus vulgaris* L.) (Wu et al., 2017), 54 *WRKY* genes in pineapple (*Ananas comosus* L.) (Xie et al., 2018), 97 *WRKY* genes in Actinidia (*Caragana intermedia* L.) (Wan et al., 2018), 94 *WRKY* genes in sorghum (*Sorghum bicolor* L.) (Baillo et al., 2020), and 224 *WRKY* genes in Camelina (*Camelina sativa* L.) (Song et al., 2020). Previously, 77 and 75 WRKY proteins have been identified from the two wild ancestral diploid genomes of cultivated tetraploid peanuts, *Arachis duranensis* and *Arachis ipaënsis* (Song et al., 2016). Recently, a study identified 158 WRKY proteins from cultivated tetraploid peanuts using an older version of *A. hypogea* and gene expression of *AhWRKY* family members in response to drought stress (Zhao et al., 2020).

Climate change and crop production are directly correlated with each other, and current climate changes significantly impact agricultural productivity (Sharma et al., 2021, 2022; Farooq et al., 2022). Mainly, different biotic diseases and abiotic environmental factors greatly affect the productivity and overall quality of various crop plants around the world (Irfan et al., 2016, 2021; Kumar et al., 2016; Jiang et al., 2017; Ansari et al., 2022; Raza et al., 2022a,b). Peanut (*Arachis hypogaea* L.) is one of the most important oil crops in the world, but its yield is severely limited by various biotic and abiotic stresses (Mishra et al., 2015; Gangurde et al., 2019). Among these, BW is the major biotic factor that significantly hampers peanut production in the field environment (Jiang et al., 2017). The BW is one of the most important diseases in peanuts, especially destructive in China. When infected with the *R. solanacearum*, peanut plants wilt and die. It usually causes a 400,000 hm^2 incidence area and 10–30% yield loss in 1 year in China (Jiang et al., 2017). This study identified 174 WRKY proteins, comprehensive analysis of gene structures, chromosome location, evolution relationship, *cis*-acting element, putative miRNAs, and expression analysis of gene response to *R. solanacearum*. These results provide insights into the evolution of the peanut WRKYs and their novel functions in peanut BW resistance. The identification and characterization of these *WRKY* genes may provide opportunities for peanut disease improvement and breeding programs in the era of climate change.

Materials and methods

Identification of the WRKY genes in peanuts

The protein data of cultivated peanuts (cv. Tifrunner) were obtained from the peanut genome database (PeanutBase, https://www.peanutbase.org/). The HMM file of the WRKY domain (PF03106) was retrieved from the Pfam database (http://pfam.sanger.ac.uk/) and was used to search the WRKY family proteins in the peanut protein database with an E-value threshold of 1×10^{-5} by simple HMM search TBtools (Toolbox for Biologists) v1.098 (Chen et al., 2020). Arabidopsis WRKY protein sequences were downloaded

from the database of The Arabidopsis Information Resource (TAIR, https://www.arabidopsis.org/). The protein sequences of AhWRKY and AtWRKY were subjected to BLAST alignment by TBtools (Toolbox for Biologists) v1.098 (E value $< 1 \times 10^{-5}$) (Chen et al., 2020). Subsequently, all non-redundant peanut WRKY protein sequences were validated for the presence of the WRKY domain by submitting them as search queries to the NCBI CDD (http://www.ncbi.nlm.nih.gov/cdd/) and SMART databases (http://smart.embl.de/). Finally, 174 AhWRKY sequences were identified and named AhWRKY1 to AhWRKY174 according to their physical locations on the chromosome.

Phylogenetic analysis

Multiple sequence alignment of AhWRKY proteins was conducted by MUSCLE with default parameters. A neighbor-joining (NJ) tree was constructed in MEGA 7.0 with the following criteria: Poisson model, pairwise deletion, and 1,000 bootstrap replications. Maximum likelihood (ML) analysis of the *AtWRKY* and *AhWRKY* gene family was conducted to draw a phylogenetic tree.

Gene structure, chromosomal distribution, and gene duplication

The MEME online program (Multiple Expectation Maximization for Motif Elicitation: http://meme-suite.org/tools/meme/) was used to identify conserved motifs in the AhWRKY proteins with a maximum motif number of 10. Information on the intron–exon structure was obtained from the peanut genome database (*A. hypogaea* cv. Tifrunner) and the TBtools software was used for visualization (Chen et al., 2020). TBtools was also used to determine the chromosomal location of the *AhWRKY* genes and draw the image. The duplication types and collinear blocks were discovered and were analyzed using One Step MCScanX and Simple Ka/Ks calculator (NJ) of Tbtools, and a diagram of gene duplication events was drawn using the Tbtools. Duplication and divergence time was calculated by the following formula as described by Bertioli et al. (2016):

$$T = Ks/2\lambda(\lambda = 8.12\times 10^{-9}). \quad (1)$$

Physiochemical parameters and promoter analysis of *AhWRKY*

The molecular weight (Mw) and isoelectric point (pI) of the full-length proteins were predicted using the pI/Mw tool (https://web.expasy.org/compute_pi/) in ExPASy (Gasteiger et al., 2003). The 2,000-base-pair (bp) sequences upstream of the start codon ATG of *AhWRKY* genes were retrieved from the peanut genome using TBtools (Chen et al., 2020) and were submitted to the online software PlantCARE to identify the *cis*-acting elements. The draft of the element distribution on each promoter was sketched using TBtools.

Prediction of putative miRNA targeting *AhWRKY* genes

The CDS of *AhWRKY* genes were employed to distinguish target miRNAs in the psRNATarget database (https://www.zhaolab.org/psRNATarget/home) with default parameters. The interaction network figure among the miRNAs and target genes was developed with the Cytoscape software (V3.8.2; https://cytoscape.org/download.html).

Gene expression analysis

The expression data of the *AhWRKY* genes in different tissues were identified using RNA-seq (Tifrunner variety) data obtained from the PeanutBase database (Clevenger et al., 2016). The read counts were transformed to TPM (Transcripts Per Kilobase of exon model per Million mapped reads) by GenomicFeatures in R, and the heatmap diagram was constructed with lg (TPM+1) using TBtools.

Two peanut cultivars (ganhua 18, resistant; and kainong 313, susceptible) were used for expression analysis against BW disease. Plant growth and *R. solanacearum* inoculation were carried out according to Chen et al. (2014). Plants were grown in 10 cm × 10 cm pots, and every pot contained three seedlings. After 21 days of sowing seeds, they were watered with 20 mL of *R. solanacearum* strain race 1 suspension (10^7 cfu ml^{-1}) in one pot. Roots of three individual seedlings were sampled at 0, 6, 12, 24, 48, 72, and 96 h post-inoculation. The samples were frozen in liquid nitrogen immediately and stored at −80°C for further analysis.

The TianGen kit (TianGen, Beijing, China) was used to extract total RNA from roots, and the experimental operations were carried out according to the developer's instructions. Approximately, 5 μg of total RNA was reverse-transcribed using the RevertAid First Strand cDNA Synthesis Kit (Thermo Fisher Scientific, USA). The primers were designed using the Primer 5.0 software (Supplementary Table 4), and the quantitative real-time qRT-PCR was performed on LightCycler 96 (Roche) using the Aidlab SYBR Green Mix kit (Aidlab, Beijing, China). The PCR protocol was conducted with a 10 μL volume, which contained 0.5 μL of upstream and downstream primers (10 μmol L^{-1}), 2 μL of cDNA template, 2 μL of double-distilled water (ddH_2O), and 5 μL of 2 × SYBR (SYBR Green qPCR Mix). The PCR program was 95°C for 120 s, followed by 40 cycles of

95°C for 5 s and 60°C for 30 s. qRT-PCR was performed with three technical repetitions, and the relative expression level was calculated using the $2^{-\Delta\Delta CT}$ method.

Results

Identification of the *AhWRKY* family

In this study, a total of 174 WRKY sequences were identified in cultivated peanuts (cv. Tifrunner) and named *AhWRKY1* to *AhWRKY174* according to their physical locations on the chromosome (Supplementary Table 1). The *AhWRKY* genes vary in length from 498 bp (*AhWRKY22* and *AhWRKY31*) to 10,044 bp (*AhWRKY59*), and their coding proteins range from 91 (*AhWRKY22*) to 1,345 (*AhWRKY59*) amino acids. The MWs of AhWRKYs were between 10.4 (AhWRKY22) and 148.6 kDa (AhWRKY132), with the majority of them ranging from 20 to 85 kDa in peanuts. The predicted pI ranged from 4.88 (AhWRKY55) to 10.08 (AhWRKY132), with an average of 7.06, among which 67 AhWRKYs had pI > 7, and 107 AhWRKYs had pI < 7.

Phylogenetic analysis of the *AhWRKY* family

To explore the evolutionary relationship between AhWRKY TFs, a phylogenetic tree was constructed using 174 AhWRKY proteins in peanuts and 74 AtWRKYs from *Arabidopsis* (Figure 1). In brief, 174 WRKY TFs were divided into four groups, group I (35), group II (107), group III (31), and group IV (1); group II was further divided into five subgroups, subgroup II-a (6), subgroup II-b (22), subgroup II-c (43), subgroup II-d (15), and subgroup II-e (21) (Figure 1; Supplementary Table 1).

Chromosomal mapping and duplication analysis of the *AhWRKY*

The mapping results showed that 174 *AhWRKYs* were found to be unevenly distributed on 20 chromosomes using genome chromosomal location analysis (Figure 2). Most genes were present on chromosomes 4 and 13, whereas 16 genes belonging to the A and B genomes, respectively, accounted for 7.47% (13 genes) and 8.05% (14 genes), 7.47% (13 genes) of the total gene numbers, and the fewest genes were scattered on chromosome 9 from the A genome and chromosome 19 of the B genome, accounting for 1.15% (2 genes) and 1.72% (3 genes), respectively.

Chromosomal mapping showed there are many gene clusters of AhWRKY in different chromosomes. For example, *AhWRKY3-9* on chr1, *AhWRKY23-27* on chr3, *AhWRKY35-40* on chr4, *AhWRKY47-49* on chr6, *AhWRKY62-67* on chr7, *AhWRKY75-77* on chr10, *AhWRKY98-100* on chr12, *AhWRKY136-139* on chr16, *AhWRKY153-155* on chr17, and *AhWRKY159-162* on chr18.

Collinearity analysis showed that among 174 *AhWRKYs*, 132 pairs of segmental duplication genes were identified; these were divided into seven groups according to the phylogenetic tree (Figure 3). Maximum segmental duplication events occurred in group II-c (34 pairs), followed by group III (22 pairs), group II-e (19 pairs), group II-b (18 pairs), group I (18 pairs), group II-d (13 pairs) and group II-a (8 pairs). Seven pairs of tandem duplication genes were detected, such as *AhWRKY99* and *AhWRKY100* in group I (Figure 3), *AhWRKY30* and *AhWRKY31, AhWRKY96* and *AhWRKY97* in group II-c, *AhWRKY64* and *AhWRKY65*, *AhWRKY66* and *AhWRKY67*, *AhWRKY76* and *AhWRKY77*, and *AhWRKY153* and *AhWRKY154* in group III. The Ka/Ks for segmental duplication was 0.05–1.21 with an average of 0.31, while the ratio of tandem duplication ranged from 0.42 to 0.94 with an average of 0.63. Only the Ka/Ks ratio of one pair (*AhWRKY119* and *AhWRKY33*) was 1.21, which indicated the gene pair was subjected to positive selection, and others were strongly subjected to pure selection. These segmental and tandem duplications may occur in 0.34–186.58 and 6.11–35.81 Mya, respectively (Figure 3; Supplementary Table 2).

Structure analysis of *AhWRKY* genes

The numbers of introns varied among 174 *AhWRKY* genes. All the *AhWRKY* family genes contain one to eight introns. Most members of group I and subgroup II-b have four introns, whereas most members of subgroup II-c, subgroup II-d, subgroup II-e, and group III have two introns. Four members of subgroup II-a have three introns, and two members have four introns. The member of group IV has two introns (Figures 4A,B; Supplementary Table 2). There was some subgroup specificity, possibly attributed to the number of changes of introns during evolution. In contrast, the number and position of the introns were relatively conserved in the same group of plant species (Figures 4A,C).

Ten conserved motifs of 174 *AhWRKY* genes were analyzed using the MEME software (Figures 4A–C). Motif 1 was dominantly present in the WRKY domain regions of most family members. The proteins of the same group showed identical numbers and arrangements of motifs, five motifs were detected in group I (motifs 3, 5, 1, 2, and 4), motif 3 in the N terminal, and motif 1 in the C terminal contained WRKY. Five and seven motifs were detected in subgroup II-a (motifs 7, 1, 2, 4, and 6) and II-b (motifs 7, 5, 1, 2, 4, 8, and 6), four motifs in subgroup II-c (motifs 5, 2, 1, and 4), II-d (motifs 9, 2, 1, and 4) and II-e (motifs 9, 2, 1, and 4), three motifs in group III (motifs 9/10, 1, and 2), and one motif in group IV (motif 3). Motifs in the same group showed great similarity, indicating the functional conservation in different groups. Comparing the intron–exon

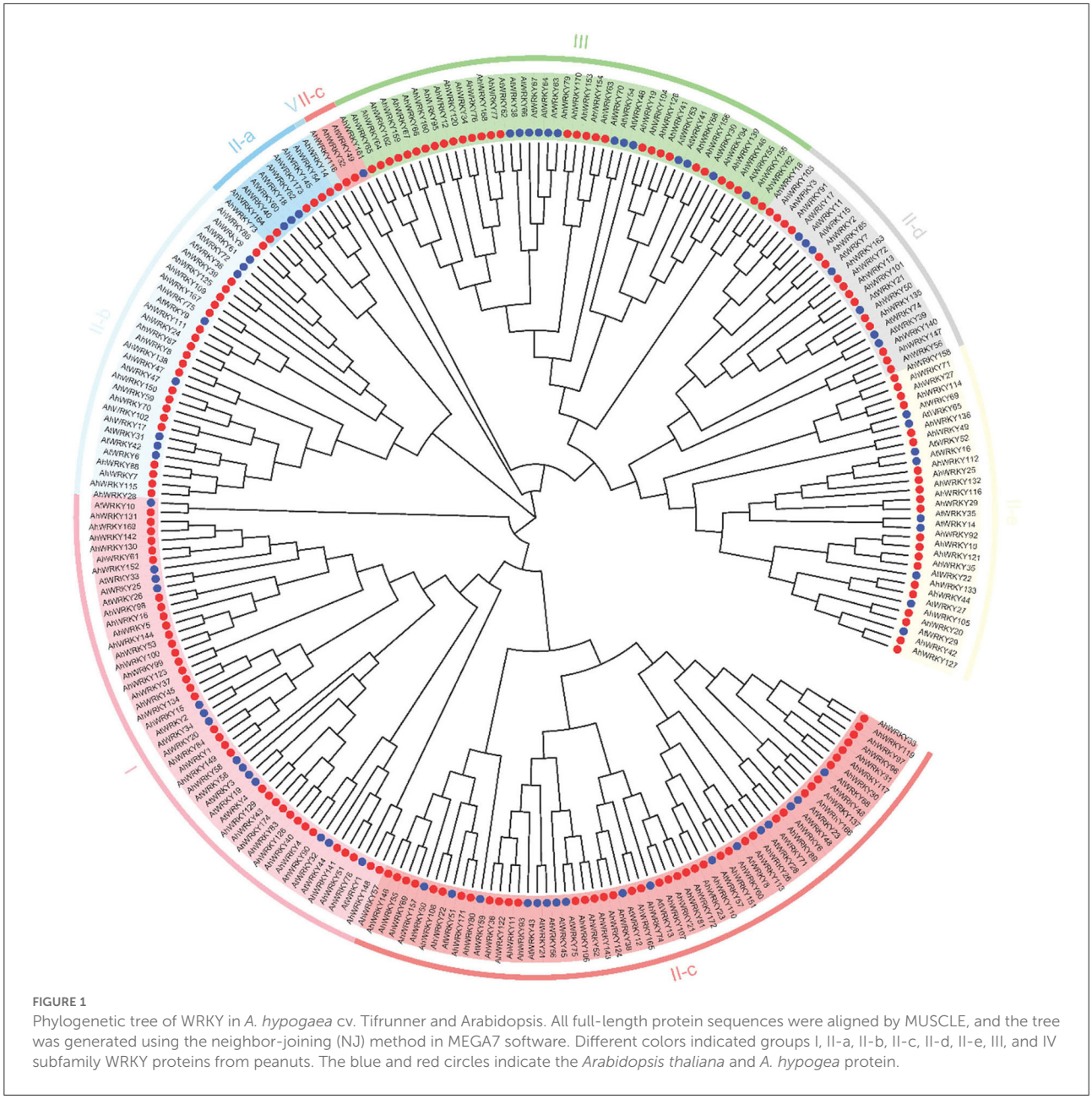

FIGURE 1
Phylogenetic tree of WRKY in *A. hypogaea* cv. Tifrunner and Arabidopsis. All full-length protein sequences were aligned by MUSCLE, and the tree was generated using the neighbor-joining (NJ) method in MEGA7 software. Different colors indicated groups I, II-a, II-b, II-c, II-d, II-e, III, and IV subfamily WRKY proteins from peanuts. The blue and red circles indicate the *Arabidopsis thaliana* and *A. hypogea* protein.

structure and conserved motif analysis, members of the same group showed great similarity in characteristics, indicating that most *AhWRKY* genes were highly conserved among groups.

Prediction analysis of *cis*-acting elements with *AhWRKY*

To further study the potential regulatory mechanism of the *AhWRKY* genes, the 2 kb upstream sequence of the *AhWRKY* genes translation start site was used to detect the *cis*-elements. A total of 55 known *cis*-elements (31 light-related elements, 11 hormone-related elements, seven tissue-specific elements, and six stress-related elements) were detected (Figure 5). MBS (drought inducibility), TC-rich repeats (defense and stress responsiveness), WUN motif (wound responsiveness), LTR (low-temperature responsiveness), ARE (essential for the anaerobic induction), and GC motif (anoxic specific inducibility) involved in stress responses are found in 52.5, 2.9, 14.9, 2.6, 12.1, and 15% of AhWRKY promoters, respectively. Meanwhile, there are a large number of hormonal response elements, including ABRE, AuxRR, and TGA-element, CGTCA

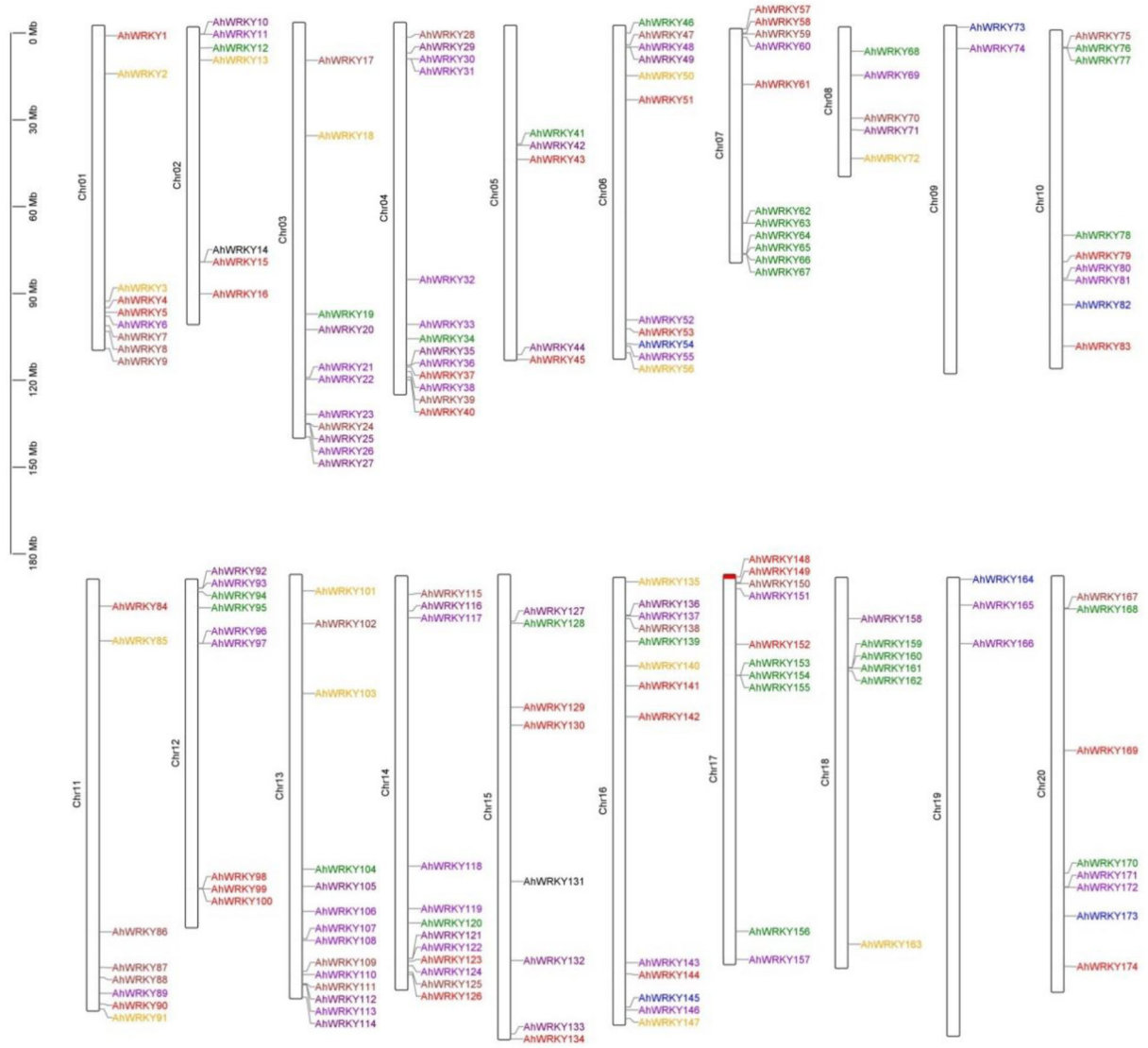

FIGURE 2
Chromosome mapping of *AhWRKY* genes. The scale represents a 30-Mb chromosomal distance. Red, sky blue, brown, DarkViolet, orange, purple, green, and blue indicated groups I, II-a, II-b, II-c, II-d, II-e, III, and IV, respectively.

motifs and TGACG-motif, GARE motifs, P-box, and TATC-box, O2 site, TCA element, and SARE. Promoters of AhWRKY possess a relatively large number of ARE elements, 83, 100, 82, 78, 73, 76, 81, and 100% family members of the group I, II-a, II-b, II-c, II-d, II-e, III, and IV possessed ARE elements. Notably, 20% of family members of group I possessed AuxRE, 91% of family members of subgroup II-b possessed ABRE elements, 54 and 48% of family members of subgroup II-c and II-e possessed TCA-element, 47% of family members of subgroup II-d possessed P-box, 84% family members of group III possessed CGTCA-motif. There was a divergence in *cis*-acting elements in promoter regions of different groups.

Expression of *AhWRKY* in different tissues of peanuts

Generally, the gene expression had a similar pattern within the same phylogenetic classes. Members of group I showed high gene expression levels in peg tip Pat, fruit Pat. 1, fruit Pat. 3, pericarp Pat. 5, and pericarp Pat. 6, and two members (*AhWRKY61* and *AhWRKY152*) were also highly expressed in root and nodule. The expression pattern of members of subgroup II-a was similar to group I, and two members (*AhWRKY163* and *AhWRKY74*) showed the same trend as *AhWRKY61* and *AhWRKY152*. Genes of subgroup II-b showed

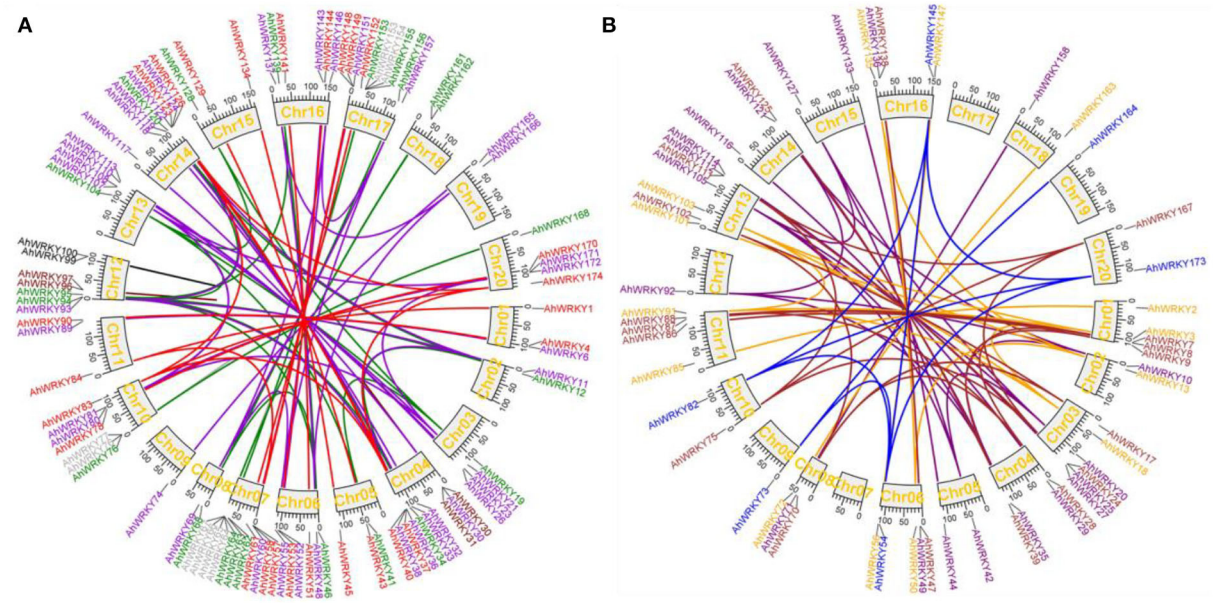

FIGURE 3
Circos figures for chromosome locations with AhWRKY duplication links. **(A)** Groups I, II-c, and III subfamily duplication links. Red, dark violet, and green lines indicated groups I, II-c, and III subfamily segmented, and black, maroon, and dark gray lines indicated groups I, II-c, and III subfamily tandem duplicated gene pairs, respectively. **(B)** Groups II-a, II-b, II-d, and II-e subfamily duplication links. Blue, brown, orange, and purple lines indicated group II-a, II-b, II-d, and II-e subfamily segmented duplicated gene pairs, respectively.

low expression levels in all tissues, but *AhWRKY115* and *AhWRKY28* had the same expression trend as *AhWRKY61* and *AhWRKY152*. Members of subgroup II-c were highly expressed in fruit Pat. 3, pericarp Pat. 5, and pericarp Pat. 6, most members of subgroup II-d were highly expressed in all tissues, and most members of subgroup II-e and group III were less expressed in all tissues (Figure 6).

AhWRKYs gene expression in response to *Ralstonia solanacearum* infection

The expression patterns of *AhWRKY* genes in group III differed between the two cultivars in response to *R. solanacearum* infection (Figure 7). One and six members of group III showed the highest and lowest expression in 6 h, eight and five in 12 h, and 13 highest in 24 h after infection with *R. solanacearum* in ganhua18. Four and eighth members of group III showed the highest and lowest expression in 6 h, seven and one in 12 h, six and three in 24 h, one highest expressed in 48 and 72 h, and five highest expressed in 96 h after infection with *R. solanacearum* in kanong313. *AhWRKY139*, *AhWRKY63*, *AhWRKY154*, *AhWRKY120*, *AhWRKY160*, *AhWRKY159*, *AhWRKY162*, *AhWRKY64*, *AhWRKY65*, and *AhWRKY161* were downregulated in ganhua18 after *R. solanacearum* infection. Whereas, *AhWRKY63*, *AhWRKY154*, *AhWRKY153*, *AhWRKY66*, *AhWRKY67*, *AhWRKY159*, *AhWRKY162*, *AhWRKY65*, *AhWRKY77*, and *AhWRKY161* were downregulated in kainong313 after *R. solanacearum* infection, these genes may negatively regulate bacterial wilt resistance in peanuts. Moreover, *AhWRKY46*, *AhWRKY94*, *AhWRKY156*, *AhWRKY68*, *AhWRKY41*, *AhWRKY128*, *AhWRKY104*, *AhWRKY19*, *AhWRKY62*, *AhWRKY155*, *AhWRKY153*, *AhWRKY170*, *AhWRKY78*, *AhWRKY34*, *AhWRKY12*, *AhWRKY95*, *AhWRKY66*, *AhWRKY67*, and *AhWRKY76* were upregulated in ganhua18 after *R. solanacearum* infection. On the other hand, *AhWRKY46*, *AhWRKY94*, *AhWRKY156*, *AhWRKY68*, *AhWRKY41*, *AhWRKY128*, *AhWRKY104*, *AhWRKY19*, *AhWRKY62*, *AhWRKY155*, *AhWRKY170*, *AhWRKY78*, *AhWRKY34*, *AhWRKY120*, *AhWRKY12*, *AhWRKY95*, *AhWRKY160*, *AhWRKY64*, *AhWRKY161*, and *AhWRKY76* were upregulated in kainong313 after *R. solanacearum* infection, indicating that these genes may positively regulate bacterial wilt resistance in peanuts (Figure 7).

After 6 h of *R. solanacearum* infection, the expressions of *AhWRKY120, AhWRKY159, AhWRKY161,* and *AhWRKY76* were downregulated by 0.07, 0.13, 0.1, and 0.28 than control in ganhua18, while that in kainong313 were increased by 66.91, 3.12, 8.19 and 6.05 than control. After 72 h of infection with the *R. solanacearum*, the expressions of *AhWRKY155, AhWRKY78,* and *AhWRKY34* were downregulated by 0.34, 0.45, and 0.24 than control in ganhua18, while that in kainong313 were increased by 17.46, 2.04, and 27.58 than control. After

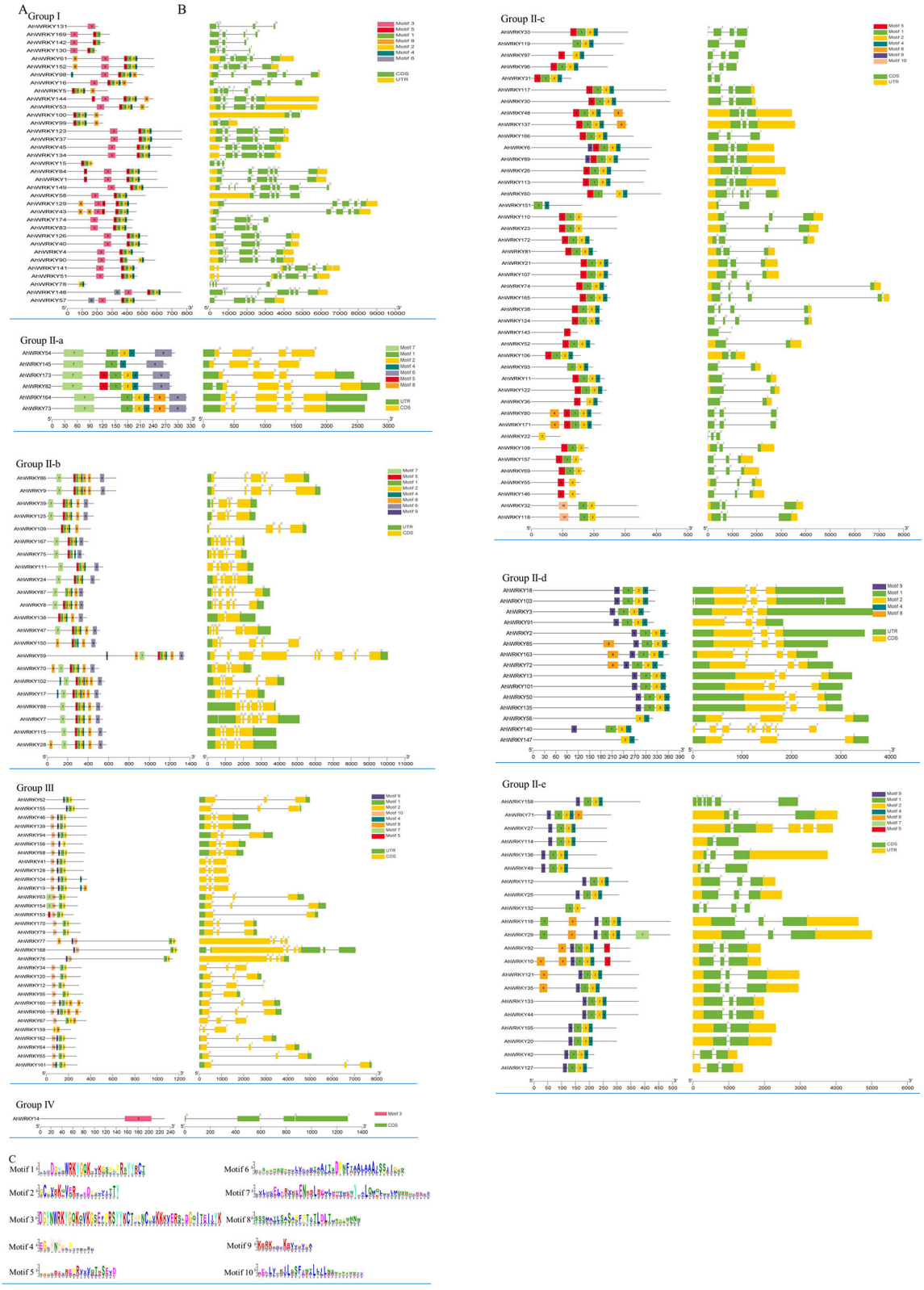

FIGURE 4
Gene structures and conserved motif analysis of *AhWRKY* genes. **(A)** The conserved motif of AhWRKY. **(B)** The exon–intron structure of AhWRKY. **(C)** The amino acid composition of each motif. Each conserved motif is represented by various-colored rectangles. Box length corresponds to motif length. Different colors represent different group members. Due to the large image size, we have presented the structures and motifs in various group-wise.

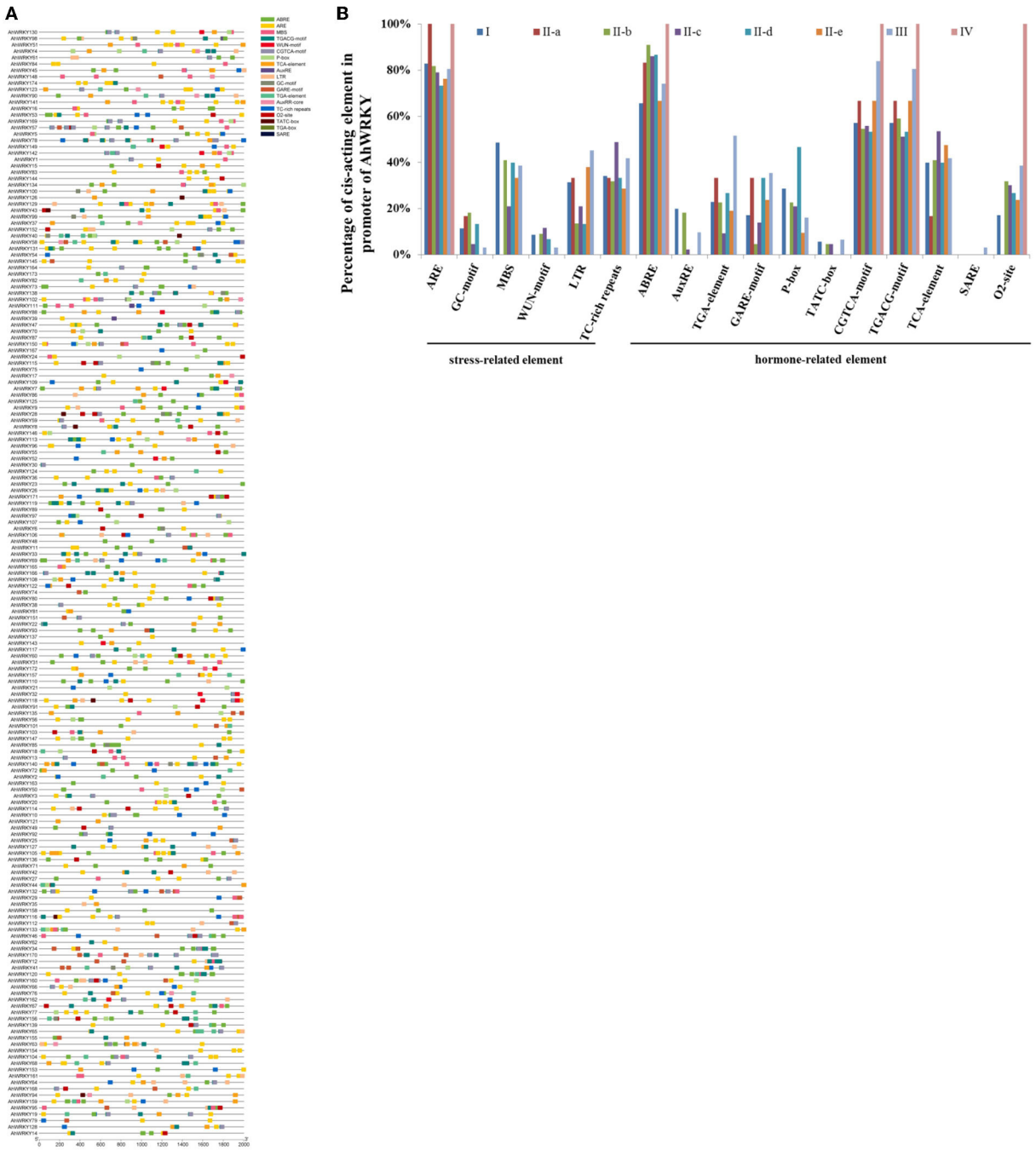

FIGURE 5
Identification of the cis-acting element in the promoter of *AhWRKY* genes. **(A)** Each type of element is represented by a number of colored rectangles. Box length corresponds to element length. Different colors represent different group members. **(B)** Percentage of each cis-acting element in the promoter of the AhWRKY.

6 h and 12 h infection with the *R. solanacearum*, the expression of *AhWRKY162* was downregulated by 0.01 and 0.02 than control in ganhua18, while that in kainong313 was increased by 4.35 and 2.11 than control. After 6 h, 12 h, and 72 h infection with the *R. solanacearum*, the expression of *AhWRKY160* was downregulated by 0.09, 0.39, and 0.21 than control in ganhua18, while that in kainong313 was increased by 5.64, 2.56, and 2.17 than control. After 6 h infection with the *R. solanacearum*, the

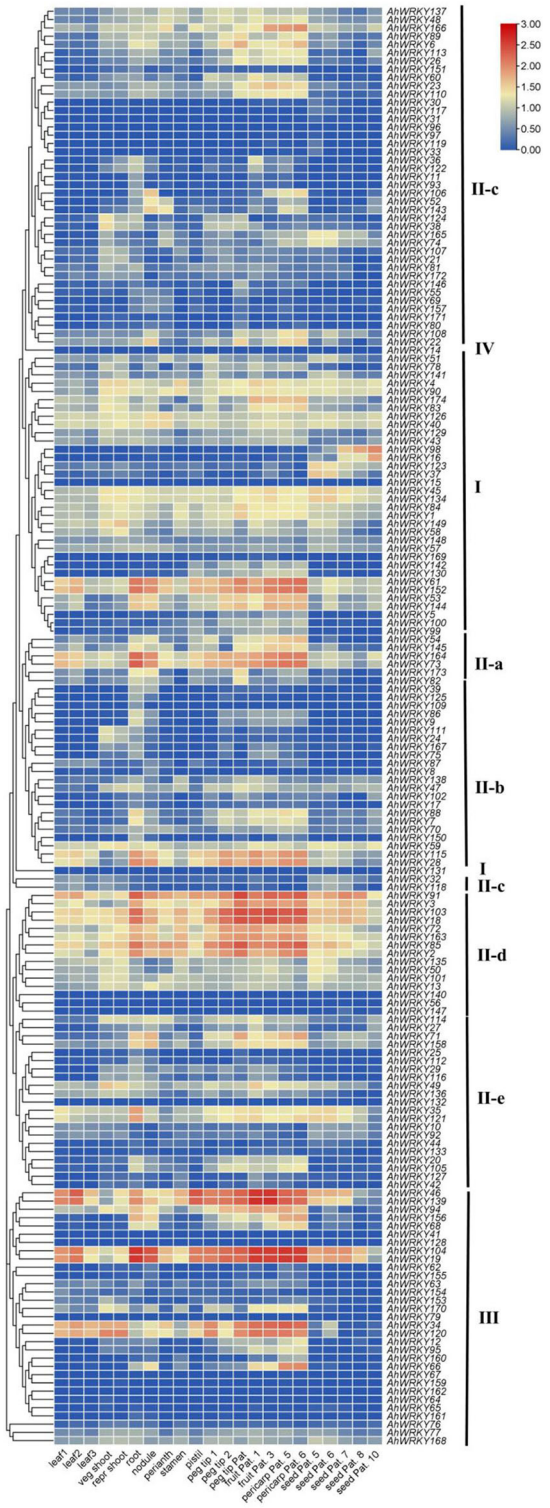

FIGURE 6
Expression profiles of *AhWRKY* genes across the different tissues. Gene expression is expressed in l g (TPM+1). Seedling leaf 10 days post-emergence (leaf 1), main stem leaf (leaf 2), lateral stem leaf (leaf 3), vegetative shoot tip from the main stem (veg shoot), reproductive shoot tip from first lateral (repr shoot), *(Continued)*

FIGURE 6 (Continued)
10-day roots (root), 25-day nodules (nodule), aerial gynophore tip (peg tip 1), subterranean peg tip (peg tip 2), Pattee 1 stalk (peg tip Pat. 1), Pattee 1 pod (fruit Pat. 1), Pattee 3 pod (fruit Pat. 3), Pattee 5 pericarp (pericarp Pat. 5), Pattee 6 pericarp (pericarp Pat. 6), Pattee 5 seed (seed Pat. 5), Pattee 6 seed (seed Pat. 6), Pattee 7 seed (seed Pat. 7), Pattee 8 seed (fruit Pat. 8), and Pattee 10 seed (seed Pat. 10).

expression of *AhWRKY153* was upregulated by 5.03 than control in ganhua18, while that in kainong313 was reduced by 0.41 than control (Figure 7). The differences in bacterial wilt resistance of two cultivars may be attributed to the expression patterns of these genes.

miRNA targeting *AhWRKY* genes

This study forecasted 18 miRNAs targeting 50 *AhWRKY* genes (Figure 8; Supplementary Table 3). The comprehensive data of all miRNAs targeted genes/sites is given in Supplementary Table 3. Overall, the results established that ahy-miR3520-5p target a maximum number of genes (13), followed by ahy-miR159 and ahy-miR156b-3p which targets six *AhWRKY* genes (Figure 8). Whereas, some genes are only targeted by one miRNA, such as *AhWRKY47, AhWRKY16, AhWRKY142,* and *AhWRKY140* (Figure 8). In further investigations, the transcript levels of these miRNAs and their targeted genes need confirmation to govern their biological acts in peanut breeding.

Discussion

As one of the most important and largest TF, WRKY TFs play a critical role in response to biotic stresses in plants (Rushton et al., 2010; Javed et al., 2020, 2022). WRKY families have been reported in many plants, but little is known regarding the functions of the WRKY family in *A. hypogaea*. There were 77, 75, and 158 WRKY proteins in *Arachis duranensis*, *Arachis ipaënsis,* and *Arachis hypogaea* with reference to the first version of the *A. hypogaea* genome, respectively (Song et al., 2016; Zhao et al., 2020). Based on the first and second versions of the *A. hypogaea* genome released on June 4, 2021, this study identified 174 *AhWRKY* genes in peanuts, 83 *WRKY* genes in the A genome, and 91 in the B genome. In our study, there were 17 more genes in *A. hypogea* genome and one fewer genes in A and B genomes than previous reports. Previous studies analyzed the expressions of *AhWRKY* under drought stress in peanuts (Zhao et al., 2020); however, this study analyzed expressions of *AhWRKY* genes in response to *R. solanacearum* infection in peanuts. The high multiplicity/unpredictability in the quantity of WRKY TFs among diverse plant species could be due to

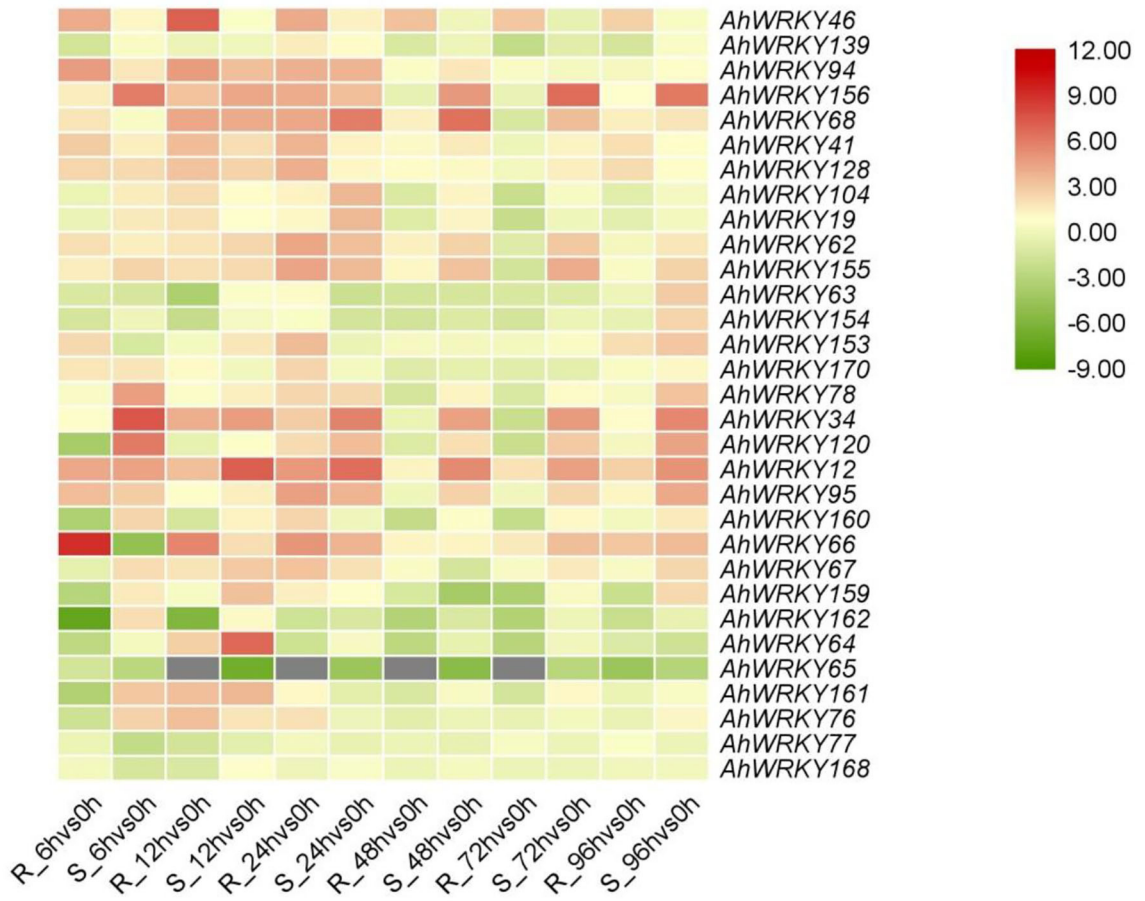

FIGURE 7
Expression of *AhWRKYs* in the two cultivars infected with *Ralstonia solanacearum*. The qRT-PCR of each gene in peanut roots infected with *Ralstonia solanacearum* in the two cultivars is shown. Heatmap showed the log2-transformed ratio values. R, Resistance; S, Susceptibility.

unalike evolutionary events or duplication of whole genomes during the evolutionary period. In particular, the distinctive reports of replicated (tandem/segmental) genes succeeding in the repetition of entire genomes could also be accountable for continuing evolutionary changeovers and crop domestication (Leister, 2004; Bertioli et al., 2016, 2019; Van De Peer et al., 2017; Bohra et al., 2022). Nevertheless, previous reports also validated that segmental and tandem repetitions, particularly for the previous events, could be important driving factors in the evolution and enlargement of WRKY TFs in diverse crop plants (Song et al., 2016; Xie et al., 2018; Zhao et al., 2020; Javed et al., 2022).

Mutations and deletions prevail in the plant WRKY domain (Wei et al., 2012). Five *WRKY* genes deleted one WRKY domain in *Helianthus annuus* L. (Li J et al., 2020). Nine *WRKY* genes deleted one WRKY domain, seven *WRKY* genes deleted zinc finger, and three *WRKY* genes deleted one WRKY motif in maize (Hu et al., 2021). Previous reports suggest that mutations also occurred in the WRKY motif of most *WRKY* genes in peanuts (Song et al., 2016; Zhao et al., 2020). In this study, there were 17 *AhWRKYs* mutated and 13 *AhWRKYs* deleted in the WRKY domain. One group I member *AhWRKY* motif changed to WRKYGEK. Seven members of subgroup II-c *AhWRKY* motif changed to WRKYGKK, and two members changed to WRKYGEK, two members changed to WRKYGRK. WRKY motif of *AhWRKY36* (subgroup II-c), *AhWRKY131* (I), *AhWRKY97* (subgroup II-e), and *AhWRKY14* (IV) changed to WRK, WRMYGQK, WHKYGKK, and GRKYGQK, respectively. Moreover, 12 *AhWRKYs* mutated and deleted in zinc fingers. Zinc finger deleted in C terminal of *AhWRKY130* (group I) and N terminal of *AhWRKY169* (group I). Zinc finger deleted in *AhWRKY145* (subgroup II-a), *AhWRKY75* (subgroup II-b), *AhWRKY150* (subgroup II-b), *AhWRKY9* (subgroup II-c), *AhWRKY143* (subgroup II-c), and *AhWRKY151* (subgroup II-c). Zinc finger changed to C-X4-C-X25-H-X-S in *AhWRKY22* (subgroup II-c),

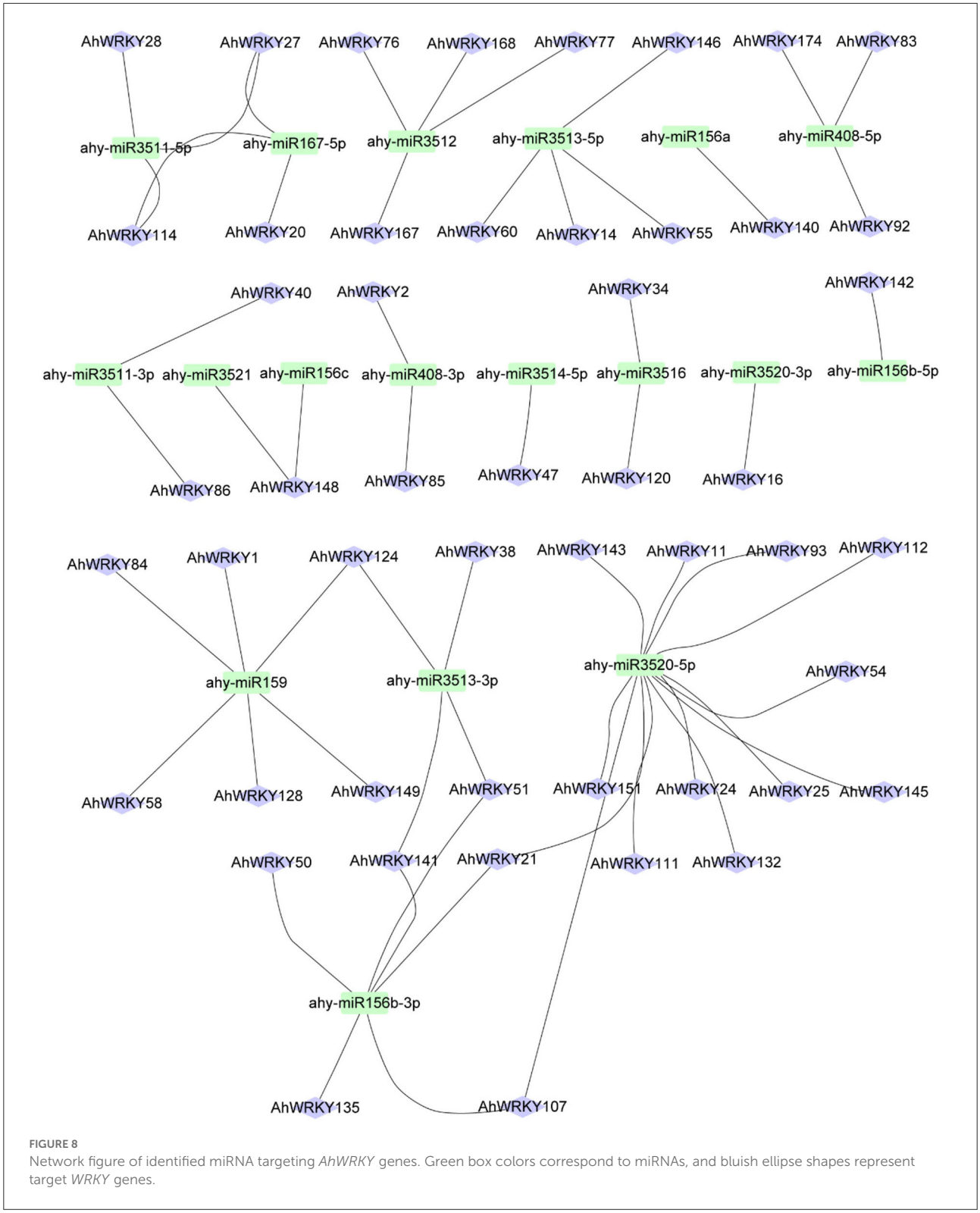

FIGURE 8
Network figure of identified miRNA targeting *AhWRKY* genes. Green box colors correspond to miRNAs, and bluish ellipse shapes represent target *WRKY* genes.

C-X5-C in *AhWRKY132* (subgroup II-e), C-X4-C-X22-H-X-Y in *AhWRKY14* (IV), and C-X4-C in *AhWRKY131* (I). There are many mutations in the zinc finger of group I and subgroup II-e and the WRKY motif of subgroup II-c presumed that the variation in members of group I, subgroup II-c, and II-e generate new functions.

Gene duplication plays an important role in the amplification and evolution of plant gene families (Cannon et al., 2004; Leister, 2004; Bertioli et al., 2016; Van De Peer et al., 2017). Among gene clusters, five pairs of tandem duplication and nine pairs of segmental duplication genes were identified; seven pairs of tandem duplication and 132 pairs of segmental duplication genes were identified in 14 and 144 *AhWRKYs* (Figure 3), which were one more tandem duplication and nine segmental duplications than the previous study (Zhao et al., 2020). The divergence of two wild ancestral diploids of cultivated tetraploid peanuts may occur in 2.16 MYA (Chen et al., 2019b). Ninety-nine pairs of segmental duplication genes occurred before the divergence of two wild ancestral diploids, 31 pairs of tandem duplication, and six pairs of segmental duplication genes occurred after the divergence of two wild ancestral diploids. The ka/ks ratios of 99.4% (173/174) of *AhWRKYs* were less than one, which suggested that most *AhWRKYs* were selected for purification. The ka/ks ratios of one gene pair, including *AhWRKY119* and *AhWRKY33,* was 1.21 (more than 1), which indicated that these genes were in a state of positive selection in peanuts, evolving rapidly, and might be very important for the evolution of peanuts.

Prediction analysis of *cis*-acting elements with *AhWRKYs* indicated many light-related, hormone-related, tissue-specific, and stress-related elements in the promoters of *AhWRKY* genes (Figure 5), which was in accordance with the previous study (Zhao et al., 2020) and speculated that *AhWRKY* is involved in various biological processes.

Tissue-specific expression suggested that genes from the same group indicated similar expression patterns (Figure 6). Tissue-specific expression was in agreement with the tissue-specific elements in the promoters of *AhWRKY* genes. For instance, *AhWRKY16* was highly expressed in seed, and an RY-element, which is a *cis*-acting regulatory element involved in seed-specific regulation in the promoter, and *AhWRKY158* was highly expressed in nodule and a nodule-site1 element, which is a nodule-specific factor binding site in its promoter (Figures 5, 6).

LRR is closely related to the disease resistance of plants (Jones and Dangl, 2006; McHale et al., 2006). It is known that some WRKY proteins contain the NBS-LRR domain (Deslandes et al., 2003; Shen et al., 2007; Liu et al., 2016), and WRKY proteins from group III are mainly involved in plant disease resistance (Kalde et al., 2003; Eulgem and Somssich, 2007). *AtWRKY52* possessed the NBS-LRR domain and WRKY domain, which is a critical gene in regulating bacterial wilt resistance (Deslandes et al., 1998, 2002). *CaWRKY58* and CaWRKY40b (II-a) negatively regulate bacterial wilt resistance, while *CaWRKY22* (II-e) and *CaWRKY27* (II-e), *CaWRKY28* (II-c), *CaWRKY30* (III), and *CaWRKY41* (III) positively regulate bacterial wilt resistance in pepper (Wang et al., 2012; Dang et al., 2014, 2019; Hussain et al., 2018, 2021; Muhammad et al., 2018; Yang et al., 2021). *SiWRKY53* (III) responded to the bacterial wilt resistance (Mishra et al., 2021). WRKY members of group III played a vital role in plant bacterial wilt resistance. In this study, *AhWRKY76* and *AhWRKY77* of group III had LRR domain. qRT-PCR results showed that *AhWRKY77* was downregulated by 0.34 than control in 12 h of ganhua18 and 0.19 than control 6 h of kainong313 after infection with the *R. solanacearum*, which may negatively regulate bacterial wilt resistance in peanuts. After *R. solanacearum* infection, *AhWRKY76* displayed lower-higher expressions, i.e., 0.28, 10.35, and 3.97 than control in 6 h, 12 h, and 24 h of ganhua18, respectively, and higher expressions by 6.05 and 3.53 than control in 6 h and 12 h in kainong313, respectively, which may contribute to explain the difference in BW resistance between the two cultivars. These outcomes suggest that *AhWRKY76* and *AhWRKY77* may play a critical role in bacterial wilt resistance in peanuts. *AhWRKY76* and *AhWRKY77* targeted by ahy-miR3512 showed that ahy-miR3512 might have a vital role in BW resistance (Figure 7).

Conclusion

In conclusion, a total of 174 *AhWRKY* genes were identified in *A. hypogaea*. The classification, chromosomal location, collinearity, protein structure, conserved motif composition, *cis*-acting elements, putative miRNAs, and phylogenetic relationship of *AhWRKYs* were systematically analyzed, which provide a basis for further study of the molecular and functional structure of *AhWRKYs*. Furthermore, the expression patterns of tissues-specific and pathogen-responsive *AhWRKYs* were obtained from RNA-seq data and qRT-PCR results, providing useful information for further functional investigations in response to biotic stresses. Ten AhWRKY genes (*AhWRKY34*, *AhWRKY76*, *AhWRKY78*, *AhWRKY120*, *AhWRKY153*, *AhWRKY155*, *AhWRKY159*, *AhWRKY160*, *AhWRKY161,* and *AhWRKY162*) from group III displayed different expression patterns in sensitive and resistant peanut genotypes infected with the *R. solanacearum*. Two AhWRKY proteins (AhWRKY76 and AhWRKY77) from group III obtained the LRR domain; *AhWRKY77* was downregulated in two cultivars, and *AhWRKY76* showed lower-higher expression ganhua18 and higher expression in kainong313. Both *AhWRKY76* and *AhWRKY77* were targeted by ahy-miR3512, which may have an important function in peanut disease resistance. The positively upregulated genes could be used for further characterization in peanuts to develop disease-smart peanut cultivars. In short, our study could help researchers better understand the function and regulatory mechanism of *AhWRKYs* genes in *A. hypogaea* during pathogen response.

Data availability statement

The datasets presented in this study can be found in online repositories. The names of the repository/repositories and accession number(s) can be found in the article/Supplementary material.

Author contributions

LY carried out the bioinformatic analysis and drafted the manuscript. LY and HJ collected the plant materials and performed the experiments. AR helped with some analysis and improved the manuscript. LY, AR, and YH participated in handling figures and tables. LY, AR, DG, and XZ edited and revised the manuscript. All authors read and approved the final version of the manuscript.

Funding

This work was supported by the Agricultural Collaborative Innovation Project of Jiangxi Province, China (JXXTCXBSJJ2022007 and JXXTCX202112), and the Third Census and Collection of Crop Germplasm Resources in China.

Conflict of interest

The authors declare that the research was conducted in the absence of any commercial or financial relationships that could be construed as a potential conflict of interest.

Publisher's note

All claims expressed in this article are solely those of the authors and do not necessarily represent those of their affiliated organizations, or those of the publisher, the editors and the reviewers. Any product that may be evaluated in this article, or claim that may be made by its manufacturer, is not guaranteed or endorsed by the publisher.

Supplementary material

The Supplementary Material for this article can be found online at: https://www.frontiersin.org/articles/10.3389/fpls.2022.986673/full#supplementary-material

References

Ansari, S., Kumar, V., Bhatt, D. N., Irfan, M., and Datta, A. (2022). N-acetylglucosamine sensing and metabolic engineering for attenuating human and plant pathogens. *Bioengineering* 9, 64. doi: 10.3390/bioengineering9020064

Baillo, E. H., Hanif, M. S., Guo, Y., Zhang, Z., Xu, P., and Algam, S. A. (2020). Genome-wide Identification of WRKY transcription factor family members in sorghum (*Sorghum bicolor* (L.) moench). *PLoS ONE* 15, e0236651. doi: 10.1371/journal.pone.0236651

Bertioli, D. J., Cannon, S. B., Froenicke, L., Huang, G., Farmer, A. D., Cannon, E. K., et al. (2016). The genome sequences of arachis duranensis and arachis ipaensis, the diploid ancestors of cultivated peanut. *Nat. Genet.* 48, 438–446. doi: 10.1038/ng.3517

Bertioli, D. J., Jenkins, J., Clevenger, J., Dudchenko, O., Gao, D., Seijo, G., et al. (2019). The genome sequence of segmental allotetraploid peanut *Arachis hypogaea*. *Nat. Genet.* 51, 877–884. doi: 10.1038/s41588-019-0405-z

Bohra, A., Tiwari, A., Kaur, P., Ganie, S. A., Raza, A., Roorkiwal, M., et al. (2022). The key to the future lies in the past: insights from grain legume domestication and improvement should inform future breeding strategies. *Plant Cell Physiol.* pcac086. doi: 10.1093/pcp/pcac086. [Epub ahead of print].

Cannon, S. B., Mitra, A., Baumgarten, A., Young, N. D., and May, G. (2004). The roles of segmental and tandem gene duplication in the evolution of large gene families in Arabidopsis thaliana. *BMC Plant Biol.* 4, 10. doi: 10.1186/1471-2229-4-10

Chen, C., Chen, H., Zhang, Y., Thomas, H. R., and Xia, R. (2020). TB tools: An integrative toolkit developed for in-teractive analyses of big biological data. *Mol. Plant* 13, 1194–1202. doi: 10.1016/j.molp.2020.06.009

Chen, X., Li, C., Wang, H., and Guo, Z. (2019a). WRKY transcription factors: evolution, binding, and action. *Phytopathol. Res.* 1, 13. doi: 10.1186/s42483-019-0022-x

Chen, X., Lu, Q., Liu, H., Zhang, J., Hong, Y., and Lan, H., et al. (2019b). Sequencing of cultivated peanut, Arachishypogaea, yields insights into genome evolution and oil improvement. *Mol. Plant.* 12, 920–934. doi: 10.1016/j.molp.2019.03.005

Chen, Y., Ren, X., Zhou, X., Huang, L., Yan, L., Lei, Y., et al. (2014). Dynamics in the resistant and susceptible peanut (*Arachis hypogaea* L.) root transcriptome on infection with the *Ralstonia solanacearum*. *BMC Genomics* 15, 1078. doi: 10.1186/1471-2164-15-1078

Clevenger, J., Chu, Y., Scheffler, B., Ozias-Akins, P. (2016). A developmental transcriptome map for allotetraploid Arachis hypogaea. *Front. Plant Sci.* 7, 1446. doi: 10.3389/fpls.2016.01446

Dang, F., Lin, J., Chen, Y., Li, G. X., and He, S. (2019). A feedback loop between CaWRKY41 and H_2O_2 coordinates the response to Ralstonia solanacearum and excess cadmium in pepper. *J. Exp. Bot.* 70, 1581–1595. doi: 10.1093/jxb/erz006

Dang, F., Wang, Y., She, J., Lei, Y., Liu, Z., Eulgem, T., et al. (2014). Overexpression of CaWRKY27, a subgroup IIe WRKY transcription factor of Capsicum annuum, positively regulates tobacco resistance to Ralstonia solanacearum infection. *Physiol. Plant.* 150, 397–411. doi: 10.1111/ppl.12093

Deslandes, L., Olivier, J., Peeters, N., Feng, D. X., Khounlotham, M., Boucher, C., et al. (2003). Physical interaction between RRS1-R, a protein conferring resistance to bacterial wilt, and PopP2, a type III ffector targeted to the plant nucleus. *Proc Natl Acad Sci USA.* 100, 8024–8029. doi: 10.1073/pnas.1230660100

Deslandes, L., Olivier, J., Theulieres, F., Hirsch, J., et al. (2002). Resistance to Ralstonia solanacearum in *Arabidopsis thaliana* is conferred by the recessive RRS1-R gene, a member of a novel family of resistance genes. *Proc. Natl. Acad. Sci. U. S. A.* 99, 2404–2409. doi: 10.1073/pnas.032485099

Deslandes, L., Pileur, F., Liaubet, L., Camut, S., Can, C., Williams, K., et al. (1998). Genetic characterization of RRS1, a recessive locus in Arabidopsis thaliana that confers resistance to the bacterial soilborne pathogen Ralstonia solanacearum. *Mol. Plant Microbe Interact.* 11, 659–667. doi: 10.1094/MPMI.1998.11.7.659

Dong, J., Chen, C., and Chen, Z. (2003). Expression profiles of the Arabidopsis WRKY gene superfamily during plant defense response. *Plant Mol. Biol.* 51, 21–37. doi: 10.1023/A:1020780022549

Eulgem, T., Rushton, P. J., Robatzek, S., and Somssich, I. E. (2000). The WRKY superfamily of plant transcription factors. *Trends Plant Sci.* 5, 199–206. doi: 10.1016/S1360-1385(00)01600-9

Eulgem, T., and Somssich, I. E. (2007). Networks of WRKY transcription factors in defense signaling. *Curr. Opin. Plant Biol.* 10, 366–371. doi: 10.1016/j.pbi.2007.04.020

Farooq, M. S., Uzair, M., Raza, A., Habib, M., Xu, Y., Yousuf, M., et al. (2022). Uncovering the research gaps to alleviate the negative impacts of climate change on food security: a review. *Front. Plant Sci.* 13, 927535. doi: 10.3389/fpls.2022.927535

Gangurde, S. S., Kumar, R., Pandey, A. K., Burow, M., and Pandey, M. K. (2019). "Climate-smart groundnuts for achieving high productivity and improved quality: current status, challenges, and opportunities", in *Genomic Designing of Climate-Smart Oilseed Crops*, ed C. Kole (Cham: Springer), 133–172. doi: 10.1007/978-3-319-93536-2_3

Gasteiger, E., Gattiker, A., Hoogland, C., Ivanyi, I., Appel, R. D., and Bairoch, A. (2003). ExPASy: the proteomics server for in-depth protein knowledge and analysis. *Nucleic Acids Re.* 31, 3784–3788. doi: 10.1093/nar/gkg563

Haider, S., Raza, A., Iqbal, J., Shaukat, M., and Mahmood, T. (2022). Analyzing the regulatory role of heat shock transcription factors in plant heat stress tolerance: a brief appraisal. *Mol. Biol. Rep.* 49, 5771–5785. doi: 10.1007/s11033-022-07190-x

He, Y., Mao, S., Gao, Y., Zhu, L., and Qian, W. (2016). Genome-wide identification and expression analysis of WRKY transcription factors under multiple stresses in Brassica napus. *PLoS ONE* 11, e0157558. doi: 10.1371/journal.pone.0157558

Hikichi, Y., Mori, Y., Ishikawa, S., Hayashi, K., Ohnish, I. K., Kiba, A., et al. (2017). Regulation involved in colonization of intercellular spaces of host plants in Ralstonia solanacearum. *Front. Plant Sci.* 8, 967. doi: 10.3389/fpls.2017.00967

Hu, W., Ren, Q., Chen, Y., Xu, G., and Qian, Y. (2021). Genome-wide identification and analysis of WRKY gene family in maize provide insights into regulatory network in response to abiotic stresses. *BMC Plant Biol.* 21, 427. doi: 10.1186/s12870-021-03206-z

Hussain, A., Khan, M. I., Albaqami, M., Mahpara, S., Noorka, I. R., Ahmed, M. A. A., et al. (2021). CaWRKY30 positively regulates pepper immunity by targeting CaWRKY40 against *Ralstonia solanacearum* inoculation through modulating defense-related genes. *Int. J. Mol. Sci.* 22, 12091. doi: 10.3390/ijms222112091

Hussain, A., Li, X., Weng, Y., Liu, Z., Ashraf, M. F., Noman, A., et al. (2018). CaWRKY22 Acts as a Positive Regulator in Pepper Response to Ralstonia Solanacearum by Constituting Networks with CaWRKY6, CaWRKY27, CaWRKY40, and CaWRKY58. *Int J Mol Sci.* 19, 1426. doi: 10.3390/ijms19051426

Irfan, M., Ghosh, S., Meli, V. S., Kumar, A., Kumar, V., Chakraborty, N., et al. (2016). Fruit ripening regulation of α-Mannosidase expression by the MADS box transcription factor RIPENING INHIBITOR and ethylene. *Front. Plant Sci.* 7, 10. doi: 10.3389/fpls.2016.00010

Irfan, M., Kumar, P., Ahmad, I., and Datta, A. (2021). Unraveling the role of tomato Bcl-2-associated athanogene (BAG) proteins during abiotic stress response and fruit ripening. *Sci. Rep.* 12, 3503. doi: 10.1038/s41598-021-01185-7

Javed, T., Shabbir, R., Ali, A., Afzal, I., Zaheer, U., and Gao, S. J. (2020). Transcription factors in plant stress responses: challenges and potential for sugarcane improvement. *Plants* 9, 491. doi: 10.3390/plants9040491

Javed, T., Zhou, J. R., Li, J., Hu, Z. T., Wang, Q. N., and Gao, S. J. (2022). Identification and expression profiling of WRKY family genes in sugarcane in response to bacterial pathogen infection and nitrogen implantation dosage. *Front. Plant Sci.* 13, 917953. doi: 10.3389/fpls.2022.917953

Jiang, G., Wei, Z., Xu, J., Chen, H., Zhang, Y., She, X., et al. (2017). Bacterial wilt in China: history, current status, and future perspectives. *Front. Plant Sci.* 8, 1549. doi: 10.3389/fpls.2017.01549

Jones, J. D., and Dangl, J. L. (2006). The plant immune system. *Nature.* 444, 323–329. doi: 10.1038/nature05286

Kalde, M., Barth, M., Somssich, I. E., and Lippok, B. (2003). Members of the Arabidopsis WRKY group III transcription factors are part of different plant defense signaling pathways. *Mol Plant Microbe Interact.* 16, 295–305. doi: 10.1094/MPMI.2003.16.4.295

Kaliyappan, R., Viswanathan, S., Suthanthiram, B., Subbaraya, U., Marimuthu Somasundram, S., and Muthu, M. (2016). Evolutionary expansion of WRKY gene family in banana and its expression profile during the infection of root lesion nematode, *Pratylenchus coffeae*. *PLoS ONE* 11, e0162013. doi: 10.1371/journal.pone.0162013

Kumar, V., Chattopadhyay, A., Ghosh, S., Irfan, M., Chakraborty, N., et al. (2016). Improving nutritional quality and fungal tolerance in soya bean and grass pea by expressing an oxalate decarboxylase. *Plant Biotechnol. J.* 14, 1394–1405. doi: 10.1111/pbi.12503

Leister, D. (2004). Tandem and segmental gene duplication and recombination in the evolution of plant disease resistance genes. *Trends Genet.* 20, 116–122. doi: 10.1016/j.tig.2004.01.007

Li, J., Islam, F., Huang, Q., Wang, J., Zhou, W., Xu, L., et al. (2020). Genome-wide characterization of WRKYgene family in *Helianthus annuus* L. and their expression profiles under biotic and abiotic stresses. *PLoS ONE* 15, e0241965. doi: 10.1371/journal.pone.0241965

Li, Z., Hua, X., Zhong, W., Yuan, Y., Wang, Y., Wang, Z., et al. (2020). Genomewide identification and expression profile analysis of WRKY family genes in the autopolyploid Saccharum spontaneum. *Plant Cell Physiol.* 61, 616–630. doi: 10.1093/pcp/pcz227

Liu, X., Inoue, H., Hayashi, N., Jiang, C. J., and Takatsuji, H. (2016). CC-NBS-LRR-type R proteins for rice blast commonly interact with specific WRKY transcription factors. *Plant Molecular Biology Reporter.* 34, 533–537. doi: 10.1007/s11105-015-0932-4

Liu, Z. Q., Shi, L. P., Yang, S., Qiu, S. S., Ma, X. L., Cai, J. S., et al. (2021). A conserved double-W box in the promoter of CaWRKY40 mediates autoregulation during response to pathogen attack and heat stress in pepper. *Mol. Plant Pathol.* 22, 3–18. doi: 10.1111/mpp.13004

McHale, L., Tan, X., Koehl, P., and Michelmore, R. W. (2006). Plant NBS-LRR proteins: adaptable guards. *Genome Biol.* 7, 212. doi: 10.1186/gb-2006-7-4-212

Mishra, G. P., Radhakrishnan, T., Kumar, A., Thirumalaisamy, P. P., Kumar, N., and Bosamia, T. C., et al (2015). Advancements in molecular marker development and their applications in the management of biotic stresses in peanuts. *Crop Protect.* 77, 74–86. doi: 10.1016/j.cropro.2015.07.019

Mishra, P., Tripathi, A. N., Kashyap, S. P., Aamir, M., and Tiwari, S. K. (2021). In silico mining of WRKY TFs through *Solanum melongena* L. and *Solanum incanum* L. transcriptomes and identification of SiWRKY53 as a source of resistance to bacterial wilt. *Plant Gene* 26, 100278. doi: 10.1016/j.plgene.2021.100278

Muhammad, I. K., Zhang, Y., Liu, Z., Hu, J., Liu, C., and Yang, S., et al. (2018). CaWRKY40b in pepper acts as a negative regulator in response to *Ralstonia solanacearum* by directly modulating defense genes including CaWRKY40. *Int. J. Mol. Sci.* 19, 1403. doi: 10.3390/ijms19051403

Raza, A., Charagh, S., García-Caparrós, P., Rahman, M. A., Ogwugwa, V. H., Saeed, F., and Jin, W. (2022b). Melatonin-mediated temperature stress tolerance in plants. *GM Crops & Food* 13, 196–217. doi: 10.1080/21645698.2022.2106111

Raza, A., Tabassum, J., Mubarik, M. S., Anwar, S., Zahra, N., Sharif, Y., et al. (2022a). Hydrogen sulfide: an emerging component against abiotic stress in plants. *Plant Biol.* 24, 540–558. doi: 10.1111/plb.13368

Rushton, P. J., Somssich, I. E., Ringler, P., and Shen, Q. J. (2010). WRKY transcription factors. *Trends Plant Sci.* 15, 247–258. doi: 10.1016/j.tplants.2010.02.006

Sharma, M., Irfan, M., Kumar, A., Kumar, P., and Datta, A. (2021). Recent insights into plant circadian clock response against abiotic stress. *J. Plant Growth Regul.* 1–14. doi: 10.1007/s00344-021-10531-y. [Epub ahead of print].

Sharma, M., Kumar, P., Verma, V., Sharma, R., Bhargava, B., and Irfan, M. (2022). Understanding plant stress memory response for abiotic stress resilience: molecular insights and prospects. *Plant Physiol. Biochem.* 179, 10–24. doi: 10.1016/j.plaphy.2022.03.004

Shen, Q. H., Saijo, Y., Mauch, S., Biskup, C., Bieri, S., Keller, B., et al. (2007). Nuclear activity of MLA immune receptors links isolate-specific and basal disease-resistance responses. *Science* 315, 1098–1103. doi: 10.1126/science.1136372

Song, H., Wang, P., Lin, J. Y., Zhao, C., Bi, Y., and Wang, X. (2016). Genome-wide identification and characterization oF WRKY gene family in peanut. *Front. Plant Sci.* 7, 534. doi: 10.3389/fpls.2016.00534

Song, Y., Cui, H., Shi, Y., Xue, J., Ji, C., Zhang, C., et al. (2020). Genome-wide identification and functional characterization of the *Camelina sativa* WRKY gene family in response to abiotic stress. *BMC Genomics* 21, 786. doi: 10.1186/s12864-020-07189-3

Van De Peer, Y., Mizrachi, E., and Marchal, K. (2017). The evolutionary significance of polyploidy. *Nat. Rev. Genet.* 18, 411–424. doi: 10.1038/nrg.2017.26

Wan, Y., Mao, M., Wan, D., Yang, Q., and Yang, F., Mandlaa, et al. (2018). Identification of the WRKY gene family and functional analysis of two genes in Caragana intermedia. *BMC Plant Biol.* 18, 31. doi: 10.1186/s12870-018-1235-3

Wang, D., Wang, L., Su, W., Ren, Y., and Su, Y. (2020). A class III WRKY transcription factor in sugarcane was involved in biotic and abiotic stress responses. *Sci. Rep.* 10, 20964. doi: 10.1038/s41598-020-78007-9

Wang, Y., Dang, F., Liu, Z., Wang, X., Eulgem, T., and Lai, Y., et al. (2012). Cawrky58, encoding a group i wrky transcription factor ofcapsicum annuum, negatively regulates resistance toralstonia solanacearuminfection. *Mol. Plant Pathol.* 14, 131–144. doi: 10.1111/j.1364-3703.2012.00836.x

Wei, K. F., Chen, J., Chen, Y. F., Wu, L. J., and Xie, D. X. (2012). Molecular phylogenetic and expression analysis of the complete WRKY transcription factor family in maize. *DNA Res.* 19, 153–164. doi: 10.1093/dnares/dsr048

Wu, J., Chen, J., Wang, L., and Wang, S. (2017). Genome-wide investigation of WRKY transcription factors involved in terminal drought stress response in common bean. *Front. Plant Sci.* 8, 380. doi: 10.3389/fpls.2017.00380

Xie, T., Chen, C., Li, C., Liu, J., Liu, C., and He, Y. (2018). Genome-wide investigation of WRKY gene family in pineapple: evolution and expression profiles during development and stress. *BMC Genomics* 19, 490. doi: 10.1186/s12864-018-4880-x

Yang, S., Zhang, Y., Cai, W., Liu, C., and Shuilin, H. E. (2021). CaWRKY28 Cys249 is required for interaction with CaWRKY40 in the regulation of pepper immunity to *Ralstonia solanacearum*. *Mol. Plant Microbe Interact.* 34, 733–745. doi: 10.1094/MPMI-12-20-0361-R

Zhang, Y., and Wang, L. (2005). The WRKY transcription factor superfamily: its origin in eukaryotes and expansion in plants. *BMC Evol Biol* 5, 1. doi: 10.1186/1471-2148-5-1

Zhao, N., He, M., Li, L., Cui, S., Hou, M., Wang, L., et al. (2020). Identification and expression analysis of WRKY gene family under drought stress in peanut (*Arachis hypogaea* L.). *PLoS ONE* 15, e0231396. doi: 10.1371/journal.pone.0231396

Zhu, H., Jiang, Y., Guo, Y., Huang, J., Zhou, M., Tang, Y., et al. (2021). A novel salt inducible WRKY transcription factor gene, *AhWRKY75*, confers salt tolerance in transgenic peanut. *Plant Physiol. Biochem.* 160, 175–183. doi: 10.1016/j.plaphy.2021.01.014

frontiers | Frontiers in Plant Science

TYPE Review
PUBLISHED 06 October 2022
DOI 10.3389/fpls.2022.1008881

OPEN ACCESS

EDITED BY
Ravi Gupta,
Kookmin University, South Korea

REVIEWED BY
Amit Kumar Mishra,
Mizoram University, India
Cheol Woo Min,
Pusan National University, South Korea

*CORRESPONDENCE
Neha Kaushik
neha.bioplasma@gmail.com
Abdel Khalid Essamadi
essamadi@uhp.ac.ma
Nagendra Kumar Kaushik
kaushik.nagendra@kw.ac.kr

SPECIALTY SECTION
This article was submitted to Crop and Product Physiology, a section of the journal Frontiers in Plant Science

RECEIVED 01 August 2022
ACCEPTED 29 August 2022
PUBLISHED 06 October 2022

CITATION
Benjamaa R, Moujanni A, Kaushik N, Choi EH, Essamadi AK and Kaushik NK (2022) *Euphorbia* species latex: A comprehensive review on phytochemistry and biological activities.
Front. Plant Sci. 13:1008881.
doi: 10.3389/fpls.2022.1008881

Euphorbia species latex: A comprehensive review on phytochemistry and biological activities

Rania Benjamaa[1], Abdelkarim Moujanni[1], Neha Kaushik[2]*, Eun Ha Choi[3], Abdel Khalid Essamadi[1]* and Nagendra Kumar Kaushik[3]*

[1]Laboratory of Biochemistry, Neurosciences, Natural Resources and Environment, Faculty of Sciences and Technologies, Hassan First University of Settat, Settat, Morocco, [2]Department of Biotechnology, College of Engineering, The University of Suwon, Hwaseong-si, South Korea, [3]Department of Electrical and Biological Physics, Plasma Bioscience Research Center, Kwangwoon University, Seoul, South Korea

The genus *Euphorbia* includes about 2,000 species commonly widespread in both temperate and tropical zones that contain poisonous milky juice fluid or latex. Many species have been used in traditional and complementary medicine for the treatment of various health issues such as dropsy, paralysis, deafness, wounds, warts on the skin, and amaurosis. The medicinal applications of these species have been attributed to the presence of various compounds, and most studies on *Euphorbia* species have focused on their latex. In this review, we summarize the current state of knowledge on chemical composition and biological activities of the latex from various species of the genus *Euphorbia.* Our aim was to explore the applications of latex extracts in the medical field and to evaluate their ethnopharmacological potential. The databases employed for data collection, are obtained through Web of Science, PubMed, Google Scholar, Science Direct and Scopus, from 1983 to 2022. The bibliographic data indicate that terpenoids are the most common secondary metabolites in the latex. Furthermore, the latex has interesting biological properties and pharmacological functions, including antibacterial, antioxidant, free radical scavenger, cytotoxic, tumor, anti-inflammatory, healing, hemostatic, anti-angiogenic, insecticidal, genotoxic, and mutagenic activities. However, the role of other components in the latex, such as phenolic compounds, alkaloids, saponins, and flavonoids, remains unknown, which limits the application of the latex. Future studies are required to optimize the therapeutic use of latex extracts.

KEYWORDS

***Euphorbiaceae*, *Euphorbia* species, latex, chemical constituents, biological applications**

Introduction

Plant latex is produced by more than 20,000 species from around 40 families (Bauer et al., 2014). It is a fluid found in specialized cells called "laticifera" that are located throughout the plant (Ramos et al., 2020) and can have different colors: white, yellow, red, or colorless. Because of its sticky properties, the latex has been implicated in the defense against herbivorous insects and used to produce rubber (Agrawal and Konno, 2009). In addition, the latex of various plant species contains a wide variety of bioactive compounds, including proteins, enzymes, alkaloids, glycosides, cardenolides, terpenoids, furanocoumarins, and starch (Konno, 2011). Moreover, the water insoluble fraction of the latex from the families *Euphorbiaceae*, *Asclepiadaceae*, and *Caricaceae* has shown lipase activity and can be used as a useful biocatalyst for several synthetic applications in the food, pharmaceutical, and detergent industries (Paques and Macedo, 2006).

Euphorbiaceae is one of the largest and oldest plant families in the world, comprising approximately 300 genera and 8,000 species (Webster, 1987). This is one of the plant families with latex-producing species (Lewinsohn, 1991). The *Euphorbia* genus (commonly called spurge) incorporates a wide variety of plants with biological and medical applications (Kemboi et al., 2020). The species are distributed in both temperate and tropical regions (Pahlevani and Mozaffarian, 2011), with endemic species such as *E. resinifera* in Morocco (Chakir et al., 2016), *E. cubensis, E. helenae, E. munizii*, and *E. podocarpifolia* in Cuba (Steinmann et al., 2007), *E. polycaulis* in Iran (Nasr et al., 2018), *E. hainanensis* in China (Tian et al., 2018), *E. fauriei* and *E. garanbiensis* in Korea and Taiwan (Ki-Ryong, 2004), and *E. boetica* in the Iberian peninsula (Narbona et al., 2007). Plants in this genus contain a white acrid, poisonous milky juice fluid or latex that comes out when cut or damaged (Bigoniya and Rana, 2008) and is extremely irritating to the skin (Salehi et al., 2019).

The latex from several *Euphorbia* species has been chemically investigated. It contains different biological compounds, such as triterpenoids (Palocci et al., 2003; Kemboi et al., 2020) diterpenes, ingenol, 12-deoxyphorbol esters (Priya and Rao, 2011), triterpene alcohols, lanosterol,(Giner et al., 2000), fatty acids, proteins, and enzymes (Spanò et al., 2012). The terpenoids are the most abundant components of this genus, which are known to have pharmacological activities, which can offer a wide range of medicinal applications.

Abbreviations: ABTS, 2,2′-azino-bis(3-ethylbenzothiazoline-6-sulphonic acid); DPPH, 2,2-diphenyl-2-picrylhydrazyl; E, *Euphorbia*; FRAP, ferric reducing antioxidant power; FTIR, Fourier-transform infrared spectroscopy; GAE, gallic acid equivalents; IC50, 50% inhibitory concentration; LC50, lethal concentration, 50 percent; MIC, minimum inhibitory concentration; MTT, (3-(4,5-dimethylthiazol-2-yl)-2,5-diphenyltetrazolium bromide); NMR, nuclear magnetic resonance spectroscopy; NO, nitric oxide; TEAC, trolox equivalent antioxidant capacity.

Furthermore, the latex of some *Euphorbia* species has been used in traditional medicine to treat wounds and warts on the skin (Özbilgin et al., 2019) as well as some nervous diseases, dropsy, paralysis, deafness, and amaurosis (Gewali et al., 1989).

To our knowledge, no literature review provides a comprehensive study on the latex of the genus Euphorbia. Here, we review the current state of knowledge on the ethnomedicinal uses, phytochemical composition, and biological activities of the latex from more than 20 species of *Euphorbia*. The main objective of this study is to present a database of knowledge and research trends on latex of the genus *Euphorbia* with the aim of providing basic data to promote future pharmacological and phytochemical studies on spurge latex.

Distribution

The genus *Euphorbia* includes several species distributed in both temperate and tropical zones (El-Ghazaly and Chaudhary, 1993). However, many species are also present in non-tropical areas such as Africa and Central and South America (Liang et al., 2014). Certain species are distributed in India, specifically in the North and West (Pascal et al., 2017). This genus is represented in Taiwan by eight species (Lin and Hsieh, 1991). There are about 90 species mostly concentrated in Iran and 91 species in Turkey (Nasseh et al., 2018), with about 70 species found in China (Liang et al., 2014). On the other hand, in Brazil, the genus is represented by about 64 species, with a degree of endemism of about 50% (31 spp.) (Steinmann et al., 2007).

Description

The genus contains several species, which can be annual or perennial, xerophytes, woody shrubs, or trees with a caustic and poisonous milky latex (Berg, 1990). They are characterized by the presence of fine or thick and fleshy or tuberous roots (Pascal et al., 2017). The fruits are basically fleshy, with explosive dehiscence (Dorsey, 2013). The species are generally recognized by their inflorescences, which are called cyathium and resemble a dicotyledonous flower. Each inflorescence contains a female flower surrounded by several male flowers and is composed of cup-like involucre formed by two bracts bearing four or five often horned glands (Prenner and Rudall, 2007).

Phytochemical profile of *Euphorbia* latex

Phytochemical investigations on different species of euphorbia have shown the presence of diversity of constituents, mainly terpenoids, enzymes and Natural Rubber. **Table 1** shows the major terpenoids and **Figures 1–6** showed the

TABLE 1 Chemical Constituents of euphorbia genus latex.

Species	Compounds	References
E. peplus	Peplusol (**1**) Obtusifoloio (**2**), lanosterol (**3**), 24-methylenelanosterol **(4),** cycloartenol **(5)** and 24-methylenecycloartano **(6**).	Giner et al., 2000
E. officinarum	7,8,12-triacetate 3-phenylacetate **(7)**, ingol 7,8,12 triacetate 3-(4-methoxyphenyl)acetate (**8**), 8 methoxyingol 7,12-diacetate 3-phenylacetate (**9**), 3S,4S,5R,7S,9R,14R-3,7-dihydroxy-4,14-dimethyl-7[8 → 9] Abeo-cholestan-8-one (10), 3β-acetoxy-norlup-20-one (**11**) and 4α,14α-dimethyl-5α-cholest-8-ene (**12**).	Daoubi et al., 2007; Smaili et al., 2017
E. obtusifolia	(2R,3R,4R,5R,7S,8S,9S,11E,13S,15R)-2,3,5,7,8,9,15-Heptahydroxyjatropha-6(17),11-diene-14-one-7,8,9-triacetate-2,5-bis(2-methylbutyrate) **(13),** (2R,3R,4R,5R,7S,8S,9S,11E,13S,15R)-2,3,5,7,8,9,15-Heptahydroxyjatropha-6(17),11-diene-14-one-7,8,9-triacetate-2-isobutyrate-5-(2-methylbutyrate) **(14),** (2R,3R,4R,5R,7S,8S,9S,11E,13S,15R)-2,3,5,7,8,9,15-Heptahydroxyjatropha-6(17),11-diene-14-one-7,8,9-triacetate-2-nicotinate-5-(2-methylbutyrate) **(15)**, (2R,3R,4R,5R,7S,8S,9S,11E,13S,15R)-2,3,5,7,8,9,15-Heptahydroxyjatropha-6(17),11-diene-14-one-8,9-diacetate-7-isobutyrate-2,5-bis(2-methylbutyrate) **(16)**, (2R,3R,4R,5R,7S,8S,9S,11E,13S,15R)-2,3,5,7,8,9,15-Heptahydroxyjatropha-6(17),11-diene-14-one-2,8,9-triacetate-7-isobutyrate-5-(2-methylbutyrate) **(17),** (2R,3R,4R,5R,7S,8S,9S,11E,13S,15R)-2,3,5,7,8,9,15-Heptahydroxyjatropha-6(17),11-diene-14-one-7,9-diacetate-8-benzoate-2,3-bis(2-methylbutyrate) **(18),** (2R,3R,4R,5R,7S,8S,9S,11E,13S,15R)-2,3,5,7,8,9,15-Heptahydroxyjatropha-6(17),11-diene-14-one-8,9-diacetate-7-isobutyrate-2,3-bis(2-methylbutyrate*)* **(19)**, 4,20-*Dideoxyphorbol* 12,13-*bis(isobutyrate)* ***(20)***, 4-*Deoxyphorbol 12,13-bis(isobutyrate)* ***(21)***, 17-*Acetoxy*-4-*deoxyphorbol* 12,13-*bis(isobutyrate)* **(22)** 17-*Acetoxy*-4,20-dideoxyphorbol *12,13*-bis(isobutyrate) ***(23)***,*4*-deoxyphorbol 12,13-bis(isobutyrate) 20-acetate **(24)** and 4-epi-4-deoxyphorbol ester: 4-Epi-4-deoxyphorbol 12,13-bis (isobutyrate) **(25).**	Marco et al., 1999
E. tirucalli L	Euphol **(26);** tirucallol **(27)**, ingenol **(28)** and 4-desoxyphorbol **(29).**	de Souza et al., 2019
E. fischeriana	12-deoxyphorbol-13-tetradecanoate **(30)**, 12-deoxyphorbol-13- (7Z)-hexadecenoate **(31)**, 12-deoxyphorbol-13-(9Z, 12Z)-octadecadienoate **(32)**, 12-deoxyphorbol-13-hexadecanoate **(33)**, 12-deoxyphorbol-13-(6Z)- octadecenoate **(34)** and 12- deoxyphorbaldehy-13-hexadecanoate **(35).**	Deng et al., 2021
E. bicolor	Resiniferatoxin (**36**) and Abietic Acid **(37).**	Basu et al., 2019
E. umbellate	Lanosterol **(38),** cycloartenol **(39),** tirucallol **(40**), taraxasterol **(41)**,lupeol **(42),** phorbol-12,13,20-triacetate **(43);** 4-β phorbol **(44);** and 3 desoxo-3,16-dihydroxy-12-desoxyphorbol 3,13,16,20-tetraacetate **(45).**	Cruz et al., 2020
E. helioscopia	7α, 9β, 15β-triacetoxy-3β-benzoyloxy-14β-hydroxyjatropha-5E, 11E-diene (**46**), euphoheliosnoid A **(47),** epieuphoscopin B **(48)**, euphoscopin C **(49)**, euphohelioscopin A **(50).**	Hua et al., 2015
E. nerifolia	9, 19-cyclolanost-22(22'), 24-diene-3β-ol (Neriifoliene) **(51),** 5α-eupha-8, 24-diaene-3β-ol (Euphol) **(52),** 9, 19-cyclolanost-20(21)-en-24-ol-3-one (Neriifolione) **(53)** and cycloartenol **(54).**	Ilyas et al., 1998; Mallavadhani et al., 2004
E. broteri	12-0-(2Z, 4E-octadienoyl)-4-deoxyphorbol-13 20-diacetate **(55),** 12-0-(2Z, 4E-octadienoyl)-phorbol-13, 20- diacetate **(56),** 20-acetyl-ingenol-3-decadienoate **(57),** 3-0-tetradecanoyl-ingenol **(58)**, 20-0-tetradecanoyl-ingenol **(59)** and 5-0-tetradecanoyl-ingeol **(60).**	Urones et al., 1988
E. lacteal	Tirucallol **(61)**	Fernandez-Arche et al., 2010
E. antiquorum	euphol 3-0-cinnamate **(62),** euphol **(63)**, 24-methylenecycloartanol **(64),** cycloeucalenol **(65),** β -Sitosterol **(66)**; 3-0-cinnamoyl-20- hydroxy derivative of lanostane or euphane (antiquol A) **(67)**, 3- epi-anhydrohtsomentof (antiquol B) **(68)**, and 4-Acetoxyphenol **(69).**	Gewali et al., 1990
E. resinifera	(2'S)-ingol 3,8-diacetate-7-(2'-hydroxy-6'- methoxyphenyl) acetate (Euphoresin A) **(70)**; (2'S)-ingol 3,8-diacetate-7-(2'-hydroxy-phenyl) acetate (Euphoresin B) **(71),** euphatexol A **(72)**, euphatexol B (27-nor-3-hydroxy-25-oxo-eupha-8, 23-diene) **(73)**, euphatexols C (3 β- hydroxyeupha-8,24-diene-1,7,11-trione) (74), euphatexol D ((24 R)-eupha-7,9,25- triene-3,24-diol) **(75)**, euphatexol E **(76),** euphatexol F (3b,7a)-dihydroxyeupha-8,24-diene-11-one) **(77),** euphatexol G (3b,7a)-dihydroxy-24-methyleneeupha-8-ene-11-one) **(78)**.3β-hydroxy-12α-methoxylanosta-7,9(11),24-triene **(79)**, 3β-hydroxy-12α-methoxy-24-methylene-lanost-7,9(11)-dien **(80),**	

(Continued)

TABLE 1 (Continued)

Species	Compounds	References
	3,7-dioxo-lanosta-8,24-diene **(81)**, and 3,7-dioxo-24-methylene-lanost-8-ene **(82).** Resiniferatoxin **(83)**	Fattorusso et al., 2002; Qi et al., 2019; Wang et al., 2019; Li et al., 2021, 2022
E. dendroides	Euphodendroidins E **(84),** euphodendroidins F (**85**), Euphodendroidin J (2R,3R,4S,5R,7R,8R,9R,13S,15R)-8,9-Diacetoxy-2,5,15-trihydroxy-3,7-dibenzoyloxy-14-oxojatropha-6(17), 11Ediene (**86**), euphodendroidins A **(87),** Euphodendroidin K, (2R,3R,4S,5R,7R,8R,9R,13S,15R)-2,8,9-Triacetoxy-15-hydroxy-7-benzoyloxy-3,5-diisobutyroyloxy-14-oxojatropha-6(17),11E-diene **(88),** Euphodendroidin L (2R,3R,4S,5R,7R,8R,9R,13S,15R)-2,3,8,9-Tetracetoxy-15-hydroxy-7-benzoyloxy-5-isobutyroyloxy-14-oxojatropha-6(17),11E-diene **(89),** jatrophane ester (**90**), Euphodendroidin M, (2R,3R,4S,5R,7R,8R,9R,13S,15R)-2,8,9-Triacetoxy-15-hydroxy-3-benzoyloxy-5,7-diisobutyroyloxy-14-oxojatropha-6-(17),11E-diene **(91),** Euphodendroidins B **(92)**, Euphodendroidin N, (2R,3R,4S,5R,7R,8R,9R,13S,15R)-2,8,9-Triacetoxy-3,15-dihydroxy-5,7-dibenzoyloxy-4-oxojatropha-6(17),11Ediene **(93),** (2R, 3R, 4S, 5R, 7R, 8R, 9R, 13S,- 15R)-2,9-diacetoxy-3, 8, 15-trihydroxy-5,7-dibenzoyloxy-14-oxojatropha-6(17), 11E-diene (euphodendroidins O) **(94),** 13α-hydroxyterracinolides G (**95**), 13α-hydroxyterracinolides B **(96)**, terracinolides J **(97)** and C **(98).**	Esposito et al., 2016
E. acrurensis	*19-Hydroxyingol 3,12-diacetate 7,8-ditiglate **(99)**, 19-Hydroxyingol 3,12,19-triacetate 8-tiglate **(100),** 19-Hydroxyingol 12,19-diacetate 8-tiglate **(101),** Ingol 3,8,12-triacetate 8-isovalerate **(102),** ingol-3,8,12-triacetate-7-angelate **(103),** Ingol 3,12-diacetate 7,8-ditiglate **(104),** ingol-3,8,12-triacetate-7-tiglat **(105),** 8-O-methyl-ingol-3,12-diacetate-7-tiglate **(106),** 3,12-di-o-acethyl-8-o-tigloyli,gol **(107),** ingenol 3-angelate 5,20- diacetate **(108)** and diester of 5-deoxyingenol **(109).***	Marco et al., 1999
E. nicaeensis	3b,5a,15b-triacetyloxy-2a-hydroxy-9a-nicotinyloxyjatropha-6 (17),11E-diene-14-one **(110)**, 2a,5a,8a-triacetyloxy-15b-hydroxy-7b-isobutanoyloxy-9a-nicotinyloxy-3b-propanoyloxyjatropha-6 (17),11E-diene-14-one **(111)**, 5a,8a,9a-triacetyloxy-15b-hydroxy-3b,7b-diisobutanoyloxy-2a-nicotinyloxyjatropha-6 (17),11Ediene-14-one **(112)**, 5a,8a,9a-triacetyloxy-15b-hydroxy-7b-isobutanoyloxy-2a-nicotinyloxy-3b-propanoyloxyjatropha-6 (17),11E-diene-14-one **(113),** euphodendrophane O **(114)**,5a,7 b,15b-triacetyloxy-9a-nicotinyloxy-3b-propanoyloxyjatropha-6 (17),11Ediene-14-one **(115),** 3b,5a,8a,15b-tetraacetyloxy-9anicotinyloxy-7b-isobutanoyloxyjatropha-6 (17),11E-diene-14-one **(116),** 5a,9adiacetyloxy-15b-hydroxy-7b-isobutanoyloxy-8a-nicotinyloxy-3bpropanoyloxyjatropha-6 (17),11E-diene-14-one **(117),** euphodendrophanes A **(118)**, B**(119),** C **(120)**, N **(121)**, F **(122),** Q**(123)**and S **(124)** 3S,24S)-tirucall-7-ene-3,24,25-triol **(125)**, (3S,24R)-tirucall-7-ene-3,24,25-triol (**126)** and inoterpene C **(127).**	Krstić et al., 2018, 2019
E. hermentiana.	3,12-O-diacetyl-7-O-benzoyl-8 methoxyingo l **(128),** 3,12-O-diacetyl-7-O-tigloyl-8- methoxyingol (**129**), 3,12-O-diacetyl-7-0-angeloyl-8-methoxyingol **(130)**, 3,7,12-0-triacetyl-8-0-benzoyl-18-hydroxyingol **(131),** 3,7,12-O-triacetyl-8-O-benzoylingol **(132),** 3,7,12-O-triacetyl-8-0-tigloylingol **(133),** 3,7,8,12-O-tetraacetylingol **(134),** 3,7,8,12,18-O-pentaacetyl-18-hydroxyngol **(135),** 3,7,12,18-O-tetraacetyl-8-o-benzoyl-18-hydroxy-ingol **(136)**,7-0-benzoyl-8-methoxy-12-0-acetylingol **(137),** 8-methoxy-12-O-acetylingol **(138),** 7-0-tigloyl-8-methoxy-12-0- acetylingol **(139),** 8-0-benzoyl-12-0-acetylingol **(140),** 12-O-acetylingol **(141),** 7,12-O-diacetyl-8-O-tigloylingol **(142)** and 8-0-tigloyl-l2-0-acetylingol **(143)**	Lin and Kinghorn, 1983
E. Drupifera	eupha- 8, 24-diene-3-ol **(144)** and 12-deoxyphorbol-20-propanoate **(145).**	Famuyiwa et al., 2014
E. polygonifolia	3β,17a,20S)-Dammara-12,24-dien-3-ol (Polygonifoliol) **(146),** (3β,20S)-Dammara-13(17),24-dien-3-ol (Isotirucallol) **(147),** Dammaradienol **(148),** Dammaradienol **(149)**, Lupeol **(150),** Lanosterol **(151),** Butyrospermol **(152),** Tirucallenol **(153)**, 24-Methylenelanosterol **(154)**, Cycloartenol **(155),** Taraxasterol **(156),** β-Amyrin **(157),** 24-Methylenecycloartanol **(158),** Taraxasterol **(159),** α-Amyrin **(160)** and Multiflorenol (**161).**	Giner and Schroeder, 2015

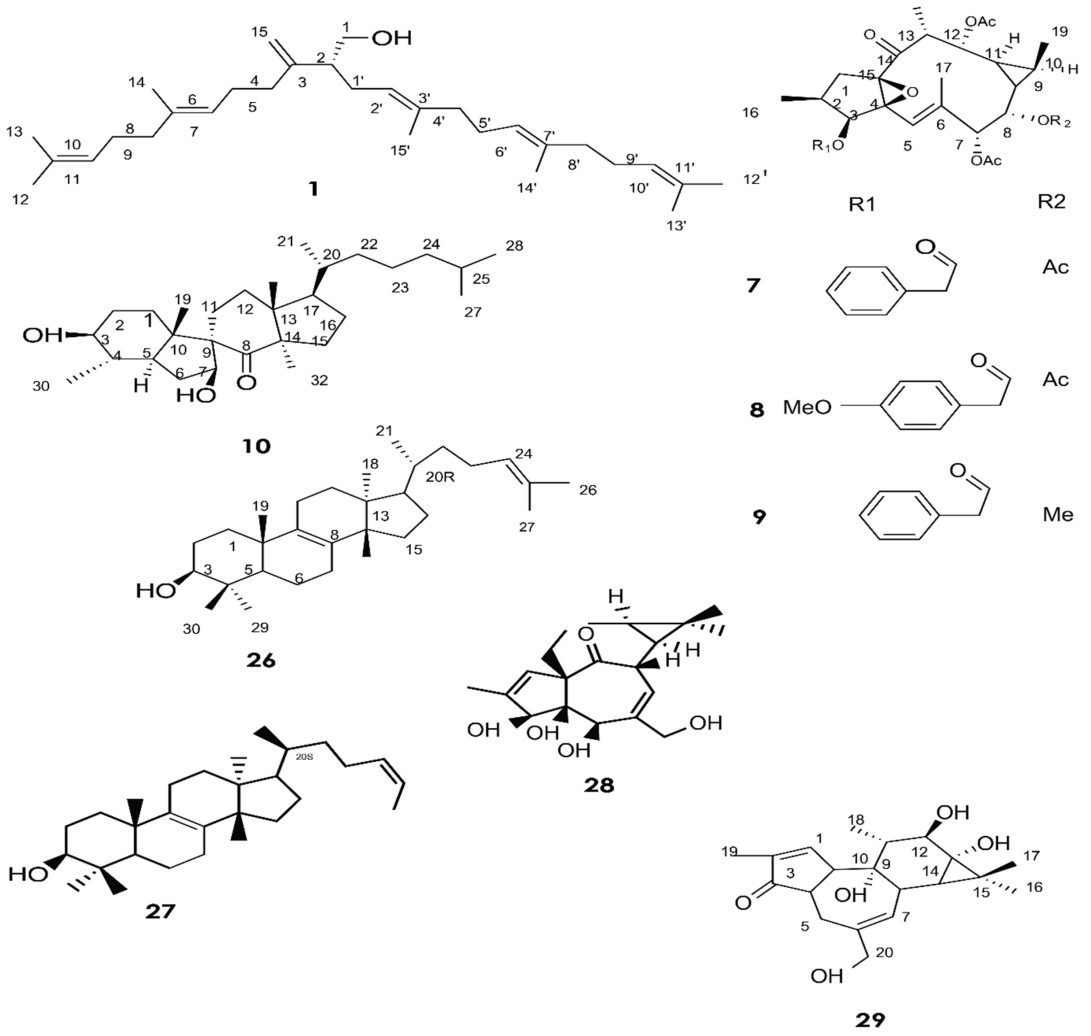

FIGURE 1
Structure of chemicals compound **1, 7-10, 26-29** (Giner et al., 2000; Daoubi et al., 2007; de Souza et al., 2019).

chemical structures of terpenoids isolated from different *Euphorbia* species.

Terpenoids

Phytochemical screening has revealed that terpenes are the main constituents isolated from the latex of different species of the *Euphorbia* genus (Shi et al., 2008). Most of them are identified using high-performance liquid chromatography (HPLC) (Deng et al., 2021), chromatography-mass spectroscopy (GC-MS) (Cruz et al., 2020), NMR spectroscopic analysis (Esposito et al., 2016), and thin layer chromatography (Daoubi et al., 2007).

A total of approximately 161 compounds have been reported from 19 species: *E. peplus, E. officinarum, E. obtusifolia, E. tirucalli L* (Compounds 1, 7–10, 26–29) (**Figure 1**), *E. fischeriana, E. bicolor, E. umbellate, E. helioscopia, E. nerifolia, E. broteri, E. lacteal, E. antiquorum* (Compounds 30–35, 46–53, 55–57, 62–68) (**Figures 2**, **3**), *E. resinifera, E. dendroides, E. acrurensis* (Compounds 70–74, 76, 78, 81, 84–94) (**Figure 4**), and (Compounds 95-98; 108-109) (**Figure 5**), *E. nicaeensis* (Compounds 110–124) (**Figure 6**), *E. hermentiana, E. Drupifera, E. polygonifolia*. Their resources from different *Euphorbia* species are shown in **Table 1**.

Giner et al. identified six triterpene alcohols from *E. peplus* latex **(1–6)** (Giner et al., 2000). Three new ingol diterpenes **(7–9)** and a novel spirotriterpene **(10)** were isolated from the dried latex of *E. officinarum* collected from Morocco. Theirs structures were elucidated by means of mass spectrometry, extensive 1D and 2D NMR (COSY, HMQC, HMBC, and NOESY), and X-ray analysis (Daoubi et al., 2007).

Other compounds have also been confirmed from the latex of *E. officinarum*, including **(11)** and **(12)**. These were

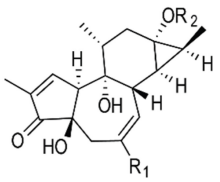

30 R_1= CH_2OH, R_2= $CO(CH_2)_{12}CH_3$

31 R_1= CH_2OH, R2= $CO(CH_2)_5CH{=}CH(CH_2)_7CH_3$

32 R_1= CH_2OH, R_2= $CO(CH_2)_7CH{=}CHCH_2CH{=}CH(CH_2)_4CH_3$

33 R_1= CH_2OH, R_2=$CO(CH_2)_{14}CH_3$

34 R_1=CH_2OH, R_2=$CO(CH_2)_4CH{=}CH(CH_2)_{10}CH_3$

35 R_1=CHO, R_2=$CO(CH_2)_{14}CH_3$

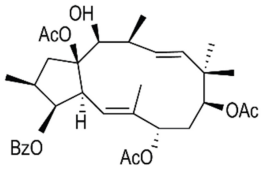

46

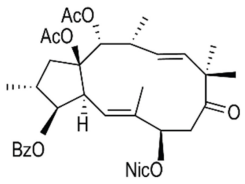

47

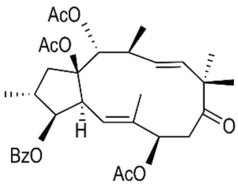

48

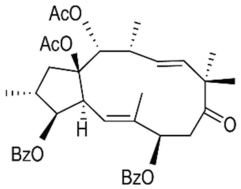

49

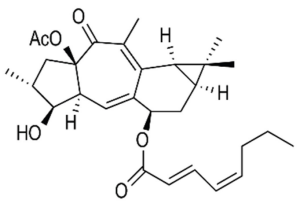

50

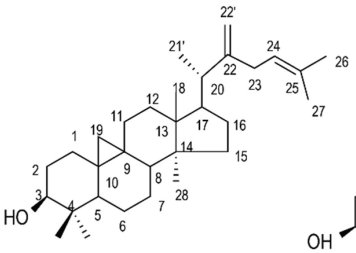

51

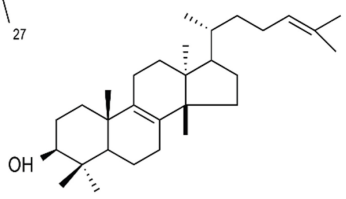

52

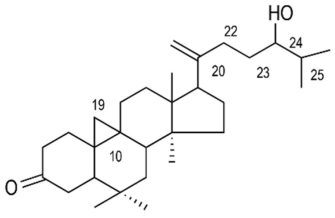

53

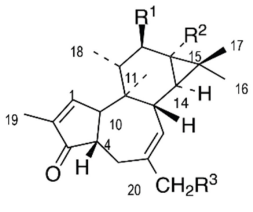

R_1	R_2	R_3
$OCO-(CH{=}CH)_2-(CH_2)_2-Me$	OAc	OAc

55

FIGURE 2
Structure of chemicals compounds **(30-35, 46-53)** and **(55)** (Urones et al., 1988; Ilyas et al., 1998; Mallavadhani et al., 2004; Hua et al., 2015; Deng et al., 2021).

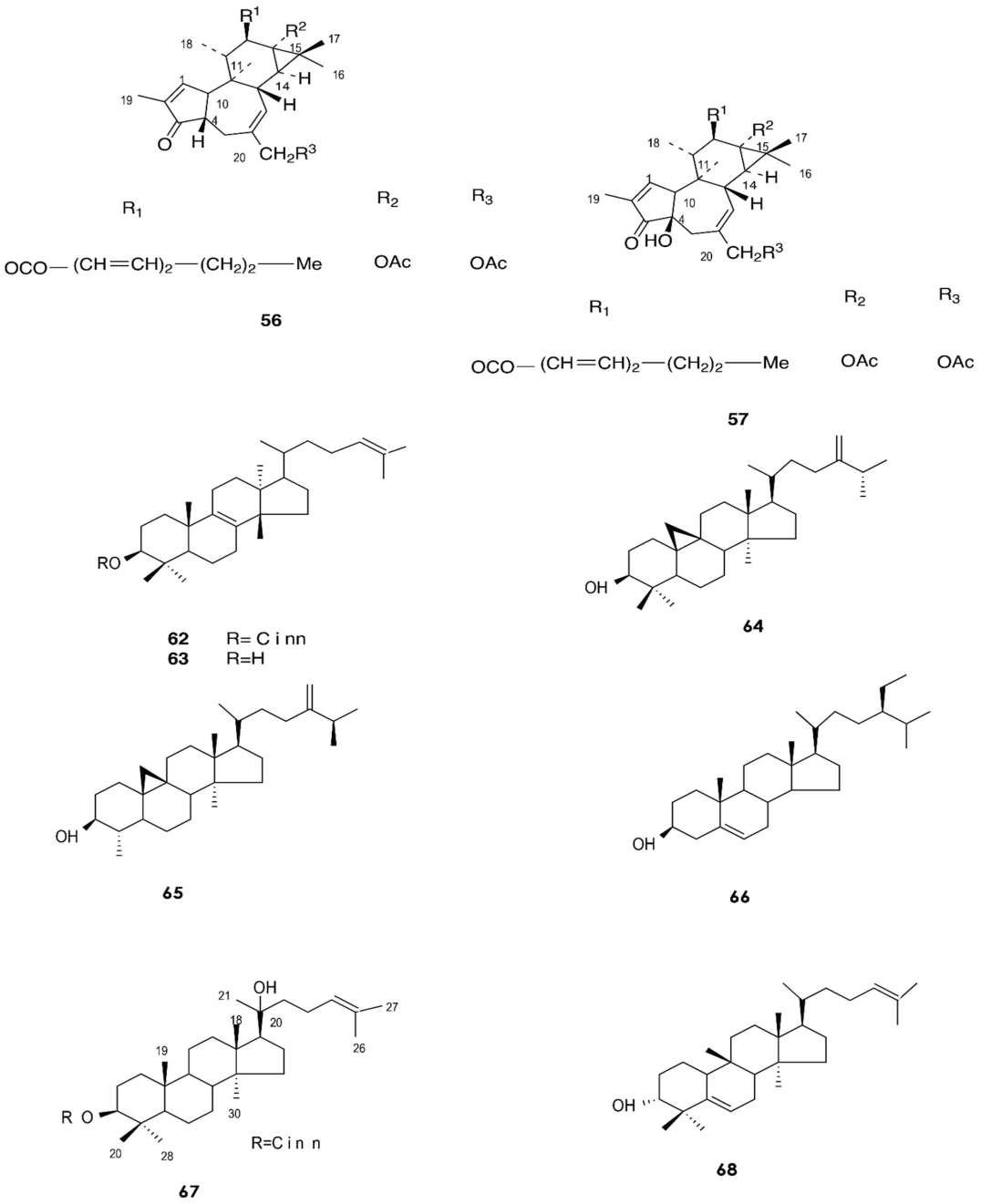

FIGURE 3
Structure of chemicals compounds **(56-57, 62-68)** (Urones et al., 1988; Gewali et al., 1990).

identified on the basis of spectroscopic data (NMR), which showed a singlet at δ 2.15 ppm assigned to the methyl of the carbonyl group at C-20 for compound **(12)** and a doublet of doublet at δ 3.41 due to the resonance of H-3 for product **(13)** (Smaili et al., 2017). Furthermore, twelve new compounds **(13–25)** were isolated from *E. obtusifolia* latex (Marco et al., 1999). Phytochemical characterization of Brazilian *E. tirucalli* latex resulted in the isolation of triterpenes such as **(26)** and **(27)** using Fourier transform-ion cyclotron resonance mass spectrometry (FT-ICR MS) and Atmospheric Pressure Chemical Ionization APCI (+) FT-ICR MS. In addition, two diterpene esters **(28, 29)** were isolated by electrospray ionization Fourier transform ion cyclotron mass spectrometry ESI (-) FT-ICR MS and ESI (-) FT-ICR MS/MS (de Souza et al., 2019).

The fresh latex collected from the roots of *E. fischeriana* has been analyzed using spectroscopic methods, HPLC, and GC-MS

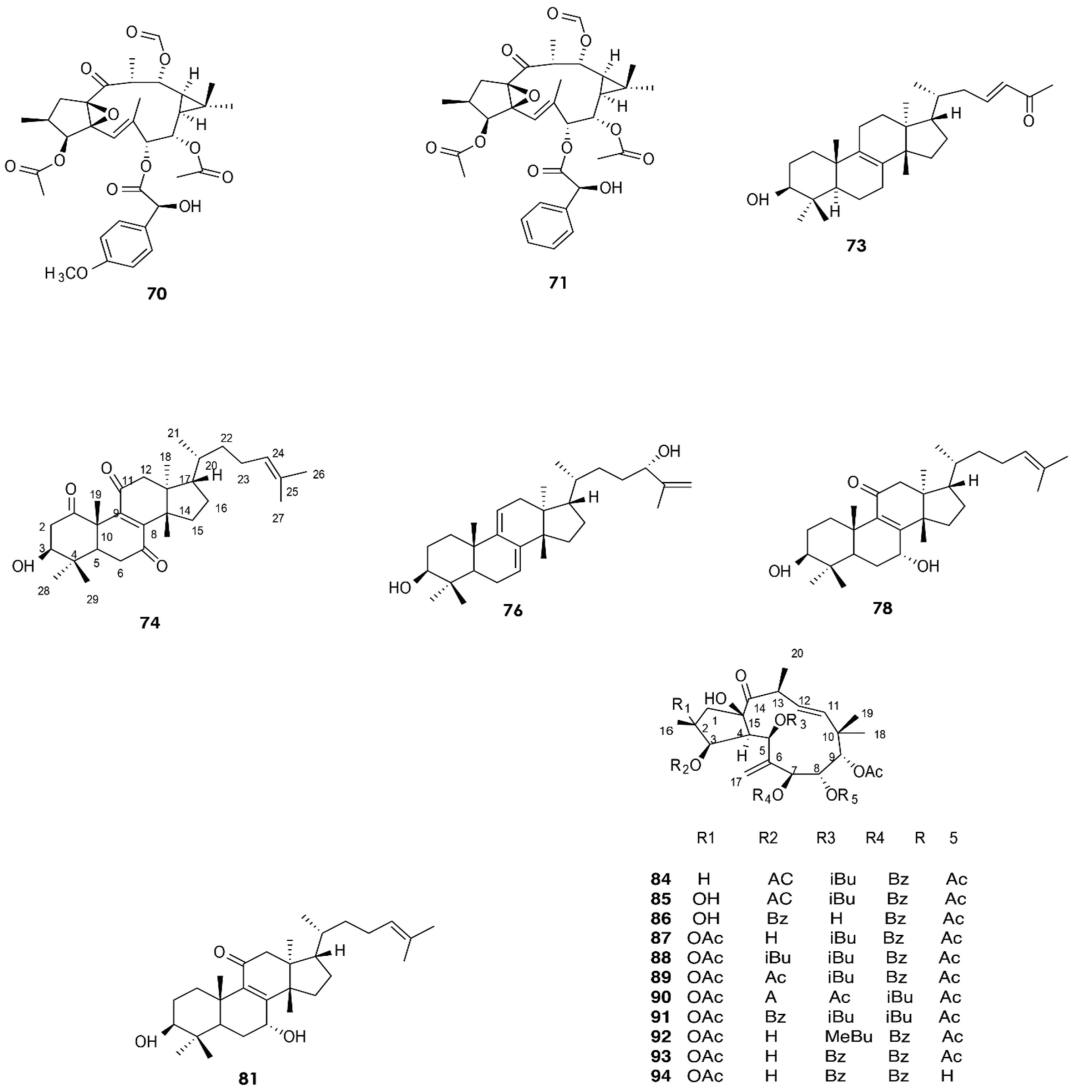

FIGURE 4
Structure of chemicals compounds **(70-74; 76; 78; 81) and (84-94)** (Esposito et al., 2016; Li et al., 2022).

analyses. The diterpenoids profile contained six aliphatic tigliane diterpenoids **(30-35)** that were identified as major compounds.

Quantitative analyses by High-Performance Liquid Chromatography with Diode-Array Detection (HPLC-DAD) revealed that compounds **(30)** and **(33)** were also present in the roots, stems, and leaves of *E. fischeriana* at varying proportions. On the other hand, **(30)** and **(33)** were mainly accumulated in the latex, with a value of greater than 232.31 ± 35.96 μg/g and 4,319.07 ± 143.26l μg/g, respectively (**Figure 7**). These two diterpenoids exhibited a marked antifeedant activity against *Helicoverpa armigera*, with EC50 values of 2.59 and 15.32 μg/cm^2, respectively (Deng et al., 2021).

Analysis by UPLC-ESI-MS/MS of latex methanolic extract samples from ***E. bicolor*** collected in Denton County, TX, USA identified two diterpenes **(36)** and **(37)** (Basu et al., 2019) responsible for the anti-inflammatory (Fernandez et al., 2001) and analgesic activity, respectively.

Compounds **(38)** to **(43)** were isolated from the hexane fraction of the latex from *E. umbellata*. On the other hand, the diterpenes **(44)** and **(45)**, which were isolated from dichloromethane and ethanol fractions, are characterized by a tigliane nucleus (Cruz et al., 2020). In 2015, a new jatrophane diterpenoid, **(48)**, and four known macrocyclic diterpenoids, **(46), (47), (49)**, and **(50)**, were isolated from the stem latex of *E. helioscopia* using reversed-phase HPLC equipped with a diode array detector and recorded at 238 nm. It was observed that **(50)** moderately inhibits the release of the cytokines TNF-α (IC_{50} = 23.7 ± 1.7 μM) and IL-6 (IC_{50} = 46.1 ± 1.1 μM) and the chemokine MCP-1 (IC_{50} = 33.7 ± 3.8 μM) by lipopolysaccharide (LPS)-induced

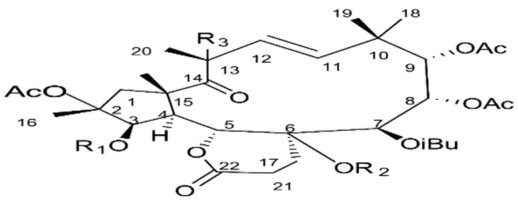

	R1	R2	R3	R4
95	Ac	Ac	OH	H
96	Ac	Ac	OH	Ac
97	Ac	iBu	H	H
98	H	Ac	H	Ac

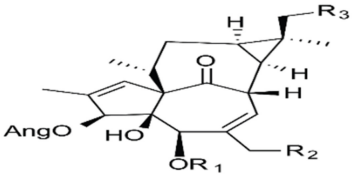

108 R_1=Ac R_2=OAc R_3= H
109 R_1=R_2=H R_3= OAc

FIGURE 5
Structure of chemicals compounds (**95-98**) and (**108-109**) (Marco et al., 1999; Esposito et al., 2016).

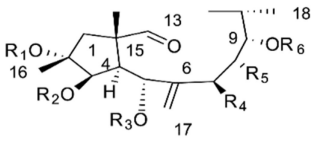

110

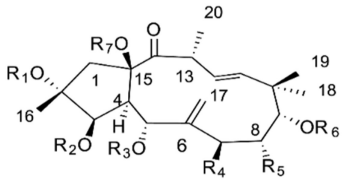

111-114

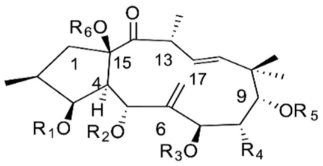

115-121

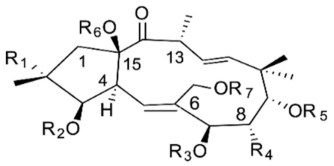

122-124

	R1	R2	R3	R4	R5	R6	R7
110	H	Ac	Ac	H	H	Nic	Ac
111	Ac	Pr	Ac	OiBu	OAc	Nic	H
112	Nic	iBu	Ac	OiBu	OAc	Ac	H
113	Nic	Pr	Ac	OiBu	OAc	Ac	H
114	Ac	iBu	Ac	OiBu	OAc	Nic	-
115	Pr	Ac	Ac	H	Nic	Ac	-
116	Ac	Ac	iBu	OAc	Nic	Ac	-
117	Pr	Ac	iBu	ONiC	Ac	H	-
118	Pr	Ac	iBu	OAc	Nic	H	-
119	iBu	Ac	iBu	OAc	Nic	H	-
120	Pr	Ac	iBu	OAc	Nic	Ac	-
121	Ac	Ac	iBu	OAc	Nic	H	-
122	OAc	Ac	iBu	Ac	Nic	Ac	Ac
123	OAc	Pr	iBu	Ac	Nic	Ac	
124	OAc	Ac	iBu	Ac	Bz	Ac	Ac

FIGURE 6
Structure of chemicals compounds (**110-124**) (Krstić et al., 2018).

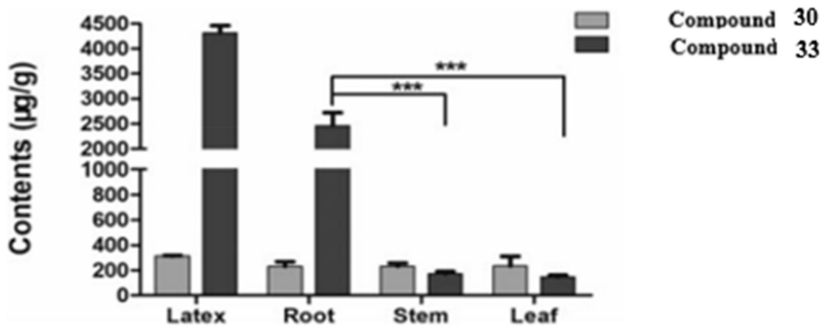

FIGURE 7
Content of compounds **30** and **33** in the different parts of *E. fischeriana* (***$p < 0.001$, student's test) (Deng et al., 2021).

RAW 264.7 macrophages (Hua et al., 2015). Compounds **(51)** and **(52)** have been reported in *E. neriifolia* (Mallavadhani et al., 2004); compounds **(53)** and **(54)** were isolated from the same species and their structures were identified using chemical and physical data (1H NMR, 13C NMR, IR, and mass spectra) (Ilyas et al., 1998).

Several studies have reported that many terpenoids from the latex of *Euphorbia* species possess biological activities. Compound (61) constitutes 0.3% of the latex obtained by incision from the leaves of *E. lacteal*. It was identified by comparing the spectroscopic data (NMR and CG-MS) from the n-hexane/ethyl ether fraction and has been suggested to exhibit an anti-inflammatory activity, as it suppresses ear edema in a mouse model and inhibits nitrite production at a concentration of 100 mM in lipopolysaccharide-stimulated mouse macrophages (Fernandez et al., 2001).

Gewali et al. reported the isolation of compounds **(62–69)** in *E. antiquorum* latex (Gewali et al., 1990).

In 2019, the two diterpenes **(70)** and **(71)** were isolated from a methanol extract of the latex of *E. resinifera Berg,* and their structures were elucidated by HR-ESI-MS, IR, UV, 1D, and 2D NMR (Wang et al., 2019). Moreover, diterpenoid **(83)** was isolated by Fattorusso et al. (2002). Twelve compounds **(70–82)** have been identified from *E. resinifera*. Two triterpenoids were isolated by Qi et al., compound **(72)**, which was reported for the first time and was shown to contain a tetrahydrofuran ring, and **(73)** (Qi et al., 2019). Furthermore, five triterpenoids **(74–78)** were discovered by Li et al. (2022), and **(79–82)** were isolated in 2021 (Li et al., 2021).

The latex of *E. dendroides* was studied for its chemical composition and anti- Chikungunya virus (CHIKV) activities. The results showed the presence of six new jatrophane esters, **(86), (88), (89), (91), (93)**, and **(94)**, and nine known compounds, **(84)**, **(85)**, **(87)**, **(92)**, **(90)**, **(95)**, **(96)**, **(97)**, and **(98)**.

In an evaluation of 15 compounds, **(90)** and **(97)** showed anti-CHIKV activity with EC50 values of 5.5 ± 1.7 and 15.0 ± 3.8 μM, respectively (Esposito et al., 2016).

Marco et al. reported in 1998 nine ingol esters **(99–107)** bearing various types of acyl groups, acetyl and tigloyl moieties, and two known ingenol esters as minor compounds in the latex of *E. acrurensis*. The structure of compounds **(99) and (104)** is characterized by the presence of two tiglate esters in C-7 and C-8. Compound **(105)** is characterized by the presence of tiglate at C-7. In contrast, compound **(103)** has an angelate residue (Marco et al., 1999).

In recent years, fifteen diterpenoids **(110–124)** were extracted from the latex of *E. nicaeensis* samples collected in Serbia (Krstić et al., 2018). Meanwhile, three tetracyclic triterpenes **(125–127)** were isolated in 2019 (Krstić et al., 2019).

Four new ingol esters **(128–131)** and compounds **(132–143)** were isolated from *E. hermentiana* latex (Lin and Kinghorn, 1983). Compounds **(144)** and **(145)** were obtained from methylated spirit extract of the *E. drupifera* latex by Famuyiwa et al., and their structures were determined by 1D-NMR and MS (Famuyiwa et al., 2014). In 2015, 16 triterpene alcohols **(146–161)** were identified by Giner et al. from *E. polygonifolia* latex (Giner and Schroeder, 2015).

Enzymes

Screening of *Euphorbia* latex has revealed the presence of many enzymes, including proteolytic enzymes that may be involved in plant defense against certain pathogens and external environmental conditions (Domsalla et al., 2010; Fais et al., 2021). The catalytic properties of lipases contained in the latex of *E. unispina* have been described by Mazou et al. (2017). The optimum temperature and pH for the hydrolytic activity of the lipases were 50°C and 5, respectively. The lipase was able to catalyze the hydrolysis of different purified Tunisian *E. peplus* triacylglycerols such as tripalmitin, trimyristin, trilaurin, tristearin, triolein, and trilinolein. In the same way, Lazreg Aref et al. studied the lipolytic activity of the latex lipase. The optimum lipase activity was obtained at 40°C and pH 8, with a molecular weight of about 40 kDa,

which was determined using electrophoresis on dodecyl gel sodium sulfate (electrophoresis on gel (SDS-PAGE) (**Figure 8**). Tributyrin (TC4) and olive oil were used as substrates to determine the specific activity of the lipase, which was found to be 249 ± 12.45 and 161.4 ± 8.07 U/mg for TC4 and olive oil, respectively. However, the lipase activity was inhibited by sodium dodecyl sulfate (Lazreg Aref et al., 2014). Moreover, the biological properties of the proteases have been reported. A serine protease with a molecular weight of 61 KDa designated as EuRP-61 was well purified from *E. resinifera* latex and characterized. The enzyme was found to have a wide pH stability range of 1–14 and a denaturation tolerance of up to 65–66°C. The fibrinogenolytic activity of EuRP-61 was investigated, and the optimal degradation of fibrinogen was found to have a Michaelis constant (Km) of 4.95 ± 0.1 μM, a maximum velocity (Vmax) of 578.1 ± 11.81 ng min^{-1}, and a catalytic efficiency (Vmax/Km) of 116.8 ± 1 ng μM^{-1} min^{-1} (Siritapetawee et al., 2020b). Siritapetawee et al. also studied the anticoagulant and antithrombotic activities of EuRP-61, and reported that this enzyme can hydrolyze human fibrin and inhibit platelet aggregation via the ADP receptor pathway (Siritapetawee et al., 2020a). Proteases such as euphorbain 1, eumiliin, mauritanicain, EuP-82, miliin, and euphorbams y-l, –2, and –3 have been purified and characterized from *E. lathyris, E. milii var.* hislopii, *E. mauritanica* L, *E. cf. lacteal, E. milii*, and *E. cyparissias*, respectively. The proteolytic activity of euphorbain1 is inhibited by diisopropyl fluorophosphates, the fibrinogenolytic activity of eumiliin is inhibited by β-mercaptoethanol and leupeptin. The mauritanicain is reduced in its proteolytic activity by aprotinin and AEBSF-HCl [4-(2-Aminoethyl)benzenesulfonylfluoride] and EuP-82 is inhibited by serine protease specific inhibitor phenylmethylsulfonyl fluoride (PMSF) (Lynn and Clevette-Radford, 1983, 1985; Fonseca et al., 2010; Moro et al., 2013; Siritapetawee et al., 2015; Flemmig et al., 2017). Furthermore, a protease has been isolated from *E. amygdaloides* latex using collapse of $(NH4)_2SO_4$ fractionation and ion-exchange chromatography. Maximum protease activity was observed at 60°C and pH 5 (Demir et al., 2005). Badgujar et al. found a clotting cysteine protease called Nivulia-II, which they purified from *E. nivulia Buch.-Ham* latex with DFPPNTCCCICC as the N-terminal amino acid sequence; the enzyme is characterized by a molecular weight of 43,670.846 Da and has an optimal activity at pH 6.3 and 50°C, which can be inhibited by common thiol blocking reagents (Badgujar and Mahajan, 2014).

Four enzymes have been purified from *E. characias* latex, an amine oxidase, a nucleotide pyrophosphatase/phosphodiesterase, a peroxidase, and a purple acid phosphatase, with molecular masses of 74, 5, 47, and 30 ± 10 kDa, respectively (Padiglia et al., 1998; Mura et al., 2008; Medda et al., 2011; Pintus et al., 2011). The serine protease purified from *E. hirta* has fibrinolytic, esterase, amidase, azocaseinolytic, fibrinogenolytic, and gelatinolytic activities. Enzyme activity was found to be inhibited by PMSF and AEBSF, and the N-terminal sequence was determined to be YAVYIGLILETAA/NNE (Patel et al., 2012). In addition, a class III endochitinase with important roles in cellular defense has been isolated from the latex of *E. characias*. This enzyme shows strong activity at 50°C and pH 5.0, and its chitinase activity can be enhanced by calcium and magnesium ions. Moreover, the enzyme was found to hydrolyze colloidal chitin, yielding N-acetyl-d glucosamine, chitobiose, and ketotriose as products (Spano et al., 2015).

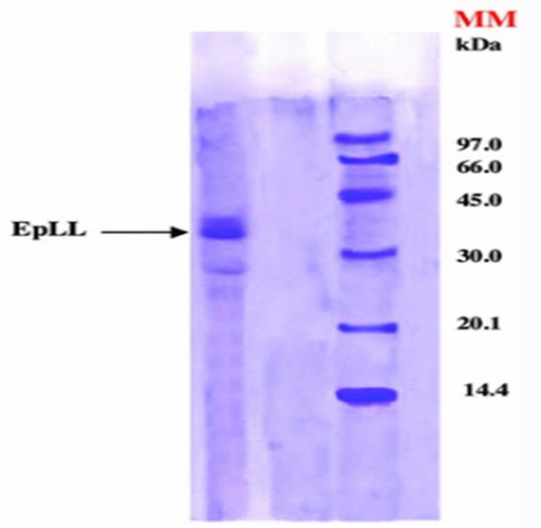

FIGURE 8
The molecular weight of the lipase from *E. peplus* latex (EPLL) obtained by Sodium dodecyl sulfate–polyacrylamide gel electrophoresis (SDS-PAGE) (Lazreg Aref et al., 2014).

Natural rubber

Natural rubber (NR) is an important polymer found in about 2,000 plant species (Arreguín, 1958). To date, *Hevea brasiliensis* is considered the most important rubber-producing plant (Laibach et al., 2015). NR from *E. characias* latex has been extracted using different solvents such as acetone, acetic acid, trichloroacetic acid, and Triton X-100, followed by successive treatments with cyclohexane/ethanol and characterized. Acetic acid has proven to be the most suitable solvent for rubber extraction, with yields of 14.3%. ^{1} H NMR, and ^{13}C NMR analysis showed that the NR has a molecular weight of 93,000 Da and contains cis-1,4-polyisoprene as shown in **Figures 9**, **10** (Spanò et al., 2012). FT-IR, NMR, and GPC analyses also revealed that the NR from *E. macroclada* latex contains cis-1,4-polyisoprene, with a molecular weight of 8.180E+2 with polydispersity of 1.287 as shown in **Figure 11** (Khan and Akhtar, 2003; Azadi et al., 2020) separated and characterized rubber hydrocarbon from *E. caducifolia* by different chemical

methods. The analysis revealed a molecular weight of 15,275–88,405 (M), iodine value of hydrocarbon of 310.91–350.80%, percentage of unsaturation of 83.40–94.10%, a refractive index of 1.49200–1.49325, and a specific gravity of 0.93102– 0.93628, and identified cis-1,4-polyisoprene (Khan and Akhtar, 2003).

Biological activities of *Euphorbia* latex

Several researchers have studied the biological activity of spurge latex extracts and their chemical constituents, both in vitro and in vivo. *Euphorbia* latex has antibacterial, antioxidant, anti-inflammatory, anti-angiogenic, wound healing, cytotoxic, hemostatic, genotoxic/mutagenic, and insecticidal activities. **Supplementary Table 1** summarizes the results of various investigations concerning the biological activities of latex from some species of the genus *Euphorbia*.

Antimicrobial activity

Several studies have explored the antibacterial activity of the latex from *Euphorbia* species (**Supplementary Table 1**). Most species in this genus exhibit moderate to strong antibacterial characteristics.

The agar well diffusion, disk diffusion, and broth microdilution methods have been applied in vitro to test the antimicrobial activity of fresh, diluted latex and some fractions isolated from latex by calculating the inhibition zone diameter and minimum inhibitory concentration (MIC). In addition, different solvents have been used to test the antimicrobial activity of latex or extracts against the Gram-positive bacteria *Bacillus pumilus*, *Staphylococcus aureus*, *Streptococcus pneumoniae*, *Bacillus subtilis*, and *Micrococcus luteus*, the Gram-negative bacteria *Escherichia coli*, *Citrobacter freundii*, *Klebsiella pneumoniae*, *Shigella flexneri, Proteus vulgaris, Pseudomonas aeruginosa, Salmonella typhi, Agrobacterium tumefaciens, Erwinia amylovora, P. syringae* pv. *tabaci*, and *Pseudomonas syringae* pv. *syringae*, and the fungal pathogens *Verticillium dahlia*, *Fusarium oxysporum* f. sp. *melonis*, and *Penicillium expansum*. In general, the fresh latex of *E. hirta* shows a promising activity against *B. pumilus* (24.98 mm), *S. aureus* (25.38 mm), *S. pneumoniae* (23.72 mm), *E. coli* (27.93 mm), *C. freundii* (23.54 mm), and *K. pneumoniae* (21.93 mm). Most of these recorded zones of inhibition are larger than those of the positive controls (vancomycin (22.29 mm), ceftriaxone (22.50 mm), ceftriaxone (22.50 mm), ciprofloxacin (22.36 mm), and levofloxacin (21.70 mm)(Hussain et al., 2014). The methanolic extract of latex from *E. antiquorum* displays moderate inhibitory effects against *E. coli* and *S. flexneri*, with inhibition zones of 5 and 4 mm respectively,

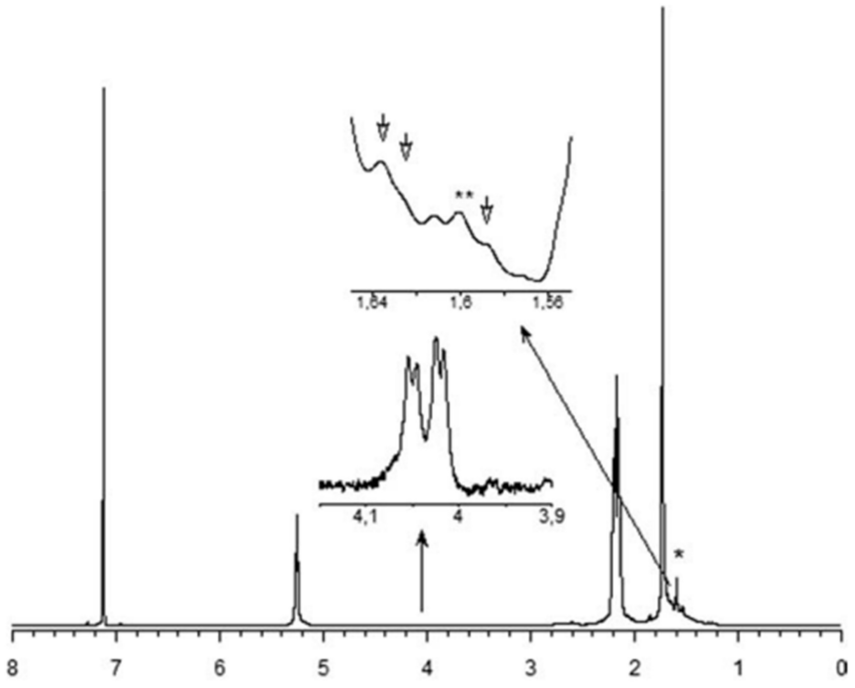

FIGURE 9
The ^{1}H NMR spectrum of rubber extracted from *E. characias* latex. Peaks at 5.31, 2.17, and 1.73 ppm are attributed to the olefinic, methylene and methyl protons, respectively, of the cis-1,4-polyisoprene (Spanò et al., 2012). * and ** indicates 1 H NMR residual signal of cyclohexane (1.43 ppm) and methyl-protons of a trans-isoprene unit (1.62 ppm), respectively.

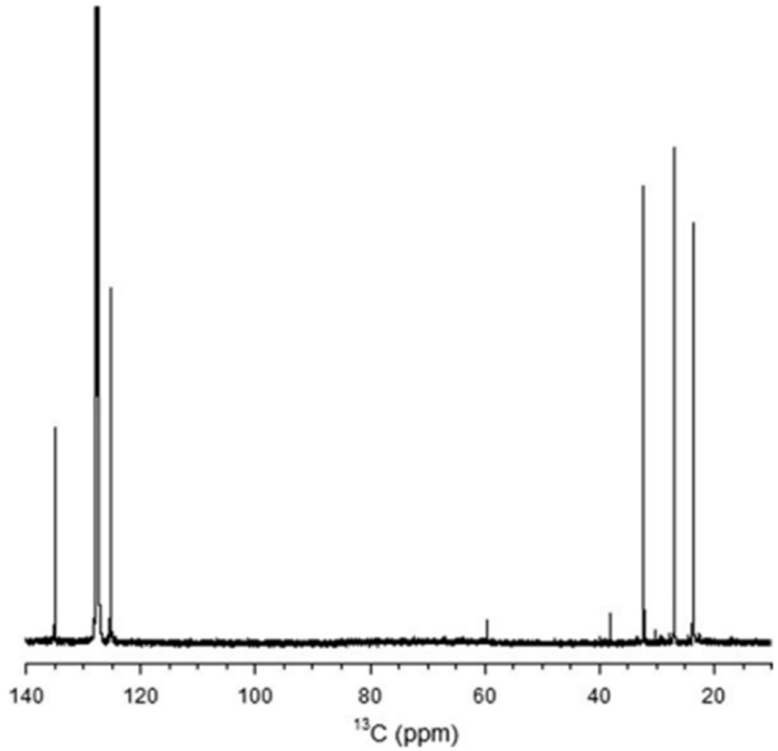

FIGURE 10
The ^{13}C NMR spectrum of rubber extracted from *E. characias* latex. The peaks at 135.2,125, 32.2, 26.4, and 23.4 arises from the two ethylenic, two methylenic, and the methyl carbon atoms of the cis-1,4-polyisoprene, respectively (Spanò et al., 2012).

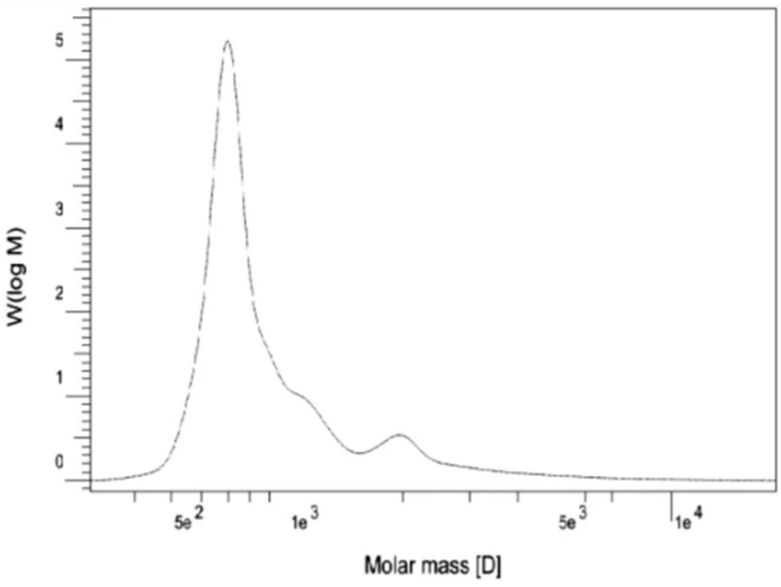

FIGURE 11
Molecular weight distribution of *E. macroclada* extracted rubber by GPC.

but not against *K. pneumonia*, *S. aureus*, or *B. subtilis*. Using the agar plug method, researchers have shown that the methanolic extract of latex from *E. antiquorum* reduces the growth of *A. fumigatus*, *C. albicans*, and *A. flavus*, with inhibition zones of 12, 10, and 5–6 mm, respectively (Sumathi et al., 2011). ML et al. examined the antimicrobial activity of different

solvent extracts (acetone, chloroform, and diethyl ether) of *E. heterophylla* latex. The acetone extract demonstrated a high zone of inhibition against most microbes, including *S. aureus*, *P. aeruginosa*, *B. subtilis*, *A. niger*, and *F. oxysporum*. The diethyl ether latex extract was more effective at inhibiting *P. vulgaris* and *Penicillium sp*.

In addition, the antimicrobial activity of the triterpene derivatives, 3β-acetoxy-norlup-20-one and 3-chloro-4α,14α-dimethyl-5α-cholest-8-ene, isolated from *E. officinarum* latex, has been determined. When used at concentrations of 100 and 200 μg/ml, they were shown to reduce conidia formation in six strains of *V. dahliae* (from 39 to 69%) as well as in *P. expansum* and *F. oxysporum* f. sp. *melonis* (from 70 to 96%). Moreover, they were also shown to inhibit the germination of all strains at concentrations of 2, 10, 100, and 200 μg/ml (ML et al., 2020).

The antibacterial activity of 3-chloro-4α, 14α-dimethyl-5α-cholest-8-ene has been demonstrated against *P. syringae* pv. *tabaci*, which causes tobacco wildfire disease, with an inhibition diameter of about 16 mm (Smaili et al., 2017). There are also reports of the antimicrobial activity of compounds other than triterpenes. For example, methyl palmitate, 5,9-hepta decadienoate, methyl 11 octadecenoate, methyl octadecenoate, and 3,7,11,15-tetramethyl-2-hexadecen-l-ol were isolated from *E. caducifolia*, and their antimicrobial activity was determined for a broad range of Gram-positive bacteria such as *S. aureus* (MIC = 262 μg/ml), *M. luteus* (MIC = 212 μg/ml), and *B. subtilis* (MIC = 187 μg/ml), Gram-negative bacteria such as *E. coli* (MIC = 225 μg/ml) and *S. typhi* (MIC = 275 μg/ml), and fungi such as *A. niger* (MIC = 150 μg/ml) and *C. albicans* (MIC = 175 μg/ml) (Goyal et al., 1970).

Antioxidant activities and free radical scavenger activity

Numerous studies have reported the antioxidant effects of *Euphorbia* latex. Phenolic compounds and secondary metabolites are generally responsible for the antioxidant properties (Koh et al., 2002). The antioxidant action of latex from *E. dendroides L.* collected in Texas, USA was studied using different in vitro assays such as 2,2-diphenyl-2-picrylhydrazyl (DPPH), Trolox equivalent antioxidant capacity (TEAC), and Ferric reducing antioxidant power (FRAP) and a concentration range of 0.625–10 μg/mL. The DPPH, FRAP, and TEAC IC_{50} antioxidant activities were 2,927.01 ± 98.03, 4,383.13 ± 95.30, and 7,580.95 ± 97.65 μmols of trolox equivalents (TE)/100 g fresh weight of sample, respectively. This antioxidant power can be attributed to the polyphenols, specifically phenolic acids, and terpenoids contained in the latex of *E. dendroids* (Smeriglio et al., 2019). Abdel-Aty et al. have reported that the antioxidant properties of *E. tirucalli* latex extracts can be attributed to phenolic and flavonoid compounds. They found that the amounts of flavonoids and phenols found in the

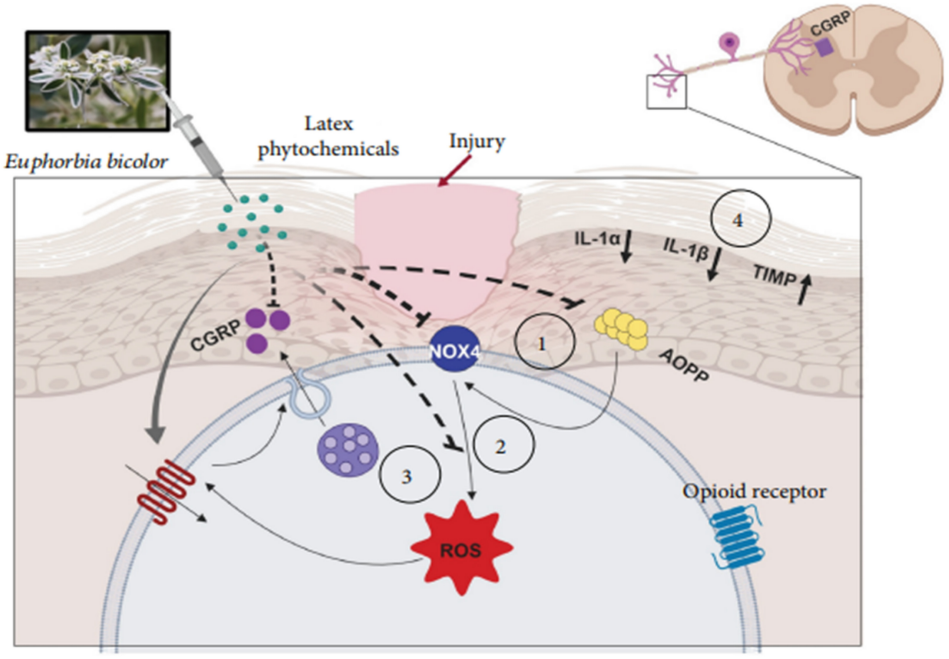

FIGURE 12
Proposed model of the mechanisms involved in *E. bicolor* latex extract-evoked peripheral, nonopioid analgesia (Basu et al., 2019).

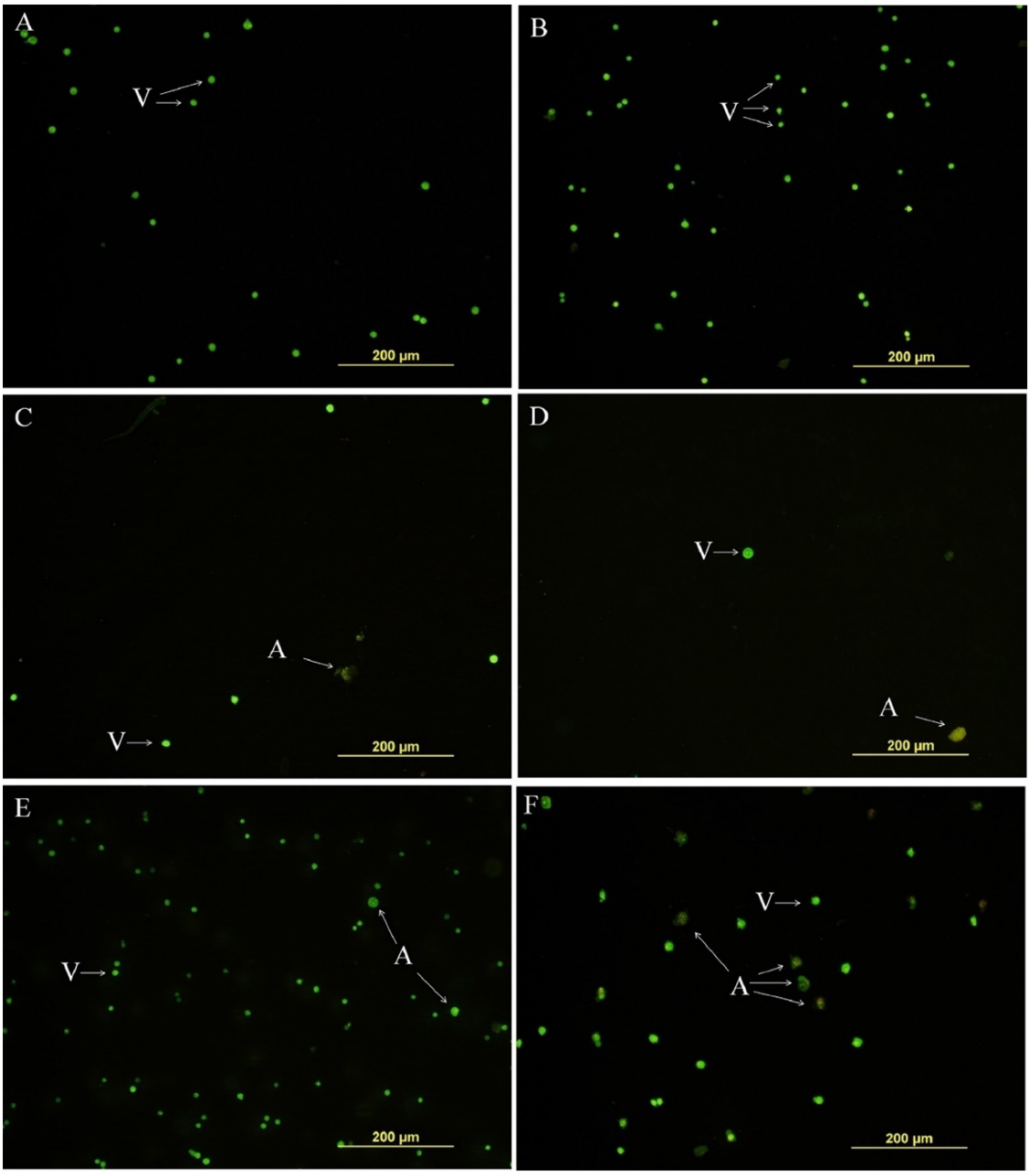

FIGURE 13
Euphol isolated from the latex of *E. tirucalli* inhibited total number of tumor cell K-562 cells after treatment (12 h). **(A)** Control cells incubated with RPMI only; **(B)** control cells incubated with DMSO (0.4%); **(C)** euphol treatment (23.4 µM); **(D)** euphol treatment (46.9 µM); **(E)** imatinib (0.5 µM); and **(F)** doxorubicin (0.085 µM). v, viable cells; a, apoptotic cells (Cruz et al., 2018).

E. tirucalli latex extracts are about 4.3 and 10.5 mg EC/g latex, respectively. These were able to scavenge free radicals from DPPH and ABTS, with IC_{50} of 6.0 and 2.0 µg GAE/ml, respectively. In addition, the phosphomolybdate assay revealed that the latex also has a high reduction capacity, with an EC_{50} value of 6.5 µg/m (Abdel-Aty et al., 2019). The latex extract of *E. bicolor* samples collected in Texas, USA showed a dose-dependent ABTS radical of 80%, a DPPH scavenging effect of 8%, and a H_2O_2 radical of 30% at the concentration of 20–100 µg/mL. Moreover, the 2,2'-azino-bis(3-ethylbenzothiazoline-6-sulphonic acid) (ABTS) radical scavenging activity of the latex extract from *E. bicolor* is strongly correlated with the concentration of flavonoids and proanthocyanidins. The DPPH and NO radical scavenging activities of the extract show strong

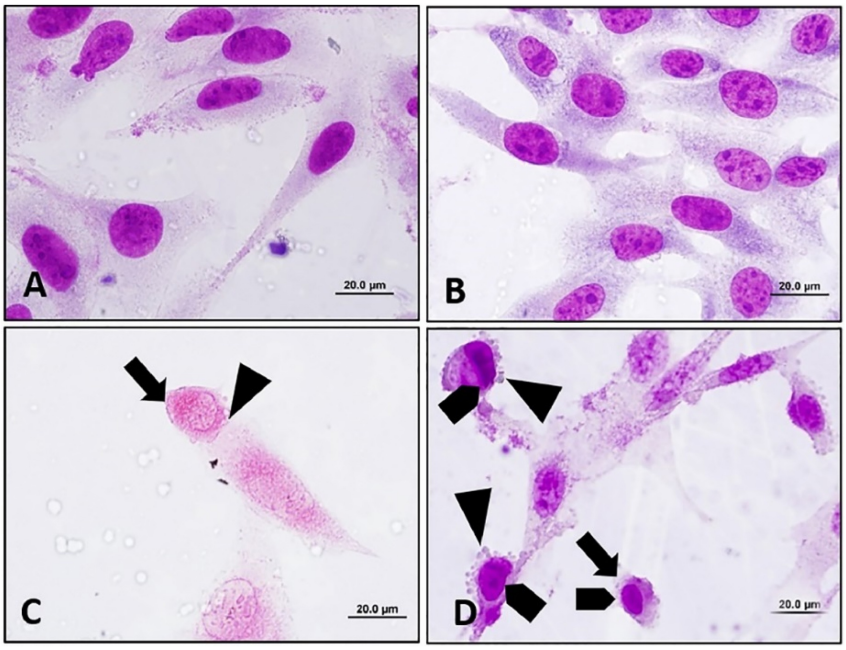

FIGURE 14
Apoptosis inducing effect of euphol extracted from *E. tirucalli* was to B16F10 cells after 24 h of treatment with different concentrations of euphol. **(A)** Control cells incubated with RPMI; **(B)** control cells incubated with DMSO (0.4%); **(C,D)** B16F10 cells treated with 70.3 and 35.2 µM of euphol. Cell rounding:, bleb formation:, chromatin condensation:. Magnification = 1,000×, bar = 20 µm (Cruz et al., 2018).

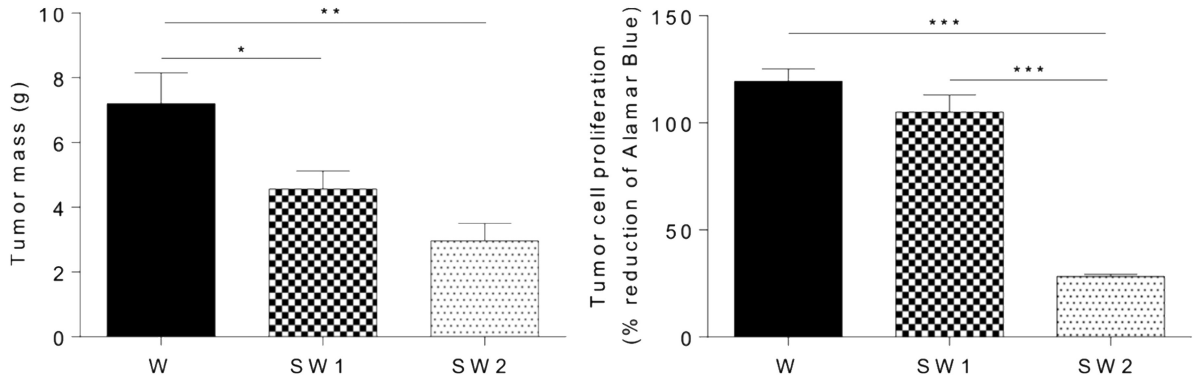

FIGURE 15
Effect of latex treatment on tumor mass and tumor cell proliferation in untreated animals with tumor (W), animals with tumor treated with 25 µL/mL aqueous solution of latex (SW1), and animals with tumor treated with 50 µL/mL aqueous solution of latex at (SW2). Data are presented as the mean + SEM. W, $n = 11$; SW1, $n = 12$; SW2, $n = 14$. *$p < 0.05$, **$p < 0.001$, and ***$p < 0.0001$ (one-way ANOVA followed by a post-hoc Tukey test) (Martins et al., 2020).

correlation with phenolic compounds and terpenoids contents. On the other hand, the H_2O_2 radical scavenging activity shows weak correlations with polyphenols contents (Basu et al., 2019).

Insecticidal activity

The use of drugs to control parasites poses many challenges, such as the resistance to insecticides developed by the parasites and the environmental damage caused by the drugs (O'Brien, 1999; Daborn and Le Goff, 2004). The insecticidal activity of *E. bupleuroides* latex samples from the east of Algeria has been evaluated against German cockroach (*Blattella germanica*)**.** The insecticidal activity against adults and larvae was dependent on the concentration and time of exposure and found to be particularly effective against males and caterpillars (Azoui et al., 2016). The insecticidal activity of xylene-latex extracts from *E. antiquorum* collected in dry, intermediate, and wet

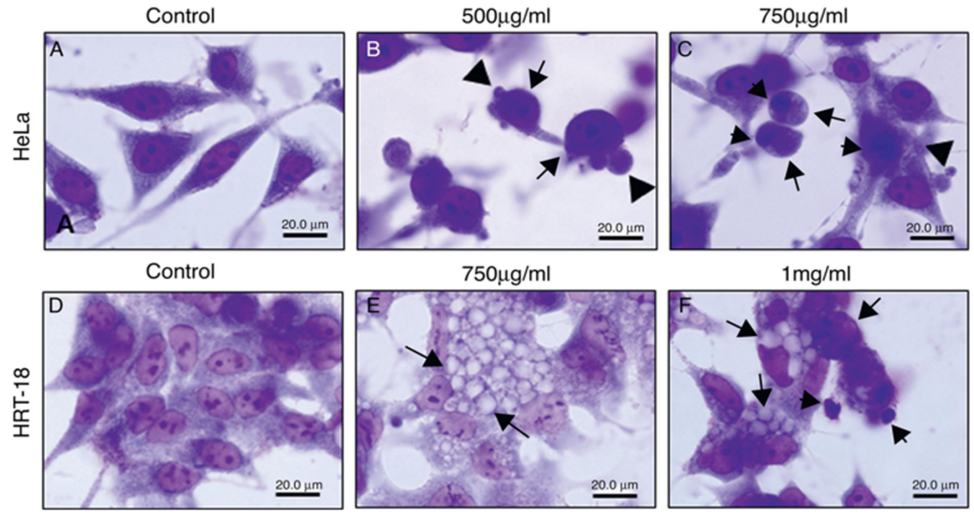

FIGURE 16
Morphological changes of HeLa and HRT-18 cells under treatment with latex of *E. umbellata* (Pax) Bruyn **(A,D)** controls; cells incubated with RPMI only. **(B)** HeLa cells incubated with 500 and **(C)** 750 µg/ml of latex. **(E)** HRT cells incubated with 750 µg/ml and **(F)** 1,000 µg/ml of latex **(**Luz et al., 2015**)**.

zones of Sri Lanka has been studied against six species of insect pests: *Myzus persicae*, *Aphis gossypii*, *Aphis craccivora*, *brown planthopper* (*Nilaparvata lugens*), *paddybug (Leptocorisa oratorius*), and *blackbug (Scotinophara lurida*) (De Silva et al., 2008). The activity against two species of predatory ladybird beetles, *Harmonia octomaculata* and *Menochilus sexmaculatus* (*Cheilomenes sexmaculatus*), and the predatory spider *Lycosa pseudoannulata*, was determined using the Potters' sprayer method. The three aphid species, *A. craccivora*, *A. gossypii*, and *M. persicae*, showed a high level of mortality toward the xylene-latex extract. On the other hand, *H. octomaculata* and *M. sexmaculatus* did not show any mortality for the xylene extract.

Anti-inflammatory activity

The latex of the *Euphorbia* genus also has anti-inflammatory effects. The anti-inflammatory effect of a hydrosoluble fraction of *E. royleana* latex was investigated using different acute and chronic test models in rats and mice, with acetylsalicylic acid (ASA) as a positive control. The latex showed a significant dose-dependent anti-inflammatory activity, as evidenced by the reduction in the volume of exudate that resulted from the migration of leukocytes, and showed a weak inhibitory effect on the formation of granulomas induced by cotton pellets (Bani et al., 2000). The anti-inflammatory effects of *E. helioscopia* latex on carrageenan-induced paw edema have been tested in mice. The latex (200 mg/kg) showed maximal anti-inflammatory (68.75%) compared to the control (2 mg/kg indomethacin) (59.38%) (Saleem et al., 2015b). Moreover, Basu, P et al. showed that *E. bicolor* latex extracts induce analgesia by reducing the levels of oxidative stress biomarkers and pro-inflammatory cytokines/chemokines in a rat model of orofacial pain. **Figure 12** shows a proposed model of the non-opioid mechanism that contributes to the peripheral analgesia induced by *E. bicolor* latex extracts. It shows that local injection of phytochemicals from *E. bicolor* latex at the site of injury may be effective in reducing oxidative stress by reducing the plasma levels of advanced oxidation protein products (AOPP) and increasing the expression of the Nox4 protein, which leads to a decrease in the levels of reactive oxygen species and consequently, the release of the pro-inflammatory peptide (Basu et al., 2019).

Cytotoxic/tumor activity

Some species of the *Euphorbia* genus exhibit antitumor activity against different cancer cell lines. The anticancer activity of the phenolic extract of *E. tirucalli* was evaluated in vitro on five cancer cell lines: MCF-7, A549, HL-60, HCT116, and HepG2. The IC_{50} values of the extract against the MCF-7 and A549 cancer cell lines were 1.65 ± 3.67 and 35.36 ± 3.82 µg/ml, respectively. In addition, it exhibited a potent cytotoxic activity against HL-60, with an IC_{50} value of 22.76 ± 2.85 µg/ml, while the IC_{50} value of doxorubicin was 21.87 ± 2.31 µg/ml. However, it had no activity against HepG2 and HCT116 cancer cells. These data suggest that these cancer cells were strongly affected by the phenolic compounds detected in the latex extract (Abdel-Aty et al., 2019). In another study of the same species; the crude latex extract of *E. tirucalli* reduced the viability of gastric adenocarcinoma cancer cells at concentrations of 100

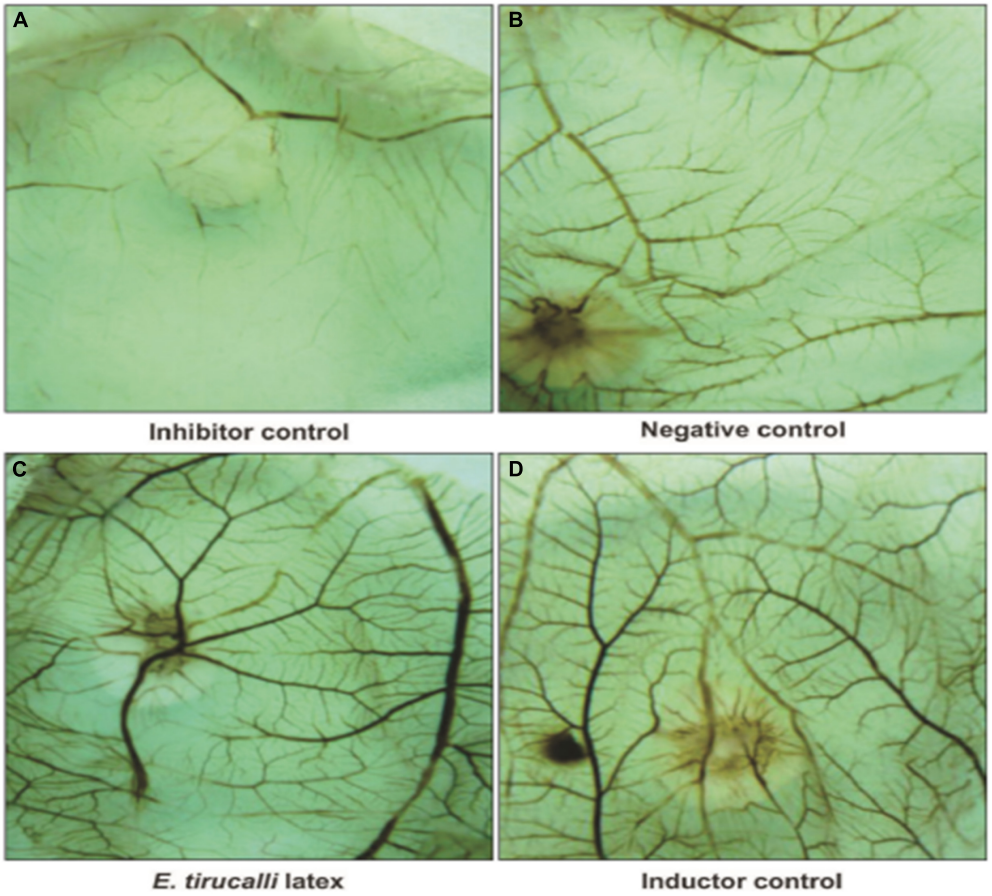

FIGURE 17
Photomicrography of Chorioallantoic membrane (CAM) vascular network formation. **(A)** Inhibitor dexamethasone; **(B)** the negative control (water); **(C)** the test solution (*E. tirucalli*); and **(D)** the inducer control (Biocure Biomembrane) (Bessa et al., 2015).

and 200 μg/mL by up to 70 and 95%, respectively. This effect could be associated with euphol, which is the main compound found in this species (de Souza et al., 2019).

Cruz et al. investigated the cytotoxic effects of euphol isolated from the latex of *E. tirucalli* against the K-562 and B16F10 cell lines using the MTT assay and morphological analysis. It was observed that this compound shows high activity against both cell lines, with IC50 values of 34.56 ± 2.12 (μM) and 53.63 ± 10.16 (μM) after 72 h against K-562 and B16F10 cells, respectively. Similarly, morphological analysis of K-562 cells showed that, compared with the negative control (DMSO treatment) and the positive control (treatment with 0.085 μM doxorubicin and 0.5 μM imatinib), the group treated with 23.4 and 46.9 μM euphol had reduced total cell counts and contained apoptotic cells, as shown in **Figure 13**. In addition, morphological analysis of B16F10 cells after 24 h of treatment showed that euphol induces cell death through apoptosis accompanied by cell rounding, membrane bleeding, and chromatin condensation (**Figure 14**; Cruz et al., 2018).

Subsequent work has recently shown that when the aqueous solution of latex from *E. tirucalli*, which contains triterpenes, is orally administered to male Wistar rats for 15 days, the tumor mass in the groups of rats treated with 25 μL latex/mL and 50 μL latex/mL latex is significantly lower than that in the control. Furthermore, a reduction of approximately 76% in tumor cell proliferation is observed in Wistar rats treated with 50 μl latex/ml ($p < 0.0001$), as determined by the Alamar Blue assay (**Figure 15**; Martins et al., 2020).

Additionally, the cytotoxic activity of *E. umbellata* latex was tested by Luz et al. This study evaluated latex cytotoxicity on human cervical adenocarcinoma (HeLa) and human ileocecal colorectal adenocarcinoma (HRT-18) cells using the 3-(4,5-Dimethylthiazol-2-yl)-2,5-diphenyltetrazolium bromide (MTT) test and neutral red. The cell viability of HRT-18 cells was reduced after 48 h when 100 to 1,000 g/ml concentrations were used. Moreover, the latex induced dose- and time-dependent cytotoxicity to HeLa cells. A photomicroscope was used to analyze the cytotoxic effects of *E. umbellata* latex on HeLa and HRT-18 cell morphology, including vacuolization,

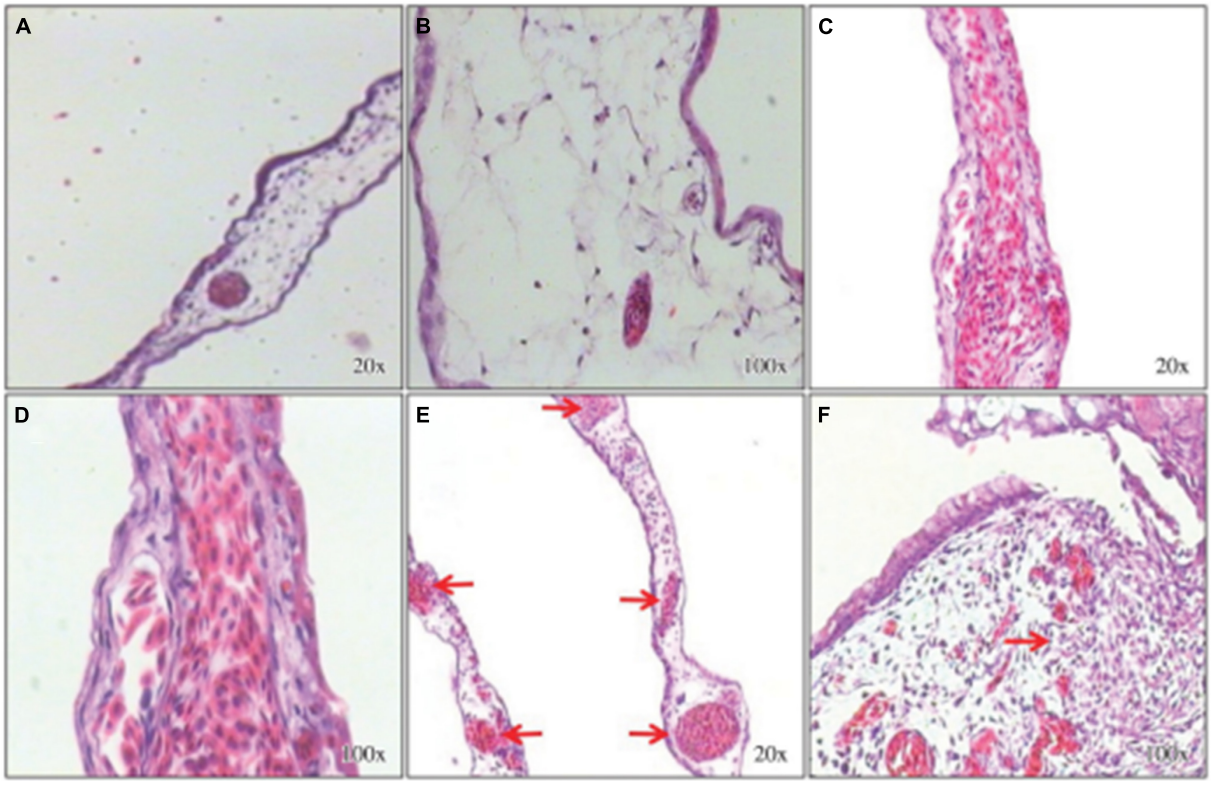

FIGURE 18
Histological sections stained with hematoxylin-eosin. Chorioallantoic membranes (CAMs) treated with the inhibitor control (dexamethasone) show few connective tissue cells and few blood vessels **(A,B)**. The inducer control (Biocure Biomembrane of Hevea brasiliensis latex) treatment induced a large number of blood vessels and inflammatory foci **(C,D)**. Treatment with the test solution of Euphorbia tirucalli latex resulted in a large number of well-organized blood vessels and inflammatory foci **(E,F)** (Bessa et al., 2015).

rounding, loss of adhesion, blebbing, nuclear condensation, and fragmentation. After 24 h, morphological alterations in HeLa and HRT-18 cells were observed and were characterized by the loss of adhesion, cellular rounding, formation of bubbles, and condensation of chromatin, showing that apoptosis is the pathway for destruction tumor (**Figure 16**; Luz et al., 2015).

Another study was carried out to determine the concentration at which the latex extract of *E. antiquorum* exhibits maximum protection and least toxicity to cells. It has been reported to be safe to normal cells such as those of *brineshrimps* (*Artemia*), *S. cerevisiae*, and chick embryo fibroblast cells, and that the toxicity of latex increases with increasing concentration.

Angiogenic and genotoxic/mutagenic activity

Angiogenesis is the growth of new vessels from an existing vascular system (Fan et al., 2006). In 2015, the pro-angiogenic activity of an aqueous *E. tirucalli* latex solution (10 mg/mL) was evaluated on chorioallantoic membranes (CAMs) of 80 fertilized chicken eggs through the application of a series of tests such as the quantification of the percentage of vascularization, histological analysis, and digital imaging; the aqueous solution significantly increased neoangiogenesis (CAM vascular network mean area and standard deviation of 46.3 ± 3.8 in the treated group versus 31.8 ± 3.0 in the control group). On the other hand, the mean surface of the vascular network in the inducer control group (51.3 ± 3.9) was not significantly ($p > 0.05$) different from that in the group treated with the *E. tirucalli* latex test. The digital images of the vascular networks of the control and the group treated with the aqueous solution of *E. tirucalli* latex are shown in **Figure 17**. The results of the histological analysis agreed with the results observed on the digital images (**Figure 18**). The positive control and *E. tirucalli* latex groups showed an increase in the number of blood vessels and an inflammatory response, whereas few blood vessels were found in the control group treated with 1% dexamethasone. Thus, the latex of *E. tirucalli* led to the activation of the inflammatory response (Bessa et al., 2015). On the other hand, the anti-angiogenic activity of *E. helioscopia* latex (100 μg/mL) has been studied in fertilized white leghorn hen eggs.

The branching of blood vessels in the latex-treated groups was similar to that in the quercetin-treated group (standard). The genotoxic and mutagenic effects of *E. helioscopia* latex at different concentrations (1,000, 200, 40, 8, and 1.6 µg/ml) was evaluated by Saleem et al. No DNA damage was observed in the lymphocytes and *S. typhimurium* reverts in latex-treated plates could not be produce at any of the doses tested (Saleem et al., 2015b).

Hemostatic and wound healing activity

Evaluation of various proteolytic activities such as protease, gelatinase, milk coagulation, and whole blood coagulation in the latex enzymatic fraction of *E. nivulia* Buch.-Ham revealed that this latex has hemostatic activity (Badgujar, 2014). Regarding proteolytic activity, the latex showed significant milk clotting activity with a value of 465.5 ± 0.37 U/g latex and protease activity with a value of 9.20 ± 0.08 U/g latex. In the gelatinase assay, the latex showed a value of 7.34 ± 0.72 U/g latex. Moreover, latex proteases have been shown to exhibit coagulation activity. Whole blood clotting times in mouse blood, human blood, and other mammals' blood samples such as those from *Capra hircus*, *Bos indicus*, *Bubalus bubalis*, and *Ovibos moschatus* were reduced by treatment with proteases present in *E. nivulia* Buch.-Ham latex. Other work has examined the wound healing activity of *E. caducifolia* latex in excision and incision wound model mice and study the effect of this latex extract on hydroxyproline and DNA content.

The results showed a complete closure of the wound in animals treated with *E. caducifolia* latex at concentrations of 2.5 and 5.0 mg/g after the 15th day. On the other hand, treatment with 10 mg/g allowed a total closure of the wound after the 14th day. Also the results of hydroxyproline content showed that the excised skin of animals treated with the latex extract with a concentration of 0.50 and 1.0 mg/g was found to have a higher amount of hydroxyproline compared to the control group, however the increase in DNA content was statistically significant only in the group treated with 10 mg/g ECL as shown in **Figure 19**.

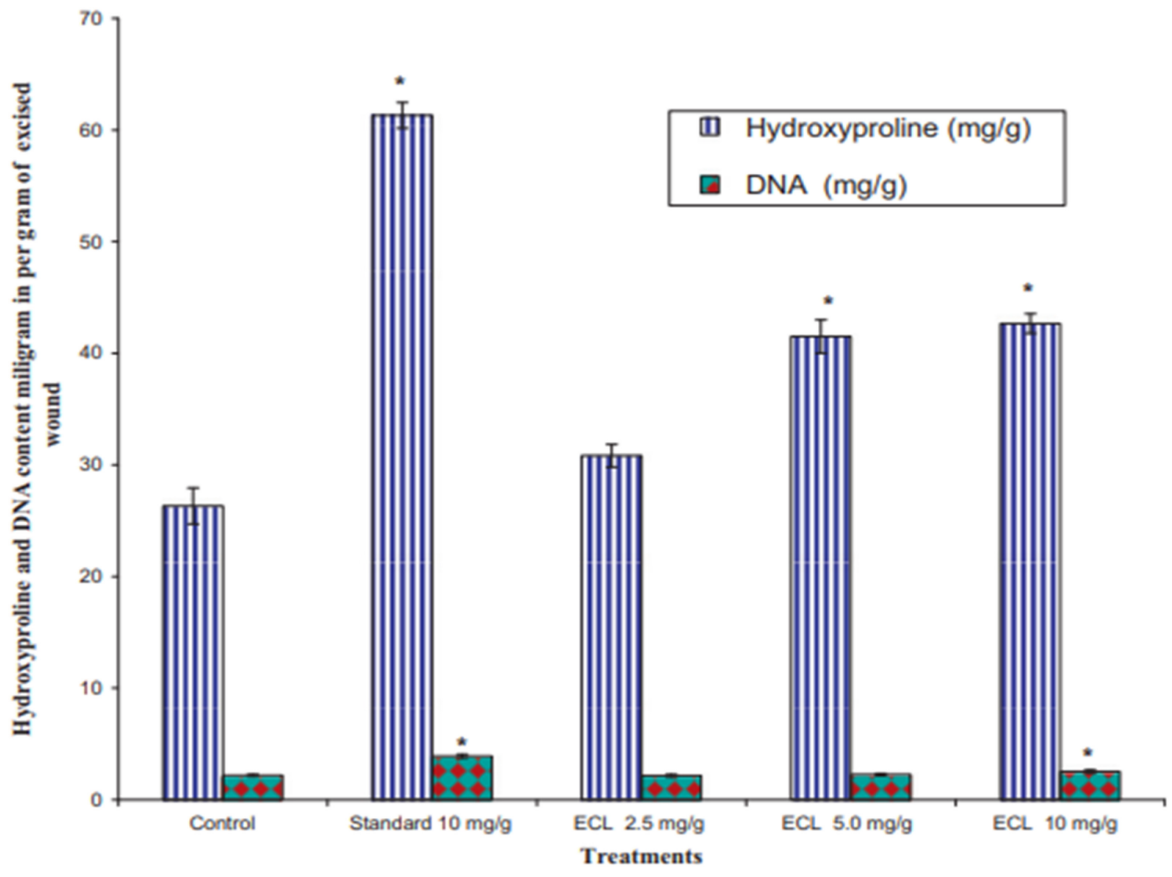

FIGURE 19
Effect of latex of *E. caducifolia* on hydroxyproline and DNA content. Values reported as Mean ± SEM (n = 6). The data were analyzed by one way ANOVA followed by and Dunnett's test. *P0.05 as compared with control group. ECL (latex of *E. caducifolia*) (Goyal et al., 2012).

In addition, the histopathological examination of excised skin showed the formation of new vessels with scattered inflammatory cells in mice treated with the latex of *E. caducifolia* (Goyal et al., 2012).

Conclusion

To our knowledge, this review represents the first report summarizing the phytochemical analysis of spurge genus latex and its pharmacological effects. *Euphorbia* is one of the largest genera in the *Euphorbiaceae* family. This review summarizes the available literature to identify compounds with pharmacological activities extracted from the latex of different species of *Euphorbia*. The major constituent secondary metabolites of *Euphorbia* species are terpenoids, and most of them have been identified using HPLC, GC-MS, and NMR spectroscopic analysis. Latex extracts from *Euphorbia* species have many pharmacological functions, including antimicrobial, anticancer, anticholinesterase, anti-inflammatory, antioxidant, cytotoxic, anti-angiogenic, genotoxic/mutagenic, and wound healing activities, which have been demonstrated in various *in vitro* and *in vivo* biological test models. However, other components such as phenolic compounds, alkaloids, saponins, and flavonoids isolated from the latex of these species have been mostly ignored, which limits the diversity of application of the latex from these plants. This review summarizes the current understanding of the biological activities of secondary metabolites from the latex of *Euphorbia* species. Our findings may promote future studies that will help to optimize the therapeutic use of latex extracts and could be useful for scientists who need unexplored species that have not yet been fully explored.

However, few studies have tested the biological activities of the latex of the genus Euphorbia in vivo conditions, further investigations are recommended in order to better understand and discover more bioactive molecules. In addition, great attention should be paid to study the pharmacokinetics and the mechanism of action of the various compounds isolated from the latex of this genus.

Author contributions

RB, AM, and AE: writing—original draft. NK and EC: writing—review and editing. NKK, NK, EC, and AE: funding and supervision. All authors contributed to the article and approved the submitted version.

Funding

This study was supported by the National Research Foundation (NRF) of Korea, funded by the Korea government (NRF-2021R1C1C1013875, 2021R1A6A1A03038785, and 2021R1F1A1055694). This study was also supported by Kwangwoon University Research Grant in 2022.

Conflict of interest

The authors declare that the research was conducted in the absence of any commercial or financial relationships that could be construed as a potential conflict of interest.

Publisher's note

Supplementary material

The Supplementary Material for this article can be found online at: https://www.frontiersin.org/articles/10.3389/fpls.2022.1008881/full#supplementary-material

References

Abdel-Aty, A. M., Hamed, M. B., Salama, W. H., Ali, M. M., Fahmy, A. S., and Mohamed, S. A. (2019). *Ficus carica*, *Ficus sycomorus* and *Euphorbia tirucalli* latex extracts: Phytochemical screening, antioxidant and cytotoxic properties. *Biocataly. Agric. Biotechnol.* 20:101199. doi: 10.1016/j.bcab.2019.101199

Agrawal, A. A., and Konno, K. (2009). Latex: A model for understanding mechanisms, ecology, and evolution of plant defense against herbivory. *Annu Rev. Ecol. Evol. Syst.* 40, 311–331. doi: 10.1146/annurev.ecolsys.110308.120307

Arreguín, B. (1958). "Rubber and latex," in *Der Stoffwechsel Sekundärer Pflanzenstoffe/The Metabolism of Secondary Plant Products*, ed. W. Ruhland (Springer), 223–248. doi: 10.1007/978-3-662-26784-4_6

Azadi, S., Bagheri, H., Mohammad Parast, B., and Ghorbani-Marghashi, M. (2020). Natural rubber identification and characterization in *Euphorbia macroclada*. *Physiol. Mol. Biol. Plants* 26, 2047–2052. doi: 10.1007/s12298-020-00880-5

Azoui, I., Frah, N., and Nia, B. (2016). Insecticidal effect of *Euphorbia bupleuroides* latex on *Blattella germanica* (Dictyoptera: Blattellidae). *Int. J. Pure Appl. Zool.* 4, 271–276.

Badgujar, S. B. (2014). Evaluation of hemostatic activity of latex from three *Euphorbiaceae* species. *J. Ethnopharmacol.* 151, 733–739. doi: 10.1016/j.jep.2013.11.044

Badgujar, S. B., and Mahajan, R. T. (2014). Nivulian-II a new milk clotting cysteine protease of *Euphorbia nivulia* latex. *Int. J Biol. Macromol.* 70, 391–398. doi: 10.1016/j.ijbiomac.2014.07.022

Bani, S., Kaul, A., Jaggi, B. S., Suri, K. A., Suri, O. P., and Sharma, O. P. (2000). Anti-inflammatory activity of the hydrosoluble fraction of *Euphorbia royleana* latex. *Fitoterapia* 71, 655–662. doi: 10.1016/S0367-326X(00)00225-2

Basu, P., Hornung, R. S., Averitt, D. L., and Maier, C. (2019). *Euphorbia bicolor* (*Euphorbiaceae*) latex extract reduces inflammatory cytokines and oxidative stress in a rat model of orofacial pain. *Oxidat. Med. Cell. Long.* 2019:8594375. doi: 10.1155/2019/8594375

Bauer, G., Friedrich, C., Gillig, C., Vollrath, F., Speck, T., and Holland, C. (2014). Investigating the rheological properties of native plant latex. *J. R. Soc. Int.* 11:20130847. doi: 10.1098/rsif.2013.0847

Berg, R. Y. (1990). Seed dispersal relative to population structure, reproductive capacity, seed predation, and distribution in *Euphorbia balsamifera* (*Euphorbiaceae*), with a note on sclerendochory. *Sommerfeltia* 11, 35–63.

Bessa, G., Melo-Reis, P. R., Araújo, L. A., Mrué, F., Freitas, G. B., Brandão, M. L., et al. (2015). Angiogenic activity of latex from *Euphorbia tirucalliLinnaeus* 1753 (plantae, *Euphorbiaceae*). *Braz. J. Biol.* 75, 752–758. doi: 10.1590/1519-6984.01214

Bigoniya, P., and Rana, A. (2008). A comprehensive phyto-pharmacological review of *Euphorbia neriifolia* linn. *Pharmacognosy Rev.* 2:57.

Chakir, A., Romane, A., Marcazzan, G. L., and Ferrazzi, P. (2016). Physicochemical properties of some honeys produced from different plants in morocco. *Arabian J. Chem.* 9, S946–S954. doi: 10.1016/j.arabjc.2011.10.013

Cruz, L. S., de Oliveira, T. L., Kanunfre, C. C., Paludo, K. S., Minozzo, B. R., Prestes, A. P., et al. (2018). Pharmacokinetics and cytotoxic study of euphol from *Euphorbia umbellata* (bruyns) pax latex. *Phytomedicine* 47, 105–112. doi: 10.1016/j.phymed.2018.04.055

Cruz, L. S., Kanunfre, C. C., de Andrade, E. A., de Oliveira, A. A., Cruz, L. S., de Faria Moss, M., et al. (2020). *Enriched terpenes* fractions of the latex of euphorbia umbellata promote apoptosis in leukemic cells. *Chem. Biodiv.* 17:e2000369. doi: 10.1002/cbdv.202000369

Daborn, P. J., and Le Goff, G. (2004). The genetics and genomics of insecticide resistance. *Trends Genet.* 20, 163–170. doi: 10.1016/j.tig.2004.01.003

Daoubi, M., Marquez, N., Mazoir, N., Benharref, A., Hernández-Galán, R., Munoz, E., et al. (2007). Isolation of new phenylacetylingol derivatives that reactivate HIV-1 latency and a novel spirotriterpenoid from *Euphorbia officinarum* latex. *Bioorganic Med. Chem.* 15, 4577–4584. doi: 10.1016/j.bmc.2007.04.009

De Silva, W., Manuweera, G. K., and Karunaratne, S. (2008). Insecticidal activity of *Euphorbia antiquorum* L. latex and its preliminary chemical analysis. *J. Natl. Sci. Found. Sri Lanka* 2008:36. doi: 10.4038/jnsfsr.v36i1.129

de Souza, L. S., Puziol, L. C., Tosta, C. L., Bittencourt, M. L., Santa Ardisson, J., Kitagawa, R. R., et al. (2019). Analytical methods to access the chemical composition of an *Euphorbia tirucalli* anticancer latex from traditional Brazilian medicine. *J. Ethnopharmacol.* 237, 255–265. doi: 10.1016/j.jep.2019.03.041

Demir, Y., Alayli, A., Yildirim, S., and Demir, N. (2005). Identification of protease from *Euphorbia amygdaloides* latex and its use in cheese production. *Preparat. Biochem. Biotechnol.* 35, 291–299. doi: 10.1080/10826060500218107

Deng, Y.-Y., Qu, B., Zhan, Z.-L., Wang, A.-Q., Zhou, W., Jia, M.-Y., et al. (2021). Bioactive tigliane diterpenoids from the latex of *Euphorbia fischeriana*. *Nat. Prod. Res.* 35, 179–187. doi: 10.1080/14786419.2019.1616728

Domsalla, A., Görick, C., and Melzig, M. F. (2010). Proteolytic activity in latex of the genus Euphorbia–a chemotaxonomic marker? *Die Pharmazie Int. J. Pharmaceut. Sci.* 65, 227–230.

Dorsey, B. L. 2013. *Phylogenetics and Morphological Evolution of Euphorbia subgenus Euphorbia*. Ph.D. dissertation, University of Michigan, Ann Arbor, MI.

El-Ghazaly, G., and Chaudhary, R. (1993). Morphology and taxonomic application of orbicules (ubisch bodies) in the genus Euphorbia. *Grana* 32, 26–32. doi: 10.1080/00173139309428975

Esposito, M., Nothias, L.-F., Nedev, H., Gallard, J.-F., Leyssen, P., Retailleau, P., et al. (2016). Euphorbia dendroides latex as a source of jatrophane esters: isolation, structural analysis, conformational study, and anti-CHIKV activity. *J. Nat. Prod.* 79, 2873–2882. doi: 10.1021/acs.jnatprod.6b00644

Fais, A., Delogu, G. L., Floris, S., Era, B., Medda, R., and Pintus, F. (2021). Euphorbia characias: Phytochemistry and biological activities. *Plants* 10:1468. doi: 10.3390/plants10071468

Famuyiwa, S. O., Oladele, A. T., Adeloye, A. O., and Fakunle, C. O. (2014). Terpenoid compounds from the latex of *Euphorbia drupifera*. *Ife J. Sci.* 16, 1–5.

Fan, T.-P., Yeh, J.-C., Leung, K. W., Yue, P. Y., and Wong, R. N. (2006). Angiogenesis: From plants to blood vessels. *Trends Pharmacol. Sci.* 27, 297–309. doi: 10.1016/j.tips.2006.04.006

Fattorusso, E., Lanzotti, V., Taglialatela-Scafati, O., Tron, G. C., and Appendino, G. (2002). Bisnorsesquiterpenoids from *Euphorbia resinifera* berg. and an expeditious procedure to obtain resiniferatoxin from its fresh latex. *Eur. J. Organic Chem.* 2002, 71–78. doi: 10.1002/1099-0690(20021)2002:1<71::AID-EJOC71>3.0.CO;2-C

Fernandez, M. A., Tornos, M. P., Garcia, M. D., De las Heras, B., Villar, A. M., and Saenz, M. T. (2001). Anti-inflammatory activity of abietic acid, a diterpene isolated from *Pimenta racemosa* var. grissea. *J. Pharmacy Pharmacol.* 53, 867–872. doi: 10.1211/0022357011776027

Fernandez-Arche, A., Saenz, M. T., Arroyo, M., De la Puerta, R., and Garcia, M. D. (2010). Topical anti-inflammatory effect of tirucallol, a triterpene isolated from *Euphorbia lactea* latex. *Phytomedicine* 17, 146–148. doi: 10.1016/j.phymed.2009.05.009

Flemmig, M., Domsalla, A., Rawel, H., and Melzig, M. F. (2017). Isolation and characterization of mauritanicain, a serine protease from the latex of *Euphorbia mauritanica* L. *Planta Med.* 234, 551–556. doi: 10.1055/s-0042-117645

Fonseca, K. C., Morais, N. C. G., Queiroz, M. R., Silva, M. C., Gomes, M. S., Costa, J. O., et al. (2010). Purification and biochemical characterization of eumiliin from *Euphorbia milii* var. hislopii latex. *Phytochemistry* 71, 708–715. doi: 10.1016/j.phytochem.2010.02.009

Gewali, M. B., Hattori, M., Tezuka, Y., Kikuchi, T., and Namba, T. (1989). Four ingol type diterpenes from *Euphorbia antiquorum* L. *Chem. Pharmaceut. Bull.* 37, 1547–1549. doi: 10.1248/cpb.37.1547

Gewali, M. B., Hattori, M., Tezuka, Y., Kikuchi, T., and Namba, T. (1990). Constituents of the latex of *Euphorbia antiquorum*. *Phytochemistry* 29, 1625–1628. doi: 10.1016/0031-9422(90)80134-3

Giner, J.-L., Berkowitz, J. D., and Andersson, T. (2000). Nonpolar components of the latex of *Euphorbia* p eplus. *J. Nat. Prod.* 63, 267–269. doi: 10.1021/np990081g

Giner, J.-L., and Schroeder, T. N. (2015). Polygonifoliol, a new tirucallane triterpene from the latex of the seaside sandmat *Euphorbia polygonifolia*. *Chem. Biodiv.* 12, 1126–1129. doi: 10.1002/cbdv.201400426

Goyal, M., Nagori, B. P., and Sasmal, D. (2012). Wound healing activity of latex of *Euphorbia caducifolia*. *J. Ethnopharmacol.* 144, 786–790. doi: 10.1016/j.jep.2012.10.006

Goyal, M., Sasmal, D., and Nagori, B. P. (1970). GCMS analysis and antimicrobial action of latex of *Euphorbia caducifolia*. *J. Complement. Med. Res.* 1, 119–119. doi: 10.5455/jice.20120618045914

Hua, J., Liu, Y.-C., Jing, S.-X., Luo, S.-H., and Li, S.-H. (2015). Macrocyclic diterpenoids from the latex of *Euphorbia helioscopia*. *Nat Prod. Commun.* 10:1934578X1501001206. doi: 10.1177/1934578X1501001206

Hussain, M., Farooq, U., Rashid, M., Bakhsh, H., Majeed, A., Khan, I. A., et al. (2014). Antimicrobial activity of fresh latex, juice and extract of *Euphorbia hirta* and *Euphorbia thymifolia*: An in vitro comparative study. *Int. J. Pharma. Sci.* 4, 546–553.

Ilyas, M., Parveen, M., and Amin, K. M. Y. (1998). Neriifolione, a triterpene from *Euphorbia neriifolia*. *Phytochemistry* 48, 561–563. doi: 10.1016/S0031-9422(98)00044-2

Kemboi, D., Peter, X., Langat, M., and Tembu, J. (2020). A review of the ethnomedicinal uses, biological activities, and triterpenoids of *Euphorbia* species. *Molecules* 25:4019. doi: 10.3390/molecules25174019

Khan, A. R., and Akhtar, T. (2003). Latexes from euphorbia caducifolia-isolation and characterisation of rubber hydrocarbon. part-I. *Biol. Sci. PJSIR* 46, 311–316.

Ki-Ryong, P. (2004). Comparisons of allozyme variation of narrow endemic and widespread species of far east *Euphorbia* (*Euphorbiaceae*). *Bot. Bull. Acad. Sin.* 2004:45.

Koh, K. J., Pearce, A. L., Marshman, G., Finlay-Jones, J. J., and Hart, P. H. (2002). Tea tree oil reduces histamine-induced skin inflammation. *Br. J. Dermatol.* 147, 1212–1217. doi: 10.1046/j.1365-2133.2002.05034.x

Konno, K. (2011). Plant latex and other exudates as plant defense systems: roles of various defense chemicals and proteins contained therein. *Phytochemistry* 72, 1510–1530. doi: 10.1016/j.phytochem.2011.02.016

Krstić, G., Jadranin, M., Todoroviæ, N. M., Pešiæ, M., Stankoviæ, T., Aljanèiæ, I. S., et al. (2018). Jatrophane diterpenoids with multidrug-resistance modulating activity from the latex of *Euphorbia nicaeensis*. *Phytochemistry* 148, 104–112. doi: 10.1016/j.phytochem.2018.01.016

Krstić, G., Novakoviæ, M., Jadranin, M., and Teševiæ, V. (2019). Tetracyclic triterpenoids from *Euphorbia nicaeensis* all. *Adv. Technol.* 8, 37–45. doi: 10.5937/savteh1902037K

Laibach, N., Hillebrand, A., Twyman, R. M., Prüfer, D., and Schulze Gronover, C. (2015). Identification of a *Taraxacum brevicorniculatum* rubber elongation

factor protein that is localized on rubber particles and promotes rubber biosynthesis. *Plant J.* 82, 609–620. doi: 10.1111/tpj.12836

Lazreg Aref, H., Mosbah, H., Fekih, A., and Kenani, A. (2014). Purification and biochemical characterization of lipase from tunisian *Euphorbia peplus* latex. *J. Am. Oil Chem. Soc.* 91, 943–951. doi: 10.1007/s11746-014-2444-z

Lewinsohn, T. M. (1991). The geographical distribution of plant latex. *Chemoecology* 2, 64–68. doi: 10.1007/BF01240668

Li, M.-M., Qi, Y.-R., Feng, Y.-P., Liu, W., and Yuan, T. (2021). Four new lanostane triterpenoids from latex of *Euphorbia resinifera*. *Zhongguo Zhong yao za zhi Zhongguo Zhongyao Zazhi China J. Chin. Mater. Med.* 46, 4744–4748.

Li, M.-M., Qi, Y.-R., Feng, Y.-P., Liu, W., and Yuan, T. (2022). Euphatexols C-G, five new triterpenoids from the latex of *Euphorbia resinifera*. *J. Asian Nat. Prod. Res.* 24, 311–320. doi: 10.1080/10286020.2021.1935894

Liang, X., Liu, Z., Cao, Y.-F., Meng, D., and Hua, H. (2014). Chemotaxonomic and chemical studies on two plants from genus of *Euphorbia*: *Euphorbia fischeriana* and *Euphorbia ebracteolata*. *Biochem. Syst. Ecol.* 57, 345–349. doi: 10.1016/j.bse.2014.09.009

Lin, L.-J., and Kinghorn, A. D. (1983). 8-methoxyingol esters from the latex of *Euphorbia hermentiana*. *Phytochemistry* 22, 2795–2799. doi: 10.1016/S0031-9422(00)97699-4

Lin, S. C., and Hsieh, C. F. (1991). A taxonomic study of the genus euphorbia. *Taiwania* 36, 57–79.

Luz, L. E., Paludo, K. S., Santos, V. L., Franco, C. R., Klein, T., Silva, R. Z., et al. (2015). Cytotoxicity of latex and pharmacobotanical study of leaves and stem of *Euphorbia umbellata* (janaúba). *Rev. Brasil. Farmacogn.* 25, 344–352. doi: 10.1016/j.bjp.2015.07.005

Lynn, K. R., and Clevette-Radford, N. A. (1983). Isolation and characterization of euphorbain 1, a proteinase from the latex of *Euphorbia lathyris*. *Biochim. Biophys. Acta (BBA) Protein Struct. Mol. Enzymol.* 746, 154–159. doi: 10.1016/0167-4838(83)90069-9

Lynn, K. R., and Clevette-Radford, N. A. (1985). Three serine proteases from the latex of *Euphorbia cyparissias*. *Phytochemistry* 24, 925–928. doi: 10.1016/S0031-9422(00)83154-4

Mallavadhani, U. V., Satyanarayana, K. V. S., Mahapatra, A., and Sudhakar, A. V. S. (2004). A new tetracyclic triterpene from the latex of *Euphorbia nerifolia*. *Nat. Prod. Res.* 18, 33–37. doi: 10.1080/1057563031000122068

Marco, J. A., Sanz-Cervera, J. F., Checa, J., Palomares, E., and Fraga, B. M. (1999). Jatrophane and tigliane diterpenes from the latex of *Euphorbia obtusifolia*. *Phytochemistry* 52, 479–485. doi: 10.1016/S0031-9422(99)00166-1

Martins, C. G., Appel, M. H., Coutinho, D. S., Soares, I. P., Fischer, S., de Oliveira, B. C., et al. (2020). Consumption of latex from *Euphorbia tirucalli* L. promotes a reduction of tumor growth and cachexia, and immunomodulation in walker 256 tumor-bearing rats. *J. Ethnopharmacol.* 255:112722. doi: 10.1016/j.jep.2020.112722

Mazou, M., Djossou, A. J., Tchobo, F. P., Villeneuve, P., and Soumanou, M. M. (2017). Catalytic properties of lipase from *Ficus trichopoda* and *Euphorbia unispina* latex: Study of their typoselectivity. *J. Appl. Biosci.* 110, 10790–10801. doi: 10.4314/jab.v110i1.9

Medda, R., Pintus, F., Spano, D., and Floris, G. (2011). Bioseparation of four proteins from euphorbia characias latex: Amine oxidase, peroxidase, nucleotide pyrophosphatase/phosphodiesterase, and purple acid phosphatase. *Biochem. Res. Int.* 2019:8594375. doi: 10.1155/2011/369484

ML, P., MK, M., and Mary, R. S. (2020). Efficacy of *Euphorbia heterophylla* latex against pathogenic bacteria and fungi. *Asian J. Pharmaceut. Clin. Res.* 2020, 141–145. doi: 10.22159/ajpcr.2020.v13i6.37341

Moro, L. P., Cabral, H., Okamoto, D. N., Hirata, I., Juliano, M. A., Juliano, L., et al. (2013). Characterization, subsite mapping and N-terminal sequence of miliin, a serine-protease isolated from the latex of *Euphorbia milii*. *Proc. Biochem.* 48, 633–637. doi: 10.1016/j.procbio.2013.02.017

Mura, A., Pintus, F., Fais, A., Porcu, S., Corda, M., Spanò, D., et al. (2008). Tyramine oxidation by copper/TPQ amine oxidase and peroxidase from *Euphorbia characias* latex. *Arch. Biochem. Biophys.* 475, 18–24. doi: 10.1016/j.abb.2008.03.034

Narbona, E., Arista, M., and Ortiz, P. L. (2007). Seed germination ecology of the perennial *Euphorbia boetica*, an endemic spurge of the southern Iberian *Peninsula*. *Ann. Bot. Fennici* 2007, 276–282.

Nasr, S., Bien, S., Soudi, M. R., Alimadadi, N., Shahzadeh Fazeli, S. A., and Damm, U. (2018). Novel *Collophorina* and *Coniochaeta* species from *Euphorbia polycaulis*, an endemic plant in Iran. *Mycol. Prog.* 17, 755–771. doi: 10.1007/s11557-018-1382-9

Nasseh, Y., Nazarova, E., and Kazempour, S. (2018). Taxonomic revision and phytogeographic studies in *Euphorbia* (*Euphorbiaceae*) in the Khorassan provinces of Iran. *Nordic J. Bot.* 36:1413. doi: 10.1111/njb.01413

O'Brien, D. J. (1999). Treatment of psoroptic mange with reference to epidemiology and history. *Vet. Parasitol.* 83, 177–185. doi: 10.1016/S0304-4017(99)00056-4

Özbilgin, S., Akkol, E. K., Süntar, I., Tekin, M., and İşcan, G. S. (2019). Wound-healing activity of some species of *Euphorbia* L. *Rec. Nat. Prod.* 13, 104–113. doi: 10.25135/rnp.81.18.03.255

Padiglia, A., Medda, R., Lorrai, A., Murgia, B., Pedersen, J. Z., Finazzi Agró, A., et al. (1998). Characterization of *Euphorbia characias* latex amine oxidase. *Plant Physiol.* 117, 1363–1371. doi: 10.1104/pp.117.4.1363

Pahlevani, A., and Mozaffarian, V. (2011). *Euphorbia iranshahri* (*Euphorbiaceae*), a new endemic species from Iran. *Adansonia* 33, 93–99. doi: 10.5252/a2011n1a6

Palocci, C., Soro, S., Cernia, E., Fiorillo, F., Belsito, C. M., Monacelli, B., et al. (2003). Lipolytic isoenzymes from *Euphorbia* latex. *Plant Sci.* 165, 577–582. doi: 10.1016/S0168-9452(03)00223-1

Paques, F. W., and Macedo, G. A. (2006). Plant lipases from latex: Properties and industrial applications. *Quimica Nova* 29, 93–99. doi: 10.1590/S0100-40422006000100018

Pascal, O. A., Bertrand, A. E. V., Esaïe, T., Sylvie, H.-A. M., and Eloi, A. Y. (2017). A review of the ethnomedical uses, phytochemistry and pharmacology of the *Euphorbia* genus. *Pharma Innov.* 6:34.

Patel, G. K., Kawale, A. A., and Sharma, A. K. (2012). Purification and physicochemical characterization of a serine protease with fibrinolytic activity from latex of a medicinal herb *Euphorbia hirta*. *Plant Physiol. Biochem.* 52, 104–111. doi: 10.1016/j.plaphy.2011.12.004

Pintus, F., Spano, D., Corongiu, S., Floris, G., and Medda, R. (2011). Purification, primary structure, and properties of *Euphorbia characias* latex purple acid phosphatase. *Biochemistry* 76, 694–701. doi: 10.1134/S0006297911060101

Prenner, G., and Rudall, P. J. (2007). Comparative ontogeny of the cyathium in *Euphorbia* (*Euphorbiaceae*) and its allies: Exploring the organ–flower–inflorescence boundary. *Am. J. Bot.* 94, 1612–1629. doi: 10.3732/ajb.94.10.1612

Priya, C. L., and Rao, K. V. B. (2011). A Review o phytochemical ad pharmacological profile of *Euphorbia tirucalli*. *Pharmacologyonline* 2, 384–390.

Qi, Y., Liu, W., Chen, Y., Guan, M., and Yuan, T. (2019). Euphatexols A and B, two unusual euphane triterpenoids from the latex of *Euphorbia resinifera*. *Tetrahedron Lett.* 60:151303. doi: 10.1016/j.tetlet.2019.151303

Ramos, M. V., Freitas, C. D. T., Morais, F. S., Prado, E., Medina, M. C., and Demarco, D. (2020). Plant latex and latex-borne defense. *Adv. Bot. Res.* 2020, 1–25. doi: 10.1016/bs.abr.2019.09.002

Saleem, U., Ahmad, B., Ahmad, M., Hussain, K., and Bukhari, N. I. (2015a). Anti-nociceptive, anti-inflammatory and anti-pyretic activities of latex and leaves methanol extract of *Euphorbia helioscopia*. *Asian Pacific J. Trop. Dis.* 5, 322–328. doi: 10.1016/S2222-1808(14)60791-X

Saleem, U., Ahmad, B., Ahmad, M., Hussain, K., Bukhari, N. I., and Ashraf, M. (2015b). Evaluation of anti-angiogenic activity of latex and extracts of *Euphorbia helioscopia* using chorioallontoic membrane (CAM) assay. *Int. J. Agric. Biol.* 2015:17.

Saleem, U., Mahmood, S., Ahmad, B., Saleem, M., and Anjum, A. A. (2015c). Estimation of genotoxic and mutagenic potential of latex and methanolic leaves extract of *Euphorbia helioscopia* by comet assay and ames test. *Asian Pacific J. Trop. Dis.* 5, S145–S150. doi: 10.1016/S2222-1808(15)60877-5

Salehi, B., Iriti, M., Vitalini, S., Antolak, H., Pawlikowska, E., Krêgiel, D., et al. (2019). Euphorbia-derived natural products with potential for use in health maintenance. *Biomolecules* 9:337. doi: 10.3390/biom9080337

Shi, Q.-W., Su, X.-H., and Kiyota, H. (2008). Chemical and pharmacological research of the plants in genus *Euphorbia*. *Chem. Rev.* 108, 4295–4327. doi: 10.1021/cr078350s

Siritapetawee, J., Khunkaewla, P., and Thumanu, K. (2020a). Roles of a protease from *Euphorbia resinifera* latex in human anticoagulant and antithrombotic activities. *Chem. Biol. Int.* 329:109223. doi: 10.1016/j.cbi.2020.109223

Siritapetawee, J., Teamtisong, K., Limphirat, W., Charoenwattanasatien, R., Attarataya, J., and Mothong, N. (2020b). Identification and characterization of a protease (EuRP-61) from *Euphorbia resinifera* latex. *Int. J. Biol. Macromol.* 145, 998–1007. doi: 10.1016/j.ijbiomac.2019.09.190

Siritapetawee, J., Sojikul, P., and Klaynongsruang, S. (2015). Biochemical characterization of a new glycosylated protease from *Euphorbia* cf. lactea latex. *Plant Physiol. Biochem.* 92, 30–38. doi: 10.1016/j.plaphy.2015.04.012

Smaili, A., Mazoir, N., Rifai, L. A., Koussa, T., Makroum, K., Benharref, A., et al. (2017). Antimicrobial activity of two semisynthetic triterpene derivatives from *Euphorbia officinarum* latex against fungal and bacterial phytopathogens. *Nat. Prod. Commun.* 12:1934578X1701200305.

Smeriglio, A., Ragusa, S., Monforte, M. T., D'angelo, V., and Circosta, C. (2019). Phytochemical analysis and evaluation of antioxidant and anti-acetylcholinesterase activities of *Euphorbia dendroides* L.(*Euphorbiaceae*) latex. *Plant Biosyst. Int. J. Dealing Aspects Plant Biol.* 153, 498–505. doi: 10.1080/11263504.2018.1498405

Spanò, D., Pintus, F., Mascia, C., Scorciapino, M. A., Casu, M., Floris, G., et al. (2012). Extraction and characterization of a natural rubber from *Euphorbia characias* latex. *Biopolymers* 97, 589–594. doi: 10.1002/bip.22044

Spano, D., Pospiskova, K., Safarik, I., Pisano, M. B., Pintus, F., Floris, G., et al. (2015). Chitinase III in *Euphorbia characias* latex: Purification and characterization. *Prot. Exp. Purificat.* 116, 152–158. doi: 10.1016/j.pep.2015.08.026

Steinmann, V. W., van Ee, B., Berry, P. E., and Gutiérrez, J. (2007). The systematic position of *Cubanthus* and other shrubby endemic species of *Euphorbia* (*Euphorbiaceae*) in cuba. *Anal. Del Jardín Bot. Mad.* 2007, 123–133. doi: 10.3989/ajbm.2007.v64.i2.167

Sumathi, S., Malathy, N., Dharani, B., Sivaprabha, J., Hamsa, D., Radha, P., et al. (2011). Antibacterial and antifungal activity of latex of *Euphorbia antiquorum*. *Afr. J. Microbiol. Res.* 5, 4753–4756. doi: 10.5897/AJMR11.043

Tarh, J. E., and Iroegbu, C. U. (2019). In-vitro anti-bacterial activity of extracts of *Euphorbia abyssinica* (desert candle) stem-bark and latex. *Rec. Adv. Biol. Res.* 3, 131–144.

Tian, X., Wang, Q., and Zhou, Y. (2018). Euphorbia section hainanensis (*Euphorbiaceae*), a new section endemic to the hainan island of china from biogeographical, karyological, and phenotypical evidence. *Front. Plant Sci.* 9:660. doi: 10.3389/fpls.2018.00660

Urones, J. G., Barcala, P. B., Cuadrado, M. J. S., and Marcos, I. S. (1988). Diterpenes from the latex of *Euphorbia broteri*. *Phytochemistry* 27, 207–212. doi: 10.1016/0031-9422(88)80615-0

Wang, S.-Y., Li, G.-Y., Zhang, K., Wang, H.-Y., Liang, H.-G., Huang, C., et al. (2019). New ingol-type diterpenes from the latex of *Euphorbia resinifera*. *J. Asian Nat. Prod. Res.* 21, 1075–1082. doi: 10.1080/10286020.2018.1498084

Webster, G. L. (1987). The saga of the spurges: A review of classification and relationships in the *Euphorbiales*. *Bot. J. Linn. Soc.* 94, 3–46. doi: 10.1111/j.1095-8339.1987.tb01036.x

frontiers | Frontiers in Plant Science

TYPE Original Research
PUBLISHED 10 October 2022
DOI 10.3389/fpls.2022.1002561

OPEN ACCESS

EDITED BY
Mohammad Irfan,
Cornell University, United States

REVIEWED BY
Aiswarya Girija,
Aberystwyth University,
United Kingdom
Rajiv Kumar,
Institute of Himalayan Bioresource Technology Council of Scientific and Industrial Research, (CSIR), India

*CORRESPONDENCE
Pranav Pankaj Sahu
sahu.p@czechglobe.cz

SPECIALTY SECTION
This article was submitted to Crop and Product Physiology, a section of the journal Frontiers in Plant Science

RECEIVED 25 July 2022
ACCEPTED 08 September 2022
PUBLISHED 10 October 2022

CITATION
Večeřová K, Oravec M, Puranik S, Findurová H, Veselá B, Opoku E, Ofori-Amanfo KK, Klem K, Urban O and Sahu PP (2022) Single and interactive effects of variables associated with climate change on wheat metabolome.
Front. Plant Sci. 13:1002561.
doi: 10.3389/fpls.2022.1002561

Single and interactive effects of variables associated with climate change on wheat metabolome

Kristýna Večeřová[1], Michal Oravec[1], Swati Puranik[1], Hana Findurová[1,2], Barbora Veselá[1], Emmanuel Opoku[1,2], Kojo Kwakye Ofori-Amanfo[1,3], Karel Klem[1], Otmar Urban[1] and Pranav Pankaj Sahu[1]*

[1]Laboratory of Ecological Plant Physiology, Global Change Research Institute of the Czech Academy of Sciences, Brno, Czechia, [2]Department of Agrosystems and Bioclimatology, Faculty of AgriSciences, Mendel University in Brno, Brno, Czechia, [3]Department of Forest Ecology, Faculty of Forestry and Wood Technology, Mendel University in Brno, Brno, Czechia

One of the key challenges linked with future food and nutritional security is to evaluate the interactive effect of climate variables on plants' growth, fitness, and yield parameters. These interactions may lead to unique shifts in the morphological, physiological, gene expression, or metabolite accumulation patterns, leading to an adaptation response that is specific to future climate scenarios. To understand such changes, we exposed spring wheat to 7 regimes (3 single and 4 combined climate treatments) composed of elevated temperature, the enhanced concentration of CO_2, and progressive drought stress corresponding to the predicted climate of the year 2100. The physiological and metabolic responses were then compared with the current climate represented by the year 2020. We found that the elevated CO_2 (eC) mitigated some of the effects of elevated temperature (eT) on physiological performance and metabolism. The metabolite profiling of leaves revealed 44 key metabolites, including saccharides, amino acids, and phenolics, accumulating contrastingly under individual regimes. These metabolites belong to the central metabolic pathways that are essential for cellular energy, production of biosynthetic pathways precursors, and oxidative balance. The interaction of eC alleviated the negative effect of eT possibly by maintaining the rate of carbon fixation and accumulation of key metabolites and intermediates linked with the Krebs cycle and synthesis of phenolics. Our study for the first time revealed the influence of a specific climate factor on the accumulation of metabolic compounds in wheat. The current work could assist in the understanding and development of climate resilient wheat by utilizing the identified metabolites as breeding targets for food and nutritional security.

KEYWORDS

climate change, wheat, metabolomics, physiology, elevated CO_2, temperature, drought

Introduction

Plants are sensitive to changes in temperature, water availability, and atmospheric CO_2 concentration (Thornton et al., 2014). As reported by the Intergovernmental Panel on Climate Change (IPCC), extreme climate events like heat waves and drought periods will become more intense and frequent, which could have devastating consequences on plant growth, development, and production (IPCC, 2018). The combinations of these climate factors may have even a more severe impact on food availability to the increasing world population. The strategy to improve the resilience of economically important crops has mostly relied on the screening of genotypes by exposing them to a single climate factor (e.g., drought, temperature, CO_2, etc.). However, the adaptive response under simultaneous exposure to multiple climate factors may vary widely, resulting in an undesired or failed crop selection process. Therefore, to prevent such crop failure in future, an assessment of the impact of combined treatments on plant's performance and adaptability is required.

Plants respond to stress by adjusting their morpho-physiological status such as by inhibiting photosynthesis (Jagtap et al., 1998), and/or altering vegetative growth and biomass allocation (Pandey et al., 2015). The molecular mechanisms of acclimation constitute the activation of genes for adaptive responses, such as the heat shock proteins (HSPs), and/or enzymes and additional transcripts facilitating detoxification and signaling of reactive oxygen species (ROS) (Rizhsky et al., 2004). In addition, under severe conditions, membrane, and protein damage lead to the accumulation of lipid peroxidation products (Jiang and Huang, 2001). This induces altered redox homeostasis and increase in ROS and consequently enhanced cellular oxidative damage (Krasensky and Jonak, 2012; Munné-Bosch et al., 2012). In addition, a wide range of different metabolites such as primary metabolites (carbohydrates, tricarboxylic acid cycle intermediates, and amino acids) essential for the growth and development, secondary metabolites (phenolics, terpenes, and nitrogen-containing compounds) along with the hormones (such as abscisic acid, jasmonic acid, salicylic acid, and ethylene) are also produced to regulate plant climate response (Fang et al., 2019; Kumar et al., 2020; Kumari et al., 2020). The primary metabolites, such as amino acids, play a pivotal role in enhancing fitness under various environmental cues. For example, the accumulation of amino acid proline is considered an indicator of adaptive behavior of plants exposed to various abiotic factors (Hayat et al., 2012; Fàbregas and Fernie, 2019; Girija et al., 2022). It helps in the maintenance of cell turgidity and reduction in electrolyte leakage to prevent cellular oxidative bursts (Hayat et al., 2012). Besides being the major metabolic resource and structural constituent of cells, carbohydrates such as sucrose and hexoses, also regulate stress-signaling and control the expression of growth as well as stress-related genes (Rosa et al., 2009). The TCA cycle intermediates are also involved in providing environmental stress tolerance attributes (Tahjib-Ul-Arif et al., 2021) and their accumulation under drought and heat stress has been reported to assist in the maintenance of physiological performance by regulating the photosynthetic rates and cellular redox status (Fernie et al., 2004; Das et al., 2017). On the other hand, secondary metabolites mitigate the plant's survival by protecting it from adverse environments (Agostini-Costa et al., 2012; Kurepin et al., 2017). For example, the antioxidants nature of flavonoids (a major class of phenylpropanoids) regulates various functions such as maintaining water homeostasis (Naing and Kim, 2021), and stomatal dynamics (Li et al., 2021) to improve the crop stress adaptability.

Identification of changes in the composition of such key compounds and derivate through the metabolomic approach serves as a powerful strategy to advance our understanding of the adaptation responses in plants (Obata and Fernie, 2012; Sardans et al., 2020; Girija et al., 2022). Various studies have provided novel insights into the metabolic signature among crop species (e.g., rice, maize, and wheat) wide-ranging across growth stages and genotypes (Peng et al., 2017; Xu et al., 2019; Chen et al., 2020). However, investigating the effects of climate change is complex because multiple interactions between various environmental factors could prompt unique shifts in the biochemical composition. A recent study in Arabidopsis revealed the difference in the metabolite accumulations under single and multi-climate factors (Zinta et al., 2018). While elevated CO_2 was found to largely enhance the cellular concentration of saccharides and amino acids, the combination with other factors caused the opposite effect on the accumulation of these compounds. Very few studies have been done to identify the shifts in metabolite pattern under combined heat and drought stress, particularly in crops (Obata et al., 2015; Templer et al., 2017). These studies revealed that most of the metabolic changes are additive, i.e., represent the sum of responses to the individual factors, and drought contributed most to such changes.

Bread wheat (*Triticum aestivum*) is a major cereal crop and widely cultivated for its grains (Shewry, 2009). The climate variability risks the livelihood and food security of about ~2 billion people who rely on wheat globally. The decline in the climate resilience of most of the wheat cultivars in the last 15 years was already observed in Europe, due to the repeated selection for few desirable traits (Kahiluoto et al., 2019). As most traits are complex and multigenic in nature, impact assessment of environmental stress on wheat crop relies not only on the type of factor exposed but also on its phenological growth stage. For example, the water availability at tillering is a critical phase in terms of grain yield potential (Curtis et al., 2002). Depending upon the severity and duration of drought stress, flowering and grain-filling phases are also considered as key stages which may result in the substantial yield loss (Farooq

et al., 2014). The flowering stage is more sensitive to temperature stress which regulates the seed-setting and grain quality (Aiqing et al., 2018). The sensitivity of wheat to any of these climate variables can result in altered metabolic processes coupled with lower biomass accumulation and grain yield (Ihsan et al., 2016). Despite the advancement in knowledge, the impact of climate factor combinations on metabolite accumulation in wheat remains ambiguous. Therefore, considering its economic importance, we aimed to examine its acclimation responses to current as well as future climate scenarios by using an experimental model of single and combined climate treatments. This work allowed us to identify the most important compounds contributing to metabolome variations in wheat leaves under multifactorial treatments and their potential to the risks associated with climate change. The key metabolites and pathways identified in this study could be the potential targets to understand their future climate-induced regulation, and development of nutritionally enriched crops.

Materials and methods

Experimental regimes and plant growth set-up

The experiment started with setting climate conditions representing the typical growth environment of Central Europe for spring wheat. Three major climate variables representing key factors associated with an ongoing climate change, i.e., air temperature, water availability and atmospheric CO_2 concentration were used. The data for air temperature (daily maximum, minimum and average) representing the years 2020 (current) and 2100 (future) were retrieved from the World Bank portal (https://climateknowledgeportal.worldbank.org/country/czech-republic/climate-data-projections). For the control set-up, an hourly dynamic of temperature (ambient temperature; aT; maximum/minimum= 24/10°C), constant CO_2 concentration (ambient CO_2; aC; 400 ± 50 ppm) and well-watered soil (water holding capacity; WHC = 90 ± 5%) conditions were maintained to mimic the environment for the year 2020. To understand the influence of individual climate variables and their combinations on acclimation responses in the year 2100, seven experimental setups were used. These included single factor treatments comprising of elevated temperature (eT), elevated CO_2 (eC) and drought (D), and combinations of two-factors (eT+D, eC+D, eC+eT) and three-factors (eC+eT+D). For these setups, the chambers were enabled with the daily air temperature of maximum/minimum= 28/12°C (eT) and CO_2 concentration of 700 ppm (eC). The applied 700 ppm CO_2 concentration as an elevated condition was based on the projections for year 2100 (Meehl et al., 2007) as well as previous studies (Reyenga et al., 2001; Jauregui et al., 2015; Soba et al., 2019). Further, a progressive drought was applied by with-holding the water supply after 7 days of optimization until WHC reached 25 ± 5% and kept constant thereafter throughout the experiment. As each setup had different evaporation rates, a minimum of 10-days continuous drought was applied depending upon the onset of 25% WHC. The pattern of daily changes in the relative humidity (RH; maximum day/night, 65/90%), maximum day light intensity (800 µmol/m^2/s) and light duration (15/9 h) were kept as constant for all experimental set-ups. The selection of light intensity (800 µmol/m^2/s) was based on previous studies conducted on wheat to study the impact of single or multiple climate factors in a growth cabinet conditions (Nuttall et al., 2018; Chavan et al., 2019).

The spring wheat cultivar Cadenza was selected for our study as it the most widely used research variety (Fernández-Gómez et al., 2020) and genomic resources are also available for further study (Walkowiak et al., 2020). Seeds after stratification (4°C/48 h) and germination (24°C/48 h) were planted in the standard substrate (TS2; Klasmann-Deilmann, Geeste, Germany). Pots (dimension: 11×11×25 cm) containing the seedlings were later transferred to climate chambers (FytoScope FS-SI 3400; PSI, Drásov, Czech Republic) for respective treatments. Seedlings were initially allowed to optimize for seven days under temperature (daily maximum/minimum= 15/10°C), constant CO_2 concentration (400 ± 50 ppm), RH (daily minimum/maximum, 65/90%), maximum/minimum light intensity (800/0 µmol/m^2/s), light duration (15/9 h) and water saturated conditions. Afterwards, they were subjected to the control and treatment/experimental set-ups (detailed above) with each setup containing at least three plants per treatment (n=3). All physiological measurements and sampling for metabolite profiling were done on the youngest fully developed leaves (second from the top) of the primary shoot at end of the tillering stage (Feekes-6) as it is an agronomically important developmental stage that contributes to grain productivity (Khadka et al., 2020). All samplings and measurements were conducted between 11.00 and 14.00 hours Central European Time (CET), when the temperature and light intensity reached maxima and relative air humidity reached a minimum for the day.

Physiological measurements

The measurements of photosynthesis and photosynthesis-related processes were done using Li-6800 gas-exchange system (LI-COR Biosciences, Lincoln, Nebraska, USA). To determine light-saturated CO_2 assimilation rate (A), stomatal conductance (Gsw), transpiration rate (Tr), and water use efficiency (WUE = A/Tr) the leaves investigated were exposed to the light intensity of 1200 µmol/m^2/s, while other microclimatic conditions inside the assimilation chamber were kept constant corresponding to daily maxima of individual treatments: CO_2 concentration (400 ppm or 700 ppm for aC and eC regimes, respectively), leaf temperature

(24°C or 28°C) and VPD (1.04 kPa and 1.32 kPa for aT and eT regimes, respectively). The measurements were conducted on three biological replicates. All data after testing for normal distribution were subject to one- or two-way analysis of variance (ANOVA) followed by *post-hoc* comparison using Tukey's multiple range test ($P \leq 0.05$). Principal component analysis (PCA) was used to analyze relations between variables. All statistical analyses were performed using the STATISTICA package version 12 (Stat Soft, Tulsa, Oklahoma, USA).

Metabolite profiling of wheat leaf at vegetative stage

The metabolomic analysis was performed using the established protocol for the metabolic studies in cereals in the laboratory of metabolomics and isotopic analyses at the CzechGlobe (Klem et al., 2019). Briefly, detached leaves at 25-days post-treatments were immediately stored in liquid nitrogen. Lyophilized samples (100 mg dry weight) were subsequently homogenized and extracted using a methanol: chloroform: H_2O solution (1:2:2). Aliquots of the polar phase were used to analyze saccharides, phenolic compounds, amino acids, phytohormones, and Krebs cycle intermediates employing an UltiMate 3000 system of high-performance liquid chromatography (HPLC) coupled with an LTQ Orbitrap XL high-resolution mass spectrometer (HRMS) (ThermoFisher Scientific, Waltham, Massachusetts, USA). The HRMS is equipped with a heated electrospray ionization source and was operated in full scan mode with a resolution of 60000. For the separation of individual compounds, a Hypersil GOLD chromatographic column (ThermoFisher Scientific, Waltham, Massachusetts, USA) of 150 mm (length), 2.1 mm (ID), and 3 µm (film thickness) was used. Moreover, gas chromatography coupled with mass spectrometry (GC-MS) was employed to analyze a spectrum of fatty acids, sterols, saccharides, and other non-polar compounds. Analyses were performed with a TSQ Quantum XLS triple Quadrupole (ThermoFisher Scientific, Waltham, Massachusetts, USA) on a Rxi-5Sil MS capillary column (Restek, Bellefonte, Pennsylvania, USA) of 30 m (length) with 5 m of integra-Guard, 0.25 mm (ID) and 0.25 µm (film thickness). The compounds detected by the chromatography were identified based on the comparison with the own mass library which had been created from the measurement of standards using HPLC-HRMS and GC-MS in full scan mode and containing about 300 compounds. The statistical analysis such as partial least squares discriminant analysis (PLS-DA), mean decrease accuracy (MDA), one-way ANOVA of the identified metabolites was done using MetaboAnalyst software (Pang et al., 2021). Correlation analyses were performed using the STATISTICA package version 12 (Stat Soft, Tulsa, Oklahoma, USA).

Results

Setting the regimes to study the impact of climate

As predicted by RCP 8.5 scenarios of IPCC, temperature, drought, and atmospheric CO_2 concentration were used as the three major factors to study the impact of climate change (Figure 1A). Current (2020) and expected future (2100) growing conditions in Central Europe corresponding to June were simulated as described in the materials and methods. The growth of plants was monitored regularly until 25 day-post treatment (DPT). The tiller and leaf number were counted after 25 DPT, however, there was no significant difference at this stage (Figure 1B).

Concentration of CO_2 determines the physiological responses

It was revealed that the pattern of change in the physiological parameters was mostly treatment-specific (Figures 2A–E). The variance (PC1 ~86%) was clearly observable due to the effect of eT (Figure 2A). Transpiration rate (*Tr*) and stomatal conductance (*Gsw*) significantly declined ($P \leq 0.05$) under eC, eC+eT and eC+D treatments in comparison to the control condition (Figures 2B, C). There was no clear trend in the pattern of the photosynthesis rate (*A*) except for an increase under eC and eC+eT+D conditions (Figure 2D). On the contrary, eC+eT treatment led to a significant reduction of *A* values. Noticeably, eC alone or in combinations with other factors significantly ($P \leq 0.05$) increased the water use efficiency (WUE), although this effect was less pronounced under eC+eT+D condition. These findings indicate a critical role of CO_2 concentration in the adjusting of physiological state under future conditions.

Metabolites accumulate differentially under various regimes

Overall, 77 metabolites were identified by GC-MS and HPLC-HRMS analysis among the leaf samples exposed to different climate regimes (Supplementary Table 1). Out of these, 44 metabolites significantly ($P \leq 0.05$) varied among the treatments (Supplementary Table 2). The most influenced metabolite groups included amino acids (16), Krebs cycle intermediates (8), phenolics (10), saccharides (4), fatty acids (3) and nitrogenous bases (3) (Supplementary Table 2). A distinct separation of metabolites between the regimes with *aT* and those with *eT* was observed, accounting for ~20% of the variation (PC1; Figure 3A). This finding indicates that

10.3389/fpls.2022.1002561

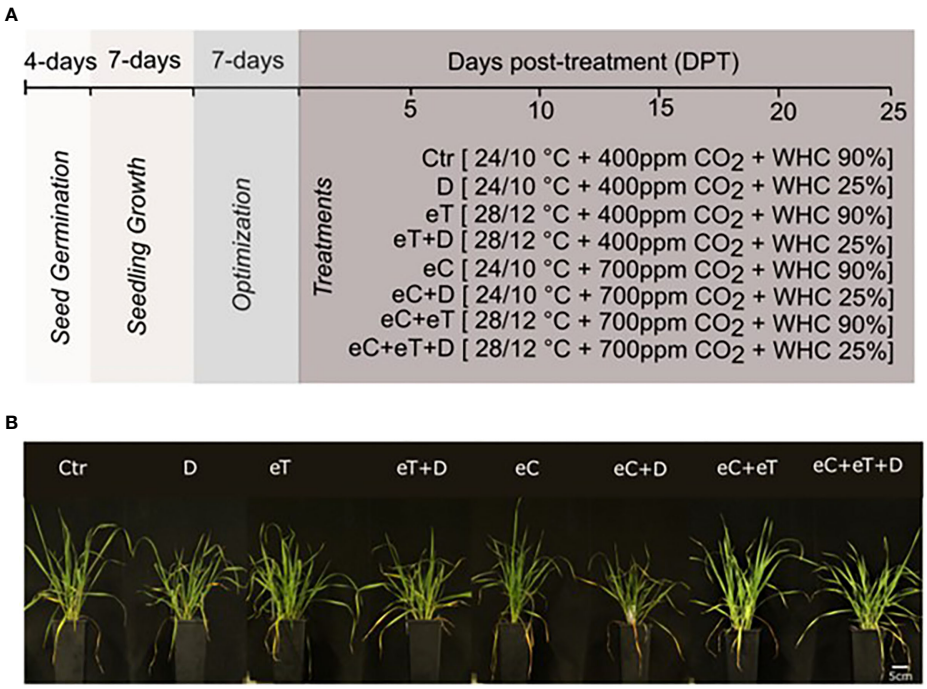

FIGURE 1
A schematic representation of experimental pipeline and developmental changes monitored in wheat cv. Cadenza. **(A)** Climate setup. Experimental setup to mimic the natural daily temperature dynamics (Tmax/Tmin) in June of years 2020 and 2100, atmospheric CO_2 concentration [ambient (400 ppm) and elevated (700 ppm)] and water availability [water holding capacity (WHC) at 25 ± 5% (Drought, D) and 90 ± 5% (water saturated pots)]. The symbol of ± indicates fluctuations in the parameters. **(B)** Phenotypic differences observed at 25 DPT showing the variable effects of treatments. The bar scale represents 5 cm. Ctr, control treatment; eC, elevated CO_2; eT, elevated temperature; D, drought; eC+eT, elevated CO_2 and elevated temperature; eC+D, elevated CO_2 and drought; eT+D, elevated temperature and drought; eC+eT+D, elevated CO_2, elevated temperature, and drought.

temperature has a strong effect on the metabolome. The main reasons for the metabolite differences in different regimes were identified by Partial least square discriminant analysis (PLS-DA). Based on their VIP scores, which is the measure of a variable's importance, the metabolites such as tyrosin (Tyr), ferulic acid (Feru), pyruvic acid (Pyru), 3-hydroxybenzoic acid (3hyd), epigallocatechin gallate (Epgg), guanine (G), uracil (U), and thymidine monophosphate (TMP) showed largest differences among all the regimes (Figure 3B). Metabolites having VIP score >1.5 were considered significant (Figure 3C). The accumulation patterns of individual metabolite categories under the subjected regimes are described in detail below. Overall, the results show a treatment-specific accumulation of metabolites during the vegetative growth stage in spring wheat.

Out of 19 amino acids detected in the metabolite profiling, 16 amino acids were significantly ($P \leq 0.05$) accumulated among the treatments (Supplementary Table 2). These included branched chain amino acids (BCAAs) such as Leucine (Leu), aromatic (Tryptophan; Try, Phenylalanine; Phe, and Tyrosine; Tyr), hydrophilic-basic (Lysine; Lys, Arginine; Arg and Histidine; His) and hydrophobic (Glycine; Gly, Proline; Pro, Hydroxy-proline; Hpro, Methionine; Met) amino acids (Supplementary Table 2). The first component (46.8%) separated the *eT* and *eC* regimes from other treatments (Figure 4A). Further, PLS-DA analysis discriminated Tyr and hydrophilic-basic amino acids from the group of all amino acids (Figure 4B). The VIP score (>1.5; $P \leq 0.05$) suggested Tyr and Lys as the key amino acids that tend to accumulate under eT and eT+D conditions in comparison to Ctr and D regimes, respectively (Figure 4C). Proline and BCAAs which accumulated primarily under eC, eC+D and eC+eT+D regimes have been reported to have osmoregulatory roles (Girija et al., 2022). On the other hand, eC alleviated the effect of eT on the accumulation of amino acids, as the accumulation of Tyr and Lys decreased under eC+eT and eC+eT+D regimes when compared to *aC* counterparts (Figure 4C).

The metabolite profiling identified 10 phenolic compounds significantly ($P \leq 0.05$) accumulated among the treatments (Supplementary Table 2). The scores plot between the first and second components identified two distinct groups related to the *aT* and *eT* regimes (Figure 4A). Based on the PLS-DA and VIP scores, 3hyd, Feru, and Epgg were identified as the key metabolites varying under treatment conditions (Figure 4B). The accumulation of these phenolics was temperature-

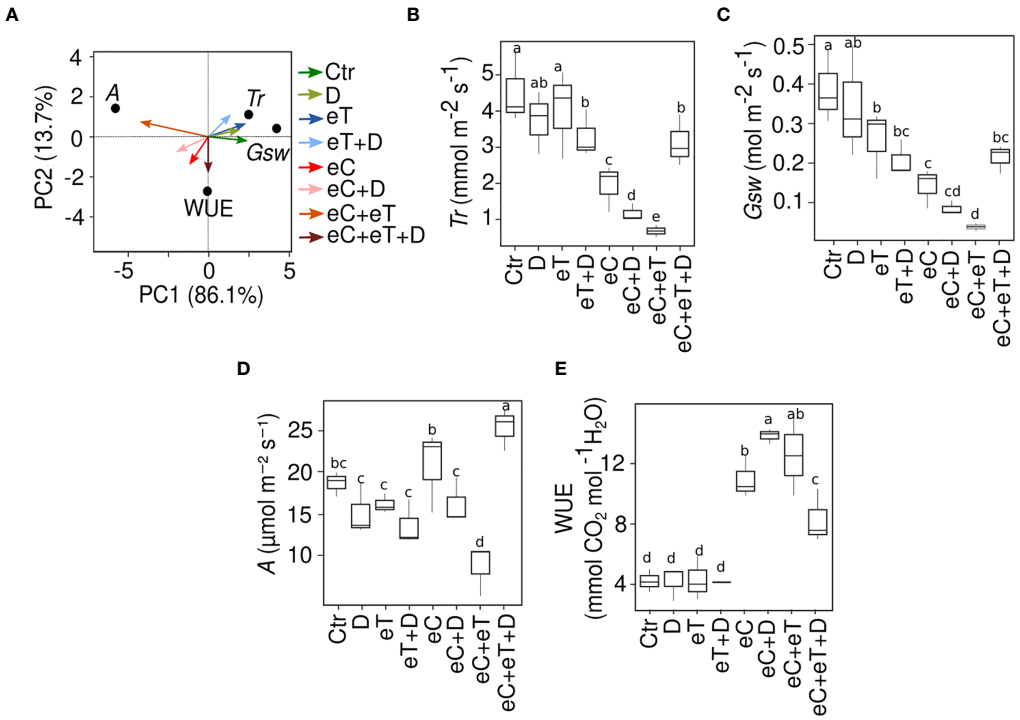

FIGURE 2
Impact of single and multiple climate variables on the physiology of wheat cv. Cadenza in tillering stage. **(A)** Principal component analysis plot of the physiological traits measured at 25 DPT. An account of **(B)** Transpiration rate, *Tr*; **(C)** Stomatal conductance, *Gsw*; **(D)** Rate of photosynthesis, *A*; **(E)** Water use efficiency, WUE, under single and combined climate variable treatments. Three biological replicates (n=3) per treatment were used to evaluate the physiological traits. The box plot shows the inter-quartile range with the mean. Values marked with the same letter do not differ according to Tukey's test multiple range tests ($P \leq 0.05$). Ctr, control treatment; eC, elevated CO_2; eT, elevated temperature; D, drought; eC+eT, elevated CO_2 and elevated temperature; eC+D, elevated CO_2, and drought; eT+D, elevated temperature, and drought; eC+eT+D, elevated CO_2, elevated temperature, and drought.

dependent and unlike amino acids, CO_2 exposure did not affect their abundance (Figure 4C). Compared with eT and eC, the effect of D on metabolome was minor or negligible.

One-way ANOVA revealed that all the Krebs cycle-related intermediates were significantly ($P \leq 0.05$) accumulated among the climate variable treatments (Supplementary Table 2). Similarly, to the phenolic compounds, the scores plot between the first and second components identified two distinct groups associated with the *aT* and *eT* regimes (Figure 4A). Acids, such as α-ketoglutaric (Ket), Pyru and malic acid (Mal), were discriminated from other Krebs cycle intermediates based on the PLS-DA and VIP score (Figure 4B). An eT treatment increased contents of Pyru and Ket, while the content of Mal decreased (Figure 4C).

Fructose (Fruc), glucose (Gluc), sucrose (Suc), and galactinol (Galc) were the most significantly ($P \leq 0.05$) accumulated saccharides among the climate variable treatments (Supplementary Table 2). The pattern of saccharide abundance showed two distinct groups associated with the *aC* and *eC* regimes (Figure 4A). Based on the PLS-DA and VIP score (> 1.0), Fruc and Gluc were identified as the most important saccharides whose abundance was mainly associated with the concentration of CO_2 (Figures 4B, C). Apart from the above metabolic compounds, nitrogenous bases such as uracil (U), guanine (G) and thymidine monophosphate (TMP) were found to be significantly ($P \leq 0.05$) accumulated (Supplementary Table 2). The most accumulated fatty acids at different regimes were identified to be linoleic acid (Lino), oleic acid (Olei), and palmitoleic acid (Palm) (Supplementary Table 2).

The correlation between the 44 significant metabolites and physiological traits was also evaluated. The analysis identified a significant negative correlation between the physiological traits (*Gsw* and *Tr*) and the accumulation of Fruc, Gluc, Arg, and shikimic acid (Shi) (Supplementary Table 3). Contrastingly, WUE showed positive correlation with these compounds.

Discussion

Changing environment causes profound physiological and metabolic changes in the plants (Gianoli and Molina-Montenegro, 2021; Zandalinas et al., 2022). While the recent

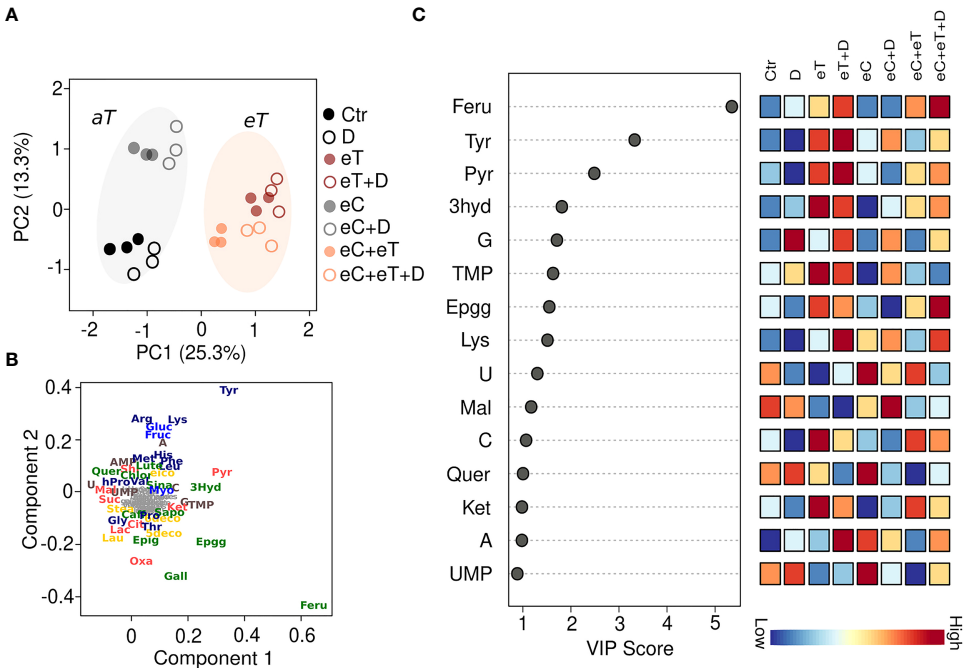

FIGURE 3
A supervised Partial Least Squares Discriminant Analysis (PLS-DA) of all the metabolites accumulated in the leaves of wheat cv. Cadenza after exposure to climate regimes. **(A)** Scores plot showing the distribution of metabolites based on the regimes. PC1 separated the metabolites based on the ambient (*aT*, gray circle) and elevated temperature (*eT*, orange circle). **(B)** Loading plot showing the metabolites discriminated based on PLS-DA. The metabolites such as phenolics (green), amino acids (dark blue), Krebs cycle intermediates (red), lipids (yellow) and nitrogenous bases (brown) have been shown. **(C)** The metabolites ranked by variable importance in projection (VIP). Ctr, control treatment; eC, elevated CO_2; eT, elevated temperature; D, drought; eC+eT, elevated CO_2 and elevated temperature; eC+ D, elevated CO_2 and drought; eT+D, elevated temperature and drought; eC+eT+D, elevated CO_2, elevated temperature and drought. The color code represents the specific metabolite families: dark blue, amino acid; light blue, saccharides; green, phenolics; yellow, fatty acids; red, Kreb's cycle acids; brown, nucleotides. Compounds in grey represent non-significant ($P \leq 0.05$) metabolites among the treatments identified by one-way ANOVA. Three biological replicates (n=3) per treatment were used in the study.

years have witnessed substantial advances in understanding the acclimation responses of wheat genotypes to various environmental drivers, most of the studies so far have mainly focused on single- or two-factor treatments, with limited possibility to assess the impacts of their mutual interactions (Zandalinas et al., 2018). Hence, the question of how plants will acclimate to a comprehensive future change in growth conditions is still far from complete. Therefore, understanding the underlying molecular mechanisms of adaptation response is crucial not only for the basic understanding of wheat stress response but also for applied wheat breeding. Through quantification of key metabolites, we reveal a differential metabolomic response against eight climate regimes (single and combined treatment) comprised of increased temperature, drought, and elevated CO_2 in spring wheat.

The general mechanism to cope with changes in the environment involves an adjustment in the physiological and molecular traits (Pandey et al., 2017; Sharma et al., 2021; Alamri et al., 2022; Sharma et al., 2022). The shift in physiological responses can be attributed to specific abiotic factors and their nature i.e., individual and combined (Zandalinas and Mittler, 2022). Gas exchange measurements suggested that at the single-factor level, the effect of eC was predominant and led to the significant changes in *Tr*, *Gsw* and WUE, while eT and D had only minor effects. Similar patterns of physiological traits were also observed under double-factor regimes combining elevated CO_2 with eT or D. As no prominent effect of eT and D on *Tr* and *Gsw* under aC was observed, this indicated that the response of these traits was mainly controlled by CO_2 enrichment either at higher temperatures or decreased soil water availability. However, the physiological pattern exhibited in single and double factor combinations inclusive of an eC regime (eC+D and eC+eT) were not replicated in the triple factor regime (eC+eT+D). This suggests that the effect of eC could have been compromised by the simultaneous counteraction of the other two factors (eT and D). Higher *A* and *Tr* were observed during eC+eT+D treatment. In general, eC and eT have opposing effects on *Tr* (Kirschbaum and McMillan, 2018). An increase in the temperature enhances the *Tr*, however,

10.3389/fpls.2022.1002561

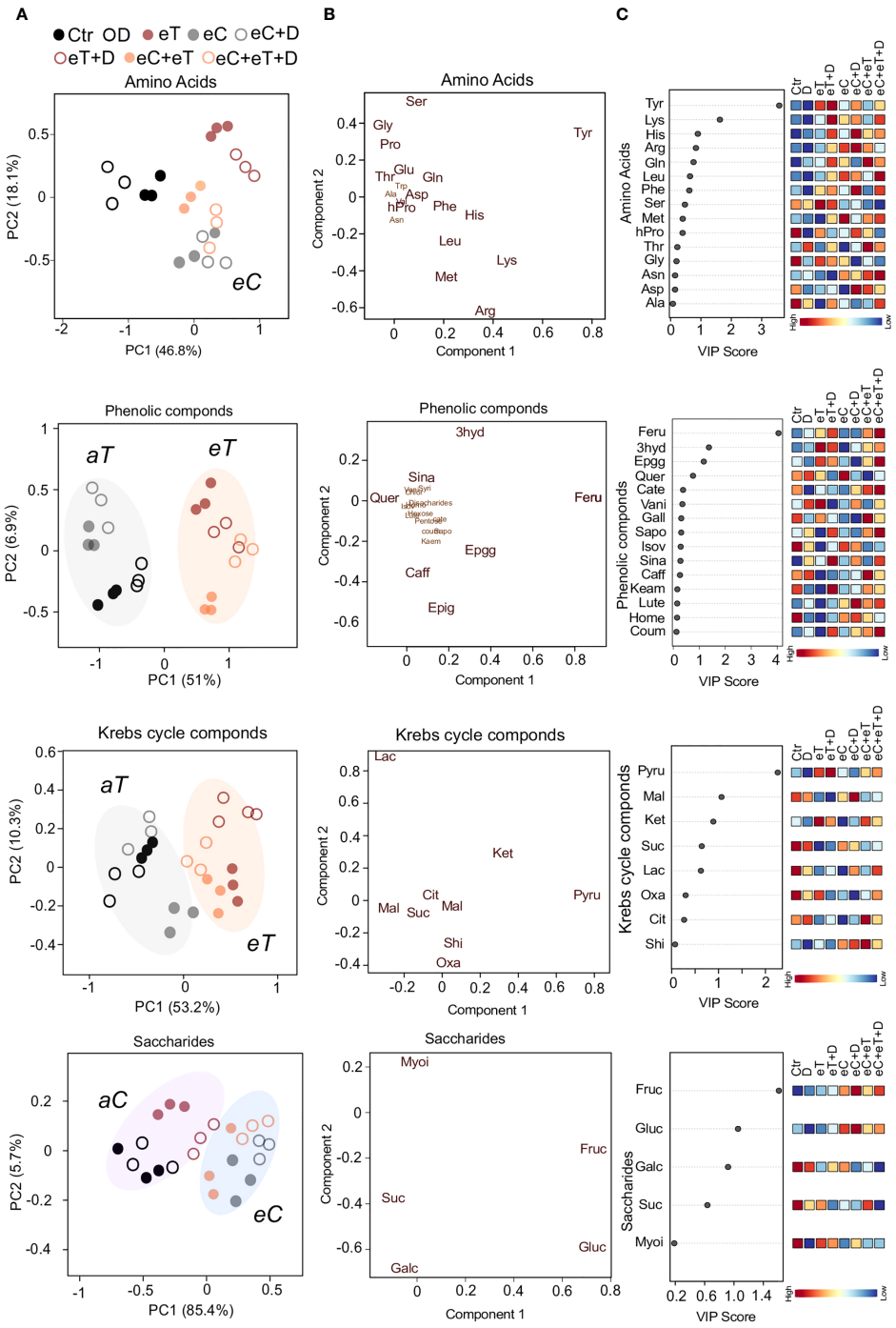

FIGURE 4
A supervised Partial Least Squares Discriminant Analysis (PLS-DA) of key metabolite categories accumulated in the leaves of wheat cv. Cadenza after exposure to climate regimes. **(A)** Scores plot showing the distribution of metabolites (amino acids; phenolics, Krebs cycle intermediates; saccharides) based on the regimes. Component 1 separated the metabolites based on the ambient temperature (aT, gray circle), elevated temperature (*eT*, orange circle). Ambient CO_2 (*aC*, purple circle), and elevated CO_2 concentrations (eC, blue circle). **(B)** Loading plot showing the metabolites (amino acids; phenolics, Krebs cycle intermediates; saccharides) discriminated based on PLS-DA. The metabolites in the bigger font significantly ($P \leq 0.05$) varied among the treatments. **(C)** The metabolites ranked by variable importance in projection (VIP). Scale bar represents high and low VIP scores corresponding to the metabolites. Ctr, control treatment; eC, elevated CO_2; eT, elevated temperature; D, drought; eC+eT, elevated CO_2 and elevated temperature; eC+ D, elevated CO_2 and drought; eT+D, elevated temperature and drought; eC+eT+D, elevated CO_2, elevated temperature and drought. Abbreviations of the metabolites are provided in Supplementary Table 1.

due to partial stomatal closure under high CO_2 concentration environment, a reduction in the *Tr* could be expected (Kirschbaum and McMillan, 2018). The increase in *Tr* under eC+eT+D in our study could be due to the influence of D, which could have helped to curtail the damage to the photosynthesis process (indicated by high *A*) through an evaporative cooling mechanism (Šigut et al., 2015).

The next focus was on investigating the metabolite accumulation to understand their role in plant acclimation under various regimes. The metabolic change patterns were highly treatment specific. For example, eC dominantly controlled the accumulation of soluble monosaccharides (Gluc and Fruc). A concomitant increase in the photosynthetic activity (*A*) was also observed in eC and the triple factor combinations eC+eT+D (Figure 2D). As monosaccharides are critical molecules for the primary carbon metabolism and the first substrates for starch biosynthesis, these results indicate that the accumulation of Gluc corresponded to the supplementary carbon fixation in these samples. The effect of higher CO_2 concentration on the accumulation of compounds related to the sugar metabolites has also been reported in Arabidopsis thaliana (Ainsworth and Rogers, 2007; Zinta et al., 2018), and crops like wheat (Levine et al., 2008) and rice (Ainsworth, 2008). Moreover, saccharides are well known to regulate the rate of transpiration, particularly *via* stomatal dynamics (Li et al., 2018). The significant correlation identified in this study between the Gluc and Fruc accumulation with *Tr* and WUE of wheat leaves under various regimes could be attributed to the stomatal function.

On the other hand, metabolites associated with the Krebs cycle and phenolics were found to be mostly dependent on the exposure of temperature (Figure 4). High-temperature stress has been found to affect the levels of pyruvic acid, fumarate, malate, and citrate in poplar and soybean (Sicher, 2013; Ren et al., 2019). The spring wheat may have an inherent capacity to withstand the projected temperature increase (4°C) in the future climate by limiting the conversion of soluble sugars to organic acids of the Krebs cycle and secondary metabolites during elevated temperatures. The increase of carbon flux under eC conditions may then be utilized for synthesizing the compounds needed for acclimation responses and defense mechanisms as has been reported previously (Kiani-Pouya et al., 2017). Moreover, at the molecular level, the expression of genes linked with saccharides, Krebs cycle intermediates, and phenolics changes dynamically upon exposure to climate change-related factors (Krasensky and Jonak, 2012; Glaubitz et al., 2015; Xalxo et al., 2020). This may consequently facilitate modifications in the levels of many saccharides and phenolic compounds imparting specific acclimation responses. Accumulation of Feru (important for cell wall rigidity and strength), 3hyd (potential antioxidant), and Epgg (flavonoid) was dominantly controlled by the high temperature (Figure 4), suggesting that these compounds may help to maintain the cellular integrity and functionality during interaction with the environment.

Amino acids are an important molecular form of organic nitrogen in plants acting as intermediates for many metabolic reactions (Trovato et al., 2021). The pattern of amino acid accumulation exhibited a unique trend where eT played a pivotal role in the accumulation of amino acids like Tyr and Lys, but their enhanced accumulation pattern diminished when combined with eCO_2 (Figure 4). CO_2 enrichment has been previously shown to reverse the effects of elevated growth temperatures on many soluble amino acids in soybean leaves (Sicher, 2013). Noticeably, the level of amino acid and Krebs cycle intermediates showed contrasting patterns in eT and eC regimes, suggesting that a subtle balance may exist between these pathways.

In general, phenolics play a pivotal role in plants as antioxidants to scavenge the ROS upon exposure to abiotic stresses (Rice-Evans et al., 1997). The increase in their cellular concentration suggests the activation of redox homeostasis to protect against the possible damage to proteins and lipids (Awasthi et al., 2015). Similar to our study, an increase in the production of phenolics, and particularly flavonoids, under heat stress has been reported previously (Wu et al., 2016). Overall, these results show that the differential accumulation of metabolites regulates plastic response under future climate scenarios.

Our study represents a comprehensive analysis of metabolite homeostasis under different climate scenarios. This study highlighted that the metabolomic acclimation of spring wheat to a single and combination of climate factors is mainly associated with temperature and CO_2 concentration. An environment with elevated CO_2 mitigated some of the effects of elevated temperature on physiological performance and metabolism possibly by maintaining the rate of carbon fixation and accumulation of key metabolites and intermediates linked with sugar metabolism, Krebs cycle, and synthesis of phenolics. Usually, drought stress is manifested by substantial changes in plant metabolome including changes in simple saccharides that have a role of osmolytes. However, in this study, the effect of D on physiology and metabolome was minor/negligible. It is possible that the drought exposure applied to the targetted stage (Feekes-6) was likely mild, or for a short duration. In conclusion, the key metabolites and pathways identified in this study and their interactions with climate variables will be helpful in understanding their future climate-induced regulation and the manipulations of potential targets for the development of climate resilient and nutritionally enriched wheat crops (Irfan and Datta, 2017). Further, a better understanding of these strategies can provide

an impetus to research on gene function discovery and biochemical evolution, which is foundational for improved metabolic engineering.

Data availability statement

The original contributions presented in the study are included in the article/Supplementary Material. Further inquiries can be directed to the corresponding author.

Author contributions

PPS and KK conceptualized the research. KV, SP, MO, HF, BV, EO, KKO-A, and PPS were involved in the methodology and analysis. SP, KV, PPS, OU and KK wrote and edited the manuscript. All authors have read and agreed to the final version of the manuscript.

Funding

This research was funded by Czech Science Foundation, grant no. 20-25845Y (awarded to PPS). A part of the research was also supported by the project SustES "Adaptation strategies for sustainable ecosystem services and food security under adverse environmental conditions" (CZ.02.1.01/0.0/0.0/16_019/0000797) to SP, BV, OU and KK. Infrastructure facilities used in the experiments were supported by the Ministry of Education, Youth and Sports of CR within the CzeCOS program, grant number LM2018123HF.

Acknowledgments

We express our gratitude to the Prof. RNDr. Ing. Michal V. Marek, Director of the Global Change Research Institute CAS, Brno for providing access to the necessary facilities and support.

Conflict of interest

The authors declare that the research was conducted in the absence of any commercial or financial relationships that could be construed as a potential conflict of interest.

Publisher's note

All claims expressed in this article are solely those of the authors and do not necessarily represent those of their affiliated organizations, or those of the publisher, the editors and the reviewers. Any product that may be evaluated in this article, or claim that may be made by its manufacturer, is not guaranteed or endorsed by the publisher.

Supplementary material

The Supplementary Material for this article can be found online at: https://www.frontiersin.org/articles/10.3389/fpls.2022.1002561/full#supplementary-material

References

Agostini-Costa, S., da, T., F., R., R., H., and Silveira, D. (2012). "Secondary metabolites," in *Chromatography and its applications* (London, UK: InTech). XXXA., M. doi: 10.5772/35705

Ainsworth, E. A. (2008). Rice production in a changing climate: A meta-analysis of responses to elevated carbon dioxide and elevated ozone concentration. *Global Change Biol.* 14, 1642–1650. doi: 10.1111/j.1365-2486.2008.01594.x

Ainsworth, E. A., and Rogers, A. (2007). The response of photosynthesis and stomatal conductance to rising [CO_2]: Mechanisms and environmental interactions. *Plant Cell Environ.* 30, 258–270. doi: 10.1111/j.1365-3040.2007.01641.x

Aiqing, S., Somayanda, I., Sebastian, S. V., Singh, K., Gill, K., Prasad, P. V. V., et al. (2018). Heat stress during flowering affects time of day of flowering, seed set, and grain quality in spring wheat. *Crop Sci.* 58, 380–392. doi: 10.2135/cropsci2017.04.0221

Alamri, S., Siddiqui, M. H., Mukherjee, S., Kumar, R., Kalaji, H. M., Irfan, M., et al. (2022). *Molybdenum-induced endogenous nitric oxide (NO) signaling coordinately enhances resilience through chlorophyll metabolism, osmolyte accumulation and antioxidant system in arsenate stressed-wheat (Triticum aestivum l.) seedlings, environmental pollution*, Vol. 292. 269–7491. doi: 10.1016/j.envpol.2021.118268

Awasthi, R., Bhandari, K., and Nayyar, H. (2015). Temperature stress and redox homeostasis in agricultural crops. *Front. Environ. Sci.* 3. doi: 10.3389/fenvs.2015.00011

Chavan, S. G., Duursma, R. A., Tausz, M., and Ghannoum, O. (2019). Elevated CO_2 alleviates the negative impact of heat stress on wheat physiology but not on grain yield. *J. Exp. Bot.* 70, 6447–6459. doi: 10.1093/jxb/erz386

Chen, J., Hu, X., Shi, T., Yin, H., Sun, D., Hao, Y., et al. (2020). Metabolite-based genome-wide association study enables dissection of the flavonoid decoration pathway of wheat kernels. *Plant Biotechnol. J.* 18, 1722–1735. doi: 10.1111/pbi.13335

Das, A., Rushton, P., and Rohila, J. (2017). Metabolomic profiling of soybeans (Glycine max L) reveals the importance of sugar and nitrogen metabolism under drought and heat stress. *Plants.* 6, 21. doi: 10.3390/plants6020021

Fàbregas, N., and Fernie, A. R. (2019). The metabolic response to drought. *J. Exp. Bot.* 70, 1077–1085. doi: 10.1093/jxb/ery437

Fang, C., Fernie, A. R., and Luo, J. (2019). Exploring the diversity of plant metabolism. *Trends Plant Sci.* 24, 83–98. doi: 10.1016/j.tplants.2018.09.006

Curtis, B. C., and Rajaram, S. (2002). Bread wheat: Improvement and production,". (Rome: Food and Agriculture Organization of the United Nations), 554.

Farooq, M., Hussain, M., and Siddique, K. H. M. (2014). Drought stress in wheat during flowering and grain-filling periods. *Crit. Rev. Plant Sci.* 33, 331–349. doi: 10.1080/07352689.2014.875291

Fernández-Gómez, J., Talle, B., Tidy, A. C., and Wilson, Z. A. (2020). Accurate staging of reproduction development in cadenza wheat by non-destructive spike analysis. *J. Exp. Bot.* 71, 3475–3484. doi: 10.1093/jxb/eraa156

Fernie, A. R., Carrari, F., and Sweetlove, L. J. (2004). Respiratory metabolism: glycolysis, the TCA cycle and mitochondrial electron transport. *Curr. Opin. Plant Biol.* 7, 254–261. doi: 10.1016/j.pbi.2004.03.007

Gianoli, E., and Molina-Montenegro, M. A. (2021). Evolution of physiological performance in invasive plants under climate change. *Evolution* 75, 3181–3190. doi: 10.1111/evo.14314

Girija, A., Han, J., Corke, F., Brook, J., Doonan, J., Yadav, R., et al. (2022). Elucidating drought responsive networks in tef (*Eragrostis tef*) using phenomic and metabolomic approaches. *Physiologia Plantarum*. 174, e13597. doi: 10.1111/ppl.13597

Glaubitz, U., Erban, A., Kopka, J., Hincha, D.K., and Zuther, E.. (2015). High night temperature strongly impacts TCA cycle, amino acid and polyamine biosynthetic pathways in rice in a sensitivity-dependent manner. *Journal of Experimental Botany*. 66, 6385–6397. doi: 10.1093/jxb/erv352

Hayat, S., Hayat, Q., Alyemeni, M. N., Wani, A. S., Pichtel, J., and Ahmad, A. (2012). Role of proline under changing environments. *Plant Signaling Behav*. 7, 1456–1466. doi: 10.4161/psb.21949

Ihsan, M. Z., El-Nakhlawy, F. S., Ismail, S. M., Fahad, S., and Daur, I. (2016). Wheat phenological development and growth studies as affected by drought and late season high temperature stress under arid environment. *Front. Plant Sci.* 7. doi: 10.3389/fpls.2016.00795

IPCC (2018). *Summary for policymakers- global warming of 1.5°C*. An IPCC Special Report on the impacts of global warming of 1.5°C above pre-industrial levels and related global greenhouse gas emission pathways, in the context of strengthening the global response to the threat of climate change, sustainable development, and efforts to eradicate poverty. V. Masson-Delmotte, P. Zhai, H.-O. Pörtner, D. Roberts, J. Skea, P.R. Shukla, et al (Geneva, Switzerland: World Meteorological Organization)

Irfan, M., and Datta, A. (2017). Improving food nutritional quality and productivity through genetic engineering. *Int. J. Cell Sci. Mol. Biol.* 2, 555576. doi: 10.19080/IJCSMB.2017.02.555576

Jagtap, V., Bhargava, S., Streb, P., and Feierabend, J. (1998). Comparative effect of water, heat and light stresses on photosynthetic reactions in *Sorghum bicolor* (L.) moench. *J. Exp. Bot.* 49, 1715–1721. doi: 10.1093/jxb/49.327.1715

Jauregui, I., Aroca, R., Garnica, M., Zamarreño, Á.M., García-Mina, J. M., Serret, M. D., et al. (2015). Nitrogen assimilation and transpiration: Key processes conditioning responsiveness of wheat to elevated [CO_2] and temperature. *Physiologia Plantarum*. 155, 338–354. doi: 10.1111/ppl.12345

Jiang, Y., and Huang, B. (2001). Drought and heat stress injury to two cool-season turfgrasses in relation to antioxidant metabolism and lipid peroxidation. *Crop Sci.* 41, 436–442. doi: 10.2135/cropsci2001.412436x

Kahiluoto, H., Kaseva, J., Balek, J., Olesen, J. E., Ruiz-Ramos, M., Gobin, A., et al. (2019). Decline in climate resilience of european wheat. *Proc. Natl. Acad. Sci. United States America*. 116, 123–128. doi: 10.1073/pnas.1804387115

Khadka, K., Earl, H. J., Raizada, M. N., and Navabi, A. (2020). A physio-morphological trait-based approach for breeding drought tolerant wheat. *Front. Plant Sci.* 11. doi: 10.3389/fpls.2020.00715

Kiani-Pouya, A., Roessner, U., Jayasinghe, N. S., Lutz, A., Rupasinghe, T., Bazihizina, N., et al. (2017). Epidermal bladder cells confer salinity stress tolerance in the halophyte quinoa and atriplex species. *Plant Cell Environ*. 40, 1900–1915. doi: 10.1111/pce.12995

Kirschbaum, M. U. F., and McMillan, A. M. S. (2018). Warming and elevated CO_2 have opposing influences on transpiration. Which is more important? *Curr. Forestry Rep*. 4, 51–71. doi: 10.1007/s40725-018-0073-8

Klem, K., Gargallo-Garriga, A., Rattanapichai, W., Oravec, M., Holub, P., Veselá, B., et al. (2019). Distinct morphological, physiological, and biochemical responses to light quality in barley leaves and roots. *Front. Plant Sci.* 10. doi: 10.3389/fpls.2019.01026

Krasensky, J., and Jonak, C. (2012). Drought, salt, and temperature stress-induced metabolic rearrangements and regulatory networks. *J. Exp. Bot.* 63, 1593–1608. doi: 10.1093/jxb/err460

Kumari, M., Joshi, R., and Kumar, R. (2020). Metabolic signatures provide novel insights to picrorhiza kurroa adaptation along the altitude in Himalayan region. *Metabolomics*. 16, 77. doi: 10.1007/s11306-020-01698-8

Kumar, R., Joshi, R., Kumari, M., Thakur, R., Kumar, D., and Kumar, S. (2020). Elevated CO_2 and temperature influence key proteins and metabolites associated with photosynthesis, antioxidant and carbon metabolism in *Picrorhiza kurroa*. *J. Proteomics*. 219, 103755. doi: 10.1016/j.jprot.2020.103755

Kurepin, L. V., Ivanov, A. G., Zaman, M., Pharis, R. P., Hurry, V., and Hüner, N. P. A. (2017). "Interaction of glycine betaine and plant hormones: protection of the photosynthetic apparatus during abiotic stress," in *Photosynthesis: Structures, mechanisms, and applications* eds. Hou, H., Najafpour, M., Moore, G, and Allakhverdiev, S. (Cham: Springer International Publishing), 185–202. doi: 10.1007/978-3-319-48873-8_9

Levine, L. H., Kasahara, H., Kopka, J., Erban, A., Fehrl, I., Kaplan, F., et al. (2008). Physiologic and metabolic responses of wheat seedlings to elevated and super-elevated carbon dioxide. *Adv. Space Res.* 42, 1917–1928. doi: 10.1016/j.asr.2008.07.014

Li, B., Fan, R., Sun, G., Sun, T., Fan, Y., Bai, S., et al. (2021). Flavonoids improve drought tolerance of maize seedlings by regulating the homeostasis of reactive oxygen species. *Plant Soil*. 461, 389–405. doi: 10.1007/s11104-020-04814-8

Li, Y., Xu, S., Wang, Z., He, L., Xu, K., and Wang, G. (2018). Glucose triggers stomatal closure mediated by basal signaling through HXK1 and PYR/RCAR receptors in arabidopsis. *J. Exp. Bot.* 69, 1471–1484. doi: 10.1093/jxb/ery024

Meehl, G. A., Stocker, T. F., Collins, W. D., Friedlingstein, P., Gaye, A. T., Gregory, J. M., et al (2007). *"Global climate projections," in Climate change 2007: The physical science basis. contribution of working group I to the fourth assessment report of the intergovernmental panel on climate change*, eds. Solomon, S. , Qin, H. L. M. D., Manning, M., Chen, Z., Marquis, M. and , and Averyt, K. B. (Cambridge, UK and New York, USA: Cambridge University Press).

Munné-Bosch, S., Queval, G., and Foyer, C. H. (2012). The impact of global change factors on redox signaling underpinning stress tolerance. *Plant Physiol.* 161, 5–19. doi: 10.1104/pp.112.205690

Naing, A. H., and Kim, C. K. (2021). Abiotic stress-induced anthocyanins in plants: Their role in tolerance to abiotic stresses. *Physiologia Plantarum*. 172, 1711–1723. doi: 10.1111/ppl.13373

Nuttall, J. G., Barlow, K. M., Delahunty, A. J., Christy, B. P., and O'Leary,G. J. (2018). Acute high temperature response in wheat. *Agron. J.* 110, 1296–1308. doi: 10.2134/agronj2017.07.0392

Obata, T., and Fernie, A. R. (2012). The use of metabolomics to dissect plant responses to abiotic stresses. *Cell. Mol. Life Sci.* 69, 3225–3243. doi: 10.1007/s00018-012-1091-5

Obata, T., Witt, S., Lisec, J., Palacios-Rojas, N., Florez-Sarasa, I., Araus, J. L., et al. (2015). Metabolite profiles of maize leaves in drought, heat and combined stress field trials reveal the relationship between metabolism and grain yield. *Plant Physiol.* 169, 2665–2683. doi: 10.1104/pp.15.01164

Pandey, P., Irulappan, V., Bagavathiannan, M. V., and Senthil-Kumar, M. (2017). Impact of combined abiotic and biotic stresses on plant growth and avenues for crop improvement by exploiting physio-morphological traits. *Front. Plant Sci.* 8. doi: 10.3389/fpls.2017.00537

Pandey, P., Ramegowda, V., and Senthil-Kumar, M. (2015). Shared and unique responses of plants to multiple individual stresses and stress combinations: Physiological and molecular mechanisms. *Front. Plant Sci.* 6. doi: 10.3389/fpls.2015.00723

Pang, Z., Chong, J., Zhou, G., de Lima Morais, D. A., Chang, L., Barrette, M., et al. (2021). MetaboAnalyst 5.0: Narrowing the gap between raw spectra and functional insights. *Nucleic Acids Res.* 49, W388–W396. doi: 10.1093/nar/gkab382

Peng, M., Shahzad, R., Gul, A., Subthain, H., Shen, S., Lei, L., et al. (2017). Differentially evolved glucosyltransferases determine natural variation of rice flavone accumulation and UV-tolerance. *Nature Communications*. 8, 1975. doi: 10.1038/s41467-017-02168-x

Ren, S., Ma, K., Lu, Z., Chen, G., Cui, J., Tong, P., et al. (2019). Transcriptomic and metabolomic analysis of the heat-stress response of *Populus tomentosa* Carr. *Forests*. 10, 383. doi: 10.3390/f10050383

Reyenga, P. J., Howden, S. M., Meinke, H., and Hall, W. B. (2001). Global change impacts on wheat production along an environmental gradient in south Australia. *Environ. Int.* 27, 195–200. doi: 10.1016/S0160-4120(01)00082-4

Rice-Evans, C., Miller, N., and Paganga, G. (1997). Antioxidant properties of phenolic compounds. *Trends Plant Sci.* 2, 152–159. doi: 10.1016/S1360-1385(97)01018-2

Rizhsky, L., Liang, H., Shuman, J., Shulaev, V., Davletova, S., and Mittler, R. (2004). When defense pathways collide. The response of arabidopsis to a combination of drought and heat stress. *Plant Physiol.* 134, 1683–1696. doi: 10.1104/pp.103.033431

Rosa, M., Prado, C., Podazza, G., Interdonato, R., González, J. A., Hilal, M., et al. (2009). Soluble sugars. *Plant Signaling Behav*. 4, 388–393. doi: 10.4161/psb.4.5.8294

Sardans, J., Gargallo-Garriga, A., Urban, O., Klem, K., Walker, T. W. N., Holub, P., et al. (2020). Ecometabolomics for a better understanding of plant responses and acclimation to abiotic factors linked to global change. *Metabolites*. 10, 239. doi: 10.3390/metabo10060239

Sharma, M., Irfan, M., Kumar, A., Kumar, P., and Datta, A. (2021). "Recent insights into plant circadian clock response against abiotic stress," *Journal of Plant Growth Regulation*. 221, 112403. doi: 10.1007/s00344-021-10531-y

Sharma, M., Kumar, P., Verma, V., Sharma, R., Bhargava, B., and Irfan, M. (2022). Understanding plant stress memory response for abiotic stress resilience: Molecular insights and prospects. *Plant Physiol. Biochem.* 179, 10–24. doi: 10.1016/j.plaphy.2022.03.004

Shewry, P. R. (2009). Wheat. *J. Exp. Bot.* 60, 1537–1553. doi: 10.1093/jxb/erp058

Sicher, R. (2013). Combined effects of CO_2 enrichment and elevated growth temperatures on metabolites in soybean leaflets: Evidence for dynamic changes of TCA cycle intermediates. *Planta*. 238, 369–380. doi: 10.1007/s00425-013-1899-8

Šigut, L., Holisova, P., Klem, K., Prtova, M., Calfapietra, C., Marek, M. V., et al (2015). Does long-term cultivation of saplings under elevated CO2

concentrationinfluence their photosynthetic response to temperature? *Ann. Bot.* 116, 929–939. doi: 10.1093/aob/mcv043

Soba, D., Ben Mariem, S., Fuertes-Mendizábal, T., Méndez-Espinoza, A. M., Gilard, F., González-Murua, C., et al. (2019). Metabolic effects of elevated CO_2 on wheat grain development and composition. *J. Agric. Food Chem.* 67, 8441–8451. doi: 10.1021/acs.jafc.9b01594

Tahjib-Ul-Arif, M., Zahan, M. I., Karim, M. M., Imran, S., Hunter, C. T. , Islam, M. S., et al. (2021). Citric acid-mediated abiotic stress tolerance in plants. *Int. J. Mol. Sci.* 7235. doi: 10.3390/ijms22137235

Templer, S. E., Ammon, A., Pscheidt, D., Ciobotea, O., Schuy, C., McCollum, C., et al. (2017). Metabolite profiling of barley flag leaves under drought and combined heat and drought stress reveals metabolic QTLs for metabolites associated with antioxidant defense. *J. Exp. Bot.* 68, 1697–1713. doi: 10.1093/jxb/erx038

Thornton, P. K., Ericksen, P. J., Herrero, M., and Challinor, A. J. (2014). Climate variability and vulnerability to climate change: A review. *Global Change Biol.* 20, 3313–3328. doi: 10.1111/gcb.12581

Trovato, M., Funck, D., Forlani, G., Okumoto, S., and Amir, R. (2021). Editorial: Amino acids in plants: Regulation and functions in development and stress defense. *Front. Plant Sci.* 12. doi: 10.3389/fpls.2021.772810

Walkowiak, S., Gao, L., Monat, C., Haberer, G., Kassa, M. T., Brinton, J., et al. (2020). Multiple wheat genomes reveal global variation in modern breeding. *Nature.* 588, 277–283. doi: 10.1038/s41586-020-2961-x

Wu, G., Johnson, S. K., Bornman, J. F., Bennett, S. J., Clarke, M. W., Singh, V., et al. (2016). Growth temperature and genotype both play important roles in sorghum grain phenolic composition. *Sci. Rep.* 6, 21835. doi: 10.1038/srep21835

Xalxo, R., Yadu, B., Chandra, J., Chandrakar, V., and Keshavkant, S. (2020). "Alteration in carbohydrate metabolism modulates thermotolerance of plant under heat stress," in *Heat stress tolerance in plants* eds. Wani, S.H. and , and Kumar, V. (New Jersey, USA: Wiley), 77–115. doi: 10.1002/9781119432401.ch5

Xu, G., Cao, J., Wang, X., Chen, Q., Jin, W., Li, Z., et al. (2019). Evolutionary metabolomics identifies substantial metabolic divergence between maize and its wild ancestor, teosinte. *Plant Cell.* 31, 1990–2009. doi: 10.1105/tpc.19.00111

Zandalinas, S. I., Balfagón, D., Gómez-Cadenas, A., and Mittler, R. (2022). Plant responses to climate change: Metabolic changes under combined abiotic stresses. *J. Exp. Bot.* 73, 3339–3354. doi: 10.1093/jxb/erac073

Zandalinas, S. I., and Mittler, R. (2022). Plant responses to multifactorial stress combination. *New Phytol.* 234, 1161–1167. doi: 10.1111/nph.18087

Zandalinas, S. I., Mittler, R., Balfagón, D., Arbona, V., and Gómez-Cadenas, A. (2018). Plant adaptations to the combination of drought and high temperatures. *Physiologia Plantarum.* 162, 2–12. doi: 10.1111/ppl.12540

Zinta, G., AbdElgawad, H., Peshev, D., Weedon, J. T., Van den Ende, W., Nijs, I., et al. (2018). Dynamics of metabolic responses to periods of combined heat and drought in arabidopsis thaliana under ambient and elevated atmospheric CO_2. *J. Exp. Bot.* 69, 2159–2170. doi: 10.1093/jxb/ery055

frontiers | Frontiers in Plant Science

TYPE Original Research
PUBLISHED 20 October 2022
DOI 10.3389/fpls.2022.990105

OPEN ACCESS

EDITED BY
Mohammad Irfan,
Cornell University, United States

REVIEWED BY
Shan Huang,
Jiangxi Agricultural University, China
Arlene Adviento-Borbe,
United States Department of Agriculture (USDA), United States

*CORRESPONDENCE
Hui Gao
gaohui@yzu.edu.cn

SPECIALTY SECTION
This article was submitted to Crop and Product Physiology, a section of the journal Frontiers in Plant Science

RECEIVED 09 July 2022
ACCEPTED 27 September 2022
PUBLISHED 20 October 2022

CITATION
Xu Q, Li J, Liang H, Ding Z, Shi X, Chen Y, Dou Z, Dai Q and Gao H (2022) Coupling life cycle assessment and global sensitivity analysis to evaluate the uncertainty and key processes associated with carbon footprint of rice production in Eastern China. *Front. Plant Sci.* 13:990105. doi: 10.3389/fpls.2022.990105

Coupling life cycle assessment and global sensitivity analysis to evaluate the uncertainty and key processes associated with carbon footprint of rice production in Eastern China

Qiang Xu[1,2,3], Jingyong Li[3], Hao Liang[4], Zhao Ding[5], Xinrui Shi[6], Yinglong Chen[1,2,3], Zhi Dou[1,2,3], Qigen Dai[1,2,3] and Hui Gao[1,2,3]*

[1]Jiangsu Key Laboratory of Crop Genetics and Physiology/Jiangsu Key Laboratory of Crop Cultivation and Physiology, Agricultural College of Yangzhou University, Yangzhou, China, [2]Jiangsu Co-Innovation Center for Modern Production Technology of Grain Crops, Yangzhou University, Yangzhou, China, [3]Research Institute of Rice Industrial Engineering Technology of Yangzhou University, Yangzhou, China, [4]College of Agricultural Engineering, Hohai University, Nanjing, China, [5]Key Laboratory of Crop Harvesting Equipment Technology of Zhejiang Province, Mechanical & Electrical Engineering College of Jinhua Polytechnic, Jinhua, China, [6]College of Agriculture, Shanxi Agricultural University, Taigu, China

An accurate and objective evaluation of the carbon footprint of rice production is crucial for mitigating greenhouse gas (GHG) emissions from global food production. Sensitivity and uncertainty analysis of the carbon footprint evaluation model can help improve the efficiency and credibility of the evaluation. In this study, we combined a farm-scaled model consisting of widely used carbon footprint evaluation methods with a typical East Asian rice production system comprising two fertilization strategies. Furthermore, we used Morris and Sobol' global sensitivity analysis methods to evaluate the sensitivity and uncertainty of the carbon footprint model. Results showed that the carbon footprint evaluation model exhibits a certain nonlinearity, and it is the most sensitive to model parameters related to CH_4 emission estimation, including EF_c (baseline emission factor for continuously flooded fields without organic amendments), SF_w (scaling factor to account for the differences in water regime during the cultivation period), and t (cultivation period of rice), but is not sensitive to activity data and its emission factors. The main sensitivity parameters of the model obtained using the two global sensitivity methods were essentially identical. Uncertainty analysis showed that the carbon footprint of organic rice production was 1271.7 ± 388.5 kg CO_2eq t^{-1} $year^{-1}$ (95% confidence interval was 663.9–2175.8 kg CO_2eq t^{-1} $year^{-1}$), which was significantly higher than that of conventional rice production (926.0 ± 213.6 kg CO_2eq t^{-1} $year^{-1}$, 95% confidence interval 582.5-1429.7 kg CO_2eq t^{-1} $year^{-1}$) (p<0.0001). The carbon footprint for organic rice had a wider range and greater uncertainty, mainly due to the greater impact of CH_4 emissions (79.8% for

organic rice versus 53.8% for conventional rice). EF_c, t, Y, and SF_w contributed the most to the uncertainty of carbon footprint of the two rice production modes, wherein their correlation coefficients were between 0.34 and 0.55 (p<0.01). The analytical framework presented in this study provides insights into future on-farm advice related to GHG mitigation of rice production.

KEYWORDS

carbon footprint, global sensitivity analysis, morris sensitivity analysis, sobol' sensitivity analysis, uncertainty analysis, life cycle assessment

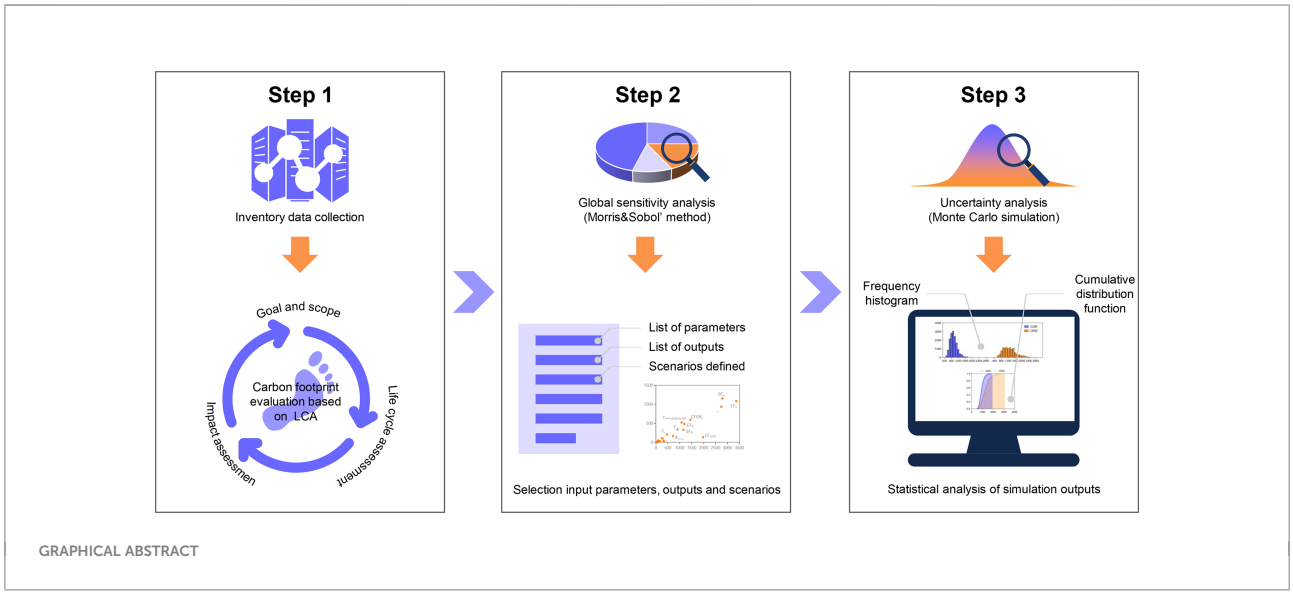

GRAPHICAL ABSTRACT

1 Introduction

Rice (*Oryza sativa L.*) is a staple food for nearly half of the world's population, and global rice consumption is projected to increase from 480 million tons (Mt) of milled rice in 2014 to nearly 550 Mt in 2030 (FAO, 2019). Driven by global population and economic growth, global rice production faces the twin challenges of increasing productivity to meet demand and reducing greenhouse gas (GHG) emissions to mitigate climate change (Yuan et al., 2021). Paddy fields are an important source of GHG emissions, accounting for about 50% of total CH_4 emissions and 10% of total N_2O emissions from cropland, respectively (Feng et al., 2021a). Carbon footprint evaluation models are important for understanding and quantifying emissions from rice production systems and give a better understanding of emission hotspots and mitigation opportunities. Such models are based on a life cycle assessment approach, the use of which typically varies in target, scope, geographic area, and time span, and can be applied to field scale (Xu Q. et al., 2020; Zhou et al., 2022), regional scale (Chen et al., 2021; Xu Z. et al., 2020), and national or global scale (Lathuillière et al., 2014) GHG assessments. Though such models draw on generic methodologies (IPCC, 2006), the rough methods required for country-level assessments are often insufficient to facilitate detailed policy analysis of the food sector. Consequently, the need for system-level assessments of GHG emissions from food production systems is growing (Singh et al., 2020; Arunrat et al., 2021).

However, the paddy field is complex, and their GHG emissions are strongly influenced by factors such as tillage practices (Xu et al., 2022), fertilization strategies (Liu et al., 2016), and irrigation regimes (Jiang Y. et al., 2019). The existing modelling methods are limited in their ability to accurately capture these complexities, which presents a significant challenge for both modelers and those seeking to leverage such methods for decision-making. Therefore, the carbon emission model of agricultural production system has considerable uncertainty, and it is necessary to conduct sensitivity analysis and uncertainty analysis on the carbon footprint evaluation model, which will help to provide reference for further optimizing parameters and reducing the uncertainty of evaluation results in the future.

Sensitivity analysis can identify high-sensitivity parameters from many input parameters, simplify low-sensitivity parameters, or increase the accuracy of high-sensitivity parameters through more accurate monitoring methods, thereby increasing the overall

accuracy of the evaluation model (Reisinger et al., 2017; Jóhannesson et al., 2020). At present, the sensitivity analysis of the carbon footprint evaluation model mainly adopts the local sensitivity method, which only changes one input parameter at a time and evaluates the impact of a single parameter change on the evaluation results. For example, a previous study explored the impact of changes in input parameters on output results in an LCA assessment of Spanish red wine production (Meneses et al., 2016). Xu et al. studied the impact of input parameter changes (± 40%) on environmental indicators such as global warming, eutrophication, and acidification, with respect to Chinese export and domestic green tea production (Xu et al., 2021). The changes in coal consumption in tea processing stage are the most sensitive to global warming and acidification, while NH_3 volatilization in tea cultivation stage is the most sensitive to eutrophication. The crops involved in the above studies were mainly derived from drylands, whose GHG emissions are significantly different from those of paddy fields. All the aforementioned studies used the local sensitivity method, which ignores the nonlinearity of the carbon footprint evaluation model to a certain extent, as well as the influence of the interaction between parameters on the output results. The global sensitivity method comprehensively considers the influence of each parameter and the interaction between parameters on the output result. The commonly used global sensitivity methods include Morris, EFAST, and Sobol' method (Saltelli et al., 2008). Currently, there is no report on the global sensitivity analysis of the carbon footprint of rice production, and it is unknown whether the sensitivity of the model parameters will be affected by management strategies.

A model is a description of a real system in nature after a series of assumptions and generalizations, which will inevitably lead to a certain amount of uncertainty. Uncertain factors such as monitoring errors, lack of key data, insufficient data representation, selection of accounting models, and allocation methods are inevitable in the carbon footprint evaluation process (De Koning et al., 2010). The uncertainty of carbon footprint assessment results often comes from the uncertainty of input parameters, including activity data, emission factors, model parameters, and scenario selection, which are propagated through the model and lead to uncertainty in estimated values (Milne et al., 2014). In ecological footprint evaluation studies lacking uncertainty analysis, the evaluation results are often questioned and are unconvincing in the interpretation stage (Zhuo et al., 2014; Zhang et al., 2021). Therefore, evaluation and quantification of the uncertainty of input parameters on the results are essential for the analysis of carbon footprint evaluation results. They can help researchers choose more reliable data sources and effectively optimize the data collection plan, and consequently, promote the application and development of product carbon footprint evaluation methods.

Given the impact of uncertainty in interpreting model outputs, as well as the importance of rice production to GHG budgets on a global scale, in this study, we aimed to identify the causes and uncertainties in modelling the farm-scaled GHG footprint affecting rice production in China. We developed a global sensitivity and uncertainty analysis method for system-scaled carbon footprint evaluation and application to rice production with different fertilization strategies, in order to achieve the following: 1) determine the most sensitive parameter in the carbon footprint evaluation of rice production, and improve the evaluation efficiency and accuracy of the model; 2) improve the robustness of the evaluation results and determine the reliability of the evaluation results through uncertainty analysis, providing technical support for further optimizing parameters and reducing the uncertainty of evaluation results in the future.

2 Materials and methods

2.1 Carbon footprint evaluation methodology

2.1.1 System boundary and functional unit

The carbon footprint was calculated by following the methodology from the IPCC Guidelines for National Greenhouse Gas Inventories (Hergoualc'h et al., 2019). The system boundary of life-cycle product carbon footprint was from cradle to farm gate, including indirect greenhouse gas (GHG) emissions from the production, transportation, and use of agricultural inputs, as well as direct GHG emissions from the farming stage. The functional unit was expressed as kg CO_2eq t^{-1} $year^{-1}$ rice product (dry matter).

2.1.2 GHG emission calculation from upstream stage

Based on Hergoualc'h et al. (2019), the GHG emissions from upstream stage was calculated by Equation (1).

$$GHG_{raw\ \ material} = \sum_{i=1}^{n}(Ai \times \varphi i) \quad (1)$$

where $GHG_{raw\ \ material}$ is the sum of GHG emissions from upstream stage (kg CO_2eq ha^{-1} $year^{-1}$); A_i refers to the amount of agri-material inputs in the upstream stage per hectare, including the inputs of rice seeds, chemical fertilizers, organic fertilizers, pesticides, herbicides, and fungicides, as well as the consumption of electricity and diesel during irrigation, land preparation, and harvesting (kg ha^{-1} or kWh ha^{-1}); and φ_i refers to the carbon emission coefficients of different agricultural materials (kg CO_2eq·$Unit^{-1}$), which were mainly derived from the Chinese Life Cycle Database (CLCD v0.8; https://efootprint.net/login) and the Swiss Ecoinvent 2.2 database (https://simapro.com/databases/ecoinvent/).

2.1.3 Field GHG emissions

The CH_4 emissions from rice cultivation were calculated using Equation (2), which is based on Hergoualc'h et al. (2019) (Tier 2).

$$Q_{CH_4} = EFi \times t \times A \quad (2)$$

where Q_{CH_4} denotes annual methane emissions from rice cultivation (kg CH_4 ha^{-1}), EF_i denotes adjusted daily emission factor for a particular harvested area (kg CH_4 ha^{-1} day^{-1}), t denotes cultivation period of rice (day); and A denotes annual harvested area of rice (ha $year^{-1}$).

Emissions from each different region can be calculated by multiplying a baseline default emissions factor with various scaling factors, as shown in Equation (3) (Hergoualc'h et al., 2019).

$$EF_i = EF_C \times SF_W \times SF_P \times SF_O \times SF_{s,r} \quad (3)$$

where EF_c is the baseline emission factor for continuously flooded fields without organic amendments; SF_w is a scaling factor to account for the differences in water regime during the cultivation period; SF_p is a scaling factor to account for the differences in water regime in the pre-season before the cultivation period; SF_O is a scaling factor that should vary for both type and amount of organic amendment applied and can be calculated by equation (4); and $SF_{s,r}$ is a scaling factor for soil type, rice cultivar, etc., if available.

The default conversion factor for farmyard manure was calculated by Equation (4) (Hergoualc'h et al., 2019):

$$SF_o = (1 + \sum_i ROA_i \times CFOA_i)^{0.59} \quad (4)$$

where SF_O is the scaling factor for both type and amount of organic amendment applied; ROA_i is the application rate of organic amendment i, in dry weight for straw and fresh weight for others in tons ha^{-1}; and $CFOA_i$ is the conversion factor for organic amendment i (in terms of its relative effect, with respect to straw applied shortly before cultivation).

Hergoualc'h et al. (2019) provided an estimation method for N_2O emission, where the direct emissions of N_2O are calculated as follows (Tier 1):

$$Q_{N_2O\ (Direct)} = [(F_{SN} + F_{ON}) \times EF_1 + F_{CR} \times EF_{1FR}] \times 44/28 \quad (5)$$

where $Q_{N_2O\ (Direct)}$ is the direct N_2O emissions (kg N_2O $year^{-1}$); F_{SN} is the annual amount of synthetic N fertilizer applied to soils (kg N $year^{-1}$); F_{ON} is the annual amount of animal manure, compost, sewage sludge and other organic N additions applied to soils (kg N $year^{-1}$); F_{CR} is the annual amount of N in crop residues (kg N $year^{-1}$); EF_1 is the emission factor for N_2O emissions from N inputs (kg N_2O-N (kg N input)$^{-1}$); and EF_{1FR} is the emission factor for N_2O emissions from N inputs to flooded rice, kg N_2O-N (kg N input)$^{-1}$.

The formula for estimating indirect N_2O emissions was as follows (Hergoualc'h et al., 2019):

$$Q_{N_2O\ (Indirect)} = [(F_{SN} \times Frac_{GASF} + F_{ON} \times Frac_{GASM})] \times EF_4 + (F_{SN} + F_{ON} + F_{CR}) \times Frac_{LEACH-(H)} \times EF_5 \times 44/28 \quad (6)$$

where $Q_{N_2O\ (Indirect)}$ denotes the indirect N_2O emissions (kg N_2O $year^{-1}$); $Frac_{GASF}$ is the fraction of synthetic N fertilizer that volatilizes as NH_3 and NO_x, kg N volatilized (kg of N applied)$^{-1}$; $Frac_{GASM}$ is the fraction of applied organic N fertilizer material (F_{ON}) that volatilizes as NH_3 and NO_x, kg N volatilized (kg of N applied or deposited)$^{-1}$; EF_4 is the emission factor for N_2O emissions from atmospheric deposition of N on soils and water surfaces, kg N–N_2O (kg NH_3–N+NO_x–N volatilized)$^{-1}$; $Frac_{LEACH-(H)}$ is the fraction of all N added to, or mineralized in, managed soils in regions where leaching or runoff occurs that is lost through leaching and runoff, kg N (kg of N additions)$^{-1}$; and EF_5 is the emission factor for N_2O emissions from N leaching and runoff, kg N_2O–N (kg N leached and runoff)$^{-1}$.

2.1.4 Calculation of carbon footprint

Yield-based carbon footprint (CF) is calculated using Equation (7):

$$CF = \left(GHG_{raw\ material} + Q_{CH_4} \times 25 + \left(Q_{N_2O\ (Direct)} + Q_{N_2O\ (Indirect)}\right) \times 298\right)/(Y/1 \quad (7)$$

where CF is the carbon footprint per unit of yield for rice production (kg CO_2eq t^{-1} $year^{-1}$); Y is the yield of rice (kg ha^{-1}). 25 and 298 are the global warming potentials of CH_4 and N_2O on a 100-year scale (IPCC, 2013).

2.2 Sensitivity analysis

2.2.1 Scenarios, data source, and selection of parameters

Sensitivity analysis was performed under two fertilization scenarios: conventional rice production (CON) and organic rice production (ORG) modes. The geographic area is in Jiangsu Province, which represents an important rice-producing area in eastern China. Collection of agricultural input data of CON and ORG was from 15 and 9 farms through survey questionnaire in 2020–2021. The questionnaire on management practices included: (1) chemical fertilizers, pesticide, fungicide, herbicide, farm yard manure, irrigation water, rice seed, electricity and diesel consumption; (2) yield of rice. In the CON mode, chemical fertilizer and pesticides were used to guarantee high productivity and pest control, while in the ORG mode, only farmyard manure was used and the use of pesticides was not permitted. Rice seed and some fuels, such as electricity and diesel, were used for agricultural operations such as land preparation and irrigation for both scenarios. The calculation of CO_2 emissions from manufacture of agricultural

machinery, i.e., tractor, combine harvester, and pump, is often omitted from carbon footprint studies (Yodkhum et al., 2017). These agricultural machines were excluded from the system in this study because of the lack of actual data on each machine's lifetime and its overall use times. Moreover, the change in soil carbon sequestration was not considered in this study due to missing data.

The parameters included in the sensitivity analysis of the carbon footprint evaluation model were divided into three categories: 1) background parameters (the carbon emission coefficients of different agricultural materials defined in Equation 1), 2) activity data (the amount of agri-material inputs defined in Equation 1), and 3) CH_4 and N_2O estimation parameters. The variation in each category parameter and emission factor would be accounted for in the final result, thereby affecting the objectivity of the final evaluation result (Sykes et al., 2019). Parameters were assumed to be independent from each other, and a uniform distribution was assigned to all parameters because initial information on the distribution characteristics was limited. Many of the previous studies have assumed a uniform distribution of data when encountering similar situations (Vanuytrecht et al., 2014; Liang et al., 2017). A total of 29 and 21 input factors for CON and ORG modes were selected, respectively, for sensitivity analysis (Table A and Table B). Lower and upper boundaries of the parameters used to design the sensitivity analysis were set according to expert knowledge and the values recommended by Hergoualc'h et al. (2019). Specifically, the upper and lower limits of the background parameters were taken from the mean value ± 10%; the upper and lower limits of the activity data were based on the maximum and minimum values of the survey data; the upper and lower limits of the CH_4 and N_2O estimation parameters were derived from the empirical values provided by Hergoualc'h et al. (2019). The effects of parameter variation on the output of the carbon footprint model were evaluated.

2.2.2 Local sensitivity analysis

Local sensitivity analysis observes the impact of input parameter changes on the output by changing the value of the input parameters one by one, while the remaining parameters remain unchanged. In this study, each input parameter was changed by ±10%, and then the change in carbon footprint was observed, so that the sensitivity (E_i) of each parameter could be obtained, as calculated by Equation (8):

$$E_i = \Delta CF / \Delta A_i \tag{8}$$

where E_i was the sensitivity of the input parameter A_i; ΔA_i denotes the change rate of the input parameter A_i (%), with the value of ±10%; and CF denotes the corresponding rate of change of the evaluation result CF when the input variable A_i has a change rate of ΔA_i. The larger the $|E|$ is, the more sensitive the evaluation result CF is to the input variable A.

2.2.3 Global sensitivity analysis

2.2.3.1 Morris method

The Morris method calculates the elementary effect (EE) of each parameter on the selected output. These elementary effects allow effects of all parameters on the same output to be compared. The Morris method uses the following Equation (9) to calculate the degree of influence (d) of each input parameter on the output result:

$$d_i(x_i, \ldots, x_k, \Delta) = \frac{[y(x_1, \ldots, x_{i-1}, x_1 + \Delta, x_{i+1}, \ldots, x_k)]}{\Delta} \tag{9}$$

where i is the number of parameters; $y(X)$ is the output result of the model; and $X=(x_1,\ldots,x_k)$ is the k-dimensional parameter input vector. Upon discretizing the parameter value range (x_{imin}, x_{imax}), each parameter can only take a value from these p values (x_{imin},x_{imin}+1/(p-1)×(x_{imax}-x_{imin}), x_{imin}+2/(p-1)×(x_{imax}-x_{imin}), …,x_{imax}), where p is the parameter level. Due to the randomness of the parameter values of the Morris method, it is easy to cause value errors; thus, r repetitions are required, and the total number of runs of the model is $r(k+1)$ times, where k represents the number of parameters. In this study, k was 29 and 21 for CON and ORG mode, respectively. The sensitivity of each parameter is measured by the mean (μ) and standard deviation (σ) of the r "elementary effects". The larger the value of μ, the more sensitive the parameter is to the output result. The value of σ represents the interaction between parameters, and the larger the value of σ, the stronger the interaction between the parameter under investigation and the other parameters.

The Morris sensitivity analysis for input samples were performed with SimLab (2010), and the evaluation of the carbon footprint model output sets was automated with SimLab (2010). The sensitivity analysis was executed by sampling r = 10 elementary effects (Morris, 1991). The model finally ran 300 and 220 times in total for CON and ORG mode, respectively.

2.2.3.2 Sobol' method

Sobol' method is a variance-based global sensitivity analysis method, which quantitatively evaluates the effect of each input parameter and the interaction between parameters on the output variable by decomposing the variance of the output variable. When there are m input parameters to be analyzed, the $D(Y)$ of the output result is defined as follows:

$$D(y) = \sum_i D_i + \sum_{1 \le i < j \le m} D_{ij} + \cdots + D_{1,2,\cdots,m} \tag{10}$$

where D_i is the variance generated by parameter i; D_{ij} is the variance produced by the interaction of parameters i and j; D_{ijk} is the variance resulting from the interaction of parameters i, j, and k; and $D_{1,2,\ldots,m}$ is the variance produced by the joint interaction of m parameters.

For parameter i, the first-order sensitivity index (S_i) can be used to reflect the sensitivity of that single parameter, and the

full-order sensitivity index (ST_i) can be used to indicate the common effect of that parameter and all other parameters. The equations to calculate these indices are as follows:

$$S_i = \frac{D_i}{D} \tag{11}$$

$$ST_i = 1 - \frac{D_{:i}}{D} \tag{12}$$

where $D_{:i}$ represents the variances of parameters other than parameter i.

The input samples for sensitivity analysis were generated with SimLab (2010), and Sobol' analysis method was executed using m = 29 and 21 input factors for CON and ORG mode, respectively, as well as a sample size of $n(m + 2)$ model input sets, where n is defined as having a range of 100 or higher (Saltelli et al., 2000). In this study, we used n = 496 for a total of 15376 and n = 490 for a total of 11270 input parameter sets for conventional rice, and organic rice, respectively.

2.3 Uncertainty analysis

Uncertainty analysis helps to increase the robustness of evaluation results (Milne et al., 2014; Sykes et al., 2019). Sobol' analysis embeds a Monte Carlo module in the SimLab (2010) software, which enables the quantification of propagation of the uncertainties in the model inputs through the model. Based on the simulation values of Sobol' analysis described above, an uncertainty analysis was conducted. Mean, median, standard deviation, minima, maxima, and 2.5% and 97.5% quantiles of carbon footprints with a 95% confidence interval were calculated, and the frequency histogram and the cumulative distribution function were also provided.

2.4 Statistical analysis

Statistical analyses were carried out using SPSS 22.0 software, and t-test of least significant difference (LSD) method was used to analyze the differences in carbon footprint between CON and ORG modes, followed by least significant difference (LSD) tests ($p< 0.05$) with a significance level of 5%. Pearson correlation analysis was used between input parameters and carbon footprint (two-tailed).

3 Results

3.1 Local sensitivity analysis

The sensitivity (E_i) of each parameter can be obtained by changing each input parameter by ±10% and then observing the change in carbon footprint (Figure 1). The impact of CH_4

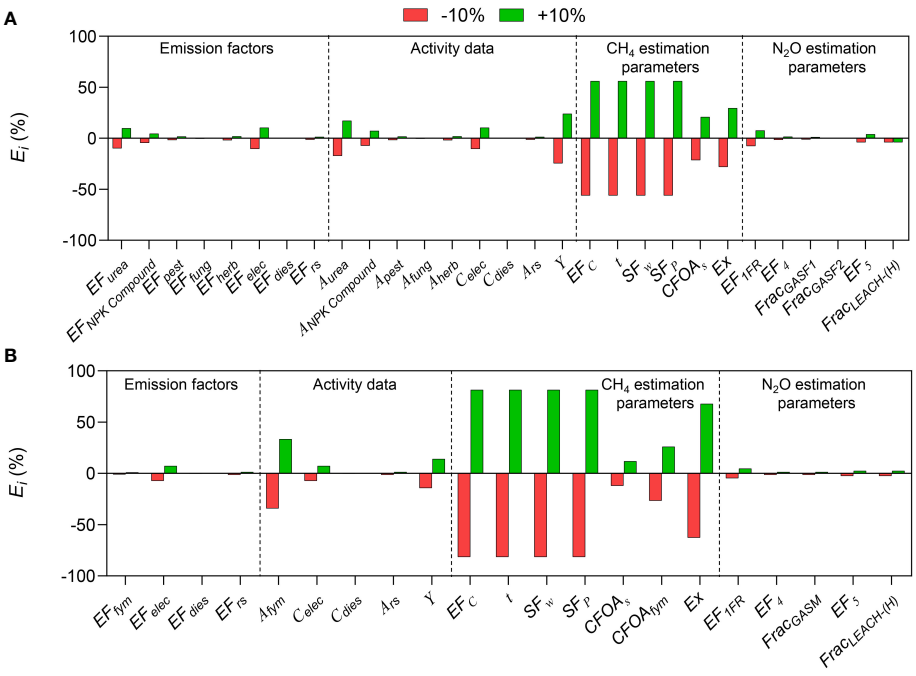

FIGURE 1
Sensitivity analysis of each parameter of the carbon footprint evaluation model to the carbon footprint by a local sensitivity analysis in **(A)** conventional and **(B)** organic rice production.

emission estimation parameters on carbon footprint is higher than that of emission factors, activity data, and N_2O emission estimation parameters. For conventional rice production mode, among the CH_4 emission estimation parameters, EF_c, t, SF_w, and SF_p had the greatest effect on carbon footprint (with an E_i of ±56.1%), followed by E_x (with an E_i of ±28.1%), $CFOA_s$ which was ranked the last (with an E_i of ±21.5%). Among activity data, the E_i of Y, A_{urea}, and C_{elec} was ±24.6%, ± 17.2%, and ±10.4%, respectively; while the E_i of other parameters were lower than ±10%. Emission factors of background database and N_2O emission estimation parameters had relatively low E_i. The trend was similar in the CON and ORG modes. The above analysis showed that it was impossible to know which parameter was the most sensitive from the local sensitivity analysis alone, as the sensitivities (E_i) of EF_c, t, SF_w, and SF_p were consistent.

3.2 Global sensitivity analysis

3.2.1 Morris sensitivity analysis

Figures 2 A–B shows the mean (μ) and variance (σ) of the Morris sensitivity index of the input parameters of the carbon footprint evaluation model to carbon footprint of CON and ORG modes. Overall, the estimation parameters of CH_4 emission generally showed greater sensitivity than emission factors of background database, activity data, and N_2O emission estimation parameters. For conventional rice production, the sensitivity of EF_c (μ=3370.0 kg CO_2eq t^{-1} $year^{-1}$, σ=1080.0 kg CO_2eq t^{-1} $year^{-1}$), SF_w (μ=2790.0 kg CO_2eq t^{-1} $year^{-1}$, σ=1150.0 kg CO_2eq t^{-1} $year^{-1}$), and t (μ=2740.0 kg CO_2eq t^{-1} $year^{-1}$, σ=930.0 kg CO_2eq t^{-1} $year^{-1}$) to carbon footprint was high among the sensitivities of CH_4 emission estimation parameters. A higher σ indicates that these three parameters interact strongly with other parameters. $CFOA_s$, EF_5, and $Frac_{LEACH\text{-}(H)}$ had relatively high sensitivity to carbon footprint, and thus, are relevant to the estimation of CH_4 and N_2O emissions. Notably, although EF_{1FR} had a relatively high μ (1980.0 kg CO_2eq t^{-1} $year^{-1}$), its low σ (132.7 kg CO_2eq t^{-1} $year^{-1}$) indicated weak interaction with other parameters. For organic rice production mode, the sensitivities of EF_c, SF_w, and t to carbon footprint were also high, among the sensitivities of various parameters. The difference is that the μ and σ of these three parameters in the ORG mode were higher than those in the CON mode, indicating that CH_4 emissions have a greater impact on the carbon footprint of the ORG mode.

3.2.2 Sobol' sensitivity analysis

The Sobol' first-order indices (S_i) and Sobol' total sensitivity (ST_i) as per Sobol' global sensitivity analysis, are shown in Figure 2C–D. Similar to the results of the Morris analysis, the sensitivity indices of CH_4 emission estimation parameters were the highest among those of all parameters associated with Sobol' sensitivity analysis. EF_c, SF_w, and t collectively explained 15.9% –27.0% and 20.9%–40.8% of the variability of carbon footprint for CON and ORG, respectively. The difference between ST_i and S_i of a parameter is the degree of influence of the interaction between that parameter and other parameters on the output results of the carbon footprint evaluation model. The larger the difference, the stronger the interaction of the parameter. EF_c, SF_w, and t indicated greater interaction with other parameters, which corresponded to the σ values noted as per the Morris analysis method. Overall, the results of the two global sensitivity analyses were consistent, and the results show that the CH_4 and N_2O emission estimation parameters were more sensitive to the carbon footprint of CON mode, whereas only the CH_4 emission estimation parameters were more sensitive to the carbon footprint of ORG mode.

3.2.3 Comparison between Morris and Sobol' method

Two methods were used for the global sensitivity analysis; correlations between the full-order sensitivity index (ST_i) values calculated as per Sobol' method and the μ values calculated as per Morris method for CON and ORG modes are shown in Figure S1. The two methods yielded r values of 0.90 for CON and 0.96 for ORG, indicating a very high correlation between the two methods used.

3.3 Uncertainty analysis

Uncertainty analysis can be used to determine the correlation between input parameters and output results, which helps increase the robustness of results during the interpretation stage in LCA studies. Thus, we conducted an uncertainty analysis based on 15360 outputs of CON and 11264 outputs of ORG using Sobol' analysis. Figure 3A shows the frequency histogram of simulation outputs of CON and ORG modes. The distributions of carbon footprints of both modes were positively skewed, with skewness of 0.82 and 0.78 for CON and ORG, respectively. Simulated carbon footprint was found to be higher for the ORG mode than the CON mode, as indicated by a steeper line for the former (Figure 3B). Figure 3C shows a violin plot of the simulated carbon footprint of the two rice production modes. The mean value was 926.0 ± 213.6 kg CO_2eq t^{-1} $year^{-1}$ for CON mode and 1271.7 ± 388.5 kg CO_2eq t^{-1} $year^{-1}$ for ORG mode, and the difference reached a significant level (p<0.0001) (Table 1). The range of carbon footprints for CON and ORG modes was 424.6–1946.9 kg CO_2eq t^{-1} $year^{-1}$ and 491.6–3092.8 kg CO_2eq t^{-1} $year^{-1}$, respectively. The 25% percentile and 75% percentile of CON mode were 772.8 kg CO_2eq t^{-1} $year^{-1}$ and 1044.3 kg CO_2eq t^{-1} $year^{-1}$, respectively, while those of ORG mode were 979.6 kg CO_2eq t^{-1} $year^{-1}$ and 1495.8 kg CO_2eq t^{-1} $year^{-1}$, respectively. The CON mode exhibited 5% and 95% CIs of 582.5 and 1429.7 kg CO_2eq t^{-1} $year^{-1}$, respectively, whereas the ORG mode exhibited

10.3389/fpls.2022.990105

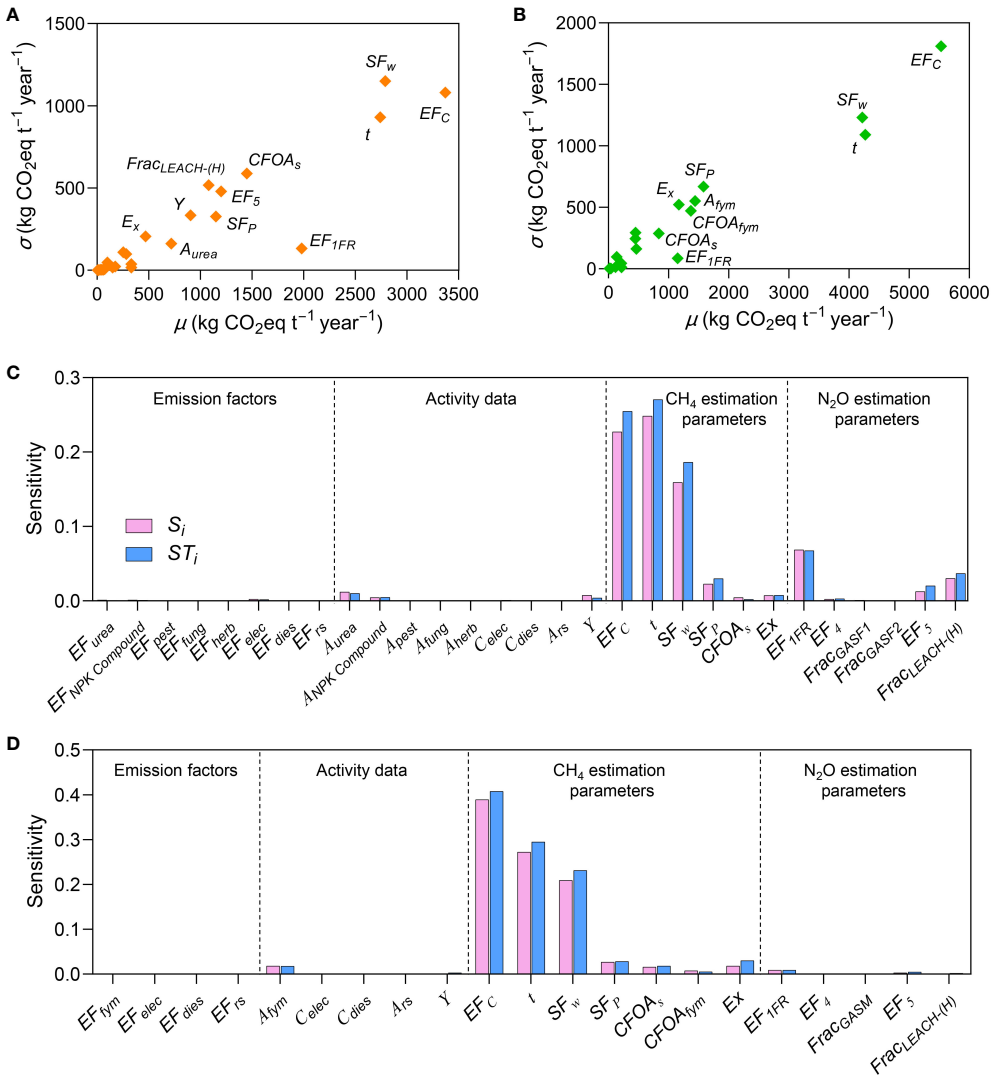

FIGURE 2
Sensitivity analysis indices of conventional (CON) and organic (ORG) rice production modes, as per global sensitivity analysis. Morris mean effect (μ) to the carbon footprint, as per Morris method in **(A)** CON and **(B)** ORG. Sobol' first-order indices (S_i), and Sobol' total sensitivity (ST_i) to, the carbon footprint, as per a Sobol' variance-based method in **(C)** CON and **(D)** ORG.

5% and 95% CIs of 663.9 and 2175.8 kg CO_2eq t^{-1} $year^{-1}$, respectively. The reason for ORG mode showing a broader range and greater uncertainty of carbon footprint results might be that it was affected by emissions of CH_4 to a greater degree. Breakdown of the system emissions into different sources is shown in Figure 3D. The emissions of CH_4 accounted for as high as 53.8% and 79.8% for the CON and ORG mode, respectively. However, the emissions of N_2O and embedded carbon emission in the production of upstream agri-materials accounted for 18.5% and 27.6% for CON mode, respectively, and 11.0% and 9.1% for ORG mode, respectively.

We ranked the top 10 input parameters with greater uncertainty affecting the carbon footprint according to the correlation coefficient (Figure 4). In addition to the CH_4 estimation parameters, the system output (Y) also contributed significantly to the uncertainty of the carbon footprint. Specifically, taking conventional rice as an example, EF_c had the largest impact on the uncertainty of the carbon footprint, with a correlation coefficient r of 0.50**; the correlation reached an extremely significant level (p<0.01). The next most influential inputs were t (r=0.45**), Y (r=–0.39**), and SF_w (r=0.35**). Several parameters related to N_2O emission estimation (EF_{1FR}, $Frac_{LEACH-(H)}$, and EF_5) had relatively larger impacts on the uncertainty of carbon footprint, while others had relatively smaller impacts. Similarly, for organic rice, the most influential inputs were EF_c (r=0.55**), t (r=0.49**), SF_w (r=–0.40**), and Y

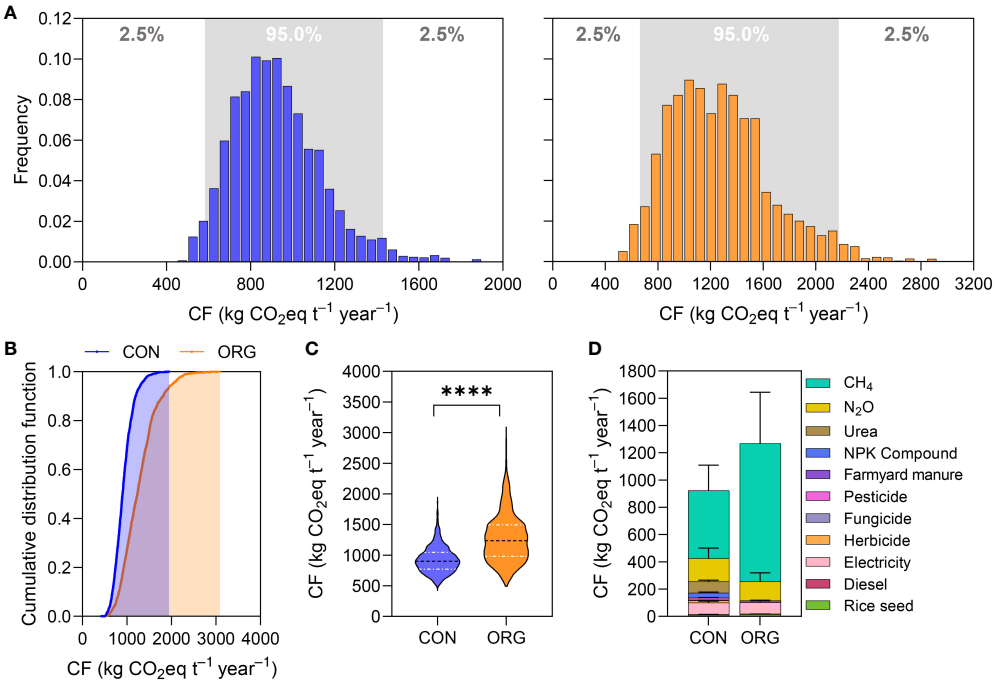

FIGURE 3
Uncertainty analysis of carbon footprint (CF) of conventional (CON) and organic (ORG) rice production. **(A)** Frequency histogram of CON (left) and ORG (right); **(B)** cumulative distribution function; **(C)** violin plot of carbon footprint based on Sobol' variance-based method. **** indicates significant difference at $p<0.0001$ level by a t-test of least significant difference (LSD) method. **(D)** Breakdown of the total CF (calculated based on Sobol' variance-based method) to the level of individual emissions sources of CON and ORG. Error bars indicate 5-95% confidence interval (CI) for each source, calculated *via* Monte Carlo simulation.

TABLE 1 **Uncertainty analysis statistics of all output responses of conventional and organic rice production modes, as determined using Sobol' global sensitivity analysis simulations.**

Item	Unit	Conventional rice	Organic rice
No. of values	–	15376	11270
Minimum	kg CO_2eq·t^{-1} $year^{-1}$	424.6	491.6
25% Percentile	kg CO_2eq·t^{-1} $year^{-1}$	772.8	979.6
Median	kg CO_2eq·t^{-1} $year^{-1}$	902.2	1235.3
75% Percentile	kg CO_2eq·t^{-1} $year^{-1}$	1044.3	1495.8
Maximum	kg CO_2eq·t^{-1} $year^{-1}$	1946.9	3092.8
Mean	kg CO_2eq·t^{-1} $year^{-1}$	926.0	1271.7
S.D.	kg CO_2eq·t^{-1} $year^{-1}$	213.6	388.5
Skewness	–	0.82	0.78
Kurtosis	–	1.12	0.71
5% CI	kg CO_2eq·t^{-1} $year^{-1}$	582.5	663.9
95% CI	kg CO_2eq·t^{-1} $year^{-1}$	1429.7	2175.8

S.D., standard deviation; CI, confidence interval.

(r=–0.34**); the correlation reached an extremely significant level ($p<0.01$). However, other parameters had relatively smaller impacts on the uncertainty of the carbon footprint, with correlation coefficient r not being more than 0.15.

4 Discussion

The current study involved a novel approach to identify and quantify the sources and effects of sensitivity and uncertainty in

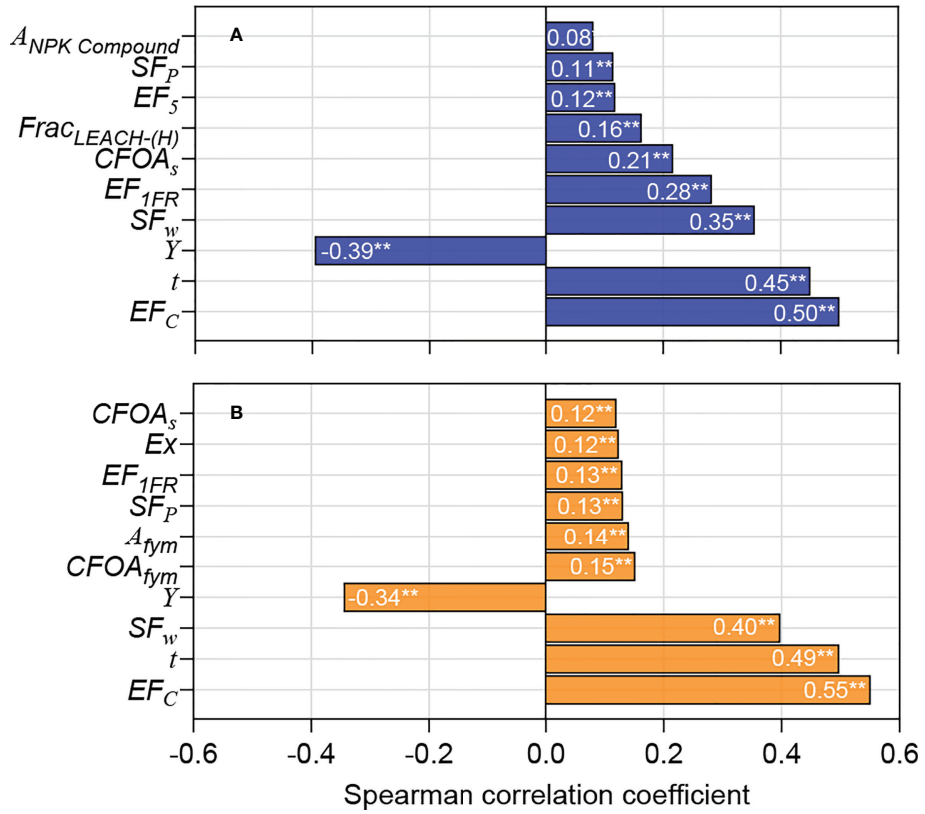

FIGURE 4
Tornado graphs showing the model inputs that according to the Pearson Rank correlation coefficient (two-tailed test), affected the uncertainty in estimated carbon footprint the most for **(A)** conventional and **(B)** organic rice production. ** indicates significant difference at $p<0.01$ level.

the carbon footprint of rice production, based on IPCC guidelines. Through the comparison of local sensitivity analysis and global sensitivity analysis of carbon footprint evaluation of rice production, in this study, we found that although the local sensitivity analysis identifies the more sensitive input parameters, the nonlinearity of the evaluation model cannot be considered satisfactory. It is impossible to determine which parameter is the most sensitive. From Figures S2–S3, it is clear that the carbon footprints of CON and ORG modes had extremely significant positive correlations with CH_4 emission, wherein the correlation coefficient r reached 0.79 and 0.91, respectively. However, there is no reliable linear correlation between the parameters (EF_c, SF_w, and t) involved in the estimation of CH_4 emissions and carbon footprint. This suggests that the carbon footprint model exhibits a certain amount of nonlinearity, and the two global sensitivity analyses used in this study (Morris and Sobol' method) account for the interaction among the input parameters.

The results of this study showed that the contribution of CH_4 emissions to the carbon footprint of CON and ORG modes was as high as 53.8% and 79.8%, respectively. This result is concordant with those of previous studies (Jiang Z. et al., 2019; Arunrat et al., 2021; Kashyap and Agarwal, 2021). Therefore, the uncertainty in the carbon footprint mainly stemmed from the uncertainty in the estimation of CH_4 emissions. CH_4 emissions from paddy field ecosystems were affected by many factors, such as soil properties, climatic factors, water and nutrient management strategies, organic substitutions, and rice varieties, with a great degree of variability (Feng et al., 2021; Yang et al., 2021). In the process of carbon footprint evaluation, when the field measurement conditions for CH_4 are not available, notable attention must be paid to the values of EF_c, SF_w, and t. The IPCC guidelines provide an estimate of the daily time step CH_4 emissions from paddy fields, and the emission factor in the model can be modified according to specific water and fertilizer management or organic substitutions. SF_w is a scaling factor that accounts for the differences in water regime during the cultivation period. CH_4 emission from paddy fields is the net effect of CH_4 generation, oxidation, and transport in soil. Water status of soil strongly affects the redox environment of paddy soil (Qian et al., 2022). Therefore, SF_w has a remarkable influence on the estimation of CH_4 emissions from paddy fields. The rice cultivation period (t) is strongly influenced by the rice variety (Feng et al., 2021; Song et al., 2022). According to the

sowing period, growth period, and maturity period, paddy can be divided into three categories: early paddy, middle paddy, and late paddy. Generally, the growth period of early paddy is 90-120 days, middle paddy is 120-150 days, and late paddy is 150-170 days (Wang, 2016). Due to the different climatic conditions in different regions, the cultivation period of the same rice variety in different regions is different. It can be seen that the variability of the parameter *t* is extremely large, which has a notable impact on the uncertainty of CH_4 emission estimation and carbon footprint evaluation results. The correlation analysis showed that the system output *Y* is significantly negatively correlated with the carbon footprint ($p<0.01$), and this parameter had a notable impact on the uncertainty of the carbon footprint (Figure 4). The value of *Y* is mainly obtained from investigation or on-field measurement; thus, it is necessary to exercise caution when collecting the data. For the accurate values of the above coefficients, analysts require extensive experience in agronomy and ecology; this is crucial for increasing the credibility of the evaluation results. Compared with the estimation parameters for CH_4 emission, the parameters related to the estimation of N_2O emission had lesser influence on the uncertainty of carbon footprint. Among all the parameters, EF_{1FR} had the greatest impact on carbon footprint. This parameter is frequently used in carbon footprint studies of crop production to quantify N_2O emissions from rice fields due to nitrogen inputs (Yodkhum et al., 2017). In the present study, the impact of EF_{1FR} on the carbon footprint of CON mode was greater compared to that of ORG model, owing to the higher exogenous nitrogen input for CON mode than that for ORG mode. Activity data and their carbon emission factors had a lower impact on the carbon footprint than that of parameters related to the estimation of CH_4 and N_2O emission. Among them, fertilizer input, electricity consumption, and system output (rice yield) had a greater impact on the carbon footprint, indicating that these coefficients should be given priority when collecting activity data.

According to the above analysis, adopting more accurate inventory data will effectively reduce the uncertainty of the evaluation results. Therefore, this study proposes the following inventory data collection optimization scheme. Factors related to greenhouse gas (especially for CH_4) estimates should be given priority, followed by activity data and their emission factors. System-scale carbon footprint evaluation should use field-measured CH_4 and N_2O emission levels as much as possible because these values correspond to specific rice varieties, management practices, and soil-climate conditions. In cases where measured values cannot be provided, experts should be consulted to determine the parameters involved in the estimation of GHG emissions. The fundamental requirement is that the basic research on the mechanism of GHG emissions from paddy fields should be strengthened, which is crucial for improving the modelling of GHG emissions. Therefore, with the continuous improvement and development of the basic database of carbon footprint evaluation in the agricultural field, the relevant carbon emission parameters will have better temporal representation, statistical representation, geographical representation, data sources, and technical representation.

The sensitivity and uncertainty analyses of the carbon footprint of rice production conducted in the current study provides a research framework that is applicable to crops in other countries or regions. We strongly recommend that emission factors or model parameters derived from local soil-climate conditions be prioritized when other regions use the analytical framework of this study. The limitations of this study are as follows. 1) In global sensitivity analysis, parameters were assumed to be independent from each other. However, in this study, there were some correlations between parameters, such as fertilizer application amount and rice yield. The global sensitivity analysis algorithm will not work if the parameters vary randomly and there is a correlation between the parameters. This is a shortcoming of this study. In future research, the parameters need to be independent of each other and the algorithm needs to be further improved, which will help to improve the credibility of the evaluation results. 2) The fertilizers in the activity data in this study are the commonly used urea and farmyard manures. The impact of activity data and their emission factors on carbon footprint uncertainty may change when new fertilizers such as nitrification inhibitors and biochar-based fertilizers are used. 3) The results of this study suggested that different fertilization scenarios have a large impact on carbon footprint uncertainty. However, this study did not consider scenarios such as different rice varieties, irrigation regimes, and tillage practices, which should be addressed in future studies.

5 Conclusions

This study provided a general approach to the sensitivity and uncertainty analysis of a system-scaled carbon footprint evaluation model for crop production, which is essential for objective, accurate, and efficient accounting of GHG emissions from crop production. Local sensitivity analysis cannot consider the nonlinearity of the carbon footprint evaluation model, while global sensitivity analysis overcomes this problem and effectively identifies the key parameters of the model. The carbon footprint evaluation model was most sensitive to model parameters related to CH_4 emission (primarily EF_c, SF_w, and *t*), while it was relatively insensitive to N_2O emission estimation parameters, activity data, and its emission factors. The main model sensitivity parameters of Morris and Sobol' global sensitivity analysis methods were essentially the same. Uncertainty analysis

results based on the Sobol' method showed that the carbon footprint of CON mode was 926.0 ± 213.6 kg CO_2eq t^{-1} $year^{-1}$ with 95% confidence interval (582.5, 1429.7), and the carbon footprint of ORG mode is 1271.7 ± 388.5 kg CO_2eq t^{-1} $year^{-1}$ with 95% confidence interval (663.9, 2175.8); the latter is extremely significantly higher than the former (p<0.0001). EF_c, t, Y, and SF_w contributed the most to the uncertainty of the carbon footprint of both rice production modes, and the correlation coefficient r was between 0.34 and 0.55; the r values for these parameters were very significant (p<0.01). Certainty can effectively improve the robustness and credibility of evaluation results. Reducing the uncertainty of these coefficients can effectively improve the robustness and credibility of the evaluation results. The analytical framework developed in the current study is applicable to other crops in different regions, and it can be used to guide researchers to formulate data inventory collection and optimization plans for carbon footprint evaluation of crop production, as well as to help policy makers assess whether the GHG mitigation is significant in future grain production.

Data availability statement

The original contributions presented in the study are included in the article/Supplementary Material. Further inquiries can be directed to the corresponding author.

Author contributions

QX: Conceptualization, methodology, formal analysis, writing - original draft, writing - review & editing, funding acquisition. JL: Visualization, data curation. HL: Methodology. ZDi: Investigation. XS: Methodology. YC: Investigation, data curation. ZDo: Investigation, data curation. QD: Supervision, funding acquisition. HG: Supervision. All authors jointly reviewed the manuscript and approved for publication. All authors contributed to the article and approved the submitted version.

Funding

The work was supported by the National Key Research and Development Project (2021YFD1700800), the Natural Science Foundation of Jiangsu Province (BK20210791), the Priority Academic Program Development of Jiangsu Higher Education Institutions (PAPD), the Lv Yang Jin Feng Research Plan of Yangzhou City (YZ-LYJF2020PHD100), and the Scientific Research Startup Foundation for Urgently-Needed Talents, Yangzhou University.

Conflict of interest

The authors declare that the research was conducted in the absence of any commercial or financial relationships that could be construed as a potential conflict of interest.

Publisher's note

All claims expressed in this article are solely those of the authors and do not necessarily represent those of their affiliated organizations, or those of the publisher, the editors and the reviewers. Any product that may be evaluated in this article, or claim that may be made by its manufacturer, is not guaranteed or endorsed by the publisher.

Supplementary material

The Supplementary Material for this article can be found online at: https://www.frontiersin.org/articles/10.3389/fpls.2022.990105/full#supplementary-material

References

Arunrat, N., Sereenonchai, S., and Wang, C. (2021). Carbon footprint and predicting the impact of climate change on carbon sequestration ecosystem services of organic rice farming and conventional rice farming: A case study in phichit province, Thailand. *J. Environ. Manage.* 289, 112458. doi: 10.1016/j.jenvman.2021.112458

Chen, X., Ma, C., Zhou, H., Liu, Y., Huang, X., Wang, M., et al. (2021). Identifying the main crops and key factors determining the carbon footprint of crop production in China 2001–2018. *Resour. Conserv. Recycl.* 172, 105661. doi: 10.1016/j.resconrec.2021.105661

De Koning, A., Schowanek, D., Dewaele, J., Weisbrod, A., and Guinée, J. (2010). Uncertainties in a carbon footprint model for detergents; quantifying the confidence in a comparative result. *Int. J. Life Cycle Assess.* 15, 79–89. doi: 10.1007/s11367-009-0123-3

FAO (2019) *FAOSTAT production data*. Available at: https://www.fao.org/faostat/en/#data.

Feng, Z. Y., Qin, T., Du, X. Z., Sheng, F., and Li, C. F. (2021a). Effects of irrigation regime and rice variety on greenhouse gas emissions and grain yields from paddy fields in central China. *Agric. Water Manage.* 250, 106830. doi: 10.1016/j.agwat.2021.106830

Feng, J., Yang, T., Li, F., Zhou, X., Xu, C., and Fang, F. (2021). Impact of tillage on the spatial distribution of CH4 and N2O in the soil profile of late rice fields. *Soil Tillage Res.* 211, 105029. doi: 10.1016/j.still.2021.105029

Hergoualc'h, K, Akiyama, H, Bernoux, M, Chirinda, N, Prado, A, Kasimir, Å, et al. (2019). *N2O emissions from managed soils, and CO2 emissions from lime and urea application*. 2019 Refinement to 2006 IPCC Guidel Natl Greenh Gas Invent. 2019, 1–48. Available at: https://www.ipcc-nggip.iges.or.jp/public/2019rf/index.html

IPCC. (2006). *Agriculture, forestry and other land use*. In: 2006 IPCC Guidelines for National Greenhouse Gas Inventories, ume 4. (Eds.) H.S. Eggleston, L. Buendia, K. Miwa, T. Ngara and K. Tanabe Institute for Global Environmental Strategies (IGES), Hayama, Japan. Available at: https://agris.fao.org/agris-search/search.do?recordID=NL2020024641

IPCC. (2013). *Climate Change 2013: the Physical Science Basis*. In: Contribution of Working Group I to the Fifth Assessment Report of the Intergovernmental Panel on Climate Change. Cambridge university Press, Cambridge, United Kingdom and New York, USA. Available at: https://doi.org/10.1017/CBO9781107415324

Jiang, Y., Carrijo, D., Huang, S., Chen, J., Balaine, N., Zhang, W., et al. (2019). Water management to mitigate the global warming potential of rice systems: A global meta-analysis. *F. Crop Res.* 234, 47–54. doi: 10.1016/j.fcr.2019.02.010

Jiang, Z., Zhong, Y., Yang, J., Wu, Y., Li, H., and Zheng, L. (2019). Effect of nitrogen fertilizer rates on carbon footprint and ecosystem service of carbon sequestration in rice production. *Sci. Total Environ.* 670, 210–217. doi: 10.1016/j.scitotenv.2019.03.188

Jóhannesson, S. E., Heinonen, J., and Davíðsdóttir, B. (2020). Data accuracy in ecological footprint's carbon footprint. *Ecol. Indic.* 111, 105983. doi: 10.1016/j.ecolind.2019.105983

Kashyap, D., and Agarwal, T. (2021). Carbon footprint and water footprint of rice and wheat production in punjab, India. *Agric. Syst.* 186, 102959. doi: 10.1016/j.agsy.2020.102959

Lathuillière, M. J., Johnson, M. S., Galford, G. L., and Couto, E. G. (2014). Environmental footprints show China and europe's evolving resource appropriation for soybean production in mato grosso, Brazil. *Environ. Res. Lett.* 9, 074001. doi: 10.1088/1748-9326/9/7/074001

Liang, H., Qi, Z., DeJonge, K. C., Hu, K., and Li, B. (2017). Global sensitivity and uncertainty analysis of nitrate leaching and crop yield simulation under different water and nitrogen management practices. *Comput. Electron. Agric.* 142, 201–210. doi: 10.1016/j.compag.2017.09.010

Liu, Q., Liu, B., Ambus, P., Zhang, Y., Hansen, V., Lin, Z., et al. (2016). Carbon footprint of rice production under biochar amendment - a case study in a Chinese rice cropping system. *GCB Bioenergy* 8, 148–159. doi: 10.1111/gcbb.12248

Meneses, M., Torres, C. M., and Castells, F. (2016). Sensitivity analysis in a life cycle assessment of an aged red wine production from Catalonia, Spain. *Sci. Total Environ.* 562, 571–579. doi: 10.1016/j.scitotenv.2016.04.083

Milne, A. E., Glendining, M. J., Bellamy, P., Misselbrook, T., Gilhespy, S., Rivas Casado, M., et al. (2014). Analysis of uncertainties in the estimates of nitrous oxide and methane emissions in the UK's greenhouse gas inventory for agriculture. *Atmos. Environ.* 82, 94–105. doi: 10.1016/j.atmosenv.2013.10.012

Morris, M. D. (1991). Factorial sampling plans for preliminary computational experiments. *Technometrics* 33, 161–174. doi: 10.1080/00401706.1991.10484804

Qian, H., Chen, J., Zhu, X., Wang, L., Liu, Y., Zhang, J., et al. (2022). Intermittent flooding lowers the impact of elevated atmospheric CO2 on CH4 emissions from rice paddies. *Agric. Ecosyst. Environ.* 329, 107872. doi: 10.1016/j.agee.2022.107872

Reisinger, A., Ledgard, S. F., and Falconer, S. J. (2017). Sensitivity of the carbon footprint of new Zealand milk to greenhouse gas metrics. *Ecol. Indic.* 81, 74–82. doi: 10.1016/j.ecolind.2017.04.026

Saltelli, A., Ratto, M., Andres, T., Campolongo, F., Cariboni, J., Gatelli, D., et al. (2008). *Global sensitivity analysis the primer, paper knowledge . toward a media history of documents* (England: John Wiley & Sons Ltd).

Saltelli, A., Tarantola, S., and Campolongo, F. (2000). Sensitivity analysis as an ingredient of modeling. *Stat. Sci.* 15, 377–395. doi: 10.1214/ss/1009213004

SimLab. (2010). *Software package for uncertainty sensitivity analysis*. Joint Research Centre of the European Commission. Available: http://simlab.jrc.ec.europea.eu

Singh, P., Singh, G., and Sodhi, G. P. S. (2020). Energy and carbon footprints of wheat establishment following different rice residue management strategies vis-à-vis conventional tillage coupled with rice residue burning in north-western India. *Energy* 200, 117554. doi: 10.1016/j.energy.2020.117554

Song, K., Zhang, G., Ma, J., Peng, S., Lv, S., and Xu, H. (2022). Greenhouse gas emissions from ratoon rice fields among different varieties. *F. Crop Res.* 277, 108423. doi: 10.1016/j.fcr.2021.108423

Sykes, A. J., Topp, C. F. E., and Rees, R. M. (2019). Understanding uncertainty in the carbon footprint of beef production. *J. Clean. Prod.* 234, 423–435. doi: 10.1016/j.jclepro.2019.06.171

Vanuytrecht, E., Raes, D., and Willems, P. (2014). Global sensitivity analysis of yield output from the water productivity model. *Environ. Model. Software* 51, 323–332. doi: 10.1016/j.envsoft.2013.10.017

Wang, D. (2016). *Climatic characters and varietal condition of high-yielding early, middle and late season rice in the middle and lower reaches of the Yangtze river* (Wuhan, Hubei Province: Huazhong Agricultural University).

Xu, Z., Chen, X., Liu, J., Zhang, Y., Chau, S., Bhattarai, N., et al. (2020). Impacts of irrigated agriculture on food–energy–water–CO2 nexus across metacoupled systems. *Nat. Commun.* 11, 5837. doi: 10.1038/s41467-020-19520-3

Xu, Q., Hu, K., Yao, Z., and Zuo, Q. (2020). Evaluation of carbon, nitrogen footprint and primary energy demand under different rice production systems. *Ecol. Indic.* 117, 106634. doi: 10.1016/j.ecolind.2020.106634

Xu, Y., Liang, L., Wang, B., Xiang, J., Gao, M., Fu, Z., et al. (2022). Conversion from double-season rice to ratoon rice paddy fields reduces carbon footprint and enhances net ecosystem economic benefit. *Sci. Total Environ.* 813, 152550. doi: 10.1016/j.scitotenv.2021.152550

Xu, Q., Yang, Y., Hu, K., Chen, J., Djomo, S. N., Yang, X., et al. (2021). Economic, environmental, and emergy analysis of china's green tea production. *Sustain. Prod. Consum.* 28, 269–280. doi: 10.1016/j.spc.2021.04.019

Yang, Y., Zhang, G., Ma, J., Huang, Q., Yu, H., Song, K., et al. (2021). Responses of the methanogenic pathway and fraction of CH4 oxidization in a flooded paddy soil to rice planting. *Pedosphere* 31, 859–871. doi: 10.1016/S1002-0160(21)60020-6

Yodkhum, S., Gheewala, S. H., and Sampattagul, S. (2017). Life cycle GHG evaluation of organic rice production in northern Thailand. *J. Environ. Manage.* 196, 217–223. doi: 10.1016/j.jenvman.2017.03.004

Yuan, S., Linquist, B. A., Wilson, L. T., Cassman, K. G., Stuart, A. M., Pede, V., et al. (2021). Sustainable intensification for a larger global rice bowl. *Nat. Commun.* 12, 7163. doi: 10.1038/s41467-021-27424-z

Zhang, L., Ruiz-Menjivar, J., Tong, Q., Zhang, J., and Yue, M. (2021). Examining the carbon footprint of rice production and consumption in hubei, China: A life cycle assessment and uncertainty analysis approach. *J. Environ. Manage.* 300, 113698. doi: 10.1016/j.jenvman.2021.113698

Zhou, Y., Liu, K., Harrison, M. T., Fahad, S., Gong, S., Zhu, B., et al. (2022). Shifting rice cropping systems mitigates ecological footprints and enhances grain yield in central China. *Front. Plant Sci.* 13. doi: 10.3389/fpls.2022.895402

Zhuo, L., Mekonnen, M. M., and Hoekstra, A. Y. (2014). Sensitivity and uncertainty in crop water footprint accounting: A case study for the yellow river basin. *Hydrol. Earth Syst. Sci.* 18, 2219–2234. doi: 10.5194/hess-18-2219-2014

frontiers | Frontiers in Plant Science

TYPE Original Research
PUBLISHED 28 November 2022
DOI 10.3389/fpls.2022.1034406

OPEN ACCESS

EDITED BY
Mohammad Irfan,
Cornell University, United States

REVIEWED BY
Ghana Shyam Challa,
Independent Researcher,
College Station, United States
Liangliang Gao,
Kansas State University, United States

*CORRESPONDENCE
William T. Hay
William.Hay@usda.gov

SPECIALTY SECTION
This article was submitted to Crop and Product Physiology, a section of the journal Frontiers in Plant Science

RECEIVED 01 September 2022
ACCEPTED 11 November 2022
PUBLISHED 28 November 2022

CITATION
Hay WT, Anderson JA, Garvin DF, McCormick SP and Vaughan MM (2022) *Fhb1* disease resistance QTL does not exacerbate wheat grain protein loss at elevated CO_2. *Front. Plant Sci.* 13:1034406. doi: 10.3389/fpls.2022.1034406

Fhb1 disease resistance QTL does not exacerbate wheat grain protein loss at elevated CO_2

William T. Hay[1*], James A. Anderson[2], David F. Garvin[2], Susan P. McCormick[1] and Martha M. Vaughan[1]

[1]Mycotoxin Prevention and Applied Microbiology Unit, National Center for Agricultural Utilization Research, Agricultural Research Service, USDA, Peoria, IL, United States, [2]Department of Agronomy & Plant Genetics, University of Minnesota, St. Paul, MN, United States

Fusarium head blight, a devastating cereal crop disease, can cause significant yield losses and contaminate grain with hazardous fungal toxins. Concerningly, recent evidence indicates that substantial grain protein content loss is likely to occur in wheat that is moderately resistant to head blight when it is grown at elevated CO_2. Although wheat breeders in North America utilize a number of resistance sources and genes to reduce pathogen damage, the *Fhb1* gene is widely deployed. To determine whether *Fhb1* is associated with the protein content loss at elevated CO_2, twelve near-isogenic spring wheat lines from either a susceptible or moderately susceptible genetic background, and with, or without the *Fhb1* QTL, were grown at ambient and elevated CO_2 conditions. The near-isogenic lines were evaluated for differences in physiology, productivity, and grain protein content. Our results showed that the *Fhb1* QTL did not have any significant effect on plant growth, development, yield, or grain protein content at ambient or elevated CO_2. Therefore, other factors in the moderately susceptible wheat genetic background are likely responsible for the more severe grain protein loss at elevated CO_2.

KEYWORDS

wheat, fusarium head blight, climate resilience, *Fhb1*, elevated CO_2, grain protein content

Introduction

Fusarium head blight (FHB), a devastating disease of cereal crops, can cause significant yield losses and contaminate grain with toxins that remain even after typical food processing (Goswami and Kistler, 2004; Bullerman and Bianchini, 2007). In North America, FHB is predominately caused by mycotoxigenic members of the

Abbreviations: FHB, Fusarium head blight; a[CO_2], Ambient CO_2; e[CO_2], Elevated CO_2; SB, Susceptible genetic background; MSB, Moderately susceptible genetic background; QTL, Quantitative trait loci.

Fusarium graminearum (*Fg*) species complex (O'Donnell et al., 2004; Ward et al., 2008). The initial infection begins through the exposed anthers and then the hyphae rapidly infiltrate into the rachis (Brown et al., 2010). There, the pathogen begins producing trichothecene mycotoxins, especially deoxynivalenol (DON), a cytotoxic virulence factor which causes plant cell death ahead of the infection and assists pathogen colonization of the wheat head (Goswami and Kistler, 2004). DON tightly binds to Eukaryotic ribosomes, preventing protein synthesis (Pestka, 2007; Wang et al., 2021). As the infection proceeds, grain yield and quality quickly diminish, leaving withered toxin-contaminated grains unsuitable for food, or feed (Argyris et al., 2003; Awad et al., 2014). Although there are no known wheat varieties that are fully resistant to FHB, a number of gene loci can provide a measure of resistance to the disease (Buerstmayr et al., 2002; Lin et al., 2004; Steiner et al., 2004; Zhu et al., 2019).

Wheat resistance to FHB is a complex quantitative trait controlled by numerous small- to medium-effect quantitative trait loci (QTL) (Buerstmayr et al., 2002; Buerstmayr et al., 2013; Steiner et al., 2019). Despite intensive study, completely FHB-resistant germplasm has not been identified, and only a limited number of QTL have been validated to confer stable FHB resistance (Wang et al., 2020). The most widely used QTL in breeding programs worldwide is *Fhb1*, which originated from Chinese wheat, primarily spring wheat cultivar Sumai 3 (Anderson et al., 2001; Rudd et al., 2001; Buerstmayr et al., 2009; Xue et al., 2011). The *Fhb1* QTL is located on the short arm of the 3B chromosome in wheat populations derived from Sumai 3 (Bai et al., 1999; Waldron et al., 1999; Anderson et al., 2001). In the U.S. and Canada, almost all FHB moderately resistant (MR) hard red spring wheat cultivars currently being used for wheat production have Sumai 3 or its derivatives as an FHB resistance source, and breeding efforts often have focused on selecting genotypes with the *Fhb1* QTL (Hao et al., 2020). While *Fhb1* does not prevent initial *Fg* infection (Type I resistance), it does slow and reduce the spread of the fungal pathogen (Type II resistance) (Lin et al., 2004; Cuthbert et al., 2006; Lin et al., 2006). The identification and functional validation of candidate genes responsible for increased resistance to FHB within the *Fhb1* locus has proven challenging and contentious (Rawat et al., 2016; He et al., 2018; Jia et al., 2018; Soni et al., 2020; Soni et al., 2021). A putative pore-forming toxin-like gene (*PFT)* was identified within the *Fhb1* locus and was predicted to encode a chimeric lectin with two agglutinin domains (Rawat et al., 2016). Transgenic expression of this gene provided a degree of resistance to FHB and the protein encoded by *PFT* was predicted to function as a plant defense protein capable of recognizing fungus-specific carbohydrates and causing membrane damage to potential pathogens. However, in experiments with twelve different wheat varieties of varying levels of FHB resistance the *PFT* gene was found in both FHB resistant and susceptible wheat (He et al., 2018). While the *PFT* gene was associated with, and explains a small part of FHB Type II resistance, it also increased in gene expression in response to abiotic plant stress, methyl jasmonate, abscisic acid, and is likely a part of a multi genic plant defense response.

In Sumai 3, plant defense against FHB is primarily due to the induction of phenylpropanoids, thickening of cell walls that reduce pathogen advancement, and synthesis of antifungal and antioxidant metabolites that reduce pathogen proliferation and DON production (Gunnaiah and Kushalappa, 2014). A recent metabolo-genomics study identified the *TaLAC4* candidate gene in the *Fhb1* locus that is predicted to encode a wheat laccase protein involved in the lignification of secondary cell walls in the wheat rachis (Soni et al., 2020). When the *TaLAC4* gene was silenced total lignin deposition declined, fungal biomass increased, and disease severity worsened. The same research group identified the *TaNAC032* transcription factor involved in regulating lignin biosynthesis, including the *TaLAC4* gene (Soni et al., 2021). When the transcription factor was silenced there was less lignin deposition in the vascular tissues of the wheat rachis and disease susceptibility increased.

Breeders have also introgressed other FHB disease resistance QTLs into wheat, such as *Fhb2, Fhb4, Fhb5, Fhb7* and numerous other minor loci associated with plant defense, kinases, nucleotide-binding and leucine rich repeats (Bent and Mackey, 2007; Brar et al., 2019a; Zhu et al., 2019; Ma et al., 2020). Alone or combined, these loci can contribute to FHB resistance. However, incorporation, and especially stacking of these resistance traits, can have negative pleiotropic effects on yield, grain quality, and grain protein content (McCartney et al., 2007; Brar et al., 2019b). Furthermore, we recently demonstrated a correlation between the degree of wheat FHB resistance and loss of grain nutritional content, particularly grain protein content, at elevated CO_2 (Hay et al., 2022).

Grain from wheat grown at elevated CO_2 typically accumulates more carbohydrates and therefore, on a relative basis, contains less protein, minerals, and lipids (Högy and Fangmeier, 2008; Ainsworth and Long, 2021). This alteration in nutritional composition is often referred to as dilution and is caused by enhanced photosynthetic carbon metabolism at elevated CO_2, as excess carbohydrates are deposited in the grain as starch (Högy and Fangmeier, 2008; Taub and Wang, 2008; Fernando et al., 2014; Broberg et al., 2017). The loss of grain protein can result in flour that is less nutritious, has reduced baking quality, and compromised end-use utility (Panozzo et al., 2014; Fernando et al., 2015). Beyond impacting food quality, alterations in wheat grain nutritional content at elevated CO_2 can cause *Fg* to significantly increase mycotoxin biosynthesis, as shown in the MR wheat cultivar Alsen (Hay et al., 2020). Moreover, numerous reports have demonstrated that rising atmospheric CO_2 is likely to increase wheat susceptibility to FHB (Váry et al., 2015; Vaughan et al., 2016; Bencze et al., 2017; Cuperlovic-Culf et al., 2019). Alarmingly, the deleterious effects of elevated CO_2 on wheat nutrition were found to be more severe for MR cultivars, compared with susceptible wheat, and was directly

correlated with the accumulation of the storage carbohydrate starch (Hay et al., 2022). It was unclear from that study whether *Fhb1* was associated with the decline in grain protein content. While most of impacted cultivars had *Fhb1*, one MR wheat cultivar Bolles, which does not contain *Fhb1*, also had significant protein losses. None of the varieties which exhibited severe protein loss at elevated CO_2 had *Fhb1* near isogenic lines (NIL) to compare. However, other *Fhb1* NIL wheat lines were readily available for comparison including one set with the Sumai 3 background.

Due to the significant utilization of the *Fhb1* locus for breeding FHB resistance into wheat, it was vital to determine whether *Fhb1* was associated with significant grain protein content loss at elevated CO_2. Based on our previous results, we hypothesized that another factor in the wheat genetic background, not *Fhb1*, was responsible for the loss in grain protein content. To test this hypothesis, two sets of near-isogenic wheat lines from either a susceptible or moderately susceptible genetic background, and either with (Fhb1+), or without (Fhb1-), the *Fhb1* QTL (Table 1), were grown in a completely random block design at ambient (400 ppm) or elevated (1000 ppm) CO_2 conditions. In addition to grain protein content, the near-isogenic lines were evaluated for differences in development, growth, and productivity. Differences between wheat genetic background or the presence of *Fhb1* were used to evaluate whether either was associated with loss of grain protein at elevated CO_2.

Materials and methods

Fhb1 near-isogenic lines

This study employed two sets of NILs to evaluate the effects of *Fhb1* in FHB susceptible or moderately susceptible wheat genetic backgrounds. The first set of NILs include the hard red spring wheat cultivars Norm, Wheaton, and Apogee. Norm (Busch et al., 1993) and Wheaton (Busch et al., 1984) were developed by USDA-ARS and the Minnesota Agricultural Experiment Station, and Apogee (Bugbee et al., 1997) was developed at Utah State University. Norm and Wheaton long have served as susceptible checks in FHB research, while Apogee has been proposed as a model for FHB research because of its short stature, rapid life cycle, and high level of FHB susceptibility (Mackintosh et al., 2006). Near-isogenic lines harboring *Fhb1* developed for each of these cultivars were also employed in this study. These were generated first by crossing Sumai 3 as the donor of *Fhb1* to each cultivar. A simple sequence repeat molecular marker locus linked to *Fhb1*, *Xgwm493* (Röder et al., 1998), was then employed to select for the presence of *Fhb1* over the course of four generations of marker-assisted backcrossing, with the cultivars serving as recurrent parents. In each cultivar's backcross pedigree, BC_4F_1 plants were surveyed for heterozygosity at *Fhb1*, based on the genotype of the linked molecular marker. A heterozygote within each cultivar's backcross pedigree that had morphological similarity to the recurrent parents was self-pollinated, and from each resultant BC_4F_2 family a single plant homozygous for *Fhb1* was identified and grown to maturity to obtain a BC_4F_3 *Fhb1* near-isogenic line for each cultivar. These *Fhb1* near-isogenic lines are designated N1 (Norm near-isogenic line), W4 (Wheaton near-isogenic line, and A73 (Apogee near-isogenic line). These NILs are predicted to be more than 95% genetically identical to their respective parental cultivars; each backcross (BC) generation increases recurrent parent homozygosity by 50% of the remaining heterozygous loci. Self-fertilization, or selfing, increases recurrent parent homozygosity by 25% of the existing heterozygous loci. For example, by BC_4, the NIL with *Fhb1* would be approximately 94% homozygous for the recurrent

TABLE 1 Breeding pedigrees for wheat genotypes in the current study.

Genotype	Background	*Fhb1* QTL	Pedigree
260-4	MSB	–	Sumai 3/Stoa RIL 63–4//MN97448
HR 45	MSB	–	Sumai 3/Stoa RIL 63–4//MN97448
HR 123	MSB	–	Sumai 3/Stoa RIL 63–4//MN97448
260-2	MSB	+	Sumai 3/Stoa RIL 63–4//MN97448
HR 56	MSB	+	Sumai 3/Stoa RIL 63–4//MN97448
HR 58	MSB	+	Sumai 3/Stoa RIL 63–4//MN97448
Apogee	SB	–	Apogee
Norm	SB	–	Norm
Wheaton	SB	–	Wheaton
A73	SB	+	Apogee*5/Sumai 3: BC_4F_3
N1	SB	+	Norm*5/Sumai 3: BC_4F_3
W4	SB	+	Wheaton*5/Sumai 3: BC_4F_3

Genetic background of wheat genotypes, as defined by whether the parental cultivars are moderately susceptible (MSB) or susceptible (SB) to FHB infection, and whether a genotype has (+), or does not have (-) the *Fhb1* QTL.

parent genome. Selfing a BC_4F_1 plant would increase this to 95.5% or so in a BC_4F_2 progeny and selfing a BC_4F_2 plant would increase this to more than 97%. For this manuscript, this set of NILs is defined as from a susceptible genetic background (SB), due to each parental cultivars' salient susceptibility to FHB infection. In previous experiments, Norm and Wheaton did not have inordinate grain protein loss at elevated CO_2, as compared with the significant protein decline observed in some wheat cultivars more resistant to FHB (Hay et al., 2020; Hay et al., 2022).

The second set of NILs was developed during the fine mapping of *Fhb1* (Liu et al., 2006). These six lines, designated as 260-2, 260-4, HR 45, HR 56, HR 58, and HR 123 all have the pedigree (Sumai 3/Stoa RIL 63–4//MN97448) and were derived from a single F_7 plant that was heterozygous for *Fhb1*. This NIL set possesses some degree of FHB resistance but were developed to have a genetic background which was only moderately susceptible to FHB; moderate susceptibility to FHB was necessary to characterize the effect of *Fhb1* on disease resistance for mapping the genomic region harboring *Fhb1*. For this manuscript, the set of NILs from the Sumai 3/Stoa RIL 63–4//MN97448 pedigree are defined as from a moderately susceptible genetic background (MSB) for comparison with the set of SB NILs derived from Norm, Wheaton and Apogee.

Growing conditions and evaluating productivity

To evaluate how the presence, or absence, of the *Fhb1* QTL impacted wheat grain protein content, the various wheat genotypes (Table 1) were grown in PGR15 environmentally controlled growth chambers (Controlled Environments INC., Manitoba, Canada). The wheat genotypes were grown in a completely random block design, with the growth chambers blocked into four pairs, each block containing a chamber set to ambient [CO_2] (420 ± 20 ppm, a[CO_2]) and a chamber set to 1000 ± 20 ppm [CO_2] (e[CO_2]). For each genotype, eight seeds were sown in a 20 × 15-cm plastic pot, filled with approximately 4 L of SunGrow Horticulture potting mix (Agawam, MA, U.S.A.), and thinned to 5 plants shortly after seedling emergence. Growth chambers were programmed to a day/night cycle of 25/23°C, respectively, with a 14 h photoperiod at 550 µmol m^{-2} s^{-1} photosynthetic photon flux density from incandescent and fluorescent light sources. The relative humidity was maintained in the range of 50-60% throughout the experiment. The plants were watered daily, and plant positions were randomized after each watering. Additionally, plants received a biweekly fertilization with soluble Peters 20-20-20 nutrient supplement (The Scotts Company, Marysville, OH, U.S.A.) until flowering. The developmental timings of heading (Feekes 10.2), flowering (Feekes 10.5.2), and maturity (Feekes 11.3) were recorded. Seed filling days were determined as the number of days from flowering to maturity. Tiller height and total number of tillers were evaluated after physiological maturity (Feekes 11.3), and grain was harvested for yield after ripening (Feekes 11.4). Remaining wheat straw was collected to gravimetrically determine above ground biomass. Wheat grain moisture and protein content was assessed by a DA 7250 near-infrared (NIR) analyzer (Perten Instruments, Springfield, IL). All local and national regulations were followed, and all relevant permissions were acquired for wheat cultivation and harvest; no genetically modified plants were used.

Statistical analyses

Results were evaluated by a generalized linear mixed model analysis of variance, with paired growth chamber blocks as a random effect (JMP V15.0), to determine significant differences between genotypes and wheat genetic background due to the effects of elevated CO_2 ($\alpha = 0.05$). Details on pairwise comparisons can be found within the table and figure legends. Principal component analysis was performed in JMP V15.0. Additionally, a permutational multivariate analysis of variance was performed in R 4.2.1 ("Prairie Trillium" release, 'Vegan' R package 2.6-2) to determine how variation was attributed to the experimental treatments.

Results

Effects of elevated CO_2 on plant development, yield, and grain protein

Grain protein content was strongly affected by elevated CO_2, particularly in MSB wheat, with significant interactions in both genotype × [CO_2] ($P = 0.0038$) and wheat genetic background × [CO_2] ($P < 0.0001$). The *Fhb1* QTL was not a significant contributing factor to differences in grain protein content ($P=0.2112$). In ambient conditions, wheat grain contained equivalent protein content ($P = 0.1351$), with the MSB and SB wheat having 16.95% and 16.21% grain protein content, respectively. At elevated CO_2, every MSB wheat genotype, except HR 56, had significant losses of grain protein content (-12.5% on average), whereas the grain protein content of SB was not impacted (-1.2% on average; Figure 1A), when compared with respective genotype at ambient conditions. Grain protein loss at elevated CO_2 was consistently worse in the MSB genetic background ($P = 0.0002$; Figure 1B), with *Fhb1* having no impact, as no significant genetic background × [CO_2] × *Fhb1* three-way interaction was found ($P = 0.8562$).

While developmental timings varied greatly by genotype, wheat heading and flowering were not significantly impacted by *Fhb1* or plant growth at elevated CO_2. However, the number of seed filling days, and the number of days till physiological

10.3389/fpls.2022.1034406

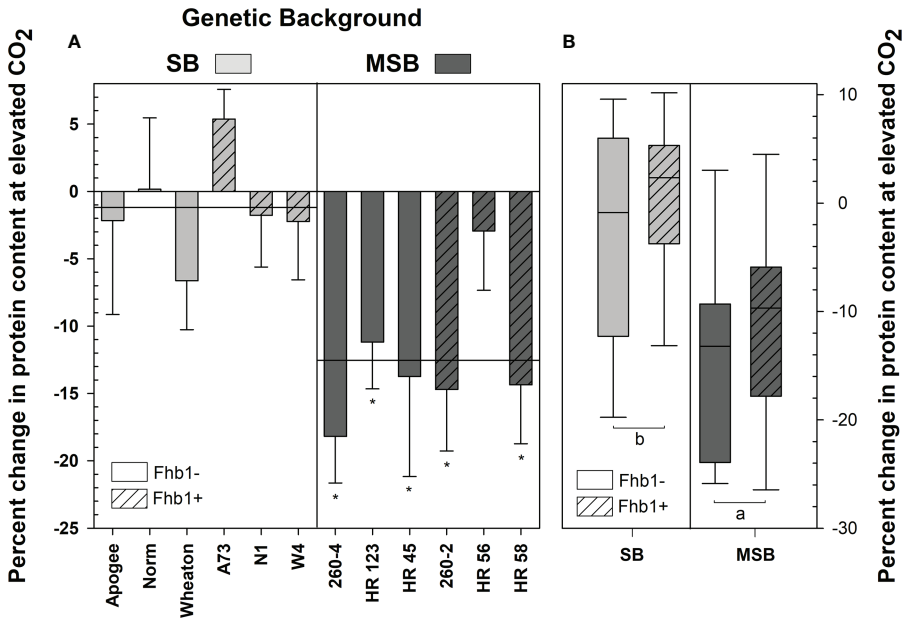

FIGURE 1
Percent change in grain protein of wheat from a *Fusarium* head blight (FHB) moderately susceptible (MSB) or susceptible (SB) genetic background with (Fhb1+) or without (Fhb1-) the *Fhb1* QTL, grown at elevated CO_2 (e[CO_2]) or ambient (a[CO_2]). **(A)** Percent change in grain protein content of wheat genotypes at e[CO_2]. Horizonal lines represent the average percent change in grain protein at e[CO_2] for each genetic background, error bars represent standard error. Asterisks (*) denote statistically significant differences in grain protein content at e[CO_2] versus a[CO_2] for a respective genotype as determined by a Student's t Test ($P<0.05$; $n = 4$), performed after a significant genotype × [CO_2] interaction was found. **(B)** Percent change in protein content by genetic background and the presence of *Fhb1*. Different letters denote statistically significant differences as determined by an ANOVA ($P<0.05$); $n = 24$ (JMP V15.0).

maturity (Feekes 11.3) were significantly reduced at elevated CO_2 for the MSB wheat, compared with the SB (Figure 2).

For the MSB wheat, the number of seed filling days was correlated with grain protein content across all CO_2 conditions (Figure 3A), however growth at elevated CO_2 significantly reduced both grain protein and seed filling days. The total seed filling days were not significantly correlated with yield in MSB (Figure 3B). MSB wheat yields increased at elevated CO_2 even as the total seed filling days and protein content declined. When examining MSB wheat only at e[CO_2] (Supplementary Figure 1), the number of seed filling days were not significantly correlated with grain protein content ($r^2 = 0.093$; $P=0.146$). Therefore, the reduced number of seed filling days at elevated CO_2 is associated, but not necessarily the direct cause of reduced grain protein content in MSB.

Wheat grown at elevated CO_2 had significantly increased plant height ($P <0.0001$), above ground biomass accumulation ($P <0.0001$), and yield per plant ($P <0.0001$). Although MSB wheat grain protein content (% protein) severely declined at elevated CO_2 (Figure 1), the improved yield caused the total amount of harvestable grain protein per plant to significantly increase at elevated CO_2. At a[CO_2] wheat had an average of 0.949 g protein/plant of total grain protein, but at e[CO_2] this average increased to 1.065 g protein/plant ($P = 0.0019$). While there were significant genotype differences, particularly due to the superdwarf habit and rapid life cycle of Apogee and A73, *Fhb1* had no significant impact on these physiological characteristics and there were no significant genetic background × [CO_2] interactions (Figure 4). The average seed weight was not impacted by growth at elevated CO_2, and therefore differences in yield were not due to changes in seed weight. Yield increases were most likely due to an increase in the number of tillers per plant, with a 27% increase at elevated CO_2 for all genotypes ($P<0.0001$), an average increase of approximately one additional tiller per plant. There was no significant impact of *Fhb1* on tiller number ($P = 0.787$), nor a significant *Fhb1* × [CO_2] interaction ($P = 0.630$). Furthermore, there was no significant genetic background × [CO_2] interaction ($P = 0.422$), and therefore, the increase in tiller number at elevated CO_2 was not associated with protein loss in MSB.

Impact of *Fhb1* or genetic background on wheat characteristics

Neither the presence of the *Fhb1* QTL in SB, nor the absence of the *Fhb1* QTL in MSB wheat had any significant effect on plant growth, development, or yield characteristics in ambient or

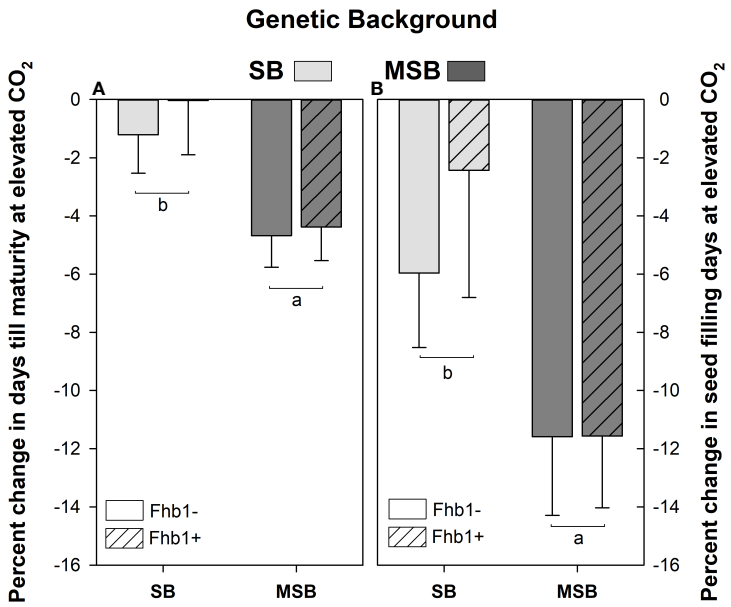

FIGURE 2
Percent change in seed filling days and days till physiological maturity for *Fusarium* head blight (FHB) moderately susceptible background (MSB) or susceptible background (SB), with (Fhb1+) or without (Fhb1-) the *Fhb1* QTL, grown at elevated CO_2 (e[CO_2]) versus ambient (a[CO_2]). **(A)** Percent change in days till physiological maturity at e[CO_2], **(B)** Percent change in seed filling days at e[CO_2]. Error bars represent standard error. Different letters denote statistically significant differences as determined by an ANOVA (P<0.05); *n* = 24 (JMP V15.0).

elevated CO_2 (Figure 5B). Above ground biomass accumulation at elevated CO_2 appeared to be impacted by *Fhb1*, but the effect was not statistically significant at an alpha level of 0.05 (P = 0.093). Wheat genetic background was the significant contributing factor in determining plant response to elevated CO_2, as protein loss was worsened by growth at elevated CO_2 in MSB, compared with SB (Figure 1, 5A).

Furthermore, a principal component analysis of the wheat traits showed that the near isogenic lines were closely clustered, regardless of the presence of the *Fhb1* QTL (Supplementary Figure 2). When determining which controlled variables, i.e. CO_2, genetic background, or *Fhb1*, were most responsible for the variance in the analysis, both genetic background (P<0.0001) and CO_2 (P<0.0001) were found to be significant and accounted for 20% and 15% of the variance, respectively. However, the *Fhb1* QTL was not significant (P = 0.611), and only accounted for 0.4% of the variance in the analysis. Therefore, the presence of *Fhb1* had no significant impact on wheat growth and productivity.

Discussion

Our results demonstrate that the *Fhb1* QTL was not associated with grain protein content loss in wheat grown at elevated CO_2. However, we found that wheat from the Sumai 3/Stoa RIL 63–4//MN97448 pedigree suffered severe grain protein loss at elevated CO_2. The Sumai 3 cultivar and its derivatives have been extensively utilized as a source of FHB resistance; however the cultivar has poor agronomic traits and breeders often have difficulty obtaining derivative breeding lines with acceptable performance (Bai et al., 2018; Zhu et al., 2019; Zhang et al., 2021). Resistance traits often incur a fitness cost, as resources used for plant self-protection become unavailable for growth or reproduction (Brown and Rant, 2013). Identifying which genes, or polygenes, are responsible for a trait is costly, difficult, and time consuming; evermore so when determining how disease resistance tradeoffs are balanced with crop performance. This defense trade-off paradigm, particularly with FHB resistance, often means the introgression of traits that only provide moderate disease resistance but are frequently associated with reduced crop performance, diminished grain protein and grain quality (McCartney et al., 2007).

However, we found that *Fhb1* had no negative impact on the agronomic traits assessed in this study; this is consistent with previous reports on wheat that had incorporated *Fhb1* from a number of Chinese donor cultivars highly resistant to FHB (Li et al., 2019; Zhang et al., 2021). It should be noted, *Fhb1* has been observed to negatively impact grain protein content in wheat, particularly when coupled with the *Fhb5* QTL (Brar et al., 2019a; Brar et al., 2019b). Sumai 3, the key parental line providing resistance factors for the genotypes in this study (Table 1), contains *Fhb1*, *Fhb2*, *Fhb5* and other minor alleles associated

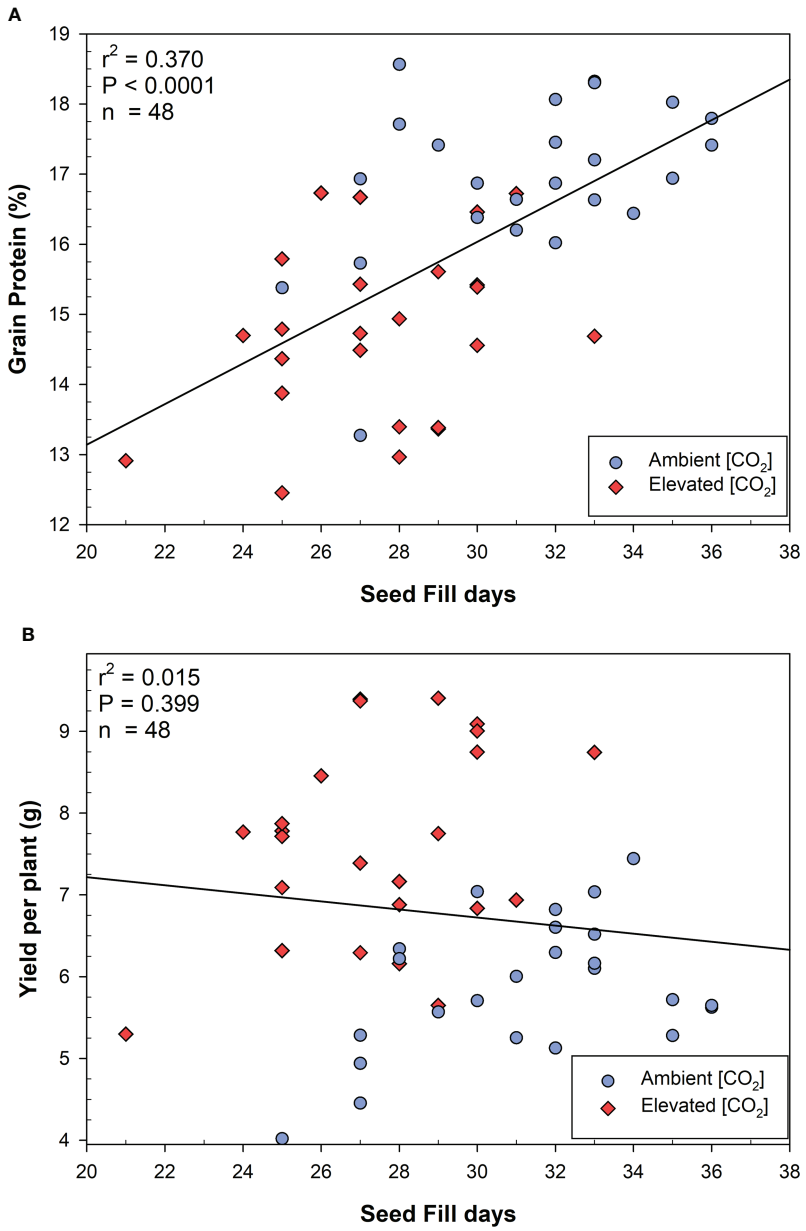

FIGURE 3
Linear correlations between **(A)** seed fill days and grain protein content, **(B)** seed fill days and yield per plant in moderately susceptible wheat. Linear fits were produced, and the analysis of variance was performed using JMP V15.0.

with cell wall thickening and Type II FHB resistance (Brar et al., 2019a). The *Fhb5* resistance loci is associated with Type I resistance, or the prevention of the initial fungal infection (Xue et al., 2011); the *Fhb1 and Fhb2* QTLs provides Type II resistance which improves wheat resistance to pathogen spread (Bai et al., 1999; Buerstmayr et al., 2002; Cuthbert et al., 2006; Yang et al., 2006). The *Fhb5* QTL has been associated with significant reductions in grain protein content when introgressed into wheat cultivars (McCartney et al., 2007; Brar et al., 2019b). However, the *Fhb2* QTL may have also been partially responsible for alterations in grain protein content, but it is currently unclear due to differences in trait conditions and wheat genetic backgrounds (Zhang et al., 2021). Further research is required to determine whether, or which, FHB resistance factor is responsible for the grain protein loss observed in MSB wheat at elevated CO_2.

Preventing grain protein loss is particularly important since the utility of wheat flour is predominately determined by grain

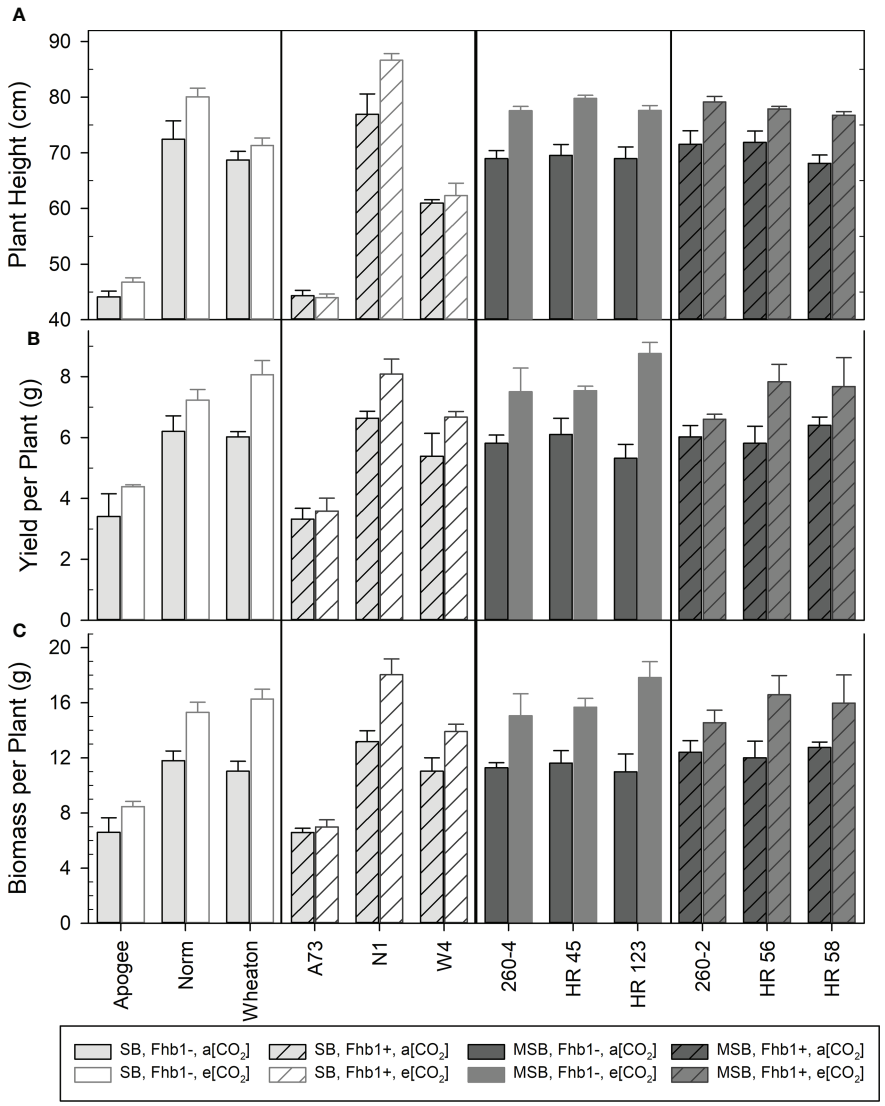

FIGURE 4
Mean plant height **(A)**, yield per plant **(B)**, and above ground biomass per plant **(C)** for various genotypes, with (Fhb1+), or without (Fhb1-), the *Fhb1* QTL, from either a moderately susceptible (MSB) or susceptible (SB) wheat genetic background at ambient (a[CO_2]), or elevated (e[CO_2]) carbon dioxide concentration. Error bars represent standard error.

protein content, as flour hydration forms a viscoelastic dough where gluten protein structure sets and determines the final processing characteristics and texture; high protein flours are chiefly utilized for breads and pastas, while lower protein flours are typically used for cakes, cookies, and pastries (Delcour et al., 2012). The large decreases in grain protein content observed at elevated CO_2 represents a concerning threat to future food quality and nutritional integrity. Environmental factors such as CO_2 concentration, as well as abiotic and biotic stresses, particularly during the critical spike formation and seed development phases, can impact yield and grain protein content to varying degrees (Fernando et al., 2014; Wang and Liu, 2021). Abiotic stresses, such as heat and drought, will reduce yield due to failures in photosynthetic competency and a lack of photosynthate during seed fill, resulting in reduced seed size, mass, total grain carbohydrate and overall yield (Begcy and Walia, 2015). Grain protein content is proportionally increased due to the inability to remobilize soluble carbohydrates, but the functional protein quality and total harvestable protein is overwhelming reduced in severe heat and drought stress (Saint Pierre et al., 2008; Farooq et al., 2011).

In contrast, rising atmospheric CO_2 can dramatically alter the primary metabolism of C3 photosynthetic crops, with increased photosynthetic rates and grain carbohydrate

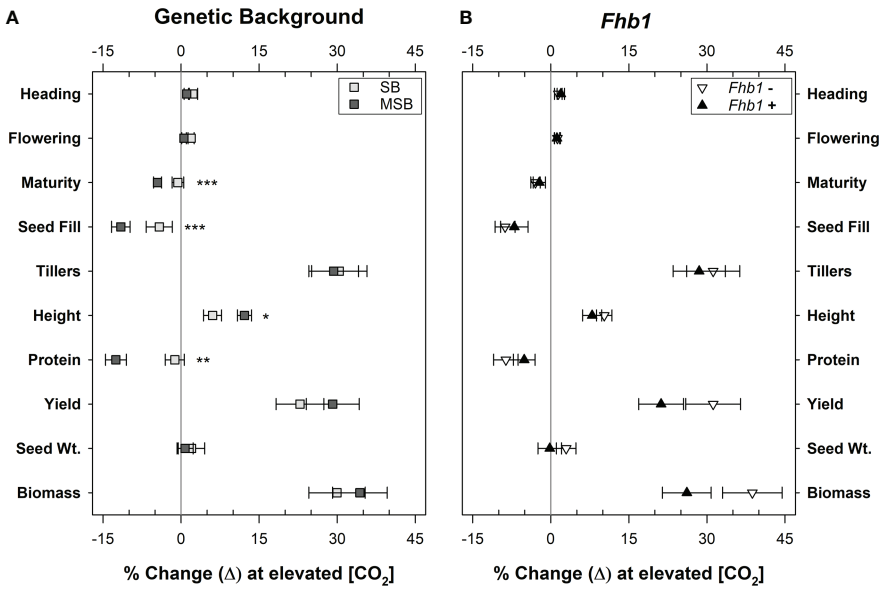

FIGURE 5
Percent change in wheat characteristics due to growth at elevated CO_2, by genetic background or the presence of the *Fhb1* QTL. Groups are **(A)**, wheat from either a moderately susceptible (MSB) or susceptible (SB) genetic background (n = 24) or **(B)**, wheat with, or without, the *Fhb1* QTL (n = 24). Points represent the mean percent change by group. Error bars represent standard error. Change in plant developmental timings, as defined by the number of days till plants achieved Heading, Flowering, Maturity and the total days of Seed Fill. Change in productivity measures, as defined by the numbers of wheat Tillers, plant Height, grain Protein, Yield per plant, the average seed weight (Seed Wt.), above ground biomass per plant (Biomass). Asterisks (*, *, ***) denote statistically significant differences in plant characteristics at elevated CO_2 ($P<0.05$, $P<0.01$, $P<0.0001$, respectively), as determined by a Student's t Test (n = 24).

deposition (Broberg et al., 2017). As observed in this study, grain protein content loss was not due to a failure of seed development or stunted seed size, as the average seed weight was not affected by elevated CO_2. The stable seed weight, even at elevated CO_2, is consistent with the wheat being sink-limited during seed fill, rather than source-limited, *i.e.*, the available photosynthate and remobilized nutrients exceeded the sink demand of the forming seed (Borrás et al., 2004). Our results demonstrated that overall yields significantly increased in all genotypes at elevated CO_2 (Figure 4 & 5), a consistent response of C3 photosynthetic crops (Ainsworth and Long, 2021). The additional photosynthate from enhanced photosynthetic carbon assimilation at elevated CO_2 is typically utilized for greater vegetative growth, and then devoted to additional seed carrying capacity (Hay et al., 2017). In wheat, the plants produce additional tillers at elevated CO_2 (Hay et al., 2022), consistent with the results of the current study. The most important component of a healthy crops' yield is the total number of seeds in the cultivated area (Borrás et al., 2004). Even though modern wheat cultivars reflect exceptional breeding progress in yield improvements they are still considered more sink than source limited, due in part to inadequate seed number and size (Foulkes et al., 2011).

Furthermore, the decline of grain protein content (Figure 1) was not due to a lack of nitrogen uptake or availability, as the total harvestable grain protein per plant (g protein/plant) was greater due to increased yields at elevated CO_2, consistent with previous studies (Ziska et al., 2004). Rather, grain protein was likely being overwhelmed by the amount of carbohydrate deposited in the grain during seed fill, as observed in our previous report (Hay et al., 2022). Seed nitrogen is predominately (65%) assimilated pre-anthesis and is remobilized from vegetative tissue, starting just before or immediately after anthesis, as photosynthetic machinery, chloroplasts, and other cellular structures are disassembled for transport (Zhou et al., 2016). Wheat with low harvest index and poor sink strength had down regulated amino acid assimilation and a depletion in N, NO_{3^-}, and amino acid content, but up-regulated starch synthesis; this resulted in the downregulation of photosynthesis and reduced plant growth response to elevated CO_2 (Aranjuelo et al., 2013). However, a lack of proper nitrogen remobilization coupled with the impairment of nitrate uptake and assimilation did not impact yield increases at elevated CO_2, but instead directly affected grain protein accumulation (Pleijel and Uddling, 2012).

Furthermore, as photosynthate builds up in the leaf tissue, due to insufficient seed sink capacity, the accumulation of leaf sugars promotes the onset of senescence (Wingler et al., 1998). The early termination of grain filling can start due to a loss of sink activity, rather than a lack of assimilate during seed fill (Kim et al., 2011). In our study, we found that the MSB wheat had

significantly reduced time for seed fill at elevated CO_2. It is not clear that this was the cause of reduced nitrogen mobilization, but it is clearly correlated (Figure 3). In the plant species *Ricinus communis*, phloem carbon export from leaves was significantly greater at night in elevated CO_2, but plants remained sink limited during the day, regardless of atmospheric CO_2 (Grimmer and Komor, 1999). The phloem vasculature connects source and sink tissues but it is tightly regulated and very sensitive to environmental conditions, which can drastically change carbon allocation to sinks (Lemoine et al., 2013). The loss of grain protein content in MSB may have been caused by a more vigorous CO_2 response which altered carbon export in relation to nitrogen remobilization from source to sink tissues. Additionally, there was no significant reduction in yield or average seed weight compared with SB, suggesting that the MSB wheat had exhausted their seed sink capacity, causing the early onset of maturity. Efforts to simply increase the seed sink size may negatively impact protein quality, and therefore it is essential to investigate the nitrogen partitioning dynamics during seed fill (Bertheloot et al., 2008). Additional research is underway to determine how genes associated with carbon/nitrogen metabolism and transport are differentially impacted by elevated CO_2 in varying wheat genetic backgrounds.

Though MSB wheat genotypes did experience a significant reduction in grain protein content at elevated CO_2, we can conclude that this was not due to the presence of the *Fhb1* QTL. *Fhb1* did not negatively impact wheat development, growth, productivity, nutritional integrity nor did it alter plant response to elevated CO_2. This research should provide plant breeders confidence in the continued utilization of *Fhb1* for enhancing FHB resistance in wheat. However, it is concerning that some wheat genetic backgrounds will suffer more severe nutrient and quality losses with rising CO_2. While our current study was focused on evaluating grain protein content, we are actively investigating how elevated CO_2 impacts gluten composition and protein functionality in additional wheat cultivars. Identifying climate resilient and disease resistant wheat traits is essential for securing future food security.

Data availability statement

The raw data supporting the conclusions of this article will be made available by the authors, without undue reservation.

Author contributions

WH planned, designed, and conducted the research efforts. Additionally, he was the primary manuscript author. JA and DG assisted in the experimental design and contributed to writing and editing the manuscript. SM assisted in sample analysis and manuscript editing. MV supervised the research, assisted with plant evaluations, and contributed to writing and editing the manuscript. All authors contributed to the article and approved the submitted version.

Funding

This work was funded by the United States Department of Agriculture.

Acknowledgments

We would like to thank Nathan Kemp and Jennifer Teresi for technical assistance with plant care and grain harvest.

Conflict of interest

The authors declare that the research was conducted in the absence of any commercial or financial relationships that could be construed as a potential conflict of interest.

Publisher's note

Disclaimer

This work was funded by the United States Department of Agriculture. Mention of trade names or commercial products in this publication is solely for the purpose of providing specific information and does not imply recommendation or endorsement by the U.S. Department of Agriculture. Authors have no conflicts of interest to declare. USDA is an equal opportunity provider and employer.

Supplementary material

The Supplementary Material for this article can be found online at: https://www.frontiersin.org/articles/10.3389/fpls.2022.1034406/full#supplementary-material

References

Ainsworth, E. A., and Long, S. P. (2021). 30 years of free-air carbon dioxide enrichment (FACE): What have we learned about future crop productivity and its potential for adaptation? *Global Change Biol.* 27 (1), 27–49. doi: 10.1111/gcb.15375

Anderson, J. A., Stack, R., Liu, S., Waldron, B., Fjeld, A., Coyne, C., et al. (2001). DNA Markers for fusarium head blight resistance QTLs in two wheat populations. *Theor. Appl. Genet.* 102 (8), 1164–1168. doi: 10.1007/s001220000509

Aranjuelo, I., Sanz-Sáez, Á., Jauregui, I., Irigoyen, J. J., Araus, J. L., Sánchez-Díaz, M., et al. (2013). Harvest index, a parameter conditioning responsiveness of wheat plants to elevated CO2. *J. Exp. Bot.* 64 (7), 1879–1892. doi: 10.1093/jxb/ert081

Argyris, J., Van Sanford, D., and TeKrony, D. (2003). Fusarium graminearum infection during wheat seed development and its effect on seed quality. *Crop Sci.* 43 (5), 1782–1788. doi: 10.2135/cropsci2003.1782

Awad, W. A., Ghareeb, K., Dadak, A., Hess, M., and Böhm, J. (2014). Single and combined effects of deoxynivalenol mycotoxin and a microbial feed additive on lymphocyte DNA damage and oxidative stress in broiler chickens. *PloS One* 9 (1), e88028. doi: 10.1371/journal.pone.0088028

Bai, G., Kolb, F. L., Shaner, G., and Domier, L. L. (1999). Amplified fragment length polymorphism markers linked to a major quantitative trait locus controlling scab resistance in wheat. *Phytopathology* 89 (4), 343–348. doi: 10.1094/PHYTO.1999.89.4.343

Bai, G., Su, Z., and Cai, J. (2018). Wheat resistance to fusarium head blight. *Can. J. Plant Pathol.* 40 (3), 336–346. doi: 10.1080/07060661.2018.1476411

Begcy, K., and Walia, H. (2015). Drought stress delays endosperm development and misregulates genes associated with cytoskeleton organization and grain quality proteins in developing wheat seeds. *Plant Sci.* 240, 109–119. doi: 10.1016/j.plantsci.2015.08.024

Bencze, S., Puskás, K., Vida, G., Karsai, I., Balla, K., Komáromi, J., et al. (2017). Rising atmospheric CO_2 concentration may imply higher risk of *Fusarium* mycotoxin contamination of wheat grains. *Mycotoxin Res.* 33 (3), 229–236. doi: 10.1007/s12550-017-0281-2

Bent, A. F., and Mackey, D. (2007). Elicitors, effectors, and r genes: the new paradigm and a lifetime supply of questions. *Annu. Rev. Phytopathol.* 45, 399–436. doi: 10.1146/annurev.phyto.45.062806.094427

Bertheloot, J., Martre, P., and Andrieu, B. (2008). Dynamics of light and nitrogen distribution during grain filling within wheat canopy. *Plant Physiol.* 148 (3), 1707–1720.

Borrás, L., Slafer, G. A., and Otegui, M. E. (2004). Seed dry weight response to source–sink manipulations in wheat, maize and soybean: a quantitative reappraisal. *Field Crops Res.* 86 (2-3), 131–146.

Brar, G. S., Brûlé-Babel, A. L., Ruan, Y., Henriquez, M. A., Pozniak, C. J., Kutcher, H. R., et al. (2019a). Genetic factors affecting fusarium head blight resistance improvement from introgression of exotic sumai 3 alleles (including Fhb1, Fhb2, and Fhb5) in hard red spring wheat. *BMC Plant Biol.* 19 (1), 1–19.

Brar, G. S., Pozniak, C. J., Kutcher, H. R., and Hucl, P. J. (2019b). Evaluation of fusarium head blight resistance genes Fhb1, Fhb2, and Fhb5 introgressed into elite Canadian hard red spring wheats: effect on agronomic and end-use quality traits and implications for breeding. *Mol. Breed.* 39 (3), 44.

Broberg, M. C., Högy, P., and Pleijel, H. (2017). CO_2-induced changes in wheat grain composition: meta-analysis and response functions. *Agronomy* 7 (2), 32.

Brown, J., and Rant, J. (2013). Fitness costs and trade-offs of disease resistance and their consequences for breeding arable crops. *Plant Pathol.* 62, 83–95. doi: 10.1111/ppa.12163

Brown, N. A., Urban, M., van de Meene, A. M. L., and Hammond-Kosack, K. E. (2010). The infection biology of *Fusarium graminearum*: Defining the pathways of spikelet to spikelet colonisation in wheat ears. *Fungal Biol.* 114 (7), 555–571. doi: 10.1016/j.funbio.2010.04.006

Buerstmayr, H., Ban, T., and Anderson, J. A. (2009). QTL mapping and marker-assisted selection for fusarium head blight resistance in wheat: a review. *Plant Breed.* 128 (1), 1–26. doi: 10.1111/j.1439-0523.2008.01550.x

Buerstmayr, H., Buerstmayr, M., Schweiger, W., and Steiner, B. (2013). "Genomics-assisted breeding for fusarium head blight resistance in wheat," in *Translational genomics for crop breeding* (John Wiley & Sons Ltd), 45–61.

Buerstmayr, H., Lemmens, M., Hartl, L., Doldi, L., Steiner, B., Stierschneider, M., et al. (2002). Molecular mapping of QTLs for fusarium head blight resistance in spring wheat. i. resistance to fungal spread (Type II resistance). *Theor. Appl. Genet.* 104 (1), 84–91.

Bugbee, B., Koerner, G., Albbrechtsen, R., Dewey, W., and Clawson, S. (1997). Registration of 'USU-Apogee'Wheat. *Crop Sci.* 37 (2), 626–626. doi: 10.2135/cropsci1997.0011183X003700020053x

Bullerman, L. B., and Bianchini, A. (2007). Stability of mycotoxins during food processing. *Int. J. Food Microbiol.* 119 (1-2), 140–146. doi: 10.1016/j.ijfoodmicro.2007.07.035

Busch, R., McVey, D., Rauch, T., Baumer, J., and Elsayed, F. (1984). Registration of Wheaton wheat. *Crop Sci.* 24 (3), 622–622. doi: 10.2135/cropsci1984.0011183X002400030054x

Busch, R., McVey, D., Wiersma, J., Warnes, D., Wilcoxson, R., and Hareland, G. (1993). Registration of 'Norm'Wheat. *Crop Sci.* 33 (4), 880–881. doi: 10.2135/cropsci1993.0011183X003300040062x

Cuperlovic-Culf, M., Vaughan, M. M., Vermillion, K., Surendra, A., Teresi, J., and McCormick, S. P. (2019). Effects of atmospheric CO_2 level on the metabolic response of resistant and susceptible wheat to fusarium graminearum infection. *Mol. Plant-Microbe Interact.* doi: 10.1094/MPMI-06-18-0161-R

Cuthbert, P. A., Somers, D. J., Thomas, J., Cloutier, S., and Brulé-Babel, A. (2006). Fine mapping Fhb1, a major gene controlling fusarium head blight resistance in bread wheat (Triticum aestivum l.). *Theor. Appl. Genet.* 112 (8), 1465–1472. doi: 10.1007/s00122-006-0249-7

Delcour, J. A., Joye, I. J., Pareyt, B., Wilderjans, E., Brijs, K., and Lagrain, B. (2012). Wheat gluten functionality as a quality determinant in cereal-based food products. *Annu. Rev. Food Sci. Technol.* 3, 469–492. doi: 10.1146/annurev-food-022811-101303

Farooq, M., Bramley, H., Palta, J. A., and Siddique, K. H. (2011). Heat stress in wheat during reproductive and grain-filling phases. *Crit. Rev. Plant Sci.* 30 (6), 491–507. doi: 10.1080/07352689.2011.615687

Fernando, N., Panozzo, J., Tausz, M., Norton, R., Fitzgerald, G., Khan, A., et al. (2015). Rising CO_2 concentration altered wheat grain proteome and flour rheological characteristics. *Food Chem.* 170, 448–454. doi: 10.1016/j.foodchem.2014.07.044

Fernando, N., Panozzo, J., Tausz, M., Norton, R. M., Neumann, N., Fitzgerald, G. J., et al. (2014). Elevated CO_2 alters grain quality of two bread wheat cultivars grown under different environmental conditions. *Agriculture Ecosyst. Environ.* 185, 24–33. doi: 10.1016/j.agee.2013.11.023

Foulkes, M. J., Slafer, G. A., Davies, W. J., Berry, P. M., Sylvester-Bradley, R., Martre, P., et al. (2011). Raising yield potential of wheat. III. optimizing partitioning to grain while maintaining lodging resistance. *J. Exp. Bot.* 62 (2), 469–486.

Goswami, R. S., and Kistler, H. C. (2004). Heading for disaster: *Fusarium graminearum* on cereal crops. *Mol. Plant Pathol.* 5 (6), 515–525. doi: 10.1111/J.1364-3703.2004.00252.X

Grimmer, C., and Komor, E. (1999). Assimilate export by leaves of ricinus communis l. growing under normal and elevated carbon dioxide concentrations: the same rate during the day, a different rate at night. *Planta* 209 (3), 275–281.

Gunnaiah, R., and Kushalappa, A. C. (2014). Metabolomics deciphers the host resistance mechanisms in wheat cultivar sumai-3, against trichothecene producing and non-producing isolates of fusarium graminearum. *Plant Physiol. Biochem.* 83 (0), 40–50. doi: 10.1016/j.plaphy.2014.07.002

Hao, Y., Rasheed, A., Zhu, Z., Wulff, B. B. H., and He, Z. (2020). Harnessing wheat Fhb1 for fusarium resistance. *Trends Plant Sci.* 25 (1), 1–3. doi: 10.1016/j.tplants.2019.10.006

Hay, W. T., Anderson, J. A., McCormick, S. P., Hojilla-Evangelista, M. P., Selling, G. W., Utt, K. D., et al. (2022). Fusarium head blight resistance exacerbates nutritional loss of wheat grain at elevated CO2. *Sci. Rep.* 12 (1), 1–13. doi: 10.1038/s41598-021-03890-9

Hay, W. T., Bihmidine, S., Mutlu, N., Le Hoang, K., Awada, T., Weeks, D. P., et al. (2017). Enhancing soybean photosynthetic CO_2 assimilation using a cyanobacterial membrane protein, ictB. *J. Plant Physiol.* 212, 58–68. doi: 10.1016/j.jplph.2017.02.003

Hay, W. T., McCormick, S. P., Hojilla-Evangelista, M. P., Bowman, M. J., Dunn, R. O., Teresi, J. M., et al. (2020). Changes in wheat nutritional content at elevated [CO_2] alter *Fusarium graminearum* growth and mycotoxin production on grain. *J. Agric. Food Chem.* 68 (23), 6297–6307. doi: 10.1021/acs.jafc.0c01308

He, Y., Zhang, X., Zhang, Y., Ahmad, D., Wu, L., Jiang, P., et al. (2018). Molecular characterization and expression of PFT, an FHB resistance gene at the Fhb1 QTL in wheat. *Phytopathology* 108 (6), 730–736. doi: 10.1094/PHYTO-11-17-0383-R

Högy, P., and Fangmeier, A. (2008). Effects of elevated atmospheric $CO_{2\ on}$ grain quality of wheat. *J. Cereal Sci.* 48 (3), 580–591. doi: 10.1016/j.jcs.2008.01.006

Jia, H., Zhou, J., Xue, S., Li, G., Yan, H., Ran, C., et al. (2018). A journey to understand wheat fusarium head blight resistance in the Chinese wheat landrace wangshuibai. *Crop J.* 6 (1), 48–59. doi: 10.1016/j.cj.2017.09.006

Kim, J., Shon, J., Lee, C.-K., Yang, W., Yoon, Y., Yang, W.-H., et al. (2011). Relationship between grain filling duration and leaf senescence of temperate rice under high temperature. *Field Crops Res.* 122 (3), 207–213. doi: 10.1016/j.fcr.2011.03.014

Lemoine, R., Camera, S. L., Atanassova, R., Dédaldéchamp, F., Allario, T., Pourtau, N., et al. (2013). Source-to-sink transport of sugar and regulation by environmental factors. *Front. Plant Sci.* 4, 272. doi: 10.3389/fpls.2013.00272

Lin, F., Kong, Z., Zhu, H., Xue, S., Wu, J., Tian, D., et al. (2004). Mapping QTL associated with resistance to fusarium head blight in the Nanda2419× wangshuibai population. i. type II resistance. *Theor. Appl. Genet.* 109 (7), 1504–1511.

Lin, F., Xue, S., Zhang, Z., Zhang, C., Kong, Z., Yao, G., et al. (2006). Mapping QTL associated with resistance to fusarium head blight in the Nanda2419× wangshuibai population. II: Type I resistance. *Theor. Appl. Genet.* 112 (3), 528–535.

Liu, S., Zhang, X., Pumphrey, M. O., Stack, R. W., Gill, B. S., and Anderson, J. A. (2006). Complex microcolinearity among wheat, rice, and barley revealed by fine mapping of the genomic region harboring a major QTL for resistance to fusarium head blight in wheat. *Funct. Integr. Genomics* 6 (2), 83–89. doi: 10.1007/s10142-005-0007-y

Li, T., Zhang, H., Huang, Y., Su, Z., Deng, Y., Liu, H., et al. (2019). Effects of the Fhb1 gene on fusarium head blight resistance and agronomic traits of winter wheat. *Crop J.* 7 (6), 799–808. doi: 10.1016/j.cj.2019.03.005

Mackintosh, C. A., Garvin, D. F., Radmer, L. E., Heinen, S. J., and Muehlbauer, G. J. (2006). A model wheat cultivar for transformation to improve resistance to fusarium head blight. *Plant Cell Rep.* 25 (4), 313–319. doi: 10.1007/s00299-005-0059-4

Ma, Z., Xie, Q., Li, G., Jia, H., Zhou, J., Kong, Z., et al. (2020). Germplasms, genetics and genomics for better control of disastrous wheat fusarium head blight. *Theor. Appl. Genet.* 133 (5), 1541–1568. doi: 10.1007/s00122-019-03525-8

McCartney, C. A., Somers, D. J., Fedak, G., DePauw, R. M., Thomas, J., Fox, S. L., et al. (2007). The evaluation of FHB resistance QTLs introgressed into elite Canadian spring wheat germplasm. *Mol. Breed.* 20 (3), 209–221. doi: 10.1007/s11032-007-9084-z

O'Donnell, K., Ward, T. J., Geiser, D. M., Kistler, H. C., and Aoki, T. (2004). Genealogical concordance between the mating type locus and seven other nuclear genes supports formal recognition of nine phylogenetically distinct species within the *Fusarium graminearum* clade. *Fungal Genet. Biol.* 41 (6), 600–623. doi: 10.1016/j.fgb.2004.03.003

Panozzo, J., Walker, C., Partington, D., Neumann, N., Tausz, M., Seneweera, S., et al. (2014). Elevated carbon dioxide changes grain protein concentration and composition and compromises baking quality. a FACE study. *J. Cereal Sci.* 60 (3), 461–470. doi: 10.1016/j.jcs.2014.08.011

Pestka, J. J. (2007). Deoxynivalenol: Toxicity, mechanisms and animal health risks. *Anim. feed Sci. Technol.* 137 (3-4), 283–298. doi: 10.1016/j.anifeedsci.2007.06.006

Pleijel, H., and Uddling, J. (2012). Yield vs. quality trade-offs for wheat in response to carbon dioxide and ozone. *Global Change Biol.* 18 (2), 596–605.

Rawat, N., Pumphrey, M. O., Liu, S., Zhang, X., Tiwari, V. K., Ando, K., et al. (2016). Wheat Fhb1 encodes a chimeric lectin with agglutinin domains and a pore-forming toxin-like domain conferring resistance to fusarium head blight. *Nat. Genet.* 48 (12), 1576–1580. doi: 10.1038/ng.3706

Röder, M. S., Korzun, V., Wendehake, K., Plaschke, J., Tixier, M.-H., Leroy, P., et al. (1998). A microsatellite map of wheat. *Genetics* 149 (4), 2007–2023. doi: 10.1093/genetics/149.4.2007

Rudd, J. C., Horsley, R. D., McKendry, A. L., and Elias, E. M. (2001). Host plant resistance genes for fusarium head blight: Sources, mechanisms, and utility in conventional breeding systems. *Crop Sci.* 41 (3), 620–627. doi: 10.2135/cropsci2001.413620x

Saint Pierre, C., Peterson, C., Ross, A., Ohm, J., Verhoeven, M., Larson, M., et al. (2008). Winter wheat genotypes under different levels of nitrogen and water stress: Changes in grain protein composition. *J. Cereal Sci.* 47 (3), 407–416. doi: 10.1016/j.jcs.2007.05.007

Soni, N., Altartouri, B., Hegde, N., Duggavathi, R., Nazarian-Firouzabadi, F., and Kushalappa, A. C. (2021). TaNAC032 transcription factor regulates lignin-biosynthetic genes to combat fusarium head blight in wheat. *Plant Sci.* 304, 110820. doi: 10.1016/j.plantsci.2021.110820

Soni, N., Hegde, N., Dhariwal, A., and Kushalappa, A. C. (2020). Role of laccase gene in wheat NILs differing at QTL-Fhb1 for resistance against fusarium head blight. *Plant Sci.* 298, 110574. doi: 10.1016/j.plantsci.2020.110574

Steiner, B., Buerstmayr, M., Wagner, C., Danler, A., Eshonkulov, B., Ehn, M., et al. (2019). Fine-mapping of the fusarium head blight resistance QTL qfhs.ifa-5A identifies two resistance QTL associated with anther extrusion. *Theor. Appl. Genet.* 132 (7), 2039–2053. doi: 10.1007/s00122-019-03336-x

Steiner, B., Lemmens, M., Griesser, M., Scholz, U., Schondelmaier, J., and Buerstmayr, H. (2004). Molecular mapping of resistance to fusarium head blight in the spring wheat cultivar frontana. *Theor. Appl. Genet.* 109 (1), 215–224. doi: 10.1007/s00122-004-1620-1

Taub, D. R., and Wang, X. (2008). Why are nitrogen concentrations in plant tissues lower under elevated CO_2? a critical examination of the hypotheses. *J. Integr. Plant Biol.* 50 (11), 1365–1374. doi: 10.1111/j.1744-7909.2008.00754.x

Váry, Z., Mullins, E., McElwain, J. C., and Doohan, F. M. (2015). The severity of wheat diseases increases when plants and pathogens are acclimatized to elevated carbon dioxide. *Global Change Biol.* 21 (7), 2661–2669. doi: 10.1111/gcb.12899

Vaughan, M., Backhouse, D., and Del Ponte, E. (2016). Climate change impacts on the ecology of *Fusarium graminearum* species complex and susceptibility of wheat to *Fusarium* head blight: a review. *World Mycotoxin J.* 9 (5), 685–700. doi: 10.3920/WMJ2016.2053

Waldron, B., Moreno-Sevilla, B., Anderson, J., Stack, R., and Frohberg, R. (1999). RFLP mapping of QTL for fusarium head blight resistance in wheat. *Crop Sci.* 39 (3), 805–811. doi: 10.2135/cropsci1999.0011183X003900030032x

Wang, X., and Liu, F. (2021). Effects of elevated co2 and heat on wheat grain quality. *Plants* 10 (5), 1027. doi: 10.3390/plants10051027

Wang, H., Sun, S., Ge, W., Zhao, L., Hou, B., Wang, K., et al. (2020). Horizontal gene transfer of *Fhb7* from fungus underlies fusarium head blight resistance in wheat. *Science*, eaba5435. doi: 10.1126/science.aba5435

Wang, W., Zhu, Y., Abraham, N., Li, X.-Z., Kimber, M., and Zhou, T. (2021). The ribosome-binding mode of trichothecene mycotoxins rationalizes their structure–activity relationships. *Int. J. Mol. Sci.* 22 (4), 1604. doi: 10.3390/ijms22041604

Ward, T. J., Clear, R. M., Rooney, A. P., O'Donnell, K., Gaba, D., Patrick, S., et al. (2008). An adaptive evolutionary shift in fusarium head blight pathogen populations is driving the rapid spread of more toxigenic fusarium graminearum in north America. *Fungal Genet. Biol.* 45 (4), 473–484. doi: 10.1016/j.fgb.2007.10.003

Wingler, A., von Schaewen, A., Leegood, R. C., Lea, P. J., and Paul Quick, W. (1998). Regulation of leaf senescence by cytokinin, sugars, and light: effects on NADH-dependent hydroxypyruvate reductase. *Plant Physiol.* 116 (1), 329–335. doi: 10.1104/pp.116.1.329

Xue, S., Xu, F., Tang, M., Zhou, Y., Li, G., An, X., et al. (2011). Precise mapping Fhb5, a major QTL conditioning resistance to fusarium infection in bread wheat (Triticum aestivum l.). *Theor. Appl. Genet.* 123 (6), 1055–1063. doi: 10.1007/s00122-011-1647-z

Yang, Z., Gilbert, J., and Procunier, J. D. (2006). Genetic diversity of resistance genes controlling fusarium head blight with simple sequence repeat markers in thirty-six wheat accessions from east asian origin. *Euphytica* 148 (3), 345–352.

Zhang, Y., Yang, Z., Ma, H., Huang, L., Ding, F., Du, Y., et al. (2021). Pyramiding of fusarium head blight resistance quantitative trait loci, Fhb1, Fhb4, and Fhb5, in modern Chinese wheat cultivars. *Front. Plant Sci.* 12.

Zhou, B., Serret, M. D., Elazab, A., Bort Pie, J., Araus, J. L., Aranjuelo, I., et al. (2016). Wheat ear carbon assimilation and nitrogen remobilization contribute significantly to grain yield. *J. Integr. Plant Biol.* 58 (11), 914–926.

Zhu, Z., Hao, Y., Mergoum, M., Bai, G., Humphreys, G., Cloutier, S., et al. (2019). Breeding wheat for resistance to fusarium head blight in the global north: China, USA and Canada. *Crop J.* 7), 730–738.

Ziska, L., Morris, C., and Goins, E. (2004). Quantitative and qualitative evaluation of selected wheat varieties released since 1903 to increasing atmospheric carbon dioxide: can yield sensitivity to carbon dioxide be a factor in wheat performance? *Global Change Biol.* 10 (10), 1810–1819.

frontiers | Frontiers in Plant Science

TYPE Review
PUBLISHED 29 November 2022
DOI 10.3389/fpls.2022.1032820

OPEN ACCESS

EDITED BY
Ravi Gupta,
Kookmin University, South Korea

REVIEWED BY
Deepu Pandita,
Government Department of School Education, India
Mehtap Yildiz,
Yüzüncü Yıl University, Turkey

*CORRESPONDENCE
Sang Ryeol Park
srpark@korea.kr

SPECIALTY SECTION
This article was submitted to Crop and Product Physiology, a section of the journal Frontiers in Plant Science

RECEIVED 31 August 2022
ACCEPTED 14 November 2022
PUBLISHED 29 November 2022

CITATION
Son S and Park SR (2022) Climate change impedes plant immunity mechanisms. *Front. Plant Sci.* 13:1032820. doi: 10.3389/fpls.2022.1032820

Climate change impedes plant immunity mechanisms

Seungmin Son and Sang Ryeol Park*

National Institute of Agricultural Sciences, Rural Development Administration, Jeonju, South Korea

Rapid climate change caused by human activity is threatening global crop production and food security worldwide. In particular, the emergence of new infectious plant pathogens and the geographical expansion of plant disease incidence result in serious yield losses of major crops annually. Since climate change has accelerated recently and is expected to worsen in the future, we have reached an inflection point where comprehensive preparations to cope with the upcoming crisis can no longer be delayed. Development of new plant breeding technologies including site-directed nucleases offers the opportunity to mitigate the effects of the changing climate. Therefore, understanding the effects of climate change on plant innate immunity and identification of elite genes conferring disease resistance are crucial for the engineering of new crop cultivars and plant improvement strategies. Here, we summarize and discuss the effects of major environmental factors such as temperature, humidity, and carbon dioxide concentration on plant immunity systems. This review provides a strategy for securing crop-based nutrition against severe pathogen attacks in the era of climate change.

KEYWORDS

carbon dioxide, climate change, crop nutritional security, humidity, pathogen, plant immunity, temperature

Introduction

Climate change is a major factor in determining where humans can live on the planet under tolerable and safe conditions (Timmermann et al., 2022). Global warming due to environmental destruction and excessive burning of fossil fuels is creating adverse conditions for the continued survival of many plant and animal species and the wellness of the human population (Román-Palacios and Wiens, 2020). The crops that have made human settlement possible since the dawn of agriculture by providing a stable source of dietary calories are now suffering from the effects of climate change (Challinor et al., 2014; Rising and Devineni, 2020). Biotic stress factors such as pathogens and insect pests reduce crop yield and quality in agricultural settings (Savary et al., 2019; Savary and Willocquet, 2020). Indeed, damage to major crop yields is estimated to reach up to 40% globally (Oerke, 2006; Savary et al., 2012). In warmer and wetter environments more amenable to pathogen growth and spread, the damage they cause can be even more

devastating (Velasquez et al., 2018). For example, bacterial blight caused by *Xanthomonas oryzae* pv. *oryzae* (*Xoo*) can decrease yield in rice (*Oryza sativa*) by up to 80% (Srinivasan and Gnanamanickam, 2005). Wheat blast caused by the fungus *Magnaporthe oryzae Triticum* can infect wheat (*Triticum aestivum*) and completely eradicate fields (Islam et al., 2020), as can banded leaf and sheath blight caused by *Rhizoctonia solani* in maize (*Zea mays*) (Haque et al., 2022). Moreover, the emergence of new pathogenic strains and the expansion of their effective damage zones due to climate change are two of the most serious threats to crop production and food security (Chaloner et al., 2021). Therefore, efficient strategies are urgently needed to reduce the impact of pathogens on crop growth and yield.

According to the disease triangle model, three factors are required for disease development: a susceptible host, a virulent pathogen, and a favorable environment (Scholthof, 2007). Of these, only plant-based strategies are available to affect one side of the triangle with current technologies. Indeed, the development of new crop cultivars conferring innate immunity will be essential for conservation of food resources. Plant breeding has traditionally been performed through laborious and time-consuming genetic crosses to introduce superior alleles into a given background (Lusser et al., 2012). However, biotechnological innovations now offer eight new plant breeding technologies (NPBTs): site-directed nucleases (SDNs), oligonucleotide-directed mutagenesis, cisgenesis and intragenesis, RNA-dependent DNA methylation, grafting, reverse breeding, Agrobacterium-mediated infiltration, and synthetic genomics (Lusser et al., 2011). Among them, SDNs are the most widely used NPBT for a broad range of crops. In particular, development of the clustered regularly interspaced short palindromic repeats (CRISPR)/CRISPR-associated nuclease 9 (Cas9) system has ushered in a new era of crop improvement (Son and Park, 2022). Therefore, understanding the molecular mechanisms and identifying novel genes conferring desired traits are essential for their targeting by NPBTs in plant breeding.

Plants have evolved varied stress responses and defense mechanisms to overcome adverse environmental conditions, about which we have gained a wealth of knowledge thanks to the efforts of countless scientists. Nevertheless, how climate change affects the molecular mechanisms related to plant immunity against pathogens is largely unknown. Luckily, this knowledge gap is beginning to be filled. In this review, we give an overview and discuss the negative effects of temperature, humidity, and carbon dioxide (CO_2) concentration on plant defense mechanisms to better understand how to design mitigation strategies.

Plant immunity system and defense signaling

Plants employ two important immune systems known as pathogen-associated molecular pattern (PAMP)-triggered immunity (PTI) and effector-triggered immunity (ETI) to perceive and respond to pathogen attacks (Thomma et al., 2011). PTI is activated mainly by plasma membrane–localized extracellular pattern recognition receptors (PRRs) that can recognize conserved PAMPs (Monaghan and Zipfel, 2012). For example, recognition of the 22–amino acid region of bacterial flagellin (flg22) by the leucine-rich repeat receptor kinase (LRR-RK) FLAGELLIN SENSING 2 (FLS2) at the plasma membrane leads to formation of a heteromer between FLS2 and BRASSINOSTEROID INSENSITIVE-ASSOCIATED KINASE 1 (BAK1), a member of the LRR receptor-like kinase (LRR-RLK) and also known as SOMATIC EMBRYOGENESIS RECEPTOR-LIKE KINASE 3 (SERK3) (Chinchilla et al., 2007). The FLS2/BAK1 complex phosphorylates the receptor-like cytoplasmic kinase BOTRYTIS-INDUCED KINASE 1 (BIK1) and mitogen-activated protein kinase (MAPK) cascade to activate the downstream signaling pathway, resulting in expression of PTI-related genes (Wang et al., 2020b). Similarly, perception of a highly conserved epitope of bacterial translation elongation factor Tu (EF-Tu) by the LRR-RK EF-Tu RECEPTOR (EFR) also results in PTI activation through heteromerization with BAK1 and phosphorylation of BIK1 (Lal et al., 2018). Moreover, the recognition of plant-derived damage-associated molecular patterns (DAMPs) and phytocytokines by LRR-RKs/RLKs is important for PTI (Hou et al., 2021; Tanaka and Heil, 2021). PTI acts as a basal defense mechanism against various types of pathogens through defense responses that include the induction of defense gene expression, reactive oxygen species (ROS) production, callose deposition, and accumulation of antimicrobial secondary metabolites (Naveed et al., 2020).

ETI is triggered following the recognition by intracellular receptor resistance (R) proteins of specific pathogen effectors that can neutralize the plant immune system in the cytoplasm (Chisholm et al., 2006; Jones and Dangl, 2006). ETI activates a prolonged and robust resistance response and rapid localized programmed cell death known as the hypersensitive response (HR) (Coll et al., 2011). Most R proteins are nucleotide-binding leucine-rich repeat proteins (NLRs) that can be classified into three groups based on their N terminus domain: Toll/interleukin-1 receptor (TIR), coiled-coil (CC), and RESISTANCE TO POWDERY MILDEW 8 (RPW8)-type CC (CC_R) domain (Monteiro and Nishimura, 2018). The ETI signal triggered by TIR-NLRs (TNLs) relies on the three acyl hydrolases ENHANCED DISEASE SUSCEPTIBILITY 1 (EDS1), PHYTOALEXIN DEFICIENT 4 (PAD4), and SENESCENCE-ASSOCIATED GENE 101 (SAG101) (Wiermer et al., 2005). EDS1 interacts directly with PAD4 or SAG101 to form exclusive heterodimers, each with distinct functions in immunity (Wagner et al., 2013; Lapin et al., 2020). It was recently revealed that helper CC_R-NLRs such as ACTIVATED DISEASE RESISTANCE 1 (ADR1) and N REQUIREMENT GENE 1 (NRG1) are required for the activation of the EDS1 complex and TNL defense signaling (i.e., EDS1–PAD4–ADR1

and EDS1–SAG101–NRG1) (Pruitt et al., 2021; Sun et al., 2021). The EDS1 pathway is involved not only in ETI but also in basal immunity and promotes salicylic acid (SA) biosynthesis and signaling (Cui et al., 2017). Therefore, EDS1 signaling plays a critical role in SA-dependent and -independent resistance. For CC-NLRs (CNLs), the plasma membrane-localized integrin-like protein NON-RACE SPECIFIC DISEASE RESISTANCE 1 (NDR1) appears to function downstream of CNLs, although several do not require NDR1 to activate ETI (van Wersch et al., 2020). Since NDR1 acts upstream of SA biosynthesis and signaling, it is also involved in SA-dependent resistance (Shapiro and Zhang, 2001).

Another plant immune response is referred to as quantitative disease resistance (QDR), which is characterized by a continuous distribution of resistance phenotypes—from highly sensitive to highly resistant—within a population (Poland et al., 2009). QDR is typically partial resistance conferred by multiple small-effect loci, while qualitative disease resistance, also referred as ETI, is complete resistance conferred by a single large-effect gene (French et al., 2016). Since multiple genes are involved in QDR, it is important in the context of the evolutionary pressure imposed by pathogens and confers broad-spectrum resistance to a wide range of pathogens including biotrophic and necrotrophic pathogens (Anderson et al., 2010; French et al., 2016). Most loci identified as quantitative trait loci for QDR are associated with the biosynthesis of the cell wall and defense compounds, thus extending beyond simple pathogen perception (Corwin and Kliebenstein, 2017).

Phytohormones participate in and control PTI and ETI. In particular, the three phytohormones SA, jasmonic acid (JA), and ethylene (ET) play critical roles in plant immunity. SA contributes significantly to innate immunity against biotrophic pathogens by evoking local and systemic resistance, whereas JA/ET play critical roles in plant resistance to necrotrophic pathogens (Glazebrook, 2005; Li et al., 2019). The SA and JA/ET defense signals can be antagonistic or synergistic (Tsuda and Katagiri, 2010). Abscisic acid (ABA) is also important for innate immunity. ABA interacts with various phytohormones during defense responses (Lee and Luan, 2012; Pieterse et al., 2012). For example, ABA suppresses SA-dependent immunity, leading to greater susceptibility against various pathogens (Berens et al., 2019). However, ABA can also increase plant disease resistance due to closure of stomata which constitutes one of the main entry routes for pathogens (Ton Mauch-Mani, 2004; Melotto et al., 2006; Flors et al., 2008). In response to the stimulus, ABA is primarily biosynthesized in vascular tissues and accumulates in guard cells through ABA transporters (e.g., ATP-binding cassette transporter G [ABCG]) (Merilo et al., 2015). In guard cells, ABA binds to its cognate receptor from the pyrabactin resistance 1/pyrabactin resistance 1-like/regulatory components of ABA receptors (PYR/PYL/RCAR) family, leading to the inactivation of type 2C protein phosphatases (PP2Cs). The alleviation of PP2C-mediated repression of SUCROSE NON-FERMENTING 1 (SNF1)-related protein kinase 2s (SnRK2s) results in activation of the downstream ABA signaling cascade (Hsu et al., 2021). For example, the PP2Cs ABA INSENSITIVE 1 (ABI1) and ABI2 inactivate OPEN STOMATA 1 (OST1), also known as SnRK2.6, thus preventing the phosphorylation of SLOW ANION CHANNEL 1 (SLAC1), which releases anions for stomatal closure. However, perception of flg22 by PRRs increases ABA levels in guard cells to inactivate ABIs, and it results in rapid stomatal closure through the activation of the OST1/SnRK2.6–SLAC1 module (Guzel Deger et al., 2015). Therefore, ABA promotes stomatal closure and prevents pathogen entry into the host plant.

ROS signaling is also important for plant immunity. ROS are highly oxidative agents, but they also act as signaling molecules that regulate biotic stress responses (e.g., systemic acquired resistance [SAR] and cell death) (Waszczak et al., 2018). ROS are generated *via* metabolic and stress signaling pathways. Metabolic ROS are produced in several intracellular compartments (e.g., chloroplast, mitochondria, peroxisomes, and apoplast) during photosynthesis and photorespiration, while signaling ROS are produced mainly by plant NADPH oxidases, mostly from members of the plasma membrane–localized respiratory burst oxidase homolog (RBOH) family (Kangasjärvi et al., 2012; Chapman et al., 2019). Pathogen recognition is accompanied by ROS production through both the metabolic and stress signaling pathways. Recognition of PAMPs by PRRs induces an initial oxidative burst that activates plant basal defenses within the infected cells; effector perception by R proteins then promotes a second oxidative burst that results in HR (Nanda et al., 2010; Torres, 2010). Therefore, ROS play a key role linking pathogen perception and plant defense responses.

However, these various plant defense systems may be adversely affected significantly by climate change, as discussed below.

The effects of temperature on PTI

Environmental factors influence not only pathogenicity but also plant disease resistance (Elad and Pertot, 2014). Temperature is perhaps the most studied climate factor modulating plant–pathogen interactions. Higher average temperatures brought upon by climate change can increase the pathogenicity of phytopathogens by raising their virulence, active geographical regions, fitness, reproduction period/rate, and epidemic risks (Agrios, 2005; Deutsch et al., 2008; Caffarra et al., 2012; Vaumourin and Laine, 2018). Temperature is also one of the most important environmental factors that shapes plant immunity against bacteria, fungi, viruses, and insects (Garrett et al., 2006). Since different host–pathogen interactions behave differently over different temperature

ranges, higher temperatures will sometimes work in favor of plant immunity. In many cases though, higher temperature will benefit the pathogen to the detriment of the host (Desaint et al., 2021).

In Arabidopsis (*Arabidopsis thaliana*), higher temperature increases early PTI signaling (through BIK1 and MAPKs) and decreases the occupancy of nucleosomes containing the histone variant H2A.Z, which modulates the plant transcriptome in response to changes in temperature (Kumar and Wigge, 2010; Cheng et al., 2013). Moderately high temperatures (23°C–32°C) will therefore activate PTI-dependent gene expression at the expense of ETI (Cheng et al., 2013). Cysteine-rich receptor-like kinases (CRKs) are one of the largest RLK subfamilies that recognizes pathogens and activates downstream signaling cascades. Recently, Wang et al. identified a CRK from wheat cultivar 'XY 6' conferring high-temperature seedling-plant resistance (Wang et al., 2021). The expression level of this gene, *TaCRK10*, was induced significantly by infection with the fungal pathogen *Puccinia striiformis f.* sp. *tritici* causing strip rust at high temperature. TaCRK10 was shown to directly phosphorylate histone H2A in wheat (TaH2A.1) and activate the SA signaling pathway, resulting in enhanced high-temperature seedling-plant resistance to *P. striiformis f.* sp. *tritici* (Wang et al., 2021). However, several studies have also indicated that PTI can be compromised at high temperature upon inhibition of flg22- and SA-induced defense responses (Rasmussen et al., 2013; Huot et al., 2017; Janda et al., 2019). Therefore, further studies are needed to understand the effect of temperature on PTI in detail.

The effects of temperature on ETI and SA-dependent immunity

Unlike PTI, much work has shown that high temperature decreases immunity evoked by ETI and QDR; this topic was well covered by a previous review (Desaint et al., 2021). Therefore, we focus here on recent important discoveries that illustrate how plant defense mechanisms are affected by high temperature.

Disruptions of NLR- and SA-mediated defense signaling by high temperature are thought to be the main reason behind diminished plant innate immunity against pathogens under these conditions. In Arabidopsis, the photoreceptor phytochrome B (phyB) also acts as a thermosensor, whereby far-red light and high temperatures lead to its inactivation (Jung et al., 2016; Legris et al., 2016). DE-ETIOLATED 1 (DET1) and CONSTITUTIVELY PHOTOMORPHOGENIC 1 (COP1), which are two key negative regulators of photomorphogenesis, promote the transcription of *PHYTOCHROME INTERACTION FACTOR 4* (*PIF4*), which encodes a basic-helix-loop-helix (bHLH) transcription factor acting as a positive regulator of growth and negative regulator of immunity (Gangappa et al., 2017; Gangappa and Kumar, 2018). phyB inhibits COP1 and PIF4 to modulate the trade-off between growth and defense. However, inactivation of phyB by high temperature results in the activation of the DET1/COP1–PIF4 module. As a result, PIF4 represses the expression of *SUPPRESSOR OF NPR1-1, CONSTITUTIVE 1* (*SNC1*), which encodes a TNL initiating ETI through the EDS1-PAD4 signaling pathway at high temperature (Gangappa et al., 2017). Since SNC1 and EDS1 play a critical role in plant defense responses such as SA biosynthesis (Zhang et al., 2003; García et al., 2010), the inhibition of *SNC1* expression at high temperature also significantly hinders SA-dependent resistance. Moreover, the SUMO E3 ligase SIZ1 (SAP and MIZ1 DOMAIN-CONTAINING LIGASE1) not only inhibits SNC1-dependent immune response but also enhances COP1 function at elevated ambient temperature (Hammoudi et al., 2018). Therefore, the activation of negative regulators (e.g., PIF4 and SIZ1) of SNC1 lead to impaired ETI and SA-dependent immunity. Recently, the transcription factor bHLH059 was identified as a temperature-responsive regulator for SA-dependent immunity acting independently of PIF4 (Bruessow et al., 2021). Relative *bHLH059* transcript level increased at 22°C compared to 16°C in Arabidopsis ecotype Columbia (Col-0). Total SA contents and resistance to *Pseudomonas syringae* pv. *tomato* (*Pst*) DC3000 decreased at 22°C relative to 16°C in Col-0, but remained similar in the *bhlh59* mutant regardless of ambient temperature. Moreover, bHLH059 has the potential to be a negative regulator involved in a defense hub associated with multiple NLRs (Mukhtar et al., 2011), hinting at a new mechanism for the temperature-mediated vulnerability of plant immune responses that should be explored in more detail.

SA is major defense phytohormone involved in PTI, ETI, and SAR; importantly, SA-dependent immunity is repressed by high temperature (Velásquez et al., 2018; Zhang and Li, 2019; Castroverde and Dina, 2021), whereas JA/ET defense signaling are enhanced under elevated temperature (Havko et al., 2020; Huang et al., 2021a). Therefore, any susceptibility to temperature in the context of plant disease resistance is mainly associated with SA signaling. SA is synthesized through the isochorismate synthase (ICS) and phenylalanine ammonia-lyase (PAL) pathways in plants (Lefevere et al., 2020). Especially, pathogen-induced SA production takes place in chloroplasts, from which it is exported to the cytoplasm *via* the SA transporter EDS5 (Serrano et al., 2013). SA activates NONEXPRESSOR OF PATHOGENESIS-RELATED GENES 1 (NPR1), the master regulator of SA signaling in the cytosol, resulting in the nuclear translocation of NPR1 to induce the expression of *pathogenesis-related* (*PR*) genes conferring disease resistance and SAR (Backer et al., 2019). Moreover, although ETI activates SA signaling, SA and NPR1 repress ETI-induced cell death *via* the formation of SA-induced NPR1 condensates to promote the degradation of proteins (e.g., NLRs, EDS1, WRKY54, and WRKY70) involved in HR (Zavaliev et al., 2020).

Huot et al. showed that inhibition of ICS1, which is also called SALICYLIC ACID-INDUCTION DEFICIENT 2 (SID2), under high-temperature conditions raised the susceptibility of Arabidopsis to *Pst* DC3000 due to the loss of SA biosynthesis and SA defense signaling (Huot et al., 2017). Furthermore, Arabidopsis disease resistance to *Pst* DC3000 increased at low temperature due to greater SA signaling that can itself be repressed by JA/ET defense signals (Li et al., 2020). However, the molecular mechanisms determining the temperature sensitivity of the SA defense signaling pathway were unknown.

Recently, two groups demonstrated different mechanisms by which the SA-mediated immune system is modulated under high temperature (Figure 1). Kim et al. showed that the expression of SA response genes is decreased under elevated temperature in various dicot (e.g., Arabidopsis, rapeseed [*Brassica napus*], tobacco [*Nicotiana tabacum*], and tomato [*Solanum lycopersicum*]) and monocot (rice) plants, with the downregulation of *CALMODULIN BINDING PROTEIN 60g* (*CBP60g*) being key for the temperature vulnerability of SA defense signaling in Arabidopsis (Kim et al., 2022). GUANYLATE BINDING PROTEIN-LIKE GTPase 3 (GBPL3) binds to the promoter region of genes involved in the plant immune system and recruits the Mediator complex and RNA polymerase II to form GBPL defense–activated condensates (GDACs) (Huang et al., 2021b). The recruitment of GBPL3 and the formation of the GDAC at the *CBP60g* and *SYSTEMIC ACQUIRED RESISTANCE DEFICIENT 1* (*SARD1*) loci, which have partially redundant functions, were necessary for their transcription, and these were attenuated by heat stress (Kim et al., 2022). Therefore, the expression of various genes (e.g., ICS1, EDS1, and PAD4) that would normally induce TNL-mediated ETI and SA biosynthesis downstream of CBP60g and SARD1 was suppressed under elevated temperature. However, and surprisingly, optimized *CBP60g* expression was sufficient to restore SA accumulation and plant immune responses at high temperature without growth or developmental penalty (Kim et al., 2022). Another group unraveled the molecular mechanism explaining the temperature vulnerability of CNLs and SA defense signaling in Arabidopsis (Samaradivakara et al., 2022). *RESISTANCE TO P. SYRINGAE PV. MACULICOLA 1* (*RPM1*) and *RESISTANCE TO P. SYRINGAE 2* (*RPS2*) encode two CNLs that recognize type III bacterial effectors indirectly through RPM1-INTERACTING PROTEIN 4 (RIN4) (Mackey et al., 2002; Mackey et al., 2003). *P. syringae* bacterial effectors such as AvrRpm1 and AvrB activate RPM1-mediated ETI through hyperphosphorylation of RIN4, while AvrRpt2 activates RPS2-mediated ETI *via* the degradation of RIN4 (Axtell and Staskawicz, 2003; Zhao et al., 2021). Plasma membrane–localized NDR1 interacts with RIN4 and is required for the activation of RPS2-based ETI in response to AvrRpt2 (Belkhadir et al., 2004; Coppinger et al., 2004; Day et al., 2006). Samaradivakara et al. showed that overexpression of *NDR1* rescues the transcript levels of *RPS2* and SA-associated genes including those of *ICS1* and *CBP60g*, which are repressed by high temperature, thus resulting in enhanced resistance to *Pst* DC3000 by maintaining ETI and SA defense signaling under elevated temperature (29°C) (Samaradivakara et al., 2022). In wheat, CNLs such as TaRPM1 and TaRPS2 also positively regulate disease resistance to *P. striiformis* f. sp. *tritici* at high temperature through the SA signaling pathway (Wang et al., 2020a; Hu et al., 2021a).

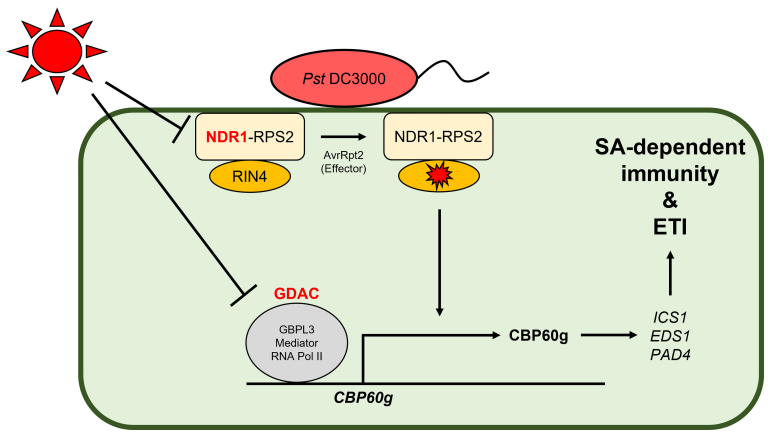

FIGURE 1
Molecular mechanisms demonstrating the negative effect of high temperature on SA-dependent immunity and ETI. In Arabidopsis, the induction of *CALMODULIN BINDING PROTEIN* 60g (CBP60g) and *NON-RACE SPECIFIC DISEASE RESISTANCE 1 (NDR1)* is necessary for innate immunity against *Pst* DC3000. However, under high temperature, the formation of guanylate binding protein-like GTPase (GBPL) defense-activated condensate (GDAC), consisting of GBPL3, Mediator, and RNA polymerase II, at the CBP60g loci (Kim et al., 2022) and the expression of *NDR1* which can increase the transcript levels of *RESISTANCE TO P. SYRINGAE 2 (RPS2)* and SA-associated genes (Samaradivakara et al., 2022) are repressed significantly, resulting in temperature vulnerability of SA-dependent immunity and ETI.

The effects of temperature on cytokinin-dependent immunity

A recent study revealed that the phytohormone cytokinin (CK) also plays an important role in plant immunity at high temperatures (Yang et al., 2022). The trade-off between growth and defense modulated by CK can result in opposite effects on plant–pathogen interactions (Choi et al., 2011). Exogenous and endogenous CK both enhance plant resistance against biotrophic pathogens through SA-dependent and -independent immune responses, therefore exerting a potentiation (or priming) defense response activated upon pathogen attack (Conrath et al., 2015; Albrecht and Argueso, 2017). Although CK displays a synergistic effect with SA, increased SA levels can inhibit CK signaling *via* a negative feedback (Argueso et al., 2012). In addition, high concentrations of CK enhance disease resistance against biotrophic oomycetes in Arabidopsis, while low concentrations raise susceptibility (Argueso et al., 2012). CK can also increase susceptibility to pathogens not only by inhibiting the plant immune system (i.e., PTI and ROS) but also by establishing source-sink relationships (Albrecht and Argueso, 2017; McIntyre et al., 2021). In pepper (*Capsicum annuum*), Yang et al. showed that infection with *Ralstonia solanacearum*, a hemibiotrophic pathogen causing bacterial wilt, activates SA signaling at an early stage and JA signaling at a later stage in roots at ambient temperature, but these responses are both impaired at high temperature (Yang et al., 2022). Instead, *isopentenyltransferase* (*IPT*) genes, including *CaIPT5*, encoding a critical enzyme in cytokinin biosynthesis, were upregulated by *R. solanacearum* infection under high temperature. Surprisingly, exogenous treatment with *trans*-zeatin (tZ), the bioactive CK, significantly enhanced disease resistance to *R. solanacearum* in pepper, tomato, and tobacco (*Nicotiana benthamiana*) under high temperature, while SA and JA did not (Yang et al., 2022). Moreover, the authors suggested that CK triggers chromatin remodeling, resulting in the upregulation of genes encoding glutathione *S*-transferase (e.g., *CaPRP1* and *CaMgst3*) and downregulation of genes involved in SA and JA signaling (e.g., *CaSTH2* and *CaDEF1* (Yang et al., 2022).

The effects of temperature on calcium ion–dependent immunity

Recently, the molecular mechanisms by which high temperature affects the calcium ion (Ca^{2+})–mediated immune system have also been reported. Ca^{2+} is an important second messenger modulating various signaling pathways, including the plant immune response (Yang and Poovaiah, 2003). Biotic/abiotic stresses increase Ca^{2+} levels in plant cells; Ca^{2+} then binds to calcium-binding proteins (CBPs) and Ca^{2+} sensors (e.g., calmodulin [CaM], calmodulin-like proteins [CMLs], calcineurin B-like proteins [CBLs], and calcium-dependent protein kinases CDPKs]) (Bose et al., 2011). The Ca^{2+}/CBP complex activates Ca^{2+} signaling by regulating the activity of signaling components such as kinases and transcription factors (Iqbal et al., 2020; Junho et al., 2020; Ma et al., 2020). Arabidopsis SIGNAL RESPONSIVE 1 (AtSR1), also known as CALMODULIN-BINDING TRANSCRIPTION ACTIVATOR 3 (CAMTA3), plays a central role in Ca^{2+} signaling–mediated immunity (Yuan et al., 2021a). AtSR1 acts as a negative regulator of the plant immune response by decreasing the expression of genes involved in ETI and/or SA signaling (e.g., *EDS1*, *NDR1*, *CBP60g*, *SARD1*, and *NPR1*) directly or indirectly (Du et al., 2009; Nie et al., 2012; Sun et al., 2020; Yuan et al., 2021b). Recently, Yuan and Poovaiah showed that the Ca^{2+} influx induced by *Pst* DC3000 is blocked in Arabidopsis at high temperature (30°C) compared to ambient temperature (18°C). In addition, the susceptibility to *Pst* DC3000 was reduced in the *atsr1* mutant plant compared to the wild type at both 18°C and 30°C (Yuan and Poovaiah, 2022). Moreover, the authors suggested that AtSR1 increases plant vulnerability to temperature by acting on stomatal and apoplastic immunity in an SA-dependent manner. In pepper, the expression of the WRKY transcription factor gene *CaWRKY40* is induced by *Ralstonia solanacearum* infection, high temperature, and major defense phytohormones (e.g., SA, JA, and ET), and CaWRKY40 enhances both *R. solanacearum* resistance and heat tolerance (DANG et al., 2013). CaWRKY40 forms positive feedback loops with CaWRKY6, BASIC LEUCINE ZIPPER 63 (CabZIP63), and CaCDPK15, all positive regulators of resistance against *R. solanacearum* and/or heat stress tolerance (Cai et al., 2015; Shen et al., 2016a; Shen et al., 2016b). Recently, two signaling components controlled by CaWRKY40 were identified as positive and negative regulators of *R. solanacearum* resistance, respectively. CaCBL1 contributes to disease resistance against *R. solanacearum* at high temperature and participates in the positive feedback loop with CaWRKY40 (Shen et al., 2020). However, pepper MILDEW-RESISTANCE LOCUS O5 (CaMLO5) has the opposite function in plant immunity and heat resistance (Yang et al., 2020). CaWRKY40 induces the expression of *CaMLO5* at high temperature, while CaWRKY40 represses it after *R. solanacearum* inoculation. CaMLO5 increases tolerance to heat stress but reduces the plant immune response against *R. solanacearum*. Moreover, the NAM/ATAF/CUC (NAC) transcription factor CaNAC2c was recently identified as being involved in temperature-responsive immunity (Cai et al., 2021). Expression of *CaNAC2c* was induced by both high temperature and *R. solanacearum* inoculation, resulting in positive effects on both thermotolerance and resistance against *R. solanacearum* but negative effects on pepper growth. CaNAC2c modulated the thermotolerance/immunity trade-off through differential and context-specific interactions with HEAT SHOCK PROTEIN 70 (CaHSP70) and CaNAC029. However, CaNAC2c/CaNAC029-mediated *R. solanacearum* resistance was impaired by ABA at high temperature, suggesting that the observed thermotolerance/immunity trade-off might be modulated by an

antagonistic interaction between ABA and JA signaling (Cai et al., 2021).

The effects of humidity on stomatal immunity

Along with temperature, humidity is an influential environmental factor during plant–pathogen interactions. In general, high humidity conditions (e.g., rainfall, high atmospheric humidity, and high soil moisture) are favorable for plant infections not only by phyllosphere pathogens but also by rhizosphere pathogens. Indeed, high humidity increases the incidence of bacterial disease and the potential threat to yield in various crops (Xin et al., 2016). In fact, humidity can be more important than temperature in predicting fungal disease outbreaks (Romero et al., 2021). Since air can maintain more water vapor at high temperature, climate change is frequently accompanied by high humidity. Therefore, understanding the effect of humidity on plant immune mechanisms will be important for ensuring food security.

By far, the main target of humidity affecting plant immunity is associated with stomatal control. Stomata consist of two guard cells that play a central role in modulating water transpiration and gas exchange between the plant and the atmosphere to balance the needs of photosynthesis while minimizing drought stress. Therefore, stomatal movements are tightly regulated in response to various environmental stimuli (e.g., humidity and CO_2) (Driesen et al., 2020). However, stomata also offer convenient portals through which pathogens can penetrate inner leaf tissues. To mitigate this threat, plants have developed sophisticated signaling networks conferring so-called stomatal immunity (Arnaud and Hwang, 2015; Murata et al., 2015). Guard cells recognize various PAMPs, resulting in PAMP-triggered stomatal closure through the activation of downstream signaling components (Figure 2A). However, according to a coevolutionary model between plants and their pathogens known as the zigzag model, some adapted pathogens have developed phytotoxins (e.g., coronatine and syringolin A) and effectors (e.g., avirulence protein B [AvrB], hrp-dependent outer protein F2 [HopF2], HopM1, HopX1, and HopZ1) to overcome stomatal immunity and use open stomata as their entry point into the leaf apoplast space (Melotto et al., 2017). Recently, Lie et al. also revealed that *Xanthomonas oryzae* pv. *oryzicola* (*Xoc*) secretes the bacterial effector AvrRxo1 to impair stomatal immunity by inducing the degradation of rice PYRIDOXAL PHOSPHATE SYNTHASE 1 (OsPDX1) involved in ABA biosynthesis (Liu et al., 2022a). Mechanisms of immunity by stomatal closure and their relationship with humidity have been covered in previous reviews (Melotto et al., 2017; Aung et al., 2018). Notably, after pathogens invade internal plant tissues, stomatal closure can support conditions of apoplast hydration auspicious for pathogen colonization. Therefore, we focus here on the most recent mechanisms regulating stomatal conductance after pathogen entry.

Since water is essential for the survival of pathogens as well as plants, pathogens have to work hard to obtain water when inside their host plants (Beattie, 2016). Water soaking is a common disease symptom visible as leaf spots caused by virulent bacterial pathogens (Davis et al., 1991; Reimers and Leach, 1991). Bacterial pathogens (e.g., *Pst* DC3000) induce water soaking to establish a favorable colonization milieu by using their effectors (e.g., WtsE, AvrHah1, HopM1, and AvrE1) (Ham et al., 2006; Schornack et al., 2008; Xin et al., 2016). For instance, Xin et al. identified two effectors (HopM1 and AvrE1) that induce water soaking in Arabidopsis and demonstrated the molecular mechanism by which HopM1 promotes apoplast hydration for bacterial proliferation (Xin et al., 2016). Arabidopsis HopM1 INTERACTOR 7 (AtMIN7), which is an ADP ribosylation factor–guanine nucleotide exchange factor (ARF-GEF) localized to the *trans*-Golgi-network/early endosome and involved in vesicle trafficking, is identified as a binding partner of HopM1 during a yeast two-hybrid (Y2H) screen and confirmed by pull-down assay (Nomura et al., 2006). AtMIN7 contributes to PTI and ETI, and the *Pst* DC3000 effector HopM1 induces its degradation through the host 26S proteasome to suppress plant innate immunity (Nomura et al., 2011). Since AtMIN7 also plays a critical role in limiting fluid loss from plant cells, HopM1-mediated AtMIN7 degradation results in apoplast hydration and provides the favorable water condition needed for *Pst* DC3000 colonization; notably, high ambient humidity is required for water soaking (Beattie, 2016; Xin et al., 2016). Moreover, HopM1 and AvrE1 increase the expression of ABA-associated genes through transcriptome reprogramming and by raising ABA contents in guard cells (Roussin-Léveillée et al., 2022). The guard cell–specific ABA transporter ABCG40 is necessary for HopM1-mediated water soaking (Roussin-Léveillée et al., 2022), while AvrE1 activates ABA signaling through the inhibition of type one protein phosphatases (TOPPs), thereby suppressing SnRK2s (Hu et al., 2022). Therefore, *Pst* DC3000 utilizes HopM1 and AvrE1 to activate ABA signaling, inducing stomatal closure for water soaking after having invaded the plant inner space.

To prevent water soaking, plants promote stomatal reopening to establish a drier apoplast environment in pathogen-infected cells (Figure 2B). In rice, the *osaba1* mutant provided genetic evidence that increased stomatal conductance can enhance disease resistance to *Xoo* (Zhang et al., 2019). OsWRKY114 negatively regulated stomatal closure and conferred innate immunity against *Xoo* by repressing ABA signaling (Son et al., 2022; Song et al., 2022). Finally, in Arabidopsis, Lie et al. elucidated the molecular mechanism of stomatal immunity by which stomata reopen following effector-triggered stomatal closure (Liu et al., 2022b). They identified a class of small peptides, named the SMALL PHYTOCYTOKINES REGULATING DEFENSE AND WATER LOSS (SCREWs), and their receptor, the PLANT SCREW UNRESPONSIVE RECEPTOR

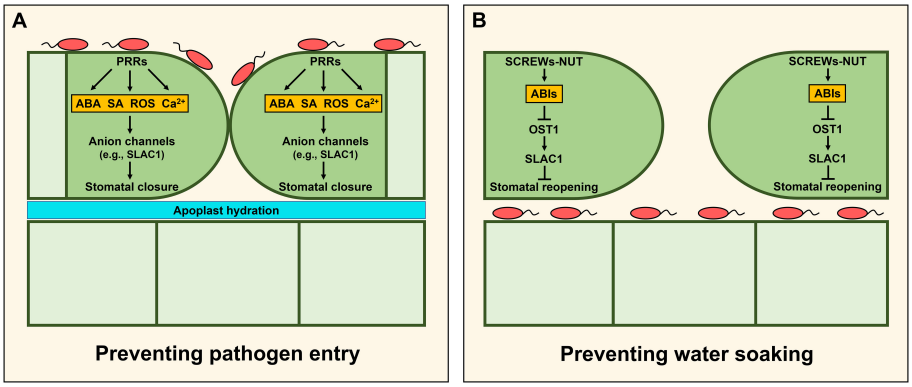

FIGURE 2
Stomatal immunity restricting pathogen entry or water soaking. **(A)** Pattern recognition receptors (PRRs)-triggered stomatal immunity. Recognition of pathogen-associated molecular patterns (PAMPs) by PRRs in guard cells promotes stomatal closure to prevent pathogen entry through activation of various signaling pathways such as ABA, SA, ROS, and Ca^{2+} (Arnaud and Hwang, 2015; Murata et al., 2015). **(B)** Stomatal immunity preventing water soaking. After pathogens invade internal plant tissues, stomatal closure can confer apoplast hydration inducing pathogen colonization. To prevent it, the secreted peptides SMALL PHYTOCYTOKINES REGULATING DEFENSE AND WATER LOSS (SCREWs) and the cognate receptor kinase PLANT SCREW UNRESPONSIVE RECEPTOR (NUT) are induced in Arabidopsis. Recognition of SCREWs by NUT increases the activity of the protein phosphatases type 2C (PP2Cs) such as ABA INSENSITIVE 1 (ABI1) and ABI2, and it results in stomatal reopening through inhibition of OST1/SnRK2.6-SLAC1 module (Liu et al., 2022b).

(NUT), a member of the LRR-RK family. Flg22 treatment increases the expression of *SCREW*s and *NUT*, and recognition of SCREWs by NUT promotes the heterodimerization of NUT with BAK1. The NUT/BAK1 complex phosphorylates and enhances the phosphatase activity of ABI1 and ABI2, thus inhibiting the OST1/SnRK2.6-SLAC1 module whose activity promotes stomatal closure. As a result, plants can increase stomatal conductance to prevent water soaking through apoplast dehydration.

The effects of carbon dioxide levels on stomatal immunity

Since the industrial revolution in the second half of the 18th century, the concentration of atmospheric CO_2 has begun to increase at an alarming rate. The Mauna Loa Observatory forecasts that the 2022 annual average CO_2 concentration will be 418.3 ± 0.5 parts per million (ppm). This trend is expected to continue and reach 730–1000 ppm by the end of the 21st century (Alley et al., 2007). Elevated CO_2 levels can increase the yield of C_3 plants by enhancing photosynthesis, but will not benefit C_4 plants (Long et al., 2006). High CO_2 levels will also affect plant–pathogen interactions. However, the effects of CO_2 concentrations on plant defense mechanisms depend on specific plant–pathogen interactions and are complex (Noctor and Mhamdi, 2017). Moreover, the detailed underlying molecular mechanisms are not yet well known. Therefore, we provide below an overview of the best-documented effects of high CO_2 on plant defense mechanisms related to stomata and photorespiration.

Like humidity, atmospheric CO_2 concentrations control stomatal immunity. CO_2 promotes stomatal closure through complex signaling networks (Zhang et al., 2018). First, atmospheric CO_2 enters guard cells *via* the PLASMA MEMBRANE INTRINSIC PROTEIN (PIP) aquaporins, followed by the conversion of CO_2 to bicarbonate (HCO_3^-) by beta carbonic anhydrases (βCAs) to activate downstream signaling events. Indeed, several studies have shown that the ubiquitous βCA enzymes are involved in the plant defense response. In Arabidopsis, genetic evidence demonstrated that βCA1 and βCA4 contribute to CO_2-induced stomatal closure by converting CO_2 into HCO_3^- (Hu et al., 2010). The CA activity of βCA1 is required for a full defense response against avirulent *Pst* DC3000 carrying the effector AvrB (Wang et al., 2009). In addition, the quintuple mutant *βca1 βca2 βca3 βca4 βca6* exhibited a partial reduction in SA sensitivity (Medina-Puche et al., 2017). However, Zhou et al. showed that, despite impaired stomatal closure preventing pathogen entry, PTI-mediated SA-dependent immunity against virulent *P. syringae* was enhanced in the *βca1 βca4* double mutant (Zhou et al., 2020). Furthermore, they revealed that the PRR-mediated downregulation of *βCA1* and *βCA4* expression was attenuated by high CO_2. These results suggest that CO_2 concentration and βCAs regulate plant immunity positively or negatively as a function of compatible and incompatible interactions with the incoming pathogen. In tobacco (*N. tabacum*), βCA SA-BINDING PROTEIN 2 (SABP2) exhibits lipase activity and confers SA-dependent immunity against tomato mosaic virus (Kumar and Klessig, 2003). Similarly, SABP3 has antioxidant activity and confers HR triggered by Pto-mediated recognition

of the effector AvrPto (Slaymaker et al., 2002). In addition, silencing of *SABP3* increases susceptibility to *Phytophthora infestans* (Restrepo et al., 2005). The expression of *CA* (accession number BQ113997) increased in potato (*Solanum tuberosum*) inoculated with an incompatible *P. infestans* strain, while it was downregulated in potato inoculated with a compatible *P. infestans* strain. Recently, Hu et al. also showed that βCA3 confers plant basal immunity in tomato (Hu et al., 2021b). High CO_2 and *Pst* DC3000 increases the induction of *βCA3* expression by the transcription factor NAC43, while the phosphorylation of the serine 207 residue of βCA3 by GRACE1 (GERMINATION REPRESSION AND CELL EXPANSION RECEPTOR-LIKE KINASE 1) results in the activation of plant basal immunity related to the cell wall regardless of stomatal movement or SA signaling.

After converting CO_2 into HCO_3^-, ABA signaling has a central role downstream of the convergence point of CO_2 for stomatal closure (Webb and Hetherington, 1997; Negi et al., 2008). Dittrich et al. argued that PYL4 and PYL5 are essential for CO_2-induced stomatal closure in Arabidopsis (Dittrich et al., 2019). However, CO_2-induced stomatal closure appears to be triggered by an ABA-independent pathway downstream of OST1/SnRK2.6 without direct activation of OST1/SnRK2.6 (Hsu et al., 2018). Another group also reported results in support of this idea. They developed a SnRK2 activity sensor called SNACS based on Förster resonance energy transfer (FRET) and showed that, although basal ABA levels and SnRK2 signaling are essential for CO_2-induced stomatal closure, CO_2 signaling did not activate SnRK2s including OST1/SnRK2.6 and PYL4 and PYL5 were also not required (Zhang et al., 2020). Therefore, it remains controversial whether CO_2 signaling can act upstream of SnRK2 in the ABA signaling cascade.

Moreover, recent studies indicated that ROS signaling is also important for CO_2 signaling for stomatal closure. In Arabidopsis, ROS signals as well as ABA signals are necessary for CO_2-induced stomatal closure (Chater et al., 2015). He et al. showed that ROS produced by both cell wall peroxidases and NADPH oxidases, together with phytohormones (SA, JA, and ABA), play an important role in CO_2-signaling during stomatal closure (He et al., 2020). However, the detailed molecular mechanisms by which ROS modulate CO_2 signaling are still unknown. Therefore, we discuss below the effects of CO_2 on ROS generation and plant immunity.

The effects of carbon dioxide on peroxisome-derived hydrogen peroxide

Photorespiration was once considered as a wasteful process because it is inefficient compared to the Calvin cycle and occurs when photosynthesis cannot operate. However, many studies have since shown photorespiration is involved in and required for various plant processes (Shi and Bloom, 2021). In particular, photorespiration has a crucial role in plant defenses due to ROS generation (Sørhagen et al., 2013). Hydrogen peroxide (H_2O_2) is a non-radical ROS that is deeply associated with plant defense responses (Smirnoff and Arnaud, 2019). It is produced mainly in leaf peroxisomes during photorespiration, with peroxisomal glycolate oxidase (GOX) and catalase (CAT) acting as major positive and negative regulators of its production, respectively (Foyer et al., 2009; Corpas et al., 2020).

Photorespiration and the Calvin cycle are competitively controlled by ribulose-1,5-bisphosphate carboxylase/oxygenase (Rubisco); thus, high CO_2 levels decrease photorespiration (Long et al., 2004; Busch, 2020). Therefore, high CO_2 would be expected to repress plant immunity. However, several studies have shown that high CO_2 can increase plant defense responses including SA and JA (Noctor and Mhamdi, 2017). In addition, CAT2 was shown to be involved in SA-mediated auxin and JA inhibition of resistance against biotrophs (Yuan et al., 2017). Recently, Williams et al. demonstrated that CO_2 influenced resistance to biotrophic and necrotrophic pathogens differently in Arabidopsis (Williams et al., 2018). Under high CO_2 conditions (1200 ppm), resistance to both the biotrophic oomycete *Hyaloperonospora arabidopsidis* and the necrotrophic fungus *Plectosphaerella cucumerina* increased compared to ambient CO_2 (400 ppm). SA appeared to play a minor role in resistance to the biotrophic pathogen, while JA conferred strong resistance against the necrotrophic pathogen. At low CO_2 (200 ppm), resistance to *H. arabidopsidis* was enhanced through photorespiration-derived H_2O_2 production, whereas resistance to *P. cucumerina* declined.

Prospects of genome editing for climate resilient crop development

Advances in biotechnology have opened up the possibility of overcoming the deleterious effects of climate change on crop plants. Induction of plant innate immunity compromised by climate change improves disease resistance to pathogen under the unfavorable environmental condition, but the constitutive activation of plant immune response retards growth and reduces crop productivity. To address this problem, scientists focused on the strategy to activate plant defense response spatiotemporally using pathogen-induced promoters and pathogen-responsive upstream open reading frames (Kim et al., 2021). However, this method cannot be free from the issue of genetically modified organisms. Therefore, the genome editing technologies based on SDNs (e.g., CRISPR/Cas9) are necessary for the development of

climate resilient crops. However, even though genome editing has successfully increased the disease resistance of various crops, there are still significant hurdle to its application to climate change adaptive crop development due to the negative effects of mutations on the crop's performance (Karavolias et al., 2021). Therefore, in order to cope with the future food resource crisis, understanding the various plant immune mechanisms affected by climate change and identifying elite genes that can improve disease resistance through genome editing will be one of the most efficient ways to develop climate resilient crops.

Conclusion

We are currently living in an unprecedented era of climate change. The consequences of this changing climate may diminish crop production and access to nutrients for all living creatures, concomitantly with the faster adaptation of microorganisms including phytopathogens due to their short life cycle and rapid propagation compared to other and more complex species, causing more severe damage to crop plants. It is clear that the damage to global crop security due to biotic stresses will pose a great challenge to human life in the future. Scientists have recently achieved remarkable progress in this field. Here, we provide an overview of the known and anticipated effects of climate change such as temperature, high humidity, and CO_2 on plant immunity mechanisms. The current efforts to understand how climate change will impact plant immune systems and to develop more efficient NPBTs will make it possible to overcome the incoming crisis through crop improvement that can minimize damage and preserve yields in future pathogen-friendly environmental conditions.

Author contributions

SS conceptualized and wrote the manuscript. SRP supervised. All authors contributed to the article and approved the submitted manuscript.

Funding

This research was funded by Research Program for Agricultural Science and Technology Development (Project No. PJ01661001), and supported by the 2022 Fellowship Program (Project No. PJ01661001) of the National Institute of Agricultural Sciences, Rural Development Administration, Republic of Korea.

Conflict of interest

The authors declare that the research was conducted in the absence of any commercial or financial relationships that could be construed as a potential conflict of interest.

Publisher's note

References

Agrios, G. N. (2005). *Plant pathology* (Burlington, MA, USA: Elsevier).

Albrecht, T., and Argueso, C. T. (2017). Should I fight or should I grow now? the role of cytokinins in plant growth and immunity and in the growth–defence trade-off. *Ann. Bot.* 119 (5), 725–735. doi: 10.1093/aob/mcw211

Alley, R., Berntsen, T., Bindoff, N. L., Chen, Z., Chidthaisong, A., Friedlingstein, P., et al. (2007). *Climate change 2007: The physical science basis. contribution of working group I to the fourth assessment report of the intergovernmental panel on climate change. summary for policymakers* (Geneva, Switzerland: IPCC Secretariat), 21.

Anderson, J. P., Gleason, C. A., Foley, R. C., Thrall, P. H., Burdon, J. B., and Singh, K. B. (2010). Plants versus pathogens: an evolutionary arms race. *Funct. Plant Biol.* 37 (6), 499–512. doi: 10.1071/FP09304

Argueso, C. T., Ferreira, F. J., Epple, P., To, J. P., Hutchison, C. E., Schaller, G. E., et al. (2012). Two-component elements mediate interactions between cytokinin and salicylic acid in plant immunity. *PloS Genet.* 8 (1), e1002448. doi: 10.1371/journal.pgen.1002448

Arnaud, D., and Hwang, I. (2015). A sophisticated network of signaling pathways regulates stomatal defenses to bacterial pathogens. *Mol. Plant* 8 (4), 566–581. doi: 10.1016/j.molp.2014.10.012

Aung, K., Jiang, Y., and He, S. Y. (2018). The role of water in plant–microbe interactions. *Plant J.* 93 (4), 771–780. doi: 10.1111/tpj.13795

Axtell, M. J., and Staskawicz, B. J. (2003). Initiation of RPS2-specified disease resistance in arabidopsis is coupled to the AvrRpt2-directed elimination of RIN4. *Cell* 112 (3), 369–377. doi: 10.1016/S0092-8674(03)00036-9

Backer, R., Naidoo, S., and Van den Berg, N. (2019). The NONEXPRESSOR OF PATHOGENESIS-RELATED GENES 1 (NPR1) and related family: mechanistic insights in plant disease resistance. *Front. Plant Sci.* 10, 102. doi: 10.3389/fpls.2019.00102

Beattie, G. A. (2016). A war over water when bacteria invade leaves. *Nature* 539 (7630), 506–507. doi: 10.1038/539506a

Belkhadir, Y., Nimchuk, Z., Hubert, D. A., Mackey, D., and Dangl, J. L. (2004). Arabidopsis RIN4 negatively regulates disease resistance mediated by RPS2 and RPM1 downstream or independent of the NDR1 signal modulator and is not required for the virulence functions of bacterial type III effectors AvrRpt2 or AvrRpm1. *Plant Cell* 16 (10), 2822–2835. doi: 10.1105/tpc.104.024117

Berens, M. L., Wolinska, K. W., Spaepen, S., Ziegler, J., Nobori, T., Nair, A., et al. (2019). Balancing trade-offs between biotic and abiotic stress responses through

leaf age-dependent variation in stress hormone cross-talk. *Proc. Natl. Acad. Sci.* 116 (6), 2364–2373. doi: 10.1073/pnas.1817233116

Bose, J., Pottosin, I. I., Shabala, S. S., Palmgren, M. G., and Shabala, S. (2011). Calcium efflux systems in stress signaling and adaptation in plants. *Front. Plant Sci.* 2, 85. doi: 10.3389/fpls.2011.00085

Bruessow, F., Bautor, J., Hoffmann, G., Yildiz, I., Zeier, J., and Parker, J. E. (2021). Natural variation in temperature-modulated immunity uncovers transcription factor bHLH059 as a thermoresponsive regulator in arabidopsis thaliana. *PloS Genet.* 17 (1), e1009290. doi: 10.1371/journal.pgen.1009290

Busch, F. A. (2020). Photorespiration in the context of rubisco biochemistry, CO_2 diffusion and metabolism. *Plant J.* 101 (4), 919–939. doi: 10.1111/tpj.14674

Caffarra, A., Rinaldi, M., Eccel, E., Rossi, V., and Pertot, I. (2012). Modelling the impact of climate change on the interaction between grapevine and its pests and pathogens: European grapevine moth and powdery mildew. *Agriculture Ecosyst. Environ.* 148, 89–101. doi: 10.1016/j.agee.2011.11.017

Cai, W., Yang, S., Wu, R., Cao, J., Shen, L., Guan, D., et al. (2021). Pepper NAC-type transcription factor NAC2c balances the trade-off between growth and defense responses. *Plant Physiol* 186 (4), 2169–2189. doi: 10.1093/plphys/kiab190

Cai, H., Yang, S., Yan, Y., Xiao, Z., Cheng, J., Wu, J., et al. (2015). CaWRKY6 transcriptionally activates CaWRKY40, regulates ralstonia solanacearum resistance, and confers high-temperature and high-humidity tolerance in pepper. *J. Exp. Bot.* 66 (11), 3163–3174. doi: 10.1093/jxb/erv125

Castroverde, C. D. M., and Dina, D. (2021). Temperature regulation of plant hormone signaling during stress and development. *J. Exp. Bot.* 72 (21), 7436–7458. doi: 10.1093/jxb/erab257

Challinor, A. J., Watson, J., Lobell, D. B., Howden, S., Smith, D., and Chhetri, N. (2014). A meta-analysis of crop yield under climate change and adaptation. *Nat. Climate Change* 4 (4), 287–291. doi: 10.1038/nclimate2153

Chaloner, T. M., Gurr, S. J., and Bebber, D. P. (2021). Plant pathogen infection risk tracks global crop yields under climate change. *Nat. Climate Change* 11 (8), 710–715. doi: 10.1038/s41558-021-01104-8

Chapman, J. M., Muhlemann, J. K., Gayomba, S. R., and Muday, G. K. (2019). RBOH-dependent ROS synthesis and ROS scavenging by plant specialized metabolites to modulate plant development and stress responses. *Chem. Res. Toxicol.* 32 (3), 370–396. doi: 10.1021/acs.chemrestox.9b00028

Chater, C., Peng, K., Movahedi, M., Dunn, J. A., Walker, H. J., Liang, Y.-K., et al. (2015). Elevated CO_2-induced responses in stomata require ABA and ABA signaling. *Curr. Biol.* 25 (20), 2709–2716. doi: 10.1016/j.cub.2015.09.013

Cheng, C., Gao, X., Feng, B., Sheen, J., Shan, L., and He, P. (2013). Plant immune response to pathogens differs with changing temperatures. *Nat. Commun.* 4 (1), 1–9. doi: 10.1038/ncomms3530

Chinchilla, D., Zipfel, C., Robatzek, S., Kemmerling, B., Nürnberger, T., Jones, J. D., et al. (2007). A flagellin-induced complex of the receptor FLS2 and BAK1 initiates plant defence. *Nature* 448 (7152), 497–500. doi: 10.1038/nature05999

Chisholm, S. T., Coaker, G., Day, B., and Staskawicz, B. J. (2006). Host-microbe interactions: shaping the evolution of the plant immune response. *Cell* 124 (4), 803–814. doi: 10.1016/j.cell.2006.02.008

Choi, J., Choi, D., Lee, S., Ryu, C.-M., and Hwang, I. (2011). Cytokinins and plant immunity: old foes or new friends? *Trends Plant Sci.* 16 (7), 388–394. doi: 10.1016/j.tplants.2011.03.003

Coll, N. S., Epple, P., and Dangl, J. L. (2011). Programmed cell death in the plant immune system. *Cell Death Differentiation* 18 (8), 1247–1256. doi: 10.1038/cdd.2011.37

Conrath, U., Beckers, G. J., Langenbach, C. J., and Jaskiewicz, M. R. (2015). Priming for enhanced defense. *Annu. Rev. Phytopathol.* 53 (1), 97–119. doi: 10.1146/annurev-phyto-080614-120132

Coppinger, P., Repetti, P. P., Day, B., Dahlbeck, D., Mehlert, A., and Staskawicz, B. J. (2004). Overexpression of the plasma membrane-localized NDR1 protein results in enhanced bacterial disease resistance in arabidopsis thaliana. *Plant J.* 40 (2), 225–237. doi: 10.1111/j.1365-313X.2004.02203.x

Corpas, F. J., González-Gordo, S., and Palma, J. M. (2020). Plant peroxisomes: A factory of reactive species. *Front. Plant Sci.* 11, 853. doi: 10.3389/fpls.2020.00853

Corwin, J. A., and Kliebenstein, D. J. (2017). Quantitative resistance: more than just perception of a pathogen. *Plant Cell* 29 (4), 655–665. doi: 10.1105/tpc.16.00915

Cui, H., Gobbato, E., Kracher, B., Qiu, J., Bautor, J., and Parker, J. E. (2017). A core function of EDS1 with PAD4 is to protect the salicylic acid defense sector in arabidopsis immunity. *New Phytol.* 213 (4), 1802–1817. doi: 10.1111/nph.14302

DANG, F. F., WANG, Y. N., Yu, L., Eulgem, T., Lai, Y., LIU, Z. Q., et al. (2013). CaWRKY40, a WRKY protein of pepper, plays an important role in the regulation of tolerance to heat stress and resistance to ralstonia solanacearum infection. *Plant Cell Environ.* 36 (4), 757–774. doi: 10.1111/pce.12011

Davis, K. R., Schott, E., and Ausubel, F. M. (1991). Virulence of selected phytopathogenic pseudomonads in arabidopsis thaliana. *Mol. Plant-Microbe Interact.* 4 (1), 477–488. doi: 10.1094/MPMI-4-477

Day, B., Dahlbeck, D., and Staskawicz, B. J. (2006). NDR1 interaction with RIN4 mediates the differential activation of multiple disease resistance pathways in arabidopsis. *Plant Cell* 18 (10), 2782–2791. doi: 10.1105/tpc.106.044693

Desaint, H., Aoun, N., Deslandes, L., Vailleau, F., Roux, F., and Berthomé, R. (2021). Fight hard or die trying: when plants face pathogens under heat stress. *New Phytol.* 229 (2), 712–734. doi: 10.1111/nph.16965

Deutsch, C. A., Tewksbury, J. J., Huey, R. B., Sheldon, K. S., Ghalambor, C. K., Haak, D. C., et al. (2008). Impacts of climate warming on terrestrial ectotherms across latitude. *Proc. Natl. Acad. Sci.* 105 (18), 6668–6672. doi: 10.1073/pnas.0709472105

Dittrich, M., Mueller, H. M., Bauer, H., Peirats-Llobet, M., Rodriguez, P. L., Geilfus, C.-M., et al. (2019). The role of arabidopsis ABA receptors from the PYR/PYL/RCAR family in stomatal acclimation and closure signal integration. *Nat. Plants* 5 (9), 1002–1011. doi: 10.1038/s41477-019-0490-0

Driesen, E., Van den Ende, W., De Proft, M., and Saeys, W. (2020). Influence of environmental factors light, CO_2, temperature, and relative humidity on stomatal opening and development: A review. *Agronomy* 10 (12), 1975. doi: 10.3390/agronomy10121975

Du, L., Ali, G. S., Simons, K. A., Hou, J., Yang, T., Reddy, A., et al. (2009). Ca2+/calmodulin regulates salicylic-acid-mediated plant immunity. *Nature* 457 (7233), 1154–1158. doi: 10.1038/nature07612

Elad, Y., and Pertot, I. (2014). Climate change impacts on plant pathogens and plant diseases. *J. Crop Improv.* 28 (1), 99–139. doi: 10.1080/15427528.2014.865412

Flors, V., Ton, J., Van Doorn, R., Jakab, G., García-Agustín, P., and Mauch-Mani, B. (2008). Interplay between JA, SA and ABA signalling during basal and induced resistance against pseudomonas syringae and alternaria brassicicola. *Plant J.* 54 (1), 81–92. doi: 10.1111/j.1365-313X.2007.03397.x

Foyer, C. H., Bloom, A. J., Queval, G., and Noctor, G. (2009). Photorespiratory metabolism: genes, mutants, energetics, and redox signaling. *Annu. Rev. Plant Biol.* 60, 455–484. doi: 10.1146/annurev.arplant.043008.091948

French, E., Kim, B.-S., and Iyer-Pascuzzi, A. S. (2016). Mechanisms of quantitative disease resistance in plants. *Semin. Cell Dev. Biol.* 56, 201–208. doi: 10.1016/j.semcdb.2016.05.015

Gangappa, S. N., Berriri, S., and Kumar, S. V. (2017). PIF4 coordinates thermosensory growth and immunity in arabidopsis. *Curr. Biol.* 27 (2), 243–249. doi: 10.1016/j.cub.2016.11.012

Gangappa, S. N., and Kumar, S. V. (2018). DET1 and COP1 modulate the coordination of growth and immunity in response to key seasonal signals in arabidopsis. *Cell Rep.* 25 (1), 29–37. e23. doi: 10.1016/j.celrep.2018.08.096

García, A. V., Blanvillain-Baufumé, S., Huibers, R. P., Wiermer, M., Li, G., Gobbato, E., et al. (2010). Balanced nuclear and cytoplasmic activities of EDS1 are required for a complete plant innate immune response. *PloS Pathog.* 6 (7), e1000970. doi: 10.1371/journal.ppat.1000970

Garrett, K. A., Dendy, S. P., Frank, E. E., Rouse, M. N., and Travers, S. E. (2006). Climate change effects on plant disease: genomes to ecosystems. *Annu. Rev. Phytopathol.* 44, 489–509. doi: 10.1146/annurev.phyto.44.070505.143420

Glazebrook, J. (2005). Contrasting mechanisms of defense against biotrophic and necrotrophic pathogens. *Annu. Rev. Phytopathol.* 43, 205. doi: 10.1146/annurev.phyto.43.040204.135923

Guzel Deger, A., Scherzer, S., Nuhkat, M., Kedzierska, J., Kollist, H., Brosché, M., et al. (2015). Guard cell SLAC 1-type anion channels mediate flagellin-induced stomatal closure. *New Phytol.* 208 (1), 162–173. doi: 10.1111/nph.13435

Ham, J. H., Majerczak, D. R., Arroyo-Rodriguez, A. S., Mackey, D. M., and Coplin, D. L. (2006). WtsE, an AvrE-family effector protein from pantoea stewartii subsp. stewartii, causes disease-associated cell death in corn and requires a chaperone protein for stability. *Mol. Plant-Microbe Interact.* 19 (10), 1092–1102. doi: 10.1094/MPMI-19-1092

Hammoudi, V., Fokkens, L., Beerens, B., Vlachakis, G., Chatterjee, S., Arroyo-Mateos, M., et al. (2018). The arabidopsis SUMO E3 ligase SIZ1 mediates the temperature dependent trade-off between plant immunity and growth. *PloS Genet.* 14 (1), e1007157. doi: 10.1371/journal.pgen.1007157

Haque, M. A., Marwaha, S., Deb, C. K., Nigam, S., Arora, A., Hooda, K. S., et al. (2022). Deep learning-based approach for identification of diseases of maize crop. *Sci. Rep.* 12 (1), 6334. doi: 10.1038/s41598-022-10140-z

Havko, N. E., Das, M. R., McClain, A. M., Kapali, G., Sharkey, T. D., and Howe, G. A. (2020). Insect herbivory antagonizes leaf cooling responses to elevated temperature in tomato. *Proc. Natl. Acad. Sci.* 117 (4), 2211–2217. doi: 10.1073/pnas.1913885117

He, J., Zhang, R.-X., Kim, D. S., Sun, P., Liu, H., Liu, Z., et al. (2020). ROS of distinct sources and salicylic acid separate elevated CO_2-mediated stomatal movements in arabidopsis. *Front. Plant Sci.* 11, 542. doi: 10.3389/fpls.2020.00542

Hou, S., Liu, D., and He, P. (2021). Phytocytokines function as immunological modulators of plant immunity. *Stress Biol.* 1 (1), 1–14. doi: 10.1007/s44154-021-00009-y

Hsu, P. K., Dubeaux, G., Takahashi, Y., and Schroeder, J. I. (2021). Signaling mechanisms in abscisic acid-mediated stomatal closure. *Plant J.* 105 (2), 307–321. doi: 10.1111/tpj.15067

Hsu, P.-K., Takahashi, Y., Munemasa, S., Merilo, E., Laanemets, K., Waadt, R., et al. (2018). Abscisic acid-independent stomatal CO_2 signal transduction pathway and convergence of CO_2 and ABA signaling downstream of OST1 kinase. *Proc. Natl. Acad. Sci.* 115 (42), E9971–E9980. doi: 10.1073/pnas.1809204115

Huang, J., Zhao, X., Bürger, M., Wang, Y., and Chory, J. (2021a). Two interacting ethylene response factors regulate heat stress response. *Plant Cell* 33 (2), 338–357. doi: 10.1093/plcell/koaa026

Huang, S., Zhu, S., Kumar, P., and MacMicking, J. D. (2021b). A phase-separated nuclear GBPL circuit controls immunity in plants. *Nature* 594 (7863), 424–429. doi: 10.1038/s41586-021-03572-6

Hu, H., Boisson-Dernier, A., Israelsson-Nordström, M., Böhmer, M., Xue, S., Ries, A., et al. (2010). Carbonic anhydrases are upstream regulators of CO_2-controlled stomatal movements in guard cells. *Nat. Cell Biol.* 12 (1), 87–93. doi: 10.1038/ncb2009

Hu, Y., Ding, Y., Cai, B., Qin, X., Wu, J., Yuan, M., et al. (2022). Bacterial effectors manipulate plant abscisic acid signaling for creation of an aqueous apoplast. *Cell Host Microbe* 30 (4), 518–529. doi: 10.1016/j.chom.2022.02.002

Hu, Z., Ma, Q., Foyer, C. H., Lei, C., Choi, H. W., Zheng, C., et al. (2021b). High CO_2- and pathogen-driven expression of the carbonic anhydrase βCA3 confers basal immunity in tomato. *New Phytol.* 229 (5), 2827–2843. doi: 10.1111/nph.17087

Huot, B., Castroverde, C. D. M., Velásquez, A. C., Hubbard, E., Pulman, J. A., Yao, J., et al. (2017). Dual impact of elevated temperature on plant defence and bacterial virulence in arabidopsis. *Nat. Commun.* 8 (1), 1–12. doi: 10.1038/s41467-017-01674-2

Hu, Y., Tao, F., Su, C., Zhang, Y., Li, J., Wang, J., et al. (2021a). NBS-LRR gene TaRPS2 is positively associated with the high-temperature seedling plant resistance of wheat against puccinia striiformis f. sp. tritici. *Phytopathology* 111 (8), 1449–1458. doi: 10.1094/PHYTO-03-20-0063-R

Iqbal, Z., Shariq Iqbal, M., Singh, S. P., and Buaboocha, T. (2020). Ca2+/calmodulin complex triggers CAMTA transcriptional machinery under stress in plants: signaling cascade and molecular regulation. *Front. Plant Sci.* 11, 598327. doi: 10.3389/fpls.2020.598327

Islam, M. T., Gupta, D. R., Hossain, A., Roy, K. K., He, X., Kabir, M. R., et al. (2020). Wheat blast: a new threat to food security. *Phytopathol. Res.* 2 (1), 1–13. doi: 10.1186/s42483-020-00067-6

Janda, M., Lamparová, L., Zubíková, A., Burketová, L., Martinec, J., and Krčková, Z. (2019). Temporary heat stress suppresses PAMP-triggered immunity and resistance to bacteria in arabidopsis thaliana. *Mol. Plant Pathol.* 20 (7), 1005–1012. doi: 10.1111/mpp.12799

Jones, J. D., and Dangl, J. L. (2006). The plant immune system. *Nature* 444 (7117), 323–329. doi: 10.1038/nature05286

Jung, J.-H., Domijan, M., Klose, C., Biswas, S., Ezer, D., Gao, M., et al. (2016). Phytochromes function as thermosensors in arabidopsis. *Science* 354 (6314), 886–889. doi: 10.1126/science.aaf6005

Junho, C. V. C., Caio-Silva, W., Trentin-Sonoda, M., and Carneiro-Ramos, M. S. (2020). An overview of the role of calcium/calmodulin-dependent protein kinase in cardiorenal syndrome. *Front. Physiol.* 11, 735. doi: 10.3389/fphys.2020.00735

Kangasjärvi, S., Neukermans, J., Li, S., Aro, E.-M., and Noctor, G. (2012). Photosynthesis, photorespiration, and light signalling in defence responses. *J. Exp. Bot.* 63 (4), 1619–1636. doi: 10.1093/jxb/err402

Karavolias, N. G., Horner, W., Abugu, M. N., and Evanega, S. N. (2021). Application of gene editing for climate change in agriculture. *Front. Sustain. Food Syst.* 5, 685801. doi: 10.3389/fsufs.2021.685801

Kim, J. H., Castroverde, C. D. M., Huang, S., Li, C., Hilleary, R., Seroka, A., et al. (2022). Increasing the resilience of plant immunity to a warming climate. *Nature* 607 (7918), 339–344. doi: 10.1038/s41586-022-04902-y

Kim, J. H., Hilleary, R., Seroka, A., and He, S. Y. (2021). Crops of the future: building a climate-resilient plant immune system. *Curr. Opin. Plant Biol.* 60, 101997. doi: 10.1016/j.pbi.2020.101997

Kumar, D., and Klessig, D. F. (2003). High-affinity salicylic acid-binding protein 2 is required for plant innate immunity and has salicylic acid-stimulated lipase activity. *Proc. Natl. Acad. Sci.* 100 (26), 16101–16106. doi: 10.1073/pnas.0307162100

Kumar, S. V., and Wigge, P. A. (2010). H2A. z-containing nucleosomes mediate the thermosensory response in arabidopsis. *Cell* 140 (1), 136–147. doi: 10.1016/j.cell.2009.11.006

Lal, N. K., Nagalakshmi, U., Hurlburt, N. K., Flores, R., Bak, A., Sone, P., et al. (2018). The receptor-like cytoplasmic kinase BIK1 localizes to the nucleus and regulates defense hormone expression during plant innate immunity. *Cell Host Microbe* 23 (4), 485–497. doi: 10.1016/j.chom.2018.03.010

Lapin, D., Bhandari, D. D., and Parker, J. E. (2020). Origins and immunity networking functions of EDS1 family proteins. *Annu. Rev. Phytopathol.* 58, 253–276. doi: 10.1146/annurev-phyto-010820-012840

Lee, S. C., and Luan, S. (2012). ABA signal transduction at the crossroad of biotic and abiotic stress responses. *Plant Cell Environ.* 35 (1), 53–60. doi: 10.1111/j.1365-3040.2011.02426.x

Lefevere, H., Bauters, L., and Gheysen, G. (2020). Salicylic acid biosynthesis in plants. *Front. Plant Sci.* 11, 338. doi: 10.3389/fpls.2020.00338

Legris, M., Klose, C., Burgie, E. S., Rojas, C. C. R., Neme, M., Hiltbrunner, A., et al. (2016). Phytochrome b integrates light and temperature signals in arabidopsis. *Science* 354 (6314), 897–900. doi: 10.1126/science.aaf5656

Li, N., Han, X., Feng, D., Yuan, D., and Huang, L.-J. (2019). Signaling crosstalk between salicylic acid and ethylene/jasmonate in plant defense: do we understand what they are whispering? *Int. J. Mol. Sci.* 20 (3), 671. doi: 10.3390/ijms20030671

Li, Z., Liu, H., Ding, Z., Yan, J., Yu, H., Pan, R., et al. (2020). Low temperature enhances plant immunity *via* salicylic acid pathway genes that are repressed by ethylene. *Plant Physiol.* 182 (1), 626–639. doi: 10.1104/pp.19.01130

Liu, Z., Hou, S., Rodrigues, O., Wang, P., Luo, D., Munemasa, S., et al. (2022b). Phytocytokine signalling reopens stomata in plant immunity and water loss. *Nature* 605 (7909), 332–339. doi: 10.1038/s41586-022-04684-3

Liu, H., Lu, C., Li, Y., Wu, T., Zhang, B., Liu, B., et al. (2022a). The bacterial effector AvrRxo1 inhibits vitamin B6 biosynthesis to promote infection in rice. *Plant Commun.* 3 (3), 100324. doi: 10.1016/j.xplc.2022.100324

Long, S. P., Ainsworth, E. A., Leakey, A. D., Nosberger, J., and Ort, D. R. (2006). Food for thought: lower-than-expected crop yield stimulation with rising CO_2 concentrations. *science* 312 (5782), 1918–1921. doi: 10.1126/science.1114722

Long, S. P., Ainsworth, E. A., Rogers, A., and Ort, D. R. (2004). Rising atmospheric carbon dioxide: plants FACE the future. *Annu. Rev. Plant Biol.* 55, 591. doi: 10.1146/annurev.arplant.55.031903.141610

Lusser, M., Parisi, C., Plan, D., and Rodríguez-Cerezo, E. (2011). *New plant breeding techniques: state-of-the-art and prospects for commercial development* (Luxembourg: Publications office of the European Union).

Lusser, M., Parisi, C., Plan, D., and Rodriguez-Cerezo, E. (2012). Deployment of new biotechnologies in plant breeding. *Nat. Biotechnol.* 30 (3), 231–239. doi: 10.1038/nbt.2142

Mackey, D., Belkhadir, Y., Alonso, J. M., Ecker, J. R., and Dangl, J. L. (2003). Arabidopsis RIN4 is a target of the type III virulence effector AvrRpt2 and modulates RPS2-mediated resistance. *Cell* 112 (3), 379–389. doi: 10.1016/S0092-8674(03)00040-0

Mackey, D., Holt, B. F.III, Wiig, A., and Dangl, J. L. (2002). RIN4 interacts with pseudomonas syringae type III effector molecules and is required for RPM1-mediated resistance in arabidopsis. *Cell* 108 (6), 743–754. doi: 10.1016/S0092-8674(02)00661-X

Ma, X., Li, Q.-H., Yu, Y.-N., Qiao, Y.-M., and Gong, Z.-H. (2020). The CBL–CIPK pathway in plant response to stress signals. *Int. J. Mol. Sci.* 21 (16), 5668. doi: 10.3390/ijms21165668

McIntyre, K. E., Bush, D. R., and Argueso, C. T. (2021). Cytokinin regulation of source-sink relationships in plant-pathogen interactions. *Front. Plant Sci.* 12, 677585. doi: 10.3389/fpls.2021.677585

Medina-Puche, L., Castelló, M. J., Canet, J. V., Lamilla, J., Colombo, M. L., and Tornero, P. (2017). β-carbonic anhydrases play a role in salicylic acid perception in arabidopsis. *PloS One* 12 (7), e0181820. doi: 10.1371/journal.pone.0181820

Melotto, M., Underwood, W., Koczan, J., Nomura, K., and He, S. Y. (2006). Plant stomata function in innate immunity against bacterial invasion. *Cell* 126 (5), 969–980. doi: 10.1016/j.cell.2006.06.054

Melotto, M., Zhang, L., Oblessuc, P. R., and He, S. Y. (2017). Stomatal defense a decade later. *Plant Physiol.* 174 (2), 561–571. doi: 10.1104/pp.16.01853

Merilo, E., Jalakas, P., Laanemets, K., Mohammadi, O., Horak, H., Kollist, H., et al. (2015). Abscisic acid transport and homeostasis in the context of stomatal regulation. *Mol. Plant* 8 (9), 1321–1333. doi: 10.1016/j.molp.2015.06.006

Monaghan, J., and Zipfel, C. (2012). Plant pattern recognition receptor complexes at the plasma membrane. *Curr. Opin. Plant Biol.* 15 (4), 349–357. doi: 10.1016/j.pbi.2012.05.006

Monteiro, F., and Nishimura, M. T. (2018). Structural, functional, and genomic diversity of plant NLR proteins: An evolved resource for rational engineering of plant immunity. *Annu. Rev. Phytopathol.* 56, 243–267. doi: 10.1146/annurev-phyto-080417-045817

Mukhtar, M. S., Carvunis, A.-R., Dreze, M., Epple, P., Steinbrenner, J., Moore, J., et al. (2011). Independently evolved virulence effectors converge onto hubs in a plant immune system network. *science* 333 (6042), 596–601. doi: 10.1126/science.1203659

Murata, Y., Mori, I. C., and Munemasa, S. (2015). Diverse stomatal signaling and the signal integration mechanism. *Annu. Rev. Plant Biol.* 66, 369–392. doi: 10.1146/annurev-arplant-043014-114707

Nanda, A. K., Andrio, E., Marino, D., Pauly, N., and Dunand, C. (2010). Reactive oxygen species during plant-microorganism early interactions. *J. Integr. Plant Biol.* 52 (2), 195–204. doi: 10.1111/j.1744-7909.2010.00933.x

Naveed, Z. A., Wei, X., Chen, J., Mubeen, H., and Ali, G. S. (2020). The PTI to ETI continuum in phytophthora-plant interactions. *Front. Plant Sci.* 11, 593905. doi: 10.3389/fpls.2020.593905

Negi, J., Matsuda, O., Nagasawa, T., Oba, Y., Takahashi, H., Kawai-Yamada, M., et al. (2008). CO_2 regulator SLAC1 and its homologues are essential for anion homeostasis in plant cells. *Nature* 452 (7186), 483–486. doi: 10.1038/nature06720

Nie, H., Zhao, C., Wu, G., Wu, Y., Chen, Y., and Tang, D. (2012). SR1, a calmodulin-binding transcription factor, modulates plant defense and ethylene-induced senescence by directly regulating NDR1 and EIN3. *Plant Physiol.* 158 (4), 1847–1859. doi: 10.1104/pp.111.192310

Noctor, G., and Mhamdi, A. (2017). Climate change, CO_2, and defense: the metabolic, redox, and signaling perspectives. *Trends Plant Sci.* 22 (10), 857–870. doi: 10.1016/j.tplants.2017.07.007

Nomura, K., DebRoy, S., Lee, Y. H., Pumplin, N., Jones, J., and He, S. Y. (2006). A bacterial virulence protein suppresses host innate immunity to cause plant disease. *Science* 313 (5784), 220–223. doi: 10.1126/science.1129523

Nomura, K., Mecey, C., Lee, Y.-N., Imboden, L. A., Chang, J. H., and He, S. Y. (2011). Effector-triggered immunity blocks pathogen degradation of an immunity-associated vesicle traffic regulator in arabidopsis. *Proc. Natl. Acad. Sci.* 108 (26), 10774–10779. doi: 10.1073/pnas.1103338108

Oerke, E.-C. (2006). Crop losses to pests. *J. Agric. Sci.* 144 (1), 31–43. doi: 10.1017/S0021859605005708

Pieterse, C. M., van der Does, D., Zamioudis, C., Leon-Reyes, A., and Van Wees, S. C. (2012). Hormonal modulation of plant immunity. *Annu. Rev. Cell Dev. Biol.* 28, 489–521. doi: 10.1146/annurev-cellbio-092910-154055

Poland, J. A., Balint-Kurti, P. J., Wisser, R. J., Pratt, R. C., and Nelson, R. J. (2009). Shades of gray: the world of quantitative disease resistance. *Trends Plant Sci.* 14 (1), 21–29. doi: 10.1016/j.tplants.2008.10.006

Pruitt, R. N., Locci, F., Wanke, F., Zhang, L., Saile, S. C., Joe, A., et al. (2021). The EDS1–PAD4–ADR1 node mediates arabidopsis pattern-triggered immunity. *Nature* 598 (7881), 495–499. doi: 10.1038/s41586-021-03829-0

Rasmussen, S., Barah, P., Suarez-Rodriguez, M. C., Bressendorff, S., Friis, P., Costantino, P., et al. (2013). Transcriptome responses to combinations of stresses in arabidopsis. *Plant Physiol.* 161 (4), 1783–1794. doi: 10.1104/pp.112.210773

Reimers, P., and Leach, J. (1991). Race-specific resistance to xanthomonas oryzae pv. oryzae conferred by bacterial blight resistance gene xa-10 in rice (Oryza sativa) involves accumulation of a lignin-like substance in host tissues. *Physiol. Mol. Plant Pathol.* 38 (1), 39–55. doi: 10.1016/S0885-5765(05)80141-9

Restrepo, S., Myers, K., Del Pozo, O., Martin, G., Hart, A., Buell, C., et al. (2005). Gene profiling of a compatible interaction between phytophthora infestans and solanum tuberosum suggests a role for carbonic anhydrase. *Mol. Plant-Microbe Interact.* 18 (9), 913–922. doi: 10.1094/MPMI-18-0913

Rising, J., and Devineni, N. (2020). Crop switching reduces agricultural losses from climate change in the united states by half under RCP 8.5. *Nat. Commun.* 11 (1), 1–7. doi: 10.1038/s41467-020-18725-w

Román-Palacios, C., and Wiens, J. J. (2020). Recent responses to climate change reveal the drivers of species extinction and survival. *Proc. Natl. Acad. Sci.* 117 (8), 4211–4217. doi: 10.1073/pnas.1913007117

Romero, F., Cazzato, S., Walder, F., Vogelgsang, S., Bender, S. F., and van der Heijden, M. G. (2021). Humidity and high temperature are important for predicting fungal disease outbreaks worldwide. *New Phytologist* 234 (5), 1553–1556. doi: 10.1111/nph.17340

Roussin-Léveillée, C., Lajeunesse, G., St-Amand, M., Veerapen, V. P., Silva-Martins, G., Nomura, K., et al. (2022). Evolutionarily conserved bacterial effectors hijack abscisic acid signaling to induce an aqueous environment in the apoplast. *Cell Host Microbe* 30 (4), 489–501. e484. doi: 10.1016/j.chom.2022.02.006

Sørhagen, K., Laxa, M., Peterhänsel, C., and Reumann, S. (2013). The emerging role of photorespiration and non-photorespiratory peroxisomal metabolism in pathogen defence. *Plant Biol.* 15 (4), 723–736. doi: 10.1111/j.1438-8677.2012.00723.x

Samaradivakara, S. P., Chen, H., Lu, Y. J., Li, P., Kim, Y., Tsuda, K., et al. (2022). Overexpression of NDR1 leads to pathogen resistance at elevated temperatures. *New Phytologist* 235 (3), 1146–1162. doi: 10.1111/nph.18190

Savary, S., Ficke, A., Aubertot, J.-N., and Hollier, C. (2012). Crop losses due to diseases and their implications for global food production losses and food security *Food Secur.* 4, 519–537. doi: 10.1007/s00203-017-1426-6

Savary, S., and Willocquet, L. (2020). Modeling the impact of crop diseases on global food security. *Annu. Rev. Phytopathol.* 58, 313–341. doi: 10.1146/annurev-phyto-010820-012856

Savary, S., Willocquet, L., Pethybridge, S. J., Esker, P., McRoberts, N., and Nelson, A. (2019). The global burden of pathogens and pests on major food crops. *Nat. Ecol. Evol.* 3 (3), 430–439. doi: 10.1038/s41559-018-0793-y

Scholthof, K. B. (2007). The disease triangle: pathogens, the environment and society. *Nat. Rev. Microbiol.* 5 (2), 152–156. doi: 10.1038/nrmicro1596

Schornack, S., Minsavage, G. V., Stall, R. E., Jones, J. B., and Lahaye, T. (2008). Characterization of AvrHah1, a novel AvrBs3-like effector from xanthomonas gardneri with virulence and avirulence activity. *New Phytol.* 179 (2), 546–556. doi: 10.1111/j.1469-8137.2008.02487.x

Serrano, M., Wang, B., Aryal, B., Garcion, C., Abou-Mansour, E., Heck, S., et al. (2013). Export of salicylic acid from the chloroplast requires the multidrug and toxin extrusion-like transporter EDS5. *Plant Physiol.* 162 (4), 1815–1821. doi: 10.1104/pp.113.218156

Shapiro, A. D., and Zhang, C. (2001). The role of NDR1 in avirulence gene-directed signaling and control of programmed cell death in arabidopsis. *Plant Physiol.* 127 (3), 1089–1101. doi: 10.1104/pp.010096

Shen, L., Liu, Z., Yang, S., Yang, T., Liang, J., Wen, J., et al. (2016a). Pepper CabZIP63 acts as a positive regulator during ralstonia solanacearum or high temperature–high humidity challenge in a positive feedback loop with CaWRKY40. *J. Exp. Bot.* 67 (8), 2439–2451. doi: 10.1093/jxb/erw069

Shen, L., Yang, S., Yang, F., Guan, D., and He, S. (2020). CaCBL1 acts as a positive regulator in pepper response to ralstonia solanacearum. *Mol. Plant-Microbe Interact.* 33 (7), 945–957. doi: 10.1094/MPMI-08-19-0241-R

Shen, L., Yang, S., Yang, T., Liang, J., Cheng, W., Wen, J., et al. (2016b). CaCDPK15 positively regulates pepper responses to ralstonia solanacearum inoculation and forms a positive-feedback loop with CaWRKY40 to amplify defense signaling. *Sci. Rep.* 6 (1), 1–12. doi: 10.1038/srep22439

Shi, X., and Bloom, A. (2021). Photorespiration: the futile cycle? *Plants* 10 (5), 908. doi: 10.3390/plants10050908

Slaymaker, D. H., Navarre, D. A., Clark, D., del Pozo, O., Martin, G. B., and Klessig, D. F. (2002). The tobacco salicylic acid-binding protein 3 (SABP3) is the chloroplast carbonic anhydrase, which exhibits antioxidant activity and plays a role in the hypersensitive defense response. *Proc. Natl. Acad. Sci.* 99 (18), 11640–11645. doi: 10.1073/pnas.182427699

Smirnoff, N., and Arnaud, D. (2019). Hydrogen peroxide metabolism and functions in plants. *New Phytol.* 221 (3), 1197–1214. doi: 10.1111/nph.15488

Song, G., Son, S., Lee, K. S., Park, Y. J., Suh, E. J., Lee, S. I., et al. (2022). OsWRKY114 negatively regulates drought tolerance by restricting stomatal closure in rice. *Plants* 11 (15), 1938. doi: 10.3390/plants11151938

Son, S., Im, J. H., Song, G., Nam, S., and Park, S. R. (2022). OsWRKY114 inhibits ABA-induced susceptibility to xanthomonas oryzae pv. oryzae in rice. *Int. J. Mol. Sci.* 23 (15), 8825. doi: 10.3390/ijms23158825

Son, S., and Park, S. R. (2022). Challenges facing CRISPR/Cas9-based genome editing in plants. *Front. Plant Sci.* 13, 902413. doi: 10.3389/fpls.2022.902413

Srinivasan, B., and Gnanamanickam, S. S. (2005). Identification of a new source of resistance in wild rice, oryza rufipogon to bacterial blight of rice caused by Indian strains of xanthomonas oryzae pv. oryzae. *Curr. Sci.* 88 (8), 1229–1231.

Sun, T., Huang, J., Xu, Y., Verma, V., Jing, B., Sun, Y., et al. (2020). Redundant CAMTA transcription factors negatively regulate the biosynthesis of salicylic acid and n-hydroxypipecolic acid by modulating the expression of SARD1 and CBP60g. *Mol. Plant* 13 (1), 144–156. doi: 10.1016/j.molp.2019.10.016

Sun, X., Lapin, D., Feehan, J. M., Stolze, S. C., Kramer, K., Dongus, J. A., et al. (2021). Pathogen effector recognition-dependent association of NRG1 with EDS1 and SAG101 in TNL receptor immunity. *Nat. Commun.* 12 (1), 1–15. doi: 10.1038/s41467-021-23614-x

Tanaka, K., and Heil, M. (2021). Damage-associated molecular patterns (DAMPs) in plant innate immunity: applying the danger model and evolutionary perspectives. *Annu. Rev. Phytopathol.* 59, 53–75. doi: 10.1146/annurev-phyto-082718-100146

Thomma, B. P., Nurnberger, T., and Joosten, M. H. (2011). Of PAMPs and effectors: the blurred PTI-ETI dichotomy. *Plant Cell* 23 (1), 4–15. doi: 10.1105/tpc.110.082602

Timmermann, A., Yun, K. S., Raia, P., Ruan, J., Mondanaro, A., Zeller, E., et al. (2022). Climate effects on archaic human habitats and species successions. *Nature* 604 (7906), 495–501. doi: 10.1038/s41586-022-04600-9

Ton, J., and Mauch-Mani, B. (2004). β-amino-butyric acid-induced resistance against necrotrophic pathogens is based on ABA-dependent priming for callose. *Plant J.* 38 (1), 119–130. doi: 10.1111/j.1365-313X.2004.02028.x

Torres, M. A. (2010). ROS in biotic interactions. *Physiol. Plant.* 138 (4), 414–429. doi: 10.1111/j.1399-3054.2009.01326.x

Tsuda, K., and Katagiri, F. (2010). Comparing signaling mechanisms engaged in pattern-triggered and effector-triggered immunity. *Curr. Opin. Plant Biol.* 13 (4), 459–465. doi: 10.1016/j.pbi.2010.04.006

van Wersch, S., Tian, L., Hoy, R., and Li, X. (2020). Plant NLRs: the whistleblowers of plant immunity. *Plant Commun.* 1 (1), 100016. doi: 10.1016/j.xplc.2019.100016

Vaumourin, E., and Laine, A.-L. (2018). Role of temperature and coinfection in mediating pathogen life-history traits. *Front. Plant Sci.* 9, 1670. doi: 10.3389/fpls.2018.01670

Velasquez, A. C., Castroverde, C. D. M., and He, S. Y. (2018). Plant-pathogen warfare under changing climate conditions. *Curr. Biol.* 28 (10), R619–R634. doi: 10.1016/j.cub.2018.03.054

Velásquez, A. C., Castroverde, C. D. M., and He, S. Y. (2018). Plant–pathogen warfare under changing climate conditions. *Curr. Biol.* 28 (10), R619–R634. doi: 10.1016/j.cub.2018.03.054

Wagner, S., Stuttmann, J., Rietz, S., Guerois, R., Brunstein, E., Bautor, J., et al. (2013). Structural basis for signaling by exclusive EDS1 heteromeric complexes with SAG101 or PAD4 in plant innate immunity. *Cell Host Microbe* 14 (6), 619–630. doi: 10.1016/j.chom.2013.11.006

Wang, Y.-Q., Feechan, A., Yun, B.-W., Shafiei, R., Hofmann, A., Taylor, P., et al. (2009). S-nitrosylation of AtSABP3 antagonizes the expression of plant immunity. *J. Biol. Chem.* 284 (4), 2131–2137. doi: 10.1074/jbc.M806782200

Wang, W., Feng, B., Zhou, J. M., and Tang, D. (2020b). Plant immune signaling: Advancing on two frontiers. *J. Integr. Plant Biol.* 62 (1), 2–24. doi: 10.1111/jipb.12898

Wang, J., Tian, W., Tao, F., Wang, J., Shang, H., Chen, X., et al. (2020a). TaRPM1 positively regulates wheat high-temperature seedling-plant resistance to puccinia striiformis f. sp. tritici. *Front. Plant Sci.* 10, 1679. doi: 10.3389/fpls.2019.01679

Wang, J., Wang, J., Li, J., Shang, H., Chen, X., and Hu, X. (2021). The RLK protein TaCRK10 activates wheat high-temperature seedling-plant resistance to stripe rust through interacting with TaH2A. 1. *Plant J.* 108 (5), 1241–1255. doi: 10.1111/tpj.15513

Waszczak, C., Carmody, M., and Kangasjärvi, J. (2018). Reactive oxygen species in plant signaling. *Annu. Rev. Plant Biol.* 69, 209–236. doi: 10.1146/annurev-arplant-042817-040322

Webb, A. A., and Hetherington, A. M. (1997). Convergence of the abscisic acid, CO_2, and extracellular calcium signal transduction pathways in stomatal guard cells. *Plant Physiol.* 114 (4), 1557–1560. doi: 10.1104/pp.114.4.1557

Wiermer, M., Feys, B. J., and Parker, J. E. (2005). Plant immunity: the EDS1 regulatory node. *Curr. Opin. Plant Biol.* 8 (4), 383–389. doi: 10.1016/j.pbi.2005.05.010

Williams, A., Pétriacq, P., Schwarzenbacher, R. E., Beerling, D. J., and Ton, J. (2018). Mechanisms of glacial-to-future atmospheric CO_2 effects on plant immunity. *New Phytol.* 218 (2), 752–761. doi: 10.1111/nph.15018

Xin, X.-F., Nomura, K., Aung, K., Velásquez, A. C., Yao, J., Boutrot, F., et al. (2016). Bacteria establish an aqueous living space in plants crucial for virulence. *Nature* 539 (7630), 524–529. doi: 10.1038/nature20166

Yang, S., Cai, W., Shen, L., Wu, R., Cao, J., Tang, W., et al. (2022). Solanaceous plants switch to cytokinin-mediated immunity against ralstonia solanacearum under high temperature and high humidity. *Plant Cell Environ.* 45 (2), 459–478. doi: 10.1111/pce.14222

Yang, T., and Poovaiah, B. (2003). Calcium/calmodulin-mediated signal network in plants. *Trends Plant Sci.* 8 (10), 505–512. doi: 10.1016/j.tplants.2003.09.004

Yang, S., Shi, Y., Zou, L., Huang, J., Shen, L., Wang, Y., et al. (2020). Pepper CaMLO6 negatively regulates ralstonia solanacearum resistance and positively regulates high temperature and high humidity responses. *Plant Cell Physiol.* 61 (7), 1223–1238. doi: 10.1093/pcp/pcaa052

Yuan, H.-M., Liu, W.-C., and Lu, Y.-T. (2017). CATALASE2 coordinates SA-mediated repression of both auxin accumulation and JA biosynthesis in plant defenses. *Cell Host Microbe* 21 (2), 143–155. 10.1016/j.chom.2017.01.007

Yuan, P., and Poovaiah, B. (2022). Interplay between Ca2+/Calmodulin-mediated signaling and AtSR1/CAMTA3 during increased temperature resulting in compromised immune response in plants. *Int. J. Mol. Sci.* 23 (4), 2175. doi: 10.3390/ijms23042175

Yuan, P., Tanaka, K., and Poovaiah, B. (2021a). Calcium/Calmodulin-mediated defense signaling: What is looming on the horizon for AtSR1/CAMTA3-mediated signaling in plant immunity. *Front. Plant Sci.* 12, 795353. doi: 10.3389/fpls.2021.795353

Yuan, P., Tanaka, K., and Poovaiah, B. (2021b). Calmodulin-binding transcription activator AtSR1/CAMTA3 fine-tunes plant immune response by transcriptional regulation of the salicylate receptor NPR1. *Plant Cell Environ.* 44 (9), 3140–3154. doi: 10.1111/pce.14123

Zavaliev, R., Mohan, R., Chen, T., and Dong, X. (2020). Formation of NPR1 condensates promotes cell survival during the plant immune response. *Cell* 182 (5), 1093–1108. e1018. doi: 10.1016/j.cell.2020.07.016

Zhang, J., De-oliveira-Ceciliato, P., Takahashi, Y., Schulze, S., Dubeaux, G., Hauser, F., et al. (2018). Insights into the molecular mechanisms of CO_2-mediated regulation of stomatal movements. *Curr. Biol.* 28 (23), R1356–R1363. doi: 10.1016/j.cub.2018.10.015

Zhang, Y., Goritschnig, S., Dong, X., and Li, X. (2003). A gain-of-function mutation in a plant disease resistance gene leads to constitutive activation of downstream signal transduction pathways in suppressor of npr1-1, constitutive 1. *Plant Cell* 15 (11), 2636–2646. doi: 10.1105/tpc.015842

Zhang, Y., and Li, X. (2019). Salicylic acid: biosynthesis, perception, and contributions to plant immunity. *Curr. Opin. Plant Biol.* 50, 29–36. doi: 10.1016/j.pbi.2019.02.004

Zhang, L., Takahashi, Y., Hsu, P.-K., Kollist, H., Merilo, E., Krysan, P. J., et al. (2020). FRET kinase sensor development reveals SnRK2/OST1 activation by ABA but not by MeJA and high CO_2 during stomatal closure. *Elife* 9, e56351. doi: 10.7554/eLife.56351

Zhang, D., Tian, C., Yin, K., Wang, W., and Qiu, J.-L. (2019). Postinvasive bacterial resistance conferred by open stomata in rice. *Mol. Plant-Microbe Interact.* 32 (2), 255–266. doi: 10.1094/MPMI-06-18-0162-R

Zhao, G., Guo, D., Wang, L., Li, H., Wang, C., and Guo, X. (2021). Functions of RPM1-interacting protein 4 in plant immunity. *Planta* 253 (1), 1–11. doi: 10.1007/s00425-020-03527-7

Zhou, Y., Vroegop-Vos, I. A., Van Dijken, A. J., van der Does, D., Zipfel, C., Pieterse, C. M., et al. (2020). Carbonic anhydrases CA1 and CA4 function in atmospheric CO_2-modulated disease resistance. *Planta* 251 (4), 75. doi: 10.1007/s00425-020-03370-w

frontiers | Frontiers in Plant Science

TYPE Original Research
PUBLISHED 11 January 2023
DOI 10.3389/fpls.2022.1054821

OPEN ACCESS

EDITED BY
Ravi Gupta,
Kookmin University, South Korea

REVIEWED BY
Peiguo Yuan,
Texas A&M University, United States
Ganesh Chandrakant Nikalje,
R. K. Talreja College of Arts, Science and Commerce, India

*CORRESPONDENCE
Amarjeet Singh
amarjeet.singh@nipgr.ac.in

SPECIALTY SECTION
This article was submitted to Crop and Product Physiology, a section of the journal Frontiers in Plant Science

RECEIVED 27 September 2022
ACCEPTED 05 December 2022
PUBLISHED 11 January 2023

CITATION
Ankit A, Singh A, Kumar S and Singh A (2023) Morphophysiological and transcriptome analysis reveal that reprogramming of metabolism, phytohormones and root development pathways governs the potassium (K^+) deficiency response in two contrasting chickpea cultivars. *Front. Plant Sci.* 13:1054821. doi: 10.3389/fpls.2022.1054821

Morphophysiological and transcriptome analysis reveal that reprogramming of metabolism, phytohormones and root development pathways governs the potassium (K^+) deficiency response in two contrasting chickpea cultivars

Ankit Ankit, Ajeet Singh, Shailesh Kumar and Amarjeet Singh*

National Institute of Plant Genome Research, New Delhi, India

Potassium (K^+) is an essential macronutrient for plant growth and development. K^+ deficiency hampers important plant processes, such as enzyme activation, protein synthesis, photosynthesis and stomata movement. Molecular mechanism of K^+ deficiency tolerance has been partly understood in model plants Arabidopsis, but its knowledge in legume crop chickpea is missing. Here, morphophysiological analysis revealed that among five high yielding desi chickpea cultivars, PUSA362 shows stunted plant growth, reduced primary root growth and low K^+ content under K^+ deficiency. In contrast, PUSA372 had negligible effect on these parameters suggesting that PUSA362 is K^+ deficiency sensitive and PUSA372 is a K^+ deficiency tolerant chickpea cultivar. RNA-seq based transcriptome analysis under K^+ deficiency revealed a total of 820 differential expressed genes (DEG's) in PUSA362 and 682 DEGs in PUSA372. These DEGs belongs to different functional categories, such as plant metabolism, signal transduction components, transcription factors, ion/nutrient transporters, phytohormone biosynthesis and signalling, and root growth and development. RNA-seq expression of randomly selected 16 DEGs was validated by RT-qPCR. Out of 16 genes, 13 showed expression pattern similar to RNA-seq expression, that verified the RNA-seq expression data. Total 258 and 159 genes were exclusively up-regulated, and 386 and 347 genes were down-regulated, respectively in PUSA362 and PUSA372. 14 DEGs showed contrasting expression pattern as they were up-regulated in PUSA362 and down-regulated in PUSA372. These include somatic embryogenesis receptor-like kinase 1, thaumatin-like protein, ferric reduction oxidase 2 and transcription factor bHLH93. Nine genes which were down-regulated in PUSA362 found to be up-regulated in PUSA372, including glutathione S-transferase like, putative calmodulin-like 19, high affinity nitrate transporter

2.4 and ERF17-like protein. Some important carbohydrate metabolism related genes, like fructose-1,6-bisphosphatase and sucrose synthase, and root growth related Expansin gene were exclusively down-regulated, while an ethylene biosynthesis gene 1-aminocyclopropane-1-carboxylate oxidase 1 (ACO1) was up-regulated in PUSA362. Interplay of these and several other genes related to hormones (auxin, cytokinin, GA etc.), signal transduction components (like CBLs and CIPKs), ion transporters and transcription factors might underlie the contrasting response of two chickpea cultivars to K^+ deficiency. In future, some of these key genes will be utilized in genetic engineering and breeding programs for developing chickpea cultivars with improved K^+ use efficiency (KUE) and K^+ deficiency tolerance traits.

KEYWORDS

potassium, deficiency, chickpea, morphophysiology, transcriptome

1 Introduction

Among different nutrients required for optimum plant growth and development, potassium (K^+) is an essential macronutrient. K^+ is crucial for various plant physiological processes, including enzyme activation, photosynthesis, protein synthesis, stomata movement, carbon metabolism and starch synthesis (Maathuis, 2009; Wang and Wu, 2013; Luan et al., 2017). In addition, K^+ plays an important role in maintaining turgor pressure and water homeostasis through K^+ movement and vacuolar storage in plants (Maathuis, 2009). K^+ status is also important for plants response to various abiotic and biotic stresses (Shabala and Pottosin, 2014; Nieves-Cordones et al., 2019; Deepika et al., 2022). Despite being the seventh most abundant element in earth crust, K^+ availability for plants is very limited. Approximately, 98% of soil K^+ exits in an unavailable state, such as primary (micas and feldspars) and secondary clay minerals, which cannot be absorbed and utilized by plants. Only 0.1-0.2% K^+ exists as water soluble form that can be absorbed by plants through roots (Hafsi et al., 2014). Such low availability of K^+ results in K^+ deficiency which leads to several physiological and developmental changes in plants, such as change in root system architecture (RSA), chlorosis which further leads to necrosis at the tip and margins of older leaves, and overall hampered growth and yield (de Bang et al., 2021). In addition, Ribulose bisphosphate carboxylase activity is reduces, and photosynthesis process and stomatal conductance are hampered (de Bang et al., 2021). Globally, most arable field soils are K^+ deficient for instance, about 75% of the paddy soils in China and 65% wheat fields in Southern Australia (Romheld and Kirby, 2010). In India, around 72% of the cultivated land soil is K^+ deficient and requires immediate supply of K^+ fertilizers to increase crop yield (Yadav and Sidhu, 2016). Unfortunately, due to low-K^+ use efficiency, crop plants utilize only about 50% of applied K^+ fertilizer (Britto and Kronzucker, 2008). Most of the unutilized fertilizer accumulate in the soil and a portion of it leaches down into the water bodies which adds to soil and water pollution, and also contributes in eutrophication (Nasr Esfahani et al., 2021). Collectively, high cost of K^+ fertilizers and their bad impact on environment and human health urge for developing crop plants with high K^+ uptake (KUpE) and use efficiency (KUE).

Chickpea (*Cicer arietinum* L.) is one of the most important legume crops known for its high nutritional value (Sagar et al., 2021). It is a self-pollinated diploid (2n = 2x = 16) cool seasoned annual pulse crop with a 738 Mb genome (Varshney et al., 2013). Among pulses, chickpea ranks third with the global production of around ~11.6 million tons *per annum*, out of which 80% is desi chickpea and 20% is Kabuli (Merga and Haji, 2019). Chickpea grain is very popular around the globe as nutrient rich seeds containing carbohydrates (50–58%), protein (15–22%), moisture (7–8%), fat (3.8–10.20%), micronutrients (<1%), amino acids like lysine and arginine, and a range of isoflavones (Jukanti et al., 2012). Importantly, India alone contributes about 70% of world's chickpea production (FAOSTAT, 2016). However, as mentioned earlier, a major proportion of soil in Indian cultivated land is deficient in K^+. Growing chickpea in K^+ deficient soil will negatively affect plant growth and development. In addition, K^+ deficiency in soil will make the plants prone to biotic and abiotic stresses (Shi et al., 2018; Nieves-Cordones et al., 2019). Collectively, these adverse effects of K^+ deficiency may severely hamper chickpea production and worldwide chickpea supply. Unfortunately, the knowledge of molecular mechanism of K^+ deficiency tolerance and K^+ uptake and homeostasis related genes in chickpea is missing. To develop improved chickpea cultivars with better KUE and K^+ deficiency tolerance, it is important to identify key K^+ uptake and homeostasis related genes. Thus, we decided to

undertake this study to understand molecular mechanism of K^+ deficiency tolerance in chickpea. The major objectives of this study are first, to analyse the response of different chickpea cultivars to K^+ deficiency and discover K^+ deficiency sensitive and tolerant cultivars. Second, to identify the key K^+ deficiency responsive genes and signaling pathways in contrasting chickpea cultivars to comprehend the molecular mechanism of K^+ deficiency response and tolerance in chickpea.

Here, we performed the morphophysiological analysis of five high yielding desi chickpea cultivars (PUSA256, PUSA362, PUSA372, ICC1882 and ICC4958) under K^+ sufficient and deficient conditions. Based on their response to K^+ deficiency, PUSA362 was identified as K^+ deficiency sensitive and PUSA372 as K^+ deficiency tolerant cultivar. To understand the molecular basis of their contrasting response to K^+ deficiency, RNA-Seq based comparative transcriptome analysis was performed in these two chickpea cultivars. K^+ deficiency responsive DEGs were identified and categorized into different functional categories based on annotations. RNA-Seq expression data was validated for few selected genes using RT-qPCR analysis. KEGG pathway analysis was performed to identify different signaling pathways affected due to K^+ deficiency in both the cultivars. Overall, this study will help to comprehend the molecular mechanism of K^+ deficiency tolerance in important legume crop chickpea.

2 Materials and methods

2.1 Plant material and growth conditions

Seeds of desi chickpea (PUSA256, PUSA362, PUSA372, ICC1882 and ICC4958) were surface sterilized and grown as described by Deepika et al. (2022). Briefly, seeds were dipped in 70% ethanol for a minute followed by two times stringent wash with sterile water. This was followed by washing with 2% sodium hypochlorite solution containing two drops of tween-20 for 15 min. Seeds were further washed many times with sterile water and left overnight in sterile water. Seeds were then kept for germination on wet Whatmann filter for 2 days in dark. Uniformly germinated seeds were transferred to 1/4th strength Hoagland media containing macronutrients- $NH_4H_2PO_4$ (250µM), KNO_3 (1.5 mM), $Ca(NO_3)_2.4H_2O$ (1mM), $MgSO_4.7H_2O$ (0.5 mM), micronutrients- H_3BO_3 (10.6 µM), $ZnSO_4.7H_2O$ (0.19 µM), $CuSO_4.5H_2O$ (0.08 µM), $H_2MoO_4{\cdot}H_2O$ (0.03 µM), $MnCl_2.4H_2O$ (2.29 µM) and Na-Fe-EDTA (3.41 µM), at pH 5.5. For K^+ deficiency, germinated seeds were transferred to media with 10 µM K^+ (KNO_3) and for K^+ sufficiency, 1.5 mM K^+ (KNO_3) and grown for ten-days. Growth media (with sufficient K^+ and deficient K^+) was replenished after every two days. Growth conditions were maintained at 12/12 h photoperiod, temperature- 23°C/18°C, 200–300 µM photons/m^2/s photon density and ~70% relative humidity. Morphological data from three replicates were captured where each replicates represent ten uniformly grown seedlings. Growth parameters, such as primary root length and shoot length were also measured from these seedlings. Based on morphological analysis, two chickpea cultivars (PUSA362 and PUSA372) were selected for further experiments.

2.2 K^+ content measurement using ICP/MS

Uniformly germinated seeds of chickpea (PUSA362 and PUSA372) were grown for seven-days in 1/4th Hoagland media. Then, half of the seedlings were transfer to K^+ sufficient (1.5 mM) and half to K^+ deficient (10µM) media. Samples (root and shoot separately) of both chickpea varieties were collected after ten-days of growth. Each sample was lyophilized and powdered, and 50mg powdered sample was dissolve in 8ml concentrated nitric acid (HNO_3) in a separate digestion tube. The samples were digested in an oven at 180°C for 35 min followed by cooling. After this, volume of each sample was made up to 50ml with sterile water. The samples were then diluted in 1:9 ratio (v/v) using 2% HNO_3. Ion content analysis in each sample was performed in ICP-MS machine (Agilent 7800). Three biological replicates for each root and shoot sample were used for the measurement of K^+ content.

2.3 RNA isolation and processing

Ten- days old chickpea seedlings grown in K^+-sufficient and K^+-deficient conditions were harvested and immediately frozen in liquid nitrogen, and stored at -80°C till RNA isolation. Total RNA was extracted from three biological replicates of each sample according to Sagar et al. (2020). RNA samples were treated with DNaseI (Thermo-Scientific) to remove any genomic DNA contamination, and samples were further purified using RNeasy MinElute Clean-up Kit (QIAGEN). Quantification of RNA samples was done using nano-spectrophotometer (Nano Drop ONE^c -Thermo Scientific) and RNA integrity was checked by loading the RNA samples on 1.2% denaturing gel in 1X MOPS buffer. RNA quality was further ensured using an Agilent 2100 RNA Bioanalyzer (Agilent, USA) and samples with RNA integrity number (RIN) > 8 were used for RNA-Seq analysis.

2.4 Library preparation for RNA-Seq and data pre-processing

The library was prepared for RNA-seq experiment using the NEB Next Ultra II RNA Library Prep Kit (NEB, Massachusetts, USA) using manufacturer instructions. Three biological replicates of each sample (K^+ sufficient and K^+ deficient) were used for RNA-seq analysis. The prepared library was quantified using Qubit 3.0 fluorometer (Thermofisher Scientific,

Massachusetts, USA) using DNA HS assay kit (Thermofisher Scientific, Massachusetts, USA). The insert size of the library was assessed using 4200 TapeStation (Agilent Technologies, CA, USA). Prepared RNA library was sequenced in Illumina Novaseq 6000 at Nucleome Informatics, Hyderabad, India. The raw RNA-seq reads in FASTQ format from all samples were subjected to quality filtering by using fastp v0.21.0 for the removal of low-quality reads (Phred score < 15; N base limit > 5) and reads with adapter contamination. The RNA-seq data has been submitted in NCBI with accession No.- PRJNA883591.

2.5 Differential gene expression analysis and functional annotation

The filtered RNA-seq data were analyzed using the new Tuxedo, an open-source pipeline (Pertea et al., 2016). The chickpea genome index was built by 'hisat2-build' utility of Hisat2 (v2.2.1) (Kim et al., 2019) by using chickpea genome (ASM33114v1), and splice and exon sites were extracted from genome annotation file. The filtered reads from all the samples were aligned to the indexes by using Hisat2 at default parameters. Further, the Stringtie (v2.1.5) software package (Pertea et al., 2015) was used for the transcriptome assembly, and quantification of expressed genes and transcripts. For each sample, the transcripts and their isoforms were assembled in separate GTF format files by using sorted BAM file as input. The transcript structures in all samples of each chickpea cultivars (PUSA362, and PUSA372) were merged by using StringTie. The merged GTF file for each sample was used for the re-estimation of transcript abundance. Gene count matrix was designed by a package Isoform Switch Analyze R (v1.18.0) (Vitting-Seerup and Sandelin, 2019) by using transcript sequences and counts data for each sample. The differential gene expression analysis was performed by using DESeq2 (v1.30.1), which normalizes libraries based on the geometric mean of the read counts, and then calculates the log2-fold change between defined conditions of samples. Differentially expressed genes (DEGs) with a $\log_2$-fold change ±1 with p-value < 0.05 were considered significant. For functional annotation of genes, the nucleotide sequence was used as input in the functional annotation pipeline of Blast2Go software package, performing the blast, mapping, and annotation of query sequences on various selected databases.

2.6 KEGG pathway analysis

Kyoto Encyclopedia of Genes and Genomes (KEGG) pathways were identified for DEGs having significant p-values. KEGG Mapper – Convert ID tool (https://www.genome.jp/kegg/mapper/convert_id.html) was used to convert NCBI gene ID (accession numbers) of each DEG to KEGG identifiers (cam ID). These KEGG identifiers were mapped to the known pathways using KEGG Mapper search tool (https://www.genome.jp/kegg/mapper/search.html). The search mode was selected as "cam", which is the KEGG organism code for *Cicer arietinum*.

2.7 RT- qPCR analysis

To validate the RNA-seq expression data, RT-qPCR analysis was performed for few selected genes. RNA samples used for RNA-seq (K^+ sufficient and K^+ deficient conditions) were also used for cDNA synthesis to perform RT-qPCR. 1µg RNA was used in a 20µl reaction for the preparation of single-strand cDNA using iScript™ cDNA Synthesis Kit (Bio-Rad) as per the manufacturer's instructions. Primers for selected DEGs were design in PRIMER EXPRESS software (PE Applied Biosystems, USA). Details of all primers are given in Table S1. The specificity of primers was confirmed by BLAST tool on NCBI and through dissociation curve analyses post RT-qPCR, as per protocol given in Singh and Pandey (2015). The expression of DEGs was detected using iTaq Universal SYBR Green super mix (Bio-Rad) according to the manufacturer's protocol in Bio-rad CFX96 Real-time PCR machine (Bio-Rad). Three biological replicates of each sample, and three technical replicates for each biological replicate were used for expression analysis. *EF1α* gene was used as endogenous control for normalization of variance among samples. Expression data was analyzed through ΔΔCt method and the average fold change was plotted on the bar graphs with the standard error.

2.8 Statistical analysis

For statistical significance of the data, all experiments including morphophysiological, expression and quantitative analysis were performed in triplicates. Mean of the morphological observations, K^+ content and expression values ± S.D (standard deviation) are represented in graphs. A two tailed student's t-test was performed for statistical significance among three replicates. The data were considered statistically significant when p-value <0.05 (denoted by *), p-value <0.01 (denoted by **) and p-value <0.005 (denoted by ***). In transcriptome analysis, DESeq2 (v1.30.1) R package was used to normalizes libraries based on the geometric mean of the read counts. DEGs with Log_2-fold changes of ±1 and p-value < 0.05 were considered statistically significant.

3 Results & discussion

3.1 Morphophysiological analysis of chickpea cultivars under K^+ deficiency

The genetically diverse germplasm is essential for breeding and development of new cultivars with desirable traits such as

KUE and K^+ deficiency tolerance. Identification of genotypes with K^+ deficiency tolerant traits has provided the suitable donor parents in several crop species (Tian et al., 2008; Wu et al., 2011). In this study, we performed the morphological analysis to evaluate and compare the effect of K^+ deficiency on five high yielding improved desi chickpea cultivars (PUSA256, PUSA362, PUSA372, ICC1882 and ICC4958). The visible symptoms of long-term K^+ deficiency include chlorosis at the tip of oldest leaves which turns into marginal necrosis (Marschner, 1995). However, mild or short duration K^+ deficiency in crop plants does not leads to visible symptoms immediately, possibly due to the significant redistribution of nutrients between mature and young developing tissues. Initially, only a reduction in growth rate is observed and, later chlorosis and necrosis begin to appear in mature leaves (Mengel et al., 2001). Accordingly, numerous studies have analyzed the root growth pattern as an effect of K^+ deficiency. It has been shown that K^+ deficiency leads to shortened primary and lateral root length along with reduction in overall growth in plants, such as Arabidopsis, rice, foxtail millet, sweet potato, pears (*pyrus betulaefolia*) and tomato (Singh et al., 2018; Zhao et al., 2018; Cao et al., 2019; Ragel et al., 2019; Yang et al., 2020). Thus, here we suitably analyze the symptoms of early K^+ deficiency i.e., change in plant growth rate, especially root and shoot growth. Out of five cultivars, PUSA362 seedlings were found to have shortest primary and lateral root length, reduced root hair numbers and stunted plant growth under K^+ deficiency when compared to sufficient K^+ condition (Figure 1A). The average height of PUSA362 plants in K^+ sufficient conditions was about 28.5cm whereas, it was approx. 17.6cm in K^+ deficient conditions. The average primary root length of PUSA362 was 15.5 cm in K^+ sufficient conditions whereas, under K^+ deficiency the average root length was found to be 8.8 cm (Figure 1B and Table S2). Similarly, the average shoot length was 13.0 cm in K^+ sufficient conditions whereas, it was only 8.5 cm under K^+ deficiency (Figure 1C). Among all the chickpea cultivars, K^+ deficiency had the negligible effect on PUSA372 as it showed no major changes in root and shoot growth under K^+ deficient and sufficient conditions. Its average primary root length was 11.53 cm and 11.9 cm, respectively under K^+ sufficiency and deficiency (Figure 1B), and shoot length was 12.0 cm and 11.7 cm under K^+ sufficiency and deficiency (Figure 1C). Further, ICP/MS analysis for K^+ content measurement in root and shoot of both cultivars provides insights into the K^+ translocation and storage status of chickpea plants under K^+ deficiency. Under sufficient K^+ conditions, the K^+ content in the root of PUSA362 was 35mg/g of dry weight, while under K^+ deficiency it was found to be 7.8mg/g (Figure 2). It infers that there is about 78% lesser K^+ content in roots of PUSA362 under K^+ deficiency. On the other hand, the K^+

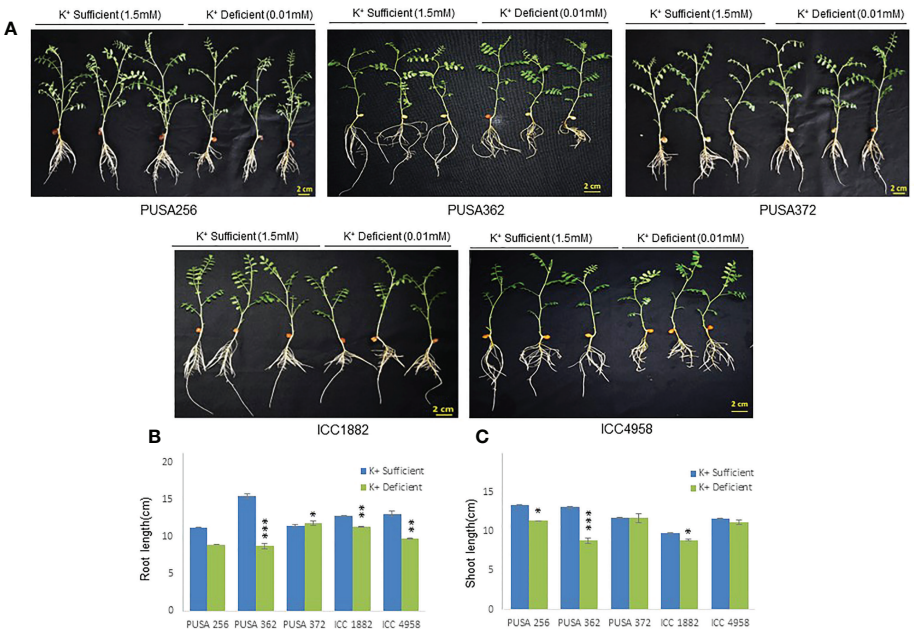

FIGURE 1
Phenotype analysis of five high yielding desi chickpea cultivars under K^+ deficiency. **(A)** Germinated seeds of desi chickpea (PUSA256, PUSA362, PUSA372, ICC1882 and ICC4958) were transferred to growth media with K^+ sufficient (1.5mM K^+) and K^+ deficient (0.01mM K^+) conditions for ten days. Phenotype was recorded after ten days of growth. **(B)** Root and **(C)** Shoot length of five chickpea cultivars under K^+ sufficient and K^+ deficient growth conditions. X-axis shows the name of chickpea cultivar and Y-axis shows the root/shoot length (cm). Each analysis was repeated three times with 10 seedlings in each sample. Asterisk (*) indicates the p-value < 0.05, and (**) p-value < 0.01 and (***) p-value < 0.005 calculated using student t-test to determine statistical significance among samples.

content in the root of PUSA372 under K^+ sufficient and K^+ deficient conditions was 27.9mg/g and 13.9 mg/g, respectively, indicating 50% lesser K^+ under K^+ deficiency. Therefore, reduction in root K^+ content was more significant in PUSA362 than in PUSA372. This indicates that PUSA362 cultivar is less efficient in K^+ uptake and storage in the root. In contrast, PUSA372 could uptake and store higher amount of K^+ in the roots. Interestingly, shoot in both the cultivars had similar K^+ content under both, K^+ sufficient (~20mg/g of dry weight) and deficient conditions (~10mg/g of dry weight). It is observed that under K deficiency, alongwith shortened root length, the root endodermis becomes suberized. The suberization process is triggered by ABA (Barberon et al., 2016) and it interferes in K^+ translocation (Chen et al., 2019). This possibly accounts for the significantly reduced K^+ content in root and shoot of PUSA362 under K^+ deficiency. Also, K^+ has a stimulatory effect on the plasma membrane located ATPase in the sieve tube. The proton pumping ATPase generates a transmembrane potential gradient and pH gradient between the lumen of the sieve tube. This gradient effectively drives the transport of sucrose from the apoplasm into the sieve tubes. Thus, K^+ plays an important role in phloem loading and phloem transport (Marschner, 1995; Römheld and Kirkby, 2010). The phloem sap which is transported from the mature leaf (source) to sink sites (roots) contains K^+ along-with Mg^{2+}, amino acids and sucrose as its major constituents (Jeschke et al., 1997). Sufficient amount of K^+ in the leaves is thus, crucial for supplying sucrose to the roots for investing in energy expenditure for root growth and development (Cakmak et al., 1994; Omondi et al., 2020). In this study, relatively low shoot K^+ content in PUSA362 may have hampered the phloem transport and sucrose supply to the roots and resulting in reduced root growth. Overall, the morphophysiological analysis concluded that PUSA362 is a K^+ deficiency sensitive chickpea cultivar while, PUSA372 is K^+ deficiency tolerant. Due to their contrasting response to K^+ deficiency, these two chickpea cultivars were selected for global transcriptome analysis to understand molecular mechanism of K^+ deficiency response in chickpea.

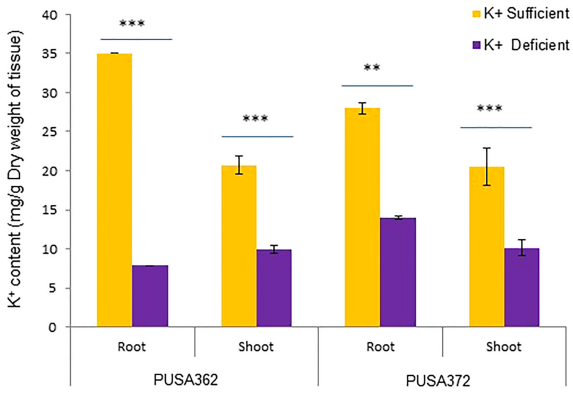

FIGURE 2
Total K^+ content in PUSA362 and PUSA372 determined using ICP-MS analysis. Graphs showing the measurement and comparison of the K^+ ion content of root and shoot samples in desi chickpea cultivars, PUSA362 and PUSA372 in response to control (1.5mM K^+) and K^+ deficient (0.01mM K^+) condition. Each bar depicts the average of K^+ content from three biological replicates of each sample. Standard error shown on bars was calculated from the standard deviation among the biological replicates. Asterisk (**) indicates the p-value < 0.01, and (***) p-value < 0.005 calculated using student t-test to determine statistical significance among sample.

3.2 RNA-seq analysis reveals K^+ deficiency related transcriptome in chickpea cultivars

Global transcriptome analysis is one of the popular methods to identify the key genes associated with a specific trait. Transcriptome analysis assists in identifying differentially expressed genes (DEGs) and provides an insight into altered cellular processes, signaling pathways and networks. Previously, RNA-seq and microarray-based transcriptome analyses have helped to understand the K^+ deficiency response in plant species, such as *Arabidopsis thaliana* (Armengaud et al., 2004), rice (Shankar et al., 2013; Zhang et al., 2017), wheat (Zhao et al., 2020), tomato (Zhao et al., 2018), cotton (Yang et al., 2021), pear (Shen et al., 2017; Yang et al., 2020), foxtail millet (*Setaria italica* L.) (Cao et al., 2019) and sweet potato (*Ipomoea batatas*) (Wang et al., 2022). However, no transcriptome base study has been undertaken so far to understand the molecular mechanism of K^+ deficiency tolerance in chickpea. Therefore, to investigate the K^+ deficiency responsive transcriptome in PUSA362 and PUSA372 cultivars, RNA-seq analysis was performed under K^+ sufficient and deficient conditions. About 303 and 307 million raw reads were generated from six samples (three K^+ sufficient, three K^+ deficient) of PUSA362 and PUSA372, respectively. Out of these, 299 and 303 million clean reads were obtained in PUSA362 and PUSA372. The Q30 values of ~ 94% for both cultivars indicated that the quality of sequencing data was good and significant. The average alignment rate for PUSA362 and PUSA372 were 91.14% and 87.56% respectively (Table 1). The analysis and identification of DEGs was performed using DESeq2 v1.30.1 package. To account for the handling errors and variations among the samples, DEGs with Log_2 fold change ±1 and a p-value of < 0.05 were considered significant. We found a total of 820 significantly expressed DEGs in PUSA362, out of which 311 genes were up-regulated and 509 were down-regulated (Figure 3 and Table S3). In PUSA372, out of a total of 682 DEGs, 207 genes were up-regulated and 475 genes were down-regulated. Most of the DEGs from both chickpea cultivars could be assigned an NCBI locus ID and annotated with a known function. For some of the DEGs, NCBI locus ID and/or known functional annotations were not available thus, they were classified as DEGs with unknown

TABLE 1 Summary of sequence assembly data analysis after RNA sequencing.

Sample name	Raw reads	Clean reads	Clean bases	Average coverage (%)	Q20 (%)	Q30 (%)	Alignment rate
PUSA362, KS1	43.791554 M	43.370770 M	6.407773 G	44.3633	97.958291	93.736127	89.34%
PUSA362, KS2	46.498322 M	46.013488 M	6.790540 G	41.4191	98.04188	93.952486	85.64%
PUSA362, KS3	65.731198 M	64.992878 M	9.630451 G	56.935	97.932701	93.660516	89.73%
PUSA362, KD1	57.020970 M	56.359848 M	8.335876 G	57.3107	98.070383	94.103813	93.71%
PUSA362, KD2	44.067446 M	43.570722 M	6.455914 G	46.3386	97.908821	93.617395	93.92%
PUSA362, KD3	45.901854 M	45.364060 M	6.697309 G	46.3855	98.184631	94.367596	94.50%
PUSA372, KS1	46.969232 M	46.360326 M	6.789864 G	40.7649	98.08786	94.228344	82.12%
PUSA372, KS2	54.918072 M	54.367048 M	8.025501 G	55.1703	97.843193	93.46048	93.13%
PUSA372, KS3	46.477222 M	45.713680 M	6.682883 G	39.0247	97.777873	93.608092	90.77%
PUSA372, KD1	48.760200 M	48.237750 M	7.112087 G	46.453	98.081043	94.010408	89.37%
PUSA372, KD2	47.119356 M	46.651980 M	6.920498 G	46.8844	97.921428	93.656282	89.38%
PUSA372, KD3	63.383762 M	62.484308 M	9.173471 G	53.1041	97.942865	93.778872	80.57%

KS – K^+ sufficient, KD – K^+ deficient.

function. These DEGs are denoted by gene name starting with "MSTRG" (Table S3). A global view of all DEG's in both varieties is presented through a volcano plot (Figure 4A). Notably, a significant number of DEGs was found to have overlapping, opposite and unique expression in both the chickpea cultivars. 258 and 159 genes were exclusively up-regulated, respectively in PUSA362 and PUSA372. While 386 and 347 unique genes were exclusively down-regulated in PUSA362 and PUSA372, respectively (Figure 4B). Interestingly, 14 genes showed contrasting expression pattern, as they were up-regulated in PUSA362 and down-regulated in PUSA372. These DEGs include somatic embryogenesis receptor-like kinase 1 (LOC113785888), thaumatin-like protein (LOC101511048), ferric reduction oxidase 2 (LOC101499003) and transcription factor bHLH93 (LOC101489960). On the other hand, 9 genes which showed down-regulation in PUSA362 were up-regulated in PUSA372, and these include glutathione S-transferase zeta class-like (LOC113784455), putative calcium-binding protein CML19 (LOC101492172), high affinity nitrate transporter 2.4 (LOC101503875) and ethylene-responsive transcription factor

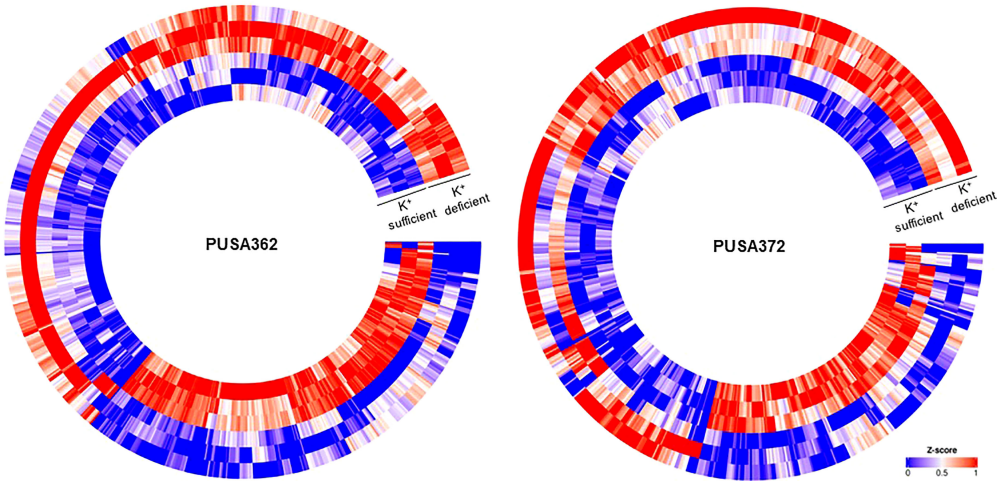

FIGURE 3
Heat map depicting complete set of DEGs of PUSA362 and PUSA372 under K^+ deficiency. Each heat-map is specific for chickpea cultivars PUSA362 and PUSA372. Three circles each of K^+ sufficient and K^+ deficient conditions represent three replicate biological samples of these conditions. Heat-map is scaled with Z-score (0-1) indicating the expression of genes across the samples.

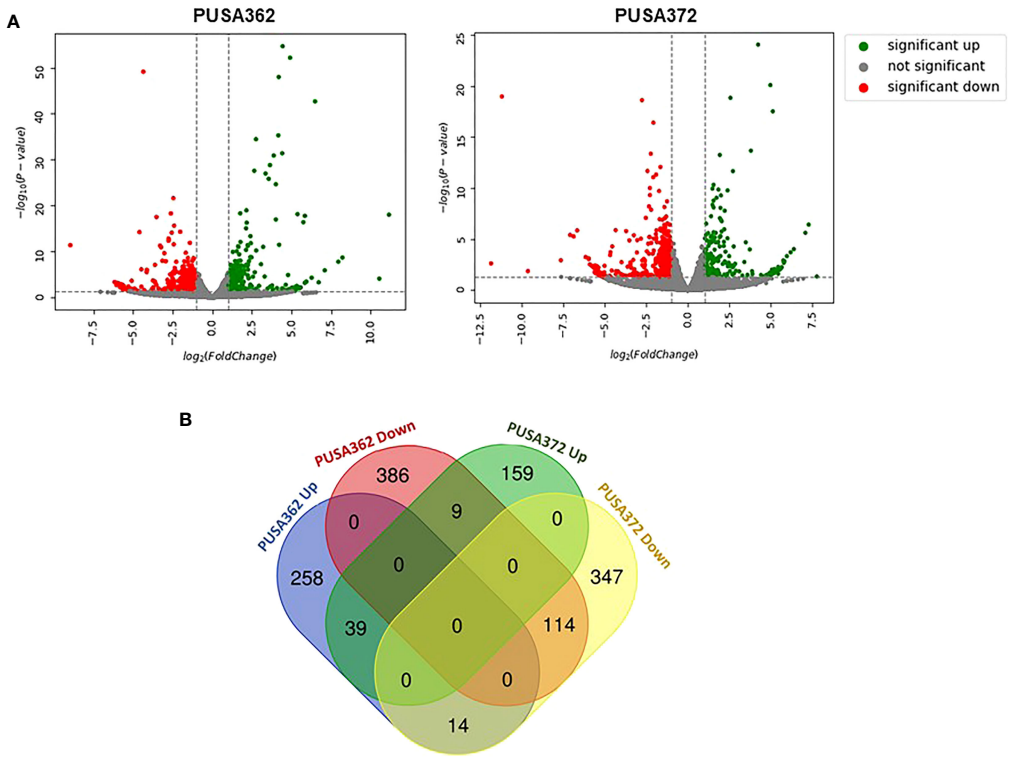

FIGURE 4
Summary of specific and overlapping expression pattern of DEGs in PUSA362 and PUSA372. **(A)** Volcano plots provides the summary of expression regulation of DEGs in PUSA362 and PUSA372 in response to K^+ deficient condition. Green dots represent significantly up-regulated DEGs, red dots represent significantly down-regulated DEGs and grey dots refers to all genes which are not significantly expressed. X-axis shows the log_2fold change of gene expression and Y-axis indicates the statistical significance in terms of -log_{10}(P-value). **(B)** Venn diagram showing the number of unique as well as commonly up-regulated and down-regulated DEGs in PUSA362 and PUSA372 variety in response to K^+ deficient condition. Mentioned numbers in each block indicates the total DEGs in corresponding group.

ERF017-like protein (LOC101496587). OA, OB, OC and OD identifiers were used for putative novel genes present in both varieties (Table S4). Thus, it is evident from transcriptome analysis that K^+ deficiency triggered the transcriptional reprogramming in different chickpea cultivars (PUSA362 and PUSA372). Interestingly, more numbers of DEGs were down-regulated than up-regulated in both the chickpea cultivars. This indicates that during short-term K^+ deficiency chickpea plants might need repression of different cellular processes, like those involved in energy expenditure and metabolism, to support the plant growth. Thus, DEGs involved in key signaling networks in each chickpea cultivars could be responsible for their contrasting morphophysiological response to K^+ deficiency.

3.3 Validation of RNA-seq expression data by RT-qPCR

To ensure the accuracy of RNA-seq data, the expression pattern of 16 randomly selected genes was verified by RT-qPCR. Out of 16 selected DEGs, 13 showed similar expression pattern by both RNA-seq and RT-qPCR methods in PUSA362 variety (Figure 5 and Table S5). These included genes like ferric reduction oxidase 2 (LOC101499003), high affinity nitrate transporter 2.4 (LOC101503875), probable inorganic phosphate transporter 1-3 (LOC101497071), putative hypoxia induced protein (LOC101488764), 1-aminocyclopropane-1-carboxylate oxidase 1 (LOC101505638) and wound-responsive family protein (LOC101510089). Similarly, in PUSA 372, 13 DEG's showed similar expression pattern by both, RNA-seq and RT-qPCR analysis. These genes included ferric reduction oxidase 2 (LOC101499003), high affinity nitrate transporter 2.4 (LOC101503875), probable inorganic phosphate transporter 1-3 (LOC101497071), peroxidase 16 (LOC101513640) and putative 12-oxophytodienoate reductase 11 (LOC101491096). In PUSA372 genes like indole-3-acetic acid-induced protein ARG7 (LOC101508549) and phosphatase 2C-like protein 44 isoform X1 (LOC101503050) showed no significant expression by RNA-seq whereas, they were found to be down-regulated by -0.1 and -0.17 Log_2fold when their expression was analyzed using RT-qPCR. Similar expression pattern of significant proportion of tested genes by both the techniques in both chickpea

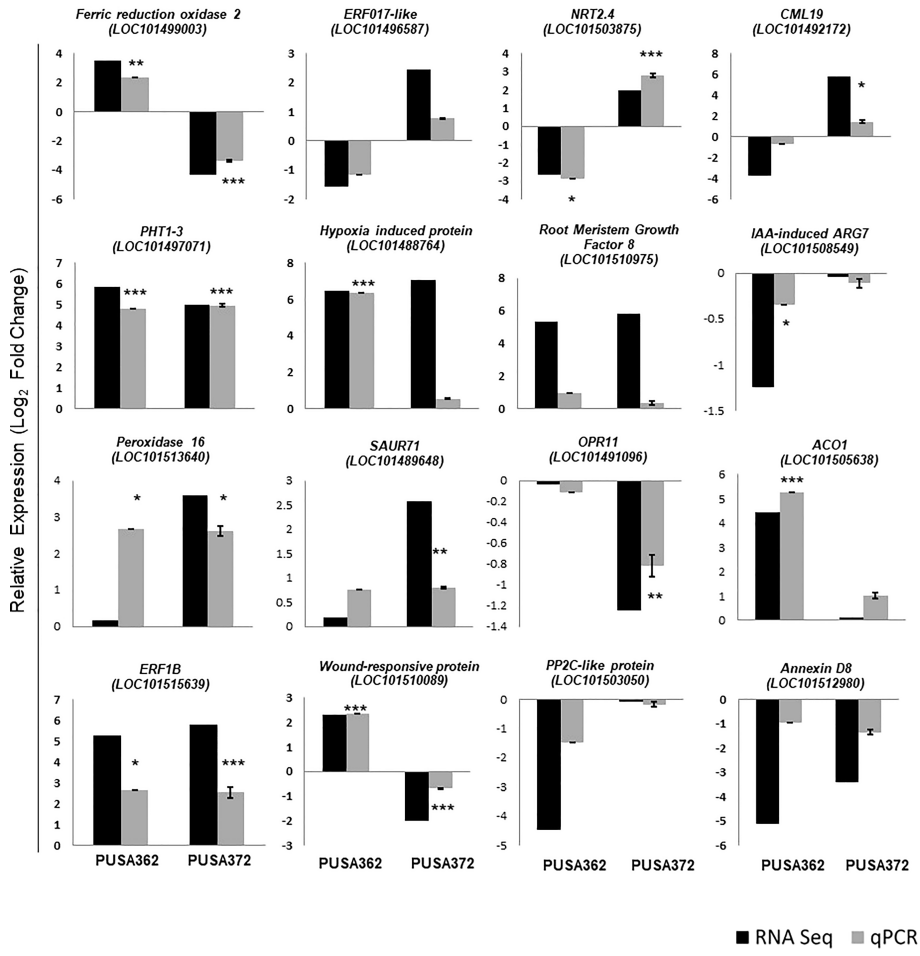

FIGURE 5
Validation of RNA-seq expression data using RT-qPCR analysis. 16 DEGs were randomly selected and their RNA-seq expression pattern was validated by RT-qPCR both in PUSA362 and PUSA372 cultivars. Each bar represents average of expression data from three biological replicates. X-axis shows the name of chickpea cultivar and Y-axis represents the relative expression in terms of log_2 fold change. Name of the genes with locus IDs are given on top of the graphs. Standard error was calculated from standard deviation among three biological replicates and is shown on each bar. Asterisks indicates the statistical significance among replicate samples with p-value as *p < 0.05, **p < 0.01 and ***p < 0.005.

cultivars make this RNA-seq expression data reliable and significant, and it confirms the differential regulation of chickpea genes under K^+ deficiency conditions. Thus, RT-qPCR expression analysis largely verified the expression pattern obtained from RNA-seq analysis in both the chickpea cultivars.

3.4 Gene ontology-based classification of DEGs

Gene Ontology (GO) enrichment analysis was performed to understand the functional relevance of K^+ deficiency responsive DEGs in chickpea. GO analysis differentiated DEGs based on their molecular functions, cellular component and biological process. Within these three main categories, a total of 24 sub-categories were identified in PUSA362, and 23 sub-categories in PUSA372 (Figure 6). DEGs in molecular functions category could be classified into 10 sub-categories in PUSA362 and into 9 sub-categories in PUSA372. Surprisingly, DEGs with molecular function of catalytic activity or acting on a protein were absent in PUSA372. Other major categories in molecular functions included, organic and heterocyclic compound binding, ion binding, transferase activity, oxidoreductase activity, hydrolase activity and transcription factor (TF) activity. Highest number of DEGs belong to heterocyclic compound binding, organic compound binding and ion binding in both the chickpea cultivars (Table S6). A significant number of DEGs (283 in PUSA362 and 233 in PUSA372) were associated with important enzymatic activity, including transferase, oxidoreductase and hydrolase. It has been well known that K^+ is required for the activation of more than 60 different types of

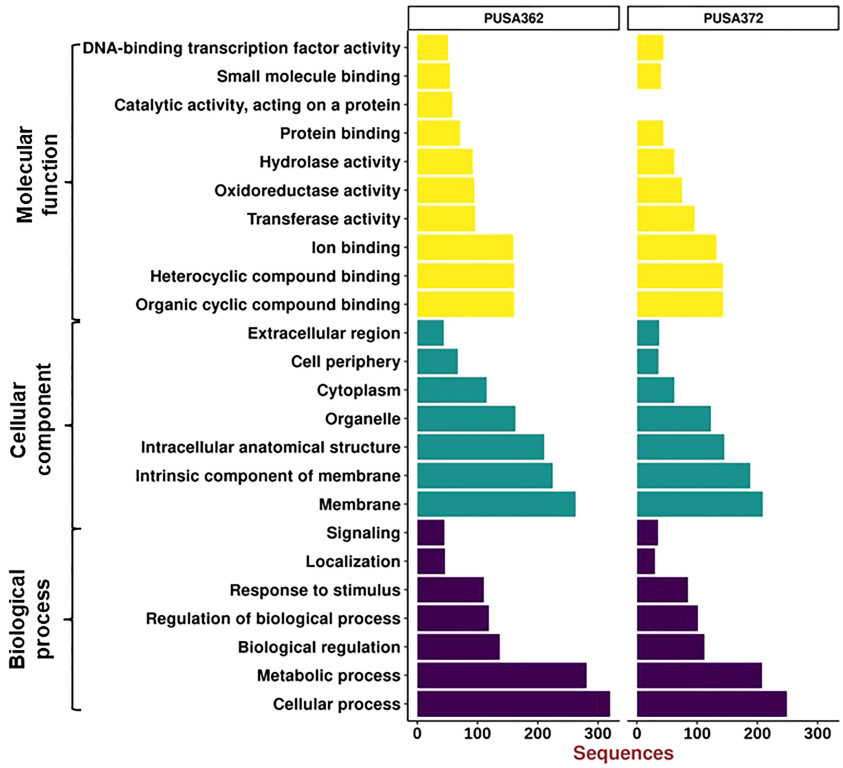

FIGURE 6
Gene Ontology enrichment analysis of DEGs of PUSA362 and PUSA372 chickpea cultivars. Each DEG's assigned with at least one GO term and categorized into three main categories and 24 total sub-categories. Three main categories include biological process, cellular component and molecular function. Y-axis indicates GO category name and X-axis shows the number of DEG sequences.

enzymes which are involved in important cellular processes, such as protein synthesis, starch synthesis, osmoregulation and photosynthesis (Hafsi et al., 2014). Association of several DEGs with important enzymatic functions indicates that K^+ deficiency may have altered the functional behavior and activities of different enzymes that could lead to modulation of important cellular processes in chickpea. In cellular component, DEGs were associated with seven different sub-categories, such as extracellular region, cell periphery, cytoplasm, organelle and cell membrane components. Highest number of DEGs was found to be associated with membrane in both the chickpea cultivars. In PUSA362, a total of 263 membrane associated DEGs were present while, 209 membrane associated DEGs were found in PUSA372. In addition, 225 and 188 DEGs were identified as intrinsic components of membrane in PUSA362 and PUSA372, respectively. This suggests that K^+ deficiency regulates several membrane associated proteins. These proteins may be involved in important cell membrane related functions, such as stress sensing/perception, membrane structure integrity, membrane lipid remodeling, ion and nutrient transport across membrane etc., in chickpea. In addition, some of the DEGs might be involved in regulating K^+ concentration around the membranes to maintain membrane potential, as K^+ is well known for its role in maintenance of membrane potential and electrical neutralization (Wang and Wu, 2013). In biological processes also, DEGs belong to seven sub-categories in both cultivars and these include, cellular processes, metabolic processes, biological pathways, response to stimulus and signaling. DEGs associated with cellular processes were highest both in PUSA362 (320 DEGs) and PUSA372(249 DEGs), followed by metabolic processes, to which 281 and 208 DEGs were associated in PUSA362 and PUSA 372, respectively (Table S6). This is again suggestive of the fact that K^+ deficiency results in modulation of numerous cellular processes and signaling networks in chickpea. Some of these important cellular processes and biological functions are discussed in upcoming sections.

3.5 DEGs are associated with different biological pathways

To understand that which biological pathways are affected in chickpea plant cell by K^+ deficiency, KEGG (http://www.

genome.jp/kegg/) pathway enrichment analysis was performed. KEGG helps to understand the biological function of DEGs by mapping them to the whole genome pathway database. In this analysis, 820 DEGs of PUSA362 were mapped to 65 pathways and 682 DEGs of PUSA372 were mapped to 49 pathways. Highest DEGs were mapped to "metabolic pathways" in both PUSA362 (55 DEGs) and PUSA372 (35 DEGs) (Figure 7 and Table S7). 29 and 13 genes that belonged to "metabolic pathways" were up-regulated while, 27 and 24 genes were down-regulated in PUSA362 and PUSA372, respectively. The pathway where second highest DEGs were mapped was "biosynthesis of secondary metabolites". In this category, 23 and 11 genes were up-regulated whereas, 21 and 22 genes were down-regulated in PUSA362 and PUSA372, respectively. A number of DEGs was mapped to various other important pathways, such as hormone signal transduction pathway, plant pathogen interaction pathway, mitogen activated protein kinases (MAPK) signaling pathway in both the chickpea cultivars. Interestingly, few genes were found to be mapped to pathways which were cultivar specific, for example, amino sugar and nucleotide sugar metabolism and carbon metabolism in PUSA362 whereas, carotenoid biosynthesis in PUSA372. Overall, GO and KEGG pathway analysis of DEGs indicate that chickpea plants respond to K^+ deficiency through alteration in metabolism, gene expression, phytohormone signaling, ion transport activity, signal transduction, RSA and root growth.

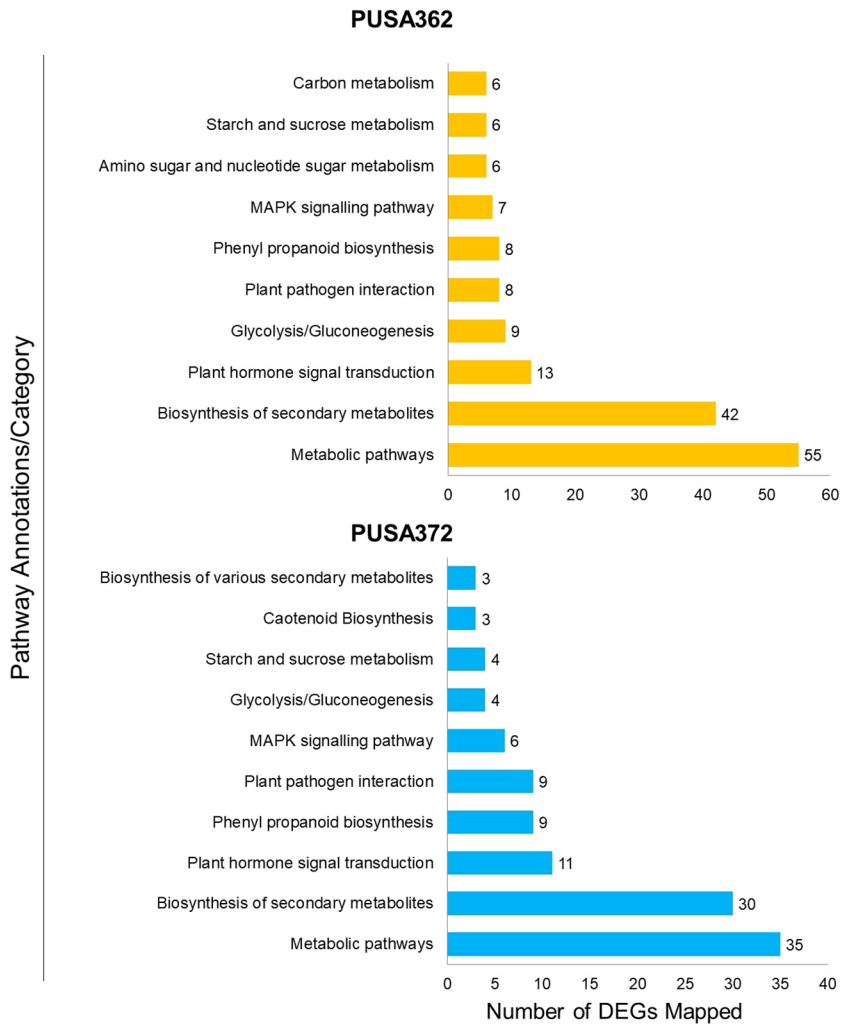

FIGURE 7
Kyoto Encyclopedia of Genes and Genomes (KEGG) pathway analysis of DEGs of both PUSA362 and PUSA372 chickpea cultivars under K^+ deficiency. The Y-axis indicates the pathway annotations/category whereas, X-axis shows the total number of DEGs mapped to corresponding pathways in each variety. A number shown against each bar indicate the total number of DEGs belonging to a particular pathway annotation/category.

3.5.1 K+ deficiency responsive metabolism related genes

Analysis revealed that about 74 DEGs in PUSA362 and 54 DEGs in PUSA372 were associated with plant metabolism. These DEGs belonged to various components of plant metabolism including metabolic pathways, secondary metabolites biosynthesis, pyruvate metabolism, glycolysis/gluconeogenesis, carbon metabolism, amino sugar and nucleotide sugar metabolism, starch and sucrose metabolism. These key genes are known to be involved in energy production, plant growth and development. K^+ serves as a co-factor for numerous important metabolic enzymes and involved in metabolite transport as a counter ion. Thus, K^+-deficiency could result in serious metabolic disorders in plants (Armengaud et al., 2009). Deficiency of K^+ has been found to alter important metabolic processes and pathways in Arabidopsis and rice, including carbohydrate metabolism, the TCA cycle, organic acid metabolism and amino acid metabolism (Armengaud et al., 2004; Shankar et al., 2013). Consistently, genes such as fructose-1,6-bisphosphatase (LOC101500563), UTP-glucose-1-phosphate uridylyltransferase (LOC101490076) and sucrose synthase (LOC101514095) which are involved in carbohydrate metabolism, glycolysis/gluconeogenesis and sucrose metabolism (Tamoi et al., 2006; Stein and Granot, 2019) were significantly down-regulated in K^+ sensitive PUSA362 chickpea. Suppression of such important genes could severely hamper the photosynthesis rate, sucrose production, and it supply to the chickpea roots. Limited availability of important carbon source sucrose may have led to energy starvation condition, and consequently retarded root and plant growth in PUSA362. Similarly, genes like phosphoserine phosphatase (LOC113786736) and cyanogenic beta-glucosidase (LOC101506343) which have crucial role in metabolism and defense against plant herbivores (Lai et al., 2015; Samuilov et al., 2018) were down regulated by -8 and -5 Log_2 fold, respectively in PUSA362. Uridine diphosphate (UDP)-glycosyltransferase (UGT) members (LOC101514581, LOC101514447) were specifically up-regulated by 3 Log_2 fold change in PUSA372 but they were not significantly expressed in PUSA362. Similarly, a UGT encoding gene was also found to be down-regulated in K^+ sensitive rice variety IR64 (Shankar et al., 2013). UGTs are known to function in metabolic pathways, secondary metabolite biosynthesis and have role in homeostasis and detoxification (Huang et al., 2021; Kulasekaran et al., 2021; Mateo-Bonmatí et al., 2021). This indicate that in addition to primary metabolism, K^+ deficiency may have negatively affected the secondary metabolite synthesis and homeostasis in PUSA362 but not in PUSA372. Interestingly, a UGT gene was also expressed differentially under iron toxicity in rice (Quinet et al., 2012), suggesting that UGT are involved in metabolic processes which are commonly affected due to variable availability of different nutrients. Other important genes which are involved in symbiotic nodule formation e.g., early nodulin-like protein (LOC101510639) and those involved in plant energy production process *via* electron transport chain e.g., NADH dehydrogenase (ubiquinone) (LOC113786610) showed more than 4 Log_2 fold up-regulation in PUSA362 (Table 2). Probable xyloglucan endotransglucosylase (LOC101490426), polygalacturonase (LOC101508055) and glucan endo-1,3-beta-glucosidase (LOC101509535) which are important components of xyloglucan metabolism and involved in cell wall assembly and growth (Babu and Bayer, 2014; Hara et al., 2014) were induced significantly in PUSA362. The cell wall is crucial for maintenance of cell structure and integrity and important barrier in plant defense against biotic factors, such as pathogens (Amtmann et al., 2008). As mentioned earlier, K^+ deficiency can weaken the plant defense and make plants prone to pathogens. Thus, in order to strengthen the defense, K^+ sensitive PUSA362 chickpea plant may want to maintain its cell wall *via* induction of cell wall associated genes. Possibly due to same reason, cell wall associated genes have been found to be induced in response to Low-K^+ stress in other plants, such as Arabidopsis (Armengaud et al., 2004), rice (Shankar et al., 2013) and sweet potato (Wang et al., 2022).Overall, alteration in expression many crucial metabolism related genes may have affected the primary metabolism particularly, carbohydrate metabolism, secondary metabolism, defence related metabolism and plant respiration, variably in PUSA362 and PUSA372.That might have resulted in diverged energy production, plant growth and development under K^+ deficiency in K^+ sensitive and tolerant chickpea cultivars.

3.5.2 K^+ deficiency related transcription factors in chickpea cultivars

Transcription factors (TFs) play important regulatory roles in several plant processes, including response to stresses, such as K^+ deficiency. In depth analysis of our transcriptome data revealed that several DEGs belong to TFs in both chickpea cultivars. In PUSA362, a total of 86 DEGs were found to encode TFs and "regulation of transcription" related proteins. Out of 86 DEGs, 28 were up-regulated and 58 were down-regulated. Similarly, 72 TF encoding DEGs were found in PUSA372, out of which 17 were up-regulated and 55 were down-regulated (Table S3). In PUSA362, most differentially expressed TF were from APETALA2 (AP2)/Ethylene Responsive Factor (ERF) (21%) and MYB (15%) family. Similarly, in PUSA372, most differentially expressed TFs belong to MYB (31%) and AP2/ERF (17%) TF family. TFs of basic helix–loop–helix (bHLH) family in PUSA372 were half (7%) compared with PUSA362 (14%). Other important differentially expressed TFs includes NAC, WRKY, bZIP and Homeobox family proteins in both chickpea cultivars (Figure 8 and Table S8). TFs belonging to AP2, MYB, ARF, bHLH and WRKY family have been found to be differentially expressed in response to K^+ deficiency in Arabidopsis (Armengaud et al., 2004) and crop plants such as rice (Shankar et al., 2013), wheat (Zhao et al., 2020), foxtail millet

10.3389/fpls.2022.1054821

TABLE 2 Details of some important K^+ deficiency responsive DEGs in PUSA362 and PUSA372 chickpea cultivars.

Gene LocusID	Function Description	Log2 fold change	Expression regulation
Metabolism related DEGs			
PUSA362			
LOC113786610	NADH dehydrogenase [ubiquinone] iron-sulfur protein 7,	4.4	Up
LOC101506343	cyanogenic beta-glucosidase	-5.6	Down
LOC101500563	fructose-1,6-bisphosphatase, cytosolic	-1.3	Down
LOC101514095	Sucrose synthase	-1.2	Down
PUSA372			
LOC101508799	putative glucose-6-phosphate 1-epimerase	2.7	Up
LOC101514581	UDP-glycosyltransferase 1	1.9	Up
LOC101489836	Alcohol dehydrogenase-like 1	-1.1	Down
LOC101506967	alpha-amylase	-1.4	Down
LOC113784595	patatin-like phospholipase	-5.4	Down
LOC101496167	seed linoleate 9S-lipoxygenase	-1.5	Down
Transcription factors			
PUSA362			
LOC101515639	Ethylene-responsive transcription factor 1B	5.2	Up
LOC101512924	Ethylene-responsive transcription factor ERF098	-2.5	Down
LOC101513362	Ethylene-responsive transcription factor RAP2-3	3.3	Up
LOC101491698	transcription factor MYB14-like	-5.6	Down
LOC101507291	transcription factor bHLH92	-5.1	Down
LOC101491267	MADS-box transcription factor 23	-4.6	Down
LOC101492395	homeobox-leucine zipper protein ATHB-40	-2.8	Down
LOC101508034	LOB domain-containing protein 41	2.2	Up
PUSA372			
LOC101499805	ethylene-responsive transcription factor ERF109	5.9	Up
LOC101515639	ethylene-responsive transcription factor 1B	5.7	Up
LOC101496258	ethylene-responsive transcription factor erf 017-like	3.7	Up
LOC101496910	ethylene-responsive transcription factor erf017-like	3.4	Up
LOC101496811	AP2-like ethylene-responsive transcription factor	-3.7	Down
LOC105851404	transcription factor MYB46	-5.0	Down
LOC101503635	transcription factor MYB98	-5.4	Down
LOC101501101	transcription factor bHLH146	-1.6	Down
LOC101492395	homeobox-leucine zipper protein ATHB-40	-1.3	Down
LOC101504817	LOB domain-containing protein 12	2.3	Up
LOC101490093	WUSCHEL-related homeobox 9	5.0	Up

(Continued)

TABLE 2 Continued

Gene LocusID	Function Description	Log2 fold change	Expression regulation
Signal transduction components			
PUSA362			
LOC101507945	CBL-interacting protein kinase 2	1.2	Up
LOC113785888	somatic embryogenesis receptor-like kinase 1	5.1	Up
LOC101510368	putative receptor-like protein kinase At4g00960	4.9	Up
LOC101504201	probable serine/threonine-protein kinase fhkB	2.7	Up
LOC101508412	probable protein phosphatase 2C 25	1.2	Up
LOC101493828	probable protein phosphatase 2C 15	-5.8	Down
LOC101503050	phosphatase 2C-like protein 44 isoform X1	-4.5	Down
LOC101500357	type I inositol polyphosphate 5-phosphatase 5	-3.8	Down
LOC101492388	calmodulin-binding receptor-like cytoplasmic kinase 2	-1.1	Down
LOC101512980	annexin D8	-5.1	Down
LOC101492172	putative calcium-binding protein CML19	-3.7	Down
LOC101507335	probable calcium-binding protein CML41	1.6	Up
LOC101501436	calcium-binding protein PBP1	1.3	Up
LOC101496110	cationic peroxidase 1	3.1	Up
LOC113784455	glutathione S-transferase zeta class-like	-5.3	Down
PUSA372			
LOC101493042	receptor-like cytosolic serine/threonine-protein kinase RBK1	1.1	Up
LOC101502405	inorganic pyrophosphatase 2-like	1.4	Up
LOC101513274	probable protein phosphatase 2C 72	1.4	Up
LOC101515110	acid phosphatase 1	1.4	Up
LOC113784622	type I inositol polyphosphate 5-phosphatase 12, X2	-5.3	Down
LOC113785888	somatic embryogenesis receptor-like kinase 1	-5.2	Down
LOC101499928	CBL-interacting serine/threonine-protein kinase 1, X1	-1.1	Down
LOC101512278	1-aminocyclopropane-1-carboxylate oxidase homolog 1-like	-1.5	Down
LOC101495667	cysteine-rich receptor-like protein kinase 10 isoform X2	-1.1	Down
LOC101492172	putative calcium-binding protein CML19	5.7	Up
LOC101515597	calcium-binding protein PBP1-like	2.6	Up
LOC101512980	annexin D8	-3.4	Down
LOC101513640	Peroxidase 16	3.6	Up
LOC101491218	peroxidase P7-like	2.1	Up
LOC101489588	probable glutathione S-transferase	-1.2	Down
Ion transport associated DEGs			
PUSA362			
LOC101497071	probable inorganic phosphate transporter 1-3	5.8	Up
LOC105851115	protein NRT1/PTR FAMILY 3.1-like	1.6	Up

(Continued)

10.3389/fpls.2022.1054821

TABLE 2 Continued

Gene LocusID	Function Description	Log2 fold change	Expression regulation
LOC101512428	vacuolar iron transporter homolog 4-like	-4.4	Down
LOC101503875	high affinity nitrate transporter 2.4	-2.6	Down
LOC101506906	high affinity nitrate transporter 2.5	-1.2	Down
LOC101497328	protein NRT1/PTR FAMILY 5.6-like	-1.2	Down
LOC101497004	protein NRT1/PTR FAMILY 2.6	-1.1	Down
LOC101495372	S-type anion channel SLAH1	-1.5	Down
PUSA372			
LOC101503875	high affinity nitrate transporter 2.4	1.9	Up
LOC101497071	probable inorganic phosphate transporter 1-3	4.9	Up
LOC101495372	S-type anion channel SLAH1	-1.9	Down
LOC101497328	protein NRT1/PTR FAMILY 5.6-like	-1.4	Down
LOC101504169	bidirectional sugar transporter SWEET3	1.5	Up
Phytohormones associated DEGs			
PUSA362			
LOC101505638	1-aminocyclopropane-1-carboxylate oxidase 1	4.4	Up
LOC101489126	auxin-responsive protein SAUR72-like	2.8	Up
LOC101513626	gibberellin 2-beta-dioxygenase	1.1	Up
LOC101509106	cytochrome P450 94C1	2.2	Up
LOC101504297	cytochrome P450 71D10-like	-1.4	Down
LOC113787771	3-epi-6-deoxocathasterone 23-monooxygenase	-1.5	Down
PUSA372			
LOC101489648	Auxin-responsive protein SAUR71	2.6	Up
LOC101489126	auxin-responsive protein SAUR72-like	2.4	Up
LOC101500571	gibberellin 20 oxidase 2-like	-2.7	Down
LOC101512278	1-aminocyclopropane-1-carboxylate oxidase homolog 1-like	-1.1	Down
LOC101510386	auxin-responsive protein SAUR50-like	-1.3	Down
LOC101501719	auxin-responsive protein SAUR68-like	-1.3	Down
DEGs associated with root growth and development			
PUSA362			
LOC101505027	expansin-A11	1.2	Up
LOC101513147	patatin-like phospholipase	5.7	Up
LOC113786110	protein MAIN-LIKE 1-like	4.6	Up
PUSA372			
LOC101500741	putative expansin-B2	7.2	Up
LOC101504687	putative expansin-A30	1.2	Up
LOC113784595	patatin-like phospholipase	-5.4	Down
LOC113786110	protein MAIN-LIKE 1-like	-5.0	Down

(Cao et al., 2019) and sweet potato (Wang et al., 2022). This indicates that these TFs have a conserved role in transcriptional reprogramming of different genes under K^+ deficiency in chickpea and other plants. TFs of AP2/ERF family are known to play an important role in regulating K^+ deficiency response in plants. Arabidopsis RAP2.11 (AP2/ERF) binds to the GCC box in the promoter of *High Affinity K⁺ Transporter 5* (*HAK5*) and regulates its expression under K^+ deficient conditions through reactive oxygen species (ROS) dependent pathway (Kim et al., 2012; Schachtman, 2015). TFs of auxin responsive factor (ARF) family have also been implicated in K^+ deficiency response. AtARF2 represses the *AtHAK5* expression under K^+ sufficient (normal) conditions while, under K^+ deficient conditions AtARF2 is phosphorylated, which relieves the repression from AtHAK5, which in turn, mediates enhanced K^+ uptake (Zhao et al., 2016). NITRATE TRANSPORTER 1/PEPTIDE TRANSPORTER FAMILY 7.3 (NPF7.3) is a proton coupled H^+/K^+ antiporter which mediates root-to-shoot K^+ translocation. AtMYB59 binds to the promoter of NPF7.3 and positively regulates its expression under external K^+/NO_3^- application (Du et al., 2019). AtMYB77 is involved in auxin signal transduction, and its expression is reduced under K^+ deficiency to regulate lateral root development (Shin et al., 2007). Importantly, AtMYB77 binds to AtHAK5 promoter and positively regulates its expression to improve K^+ uptake by roots (Feng et al., 2021). Similarly, bHLH122 and WRKY33 TFs regulate the expression of an Arabidopsis K^+ transporter, K^+ UPTAKE 2 (KUP2) (Rajappa et al., 2020). Like Arabidopsis, these important TFs could be involved in regulating expression of K^+ transporters, such as HAKs, KUP and NPF7.3 in chickpea, and may contribute to enhanced K^+ uptake, root-shoot translocation and redistribution under K^+ deficient conditions. In addition, TFs could also regulate the expression of development related genes, such as those involved in root growth.

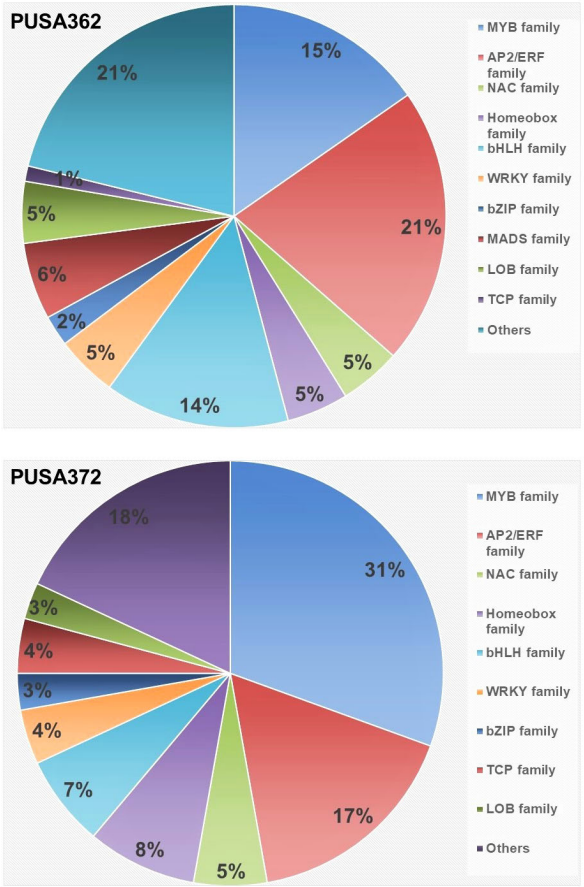

FIGURE 8
Distribution of K^+ deficiency responsive, differentially expressed transcription factor in PUSA362 and PUSA372 cultivars. Color legends and corresponding names of different transcription factor family are denoted on the right. Numbers in the different color compartments of pi-chart indicate total TF from different family as DEGs.

3.5.3 K^+ deficiency related signal transduction components

High amount of ROS is known to be accumulated under K^+ deficiency, and it interferes in the normal function of proteins and lipids which leads to cell damage (Mittler, 2017). Although, accumulation of ROS may lead to oxidative stress that can be damaging to cells, ROS is known as an important signaling molecules. Therefore, in plant cell several proteins function to strike a balance between ROS production and detoxification (Sagi and Fluhr, 2006; Vellosillo et al., 2010; Sharma et al., 2012). Peroxidases and glutathione S-transferase (GST) are involved in this process and both act as ROS scavengers. In Arabidopsis roots, the expression of a peroxidase encoding gene *ATP19a* was significantly reduced under K^+ deficiency (Armengaud et al., 2004). In rice, the expression of GST encoding genes was found to be down-regulated under K^+ deficiency (Shankar et al., 2013). Similarly, several peroxidase and GST genes were differentially expressed in wheat under K^+ deficiency conditions. In this study, several members of peroxidase family and GSTs were found to be differentially expressed in both chickpea cultivars. For example, GST encoding gene LOC113784455 showed -5.29 Log_2 fold down-regulation in PUSA362 and 3.08 Log_2 fold up-regulation in PUSA372. This infers that like in other plants, peroxidase and GST *via* ROS scavenging regulate the ROS accumulation and homeostasis to prevent the chickpea plants from oxidative damage due to low-K^+ stress.

K^+ deficiency is known to trigger Ca^{2+} signaling in plants. Several Ca^{2+} signaling components, such as calmodulin (CaM), calcineurin B-like (CBL), CBL-interacting protein kinases (CIPKs) have been found to be induced under K^+ deficiency and regulating K^+ deficiency response in plants (Armengaud et al., 2004; Lee et al., 2007; Pandey et al., 2007; Singh et al., 2018). In this study, a CIPK gene (LOC101507945) was up-regulated in PUSA362 whereas, another CIPK member (LOC101499928) was significantly down-regulated in PUSA372. In depth analysis revealed that more phosphorylation related genes are up-regulated in PUSA362 than in PUSA372. Genes encoding protein phosphatase 2C (PP2C) (LOC101493828, LOC101503050) were down-regulated by -5.8 and -4.4 Log_2 fold in PUSA362. In PUSA372, type I inositol polyphosphate 5-phosphatase was found to be down-regulated by -5.8 Log_2 fold (Table 2). This indicates that besides transcriptional regulation, post-translational regulation of genes is critical of K^+ deficiency tolerance in chickpea. It is well known that signaling components, such as kinases and phosphatases play an important role in regulating K^+ uptake and transport in plants. Primarily, kinases such as CIPKs and phosphatases of PP2C family post-translationally regulate K^+ transporters and channels like HAK5 and Arabidopsis K^+ transporter 1 (AKT1) in response to K^+ deficiency (Singh et al., 2016; Singh et al., 2018; Ankit and Singh, 2022). CIPK23 in complex with CBL1 and CBL9 phosphorylates and activates AKT1, to enhance root K^+ uptake under K^+ deficient conditions (Lee et al., 2007). Also, CIPK6 interacts with CBL4 and regulate the translocation of K^+ channel AKT2 to plasma membrane, that ultimately enhance AKT2 activity (Held et al., 2011; Singh et al., 2016). In addition, Ca^{2+} sensor proteins such as CBLs have been implicated in K^+ deficiency response. For example, CBL2 and CBL3 which interact with four CIPKs (CIPK3, 9, 23 and 26) in Arabidopsis, regulate K^+ homeostasis through activating TPK (two-pore K) channel mediated vacuolar K^+ efflux to the cytoplasm (Tang et al., 2020). PP2C-type phosphatase like AKT1 INTERACTING PROTEIN PHOSPHATASE 1 (AIP1) dephosphorylate AKT1 and functions as a negative regulator of AKT1 channel activity under K^+ deficiency (Lee et al., 2007; Singh et al., 2015). Similarly, AP2C1 (PP2C), interacts with and dephosphorylates an autophosphorylated CIPK9 (a positive regulator of K^+ deficiency tolerance), thus, its function as a negative regulator of K^+ deficiency tolerance in Arabidopsis (Singh et al., 2018). AtPP2CA which is involved in ABA signaling, inhibits gated outwardly-rectifying K^+ (GORK) channels K^+ efflux activity independent of its phosphorylation status (Lefoulon et al., 2016). Here, we found that PP2Cs; LOC101493828, LOC101503050 were strongly down-regulated in PUSA362 whereas, five other phosphatases (LOC101502405, LOC101515110, LOC101513274, LOC101504848 and LOC113785826) were significantly up-regulated in PUSA372. We also found genes encoding calcium uniporter, Annexin D, Ca^{2+} binding proteins, like PINOID-BINDING PROTEIN (PBP), CaM-like (CML), CaM binding protein (CBP), etc. as DEGs in both chickpea cultivars. One calcium uniporter (LOC101508599) was found to be up-regulated in PUSA362. While, Annexin D4 and D8 were down-regulated in both, PUSA362 (-5.1 and -1.3 Log_2fold) and PUSA372 (-3.4 and -1.5 Log_2fold) (Table 2). Thus, signaling components like CBL, CaM, CML, CIPK and PP2C may regulate various K^+ transporters and channels *via* Ca^{2+} signaling, to improve K^+ uptake and transport in chickpea, thereby contribute to better KUE. Overall, these findings infer that like in other plants, a conserved CBL-CIPK-PP2C signaling module might be involved in regulating K^+ uptake and transport in chickpea.

3.5.4 K^+ deficiency responsive ion/nutrient transport related genes

K^+ deficiency could have disturbed the homeostasis of different ions and nutrients as several ion/nutrient transporters were identified as DEGs in both chickpea cultivars. These DEGs belonged to ABC transporters, metal transporters, anion channels, transporters for nitrate, phosphate and zinc. An important inorganic phosphate (Pi) transporter (LOC101497071) was up-regulated by 5.8 and 4.97 Log_2 fold in PUSA362 and PUSA372, respectively (Table 2). Members of dual-affinity nitrate transporter/peptide transporter (NRT1/PTR) family were differentially expressed in both the cultivars. High affinity nitrate transporters, LOC101503875 and LOC101506906 were down-regulated in PUSA362 whereas, LOC101503875 was up-regulated significantly in PUSA372. Different members of S-type anion channel (SLAH1) family were down-regulated in both

varieties. One of the vacuolar iron transporters homolog 4-like (LOC101512428) was down-regulated specifically in PUSA362 by -4.3 Log_2 fold. The flux of different ions, metals or solutes is regulated to maintain their homeostasis, osmoticum in the cell and neutralization of the charges across cell membrane. Under K^+ deficiency, these physiological processes are disturbed and plant cell tends to normalize them *via* different transporters and channels (Walker et al., 1996; Gierth and Mäser, 2007). Thus, differential regulation of several genes encoding ion/metal/solute transporter/channels might be required to maintain the ion homeostasis and membrane potential under K^+ deficiency in chickpea. Carbohydrate transporter SWEET proteins encoding genes LOC101488880 and LOC101497351 were up-regulated in PUSA362 and PUSA372, respectively. SWEET transporters function as uniporters and mediate sugar diffusion across cell membranes. They mediate sucrose efflux from phloem parenchyma into the phloem apoplasm thus, they are involved in phloem loading (Chen, 2014). As discussed earlier, we found evidence of significant modulation of carbohydrate metabolism under K^+ deficiency in chickpea. These SWEET transporters could be an important part of the carbohydrate metabolism process. They may help to maintain a sustained supply of sucrose from source to sink for energy production in chickpea under low-K^+ conditions. In Arabidopsis, most of the K^+ uptake occur through AKT1, HAK5 and KUP7 transporters (Ankit et al., 2022). The expression level of these transporters in different plants has been found to increase in response to K^+ deprivation (Ankit and Singh, 2022). Surprisingly, in this study we did not find these transporters genes as DEGs in chickpea. NRT1/PTR members which are found as DEGs here, are known to be involved in nitrate uptake through roots. However, *NRT1/PTR* expression levels is dependent on the external K^+ level in many plants (Ma et al., 2012; Ruan et al., 2015; He et al., 2020; Yang et al., 2020). K^+ and NO_3^- have been shown to be coupled during root uptake and transport towards shoots (Ruffel, 2018). NRT1.5/NPF7.3 functions as a proton-coupled H^+/K^+ antiporter which can mediates root-to-shoot K^+ translocation in Arabidopsis (Li et al., 2017). Another Arabidopsis nitrate transporter NRT1.1/NPF6.3 coordinates K^+ uptake and its translocation from root towards shoots (Bouguyon et al., 2016). This suggest that in chickpea, instead of traditional HAK/AKT/KUP mediated K^+ transport, a co-transport mechanism of K^+ and NO_3^- may regulate K^+ uptake and transport. Importantly, ion transporters may not always be regulated transcriptionally. They might also be regulated post-translationally *via* reversible phosphorylation mechanism by kinases and phosphatases. As discussed earlier, we found several kinases and phosphatases as DEGs which is evidence of significant amount of reversible phosphorylation (post-translational modifications) under K^+ deficiency in chickpea. However, detail functional investigations are required to establish these assumptions, and to completely understand the K^+ transport mechanism in chickpea.

3.5.5 K^+ deficiency responsive phytohormones biosynthesis and signaling genes

Transcriptome data analysis revealed that K^+ deficiency resulted in modulation of various phytohormones pathways in chickpea. Several genes associated with phytohormone biosynthesis and signaling were found to be differentially expressed in both chickpea cultivars under K^+ deficiency. In PUSA362, total 44 DEGs were associated with phytohormone, out of which 15 were up-regulated and 29 were down-regulated. In PUSA372, out of total 32 phytohormone related DEGs, only 5 genes were up-regulated and 28 were down-regulated. Ethylene is one of the crucial and early responsive phytohormones to K^+ deficiency. Ethylene biosynthesis genes are readily induced under K^+ deficiency and ethylene content is significantly increased as early as 6 hours of K^+ deficiency in Arabidopsis. Ethylene regulates plants response to K^+ deficiency, including HAK5 expression, ROS production and primary root growth inhibition (Jung et al., 2009; Schachtman, 2015). We found that a gene encoding for important ethylene biosynthesis enzyme, 1-aminocyclopropane-1-carboxylate oxidase 1 (ACO1) (LOC101505638) was up-regulated by 4.44 Log_2 fold change in PUSA362 (Table 2). Interestingly, an ACO member (LOC101512278) was down-regulated in PUSA372. It is well known that external addition of ethylene or auxin inhibits the primary root growth and root hair elongation, a phenotype similar to one observed in K^+ deficient plants (Jung et al., 2009; Muday et al., 2012). Importantly, K^+ deficiency induced inhibition of primary root growth could be reversed in mutants insensitive to auxin (Cao et al., 1993). Interestingly, evidence suggest that ethylene and auxin may function together or cross-talk to regulate root growth development either synergistically or antagonistically (Muday et al., 2012). Also, K^+ deficiency induced ethylene signal supports auxin biosynthesis and its transport to roots, where auxin accumulates in root elongation zone to inhibit primary root growth and to enhance root hair elongation (Muday et al., 2012; Wang and Wu, 2013). This indicates that ethylene and auxin are crucial in determining the root morphology and RSA under K^+ deficiency. We also found the evidence of involvement of auxin signaling in K^+ deficiency response in chickpea. Small auxin up-regulated RNA (SAUR) is one of the largest families of early auxin responsive genes in higher plants (Ren and Gray, 2015). In PUSA362, many SAUR genes (LOC101489126, LOC101509958, LOC101489202, LOC101488509, and LOC101492206) were significantly up-regulated while, some other genes related to auxin response and signaling (LOC101496738, LOC101494568, LOC101508549, LOC101505229, LOC101510386) were significantly down-regulated. Similarly, in PUSA372 auxin responsive SAUR protein encoding genes (LOC101489648, LOC101489126 and LOC101489202) were up-regulated whereas, other auxin signaling and response genes (LOC101508549, LOC101510386, LOC113785858 etc.) were

down-regulated. Brassinosteroids (BRs) are also involved in root growth and development in plants (Wei and Li, 2016). Recent transcriptome study showed that various BR related genes were differentially expressed under K^+ deficient conditions in cotton, and they were implicated in cotton root growth (Yang et al., 2021). In this study, many BR biosynthesis and signaling genes were found to be differentially expressed in both cultivars. BR biosynthesis genes like 3-epi-6-deoxocathasterone23-monooxygenase were down-regulated in both varieties. BR homeostasis related gene cytochrome P450 85A (LOC101510551) was up-regulated, and one beta-amyrin 11-oxidase (LOC101495501) was down-regulated in PUSA362. Like BR, jasmonic acid (JA)has been known to regulate various facets of root growth. It acts as a negative regulator of primary root growth (Chen et al., 2011; Kamali and Singh, 2022), and positive regulator of lateral root (Cai et al., 2014) and root hair growth (Han et al., 2020). JA biosynthesis and signaling genes have been shown to induced in response to K^+ deficiency in different plants (Armengaud et al., 2004; Li et al., 2017; Deepika and Singh, 2021; Deepika et al., 2022). In this study, JA related gene (LOC101509106) was significantly up-regulated whereas, JA biosynthesis gene (LOC101491096) was down-regulated in PUSA362. Also, various JA catabolism related cytochrome p450 family members were differentially expressed in response to K^+ deficiency, for example, in PUSA362, LOC101498230, LOC101504297 and in PUSA372, LOC101498230, LOC101504297 were down-regulated. This indicates that K^+ deficiency stimulated JA accumulation in chickpea is controlled by fine-tuning of JA biosynthesis and catabolism related genes. Variable expression of these genes and accumulation of physiologically significant level of JA may influence the root growth and RSA in chickpea. Besides, gibberellin related gibberellin 2-beta-dioxygenase (LOC101513626) and putrescine related ornithine decarboxylase (LOC101494284) genes were significantly up-regulated in PUSA362. While, genes such as gibberellin 20 oxidase (LOC101492441, LOC101500571, and LOC101491320), genes related to abscisic acid (ABA) (LOC101506315, LOC101505927, LOC101490679) and cytokinin (LOC101495234, LOC101498288) were-down-regulated in PUSA372. Identification of ethylene, auxin, GA, ABA, BR and JA biosynthesis and signaling genes as DEGs under K^+ deficiency suggests that differential regulation of these genes and reprogramming of these phytohormones pathway could be essential for root growth, RSA changes and overall plant growth in chickpea. Variable expression of these important genes could be one of the reasons of the contrasting growth pattern of two chickpea cultivars under K^+ deficiency.

3.5.6 K^+ deficiency responsive genes associated with root growth and development

Our morphological analysis revealed that K^+ deficiency results in inhibition of primary and lateral root growth in chickpea. It's expected that the expression of root growth and development related genes might have altered under K^+ deficiency in chickpea. Consistently, EXPANSIN genes were found to be up-regulated in both chickpea varieties. Expansin family proteins are known to catalyze long-term expansion of cell walls, thus they regulate cell expansion in plants particularly in processes like primary root elongation and root growth (Lee et al., 2003). In PUSA362, EXPANSIN (LOC101505027) was up-regulation by 1.1 Log_2fold whereas, in PUSA372 EXPANISN (LOC101504687 and LOC101500741) were up-regulated by 1.2 and 7.2 Log_2fold (Table 2). In contrast, LOC101489892 was down-regulated by -1.4 Log_2fold in PUSA362, whereas no EXPANSIN gene was down-regulated in PUSA372. A leucine-rich repeat (LRR)- extensin (LRX) gene (MSTRG.17226) showed up-regulation by 5.5 Log_2fold in PUSA362 while, another member of same family (LOC101515776) was down-regulated by -3.4 Log_2fold in PUSA372.Extensins are the important constituents of the plant cell wall and are involved in cell wall remodeling during cell expansion (Herger et al., 2019). In Arabidopsis, two members of LRX family; *LRX1* and *LRX2* express mainly in root hairs. The *lrx1* mutant was shown to develop root hairs that were deformed and frequently burst. Interestingly, the *lrx2* mutant develops root hairs similar to wild type, however, the *lrx1lrx2* double mutant show more severe phenotype than *lrx1* in terms of hampered root hair development (Baumberger et al., 2001). This indicates synergistic interaction of LRX1 and LRX2 in root hair development. In addition to root hairs, LRX2 has also been implicated in lateral root formation. Similarly, *LRX6* has been found to express during lateral root formation (Baumberger et al., 2003), however, its exact role in root development needs to be investigated. Thus, differentially expressed cell wall- related LRX in chickpea may regulate mechanical stability of cell wall, and support cell expansion during root hair and lateral root development. Peptide hormone, root meristem growth factor 1 (RGF1) is involved in maintaining stem cell niche and root meristem size through ROS signaling in Arabidopsis (Yamada et al., 2020). A RGF gene (LOC101510975) was strongly up-regulated in both chickpea cultivars under K^+ deficiency, however, another RGF (LOC101507205) showed down-regulation in PUSA362. RADIALIS (LOC113785428, LOC101513794, LOC101491616, LOC101493531, LOC101491616) genes involved in formation of root endodermis (Kaashyap et al., 2018) were found to be down-regulated in both varieties. Overall, the interplay of these important regulators of root development and those which regulate metabolism, signal transduction, phytohormones and TFs could have resulted into variable root growth pattern and RSA in PUSA362 and PUSA372 chickpea cultivars. In future, detail functional investigation and genetic engineering using these crucial genes may help in achieving chickpea plants with desired RSA and improved KUE and K^+ deficiency tolerance traits.

4 Conclusion

In conclusion, among five different chickpea cultivars PUSA362 had shortened primary roots and stunted plant growth under K^+

deficiency while, PUSA372 had negligible effect on root and overall plant growth. In addition, K^+ content analysis indicated impaired K^+ uptake and transportation in PUSA362, but not in PUSA372. These evidences suggest that PUSA362 is a K^+ deficiency sensitive chickpea cultivar while, PUSA372 is K^+ deficiency tolerant. Global transcriptome analysis revealed hundreds of K^+ deficiency responsive genes in PUSA362 and PUSA372. Some crucial genes related to plant metabolism, such as fructose-1,6-bisphosphatase and sucrose synthase were repressed in PUSA362, which could result in low carbohydrate and sucrose level, consequently, hampered transportation of sucrose from shoot (source) to root (sink) and low available energy. Thus, PUSA362 plants may have diverted their limited energy sources in combating K^+ deficiency than supporting plant growth and resulting in hampered root growth and overall plant growth. An ethylene biosynthesis gene, ACO was up-regulated in PUSA362 while, an ACO gene was down-regulated in PUSA372. As ethylene is known to trigger ROS production and inhibit primary root growth, accumulation of ethylene could be one of the possible reasons for impaired primary root growth in PUSA362 under K^+ deficiency. Also, an expansin gene which promote root development by controlling cell expansion was down-regulated in PUSA362 but not in PUSA372. In addition to these, interplay of several other hormone related genes (particularly auxin), signal transduction components (like CBLs, CIPKs, PP2C) and TFs (AP2, ARF, MYBs) may determine the chickpea plants response to K^+ deficiency in two contrasting cultivars. However, adaptive response to stress, such as K^+ deficiency is a complex trait and may not be completely understood by transcriptional changes. Several other important factors, such as genetic and physiological events, post-translational modifications and epigenetic regulations are potential determinants of an adaptive response. In future, detail functional investigation of some of these key genes and their utilization in genetic engineering and breeding programs will help in understanding the genetic, physiological and molecular basis of K^+ deficiency tolerance in chickpea. The knowledge so generated will help in developing chickpea plants with better KUE and K^+ deficiency tolerance traits.

Data availability statement

The datasets presented in this study can be found in online repositories. The names of the repository/repositories and accession number(s) can be found in the article/Supplementary Material.

Author contributions

AS conceptualized and design the study. AA performed the wet lab experiments. AA, AjS, SK, and AS analyzed the data. AS and AA wrote the manuscript. All authors read and approved the final version of manuscript.

Acknowledgments

Authors are thankful to Dr. Swarup K. Parida, Scientist, NIPGR, New Delhi for providing the seeds of five desi chickpea cultivars. The financial support from NIPGR core grant and Science and Engineering Research Board (SERB)—Department of Science and Technology (DST), Government of India (Grant No. CRG/2021/000694) to AS lab is also acknowledged. DBT—eLibrary Consortium (DeLCON) is acknowledged for providing e-resources.

Conflict of interest

The authors declare that the research was conducted in the absence of any commercial or financial relationships that could be construed as a potential conflict of interest.

Publisher's note

Supplementary material

The Supplementary Material for this article can be found online at: https://www.frontiersin.org/articles/10.3389/fpls.2022.1054821/full#supplementary-material

References

Amtmann, A., Troufflard, S., and Armengaud, P. (2008). "The effect of potassium nutrition on pest and disease resistance in plants," in *Physiologia plantarum*, vol. 133. , 682–691. doi: 10.1111/j.1399-3054.2008.01075.x

Ankit, A., Kamali, S., and Singh, A. (2022). Genomic & structural diversity and functional role of potassium (K+) transport proteins in plants. International journal of biological macromolecules, 208, 844–857. doi: 10.1016/j.ijbiomac.2022.03.179

Ankit,, and Singh, A. (2022). "Potassium (K+) transporters in plants: regulation and functional role in k+ uptake and homeostasis," in *Cation transporters in plants*. Ed. S. K. B. T. Upadhyay (Academic Press), 29–47. doi: 10.1016/B978-0-323-85790-1.00013-0

Armengaud, P., Breitling, R., and Amtmann, A. (2004). The potassium-dependent transcriptome of arabidopsis reveals a prominent role of jasmonic

acid in nutrient signaling. *Plant Physiol.* 136, 2556–2576. doi: 10.1104/pp.104.046482

Armengaud, P., Sulpice, R., Miller, A. J., Stitt, M., Amtmann, A., and Gibon, Y. (2009). Multilevel analysis of primary metabolism provides new insights into the role of potassium nutrition for glycolysis and nitrogen assimilation in arabidopsis roots. *Plant Physiol.* 150, 772–785. doi: 10.1104/pp.108.133629

Babu, Y., and Bayer, M. (2014). Plant polygalacturonases involved in cell elongation and separation-the same but different? *Plants (Basel Switzerland)* 3, 613–623. doi: 10.3390/plants3040613

Barberon, M., Vermeer, J. E. M., De Bellis, D., Wang, P., Naseer, S., Andersen, T. G., et al. (2016). Adaptation of root function by nutrient-induced plasticity of endodermal differentiation. *Cell* 164, 447–459. doi: 10.1016/j.cell.2015.12.021

Baumberger, N., Doesseger, B., Guyot, R., Diet, A., Parsons, R. L., Clark, M. A., et al. (2003). Whole-genome comparison of leucine-rich repeat extensins in arabidopsis and rice. a conserved family of cell wall proteins form a vegetative and a reproductive clade. *Plant Physiol.* 131, 1313–1326. doi: 10.1104/pp.102.014928

Baumberger, N., Ringli, C., and Keller, B. (2001). The chimeric leucine-rich repeat/extensin cell wall protein LRX1 is required for root hair morphogenesis in *Arabidopsis thaliana*. *Genes Dev.* 15, 1128–1139. doi: 10.1101/gad.200201

Bouguyon, E., Perrine-Walker, F., Pervent, M., Rochette, J., Cuesta, C., Benkova, E., et al. (2016). Nitrate controls root development through posttranscriptional regulation of the NRT1.1/NPF6.3 transporter/sensor. *Plant Physiol.* 172, 1237–1248. doi: 10.1104/pp.16.01047

Britto, D. T., and Kronzucker, H. J. (2008). Cellular mechanisms of potassium transport in plants. *Physiol. Plant* 133, 637–650. doi: 10.1111/j.1399-3054.2008.01067.x

Cai, X.-T., Xu, P., Zhao, P.-X., Liu, R., Yu, L.-H., and Xiang, C.-B. (2014). Arabidopsis ERF109 mediates cross-talk between jasmonic acid and auxin biosynthesis during lateral root formation. *Nat. Commun.* 5, 5833. doi: 10.1038/ncomms6833

Cakmak, I., Hengeler, C., and Marschner, H. (1994). Changes in phloem export of sucrose in leaves in response to phosphorus, potassium and magnesium deficiency in bean plants. *J. Exp. Bot.* 45, 1251–1257. doi: 10.1093/jxb/45.9.1251

Cao, Y., Glass, A. D., and Crawford, N. M. (1993). Ammonium inhibition of Arabidopsis root growth can be reversed by potassium and by auxin resistance mutations aux1, axr1, and axr2. *Plant physiology* 103 (3), 983–989. doi: 10.1104/pp.102.3.983

Cao, X., Hu, L., Chen, X., Zhang, R., Cheng, D., Li, H., et al. (2019). Genome-wide analysis and identification of the low potassium stress responsive gene SiMYB3 in foxtail millet (*Setariaitalica l.*). *BMC Genomics* 20, 136. doi: 10.1186/s12864-019-5519-2

Chen, L.-Q. (2014). SWEET sugar transporters for phloem transport and pathogen nutrition. *New Phytol.* 201, 1150–1155. doi: 10.1111/nph.12445

Chen, A., Husted, S., Salt, D. E., Schjoerring, J. K., and Persson, D. P. (2019). The intensity of manganese deficiency strongly affects root endodermal suberization and ion homeostasis. *Plant Physiol.* 181 (2), 729–742. doi: 10.1104/pp.19.00507

Chen, Q., Sun, J., Zhai, Q., Zhou, W., Qi, L., Xu, L., et al. (2011). The basic helix-loop-helix transcription factor MYC2 directly represses PLETHORA expression during jasmonate-mediated modulation of the root stem cell niche in arabidopsis. *Plant Cell* 23 (9), 3335–3352. doi: 10.1105/tpc.111.089870

de Bang, T. C., Husted, S., Laursen, K. H., Persson, D. P., and Schjoerring, J. K. (2021). The molecular–physiological functions of mineral macronutrients and their consequences for deficiency symptoms in plants. *New Phytol.* 229, 2446–2469. doi: 10.1111/nph.17074

Deepika, D., Ankit,, Jonwal, S., Mali, K. V., Sinha, A. K., and Singh, A. (2022). Molecular analysis indicates the involvement of jasmonic acid biosynthesis pathway in low-potassium (K^+) stress response and development in chickpea (*Cicer arietinum*). *Environ. Exp. Bot.* 194, 104753. doi: 10.1016/j.envexpbot.2021.104753

Deepika, and Singh, A. (2021). Expression dynamics indicate the role of jasmonic acid biosynthesis pathway in regulating macronutrient (N, p and k^+) deficiency tolerance in rice (*Oryza sativa l.*). *Plant Cell Rep.* 40, 1495–1512. doi: 10.1007/s00299-021-02721-5

Du, X.-Q., Wang, F.-L., Li, H., Jing, S., Yu, M., Li, J., et al. (2019). The transcription factor MYB59 regulates K^+/NO_3^- translocation in the arabidopsis response to low k^+ stress. *Plant Cell* 31, 699–714. doi: 10.1105/tpc.18.00674

FAOSTAT (2016). Available at: http://www.fao.org/faostat/en/#home.

Feng, C.-Z., Luo, Y.-X., Wang, P.-D., Gilliham, M., and Long, Y. (2021). MYB77 regulates high-affinity potassium uptake by promoting expression of HAK5. *New Phytol.* 232, 176–189. doi: 10.1111/nph.17589

Gierth, M., and Mäser, P. (2007). Potassium transporters in plants-involvement in k^+ acquisition, redistribution and homeostasis. *FEBS Lett.* 581, 2348–2356. doi: 10.1016/j.febslet.2007.03.035

Hafsi, C., Debez, A., and Abdelly, C. (2014). Potassium deficiency in plants: effects and signaling cascades. *Acta Physiol. Plant* 36, 1055–1070. doi: 10.1007/s11738-014-1491-2

Han, X., Zhang, M., Yang, M., and Hu, Y. (2020). Arabidopsis JAZ proteins interact with and suppress RHD6 transcription factor to regulate jasmonate-stimulated root hair development. *Plant Cell* 32, 1049–1062. doi: 10.1105/tpc.19.00617

Hara, Y., Yokoyama, R., Osakabe, K., Toki, S., and Nishitani, K. (2014). Function of xyloglucan endotransglucosylase/hydrolases in rice. *Ann. Bot.* 114, 1309–1318. doi: 10.1093/aob/mct292

Held, K., Pascaud, F., Eckert, C., Gajdanowicz, P., Hashimoto, K., Corratgé-Faillie, C., et al. (2011). Calcium-dependent modulation and plasma membrane targeting of the AKT2 potassium channel by the CBL4/CIPK6 calcium sensor/protein kinase complex. *Cell Res.* 21, 1116–1130. doi: 10.1038/cr.2011.50

He, Y., Li, R., Lin, F., Xiong, Y., Wang, L., Wang, B., et al. (2020). Transcriptome changes induced by different potassium levels in banana roots. *Plants* 9, 1–24. doi: 10.3390/plants9010011

Herger, A., Dünser, K., Kleine-Vehn, J., and Ringli, C. (2019). Leucine-rich repeat extensin proteins and their role in cell wall sensing. *Curr. Biol.* 29, R851–R858. doi: 10.1016/j.cub.2019.07.039

Huang, X.-X., Zhao, S.-M., Zhang, Y.-Y., Li, Y.-J., Shen, H.-N., Li, X., et al. (2021). A novel UDP-glycosyltransferase 91C1 confers specific herbicide resistance through detoxification reaction in arabidopsis. *Plant Physiol. Biochem. PPB* 159, 226–233. doi: 10.1016/j.plaphy.2020.12.026

Jeschke, W. D., Kirkby, E. A., Peuke, A. D., Pate, J. S., and Hartung, W. (1997). Effects of p deficiency on assimilation and transport of nitrate and phosphate in intact plants of castor bean (*Ricinus communis l.*). *J. Exp. Bot.* 48, 75–91. doi: 10.1093/jxb/48.1.75

Jukanti, A. K., Gaur, P. M., Gowda, C. L. L., and Chibbar, R. N. (2012). Nutritional quality and health benefits of chickpea (*Cicer arietinum l.*): A review. *Br. J. Nutr.* 108, S11–26. doi: 10.1017/S0007114512000797

Jung, J. Y., Shin, R., and Schachtman, D. P. (2009). Ethylene mediates response and tolerance to potassium deprivation in arabidopsis. *Plant Cell* 21, 607–621. doi: 10.1105/tpc.108.063099

Kaashyap, M., Ford, R., Kudapa, H., Jain, M., Edwards, D., Varshney, R., et al. (2018). Differential regulation of genes involved in root morphogenesis and cell wall modification is associated with salinity tolerance in chickpea. *Sci. Rep.* 8, 4855. doi: 10.1038/s41598-018-23116-9

Kamali, S., and Singh, A. (2022). Jasmonates as emerging regulators of plants response to variable nutrient environment. *CRC. Crit. Rev. Plant Sci.* 41, 271–285. doi: 10.1080/07352689.2022.2109866

Kim, D., Paggi, J. M., Park, C., Bennett, C., and Salzberg, S. L. (2019). Graph-based genome alignment and genotyping with HISAT2 and HISAT-genotype. *Nat. Biotechnol.* 37, 907–915. doi: 10.1038/s41587-019-0201-4

Kim, M. J., Ruzicka, D., Shin, R., and Schachtman, D. P. (2012). The arabidopsis AP2/ERF transcription factor RAP2.11 modulates plant response to low-potassium conditions. *Mol. Plant* 5, 1042–1057. doi: 10.1093/mp/sss003

Kulasekaran, S., Cerezo-Medina, S., Harflett, C., Lomax, C., de Jong, F., Rendour, A., et al. (2021). A willow UDP-glycosyltransferase involved in salicinoid biosynthesis. *J. Exp. Bot.* 72, 1634–1648. doi: 10.1093/jxb/eraa562

Lai, D., Pičmanová, M., Abou Hachem, M., Motawia, M. S., Olsen, C. E., Møller, B. L., et al. (2015). Lotus japonicus flowers are defended by a cyanogenic β-glucosidase with highly restricted expression to essential reproductive organs. *Plant Mol. Biol.* 89, 21–34. doi: 10.1007/s11103-015-0348-4

Lee, D. K., Ahn, J. H., Song, S. K., Choi, Y. D., and Lee, J. S. (2003). Expression of an expansin gene is correlated with root elongation in soybean. *Plant Physiol.* 131 (3), 985–997. doi: 10.1104/pp.009902

Lee, S. C., Lan, W.-Z., Kim, B.-G., Li, L., Cheong, Y. H., Pandey, G. K., et al. (2007). A protein phosphorylation/dephosphorylation network regulates a plant potassium channel. *Proc. Natl. Acad. Sci.* 104, 15959–15964. doi: 10.1073/pnas.0707912104

Lefoulon, C., Boeglin, M., Moreau, B., Véry, A.-A., Szponarski, W., Dauzat, M., et al. (2016). The arabidopsis AtPP2CA protein phosphatase inhibits the GORK k^+ efflux channel and exerts a dominant suppressive effect on phosphomimetic-activating mutations. *J. Biol. Chem.* 291, 6521–6533. doi: 10.1074/jbc.M115.711309

Li, G., Wu, Y., Liu, G., Xiao, X., Wang, P., Gao, T., et al. (2017). Large-Scale proteomics combined with transgenic experiments demonstrates an important role of jasmonic acid in potassium deficiency response in wheat and rice. *Mol. Cell. Proteomics* 16, 1889–1905. doi: 10.1074/mcp.RA117.000032

Li, H., Yu, M., Du, X.-Q., Wang, Z.-F., Wu, W.-H., Quintero, F. J., et al. (2017). NRT1.5/NPF7.3 functions as a proton-coupled H^+/K^+ antiporter for k^+ loading into the xylem in arabidopsis. *Plant Cell* 29, 2016–2026. doi: 10.1105/tpc.16.00972

Luan, M., Tang, R. J., Tang, Y., Tian, W., Hou, C., Zhao, F., et al. (2017). Transport and homeostasis of potassium and phosphate: Limiting factors for sustainable crop production. *J. Exp. Bot.* 68, 3091–3105. doi: 10.1093/jxb/erw444

Maathuis, F. J. (2009). Physiological functions of mineral macronutrients. *Curr. Opin. Plant Biol.* 12, 250–258. doi: 10.1016/j.pbi.2009.04.003

Marschner, H. (1995). *Mineral nutrition of higher plants. 2nd ed.* (London: Academic Press, Elsevier), 889.

Mateo-Bonmatí, E., Casanova-Sáez, R., Šimura, J., and Ljung, K. (2021). Broadening the roles of UDP-glycosyltransferases in auxin homeostasis and plant development. *New Phytol.* 232, 642–654. doi: 10.1111/nph.17633

Ma, T.-L., Wu, W.-H., and Wang, Y. (2012). Transcriptome analysis of rice root responses to potassium deficiency. *BMC Plant Biol.* 12, 161. doi: 10.1186/1471-2229-12-161

Mengel, K., Kirkby, E. A., Kosegarten, H., and Appel, T. (2001). "Potassium," in *Principles of plant nutrition*. Eds. K. Mengel, E. A. Kirkby, H. Kosegarten and T. Appel (Dordrecht: Springer Netherlands), 481–511. doi: 10.1007/978-94-010-1009-2_10

Merga, B., and Haji, J. (2019). *Economic importance of chickpea: Production, value, and world trade. Cogent Food Agric.* 5, 1. doi: 10.1080/23311932.2019.1615718

Mittler, R. (2017). ROS are good. *Trends Plant Sci.* 22, 11–19. doi: 10.1016/j.tplants.2016.08.002

Muday, G. K., Rahman, A., and Binder, B. M. (2012). Auxin and ethylene: collaborators or competitors? *Trends Plant Sci.* 17, 181–195. doi: 10.1016/j.tplants.2012.02.001

Nasr Esfahani, M., Inoue, K., Nguyen, K. H., Chu, H. D., Watanabe, Y., Kanatani, A., et al. (2021). Phosphate or nitrate imbalance induces stronger molecular responses than combined nutrient deprivation in roots and leaves of chickpea plants. *Plant Cell Environ.* 44, 574–597. doi: 10.1111/pce.13935

Nieves-Cordones, M., Ródenas, R., Lara, A., Martínez, V., and Rubio, F. (2019). The combination of k^+ deficiency with other environmental stresses: What is the outcome? *Physiol. Plant* 165, 264–276. doi: 10.1111/ppl.12827

Omondi, J. O., Lazarovitch, N., Rachmilevitch, S., Kukew, T., Yermiyahu, U., and Yasuor, H. (2020). Potassium and storage root development: focusing on photosynthesis, metabolites and soluble carbohydrates in cassava. *Physiol. Plant* 169, 169–178. doi: 10.1111/ppl.13060

Pandey, G. K., Cheong, Y. H., Kim, B.-G., Grant, J. J., Li, L., and Luan, S. (2007). CIPK9: a calcium sensor-interacting protein kinase required for low-potassium tolerance in arabidopsis. *Cell Res.* 17, 411–421. doi: 10.1038/cr.2007.39

Pertea, M., Kim, D., Pertea, G. M., Leek, J. T., and Salzberg, S. L. (2016). Transcript-level expression analysis of RNA-seq experiments with HISAT, StringTie and ballgown. *Nat. Protoc.* 11, 1650–1667. doi: 10.1038/nprot.2016.095

Pertea, M., Pertea, G. M., Antonescu, C. M., Chang, T.-C., Mendell, J. T., and Salzberg, S. L. (2015). StringTie enables improved reconstruction of a transcriptome from RNA-seq reads. *Nat. Biotechnol.* 33, 290–295. doi: 10.1038/nbt.3122

Quinet, M., Vromman, D., Clippe, A., Bertin, P., Lequeux, H., Dufey, I., et al. (2012). Combined transcriptomic and physiological approaches reveal strong differences between short- and long-term response of rice (*Oryza sativa*) to iron toxicity. *Plant Cell Environ.* 35, 1837–1859. doi: 10.1111/j.1365-3040.2012.02521.x

Ragel, P., Raddatz, N., Leidi, E. O., Quintero, F. J., and Pardo, J. M. (2019). Regulation of k^+ nutrition in plants. *Front. Plant Sci.* 10, 281. doi: 10.3389/fpls.2019.00281

Rajappa, S., Krishnamurthy, P., and Kumar, P. P. (2020). Regulation of AtKUP2 expression by bHLH and WRKY transcription factors helps to confer increased salt tolerance to *Arabidopsis thaliana* plants. *Front. Plant Sci.* 11. doi: 10.3389/fpls.2020.01311

Ren, H., and Gray, W. M. (2015). SAUR proteins as effectors of hormonal and environmental signals in plant growth. *Mol. Plant* 8, 1153–1164. doi: 10.1016/j.molp.2015.05.003

Römheld, V., and Kirkby, E. A. (2010). Research on potassium in agriculture: Needs and prospects. *Plant Soil* 335, 155–180. doi: 10.1007/s11104-010-0520-1

Ruan, L., Zhang, J., Xin, X., Zhang, C., Ma, D., Chen, L., et al. (2015). Comparative analysis of potassium deficiency-responsive transcriptomes in low potassium susceptible and tolerant wheat (*Triticum aestivum l.*). *Sci. Rep.* 5, 10090. doi: 10.1038/srep10090

Ruffel, S. (2018). Nutrient-related long-distance signals: Common players and possible cross-talk. *Plant Cell Physiol.* 59, 1723–1732. doi: 10.1093/pcp/pcy152

Sagar, S., Biswas, D. K., and Singh, A. (2020). Genomic and expression analysis indicate the involvement of phospholipase C family in abiotic stress signaling in chickpea (*Cicer arietinum*). *Gene* 753, 144797. doi: 10.1016/j.gene.2020.144797

Sagar, S., Deepika,, Biswas, D. K., Chandrasekar, R., and Singh, A. (2021). Genome-wide identification, structure analysis and expression profiling of phospholipases d under hormone and abiotic stress treatment in chickpea (*Cicer arietinum*). *Int. J. Biol. Macromol.* 169, 264–273. doi: 10.1016/j.ijbiomac.2020.12.102

Sagi, M., and Fluhr, R. (2006). Production of reactive oxygen species by plant NADPH oxidases. *Plant Physiol.* 141, 336–340. doi: 10.1104/pp.106.078089

Samuilov, S., Rademacher, N., Brilhaus, D., Flachbart, S., Arab, L., Kopriva, S., et al. (2018). Knock-down of the phosphoserine phosphatase gene effects rather n-than s-metabolism in *Arabidopsis thaliana*. *Front. Plant Sci.* 9. doi: 10.3389/fpls.2018.01830

Schachtman, D. P. (2015). The role of ethylene in plant responses to k^+ deficiency. *Front. Plant Sci.* 6. doi: 10.3389/fpls.2015.01153

Shabala, S., and Pottosin, I. (2014). Regulation of potassium transport in plants under hostile conditions: Implications for abiotic and biotic stress tolerance. *Physiol. Plant.* 151, 257–279. doi: 10.1111/ppl.12165

Shankar, A., Singh, A., Kanwar, P., Srivastava, A. K., Pandey, A., Suprasanna, P., et al. (2013). Gene expression analysis of rice seedling under potassium deprivation reveals major changes in metabolism and signaling components. *PloS One* 8, 18–21. doi: 10.1371/journal.pone.0070321

Sharma, P., Jha, A. B., Dubey, R. S., and Pessarakli, M. (2012). Reactive oxygen species, oxidative damage, and antioxidative defense mechanism in plants under stressful conditions. *J. Bot.* 2012, 217037. doi: 10.1155/2012/217037

Shen, C., Wang, J., Shi, X., Kang, Y., Xie, C., Peng, L., et al. (2017). Transcriptome analysis of differentially expressed genes induced by low and high potassium levels provides insight into fruit sugar metabolism of pear. *Front. Plant Sci.* 8. doi: 10.3389/fpls.2017.00938

Shi, X., Long, Y., He, F., Zhang, C., Wang, R., Zhang, T., et al. (2018). The fungal pathogen *Magnaporthe oryzae* suppresses innate immunity by modulating a host potassium channel. *PloS Pathog.* 14, 1–21. doi: 10.1371/journal.ppat.1006878

Shin, R., Burch, A. Y., Huppert, K. A., Tiwari, S. B., Murphy, A. S., Guilfoyle, T. J., et al. (2007). The arabidopsis transcription factor MYB77 modulates auxin signal transduction. *Plant Cell* 19, 2440–2453. doi: 10.1105/tpc.107.050963

Singh, A., Jha, S. K., Bagri, J., and Pandey, G. K. (2015). ABA inducible rice protein phosphatase 2C confers ABA insensitivity and abiotic stress tolerance in arabidopsis. *PloS One* 10, e0125168. doi: 10.1371/journal.pone.0125168

Singh, A., and Pandey, G. K. (2015). Primer design using primer express® for SYBR green-based quantitative PCR. *Methods Mol. Biol.* 1275, 153–164. doi: 10.1007/978-1-4939-2365-6_11

Singh, A., Pandey, A., Srivastava, A. K., Tran, L. S., and Pandey, G. K. (2016). Plant protein phosphatases 2C: from genomic diversity to functional multiplicity and importance in stress management. *Crit. Rev. Biotechnol.* 36, 1023–1035. doi: 10.3109/07388551.2015.1083941

Singh, A., Yadav, A. K., Kaur, K., Sanyal, S. K., Jha, S. K., Fernandes, J. L., et al. (2018). A protein phosphatase 2C, AP2C1, interacts with and negatively regulates the function of CIPK9 under potassium-deficient conditions in arabidopsis. *J. Exp. Bot.* 69, 4003–4015. doi: 10.1093/jxb/ery182

Stein, O., and Granot, D. (2019). An overview of sucrose synthases in plants. *Front. Plant Sci.* 10. doi: 10.3389/fpls.2019.00095

Tamoi, M., Nagaoka, M., Miyagawa, Y., and Shigeoka, S. (2006). Contribution of fructose-1,6-bisphosphatase and sedoheptulose-1,7-bisphosphatase to the photosynthetic rate and carbon flow in the Calvin cycle in transgenic plants. *Plant Cell Physiol.* 47, 380–390. doi: 10.1093/pcp/pcj004

Tang, R.-J., Zhao, F.-G., Yang, Y., Wang, C., Li, K., Kleist, T. J., et al. (2020). A calcium signalling network activates vacuolar k^+ remobilization to enable plant adaptation to low-K environments. *Nat. Plants* 6, 384–393. doi: 10.1038/s41477-020-0621-7

Tian, X.-l., Wang, G.-W., Zhu, R., Yang, P.-Z., Duan, L.-S., and Li, Z.-H. (2008). Conditions and indicators for screening cotton (*Gossypium hirsutum l.*) varieties tolerant to low potassium. *Acta Agron. Sin.* 34, 1435–1443. doi: 10.1016/S1875-2780(08)60050-4

Varshney, R. K., Song, C., Saxena, R. K., Azam, S., Yu, S., Sharpe, A. G., et al. (2013). Draft genome sequence of chickpea (*Cicer arietinum*) provides a resource for trait improvement. *Nat. Biotechnol.* 31, 240–246. doi: 10.1038/nbt.2491

Vellosillo, T., Vicente, J., Kulasekaran, S., Hamberg, M., and Castresana, C. (2010). Emerging complexity in reactive oxygen species production and signaling during the response of plants to pathogens. *Plant Physiol.* 154, 444–448. doi: 10.1104/pp.110.161273

Vitting-Seerup, K., and Sandelin, A. (2019). IsoformSwitchAnalyzeR: analysis of changes in genome-wide patterns of alternative splicing and its functional consequences. *Bioinformatics* 35, 4469–4471. doi: 10.1093/bioinformatics/btz247

Walker, D. J., Leigh, R. A., and Miller, A. J. (1996). Potassium homeostasis in vacuolate plant cells. *Proc. Natl. Acad. Sci. U. S. A.* 93, 10510–10514. doi: 10.1073/pnas.93.19.10510

Wang, F., Tan, W.-F., Song, W., Yang, S.-T., and Qiao, S. (2022). Transcriptome analysis of sweet potato responses to potassium deficiency. *BMC Genomics* 23, 655. doi: 10.1186/s12864-022-08870-5

Wang, Y., and Wu, W. H. (2013). Potassium transport and signaling in higher plants. *Annu. Rev. Plant Biol.* 64, 451–476. doi: 10.1146/annurev-arplant-050312-120153

Wei, Z., and Li, J. (2016). Brassinosteroids regulate root growth, development, and symbiosis. *Mol. Plant* 9, 86–100. doi: 10.1016/j.molp.2015.12.003

Wu, J., Zhang, X., Li, T., Yu, H., and Huan, P. (2011). Differences in the efficiency of potassium (K^+) uptake and use in barley varieties. *Agric. Sci. China* 10, 101–108. doi: 10.1016/S1671-2927(11)60312-X

Yadav, B. K., and Sidhu, A. S. (2016). "Dynamics of potassium and their bioavailability for plant nutrition," in *Potassium solubilizing microorganisms for sustainable agriculture*. Eds. V. S. Meena, B. R. Maurya, J. P. Verma and R. S. Meena (New Delhi: Springer India), 187–201. doi: 10.1007/978-81-322-2776-2_14

Yamada, M., Han, X., and Benfey, P. N. (2020). RGF1 controls root meristem size through ROS signalling. *Nature* 577, 85–88. doi: 10.1038/s41586-019-1819-6

Yang, H., Li, Y., Jin, Y., Kan, L., Shen, C., Malladi, A., et al. (2020). Transcriptome analysis of *pyrus betulaefolia* seedling root responses to short-term potassium deficiency. *Int. J. Mol. Sci.* 21, 1–17. doi: 10.3390/ijms21228857

Yang, D., Li, F., Yi, F., Eneji, A. E., Tian, X., and Li, Z. (2021). Transcriptome analysis unravels key factors involved in response to potassium deficiency and feedback regulation of k^+ uptake in cotton roots. *Int. J. Mol. Sci.* 22, 3133. doi: 10.3390/ijms22063133

Zhang, X., Jiang, H., Wang, H., Cui, J., Wang, J., Hu, J., et al. (2017). Transcriptome analysis of rice seedling roots in response to potassium deficiency. *Sci. Rep.* 7, 5523. doi: 10.1038/s41598-017-05887-9

Zhao, X., Liu, Y., Liu, X., and Jiang, J. (2018). Comparative transcriptome profiling of two tomato genotypes in response to potassium-deficiency stress. *Int. J. Mol. Sci*. 19 (8), 2402. doi: 10.3390/ijms19082402

Zhao, Y., Sun, R., Liu, H., Liu, X., Xu, K., Xiao, K., et al. (2020). Multi-omics analyses reveal the molecular mechanisms underlying the adaptation of wheat (*Triticum aestivum l.*) to potassium deprivation. *Front. Plant Sci.* 11. doi: 10.3389/fpls.2020.588994

Zhao, S., Zhang, M.-L., Ma, T.-L., and Wang, Y. (2016). Phosphorylation of ARF2 relieves its repression of transcription of the k^+ transporter gene HAK5 in response to low potassium stress. *Plant Cell* 28, 3005–3019. doi: 10.1105/tpc.16.00684

frontiers | Frontiers in Plant Science

TYPE Original Research
PUBLISHED 30 January 2023
DOI 10.3389/fpls.2023.1107970

OPEN ACCESS

EDITED BY
Ravi Gupta,
Kookmin University, Republic of Korea

REVIEWED BY
Kaiyang Zhong,
Southwestern University of Finance and Economics, China
Decai Tang,
Nanjing University of Information Science and Technology, China
Jialu You,
Shanghai University of Finance and Economics, China

*CORRESPONDENCE
Qingning Lin
linqingning@caas.cn

SPECIALTY SECTION
This article was submitted to Crop and Product Physiology, a section of the journal Frontiers in Plant Science

RECEIVED 25 November 2022
ACCEPTED 03 January 2023
PUBLISHED 30 January 2023

CITATION
Li J and Lin Q (2023) Threshold effects of green technology application on sustainable grain production: Evidence from China.
Front. Plant Sci. 14:1107970.
doi: 10.3389/fpls.2023.1107970

Threshold effects of green technology application on sustainable grain production: Evidence from China

Jingdong Li[1,2] and Qingning Lin[3]*

[1]Institute of Geographic Sciences and Natural Resources Research, Chinese Academy of Sciences, Beijing, China, [2]Key Laboratory of Regional Sustainable Development Modeling, Chinese Academy of Sciences, Beijing, China, [3]Institute of Agricultural Economics and Development, Chinese Academy of Agricultural Sciences, Beijing, China

Sustainable production is considered as an important approach to solve the dilemma of food insecurity. Green technologies have made contributions to improving food production and reducing environmental pollution. Studying the effects of green technologies on sustainable food production has great significance. The paper started with the influence mechanism of green technology application on the green total factor productivity of grain (GTFPG). With the GTFPG, green technology efficiency change of grain (GECG) and green technical progress change of grain (GTCG) measured, threshold models were constructed to explore the nonlinear impacts of various green technologies on GTFPG and the influence paths. Results indicated that the differences of GTFPG among provinces in China were decreased mainly due to the changes of GTCG, while the regional differences of GECG remained small. The impacts of green technologies had threshold effects that depended on the ecological effects of green technologies in different application stages, and were significantly different in the major and non-major grain producing areas. Meanwhile, significant differences existed in the influence paths of green technologies. In the major grain producing areas, green technologies were more likely to improve GTFPG through the GTCG path; while in the non-major grain producing areas, the GECG path and the GTCG path were both important to improve GTFPG. The differences of green technologies' threshold effects and influence paths in the major and non-major grain producing areas were caused by regional technology preference, resource endowment and technology compatibility. This study emphasizes that the development of green technologies should fully consider the resource endowment and economic development of different regions, as well as the applicability and adoption rate of green technologies.

KEYWORDS

green technology, grain production, green total factor productivity, influence mechanism, threshold effects

1 Introduction

Sustainable food security has been the foundation for global economic and social development. From Millennium Development Goals (MDGs) proposed by the United Nations to Sustainable Development Goals (SDGs), the focus of food security has shifted from extreme poverty and hunger to food security and nutrition improvement within the framework of sustainable agriculture (UN, 2001; UN, 2015; Clapp et al., 2022). However, shocks from pandemics, conflicts, natural disasters, climate change, and energy crisis have intensified the risk of global food insecurity (FSIN, 2022; Li and Song, 2022), further frustrating the progress of SDGs 1 and SDGs 2 (FAO et al., 2022).

In the complex natural, economic and social environment, sustainable production is considered as an important way out of food insecurity dilemma (Rahman et al., 2021; ECOSOC, 2022). Extensive management of traditional agriculture features high resource input and high energy consumption (Jin et al., 2012; Nagothu, 2018). Its pursuit of maximized output has brought about resource waste, land overdraft, non-point source pollution, greenhouse gas emissions, etc. (Shen et al., 2018; Li and Lin, 2022), especially in Asia, where extensive agricultural production mode is expected to increase greenhouse gas emissions by 37% in 2050 (Frank et al., 2019). Sustainable agriculture highlights the use of advanced technologies and management to ensure the quality of agricultural products and ecological security, and improve comprehensive economic benefits (Liu et al., 2020; Guo et al., 2022a). It takes into accounts economy, society and environment (Elkington, 1994; Purvis et al., 2019), and strikes a balance between agricultural development and environmental sustainability (Shah et al., 2021).

With the wide application of total factor productivity analysis in agricultural development (Liu and Feng, 2019), especially the proposal of green total factor productivity (GTFP), researchers can better measure and study sustainable development of agriculture (Chen et al., 2021). GTFP is also regarded as an ideal indicator for studying sustainable development of agriculture (Chen et al., 2021; Liu et al., 2022). GTFP takes the negative impact of agricultural production on the environment as an undesirable output (Tugcu and Tiwari, 2016; Yu et al., 2022), and incorporates it into the calculation framework. Stochastic Frontier Analysis (SFA) and Data Envelopment Analysis (DEA) are the main methods to measure GTFP (Tang et al., 2017; Shi and Li, 2019; Baležentis et al., 2021). DEA does not rely on the form of production function, and can be adapted to the efficiency calculation of complex systems with multiple input and output variables (Johnes, 2015; Song et al., 2018; He et al., 2021). Considering the diversity of factor inputs and undesirable outputs in agricultural production, DEA method is more suitable for measuring GTFP (Liu and Feng, 2019).

As to the improvement of GTFP, current research mostly discusses it from the perspective of output side and input side. The first is to increase agricultural output and reduce undesirable output at the output end. For example, relevant studies believe that environmental regulation can reduce unexpected output, thereby improving green production efficiency (Xie et al., 2017; Tang et al., 2022). The second is to reduce the use of pollutants at the input side and improve the utilization efficiency of energy chemicals. The innovation of physicochemical technology can improve the utilization efficiency of input factors such as chemical fertilizers and pesticides (Wang et al., 2021a). The promotion of green technologies (or clean technologies) can optimize the allocation of production factors, reduce the use of pollutants such as chemical fertilizers and pesticides, and effectively improve the conversion efficiency of energy chemicals (Midingoyi et al., 2018; Eanes et al., 2019). In sustainable agriculture practice, improvement of agricultural production efficiency through green technologies has drawn much attention (Shah et al., 2021; Rahman et al., 2021). Green technologies are involved in all sectors of grain production, processing, storage and transportation (MARAPRC, 2018). Among them, green technologies in the production link include that in plowing, sowing, fertilization, irrigation, etc. (Midingoyi et al., 2018; He et al., 2021; Mao et al., 2021; Zhao et al., 2021). These green technologies have played a significant role in improving grain production and reducing greenhouse gas emissions and non-point source pollution (Zhuang et al., 2019; Zhu et al., 2021; Chen et al., 2022).

With the greatest population, China has made remarkable progress in the continuous improvement of agricultural production value and grain output (Liu and Feng, 2019), achieving food security for 18% of the world's population with only 9% of the world's arable land and 6% of the world's water resources (Wang et al., 2018). With the increasing pressures of population growth, resource shortage, carbon emissions and environmental destruction, the green production of grain has been an important approach to achieve sustainable food security in China (Rahman et al., 2021; ECOSOC, 2022). However, literatures on the green production of grain are still relatively insufficient, especially in green productivity estimation and its influencing factors. The existing researches showed that China's green productivity of grain shows a trend of fluctuating growth (Xue and Gu, 2022), which was affected by agricultural labor force, technological innovation, storage policy and other factors (Wang and Yang, 2020; Gao, 2022; Li and Lin, 2022). Nevertheless, China's agriculture is dominated by extensive management, and agricultural development and food security are achieved at the cost of high energy consumption and serious environmental pollution (Yang et al., 2018). Compared with the mechanized production and industrialized operation in developed countries such as the United States, China's grain production features small-scale farmers (Guo et al., 2022b), a lower degree of mechanization (Qiu and Luo, 2021), and large gap in relevant technical level and management experience with those countries (Si et al., 2021). This leads to the negative impact of China's agricultural mechanization on energy-environment efficiency (Jiang et al., 2020). There is a long-term correspondence between the improvement of agricultural mechanization and increase of energy consumption and carbon emissions (Fabiani et al., 2020), the application of green technologies in agricultural mechanized production is of great significance for improving GTFP (Li et al., 2020; He et al., 2021).

Actually, the impacts of technology application on GTFP are nonlinear (Luan et al., 2019; He et al., 2021). Due to the lag effect of technology application (Mao et al., 2021), green technologies can only play a role in increasing production, improving environment and reducing pollution after a period of application (Huisingh et al., 2015; Chen et al., 2017; Gao et al., 2018).When machinery and energy are overused, the continuous application of green technology will also lead to low productivity and increased carbon emissions (Silva-Olaya et al., 2013; Zhao et al., 2018; Min et al., 2021), that is, the impacts of

green technology application on GTFP has a threshold effect. As an important part of agricultural modernization (Houssou et al., 2013), mechanization has made great contributions to China's food security (Min et al., 2021; Yang et al., 2022a). The application of green technologies in agricultural mechanization also has threshold restrictions. Appropriate application conditions and adoption rates will promote green production (Zhang et al., 2020; He et al., 2021), while inappropriate conditions and excessive application will also have negative impacts on the environment (Min et al., 2021; He et al., 2021). Therefore, studying the threshold impacts of green technologies on grain green productivity in agricultural mechanization has great significance (He et al., 2021), which is very scarce and necessary.

The main contributions of this paper are as follows: according to the difference of ecological effects, the application of green technology was divided into the initial development stage, the ecological efficiency stage and the overuse stage, so as to build a mechanism framework of the nonlinear effects of green technology application on the green total factor productivity of grain (GTFPG); it took carbon emissions and non-point source pollution as undesirable output, and used the Super Epsilon Based Measure (Super-EBM) model and the Global Malmquist Lunberger (GML) productivity index to calculate the GTFPG, the green technology efficiency change of grain (GECG) and the green technical progress change of grain (GTCG); the correlations between GTFPG and green technologies were analyzed with pattern evolution, kernel density curve and box plot; by matching the ecological effects of green technologies in different application stages with their threshold results, we could better comprehend the nonlinear effects of green technologies on GTFPG; besides, the paper investigated the different influence paths of various green technologies on GTFPG in the major and non-major grain producing areas, and revealed that regional technology preference, resource endowment and technology compatibility diversified the influence paths of green technologies. The paper highlights the threshold effect of green technology application on GTFPG. Therefore, the development of green technologies should take into full account the productivity, resource endowment of different regions, and applicability of green technologies. Adoption rate of green technologies should be reasonably controlled. It is hoped that this paper will provide theoretical basis and practical experience for sustainable development of grain in China.

2 Materials and methods

2.1 Green total factor productivity and its decomposition

GTFP has been widely used as an ideal index to measure agricultural green development (Chen et al., 2021; Chen et al., 2021; Liu et al., 2022). To calculate GTFP, first green production efficiency is obtained through DEA, and then GTFP and its decomposition (GECG and GTCG) are obtained through GML productivity index.

2.1.1 Green productivity

The production frontier function of DEA model may be parallel to the coordinate axis, resulting in disparities between the DMU falling on these parallel functions and the strong effective target value, including the Proportionate Movement part and the Slack Movement part. However, the radial DEA model can only solve the Proportionate Movement part, which leads to the deviation of the efficiency measurement value. Therefore, the non-radial DEA model can fully consider the Slack Movement part, realize the compatibility of the Proportionate Movement part and the Slack Movement part, and ensure the original information of the efficiency frontier's projection values (Cheng, 2014). Therefore, the paper chooses the Epsilon Based Measure (EBM) model constructed by Tone and Tsutsui (2010) to measure green productivity. Meanwhile, in order to distinguish the differences between decision-making units (DMUs) with the same efficiency of 1, the paper finally follows the research methods of Wu et al. (2020) and Zhao et al. (2022), and uses the Super-EBM model to calculate the green productivity of grain. The Super-EBM model can be expressed as:

$$\tilde{E} = \min \left[\frac{\theta - \epsilon_x \sum_{i=1}^{m} \frac{w_i^- s_i^-}{x_{ik}}}{\phi + \epsilon_y \sum_{r=1}^{q} \frac{w_r^{g+} s_r^{g+}}{y_{rk}} + \epsilon_v \sum_{t=1}^{p} \frac{w_t^{b-} s_t^{b-}}{v_{tk}}} \right] \quad (1)$$

$$\begin{cases} \sum_{j=1, j\neq k}^{n} x_{ij}\lambda_j - s_i^- \leq \theta \cdot x_{ik}, \quad i = 1, \ldots, m \\ \sum_{j=1, j\neq k}^{n} y_{rj}\lambda_j - s_r^{g+} \geq \phi \cdot y_{rk}, \quad r = 1, \ldots, q \\ \sum_{j=1, j\neq k}^{n} v_{tj}\lambda_j - s_t^{b-} \leq v_{tk}, \quad t = 1, \ldots, p \\ \lambda \geq 0,\ s^- \geq 0,\ s^{g+} \geq 0,\ S^{b-} \geq 0 \end{cases} \quad (2)$$

where $\tilde{E}$ represents the value of green productivity of grain; x_{ij} is the input variable matrix, with specific indicators including planting area, fertilizer, pesticide, agricultural film, diesel oil, seed, electricity for irrigation, labor and machinery (Liu and Feng, 2019; He et al., 2021; Li and Lin, 2022); y_{rj} represents the desirable output, which is expressed in grain production; v_{tj} represents the undesirable output, including carbon emissions and non-point source pollutions (the measurement of carbon emissions follows the methods of Liu et al., 2013 and Chen et al., 2021; and the measurement of non-point source pollutions follows the methods of Chen et al., 2006 and Zou et al., 2020); s_i^-, s_r^{g+} and s_t^{b-} are slacks of inputs, slacks of desirable outputs and slacks of undesirable outputs respectively; w_i^- , w_r^{g+} and w_t^{b-} represent the relative importance of various input indicators, desirable outputs and undesirable outputs, with $\sum_{i=1}^{m} w_i^- = 1 (w_i^- \geq 0)$, $\sum_{i=1}^{m} w_r^{g+} = 1 (w_r^{g+} \geq 0)$ and $\sum_{i=1}^{m} w_t^{b-} = 1 (w_t^{b-} \geq 0)$; θ represents the efficiency value under input orientation; φ represents the efficiency value under output orientation; ε is the importance of the non-radial part, $\varepsilon \in [0, 1]$.

2.1.2 Global malmquist-luenberger productivity index

In order to better reflect the change state of productivity, this paper measures the green total factor productivity of grain (GTFPG) with the help of the Global Malmquist Lunberger (GML) index proposed by Oh (2010) based on the calculation of green productivity by the Super-EBM model, and decomposes it into the green technology efficiency change of grain (GECG) index and the green technical progress change of grain (GTCG) index, then GTFPG = GECG×GTCG. GTFPG, GECG and GTCG can be expressed as:

$$GECG_{i,t+1} = \frac{1 + E_c^{it}(x^{it}, y^{it}, b^{it})}{1 + E_C^{i,t+1}(x^{i,t+1}, y^{i,t+1}, b^{i,t+1})} \quad (3)$$

$$GTCG_{i,t+1} = \frac{1 + E_C^{i,t+1}(x^{i,t+1}, y^{i,t+1}, b^{i,t+1})}{1 + E_G^{it}(x^{i,t+1}, y^{i,t+1}, b^{i,t+1})} \times \frac{1 + E_G^{it}(x^{it}, y^{it}, b^{it})}{1 + E_C^{it}(x^{it}, y^{it}, b^{it})} \quad (4)$$

$$GTFPG_{i,t+1} = \frac{1 + E_G^{it}(x^{it}, y^{it}, b^{it})}{1 + E_G^{it}(x^{i,t+1}, y^{i,t+1}, b^{i,t+1})} = GEC_{i,t+1} \times GTC_{i,t+1} \quad (5)$$

where the values of GTFPG, GECG and GTCG are greater than 0; when GTFPG > 1, means the GTFPG increases; on the contrary, means the GTFPG decreases. The values of GECG and GTCG have the same meaning.

2.2 Green technologies and the mechanism of their impacts

2.2.1 Selection of green technologies

Based on the research of He et al. (2021) and Zhai et al. (2021), this study selects six green technologies from plowing, sowing, fertilization and irrigation in agricultural mechanized production. They are the mechanical deep-plowing and subsoiling (MDPS) in plowing stage, the precision and small quantity sowing (PSQS) and mechanized no-tillage sowing (MNTS) in sowing stage, the mechanized straw returning(MSRE) and mechanical fertilizer deep distributing (MFDD) in fertilization stage, and the water-saving irrigation (WSIR) in irrigation stage. Application of green technologies requires certain conditions. Suitable conditions and appropriate adoption ratio will promote their ecological effects (Gao et al., 2018; Zhang et al., 2020; He et al., 2021), while mismatched conditions and excessive application will have a negative impact on the environment (Zhao et al., 2018; Wang et al., 2020a; Min et al., 2021; He et al., 2021). The application conditions (Yang et al., 2019; CPGPRC, 2007; Duan et al., 2022a; Yin et al., 2016; Tian et al., 2019; Zhao et al., 2020; Wang, 2021; Chen et al., 2022; Zhuang et al., 2019), ecological effects (CPGPRC, 2007; Shao et al., 2016; Wang et al., 2015; Wang et al., 2020a; Chen et al., 2020; Karayel, 2009; Li et al.,2015; Chaudhary et al., 2021; Keshavarz Afshar and Dekamin, 2022; Zhang et al., 2022; Sun et al., 2018; Hu et al., 2022; Zhu et al., 2021; Zhong et al., 2021; Wu et al., 2021; Gaihre et al., 2015; Miah et al., 2016; Man et al., 2014; Wang et al., 2020b; Zhuang et al., 2019) and negative impacts (Baumhardt et al., 2008; Ding et al., 2018; CPGPRC, 2007; Chen et al., 2022; Rahim et al., 2021; Peixoto et al., 2020; Sun et al., 2022; Pisante et al., 2014; Wang et al., 2021b; Wang et al., 2021a; Li et al., 2018; Hu et al., 2022; Yang et al., 2020; Zhao et al., 2021; Xia et al., 2022; Zhuang et al., 2019; Wang et al., 2022) of each green technology are shown in Table S1.

2.2.2 The influence mechanism of green technology application on GFTPG

Efficient and environment-friendly, green technologies have a long-term industrial ripple effect on the agricultural sector and have become an important part of the green development platform, affecting people's perception of sustainable development and research on GFTPG (Wang et al., 2021a; Zhu et al., 2021; Chen et al., 2022). This paper decomposes GFTPG into the green technology efficiency change of grain (GECG) and the green technical progress change of grain (GTCG), and discusses the impacts of technology application, as well as platform construction and perception promotion driven by it, on GECG and GTCG respectively. Green technology application is divided into different stages according to its ecological effects, to better understand the influence mechanism of green technologies on GFTPG. The influence mechanism of green technology application on GFTPG is shown in Figure 1.

The impacts of green technology application on GECG. First, in the initial stage of green technology application, the Diseconomies of Scale may lead to the decline of GECG (Zhong et al., 2022). The Diseconomies of Scale is reflected in the increase of average cost and decrease of yield and income, due to the allocation of new equipment, low technical level and lack of management experience (Zhang et al., 2016; Si et al., 2021; Zhong et al., 2022), that is, the Internal Diseconomies of technology application. Secondly, with increasing application rate, green platform is gradually formed (Reza-Gharehbagh et al., 2022), which helps to connect technology developers and users and provide supporting social services, thereby accelerating the application of green technology and reducing cost (Totin et al., 2020), namely the Learning Effects of technology application and the Synergy Effects of green platform. Additionally, the green platform will bring inertia to the application of green technology (Inertial Actions). Combined with the sunk cost and application threshold of new technology (Zhang et al., 2016; Mañez and Love, 2020), it will increase the Path Dependences of green technology application, and aggravate the overuse and mismatch of technologies (Amplification Effects), thereby reducing GECG. Finally, the large-scale application of green technologies has accelerated promotion of green concepts. More subjects have participated in green production, which promotes popularization of green technologies and improvement of regional GECG (Promoting Effects). However, attention should also be paid to the contradiction between standardized machinery and diversified demand in green production, as well as the mismatch between rising technology adoption rate and the level of social services (Zhuang et al., 2019; Wang et al., 2021b; Zhang et al., 2021), all of which will hinder the improvement of GECG.

The impacts of green technology application on GTCG. First, the development and application of green technologies has Spillover Effects (Pan et al., 2021), which is reflected in the fact that the increase of green technology adoption rate in a region will promote the development of related technologies in its surrounding areas, and can trigger the Facilitation Effects of technology application. However, the Spillover Effects may also lead to overuse of the technology throughout the planting industry. Pursue the growth of green technology adoption rate while ignoring the application threshold and applicable conditions ultimately leads to the grain output decrease and environmental pollution, that is, the External Diseconomies of technology application (Zhong et al., 2022). Secondly, the green platform built for the application of green technology can arouse the enthusiasm of participants (especially the proportion of ordinary farmers), strengthen rural collective action, stimulate the initiative of enterprises in green technology research and development, promote the application and integration of green technology in various production links (Wang et al., 2022), and

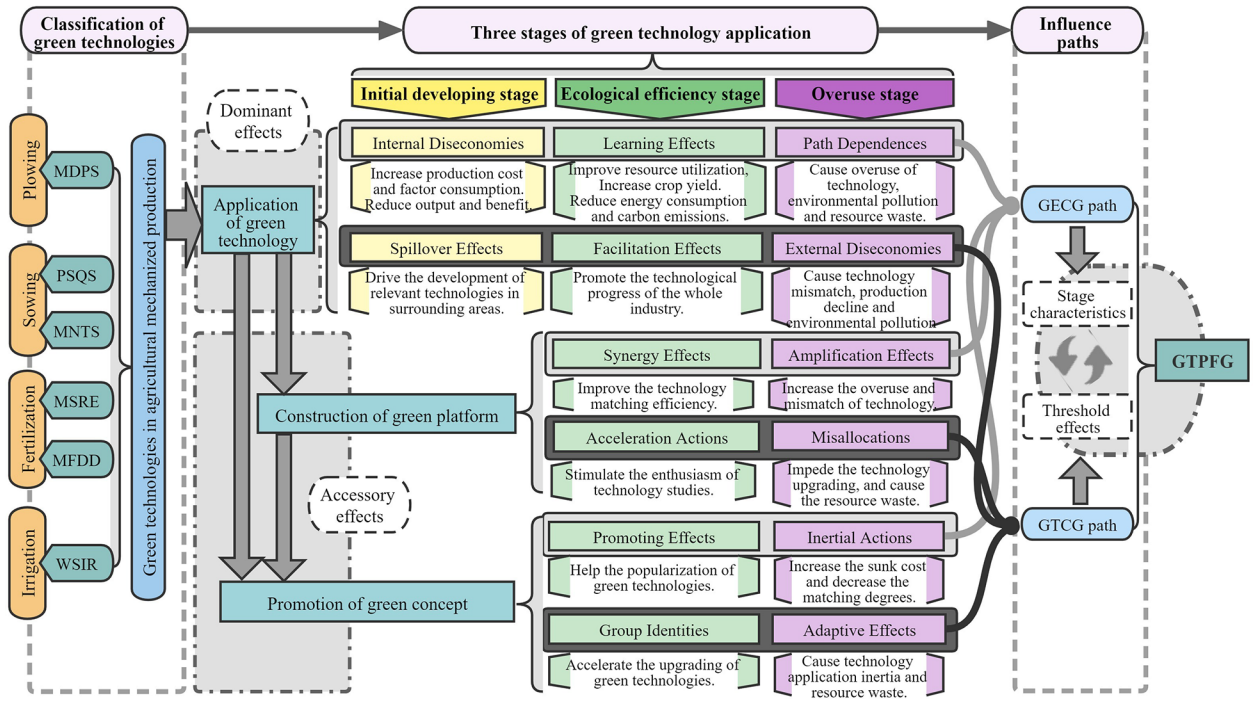

FIGURE 1
The influence mechanism of green technology application on GFTPG.

thus accelerate the development and promotion of new technologies (Acceleration Actions). However, excessive emphasis on the role of green platforms will also lead to resource Misallocations. Finally, the high adoption rate of green technologyies reflects the Group Identities with green development concept, which can effectively promote the upgrading and progress of the overall agricultural green technology, and promote the improvement of GTCG. However, when the concept of green development does not match the actual production, it cannot effectively improve GTCG (Adaptive Effects). For example, when mechanical equipment, operation level, natural conditions and social services cannot support green technology to exert its ecological effect, excessive pursuit of high adoption rate will lead to increase of cost, decrease of benefit and waste of resources (He et al., 2021; Min et al., 2021), which will also lead to External Diseconomies of technology application.

The impacts of green technology adoption on GTFPG. The analysis above shows that the impacts of adoption rate of green technologies on GECG and GTCG has threshold effects, which will also be reflected in the impacts on GTFPG. The threshold effects can be understood as its different impacts on GTFPG at different stages: the initial development stage, ecological efficiency stage and overuse stage. Specifically, in the initial developing stage, the application of green technologies is in the experimental and demonstration period. Construction of green platforms and promotion of green concepts just get started. Supporting machinery, technology, management and social services are at a low level. The resulting Diseconomies of Scale (Internal and External Diseconomies) hinder the improvement of GTFPG. In the ecological efficiency stage, technology, machinery configuration and management are improved. Green platforms are enhanced, green concept is widely recognized, and rural collective action is further strengthened. The marginal cost of production is reduced, and resource allocation is more reasonable. Green technology is upgraded and promoted faster, and starts to exhibit its ecological effect, thus effectively improving GTFPG. During the overuse stage of green technologies, due to the high level of green technology application, platform construction and concept identity in the area with high green technology adoption rate, and the sunk cost of technology application decision, Path Dependences may occur, which hinders the upgrading and improvement of green technologies. Meanwhile, ignoring the improvement of quality and efficiency of traditional agricultural technology, as well as the resource allocation in areas where green technology is not applicable, may also cause resource Misallocations, and lead to Diseconomies of Scale (Internal and External Diseconomies), which hinders the improvement of GTFPG. Due to the differences in application conditions, applicability and negative effects of various green technologies, theirs impacts on GTFPG have different threshold effects.

2.3 Model construction and data sources

2.3.1 Threshold model

Considering that the effects of green technology application have hysteresis (Chen et al., 2017; Gao et al., 2018; Mao et al., 2021), and require appropriate application conditions and proportions (Zhang et al., 2020; Min et al., 2021), otherwise it will have negative impacts on the environment (Wang et al., 2020a; He et al., 2021), thus, there are threshold effects of green technology on GTFPG. This paper refers to the threshold model proposed by Hansen (1999) to explore the nonlinear effects of green technology application on GTFPG. The single-threshold model can be expressed as:

$$y_{it} = \alpha_i + \beta_1 X_{it} I(thre_{it} \le \gamma) + \beta_2 X_{it} I(thre_{it} > \gamma) + \epsilon_{it} \quad (6)$$

where X_{it} represents the set of explanatory variables; β_1 and β_2 are coefficient estimates; $thre_{it}$ represents the threshold variable (which can be a part of X_{it}), and γ is the threshold value; $I(*)$ is the indicating function, when the inequality in brackets is ture, $I(*)=1$, otherwise, $I(*)=0$.

The double-threshold model can be expressed as:

$$y_{it} = \alpha_i' + \beta_1' X_{it} I(thre_{it}' \le \gamma_1) + \beta_2' X_{it} I(\gamma_1 < thre_{it}' \le \gamma_2) + \beta_3' X_{it} I(thre_{it}' > \gamma_2) + \epsilon_{it} \quad (7)$$

where β_1', $\beta_2'$and β_3' are coefficient estimates; $thre_{it}'$ represents the threshold variable, γ_1 and γ_2 represent two threshold values.

2.3.2 Control variables selection

Considering that the GTFPG is affected by various factors, in order to remove the interference of other factors on green technology, this paper uses the research approaches of Xu et al. (2020); He et al. (2021); Yang et al. (2022b), and Li and Lin (2022) selects control variables from production condition, production decision, agglomeration capacity, financial support, economic development and natural disaster. Production condition increases the marginal desirable output or reduce the undesirable output by matching with the productivity level (Jiang et al., 2020; Li and Lin, 2022), and agricultural mechanization level and irrigation level are selected as proxy variables; production decision affects productivity by changing the proportion of production elements and production scales (Jiang et al., 2020; Liu et al., 2020; Li et al., 2020), and planting structure and rural income level are selected as proxy variables; agglomeration capacity improves resource utilization efficiency through knowledge spillover and energy structure optimization (Li and Lin, 2022; Yang et al., 2022b), and grain production agglomeration is selected as the proxy variable; financial expenditure affects productivity by improving production input, management level and service quality (Chen et al., 2021; He et al., 2021), and agricultural fiscal level and agricultural investment level are selected as proxy variables; economic development improves green productivity by influencing the adoption of green technologies and environmental awareness (Xu et al., 2020; Liu et al., 2022), and urbanization level and trade dependence level are selected as proxy variables; natural disasters have directly led to the decline of grain output and the increase of energy and chemical products input (Chen et al., 2021; He et al., 2021; Liu et al., 2022), and disaster incidence level, temperature fluctuation level and precipitation fluctuation level are selected as proxy variables. The specific calculation method of each control variable is shown in Table S2.

2.3.3 Data sources

The paper selects rice, wheat and maize as the representative varieties of grain. In 2020, the total output of rice, wheat and maize was 606.7786 million tons, accounting for 90.633% of the total grain output, so it can substitute for grain crops for research. Limited by the availability of green technology data, the sample period selected in this paper is from 2000 to 2020. Tianjin, Hebei, Shanxi, Inner Mongolia, Liaoning, Jilin, Heilongjiang, Jiangsu, Zhejiang, Anhui, Fujian, Jiangxi, Shandong, Henan, Hubei, Hunan, Guangdong, Guangxi, Hainan, Sichuan, Guizhou, Yunnan, Shaanxi, Gansu, Qinghai, Ningxia and Xinjiang are selected as the research areas. In 2020, the staple food (rice, wheat and maize) output of these 27 provinces was 582.442 million tons, accounting for 95.989% of China's total staple grain output, so the samples are highly representative. Additionally, Chinese government set up major grain producing areas, funds, technology, talent flew to these areas and promoted the annual growth of grain production (Yang et al., 2021; Li and Lin, 2022). Therefore, it is necessary to examine the changes of green total factor productivity of grain in the major grain producing areas and non-major grain producing areas respectively (He et al., 2021). The major grain producing areas were divided according to the definition of SCPRC (2017). The distribution of these areas is shown in Figure 2.

The data of green technologies comes from the China Agricultural Machinery Industry Yearbook; the data of staple grain production and planting area are from the National Bureau of Statistics of China; the input data in the grain production process are from the Ministry of Agriculture and Rural Affairs of China, the China Rural Statistical Yearbooks and the provincial Statistical Yearbooks; the original data of the control variables are from the National Bureau of Statistics of China and the provincial Statistical Yearbooks, and are calculated according to Table S3. In order to eliminate the inflation impacts, the data measured in monetary units in this paper are reduced by the consumer price index (CPI) based on 2000 to obtain the real values. The descriptive statistics of each variable are shown in Table S3.

3 Results and analysis

3.1 Measurement of GTFPG, GECG and GTCG

3.1.1 Spatial-temporal pattern analysis

China's GTFPG shows an 'N' shaped trend from 2000 to 2020 (Figure 3). GTFPG was on the rise from 2000 to 2005, and that of grain planting areas in northern China was significantly higher than that in southern China. From 2005 to 2010, overall GTFPG decreased significantly, and that in Inner Mongolia-Northeast China was higher. From 2010 to 2015, overall GTFPG gradually recovered, and that in Inner Mongolia-Northeast China grain producing areas was still high, while that in the middle and lower reaches of the Yangtze River areas (Anhui, Hubei, Hunan) increased significantly. From 2015 to 2020, areas with higher GTFPG gathered along the Yellow River (Qinghai, Shanxi, Shaanxi, Gansu, Ningxia) and Huang-Huai-Hai area (Hebei, Henan, Shandong). China's GECG showed a 'U' shaped trend from 2000 to 2020 (Figure 3). The regions with higher GECG gathered to the provinces along the Yellow River, the lower reaches of the Yangtze River, and the Huang-Huai-Hai grain production areas. China's GTCG showed an 'M' shaped trend from 2000 to 2020. The regions with higher GTCG gathered in southwestern China (Yunnan, Guizhou) and central and western China (Qinghai, Sichuan).

The application of various green technologies has obvious spatial agglomeration (Figure 3). From 2000 to 2020, MDPS had a higher adoption rate in the northern areas than in the south, and formed the distribution pattern centered around Xinjiang, Northeast producing areas (Heilongjiang, Jilin) and the areas along the Yellow River. PSQS

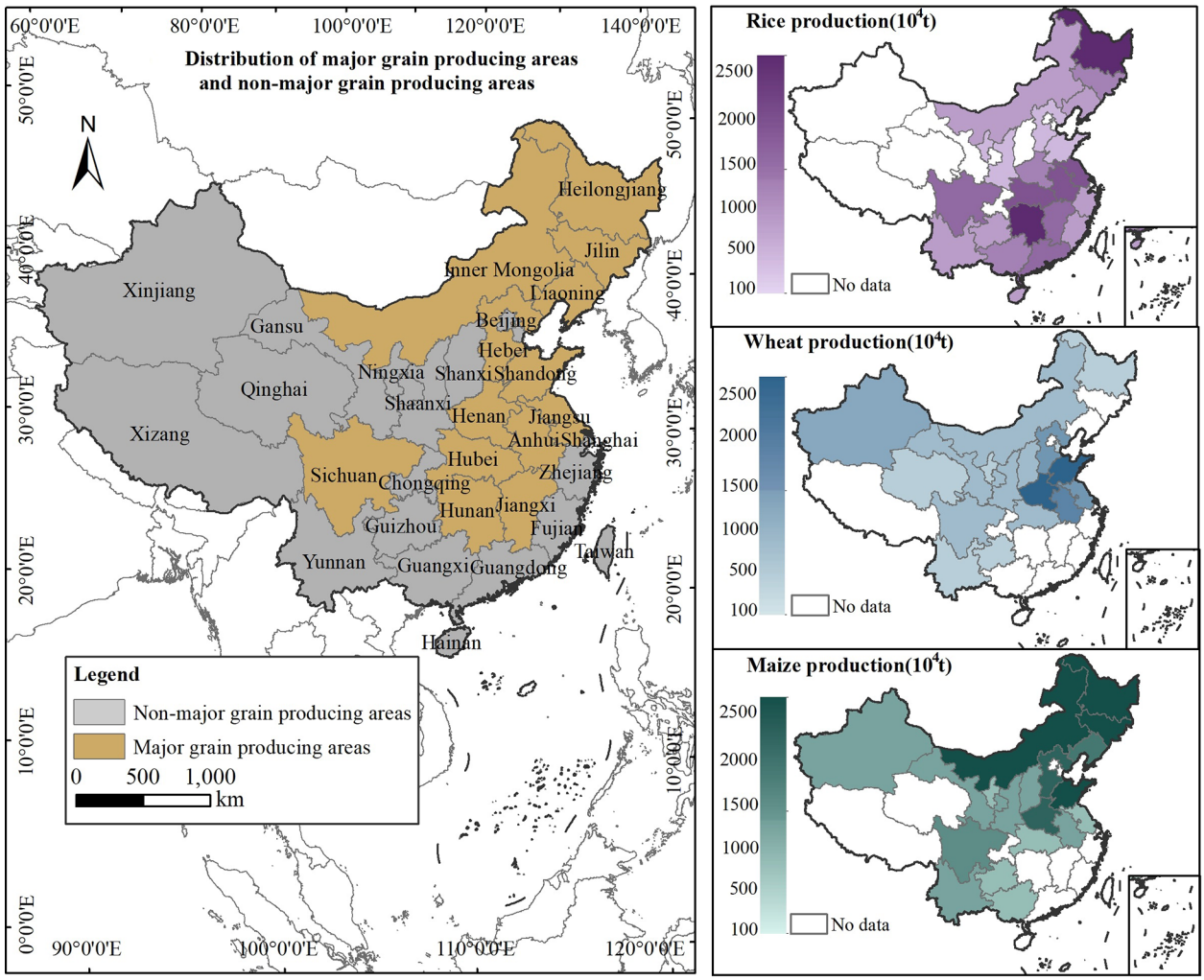

FIGURE 2
Distribution of the research areas.

had a higher adoption rate in the northern producing areas than in the southern areas, and formed the distribution pattern centered on the Inner Mongolia-Northeast producing areas. Besides, its adoption rate in Xinjiang and Huang-Huai-Hai area was also relatively high. MNTS gradually formed the distribution pattern centered on the Huang-Huai-Hai area. The adoption rate of MNTS in the arid and semi-arid regions of the north was significantly higher than that in the south. MSRE formed the distribution pattern centered on the Huang-Huai-Hai area and the lower reaches of the Yangtze River. MFDD had significantly higher adoption rate in the north than in the south, and formed the distribution pattern centered on the Inner Mongolia-Northeast region. The distribution of WSIR is centered on the eastern coastal provinces, and it had high adoption rate in Xinjiang.

Comparison of the spatial distribution of GTFPG and green technologies shows that, in different periods, there is correlation between GTFPG and green technologies in terms of spatial evolution, as well as obvious regional differences. For example, the concentration of high GTFPG in some northern producing areas from 2000 to 2005 may be correlated with changes in the adoption rates of MDPS, MNTS, and MSRE in these provinces. However, the change of GTFPG is also affected by financial support, agricultural investment, natural disasters, etc. Therefore, there is no simple correspondence between GTFPG and the change of green technology adoption rates. Investigation into the impacts of green technologies on GTFPG and the influence paths requires fitting analysis through multiple regressions.

3.1.2 Regional differences analysis

This paper further analyzes the dynamic difference of sustainable grain production in China by means of three-dimensional kernel density function. The kernel density curves of GTFPG, GECG and GTCG in the whole region are shown in Figures 4A– C. The integral area of GTFPG kernel density curve in the whole region changed from 'low-wide' to 'high-narrow', which means that provincial difference of GTFPG shrank. The peak of the kernel density curve of GECG is significantly higher than that of GTFPG, indicating small regional differences of GECG. The peak of the kernel density curve of GTCG in the whole region increased first and then decreased, which reflects that the regional difference of GTCG decreases first and then increases. Similarly, it can be concluded that the regional difference of GTFPG in the major grain producing areas decreased (Figure 4D); the regional difference of GECG in the main grain producing areas

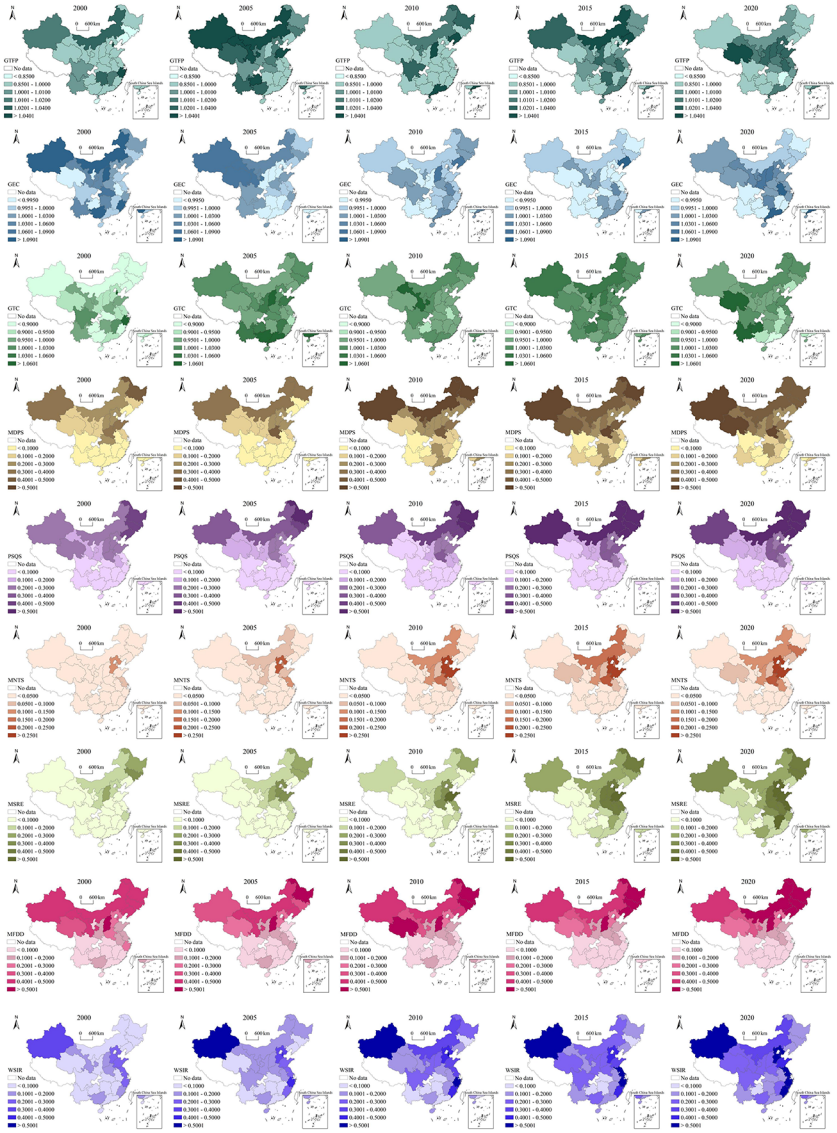

FIGURE 3
Spatial-temporal pattern of GTFPG, GECG, GTCG and green technologies from 2000 to 2020.

has increased, but the overall level was still low (Figure 4E). The increase of GECG agglomeration in the major grain producing areas leads to the decrease of regional differences of GTFPG (Figure 4F). The regional difference of GTFPG in the non-major grain producing areas is greater than that in the whole region and in the major grain producing areas (Figure 4G). The overall regional difference of GECG in the non-major grain producing areas is small (Figure 4H). The regional difference of GTCG in the non-major grain producing areas is large (Figure 4I). In summary, the difference of GTFPG among provinces in China gradually decreases, which is mainly attributed to the regional differences of GTCG, while the regional differences of GECG remain small.

Based on the analysis of the difference of the whole sample through kernel density curve, this paper uses box plot to analyze the differences in GTFPG, GECG, GTCG and green technology adoption rate between major grain producing areas and the non-major producing areas, as shown in Figure 5. Firstly, differences in the change of GTFPG from 2000 to 2020 show that sample dispersion of GTFPG in both major and non-major grain producing areas was significantly reduced (Figure 5A). In 2000, the median of GTFPG in the major grain producing areas (0.954) was significantly lower than that in the non-major grain producing areas (0.985). In 2020, the median of GTFPG in the major grain producing areas (1.005) increased slightly and was roughly equal to that in the non-major grain producing areas (1.002). The median of GECG in the major grain producing areas and non-grain producing areas shows a fluctuating upward trend (Figure 5B). The median of GTCG increased first and then decreased (Figure 5C).

Secondly, differences in green technology adoption rate from 2000 to 2020 show that major grain producing areas and non-major grain producing areas have obvious different preference for green technologies. In summary, the adoption rate of all green technologies in the major grain producing areas has increased. Compared with non-major grain producing areas, the adoption

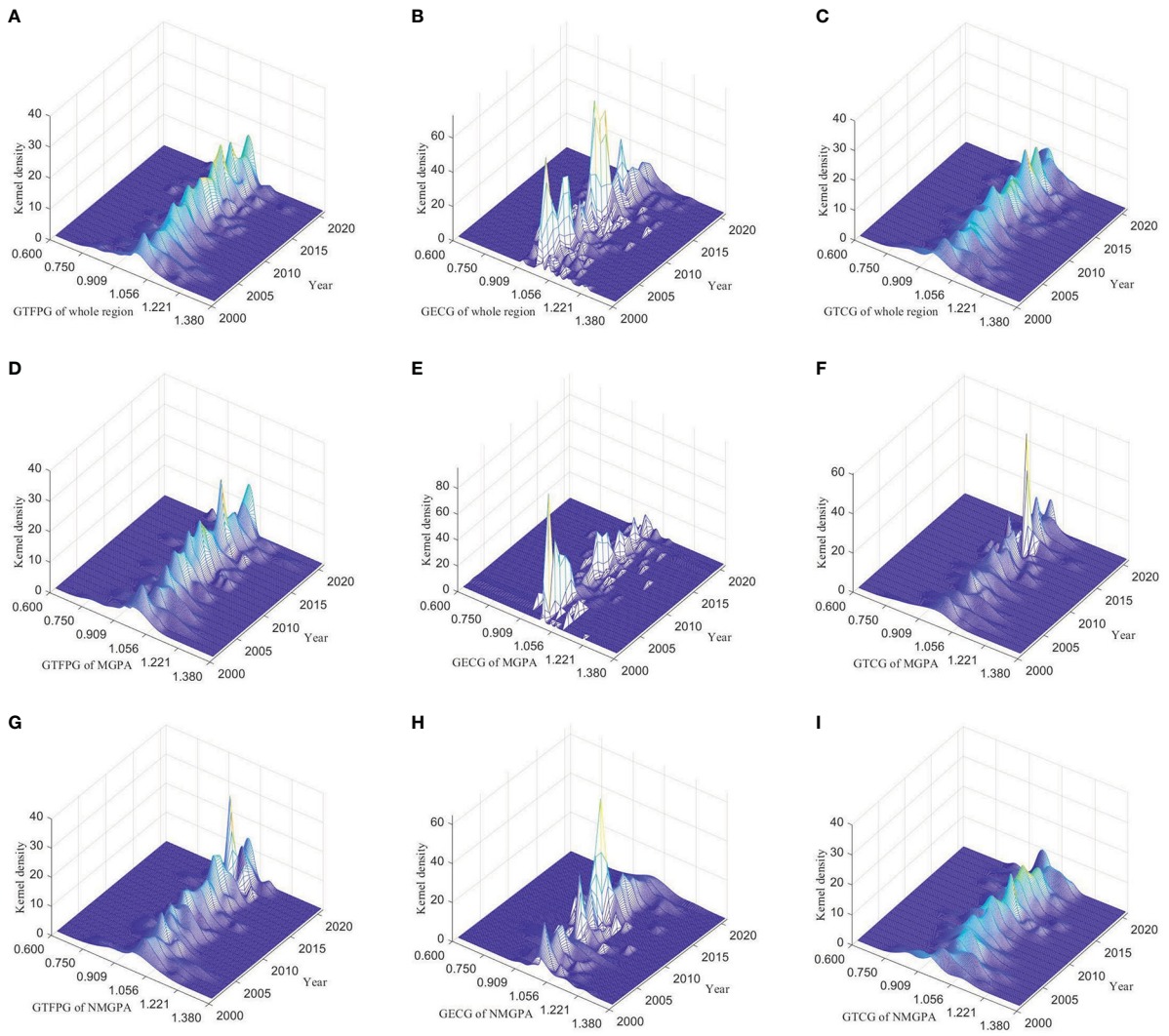

FIGURE 4
Three-dimensional kernel density curves of GTFPG, GECG and GTCG. MGPA: major grain producing areas; NMGPA: non-major grain producing areas. **(A–C)** are kernel density curves of GTFPG, GECG and GTCG of the whole region respectively. **(D–F)** are kernel density curves of GTFPG, GECG and GTCG of the major grain producing areas respectively. **(G–I)** are kernel density curves of GTFPG, GECG and GTCG of the non-major grain producing areas respectively.

rates of MDPS, PSQS, MNTS and MSRE in the major grain producing areas are higher. The adoption rates of MDPS and WSIR in the non-major grain producing areas have increased more significantly, and that of MSRE has increased faster than that in the major grain producing areas (Figures 5D–I). In order to study quantitatively the impacts, influence paths and regional differences of green technologies, this paper further analyzes the threshold results of GTFPG, GECG and GTCG.

3.2 Threshold analysis of GTFPG

Before we use the threshold model for empirical analysis, it is necessary to test the threshold effect of the constructed model, and the test results are shown in Tables S4–S6. All green technologies (MDPS, PSQS, MNTS, MSRE, MFDD, WSIR) show threshold effects on GTFPG, GECG and GTCG, reflecting that application of green technologies has a non-linear effect on GTFPG as well as its decomposition during agricultural mechanization.

3.2.1 Threshold analysis of GTFPG in the whole region

The threshold model results of GTFPG in the whole region are shown in Table 1. The results show that all green technologies have double threshold effects on GTFPG. MFDD and WSIR have only positive impact on it. MDPS, PSQS and MSRE have both positive and negative impact, and MNTS has only negative impact. MDPS has the greatest positive impact on GTFPG (1.568). MFDD and WSIR have great positive impact on GTFPG, while NTS and MSRE have great negative impact (only the coefficients that passed the significance test were compared).

In Model 1, when MDPS ≤ 0.029, the application of MDPS has not yet formed scale effect due to the high application cost (Internal Diseconomies) and greenhouse gas emissions (External Diseconomies) in mechanical operations, which results in a negative impact on GTFPG. When 0.029< MDPS ≤ 0.296, economies of scale and environmental benefits gradually emerge (Table 1), thereby effectively increasing GTFPG. However, MDPS is heavy-duty mechanical operation and is limited by soil texture.

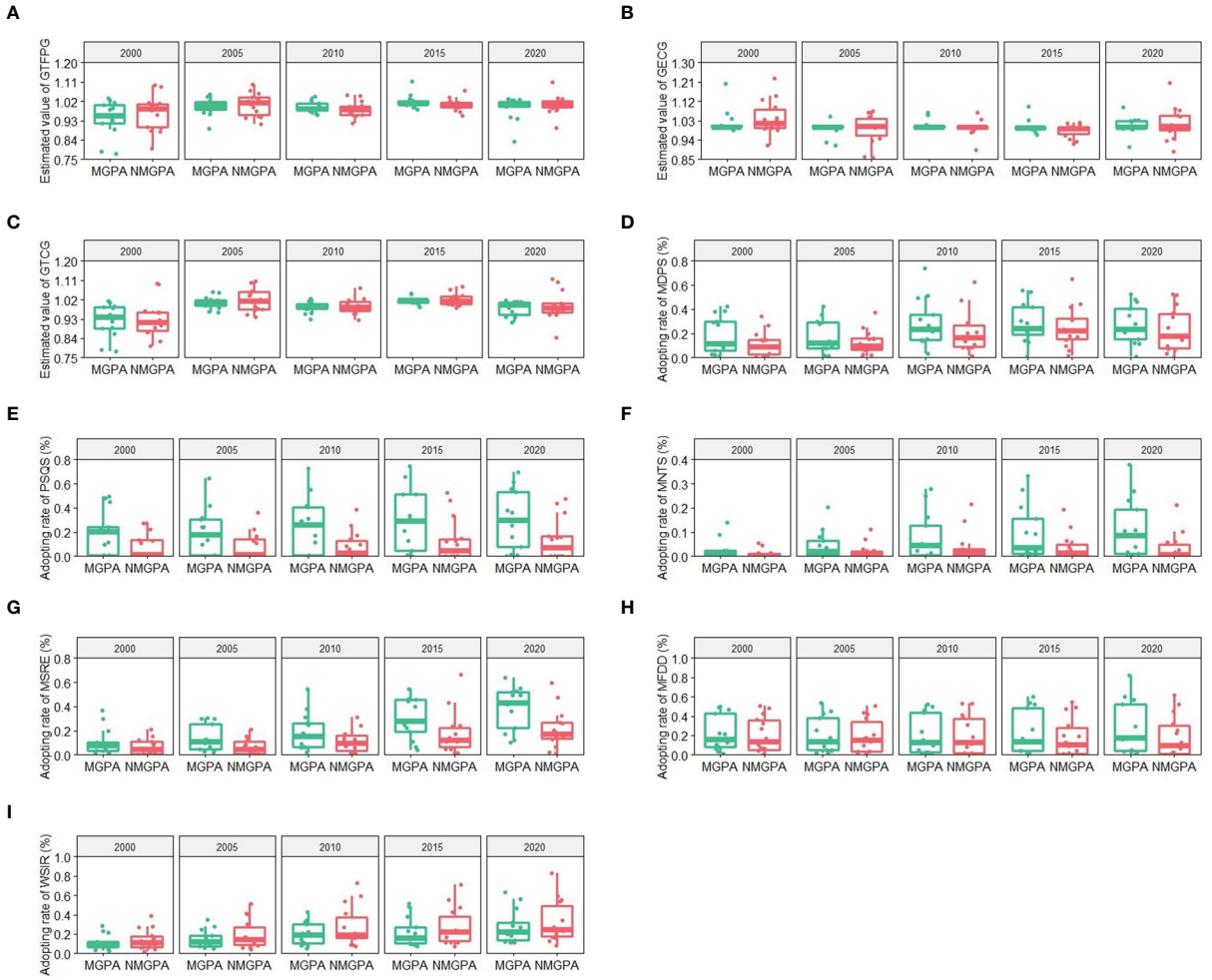

FIGURE 5
Regional difference of GTFPG, GECG, GTCG and green technologies from 2000 to 2020. MGPA: major grain producing areas; NMGPA: non-major grain producing areas. **(A–C)** are estimated values of GTFPG, GECG and GTCG in the major and non-major grain producing areas respectively. **(D–I)** are adoption rates of MDPS, PSQS, MNTS, MSRE, MFDD and WSIR in the major and non-major grain producing areas respectively.

Therefore, overuse of MDPS does not improve GTFPG (He et al., 2021), which can explain why the positive effect on GTFPG is no longer significant when MDPS > 0.296.

The impacts of PSQS are similar to that of MDPS (Model 2). The high application cost of PSQS in the initial development stage decreases GTFPG due to its Diseconomies of Scale. When 0.018< PSQS ≤ 0.444, promotion of PSQS improves GTFPG by increasing seed efficiency, reducing herbicide use, and stabilizing crop yields (Karayel, 2009; Li et al., 2015; Chen et al., 2022). However, PSQS has high requirements for production conditions, technology and management (CPGPRC, 2007). Overuse of PSQS will bring more emissions and wastes, so its positive impact is no longer significant when PSQS > 0.444.

MNTS only has negative impacts on GTFPG no matter how the adoption rate changes (Model 3). The application of MNTS is not yet mature, because of seed quality, mechanical configuration and operation technology, in which China lags behind the developed countries. Large-scale application of MNTS leads to a cost surge, production decline and resources waste (Pisante et al., 2014; Wang et al., 2021b), and causes serious External Diseconomies.

MSRE has a significant positive impact on GTFPG only in the range of 0.087-0.209 (Model 4). In the initial stage, MSRE application has prominent Internal Diseconomies (Jin et al., 2020; Aguiar et al., 2021), thereby significantly reducing GTFPG. In the ecological efficiency stage, ecological effect of MSRE application gradually emerges, thus significantly improving GTFPG. The overuse of MSRE leads to Misallocations and resource waste, which is not conducive to the GTFPG improvement.

The positive effect of MFDD on GTFPG changes from insignificant to significant in different threshold intervals (Model 5). The threshold effect of MFDD on GTFPG shows that the Learning Effects and Facilitation Effects are more prominent, and the External Diseconomies are not significant, so continuous increase of MFDD adoption rate is effective for the improvement of GTFPG.

The positive impacts of WSIR on GTFPG change from insignificant to significant, and then to insignificant (Model 6). The

TABLE 1 The threshold model results of GTFPG in the whole region.

	Model 1	Model 2	Model 3	Model 4	Model 5	Model 6
MDPS≤γ_1	-0.436 (0.905)					
γ_1<MDPS≤γ_2	1.568 (0.728)**					
MDPS>γ_2	0.011 (0.024)					
PSQS≤γ_1		-0.564 (0.607)				
γ_1<PSQS≤γ_2		0.082 (0.038)**				
PSQS>γ_2		0.032 (0.024)				
MNTS≤γ_1			-0.095 (0.358)			
γ_1<MNTS≤γ_2			-1.907 (0.536)***			
MNTS>γ_2			-0.052 (0.050)			
MSRE≤γ_1				-2.605 (1.225)**		
γ_1<MSRE≤γ_2				0.291 (0.123)**		
MSRE>γ_2				-0.025 (0.027)		
MFDD≤γ_1					0.034 (0.057)	
γ_1<MFDD≤γ_2					0.164 (0.051)***	
MFDD>γ_2					0.041 (0.021)*	
WSIR≤γ_1						0.046 (0.071)
γ_1<WSIR≤γ_2						0.147 (0.061)**
WSIR>γ_2						0.014 (0.027)
UR	0.021 (0.010)**	0.043 (0.019)**	0.028 (0.016)*	0.038 (0.031)	0.022 (0.012)*	0.026 (0.049)
AM	0.219 (0.031)***	0.054 (0.026)**	0.078 (0.014)***	0.019 (0.001)**	0.039 (0.014)***	0.071 (0.019)***
IR	0.088 (0.027)***	0.020 (0.017)	0.042 (0.020)**	0.038 (0.015)**	0.021 (0.015)	0.029 (0.020)
PS	0.031 (0.040)	0.069 (0.040)*	0.049 (0.026)*	-0.020 (0.033)	-0.025 (0.042)	-0.024 (0.040)
AF	-0.044 (0.016)***	-0.063 (0.045)	-0.037 (0.018)**	0.060 (0.075)	-0.013 (0.007)*	0.012 (0.015)
AI	0.054 (0.029)*	0.037 (0.132)	0.116 (0.125)	0.132 (0.127)	0.059 (0.129)	0.132 (0.075)*
RI	0.034 (0.060)	-0.018 (0.069)	0.025 (0.058)	-0.112 (0.059)*	-0.015 (0.062)	0.031 (0.058)
PA	-0.021 (0.012)*	-0.026 (0.012)**	-0.019 (0.017)	-0.009 (0.012)	-0.019 (0.011)*	-0.014 (0.013)
TD	-0.013 (0.013)	-0.013 (0.013)	-0.014 (0.013)	-0.016 (0.009)*	-0.015 (0.013)	-0.011 (0.013)
DI	-0.073 (0.018)***	-0.076 (0.018)***	-0.068 (0.018)***	-0.071 (0.018)***	-0.078 (0.018)***	-0.071 (0.018)
TF	0.016 (0.044)	0.014 (0.044)	0.028 (0.044)	0.050 (0.045)	0.054 (0.045)	0.027 (0.044)
PF	0.016 (0.011)	0.013 (0.011)	0.017 (0.010)*	0.013 (0.011)	0.019 (0.011)*	0.016 (0.011)
γ_1	0.029	0.018	0.027	0.087	0.152	0.161
γ_2	0.296	0.444	0.133	0.209	0.317	0.395
R^2	0.557	0.610	0.620	0.541	0.643	0.535

The standard error of coefficient estimation is shown in brackets, '*', '**', '***' represent the significance levels of 10%, 5% and 1%, respectively.

Diseconomies of Scale significantly increases costs and emissions (Moinet et al., 2017), which difficult to increase GTFPG in the initial development stages. When 0.161< WSIR ≤ 0.395, the ecological effects appear, which promote the GTFPG growth. High cost of application makes it difficult to promote WSIR (Zhuang et al., 2019). Recent outflow of rural labor force has led to a decline in rural collective action, which is not conducive to the facility maintenance and technical renewal (Wang et al., 2022). Therefore, its positive impact is no longer significant when WSIR > 0.395.

3.2.2 Threshold analysis of GTFPG in the major grain producing areas

MDPS has the greatest positive impact (1.882), and MNTS has the greatest negative impact (-1.309). Compared with the threshold results

TABLE 2 The threshold model results of GTFPG in the major grain producing areas.

	Model 7	Model 8	Model 9	Model 10	Model 11	Model 12
MDPS≤γ_1	1.882 (1.139)*					
γ_1<MDPS≤γ_2	0.701 (0.250)***					
MDPS>γ_2	0.290 (0.191)					
PSQS≤γ_1		3.207 (2.427)				
γ_1<PSQS≤γ_2		1.029 (0.508)**				
PSQS>γ_2		0.320 (0.425)				
MNTS≤γ_1			0.581 (0.285)**			
γ_1<MNTS≤γ_2			-1.309 (0.487)***			
MNTS>γ_2			-0.076 (0.068)			
MSRE≤γ_1				-0.040 (0.133)		
γ_1<MSRE≤γ_2				—		
MSRE>γ_2				0.388 (0.193)**		
MFDD≤γ_1					0.045 (0.045)	
γ_1<MFDD≤γ_2					—	
MFDD>γ_2					0.184 (0.054)***	
WSIR≤γ_1						-0.045 (0.108)
γ_1<WSIR≤γ_2						0.140 (0.061)**
WSIR>γ_2						0.052 (0.058)
Control variables	Control	Control	Control	Control	Control	Control
γ_1	0.091	0.050	0.172	0.114	0.162	0.195
γ_2	0.289	0.264	0.339	—	—	0.466
R^2	0.627	0.471	0.610	0.436	0.468	0.573

The standard error of coefficient estimation is shown in brackets, '*', '**', '***' represent the significance levels of 10%, 5% and 1%, respectively; "—" represent no data.

of the whole region, the positive impacts of PSQS, MNTS and MSRE on GTFPG in the major grain producing areas are significantly improved, while the positive impacts of MDPS, MFDD and WSIR are not significantly increased (Table 2).

MDPS can have a great positive impact on GTFPG in the initial development stage (MDPS ≤ 0.289), but the positive impact decreases with the increase of its adoption rate (Model 7). It shows that the mismatch between agricultural mechanization and grain productivity exists even in the major grain producing areas (He et al., 2021).

When 0.050< PSQS ≤ 0.264, its positive effect on GTFPG is remarkably higher than that in the whole region (Model 8). This reflects the importance of the promotion and adoption of PSQS in the major grain producing areas for the improvement of GTFPG.

It has a significant positive impact on GTFPG when MNTS ≤ 0.172 (Model 9). Compared with the whole region results, the MNTS application in the major grain producing areas can have a significant positive impact on GTFPG in a longer period.

When MSRE > 0.114, it has a significant positive impact on GTFPG (Model 10). The increase of MSRE adoption rate doesn't lead to a negative impact on GTFPG, reflecting that the development of MSRE in the major grain producing areas provides continuous impetus for the improvement of GTFPG.

It has a significant positive impact on GTFPG when MFDD > 0.162. This positive impact is remarkably higher than that in the whole region, reflecting that the application of MFDD has a greater Promoting Effects on GTFPG in the major grain producing areas (Model 11).

When 0.195< WSIR ≤ 0.466, it has a significant positive impact on GTFPG (Model 12). Although the positive impact of WSIR on GTFPG is not significantly improved, the application of this technology plays an important role in improving GTFPG in terms of the impact levels and the threshold value ranges, in both major and non-major producing areas.

3.2.3 Threshold analysis of GTFPG in the non-major grain producing areas

In non-major grain production areas, all green technologies have double threshold impact on GTFPG except MDPS (Table 3). WSIR has the greatest positive impact and MFDD the greatest negative impact.

The positive impact of MDPS on GTFPG lasts longer though its impact level is much smaller than that in the whole region and major grain producing areas (Model 13).

TABLE 3 The threshold model results of GTFPG in the non-major grain producing areas.

	Model 13	Model 14	Model 15	Model 16	Model 17	Model 18
MDPS≤γ_1	-0.714 (0.273)***					
γ_1<MDPS≤γ_2	—					
MDPS>γ_2	0.341 (0.153)**					
PSQS≤γ_1		0.044 (0.059)				
γ_1<PSQS≤γ_2		0.067 (0.031)**				
PSQS>γ_2		-0.052 (0.061)				
MNTS≤γ_1			-0.381 (0.613)			
γ_1<MNTS≤γ_2			0.582 (0.283)**			
MNTS>γ_2			0.025 (0.113)			
MSRE≤γ_1				-0.584 (0.202)***		
γ_1<MSRE≤γ_2				0.491 (0.239)**		
MSRE>γ_2				0.133 (0.064)		
MFDD≤γ_1					-1.308 (0.537)**	
γ_1<MFDD≤γ_2					0.260 (0.075)***	
MFDD>γ_2					0.089 (0.135)	
WSIR≤γ_1						0.631 (0.246)***
γ_1<WSIR≤γ_2						0.131 (0.073)*
WSIR>γ_2						-0.024 (0.052)
Control variables	Control	Control	Control	Control	Control	Control
γ_1	0.068	0.101	0.055	0.093	0.036	0.079
γ_2	—	0.459	0.250	0.206	0.295	0.299
R^2	0.379	0.345	0.494	0.475	0.526	0.464

The standard error of coefficient estimation is shown in brackets, '*', '**', '***' represent the significance levels of 10%, 5% and 1%, respectively; "—" represent no data.

The positive impact of PSQS on GTFPG is remarkably smaller than that in the whole region and major grain producing areas, reflecting the limited ability of PSQS to increase GTFPG in the non-major grain producing areas (Model 14).

Compared with the major grain producing areas, the green effect of MNTS application in the non-major grain producing areas is more significant (Model 15), and the increase of MNTS adoption rate in the northern arid and semi-arid non-major grain producing areas is a good illustration.

The positive impact of MSRE on GTFPG is remarkably greater than that in the major grain producing areas (Model 16), meaning that the development and application of MSRE in the non-major grain producing areas has significantly improved GTFPG.

The positive effect is remarkably higher than that in the major grain producing areas, indicating that the application of MFDD in the non-major grain producing areas makes grain production more sustainable (Model 17).

With the increase of WSIR adoption rate, the positive effect gradually decreases (Model 18). It reflects that the application of WSIR is of great significance to improve sustainable development of grain in the non-major grain producing areas, and the agglomeration of provinces with high WSIR adoption rate to some non-major grain producing areas is a good illustration.

3.3 Threshold analysis of GECG

3.3.1 Threshold analysis of GECG in the whole region

The threshold results of GECG in the whole region (Table 4) shows that MDPS, MSRE, MFDD and WSIR have double threshold effects on GECG, while PSQS and MNTS have single threshold effects on GECG. Among them, MFDD has the greatest positive effect (1.025), and MNTS has the greatest negative effect (-0.793). In Model 19, the positive impact of MDPS on GECG gradually decreases with increasing application. When PSQS > 0.120, it has an insignificant positive impact on GECG, reflecting that PSQS can't significantly increase GTFPG by affecting GECG (Model 20). Similarly, when MNTS > 0.096, it has an insignificant positive impact on GECG, which reflects that MNTS has no significant effect on GTFPG by affecting GECG (Model 21). MSRE has only a negative impact on GECG, indicating that MSRE decreases GTFPG

TABLE 4 The threshold model results of GECG in the whole region.

	Model 19	Model 20	Model 21	Model 22	Model 23	Model 24
MDPS≤γ_1	0.498 (0.212)**					
γ_1<MDPS≤γ_2	0.193 (0.065)***					
MDPS>γ_2	0.026 (0.021)					
PSQS≤γ_1		-0.374 (0.180)**				
γ_1<PSQS≤γ_2		—				
PSQS>γ_2		0.032 (0.022)				
MNTS≤γ_1			-0.793 (0.315)***			
γ_1<MNTS≤γ_2			—			
MNTS>γ_2			0.051 (0.043)			
MSRE≤γ_1				-0.091 (0.133)		
γ_1<MSRE≤γ_2				-0.465 (0.153)***		
MSRE>γ_2				-0.004 (0.024)		
MFDD≤γ_1					-0.073 (1.379)	
γ_1<MFDD≤γ_2					1.025 (0.376)***	
MFDD>γ_2					0.028 (0.019)	
WSIR≤γ_1						-0.455 (0.168)***
γ_1<WSIR≤γ_2						0.169 (0.061)***
WSIR>γ_2						-0.020 (0.024)
UR	0.013 (0.045)	0.069 (0.044)	-0.039 (0.044)	0.010 (0.046)	-0.017 (0.024)	0.015 (0.044)
AM	-0.012 (0.005)***	-0.028 (0.012)	-0.011 (0.013)	-0.006 (0.011)	-0.019 (0.014)	-0.011 (0.011)
IR	0.049 (0.015)***	0.048 (0.014)***	0.081 (0.044)*	0.013 (0.014)	0.012 (0.014)	0.045 (0.018)***
PS	-0.028 (0.034)	-0.013 (0.044)	-0.017 (0.031)	-0.029 (0.029)	-0.023 (0.013)*	-0.011 (0.035)
AF	-0.091 (0.104)	-0.069 (0.124)	-0.046 (0.140)	-0.033 (0.019)*	-0.085 (0.014)	-0.033 (0.014)
AI	0.029 (0.119)	0.050 (0.041)	0.059 (0.031)*	0.082 (0.113)	0.085 (0.117)	0.060 (0.033)*
RI	0.011 (0.054)	0.030 (0.063)	-0.070 (0.052)	-0.050 (0.053)	-0.021 (0.057)	0.006 (0.052)
PA	-0.019 (0.011)*	-0.018 (0.011)*	-0.013 (0.011)	-0.085 (0.031)***	-0.053 (0.026)**	-0.069 (0.012)
TD	-0.045 (0.117)	-0.046 (0.101)	-0.021 (0.061)	-0.058 (0.101)	-0.028 (0.016)*	-0.074 (0.111)
DI	-0.028 (0.016)*	-0.029 (0.015)**	-0.023 (0.013)*	-0.021 (0.016)	-0.024 (0.014)*	-0.021 (0.012)*
TF	0.015 (0.039)	0.017 (0.039)	0.015 (0.039)	0.051 (0.041)	0.014 (0.039)	0.008 (0.039)
PF	0.016 (0.009)*	0.014 (0.008)*	0.016 (0.009)*	0.015 (0.099)	0.016 (0.009)*	0.014 (0.009)
γ_1	0.067	0.120	0.096	0.109	0.032	0.067
γ_2	0.346	—	—	0.386	0.122	0.146
R^2	0.421	0.325	0.366	0.430	0.396	0.448

The standard error of coefficient estimation is shown in brackets, '*', '**', '***' represent the significance levels of 10%, 5% and 1%, respectively; "—" represent no data.

by affecting GECG (Model 22). When 0.032< MFDD ≤ 0.122, it has the greatest positive impact on GECG, and when MFDD > 0.122, the impact is no longer significant. It reflects that MFDD can't continue to improve GTFPG through GECG with increasing application (Model 23). Likewise, the threshold results of WSIR for GECG also reflect that as WSIR applications increases, the approach of improving GTFPG by affecting GECG is no longer effective (Model 24).

3.3.2 Threshold analysis of GECG in the major grain producing areas

The threshold results of GECG in the major grain producing areas (Table 5) show that MDPS, MSRE, MFDD and WSIR have double threshold effects on GECG, while PSQS and MNTS have single threshold effects on GECG. In the major grain producing areas, the positive impact of MDPS on GECG is remarkably higher than that in the whole region. PSQS only has a negative impact on GECG, and the

TABLE 5 The threshold model results of GECG in the major grain producing areas.

	Model 25	Model 26	Model 27	Model 28	Model 29	Model 30
MDPS≤γ_1	0.753 (0.117)					
γ_1<MDPS≤γ_2	0.353 (0.124)***					
MDPS>γ_2	-0.059 (0.044)					
PSQS≤γ_1		-1.495 (0.442)***				
γ_1<PSQS≤γ_2		—				
PSQS>γ_2		-0.022 (0.082)				
MNTS≤γ_1			6.551 (2.253)***			
γ_1<MNTS≤γ_2			—			
MNTS>γ_2			0.091 (0.074)			
MSRE≤γ_1				0.299 (0.141)**		
γ_1<MSRE≤γ_2				0.099 (0.050)**		
MSRE>γ_2				0.071 (0.046)		
MFDD≤γ_1					0.089 (0.184)	
γ_1<MFDD≤γ_2					1.167 (0.582)**	
MFDD>γ_2					0.059 (0.112)	
WSIR≤γ_1						-0.019 (0.135)
γ_1<WSIR≤γ_2						0.270 (0.131)**
WSIR>γ_2						0.058 (0.085)
Control variables	Control	Control	Control	Control	Control	Control
γ_1	0.117	0.103	0.085	0.121	0.152	0.046
γ_2	0.375	—	—	0.513	0.425	0.194
R^2	0.563	0.484	0.463	0.442	0.441	0.562

The standard error of coefficient estimation is shown in brackets, '**', '***' represent the significance levels of 5% and 1%, respectively; "—" represent no data.

impact is greater than that in the whole region. In the initial development stage (MNTS ≤ 0.085), MNTS can have a great positive impact on GECG, but in other stages (MNTS > 0.085), the positive impact is not significant. With the increasing application of MSRE, its positive impact on GECG gradually decreases, but the overall impact is significantly higher than that in the whole region. The positive impact of both MFDD and WSIR on GECG in ecological efficiency stage is greater than that in the whole region.

3.3.3 Threshold analysis of GECG in the non-major grain producing areas

The threshold results of GECG in the non-major grain producing areas (Table 6) show that MDPS, PSQS, MSRE and WSIR have double threshold effects on GECG, while MNTS and MFDD have single threshold effect on GECG. In the non-major grain producing areas, the positive effects of MDPS, MNTS and WSIR on GECG are smaller than those in the whole region and major grain producing areas, indicating that these technologies have poor effects on improving GTFPG through GECG in the non-major grain producing areas. Besides, the positive impact of PSQS and MFDD on GECG is greater than that in the whole region and major grain producing areas, reflecting that PSQS and MFDD can better improve GTFPG through GECG in the non-major grain producing areas. MSRE has only a negative impact on GECG, and the impact is greater than that in the whole region, indicating that MSRE significantly reduced GTFPG through GECG in the non-major grain producing areas.

3.4 Threshold analysis of GTCG

3.4.1 Threshold analysis of GTCG in the whole region

The threshold results of GTCG in the whole region shows that only MFDD has a double threshold effect on GTCG, while MDPS, MNTS, MSRE and WSIR have single threshold effects (Table 7). PSQS does not have a threshold effect. PSQS has the greatest positive effect on GTCG (0.239), while MSRE has the greatest negative effect (-1.587). In Model 37, the application of MDPS has a negative impact on GTCG, and the negative impact becomes more remarkable with increasing application. Compared with the effect of PSQS on GECG, PSQS mainly improves GTFPG through GTCG (Model 38). MNTS can significantly increase GTCG only in the initial development stage. Increase of MNTS adoption rate hinders the improvement of GTCG (Model 39). In Model 40, the impact of

TABLE 6 The threshold model results of GECG in the non-major grain producing areas.

	Model 31	Model 32	Model 33	Model 34	Model 35	Model 36
MDPS≤γ_1	0.062 (0.103)					
γ_1<MDPS≤γ_2	0.188 (0.108)*					
MDPS>γ_2	-0.066 (0.079)					
PSQS≤γ_1		6.142 (5.528)				
γ_1<PSQS≤γ_2		0.237 (0.133)*				
PSQS>γ_2		0.018 (0.091)				
MNTS≤γ_1			-1.422 (0.810)*			
γ_1<MNTS≤γ_2			—			
MNTS>γ_2			0.086 (0.218)			
MSRE≤γ_1				-0.833 (0.242)***		
γ_1<MSRE≤γ_2				-0.248 (0.122)**		
MSRE>γ_2				-0.093 (0.078)		
MFDD≤γ_1					5.889 (2.221)***	
γ_1<MFDD≤γ_2					—	
MFDD>γ_2					0.039 (0.067)	
WSIR≤γ_1						-0.820 (0.348)**
γ_1<WSIR≤γ_2						-0.301 (0.135)**
WSIR>γ_2						0.131 (0.168)
Control variables	Control	Control	Control	Control	Control	Control
γ_1	0.122	0.106	0.123	0.086	0.122	0.067
γ_2	0.414	0.274	—	0.142	—	0.144
R^2	0.453	0.463	0.441	0.496	0.480	0.464

The standard error of coefficient estimation is shown in brackets, '*', '**', '***' represent the significance levels of 10%, 5% and 1%, respectively; "—" represent no data.

MSRE on GTCG changed from a significant negative impact to significant positive in different threshold intervals, indicating that the large-scale application of MSRE could effectively improve GTCG. This is also why MSRE can improve GEFPG significantly when 0.087< MSRE ≤ 0.209 in Model 4. When MFDD >0.064, the GTCG level is significantly improved, reflecting that increasing application of MFDD can improve GTFPG through GTCG (Model 41). The threshold results of WSIR on GTCG reflect that the increase of WSIR applications improves GTFPG through GTCG (Model 42).

3.4.2 Threshold analysis of GTCG in the major grain producing areas

The threshold results of GTCG in the major grain producing areas (Table 8) show that only the impact of MDPS on GTCG has single threshold effect, and that of other green technologies has double threshold effect. In the major grain producing areas, the positive impact of MDPS on GTCG is remarkably higher than that in the whole region. PSQS has a positive impact on GTCG, but the impact is smaller than that in the whole region. When MNTS > 0.090, its impact on GTCG is significantly negative and the negative effect is higher than that in the whole region. With increasing application of MSRE, its positive impact on GTCG gradually decreases, and eventually turns to the insignificant negative impact, but the overall impact levels are higher than that in the whole region. With increasing application of MFDD, its positive impact on GTCG gradually decreases and eventually becomes an insignificant negative impact. The impact of WSIR on GTCG in the major grain producing areas is negative in all threshold intervals.

3.4.3 Threshold analysis of GTCG in the non-major grain producing areas

The threshold results of GTCG in the non-major grain producing areas (Table 9) show that the impact of PSQS and MFDD on GTCG has double threshold effect, and the impact of other green technologies has single threshold effect. In the non-major grain producing areas, MDPS has a negative impact on GTCG, and the impact is especially significant when MDPS ≤ 0.178. Compared with that in the whole region and major grain producing areas, the impact of PSQS on GTCG is positive only when it is smaller than the first threshold value. MNTS, MSRE, MFDD and WSIR have a positive impact on GTCG, and the positive impact of MFDD and WSIR is higher than that in the whole region and the major grain producing areas.

TABLE 7 The threshold model results of GTCG in the whole region.

	Model 37	Model 38	Model 39	Model 40	Model 41	Model 42
MDPS≤γ_1	-0.451 (0.488)					
γ_1<MDPS≤γ_2	—					
MDPS>γ_2	-1.364 (0.509)***					
PSQS≤γ_1		—				
γ_1<PSQS≤γ_2		—				
PSQS>γ_2		0.239 (0.124)*				
MNTS≤γ_1			0.201 (0.116)*			
γ_1<MNTS≤γ_2			—			
MNTS>γ_2			-0.017 (0.051)			
MSRE≤γ_1				-1.587 (0.787)**		
γ_1<MSRE≤γ_2				—		
MSRE>γ_2				0.161 (0.026)***		
MFDD≤γ_1					-0.763 (0.295)***	
γ_1<MFDD≤γ_2					0.129 (0.043)***	
MFDD>γ_2					0.042 (0.021)**	
WSIR≤γ_1						0.097 (0.075)
γ_1<WSIR≤γ_2						—
WSIR>γ_2						0.152 (0.073)**
UR	0.021 (0.050)	0.026 (0.049)	0.031 (0.049)	0.055 (0.031)*	0.035 (0.049)	0.024 (0.049)
AM	0.014 (0.012)	0.013 (0.013)	0.018 (0.011)*	0.027 (0.011)***	0.023 (0.016)	0.016 (0.009)*
IR	0.013 (0.017)	0.069 (0.105)	0.125 (0.051)***	0.012 (0.016)	0.018 (0.011)*	-0.003 (0.020)
PS	0.014 (0.037)	0.007 (0.017)	0.007 (0.036)	-0.055 (0.032)*	0.037 (0.041)	-0.014 (0.009)
AF	0.038 (0.016)***	0.021 (0.012)*	0.085 (0.019)***	0.004 (0.015)	0.031 (0.017)*	0.034 (0.016)**
AI	0.192 (0.113)*	0.172 (0.110)*	0.044 (0.124)	0.034 (0.124)	0.140 (0.068)*	0.028 (0.015)*
RI	-0.013 (0.059)	-0.035 (0.068)	-0.013 (0.027)	-0.017 (0.059)	0.044 (0.026)*	-0.008 (0.058)
PA	-0.005 (0.011)	-0.019 (0.011)*	-0.012 (0.013)	-0.072 (0.124)	-0.070 (0.111)	-0.071 (0.013)
TD	-0.075 (0.110)	-0.012 (0.013)	-0.076 (0.102)	-0.099 (0.130)	-0.031 (0.136)	-0.058 (0.013)
DI	-0.056 (0.018)***	-0.052 (0.018)***	-0.057 (0.018)***	-0.056 (0.017)***	-0.054 (0.018)***	-0.050 (0.018)***
TF	0.011 (0.043)	0.008 (0.043)	0.015 (0.044)	0.029 (0.044)	0.032 (0.044)	0.013 (0.044)
PF	0.006 (0.010)	-0.007 (0.010)	0.006 (0.011)	0.007 (0.011)	0.007 (0.011)	0.004 (0.010)
γ_1	0.095	—	0.081	0.025	0.064	0.141
γ_2	—	—	—	—	0.377	—
R^2	0.345	0.490	0.401	0.344	0.465	0.309

The standard error of coefficient estimation is shown in brackets, '*', '**', '***' represent the significance levels of 10%, 5% and 1%, respectively; "—" represent no data.

4 Discussions

The concept of major grain producing areas has attracted more resources to the provinces in these areas, and has profoundly affected the behavior and decision-making of producers (SCPRC, 2017; Yang et al., 2021). Besides, the resource wastes and environmental pressures caused by the continuous growth of grain production in major producing areas (Yang et al., 2021; Li and Lin, 2022), arouse more attention to the coordinated use of various green technologies. Additionally, the influence paths of green technology on the promotion of GTFPG also vary in different areas, due to regional differences in development and applicability of green technologies (Si et al., 2021; He et al., 2021).

TABLE 8 The threshold model results of GTCG in the major grain producing areas.

	Model 43	Model 44	Model 45	Model 46	Model 47	Model 48
MDPS≤γ_1	4.307 (1.542)***					
γ_1<MDPS≤γ_2	—					
MDPS>γ_2	-0.029 (0.048)					
PSQS≤γ_1		1.279 (0.933)				
γ_1<PSQS≤γ_2		0.109 (0.051)**				
PSQS>γ_2		0.028 (0.094)				
MNTS≤γ_1			2.542 (5.026)			
γ_1<MNTS≤γ_2			-7.663 (2.346)***			
MNTS>γ_2			-0.131 (0.076)*			
MSRE≤γ_1				1.193 (0.493)**		
γ_1<MSRE≤γ_2				0.104 (0.059)*		
MSRE>γ_2				-0.064 (0.144)		
MFDD≤γ_1					1.112 (0.443)**	
γ_1<MFDD≤γ_2					0.292 (0.174)*	
MFDD>γ_2					-0.092 (0.120)	
WSIR≤γ_1						-4.718 (1.326)
γ_1<WSIR≤γ_2						-0.501 (0.247)
WSIR>γ_2						-0.021 (0.092)
Control variables	Control	Control	Control	Control	Control	Control
γ_1	0.117	0.103	0.090	0.037	0.049	0.093
γ_2	—	0.444	0.145	0.352	0.371	0.176
R^2	0.335	0.329	0.347	0.344	0.368	0.351

The standard error of coefficient estimation is shown in brackets, '*', '**', '***' represent the significance levels of 10%, 5% and 1%, respectively; "—" represent no data.

4.1 Green technologies in plowing

The adoption rate of MDPS in the major grain producing areas is higher, especially in Northwest, Northeast and Yellow River production areas, reflecting that the major grain producing areas pay more attention to the green technology application in plowing.

During the ecological efficiency stage of MDPS, the ecological effects of technology application in the major grain producing areas are greater than those in the non-major grain producing areas, which is consistent with He et al. (2021). Moreover, there is overuse of MDPS in the major grain producing areas, which may be a result of resource Misallocations caused by Path Dependences or External Diseconomies (Li et al., 2017; Xie et al., 2021). However, there is no overuse of MDPS in the non-major grain producing areas, which may be related to its advantages in mechanization, proficiency of technical staff and social services (especially provinces with higher level of economic development).

In the major grain producing areas, MDPS mainly affects GTFPG through the GTCG path in the initial development stage, which indicates that the Spillover Effects are more significant in this period; MDPS improves GTFPG mainly through the GECG path in the ecological efficiency stage, which may be related to the Learning Effects, Synergy Effects and Promoting Effects generated by the MDPS application (Figure 1). In the non-major grain producing areas, MDPS increases GTFPG mainly through the GECG path. The green technology efficiency change caused by the MDPS application is more prominent in the major grain producing areas. However, the contribution of MDPS to green technical progress change is very limited, and the Diseconomies of Scale caused by technological upgrading are especially serious in the non-major grain producing areas.

4.2 Green technologies in sowing

High adoption rate of PSQS agglomerates in Inner Mongolia-Northeast China, Xinjiang and Huang-Huai-Hai area, and high adoption rate of MNTS gathers in Huang-Huai-Hai area, reflecting that the importance attached to green sowing technologies by major grain producing areas.

The difference between PSQS and MNTS threshold results can reflect that the ecological effect of PSQS application is better than that of MNTS, especially in the major grain producing areas, which is consistent with Li et al. (2015) and Chen et al. (2022), and also

TABLE 9 The threshold model results of GTCG in the non-major grain producing areas.

	Model 49	Model 50	Model 51	Model 52	Model 53	Model 54
MDPS≤γ_1	-4.386 (2.017)**					
γ_1<MDPS≤γ_2	—					
MDPS>γ_2	-0.024 (0.096)					
PSQS≤γ_1		1.446 (0.308)***				
γ_1<PSQS≤γ_2		-0.221 (0.119)*				
PSQS>γ_2		-0.016 (0.110)				
MNTS≤γ_1			0.611 (0.287)**			
γ_1<MNTS≤γ_2			—			
MNTS>γ_2			0.084 (0.196)			
MSRE≤γ_1				0.286 (0.142)**		
γ_1<MSRE≤γ_2				—		
MSRE>γ_2				0.082 (0.095)		
MFDD≤γ_1					1.688 (0.737)**	
γ_1<MFDD≤γ_2					0.254 (0.126)**	
MFDD>γ_2					0.055 (0.083)	
WSIR≤γ_1						0.041 (0.082)
γ_1<WSIR≤γ_2						—
WSIR>γ_2						0.374 (0.185)**
Control variables	Control	Control	Control	Control	Control	Control
γ_1	0.178	0.104	0.182	0.134	0.036	0.143
γ_2	—	0.273	—	—	0.291	—
R^2	0.427	0.452	0.424	0.429	0.412	0.491

The standard error of coefficient estimation is shown in brackets, '*', '**', '***' represent the significance levels of 10%, 5% and 1%, respectively; "—" represent no data.

explains the higher adoption rate of PSQS. The application of MNTS has high requirements for natural conditions, mechanical configuration, seed quality and technical levels (Duan et al., 2022a). Improper application of MNTS brings serious External Diseconomies, which limits its ecological effects and application scopes.

In the major grain producing areas, PSQS mainly improves GTFPG through the GTCG path, which indicates that the Facilitation Effects, Acceleration Actions and Group Identities caused by the PSQS application are more prominent (Figure 1); however, MNTS application features high operational risk, long investment return period, and high operational requirements (Zhang et al., 2021; Wang et al., 2021b), which lead to the External Diseconomies, Misallocation and Adaptive Effects, and mainly improve GTFPG through the GTCG path. In the non-major grain producing areas, some economically developed and highly mechanized provinces can support the mature application of PSQS, and are more prominent in the Learning effects, Synergy Effects and Promoting effects, which lead to improve GTFPG through the GECG path. Meanwhile, the arid and semi-arid areas in the non-major grain producing areas are suitable for the promotion and application of MNTS (Zhang et al., 2018), which bring significant Facilitation Effects, Acceleration Actions and Group identities, and mainly improve GTFPG through the GTCG path. This also explains the increase of MNTS adoption rate in Qinghai, Shanxi and Shaanxi in recent years.

4.3 Green technologies in fertilization

The adoption rate of MSRE in the major grain producing areas is significantly higher than that in the non-major grain producing areas, while the adoption rate of MFDD in the two areas is similar, which reflects that major grain producing areas pay more attention to the green fertilization technologies.

In the major grain producing areas, MSRE and MFDD can continuously improve GTFPG (the increase in technology adoption rate does not cause a negative threshold effect), and the ecological effect of MSRE is greater. In the non-major grain producing areas, MSRE and MFDD only have significant positive impacts on GTFPG between the first and second threshold values, and the effects are greater than that in the major grain producing areas, and MSRE has more obvious advantages. While, there are overuse of the two green technologies in the non-major grain producing areas.

Application of MSRE requires complex conditions (Table S1), and more straw returning brings higher production costs under the intensive

production and rotation system (Yang et al., 2020), resulting in significant Path Dependences and Inertial Actions (Figure 1). In addition to the imperfect subsidy system (Huang et al., 2019), MSRE can't continuously increase GECG. Therefore, MSRE improves GTFPG mainly through the GTCG path in both major and non-major grain producing areas. The differences in the influence paths of MFDD in major and non-major grain producing areas are caused by different natural conditions, economic development, technological levels, and green conception. Especially in the ecological efficiency stage of MFDD application, the Learning Effects, Synergy Effects and Promoting Effects of MFDD application in the major grain producing areas are more prominent; while, the Facilitation Effects, Acceleration Actions and Group identities are more prominent in non-major grain producing areas.

4.4 Green technologies in irrigation

The adoption rate of WSIR in the non-major grain producing areas is slightly higher than that in the major grain producing areas, but with higher sample dispersion. This indicates that the non-major grain producing areas attach great importance to the development of green irrigation technologies.

The difference in the threshold effects of WSIR reflects the obvious External Diseconomies in the initial stage of WSIR application in the major grain producing areas, which supports the conclusions of Zhuang et al. (2019) and Chen et al. (2022). However, it shows better green effects in ecological efficiency stage, which explains the high adoption rate of WSIR in the major grain producing areas. In the non-major grain producing areas, WSIR has significant ecological effects in the initial stage. It may be related to the water-saving effects of WSIR in water-deficient areas, especially in Xinjiang, Qinghai, Gansu and Shaanxi (Zhuang et al., 2019; Duan et al., 2022b; Guo et al., 2022a). Moreover, the reason why the overuse stage of WSIR is advanced in the non-major grain producing areas may be that the rural labor transfer reduces collective actions, and is not conducive to the maintenance of irrigation facilities and green efficiency improvement, which supporting the conclusions of Wang et al. (2022).

As an important practice of sustainable agricultural production (Zhuang et al., 2019), the application of WSIR has brought significant green efficiency improvement to major grain producing areas (Man et al., 2014; Wang et al., 2020b). Moreover, External Diseconomies, Misallocation and Adaptive Effects limit the contribution of WSIR to the green technology progress in the major grain producing areas. Regions in the non-major grain producing areas vary greatly in precipitation, so choosing the appropriate water-saving irrigation method is the key to achieving green production (Zhuang et al., 2019; Chen et al., 2022). Therefore, the applications and upgrading of various water-saving technologies in the non-major grain producing areas in recent years have enabled WSIR to make a greater contribution to green technology progress in these areas, which supporting the conclusions of Zhuang et al. (2019).

5 Conclusions

This paper took the influence mechanism of green technologies on GTFPG as the entry point, selected green technologies from the plowing, sowing, fertilization, and irrigation section in agricultural mechanized production, and constructed threshold models to explore the impacts of various green technologies on GTFPG and the influence paths. The main conclusions are as follows:

(1) GTFPG and green technologies exhibited correlations as well as regional differences in spatial evolution. The difference of GTFPG among provinces in China gradually decreased, which was mainly caused by the regional difference of GTCG, while the regional difference of GECG remained small. Major grain producing areas and non-major grain producing areas had different preferences for green technologies. Major grain producing areas paid more attention to the green technologies in plowing, sowing and fertilization; while, the green irrigation technology was more widely used in non-major grain producing areas.

(2) In the major grain producing areas, MDPS had the greatest positive impact on GTFPG. In the non-major grain producing areas, the positive impact of WSIR was greatest. In plowing, MDPS had greater ecological effects in the major grain producing areas than in the non-major grain producing areas; however, the overuse of MDPS occurred in the major grain producing areas, but not in the non-major grain producing areas. In sowing, PSQS had better ecological effects than MNTS, especially in the major grain producing areas; the negative impact of MNTS was more significant in the major grain producing areas. In fertilization, overuse of MSRE and MFDD never occurred in the major grain producing areas; in the ecological efficiency stage, MSRE and MFDD had greater positive impacts on GTFPG in the non-major grain producing areas. In irrigation, WSIR showed better ecological effects in the major grain producing areas, and the negative impacts of its overuse were greater in the non-major grain producing areas.

(3) There were significant differences in the influence paths of green technologies on GTFPG of major grain producing areas and non-major grain producing areas. In the major grain producing areas, MDPS (in the ecological efficiency stage), MFDD (in the ecological efficiency stage) and WSIR mainly improved GTFPG through the GECG path; MDPS (in the initial development stage), PSQS, MNTS, MSRE (in the initial development and ecological efficiency stage), and MFDD (in the initial development stage) mainly affected GTFPG through the GTCG path. In the non-major grain production areas, MDPS, PSQS and MFDD (in the initial development stage) increased GTFPG mainly through the GECG path; MNTS, MSRE, MFDD (in the ecological efficiency stage) and WSIR mainly improved GTFPG through the GTCG path.

Data availability statement

The raw data supporting the conclusions of this article will be made available by the authors, without undue reservation.

Author contributions

JL: Conceptualization, methodology, software, validation, investigation, resources, data analysis, writing-original draft preparation, writing-review and editing, visualization, funding acquisition. QL: Conceptualization, software, writing-review and

editing, supervision, validation, project administration. All authors contributed to the article and approved the submitted version.

Funding

The work was supported by the Priority Research Program of Chinese Academy of Sciences.

Conflict of interest

The authors declare that the research was conducted in the absence of any commercial or financial relationships that could be construed as a potential conflict of interest.

Publisher's note

Supplementary material

The Supplementary Material for this article can be found online at: https://www.frontiersin.org/articles/10.3389/fpls.2023.1107970/full#supplementary-material

References

Aguiar, A., Milessi, T. S., Mulinari, D. R., Lopes, M. S., da Costa, S. M., and Candido, R. G. (2021). Sugarcane straw as a potential second generation feedstock for biorefinery and white biotechnology applications. *Biomass Bioenerg.* 144, 105896. doi: 10.1016/j.biombioe.2020.105896

Baležentis, T., Blancard, S., Shen, Z., and Štreimikienė, D. (2021). Analysis of environmental total factor productivity evolution in european agricultural sector. *Decis. Sci.* 52 (2), 483–511. doi: 10.1111/deci.12421

Baumhardt, R. L., Jones, O. R., and Schwartz, R. C. (2008). Long-term effects of profile-modifying deep plowing on soil properties and crop yield. *Soil Sci. Soc. America J.* 72 (3), 677–682. doi: 10.2136/sssaj2007.0122

Chaudhary, V., Chandra, R., Chaudhary, R., and Bhattacharyya, R. (2021). Global warming potential and energy dynamics of conservation tillage practices for different rabi crops in the indo-gangetic plains. *J. Environ. Manage.* 296, 113182. doi: 10.1016/j.jenvman.2021.113182

Chen, M., Chen, J., and Lai, S. (2006). Inventory analysis and spatial feature recognition of agricultural and rural pollution in China. *China Environ. Sci.* 6, 751–755. doi: 10.1016/S0379-4172(06)60102-9

Cheng, G. (2014). *Data envelopment analysis method and MaxDEA software* (Beijing: Intellectual Property Publishing House).

Chen, Y., Miao, J., and Zhu, Z. (2021). Measuring green total factor productivity of china's agricultural sector: A three-stage SBM-DEA model with non-point source pollution and CO_2 emissions. *J. Clean. Prod.* 318, 128543. doi: 10.1016/j.jclepro.2021.128543

Chen, L., Xin, J., Liu, J., Yuan, M., Liu, S., Jiang, W., et al. (2017). Changes in bacterial community of soil induced by long-term straw returning. *Sci. Agric.* 74, 349–356. doi: 10.1590/1678-992X-2016-0025

Chen, M., Xue, W., and Chen, J. (2022). Platform subsidy policy design for green product diffusion. *J. Clean. Prod.* 359, 132039. doi: 10.1016/j.jclepro.2022.132039

Chen, J., Pang, D., Jin, M., Luo, Y., Li, H., Li, Y., et al. (2020). Improved soil characteristics in the deeper plough layer can increase grain yield of winter wheat. *J. Integr. Agriculture.* 19 (5), 1215–1226. doi: 10.1016/S2095-3119(19)62679-1

Clapp, J., Moseley, W. G., Burlingame, B., and Termine, P. (2022). Viewpoint: The case for a six-dimensional food security framework. *Food Policy.* 106, 102164. doi: 10.1016/j.foodpol.2021.102164

CPGPRC. (2007). *Agricultural science popularization: high-yield cultivation technology of wheat precision and small quantity sown*. Available at: http://www.gov.cn/govweb/fwxx/kp/2007-10/10/content_771816.htm.

Ding, J., Wei, H., Yang, Y., Zhang, J., and Wu, J. (2018). Effects of conservation tillage on soil water condition and winter wheat yield in farmland. *Chin. J. Appl. Ecol.* 29, 2501–2508. doi: 10.13287/j.1001-9332.201808.005

Duan, P., Liu, R., and Chen, S. D. (2022b). Payment decisions on water-saving irrigation services and farming households'incomes: Based on survey data in the ecologically fragile areas of xinjiang, China. *Resour. Sci.* 44 (4), 833–846. doi: 10.18402/resci.2022.04.15

Duan, Y., Wu, M., LV, J., Xiang, W., Yan, B., Ma, L., et al. (2022a). Research status and development suggestions of no-tillage seeding anti-blocking technology. *J. Agric. Sci. Technol.* 24 (2), 124–135. doi: 10.13304/j.nykjdb.2021.0370

Eanes, F. R., Singh, A. S., Bulla, B. R., Ranjan, P., Fales, M., Wickerham, B., et al. (2019). Crop advisers as conservation intermediaries: perceptions and policy implications for relying on nontraditional partners to increase U.S. farmers' adoption of soil and water conservation practices. *Land Use Policy* 81 (10), 360–370. doi: 10.1016/j.landusepol.2018.10.054

ECOSOC. (2022). Progress report on the 10 year framework of programmes on sustainable consumption and production patterns.. In: *United Nations Conference on Sustainable Development*, Rio, Brazil. Available at: https://sdgs.un.org/sites/default/files/publications/1444HLPF_10YFP2.pdf.

Elkington, J. (1994). Towards the sustainable corporation: Win-win-win business strategies for sustainable development. *California Manage. Rev.* 36 (2), 90–100. doi: 10.2307/41165746

Fabiani, S., Vanino, S., Nino, P., and Napoli, R. (2020). Water energy food nexus approach for sustainability assessment at farm level: an experience from an intensive agricultural area in central italy. *Environ. Sci. Policy* 104, 1–12. doi: 10.1016/j.envsci.2019.10.008

FAO, IFAD, UNICEF, WFP and WHO. (2022). "The state of food security and nutrition in the world 2022," in *Repurposing food and agricultural policies to make healthy diets more affordable* (Rome: FAO). doi: 10.4060/cc0639en

Frank, S., Havlík, P., Stehfest, E., van Meijl, H., Witzke, P., Perez-Domínguez, I., et al. (2019). Agricultural non-CO2 emission reduction potential in the context of the 1.5 0C target. *Nat. Climate Change* 9, 66e72. doi: 10.1038/s41558-018-0358-8

FSIN. (2022). *Global report on food crises*. Available at: https://www.fsinplatform.org/sites/default/files/resources/files/GRFC%202022%20KM%20ENG%20ARTWORK.pdf (Accessed September 12, 2022).

Gaihre, Y., Singh, U., Islam, S., Huda, A., Islam, M., Satter, M., et al. (2015). Impacts of urea deep placement on nitrous oxide and nitricoxide emissions from rice fields in bangladesh. *Geoderma*. 259, 370–379. doi: 10.1016/j.geoderma.2015.06.001

Gao, W. (2022). Research on green innovation driving mechanism for high-quality development of grain industry. *J. Jiangxi Univ. Finance Econ.* 3, 73–86. doi: 10.13,676/j.cnki.cn36-1224/f.2022.03.002

Gao, L., Zhang, W., Mei, Y., Abdoul, G., Song, Y., and Jin, S. (2018). Do farmers adopt fewer conservation practices on rented land? evidence from straw retention in China. *Land Use Policy*. 79, 609–621. doi: 10.1016/j.landusepol.2018.08.026

Guo, Z., Chen, X., and Zhang, Y. (2022b). Impact of environmental regulation perception on farmers' agricultural green production technology adoption: A new perspective of social capital. *Technol. Soc.* 71, 102085. doi: 10.1016/j.techsoc.2022.102085

Guo, Y., Qiu, L., and Yao, S. (2022a). Analysis of the impact of irrigation water-saving techniques adoption on Farmers'Agricultural income. *On Econ. Problems* 04), 93–100. doi: 10.16011/j.cnki.jjwt.2022.04.008

Hansen, B. E. (1999). Threshold effects in non-dynamic panels: estimation, testing, and inference. *J. Econom.* 93 (2), 345–368. doi: 10.1016/S0304-4076(99)00025-1

He, P., Zhang, J., and Li, W. (2021). The role of agricultural green production technologies in improving low-carbon efficiency in china: necessary but not effective. *J. Environ. Manage.* 293, 112837. doi: 10.1016/j.jenvman.2021.112837

Houssou, N., Diao, X., Cossar, F., Kolavalli, S., Jimah, K., and Aboagye, P. (2013). Agricultural mechanization in ghana: Is specialized agricultural mechanization service provision a viable business model? *Am. J. Agric. Economics* 95 (5), 1237–1244. doi: 10.1093/ajae/aat026

Huang, X., Cheng, L., Chien, H., Jiang, H., Yang, X., and Yin, C. (2019). Sustainability of returning wheat straw to field in hebei, Shandong and jiangsu provinces: a contingent valuation method. *J. Clean. Prod.* 213, 1290–1298. doi: 10.1016/j.jclepro.2018.12.242

Huisingh, D., Zhang, Z., Moore, J. C., Qiao, Q., and Li, Q. (2015). Recent advances in carbon emissions reduction: policies, technologies, monitoring, assessment and modeling. *J. Clean. Prod.* 103, 1–12. doi: 10.1016/j.jclepro.2015.04.098

Hu, J., Xue, L., Qian, C., Xue, L., and Cao, S. (2022). Effects of oxygen enrichment on surface water nutrient dynamics and greenhouse gas emissions in paddy fields with different straw returning. *Environ. Sci.* doi: 10.13227/j.hjkx.202204079

Jiang, M., Hu, X., Chunga, J., Lin, Z., and Fei, R. (2020). Does the popularization of agricultural mechanization improve energy-environment performance in china's agricultural sector? *J. Clean. Prod.* 276 (1), 124210. doi: 10.1016/j.jclepro.2020.124210

Jin, L. B., Cui, H. Y., Li, B., Zhang, J. W., Dong, S. T., and Liu, P. (2012). Effects of integrated agronomic management practices on yield and nitrogen efficiency of summer maize in north China. *Field Crops Res.* 134, 30–35. doi: 10.1016/j.fcr.2012.04.008

Jin, Z., Shah, T., Zhang, L., Liu, H., Peng, S., and Nie, L. (2020). Effect of straw returning on soil organic carbon in rice–wheat rotation system: A review. *Food Energy Secur.* 9 (2), e200. doi: 10.1002/fes3.200

Johnes, J. (2015). Operational research in education. *Eur. J. Oper. Res.* 243, 683–696. doi: 10.1016/j.ejor.2014.10.043

Karayel, D. (2009). Performance of a modified precision vacuum seeder for no-till sowing of maize and soybean. *Soil tillage Res.* 104 (1), 121–125. doi: 10.1016/j.still.2009.02.001

Keshavarz Afshar, R., and Dekamin, M. (2022). Sustainability assessment of corn production in conventional and conservation tillage systems. *J. Clean. Prod.* 351, 131508. doi: 10.1016/j.jclepro.2022.131508

Li, Q., Bian, C., Liu, X., Ma, C., and Liu, Q. (2015). Winter wheat grain yield and water use efficiency in wide-precision planting pattern under deficit irrigation in north China plain. *Agric. Water Manage.* 153, 71–76. doi: 10.1016/j.agwat.2015.02.004

Li, H., Dai, M., Dai, S., and Dong, X. (2018). Current status and environment impact of direct straw return in china's cropland – a review. *Ecotoxicol. Environ. Safety* 159, 293–300. doi: 10.1016/j.ecoenv.2018.05.014

Li, J., and Lin, Q. (2022). Can the adjustment of china's grain purchase and storage policy improve its green productivity? *Int. J. Environ. Res. Public Health* 19, 6310. doi: 10.3390/ijerph19106310

Li, T., Long, H., Zhang, Y., Ge, D., and Li, Y. (2017). Analysis of the spatial mismatch of grain production and farmland resources in China based on the potential crop rotation system. *Land Use Policy.* 60, 26–36. doi: 10.1016/j.landusepol.2016.10.013

Li, J., and Song, Z. (2022). Dynamic impacts of external uncertainties on the stability of the food supply chain: Evidence from China. *Foods* 11, 2552. doi: 10.3390/foods11172552

Liu, Y., and Feng, C. (2019). What drives the fluctuations of "green" productivity in china's agricultural sector? a weighted Russell directional distance approach. *Res. Conserv. Recy.* 147, 201–213. doi: 10.1016/j.resconrec.2019.04.013

Liu, Z., Guan, D., Crawford-Brown, D., Zhang, Q., He, K., and Liu, J. (2013). Energy policy: A low-carbon road map for China. *Nat. (London)* 500 (7461), 143–145. doi: 10.1038/500143a

Liu, S., Lei, P., Li, X., and Li, Y. (2022). A nonseparable undesirable output modified three-stage data envelopment analysis application for evaluation of agricultural green total factor productivity in China. *Sci. Total Environ.* 838, 155947. doi: 10.1016/j.scitotenv.2022.155947

Liu, Y., Sun, D., Wang, H., Wang, X., Yu, G., and Zhao, X. (2020). An evaluation of china's agricultural green production: 1978-2017. *J. Clean. Prod.* 243, 118483.1–118483.12. doi: 10.1016/j.jclepro.2019.118483

Li, M., Wang, J., Zhao, P., Chen, K., and Wu, L. (2020). Factors affecting the willingness of agricultural green production from the perspective of farmers' perceptions. *Sci. total environ.* 738, 140289. doi: 10.1016/j.scitotenv.2020.140289

Luan, B., Huang, J., and Zou, H. (2019). Domestic R&D, technology acquisition, technology assimilation and china's industrial carbon intensity: evidence from a dynamic panel threshold model. *Sci. Total Environ.* 693, 133436.1–133436.11. doi: 10.1016/j.scitotenv.2019.07.242

Maňez, J. A., and Love, J. H. (2020). Quantifying sunk costs and learning effects in R&Dd persistence. *Res. Policy.* 49, 104004. doi: 10.1016/j.respol.2020.104004

Man, J., Wang, D., White, P., and Yu, Z. (2014). The length of micro-sprinkling hoses delivering supplemental irrigation affects photosynthesis and dry matter production of winter wheat. *Field Crops Res.* 168, 65–74. doi: 10.1016/j.fcr.2014.08.012

Mao, H., Zhou, L., Ying, R., and Pan, D. (2021). Time preferences and green agricultural technology adoption: Field evidence from rice farmers in China. *Land Use Policy.* 109, 105627. doi: 10.1016/j.landusepol.2021.105627

MARAPRC. (2018). *Technical guidelines for agricultural green development(2018-2030)*. Available at: http://www.moa.gov.cn/govpublic/KJJYS/201807/t20180706_6153629.htm.

Miah, M., Gaihre, Y., Hunter, G., Singh, U., and Hossain, S. (2016). Fertilizer deep placement increases rice production: evidence from farmers' fields in southern bangladesh. *Agron. J.* 108 (2), 805–812. doi: 10.2134/agronj2015.0170

Midingoyi, S., Kassie, M., Muriithi, B., Diiro, G., and Ekesi, S. (2018). Do farmers and the environment benefit from adopting integrated pest management practices? evidence from Kenya. *J. Agric. Econ.* 70, 452–470. doi: 10.1111/1477-9552.12306

Min, S., Paudel, K. P., and Chen, F. B. (2021). Mechanization and efficiency in rice production in china. *J. Integr. Agri.* 20 (7), 1996–2008. doi: 10.1016/S2095-3119(20)63439-6

Moinet, G., Cieraad, E., Turnbull, M., and Whitehead, D. (2017). Effects of irrigation and addition of nitrogen fertiliser on net ecosystem carbon balance for a grassland. *Sci. Total Environ.* 579, 1715e1725. doi: 10.1016/j.scitotenv.2016.11.199

Nagothu, U. S. (2018). "Summary: sustainable intensification of agriculture, technology and policy options," in *Agricultural development and sustainable intensification* (London, New York: Routledge), 274–296.

Oh, D. (2010). A global malmquist-luenberger productivity index. *J. Product. Anal.* 34, 183–197. doi: 10.1007/s11123-010-0178-y

Pan, X., Wei, Z., Han, B., and Shahbaz, M. (2021). The heterogeneous impacts of interregional green technology spillover on energy intensity in china. *Energy Econ.* 96, 105133. doi: 10.1016/j.eneco.2021.105133

Peixoto, D. S., Silva, L., Melo, L. B. B., Azevedo, R. P., Araujo, B. C. L., Carvalho, T. S., et al. (2020). Occasional tillage in no-tillage systems: a global meta-analysis. *Sci. total environ.* 745, 140887. doi: 10.1016/j.scitotenv.2020.140887

Pisante, M., Stagnari, F., Acutis, M., Bindi, M., Brilli, L., Stefano, V. D., et al. (2014). "Conservation agriculture and climate change," in *Conservation agriculture*. Eds. M. Farooq and K. Siddique (Switzerland: Springer, Cham).

Purvis, B., Mao, Y., and Robinson, D. (2019). Three pillars of sustainability: in search of conceptual origins. *Sustain. Sci.* 14 (3), 681–695. doi: 10.1007/s11625-018-0627-5

Qiu, T., and Luo, B. (2021). Do small farms prefer agricultural mechanization services? evidence from wheat production in china. *Appl. Econ.* 53 (26), 2962–2973. doi: 10.1080/00036846.2020.1870656

Rahim, H., Ghazali, M., Bookeri, M., Abu Bakar, B., Ariff, E., Rahman, M., et al. (2021). Economic potential of rice precision farming in malaysia: The case study of felcra seberang perak. *Precis. Agri.* 23 (3), 812–829. doi: 10.1007/s11119-021-09862-3

Rahman, H., Haque, K. M. S., and Khan, Z. H. (2021). A review on application of controlled released fertilizers influencing the sustainable agricultural production: A cleaner production process. *Environ. Technol. Innov.* 23, 101697. doi: 10.1016/j.eti.2021.101697

Reza-Gharehbagh, R., Hafezalkotob, A., Makui, A., and Sayadi, M. (2022). Financing green technology development and role of digital platforms: Insourcing vs. outsourcing. *Technol. Soc.* 69, 101967. doi: 10.1016/j.techsoc.2022.101967

SCPRC. (2017). Available at: http://www.gov.cn/zhengce/content/2017-02/04/content_5165309.htm.

Shah, S. M., Liu, G., Yang, Q., Casazza, M., Agostinho, F., Giannetti, B. F., et al. (2021). Sustainability assessment of agriculture production systems in pakistan: a provincial-scale energy-based evaluation. *Ecol. Model.* 455, 109654. doi: 10.1016/j.ecolmodel.2021.109654

Shao, Y., Xie, Y., Wang, C., Yue, J., Yao, Y., Li, X., et al. (2016). Effects of different soil conservation tillage approaches on soil nutrients, water use and wheat-maize yield in rainfed dry-land regions of north China. *Eur. J. Agron.* 81, 31–45. doi: 10.1016/j.eja.2016.08.014

Shen, Z., Baležentis, T., Chen, X., and Valdmanis, V. (2018). Green growth and structural change in Chinese agricultural sector during 1997–2014. *China Econ. Rev.* 51, 83–96. doi: 10.1016/j.chieco.2018.04.014

Shi, X., and Li, L. (2019). Green total factor productivity and its decomposition of Chinese manufacturing based on the MML index:2003–2015. *J. Clean. Prod.* 222, 998–1008. doi: 10.1016/j.jclepro.2019.03.080

Si, R., Aziz, N., Liu, M., and Lu, Q. (2021). Natural disaster shock, risk aversion and corn farmers' adoption of degradable mulch film: evidence from zhangye, china. *Int. J. Climate Change Strat. Manage.* 13, 60–77. doi: 10.1108/IJCCSM-08-2020-0090

Silva-Olaya, A., Cerri, C., La Scala, N. Jr., Dias, C., and Cerri, C. (2013). Carbon dioxide emissions under different soil tillage systems in mechanically harvested sugarcane. *Environ. Res. Lett.* 8 (1), 1–8. doi: 10.1088/1748-9326/8/1/015014

Song, M., Fisher, R., Wang, J., and Cui, L. (2018). Environmental performance evaluation with big data: Theories and methods. *Ann. Operations Res.* 270 (1–2), 459–472. doi: 10.1007/s10479-016-2158-8

Sun, J., Wang, Z., Du, Y., Zhang, E., Gan, H., Sun, D., et al. (2022). Optimized tillage improves yield and energy efficiency while reducing carbon footprint in winter wheat-summer maize rotation systems. *Sci. Total Environ.* 820, 153278. doi: 10.1016/j.scitotenv.2022.153278

Sun, M., Ren, A., Gao, Z., Wang, P., Mo, F., Xue, L., et al. (2018). Long-term evaluation of tillage methods in fallow season for soil water storage, wheat yield and water use efficiency in semiarid southeast of the loess plateau. *Field Crops Res.* 218, 24–32. doi: 10.1016/j.fcr.2017.12.021

Tang, D., Shan, Z., He, J., and Zhao, Z. (2022). How do environmental regulations and outward foreign direct investment impact the green total factor productivity in China? a mediating effect test based on provincial panel data. *Int. J. Environ. Res. Public Health* 19, 15717. doi: 10.3390/ijerph192315717

Tang, D., Tang, J., Xiao, Z., Ma, T., and Bethel, B. J. (2017). Environmental regulation efficiency and total factor productivity–effect analysis based on chinese data from 2003 to 2013. *Ecol. Indic.* 73, 312–318. doi: 10.1016/j.ecolind.2016.08.040

Tian, P., Sui, P., Lian, H., Wang, Z., Meng, G., Sun, Y., et al. (2019). Maize straw returning approaches affected straw decomposition and soil carbon and nitrogen storage in northeast china. *Agron. (Basel).* 9 (12), 818. doi: 10.3390/agronomy9120818

Tone, K., and Tsutsui, M. (2010). An epsilon-based measure of efficiency in dea-a third pole of technical efficiency. *Eur. J. Oper. Res.* 207, 1554–1563. doi: 10.1016/j.ejor.2010.07.014

Totin, E., Van Mierlo, B., and Klerkx, L. (2020). Scaling practices within agricultural innovation platforms: Between pushing and pulling. *Agric. Syst.* 179, 102764. doi: 10.1016/j.agsy.2019.102764

Tugcu, C., and Tiwari, A. (2016). Does renewable and/or non-renewable energy consumption matter for total factor productivity (TFP) growth? evidence from the BRICS. *Renewable Sustain. Energy Rev.* 65, 610–616. doi: 10.1016/j.rser.2016.07.016

UN. (2001). Road map towards the implementation of the united nations millennium declaration. Available at: https://mdgs.un.org/unsd/mdg/Resources/Static/Products/SGReports/56_326/a_56_326e.pdf.

UN. (2015). *Transforming our world: the 2030 agenda for sustainable development*. Available at: https://documents-dds-ny.un.org/doc/UNDOC/GEN/N15/291/89/PDF/N1529189.pdf?OpenElement.

Wang, N. (2021). Mechanized technology for deep application of chemical fertilizer to corn in heilongjiang province. *New Agric.* 14, 66.

Wang, H., Fang, L., Mao, H., and Chen, S. (2022). Can e-commerce alleviate agricultural non-point source pollution? — A quasi-natural experiment based on a china's e-commerce demonstration city. *Sci. Total Environ.* 846, 157423. doi: 10.1016/j.scitotenv.2022.157423

Wang, S., Huang, X., Zhang, Y., Yin, C., and Richel, A. (2021a). The effect of corn straw return on corn production in northeast China: An integrated regional evaluation with meta-analysis and system dynamics. *Res. Conserv. Recy.* 167, 105402. doi: 10.1016/j.resconrec.2021.105402

Wang, Y., Su, Y., and Shu, Q. (2022). Labor out-migration, rural collective action and rural revitalization. *J. Tsinghua University(Philos. Soc. Sci.)* 37, 173–187. doi: 10.13613/j.cnki.qhdz.003150

Wang, S., Wang, H., Hafeez, M. D., Zhang, Q., Yu, Q., Wang, R., et al. (2020a). No-tillage and subsoiling increased maize yields and soil water storage under varied rainfall distribution: A 9-year site-specific study in a semi-arid environment. *Field Crops Res.* 255, 107867. doi: 10.1016/j.fcr.2020.107867

Wang, Q., Xu, Q., Lu, C., Li, H., and He, J. (2021b). Research status and development of key technologies for no-tillage seeding intellectualization. *J. South China Agric. Univ.* 42 (6), 27–35.

Wang, S., and Yang, Z. (2020). The effect of the aging of agricultural labor force on the change of grain green total factor productivity. *Res. Agric. Modern.* 41 (3), 396–406. doi: 10.13872/j.1000-0275.220.0037

Wang, Y., Yang, J., Liang, J., Qiang, Y., Fang, S., Gao, M., et al. (2018). Analysis of the environmental behavior of farmers for non-point source pollution control and management in a water source protection area in China. *Sci. Total Environ.* 633, 1126–1135. doi: 10.1177/0954407012475272

Wang, X., Yang, H., Liu, J., Wu, J., Chen, W., Wu, J., et al. (2015). Effects of ditch-buried straw return on soil organic carbon and rice yields in a rice-wheat rotation system. *Catena* 127, 56–63. doi: 10.1016/j.catena.2014.10.012

Wang, H., Zhang, Y., Zhang, Y., McDaniel, M., Sun, L., Su, W., et al. (2020b). Water-saving irrigation is a 'win-win' management strategy in rice paddies – with both reduced greenhouse gas emissions and enhanced water use efficiency. *Agric. Water Manage.* 228, 105889. doi: 10.1016/j.agwat.2019.105889

Wu, D., Wang, Y., and Qian, W. (2020). Efficiency evaluation and dynamic evolution of china's regional green economy: A method based on the super-PEBM model and DEA window analysis. *J. Clean. Prod.* 264, 121630. doi: 10.1016/j.jclepro.2020.121630

Wu, P., Liu, F., Li, H., Cai, T., Zhang, P., and Jia, Z. (2021).). suitable fertilizer application depth can increase nitrogen use efficiency and maize yield by reducing gaseous nitrogen losses. *Sci. Total Environment.* 781, 146787. doi: 10.1016/j.scitotenv.2021.146787

Xia, H., Riaz, M., Zhang, M., Liu, B., Li, Y., El-Desouki, Z., et al. (2022). Biochar-n fertilizer interaction increases n utilization efficiency by modifying soil C/N component under n fertilizer deep placement modes. *Chemo. (Oxford).* 286, 131594. doi: 10.1016/j.chemosphere.2021.131594

Xie, R., Yuan, Y., and Huang, J. (2017). Different types of environmental regulations and heterogeneous influence on "green" productivity: evidence from China. *Ecol. Econ.* 132, 104–112. doi: 10.1016/j.ecolecon.2016.10.019

Xie, F., Zhang, B., and Wang, N. (2021). Non-linear relationship between energy consumption transition and green total factor productivity: A perspective on different technology paths. *Sustain. Prod. Consump.* 28, 91–104. doi: 10.1016/j.spc.2021.03.036

Xu, B., Chen, W., Zhang, G., Wang, J., Ping, W., Luo, L., et al. (2020). How to achieve green growth in china's agricultural sector. *J. Clean. Prod.* 271, 122770. doi: 10.1016/j.jclepro.2020.122770

Xue, X., and Gu, X. (2022). Research on the threshold effect of non-grain on grain green total factor productivity. *Chin. J. Agric. Resour. Reg. Plan.* 43 (7), 17–26.

Yang, X., Cheng, L., Huang, X., Zhang, Y., and Lebailly, P. (2020). Incentive mechanism to promote corn stalk return sustainably in henan, china. *Sci. Total Environ.* 738, 139775. doi: 10.1016/j.scitotenv.2020.139775

Yang, C., Hu, P., Diao, B., Cheng, J., and Cui, H. (2021). Environmental performance evaluation of policies in main grain producing areas:from the perspective of agricultural carbon emissions. *China Popul. Resour. Environ.* 31 (12), 35–44.

Yang, Y., Shi, L., and Zhang, X. (2019). Application of mechanized deep tillage and subsoiling technology and types of machinery. *Agric. Machin. Using Maintenance* 8, 102. doi: 10.14031/j.cnki.njwx.2019.08.065

Yang, H., Wang, X., and Bin, P. (2022b). Agriculture carbon-emission reduction and changing factors behind agricultural eco-efficiency growth in China. *J. Clean. Prod.* 334, 130193. doi: 10.1016/j.jclepro.2021.130193

Yang, Z., Wang, D., Du, T., Zhang, A., and Zhou, Y. (2018). Total-factor energy efficiency in china's agricultural sector: Trends, disparities and potentials. *Energies (Basel)* 11 (4), 853. doi: 10.3390/en11040853

Yang, Z., Zhu, Y., Zhang, J., Li, X., Ma, P., Sun, J., et al. (2022a). Comparison of energy use between fully mechanized and semi-mechanized rice production in southwest china. *Energy* 245, 123270. doi: 10.1016/j.energy.2022.123270

Yin, C., Huang, X., Zhao, J., Cheng, L., Chang, Z., and Chien, H. (2016). Analysis of the willingness to accept for maize straw returned to field: based on farmer's survey in hebei and shandong provinces. *Chin. J. Agric. Resour. Regional Planning.* 37 (7), 87–95.

Yu, D., Liu, L., Gao, S., Yuan, S., Shen, Q., and Chen, H. (2022). Impact of carbon trading on agricultural green total factor productivity in China. *J. Clean. Prod.* 367, 132789. doi: 10.1016/j.jclepro.2022.132789

Zhai, L., LÜ, L., Dong, Z., Zhang, L., Zhang, J., Jia, X., et al. (2021). The water-saving potential of using micro-sprinkling irrigation for winter wheat production on the north China plain. *J. Integr. Agri.* 20 (6), 1687–1700. doi: 10.1016/S2095-3119(20)63326-3

Zhang, W., Cao, G., Li, X., Zhang, H., Wang, C., Liu, Q., et al. (2016). Closing yield gaps in China by empowering smallholder farmers. *Nat. (London)* 537 (7622), 671–674. doi: 10.1038/nature19368

Zhang, Q., Chu, Y., Xue, Y., Ying, H., Chen, X., Zhao, Y., et al. (2020). Outlook of china's agriculture transforming from smallholder operation to sustainable production. *Global Food Secur.* 26, 100444. doi: 10.1016/j.gfs.2020.100444

Zhang, M., Dong, S., Zhu, J., and Zhao, H. (2021). Research on the influence of socialized service of mid-production. *J. Maize Sci.* 06), 175–183. doi: 10.13597/j.cnki.maize.science.20210625

Zhang, M., Song, D., Pu, X., Dang, P., Qin, X., and Siddique, K. (2022). Effect of different straw returning measures on resource use efficiency and spring maize yield under a plastic film mulch system. *Eur. J. Agro.* 134, 126461. doi: 10.1016/j.eja.2022.126461

Zhang, C., Wu, N., Zhang, Y., Wu, H., Gu, F., and Hu, Z. (2018). Development status and trend of no tillage seeding technology at home and abroad. *Jiangsu Agric. Sci.* 46 (16), 1–5. doi: 10.15889/j.issn.1002-1302.2018.16.001

Zhao, T., Xiao, H., Zhao, H., Dai, J., Zhao, L., Zhang, M., et al. (2020). Response of maize yield, biological traits and nutrient utilization and soil fertility to fertilization depth in guizhou. *J. Irrig. Drain.* 39, 21–25. doi: 10.13522/j.cnki.ggps.2019113

Zhao, Y., Xiong, X., and Wu, C. (2021). Effects of deep placement of fertilizer on periphytic biofilm development and nitrogen cycling in paddy systems. *Pedosphere* 31 (1), 125–133. doi: 10.1016/S1002-0160(20)60051-0

Zhao, P., Zeng, L., Li, P., Lu, H., Hu, H., Li, C., et al. (2022). China's transportation sector carbon dioxide emissions efficiency and its influencing factors based on the EBM DEA model with undesirable outputs and spatial durbin model. *Energy* 238, 121934. doi: 10.1016/j.energy.2021.121934

Zhao, R., Liu, Y., Tian, M., Ding, M., Cao, L., Zhang, Z., et al. (2018). Impacts of water and land resources exploitation on agricultural carbon emissions: The water-land-energy-carbon nexus. *Land Use Policy* 72, 480–492. doi: 10.1016/j.landusepol.2017.12.029

Zhong, M., Huang, G., He, R., Lund, H., and Kaiser, M. J. (2022). The technological innovation efficiency of china's lithium-ion battery listed enterprises: evidence from a three-stage dea model and micro-data. *Energy* 246, 123331. doi: 10.1016/j.energy.2022.123331

Zhong, X., Peng, J., Kang, X., Wu, Y., Luo, G., Hu, W., et al. (2021). Optimizing agronomic traits and increasing economic returns of machine-transplanted rice with side-deep fertilization of double-cropping rice system in southern china. *Field Crops Res.* 270, 108191. doi: 10.1016/j.fcr.2021.108191

Zhuang, Y., Zhang, L., Li, S., Liu, H., Zhai, L., Zhou, F., et al. (2019). Effects and potential of water-saving irrigation for rice production in China. *Agric. Water Manage.* 217, 374–382. doi: 10.1016/j.agwat.2019.03.010

Zhu, C., Ouyang, Y., Diao, Y., Yu, J., Luo, X., Zheng, J., et al. (2021). Effects of mechanized deep placement of nitrogen fertilizer rate and type on rice yield and nitrogen use efficiency in chuanxi plain, China. *J. Integr. Agri.* 20 (2), 581–592. doi: 10.1016/S2095-3119(20)63456-6

Zou, L., Liu, Y., Wang, Y., and Hu, X. (2020). Assessment and analysis of agricultural non-point source pollution loads in China: 1978–2017. *J. Environ. Manage.* 263, 110400. doi: 10.1016/j.jenvman.2020.110400

frontiers | Frontiers in Plant Science

TYPE Original Research
PUBLISHED 31 May 2023
DOI 10.3389/fpls.2023.1176293

OPEN ACCESS

EDITED BY
M. Iqbal R. Khan,
Jamia Hamdard University, India

REVIEWED BY
Zhenwei Song,
CAAS, China
Wei Hu,
Nanjing Agricultural University, China
Chandra Shekhar Seth,
University of Delhi, India

*CORRESPONDENCE
Xinglong Dai
adaisdny@163.com

RECEIVED 28 February 2023
ACCEPTED 04 May 2023
PUBLISHED 31 May 2023

CITATION
Zhang X, Liu M, Zheng F, Dong Y, Hua Y, Chu J, He M and Dai X (2023) Optimizing sowing patterns in winter wheat can reduce N_2O emissions and improve grain yield and NUE by enhancing N uptake. *Front. Plant Sci.* 14:1176293. doi: 10.3389/fpls.2023.1176293

Optimizing sowing patterns in winter wheat can reduce N_2O emissions and improve grain yield and NUE by enhancing N uptake

Xiu Zhang[1], Manyu Liu[1,2], Feina Zheng[1], Yuanjie Dong[3], Yifan Hua[1,4], Jinpeng Chu[1], Mingrong He[1] and Xinglong Dai[1]*

[1]College of Agronomy, Shandong Agricultural University, Tai'an, Shandong, China, [2]Agricultural and Rural Bureau of Mengyin County, Linyi, Shandong, China, [3]College of Resources and Environment, Shandong Agricultural University, Tai'an, Shandong, China, [4]College of Agriculture, Nanjing Agricultural University, Nanjing, Jiangsu, China

Increasing nitrogen (N) input is essential to satisfy the rising global wheat demand, but this increases nitrous oxide (N_2O) emissions, thereby exacerbating global climate change. Higher yields accompanied by reduced N_2O emissions are essential to synergistically reduce greenhouse warming and ensure global food security. In this study, we conducted a trial using two sowing patterns (conventional drilling sowing [CD] and wide belt sowing [WB], with seedling belt widths of 2–3 and 8–10 cm, respectively) with four N rates (0, 168, 240, and 312 kg ha^{-1}, hereafter N0, N168, N240, and N312, respectively) during the 2019–2020 and 2020–2021 growing seasons. We investigated the impacts of growing season, sowing pattern, and N rate on N_2O emissions, N_2O emissions factors (EFs), global warming potential (GWP), yield-scaled N_2O emissions, grain yield, N use efficiency (NUE), plant N uptake and soil inorganic N concentrations at jointing, anthesis, and maturity. The results showed that sowing pattern and N rate interactions influenced the N_2O emissions markedly. Compared to CD, WB significantly reduced cumulative N_2O emissions, N_2O EFs, GWP, and yield-scaled N_2O emissions for N168, N240, and N312, with the largest reduction seen at N312. Furthermore, WB markedly improved plant N uptake and reduced soil inorganic N compared to CD at each N rate. Correlation analyses indicated that WB mitigated the N_2O emissions at various N rates mainly through efficient N uptake and reduced soil inorganic N. The highest grain yield occurred under a combination of WB and N312, under which the yield-scaled N_2O emissions were equal to the local management (sowing with CD at N240). In conclusion, WB sowing could synergistically decrease N_2O emissions and obtain high grain yields and NUEs, especially at higher N rates.

KEYWORDS

N rate, wide belt sowing, N_2O emissions, grain yield, plant N uptake, soil inorganic N concentration, winter wheat (*Triticum aestivum* L.)

1 Introduction

With an expanding world population, it is estimated that major cereal crops must increase by approximately 50% to meet the expected food demand by 2050 (vanDijk et al., 2021). However, limited land area for agriculture means that the only way to increase grain yield is to achieve a higher yield per unit of land area (Godfray et al., 2011). The nutrients compositions and quality of soil, especially nitrogen (N) nutrition, has a significant impact on crops productivity, thereby grain yield (Duan et al., 2019). It is foreseeable that more synthetic N fertilizers will be needed to meet the increasing grain yield demands of an increased global population (Kong et al., 2021).

Global warming caused by greenhouse gases is currently a research hotspot (Kim et al., 2013; Seth and Misra, 2014). It may exacerbate the occurrence of abiotic stresses, such as salt, drought, and so on (Zhu, 2016; Shultana et al., 2022). Application of exogenous matters, like inorganic N, may alleviate these abiotic stresses (Krapp, 2015; Agnihotri and Seth, 2016).

N_2O, one of the most important greenhouse gases, is produced in soils, and approximately 60% of global N_2O emissions originate from agriculture, mainly due to N fertilizer application to soils (Millar et al., 2018). N_2O causes global warming, destroys the ozone layer, and increases ultraviolet radiation on the ground (IPCC, 2021). When seeking for the high yield or alleviating these abiotic stress in crop production, the application of N fertilizer may increase N_2O emissions, because the soil NH_4^+ and NO_3^- concentrations increase (Millar et al., 2018; Takeda et al., 2021), both of which are the substrates of nitrification and denitrification processes in soil and closely related to N_2O emissions (Subbarao et al., 2017; Zhang et al., 2019).

Therefore, increasing wheat yield while mitigating the cumulative N_2O emissions caused by N fertilizer application is essential to ensure food security and slow global warming (Ying et al., 2019). The application of urease and nitrification inhibitors (Recio et al., 2019; Wang et al., 2021), control-released fertilization (Ji et al., 2012), and partial substitution of chemical N with manure (Kong et al., 2021; Zhang et al., 2021) could synergistically increase wheat yield and reduce N_2O emissions. However, these measures will increase production costs.

Compared to conventional drilling sowing (CD), wide belt sowing (WB) is an optimized sowing pattern that increases the belt of wheat seedlings from 2–3 to 8–10 cm by altering the width of the furrow opener moldboard without increasing other costs. This improves spatial uniformity and reduces intraspecific competition within seedling belts (Liu et al., 2020; Lv et al., 2020), and results in enhanced water, N, radiation use efficiency, and grain yield of winter wheat (Li et al., 2015; Liu et al., 2020; Wang et al., 2022; Zheng et al., 2023). In particular, the enhanced ability to absorb N offers the possibility of reducing nitrous oxide emissions. However, there are insufficient data on how WB affects the N_2O emissions of winter wheat.

Therefore, we hypothesized that sowing winter wheat as WB instead of CD with N fertilizer input would result in improved grain yield alongside reduced N_2O emissions. This would be due to the reduced concentrations of inorganic N in the soil through enhanced N uptake. We evaluated the interaction between sowing pattern and the application of different N rates on grain yield and N_2O emissions. To this end, we used two sowing patterns (CD and WB) at N rates of 0, 168, 240, and 312 kg ha^{-1} under field conditions. We also investigated the N uptake and soil inorganic N concentrations at jointing, anthesis, and maturity stages to elucidate the processes involved in decreasing N_2O emissions using the optimized sowing pattern.

2 Materials and methods

2.1 Study site and growth conditions

During the 2019–2020 and 2020–2021 winter wheat growing seasons, field experiments were conducted in Dongwu Village (35° 57'N, 117°03'E), Dawenkou, Daiyue District, Tai'an, Shandong Province, China. Summer maize was the previous crop grown at the study site, and all remaining straw was plowed into the field. The soil was characterized as a sandy loam (typic Cambisols; FAO, 2003) with a pH of 7.2. Before sowing wheat in 2019–2020, the total N, alkali-hydrolyzable N, available P_2O_5, available K_2O, and organic matter in the top 20 cm of the soil were 1.11 g kg^{-1}, 111.00 mg kg^{-1}, 34.69 mg kg^{-1}, 98.47 mg kg^{-1}, and 16.70 g kg^{-1}, respectively. Climatic data, including rainfall and temperature, are shown in Figure S1.

2.2 Experimental design

Seeds of two winter wheat cultivars, Tainong18 (T18) and Taimai198 (T198), were sown on 15 October 2019 and 17 October 2020 and harvested on 8 June 2020 and 10 June 2021, respectively. We used two sowing patterns (Figure S2; CD and WB) and four N rates (0, 168, 240, and 312 kg ha^{-1}; hereafter, N0, N168, N240, and N312, respectively). The CD sowing pattern at N240 is widely used in local agricultural production. Treatments of each cultivar were arranged in a split-plot design with the N rate as the main plot and sowing pattern as the subplot (n = 4). The length and width of each subplot were 22.0 m and 3.0 m (12 rows spaced 25 cm apart), respectively. The basal/topdressing of N fertilizer (applied as urea, 46% N) in a 4:6 ratio, and the topdressing N was applied at jointing (Table S1). The crops were irrigated after sowing, at jointing and anthesis in both growing seasons, at a rate of 60 mm each time.

2.3 Measurement methods

2.3.1 Grain yield, inorganic N concentrations in the soil, and plant N uptake

Grain yield was measured at maturity by manually cutting all spikes in 3.0 m^2 rows in each plot as described by Li et al. (2015) and adjusted to 13% moisture content. The inorganic N concentrations in the soil and plant N uptake were measured according to Shi et al. (2012). We collected soil samples randomly from five locations in each plot before sowing, and at the jointing, anthesis, and maturity

stages to estimate the inorganic N. Fifty single plants or stems were sampled at all three stages to determine the aboveground N accumulation (AGN). The plant N uptake during growth was calculated according to the AGN of the latter growth stage minus that of the previous growth stage. NUE, N uptake efficiency (UPE), and N utilization efficiency (UTE) were calculated according to Moll et al. (1982). The formulas for calculating these indexes are provided in the Supplementary Material.

2.3.2 N_2O emissions flux and calculation of N_2O emissions-related indicators

We used the closed chamber-gas chromatography method to measure the N_2O emissions flux, according to Lyu et al. (2019). In this study, the chambers included a chamber base of 54 cm length × 22 cm wide and 26 cm high with a 3 cm width water channel and a cover box of 56 cm × 24 cm × 90 cm. Gas was sampled daily for 5 days after base fertilization, and sampling frequency was reduced to once every 7 days for approximately 1 month after irrigation (after sowing) or rainfall > 20 mm and then three times a month until the next fertilization event. Gas samples were also measured daily following topdressing for 5 days and every 2 days after that for five times until irrigation at the anthesis stage. Gas samples were also measured after irrigation or rainfall > 20 mm every 7 days until maturity.

The N_2O flux formula was calculated according to the adapted equation by Duan et al. (2019). The cumulative N_2O emissions, fertilizer-induced N_2O emissions factor (EF), and the yield-scaled N_2O were computed referring to the equation in Huang et al. (2017). The N_2O global warming potential (GWP) was calculated as the cumulative N_2O emissions multiplied by 273, according to IPCC (2021). The formulas for calculating these indexes are provided in the Supplementary Material.

2.4 Statistical analysis

Analyses of variance and multiple comparisons were determined according to the least significant difference at 0.05 and a probability level with DPS 7.05 (Zhejiang University, Hangzhou, China). We used Microsoft Excel 2013 (Microsoft, Redmond, WA, USA) to create the tables and SigmaPlot 14.0 (Systat Software, San Jose, CA, USA) to generate the figures.

3 Results

3.1 Grain yield and NUE

The winter wheat grain yield was significantly affected by growing season, cultivars, N rates, sowing patterns, and the following interactions: growing season × N rate, cultivar× N rate, N rate × sowing pattern, and growing season × cultivar × N rate (Table S2). The grain yield increased significantly with an increased N rate from N0 to N312 (Table 1). WB significantly increased the grain yield at N168, N240, and N312 compared to CD, despite the increase showing a decreasing trend with the increased N rate. In 2019–2020, WB increased grain yields by 10.43%, 8.22%, and 5.44%, and by 10.31%, 7.67%, and 6.63% at N168, N240, and N312 for cultivars T18 and T198, respectively. In 2020–2021, the grain yields in WB increased by 9.18%, 8.24%, and 7.22%, and by 8.44%, 6.85%, and 5.74% for T18 and T198, respectively. WB at N312 showed the highest yield of all the treatments. Compared to local management (sowing with CD at N240), WB at N312 increased the grain yields of T18 and T198 by 8.03% and 13.53% in 2019–2020 and 15.16% and 13.06% in 2020–2021, respectively.

The NUE of winter wheat was significantly influenced by growing season, cultivar, N rates, sowing patterns, and the interactions of growing season × cultivar, growing season × N rate, cultivar× N rate, N rate × sowing pattern, growing season × cultivar× N rate, and growing season × N rate × sowing pattern (Table S2). It significantly decreased with N rates increased from N168 to N312 (Table 1). WB significantly improved it at N168, N240, and N312 compared to CD, despite the extent of the increase showing a decreasing trend with the increased N rate. In 2019–2020, WB increased the NUE by 10.43%, 8.22%, and 5.44%, and by 10.31%, 7.67%, and 6.63% at N168, N240, and N312 for cultivars T18 and T198, respectively. In 2020–2021, the NUE in WB increased by 9.18%, 8.24%, and 7.22%, and by 8.44%, 6.85%, and 5.74% for T18 and T198, respectively.

Under each sowing pattern, the UPE and UTE decreased gradually with the increased N rate. Compared to CD, WB markedly increased the UPE at N168, N240, and N312. The UPE was increased by an average of 11.42%, 9.83%, and 7.71%, and by 10.88%, 8.52%, and 7.87%, at N168, N240, and N312 for the T18 and T198 cultivars, respectively, across two growing seasons. However, the UTE for either cultivar was not significantly different between CD and WB at each N rate.

3.2 N_2O emissions

3.2.1 N_2O emissions dynamics

The dynamic changes in the N_2O fluxes are presented in Figure 1. The N_2O dynamics were considerably affected by the sowing patterns and N rates over the two growing seasons. N_2O gradually increased with the increased N rate when sown using the same sowing pattern. Then it usually spiked after the input of basal fertilizer and topdressing fertilizer and after rainfall (> 20 mm) or irrigation (arrows numbered 1 to 5). The N_2O emissions were higher in CD than in WB, and CD at N312 had the highest N_2O flux.

N_2O flux peaked after topdressing and was lower in WB at each N rate compared to CD. In 2019–2020, the highest fluxes were 12.98, 18.20, 26.00, and 29.04 μg m^{-2} h^{-1} and 12.75, 18.75, 25.77, and 30.56 μg m^{-2} h^{-1} for N0, N168, N240, and N312 of the T18 and T198 cultivars, respectively, when sown in CD. However, when sown in WB, they were 11.20, 17.53, 24.30, and 26.77 μg m^{-2} h^{-1} and 11.82, 17.30, 25.13, and 27.94 μg m^{-2} h^{-1} for cultivars T18 and T198, respectively. In 2020–2021, the highest fluxes were 6.32, 17.90, 27.67, and 31.03 μg m^{-2} h^{-1} and 6.51, 19.14, 26.61, and 31.19 μg m^{-2} h^{-1} for N0, N168, N240, and N312 of cultivars T18 and T198, respectively, when sown in CD. However, they were 6.20, 16.36, 26.67, and 28.65 μg m^{-2} h^{-1} and 6.54, 17.65, 25.64, and 28.51 μg m^{-2} h^{-1}, respectively, for cultivars T18 and T198 when sown in WB. The flux gradually decreased following the peak pulse.

10.3389/fpls.2023.1176293

TABLE 1 Effects of sowing pattern and N rate on grain yield, N use efficiency (NUE), N uptake efficiency (UPE), and N utilization efficiency (UTE) of winter wheat.

Growing season	Cultivar	N rate (kg ha^{-1})	Sowing pattern	Grain yield (kg ha^{-1})	NUE (kg kg^{-1})	UPE (%)	UTE (kg kg^{-1})
2019–2020	Tainong18	0	Conventional drilling	7254.94e	41.50b	88.86b	46.61a
			Wide belt	7754.59d	44.60a	91.88a	48.59a
		168	Conventional drilling	8412.29c	24.56d	72.05d	33.73b
			Wide belt	9289.77a	27.13c	80.59c	33.72b
		240	Conventional drilling	8656.55bc	20.92f	66.45f	31.49c
			Wide belt	9368.07a	22.60e	73.05d	30.95c
		312	Conventional drilling	8868.76b	18.25h	64.68g	28.36d
			Wide belt	9351.27a	19.25g	69.16e	28.32d
	Taimai198	0	Conventional drilling	7279.05f	41.80b	75.03b	55.94a
			Wide belt	7952.01e	45.66a	80.78a	57.17a
		168	Conventional drilling	8636.00d	25.24d	66.88d	37.84b
			Wide belt	9526.40c	27.84c	74.88b	37.10b
		240	Conventional drilling	9318.82c	22.50f	64.43e	34.78c
			Wide belt	10033.43b	24.23e	70.53c	34.36c
		312	Conventional drilling	9921.35b	20.41h	63.05e	32.23d
			Wide belt	10579.47a	21.76g	68.42d	31.96d
2020–2021	Tainong18	0	Conventional drilling	4562.38f	31.74c	77.96e	40.13a
			Wide belt	4808.72e	33.45b	84.28d	39.67a
		168	Conventional drilling	9049.36d	31.70c	91.40b	34.68b
			Wide belt	9880.08c	34.60a	101.53a	34.11b
		240	Conventional drilling	9784.59c	26.42e	79.71e	33.14c
			Wide belt	10591.14b	28.59d	87.46c	32.70c
		312	Conventional drilling	10512.10b	22.64g	72.96f	31.04d
			Wide belt	11270.99a	24.27f	79.15e	30.71d
	Taimai198	0	Conventional drilling	3956.82f	27.53f	75.40d	36.56ab
			Wide belt	4257.15e	29.61d	82.32c	36.18b
		168	Conventional drilling	9662.91d	33.84b	90.86b	37.27a
			Wide belt	10478.41c	36.70a	99.90a	36.74ab
		240	Conventional drilling	10648.62c	28.75e	84.12c	34.18c
			Wide belt	11378.58b	30.72c	90.80b	33.84c
		312	Conventional drilling	11386.15b	24.52h	77.44d	31.67d
			Wide belt	12039.84a	25.93g	82.89c	31.29d

Different letters within a column for the same season and cultivar indicate significant differences ($P < 0.05$).

3.2.2 Cumulative N_2O emissions

The cumulative N_2O and GWP of N_2O emissions were significantly influenced by the growing season, cultivar, N rate, and sowing pattern. Only the growing season × N rate and N rate × sowing pattern interactions significantly affected this measure (Table S2). The cumulative N_2O emissions were 0.21–0.91 kg N ha^{-1} with an average of 0.60 kg N ha^{-1} for cultivar T18 and 0.19–0.87 kg N ha^{-1} with an average of 0.57 kg N ha^{-1} for cultivar T198, across two growing seasons (Figure 2). The GWP was 57.33–248.43 kg CO_2-eq ha^{-1} with an average of 163.80 kg CO_2-eq ha^{-1} for cultivar

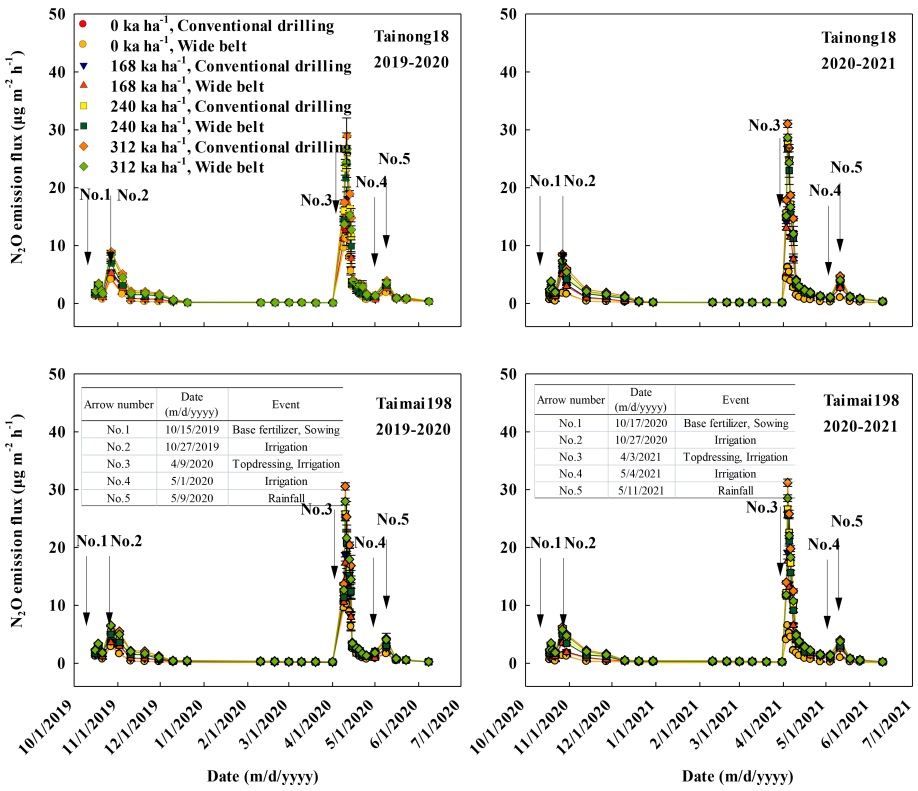

FIGURE 1
Effects of sowing pattern and N rate on the nitrous oxide (N_2O) emissions fluxes of winter wheat. The rainfall events all exceeded 20 mm.

T18 and 51.87–237.51 kg CO_2-eq ha^{-1} with an average of 155.61 kg CO_2-eq ha^{-1} for cultivar T198, across two growing seasons (Figure S3).

Under each sowing pattern, the cumulative N_2O emissions increased exponentially as the N rate increased from N0 to N312. WB significantly reduced the values at N168, N240, and N312 compared to CD and had a lower exponential equation slope (Figure 2), indicating that WB could slow the increase in N_2O emissions resulting from the increased N rate. Therefore, the reduction in cumulative N_2O emissions in WB significantly improved as the N rates increased and peaked at an N312. In 2019–2020, WB decreased the values by 6.29%, 8.31%, and 11.90%, and by 5.00%, 7.58%, and 9.61% for cultivars T18 and T198 at N168, N240, and N312, respectively. In 2020–2021, WB decreased the values by 4.69%, 7.07%, and 7.99%, and by 4.48%, 6.23%, and 7.64% for cultivars T18 and T198 at N168, N240, and N312, respectively. CD at N312 showed the highest cumulative N_2O emissions. The GWP response of N_2O emissions to sowing pattern and N rate showed the same trend as the cumulative N_2O emissions (Figure S3).

As shown in Figure 3 and Table S3, the cumulative N_2O emissions during the stages from sowing to jointing, jointing to anthesis, and anthesis to maturity were 0.10–0.36, 0.13–0.38, and 0.05–0.17 kg N ha^{-1} with averages of 0.21, 0.27, and 0.11 kg N ha^{-1} for cultivar T18. For cultivar T198, these were 0.09–0.33, 0.13–0.37, and 0.05–0.16 kg N ha^{-1} with averages of 0.21, 0.26, and 0.11 kg N ha^{-1}, respectively, across two growing seasons. The biggest proportion of cumulative N_2O emissions was that from jointing to anthesis (39.22–47.44% with an average of 44.60%), followed by sowing to jointing (30.35–40.62% with an average of 36.32%) and anthesis to maturity (15.67–22.95% with an average of 19.08%).

The cumulative N_2O emissions in WB during these three stages were all lower than in CD at N168, N240, and N312. Like the total cumulative N_2O emissions, the amount and proportion of the reduced cumulative N_2O emissions during the three stages also improved with increasing N rates and had the highest reduction at N312. The largest difference in N_2O emissions for the two sowing patterns occurred from jointing to anthesis (0.011–0.043 kg N ha^{-1} with 0.025 kg N ha^{-1} on average), followed by sowing to jointing (0.007–0.041 kg N ha^{-1} with 0.021 kg N ha^{-1} on average), and anthesis to maturity (0.005–0.020 kg N ha^{-1} with 0.011 kg N ha^{-1} on average) across two growing seasons, for both cultivars and with N168, N240, and N312.

3.3 N_2O emissions factors

The N_2O EFs were significantly influenced by the main effects of growing seasons, cultivar, N rate, and sowing pattern. Only the interactions of growing season × N rate and N rate × sowing pattern significantly affected the N_2O EFs (Table S2). The N_2O EFs were 0.09–0.22% with an average of 0.17% for cultivar T18 and 0.09–0.22% with an average of 0.16% for cultivar T198 across two growing seasons (Figure 4). They were much higher in 2020–2021 (0.20%) than in 2019–2020 (0.13%), mainly due to the lower

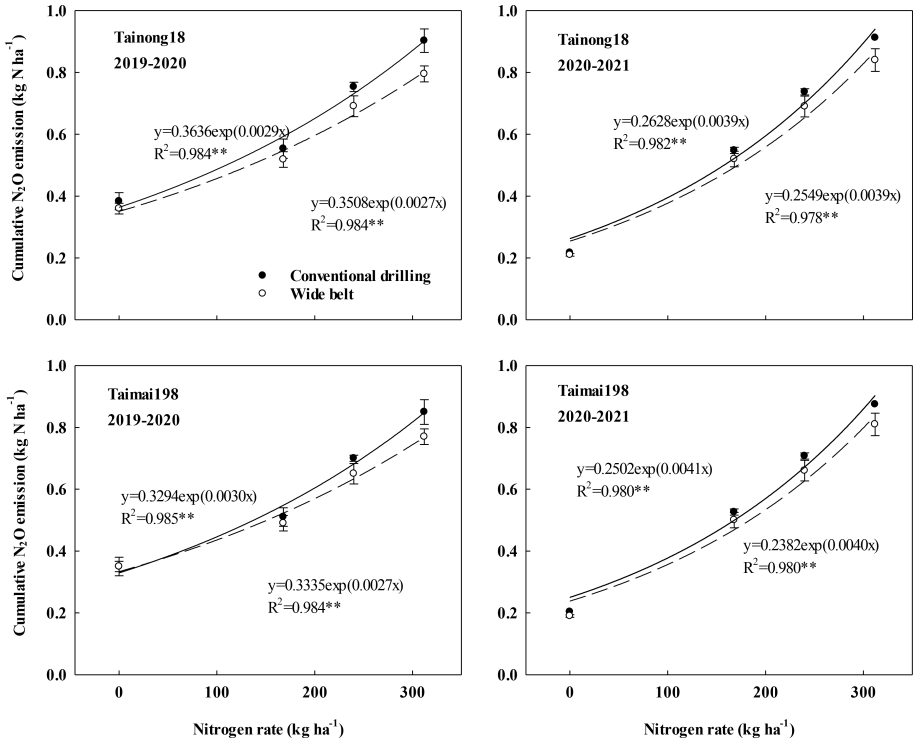

FIGURE 2
Effects of sowing patterns and N rates on cumulative nitrous oxide (N_2O) emissions of winter wheat.

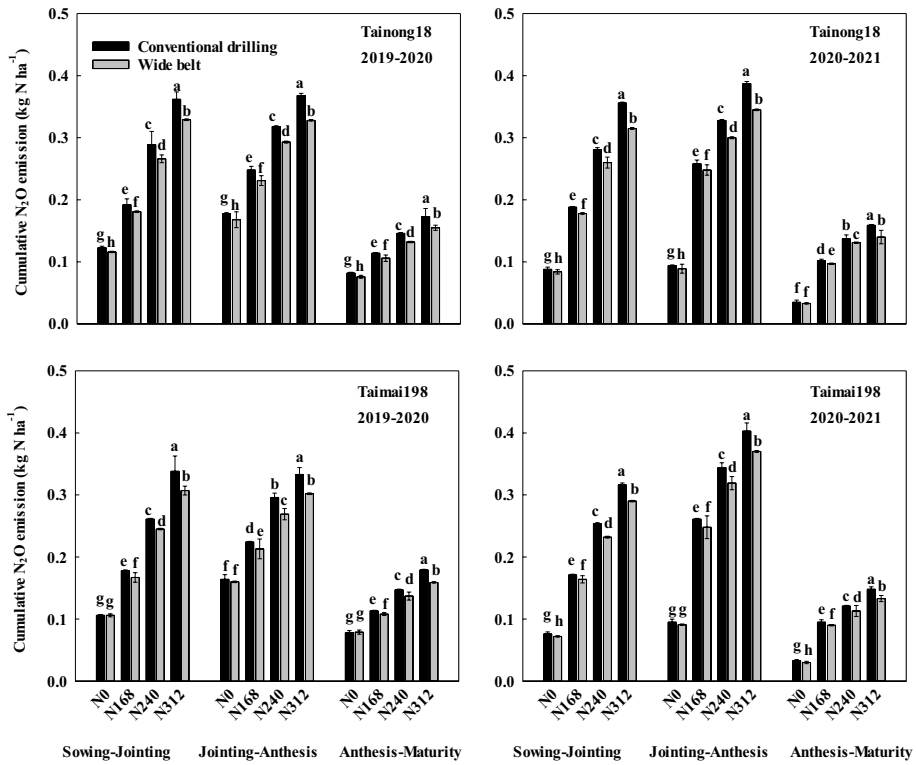

FIGURE 3
Effects of sowing patterns and N rates on cumulative nitrous oxide (N_2O) emissions during different growth stages of winter wheat. N0, N168, N240, and N312 indicate N rates of 0, 168, 240, and 312 kg ha^{-1}. Different letters within the same growth stage for the same season and cultivar indicate significant differences at $P < 0.05$.

cumulative N_2O emissions at N0 in the second growing season as a result of continuous not applying N fertilizer. Meanwhile, there was a parabolic change as the N rate increased from N168 to N312 under each sowing pattern.

The N_2O EFs peaked at 293.20–319.00 kg ha^{-1} with an average of 305.63 kg ha^{-1} in CD, which was higher than that in WB (275.92–295.49 kg ha^{-1} with 283.55 kg ha^{-1} on average). WB significantly decreased the N_2O EFs at N168, N240, and N312 compared to CD and showed a lower slope in the parabolic equation (Figure 4). Hence it reduced the increase in EFs resulting from the increased N rate. The extent of this reduction was significantly improved as the N rates increased and was highest at N312. In 2019–2020, WB decreased the EFs by 6.47%, 10.49%, and 16.09%, and by 13.66%, 14.16%, and 15.68% for cultivars T18 and T198 at N168, N240 and N312, respectively. In 2020–2021, WB decreased the values by 4.36%, 7.85%, and 8.86%, and by 4.19%, 6.76%, and 8.47% for cultivars T18 and T198 at N168, N240, and N312, respectively. CD at N312 had the highest N_2O EFs. WB at N312 decreased the EFs of T18 and T198 by 9.40% and 8.53% in 2019–2020 and by 6.32% and 6.21% in 2020–2021, respectively, compared to the local management (sowing using CD at N240).

3.4 Yield-scaled N_2O emissions

The yield-scaled N_2O emissions were significantly influenced by the effects of the growing season, cultivar, N rate and sowing pattern, and the two-way interactions except for growing season × sowing pattern (Table S2). Across two growing seasons, the values were 42.77–101.78 mg kg^{-1} with 67.09 mg kg^{-1} on average for cultivar T18 and 43.41–85.69 mg kg^{-1} with 60.56 mg kg^{-1} on average for cultivar T198, respectively (Figure 5).

The yield-scaled N_2O emissions increased exponentially as the N rate increased from N0 to N312 under the same sowing pattern. WB significantly reduced the values at each N rate compared to CD. The lower slope of the exponential equation indicated that WB could slow the increment of these emissions resulting from the increased N rate (Figure 5). Therefore, the reduction of yield-scaled N_2O emissions in WB significantly improved as the N rates increased and were highest at N312. In 2019–2020, WB decreased this measure by 12.26%, 15.15%, 15.28%, and 16.44% and by 9.25%, 13.88%, 14.16%, and 15.23% for cultivars T18 and T198 at N0, N168, N240, and N312, respectively. In 2020–2021, the values decreased by 10.06%, 12.70%, 14.15%, and 14.19% and by 11.63%, 11.91%, 12.25%, and 12.66% for cultivars T18 and T198 at N0, N168, N240, and N312 kg ha^{-1}, respectively. Furthermore, the reductions with seedling belt optimization were greater than those of cumulative N_2O emissions. CD at N312 kg ha^{-1} obtained the highest yield-scaled N_2O emissions. The emissions of WB at N312 were equal to the local management system (sowing with CD at N 240).

3.5 N uptake and soil inorganic N concentrations

3.5.1 N uptake during different growth stages

The N uptake during the three growth stages increased with increasing N rates and peaked at N312 (Figure 6). The uptake

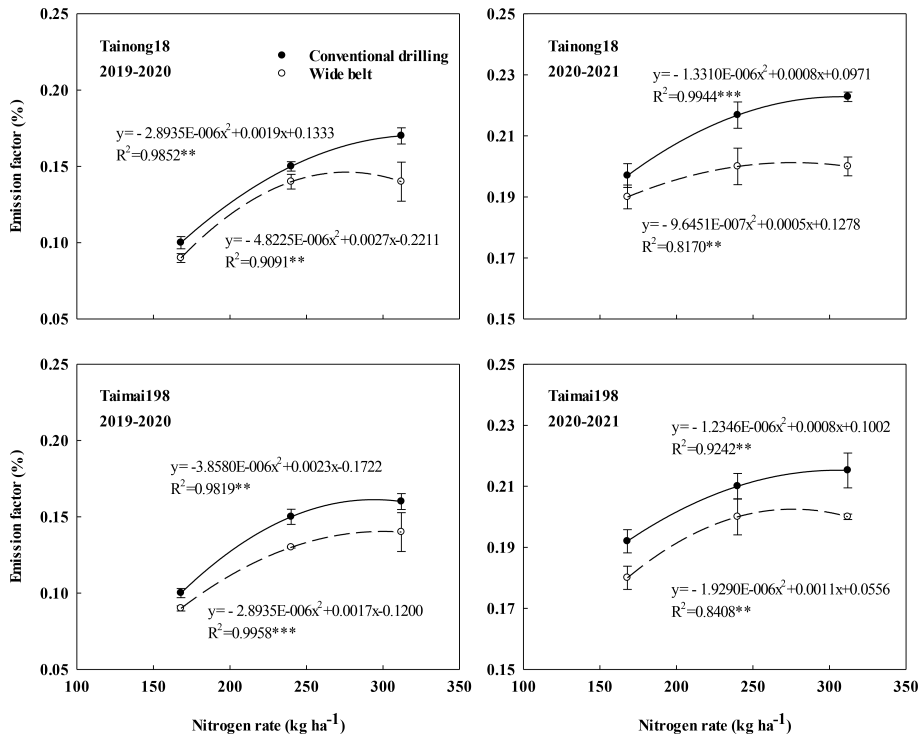

FIGURE 4
Effects of sowing patterns and N rates on the nitrous oxide emission factor of winter wheat.

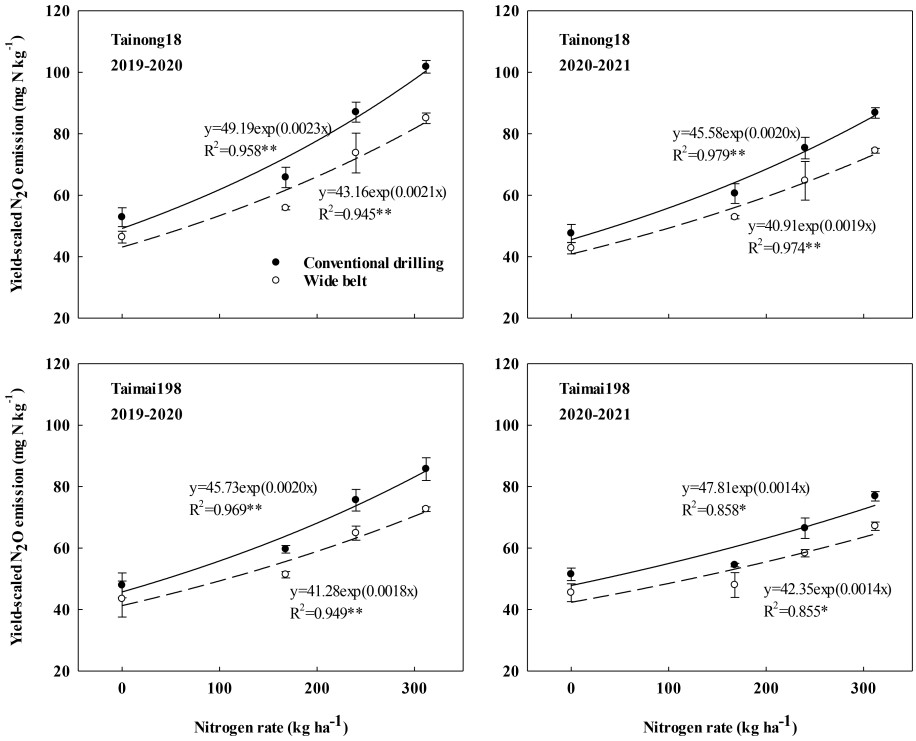

FIGURE 5
Effects of sowing pattern and N rate on yield-scaled nitrous oxide (N_2O) emissions of winter wheat.

during the three growth stages was higher in WB than in CD. At N168, N240, and N312, the differences in uptake for the two sowing patterns were 9.53, 8.74, and 5.99 kg ha^{-1} for T18 and 9.36, 7.06, and 6.22 kg ha^{-1} for T198 during sowing to jointing, 8.39, 7.90, and 7.93 kg ha^{-1} for T18 and 7.41, 6.99, and 6.97 kg ha^{-1} for T198 during jointing to anthesis, and 11.13, 11.39, and 11.33 kg ha^{-1} for T18 and 9.83, 10.94, and 12.52 kg ha^{-1} for T198 during anthesis to maturity, respectively, across two growing seasons.

3.5.2 Soil inorganic N concentrations at different stages

The inorganic N concentrations in the soil at the three stages increased with increasing N rates and peaked at N312 (Figure 7). The concentrations at the three growth stages were lower in WB than in CD. At N168, N240, and N312, the differences were 13.18, 10.84, and 8.80 kg ha^{-1} for T18 and 15.31, 9.65, and 7.03 kg ha^{-1} for T198 at jointing, 19.63, 15.48, and 12.13 kg ha^{-1} for T18 and 22.81, 12.56, and 10.50 kg ha^{-1} for T198 at anthesis, and 18.07, 14.02, and 10.52 kg ha^{-1} for T18 and 21.00, 10.82, and 7.06 kg ha^{-1} for T198 at maturity, respectively, across two growing seasons.

3.6 Correlation analyses

We conducted correlation analyses between the cumulative N_2O emissions and plant N uptake and soil inorganic N concentrations at N168, N240, and N312, respectively (Table 2). The N_2O emissions were significantly negatively related to plant N uptake during the growth stages of sowing to jointing, jointing to anthesis, and anthesis to maturity. However, they were significantly positively related to the soil inorganic N concentrations at jointing, anthesis, and maturity for N168, N240, and N312.

4 Discussion

4.1 Influences of WB on grain yield and N uptake and utilization at different N rates

High wheat yields and NUE are based on plant N uptake (Duan et al., 2019). The arrangement of the wheat plants in the field may significantly affect growth and N uptake (Lu et al., 2020). WB sowing increased the belt of wheat seedlings and reduced the intraspecific competition of plants within the belts (Liu et al., 2020). This benefitted the growth of tillers and roots and resulted in an efficient N absorption capacity during the whole wheat growing season (Lv et al., 2020). In the present study, WB markedly improved grain yield and NUE at N168, N240, and N312, due to the improved plant N uptake, in line with Wang et al. (2022) and Zheng et al. (2023). This may be related to the improved activity of N assimilation enzymes in WB sowing, because higher activities of N assimilation enzymes, such as nitrate reductase, nitrite reductase, glutamine synthetase, glutamate synthase, are beneficial for crop N assimilation and absorption (Chandna et al., 2012; Agnihotri and Seth, 2016; Gupta and Seth, 2019). Furthermore, the combination of WB at N312 obtained the highest yield (most >11,000 kg ha^{-1}), demonstrating that WB can be used to gain high grain yield at various N rates, especially at higher N rates.

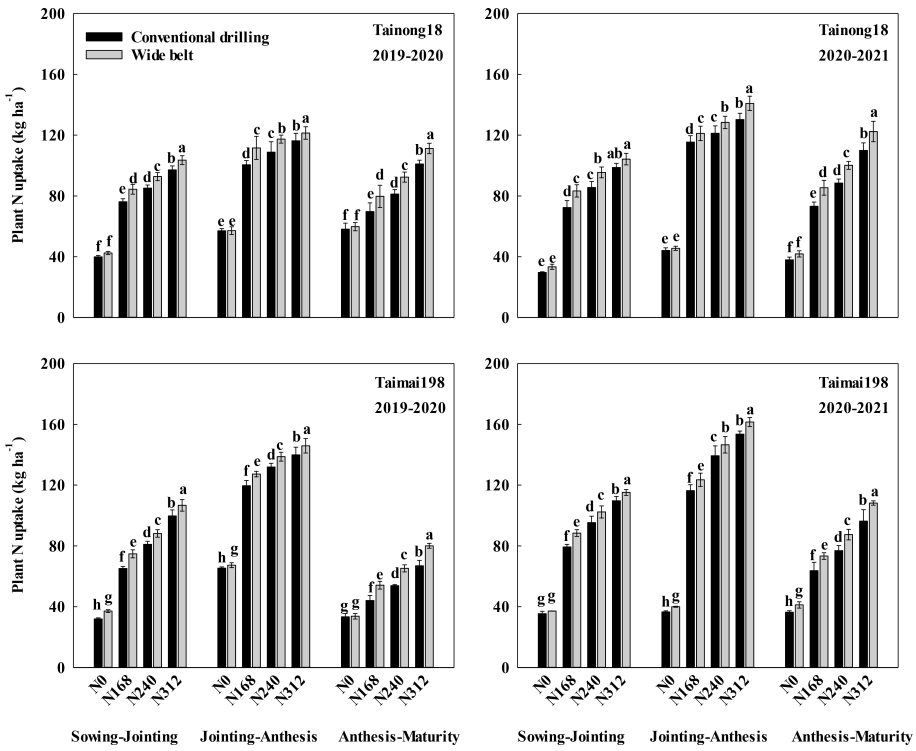

FIGURE 6
Effects of sowing pattern and N rate on plant N uptake during different winter wheat growth stages. N0, N168, N240, and N312 are N rates of 0, 168, 240, and 312 kg ha^{-1}. Different letters within the same growth stage for the same season and cultivar indicate significant differences ($P < 0.05$).

4.2 Influences of WB on N_2O emissions at different N rates

N_2O emissions exhibited seasonal variation, and some studies have found that the cumulative N_2O emissions at each winter wheat growing stage gradually decreased and were concentrated during the sowing to the greening stage (Liu et al., 2015). Nevertheless, Ji et al. (2012) demonstrated that they were higher from the greening to maturity stage than from the sowing to greening stage. This discrepancy may be due to the differences in specific basal/topdressing fertilizer ratios, temperature, rainfall, irrigation, or other factors. In our study, these emissions were concentrated at jointing to anthesis, followed by sowing to jointing, and anthesis to maturity. Furthermore, the reduced cumulative N_2O emissions in the three growth stages followed a similar pattern in WB compared to CD. This was probably due to the 60% N topdressing (60% of total N fertilizer), irrigation at the jointing stage (60 mm), and suitable temperature (average 12.6°C) during the jointing to anthesis growth stage. These conditions favor soil nitrification and denitrification (Pan et al., 2022) and produce more N_2O emissions.

N fertilization contributes to N_2O emissions (Rahman et al., 2021). Despite a linear relationship between the cumulative N_2O emissions and N rates (Kim et al., 2013), there is overwhelming evidence in the literature indicating that cumulative N_2O emissions increase exponentially as the N rate increases, including evidence for grain crops around the world (Shcherbak et al., 2014), tropical sugarcane in Australia (Takeda et al., 2021), and spring wheat in New Mexico (Millar et al., 2018). Therefore, mitigation of N_2O emissions at higher N input may be more difficult because some simple measures, such as supplementing with phosphate fertilizer (Shen and Zhu, 2022) and changing from conventional to no tillage (Campanha et al., 2019), mitigated N_2O emissions at relatively low N input, but not at higher N rates. An exponential relationship was also found in the present study. Although the sowing pattern did not influence the exponential relationship between an increase in N_2O emissions and increased N rates, WB initially decreased the N_2O emissions for N168, N240, and N312 compared to CD and slowed the increase in cumulative N_2O emissions resulting from the increased N rate. As a result, WB had greater N_2O emissions at N312 compared to CD, indicating that WB could be used to reduce N_2O emissions at various N rates, especially higher ones. A similar relationship was also observed between the GWP of N_2O emissions and interactions of N rate and sowing pattern.

N_2O EFs are used to estimate the direct N_2O emissions in field crops, reflecting the differences in management patterns (Yue et al., 2019). The EFs in the present study were 0.09–0.22% when N rates increased from N168 to N312, like the reference values in Yan et al. (2015). Rahman et al. (2021) found that N_2O EFs were linearly correlated with increasing N rates; however, other studies have demonstrated an exponential (Grace et al., 2016) or hyperbolic relationship (Kim et al., 2013) between EFs and N rates. Nevertheless, we observed a parabolic response, and the N rate at which N_2O EFs theoretically peaked in WB (275.92–295.49 kg ha^{-1} with 283.55 kg ha^{-1} on average) was lower than that in CD (293.20–319.00 kg ha^{-1} with 305.63 kg ha^{-1} on average). This was probably due

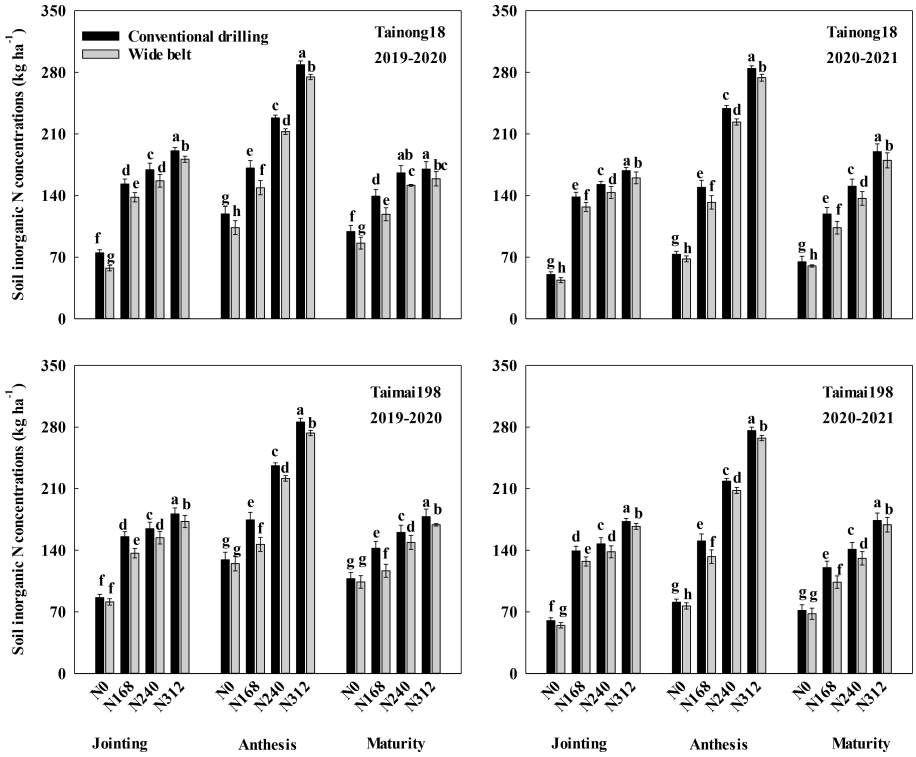

FIGURE 7
Effects of sowing pattern and N rate on soil inorganic N concentrations during different growth stages of winter wheat. N0, N168, N240, and N312 are N rates of 0, 168, 240, and 312 kg ha^{-1}. Different letters within the same growth stage for the same season and cultivar indicate significant differences ($P < 0.05$).

to the reduced cumulative N_2O emissions in WB as the N rates increased.

4.3 N uptake, soil N concentrations, and their relationship with N_2O emissions

Efficient N uptake and decreased concentrations of inorganic N in the soil may reduce N_2O emissions (Xu et al., 2022). A review of 12 leading cultivars used in China's major winter wheat cropping regions since the 1940s found that new wheat cultivars have a higher capacity to increase N uptake and reduce N_2O emissions than older wheat cultivars (Ying et al., 2019). Chen et al. (2021) also demonstrated that new wheat cultivars reduce N_2O emissions mainly through their higher productivity and N uptake and lower soil inorganic N availability. Similarly, the application of control-released fertilization also mitigates N_2O emissions by maintaining the substrate content of inorganic N at a lower level in the soil than conventional fertilizers (Zhang et al., 2019).

At N168, N240, and N312, changing the sowing pattern from CD to WB markedly increased plant N uptake during the growth stages of sowing to jointing, jointing to anthesis, and anthesis to maturity and reduced the soil N concentrations at jointing, anthesis, and maturity. This was mainly due to WB-associated efficient N uptake capacity throughout the wheat growing season (Lv et al., 2020). Meanwhile, the cumulative N_2O emissions during the different stages were significantly negatively related to the N uptake and positively related to the inorganic N concentrations in the soil, indicating that WB mitigated N_2O emissions mainly through efficient N uptake and reduced soil inorganic N concentrations.

4.4 Influences of WB on yield-scaled N_2O emissions at different N rates

N is an essential nutrient for crop production. Higher N fertilizer rates can often result in higher grain yields, resulting in a corresponding increase in N_2O emissions (Millar et al., 2018). Unilaterally focusing on reducing the N_2O emissions by reducing N rates may be counterproductive and lead to low grain yields (Duan et al., 2019). While meeting agricultural production needs, practices that minimize N_2O emissions must be identified (Kim et al., 2022). Yield-scaled N_2O emissions could be used as a benchmark to meet the critical global challenge of reducing N_2O emissions while ensuring food security (Kong et al., 2021).

Field studies have reported an exponential increase between yield-scaled N_2O emissions and increased N rates (Ma et al., 2010; Ji et al., 2012). We observed a similar relationship regardless of the sowing pattern, mainly due to the exponentially increased N_2O emissions ($R^2 = 0.89$, $P < 0.01$). Therefore, it is necessary to exploit efficient measures to reduce the yield-scaled N_2O emissions when a specific N fertilizer is applied to achieve a high yield. New crop genotypes can increase plant N uptake (Chen et al., 2021), and other methods, such as new controlled-release fertilizers (Ji et al., 2012),

TABLE 2 Results of correlation analyses of cumulative nitrous oxide emissions during different growth stages with plant N uptake and soil inorganic N concentrations.

N rate (kg ha^{-1})	Growth stage	Plant N uptake during growth stage	Soil inorganic N concentrations at the growth stage
168	Sowing-jointing/Jointing	-0.49*	0.47*
	Jointing-anthesis/Anthesis	-0.58**	0.41*
	Anthesis-maturity/Maturity	-0.72**	0.46*
240	Sowing-jointing/Jointing	-0.55**	0.46*
	Jointing-anthesis/Anthesis	-0.49*	0.41*
	Anthesis-maturity/Maturity	-0.61**	0.48*
312	Sowing-jointing/Jointing	-0.86**	0.46*
	Jointing-anthesis/Anthesis	-0.51**	0.51*
	Anthesis-maturity/Maturity	-0.73**	0.50*

* and ** indicate significance at $P < 0.05$ and 0.01, respectively.

partial substitution of chemical N with manure (Kong et al., 2021), and the addition of urease and nitrification inhibitors (Wang et al., 2021) can reduce the concentrations of inorganic N in the soil. All these measures would effectively decrease yield-scaled N_2O emissions and improve yields. Meanwhile, in the present study, WB significantly reduced the yield-scaled N_2O emissions at N168, N240, and N312 compared to CD due to the increased grain yield and reduced N_2O emissions caused by the efficient N uptake and reduced soil N concentrations. Furthermore, we observed an increased reduction in yield-scaled N_2O emissions in WB at high N rates, indicating that WB could play an important role in reducing such emissions when more synthetic N fertilizers are applied to in an effort to obtain high yields in the future. Besides, the yield-scaled N_2O emissions were not significantly different between WB at N312 and the local management system (sowing using CD at N240); however, the grain yield was much higher. In conclusion, WB sowing can decrease N_2O emissions and synergistically obtain high grain yields and NUEs, especially at higher N rates.

Although the application of higher N rates can improve the yield of winter wheat, it also reduces NUE and increases N_2O emissions, regardless of sowing pattern. Moreover, higher N fertilizer application may decrease profits and increase carbon emissions considering the manufacture and transport of agricultural products. Therefore, more attention should be paid to the joint goals of increasing grain yield and reducing N rate. Combining WB sowing with the use of new controlled-release fertilizers or partial substitution of chemical N with manure may be efficient pathways to synergistically improve grain yield and reduce N input in the future.

5 Conclusions

WB sowing significantly increased the N uptake of winter wheat and reduced soil inorganic N concentrations, thereby markedly decreasing the cumulative N_2O emissions, N_2O EFs, GWP of N_2O, and grain yield-scaled N_2O emissions, and increased grain yield and NUE at N168, N240, and N312 compared to CD. Furthermore, these N_2O emissions indices showed a larger reduction at higher N rates. Therefore, optimizing the seeding belt of wheat seedlings with high N rate input is an efficient way to mitigate greenhouse gases and improve yields and NUE. Our study shows the feasibility of attaining both high yield and low N_2O emissions. However, more attention should be paid to the issues of increasing grain yield and reducing N rate in the future.

Data availability statement

The original contributions presented in the study are included in the article/Supplementary Material. Further inquiries can be directed to the corresponding author.

Author contributions

XD designed the experiments, managed the projects and guided the writing of the article. XZ and ML performed the experiments. XZ performed the data analysis and wrote the manuscript. FZ, YH and JC provided help on the experiments. YD and MH gave useful suggestions during the process of this experiments and article. All of authors listed have approved the manuscript that is enclosed.

Funding

This work was supported by the Key Research and Development Program of Shandong Province (LJNY202103), National Natural Science Foundation of China (31801298), the Natural Science Foundation of Shandong Province (ZR2018BC034).

Conflict of interest

The authors declare that the research was conducted in the absence of any commercial or financial relationships that could be construed as a potential conflict of interest.

Publisher's note

All claims expressed in this article are solely those of the authors and do not necessarily represent those of their affiliated organizations, or those of the publisher, the editors and the reviewers. Any product that may be evaluated in this article, or claim that may be made by its manufacturer, is not guaranteed or endorsed by the publisher.

Supplementary material

The Supplementary Material for this article can be found online at: https://www.frontiersin.org/articles/10.3389/fpls.2023.1176293/full#supplementary-material

References

Agnihotri, A., and Seth, C. S. (2016). Exogenously applied nitrate improves the photosynthetic performance and nitrogen metabolism in tomato (*Solanum lycopersicum* l. cv pusa rohini) under arsenic (V) toxicity. *Physiol. Mol. Biol. Pla.* 22, 341–349. doi: 10.1007/s12298-016-0370-2

Campanha, M. M., de Oliveira, A. D., Marriel, I. E., Marques, M., Malaquias, J. V., Landau, E. C., et al. (2019). Effect of soil tillage and N fertilization on N_2O mitigation in maize in the Brazilian Cerrado. *Sci. Total Environ.* 692, 1165–1174. doi: 10.1016/j.scitotenv.2019.07.315

Chandna, R., Hakeem, K. R., Khan, F., Ahmad, A., and Iqbal, M. (2012). Variability of nitrogen uptake and assimilation among N-efficient and N-inefficient wheat (*Triticum aestivum* L.) genotypes. *J. Plant Interac.* 7, 367–375. doi: 10.1080/17429145.2011.641229

Chen, H., Zheng, C., Chen, F., Qiao, Y., Du, S., Cao, C., et al. (2021). Less N_2O emission from newly high-yielding cultivars of winter wheat. *Agr. Ecosyst. Environ.* 320, 107557. doi: 10.1016/j.agee.2021.107557

Duan, J., Shao, Y., He, L., Li, X., Hou, G., Li, S., et al. (2019). Optimizing nitrogen management to achieve high yield, high nitrogen efficiency and low nitrogen emission in winter wheat. *Sci. Total Environ.* 697, 134088. doi: 10.1016/j.scitotenv.2019.134088

FAO. (2003). European Communities, International Soil Reference and Information Centre (FAO, EC, ISRIC). *WRB map World Soil Resour.* 1, 25 000 000. (Rome, Italy: FAO). Available at: https://www.fao.org/soils-portal/resources/world-soil-resources-reports/zh/.

Godfray, H. C. J., Pretty, J., Thomas, S. M., Warham, E. J., and Beddington, J. R. (2011). Linking policyon climate and food. *Science.* 331, 1013–1014. doi: 10.1126/science.1202899

Grace, P., Shcherbak, I., Macdonald, B., Scheer, C., and Rowlings, D. (2016). Emission factors for estimating fertiliser-induced nitrous oxide emissions from clay soils in australia's irrigated cotton industry. *Soil Res.* 54, 598–603. doi: 10.1071/SR16091

Gupta, P., and Seth, C. S. (2019). Nitrate supplementation attenuates as (V) toxicity in *Solanum lycopersicum* l. cv pusa rohini: insights into as (V) sub-cellular distribution, photosynthesis, nitrogen assimilation, and DNA damage. *Plant Physiol. Bioch.* 139, 44–55. doi: 10.1016/j.plaphy.2019.03.007

Huang, T., Yang, H., Huang, C., and Ju, X. (2017). Effect of fertilizer N rates and straw management on yield-scaled nitrous oxide emissions in a maize-wheat double cropping system. *Field Crop Res.* 204, 1–11. doi: 10.1016/j.fcr.2017.01.004

IPCC (2021). *Climate change 2021: the physical science basis: working group I contribution to the sixth assessment report of the intergovernmental panel on climate change* (Cambridge, New York: Cambridge University Press).

Ji, Y., Liu, G., Ma, J., Li, X., Xu, H., and Cai, Z. (2012). Effect of controlled-release fertilizer (CRF) on nitrous oxide emission during the wheat growing feriod. *Acta Pedologica Sin. (in Chin. English abstract).* 49, 526–534.

Kim, D. G., Giltrap, D., and Sapkota, T. B. (2022). Understanding response of yield-scaled N_2O emissions to nitrogen input: data synthesis and introducing new concepts of background yield-scaled N_2O emissions and N_2O emission-yield curve. *Field Crop Res.* 290, 108737. doi: 10.1016/j.fcr.2022.108737

Kim, D. G., Hernandez-Ramirez, G., and Giltrap, D. (2013). Linear and nonlinear dependency of direct nitrous oxide emissions on fertilizer nitrogen input: a meta-analysis. *Agr. Ecosyst. Environ.* 168, 53–65. doi: 10.1016/j.agee.2012.02.021

Kong, D., Jin, Y., Yu, K., Swaney, D. P., and Zou, J. (2021). Low N_2O emissions from wheat in a wheat-rice double cropping system due to manure substitution are associated with changes in the abundance of functional microbes. *Agr. Ecosyst. Environ.* 311, 107318. doi: 10.1016/j.agee.2021.107318

Krapp, A. (2015). Plant nitrogen assimilation and its regulation: a complex puzzle with missing pieces. *Curr. Opin. Plant Biol.* 25, 115–122. doi: 10.1016/j.pbi.2015.05.010

Li, Q., Bian, C., Liu, X., Ma, C., and Liu, Q. (2015). Winter wheat grain yield and water use efficiency in wide-precision planting pattern under deficit irrigation in north China plain. *Agr. Water Manage.* 153, 71–76. doi: 10.1016/j.agwat.2015.02.004

Liu, Y., Li, Y., Peng, Z., Wang, Y., Ma, S., Guo, L., et al. (2015). Effects of different nitrogen fertilizer management practices on wheat yields and N_2O emissions from wheat fields in north China. *J. Integr. Agr.* 14, 1184–1191. doi: 10.1016/S2095-3119(14)60867-4

Liu, X., Wang, W., Lin, X., Gu, S., and Wang, D. (2020). The effects of intraspecific competition and light transmission within the canopy on wheat yield in a wide-precision planting pattern. *J. Integr. Agr.* 19, 1577–1585. doi: 10.1016/S2095-3119(19)62724-3

Lu, P., Jiang, B. W., and Weiner, J. (2020). Crop spatial uniformity, yield and weed suppression. *Adv. Agron.* 161, 117–178. doi: 10.1016/bs.agron.2019.12.003

Lv, X., Zhang, Y., Li, H., Fan, S., Feng, B., and Kong, L. (2020). Wheat belt-planting in China: an innovative strategy to improve production. *Plant Prod. Sci.* 23, 12–18. doi: 10.1080/1343943X.2019.1698972

Lyu, X., Wang, T., Ma, Z., Zhao, C., Siddique, K. H. M., and Ju, X. (2019). Enhanced efficiency nitrogen fertilizers maintain yields and mitigate global warming potential in an intensified spring wheat system. *Field Crop Res.* 244, 107624. doi: 10.1016/j.fcr.2019.107624

Ma, B. L., Wu, T. Y., Tremblay, N., Deen, W., Morrison, M. J., Mclaughlin, N. B., et al. (2010). Nitrous oxide fluxes from corn fields: on-farm assessment of the amount and timing of nitrogen fertilizer. *Global Change Biol.* 16, 156–170. doi: 10.1111/j.1365-2486.2009.01932.x

Millar, N., Urrea, A., Kahmark, K., Shcherbak, I., Robertson, G. P., and Ortiz-Monasterio, I. (2018). Nitrous oxide (N_2O) flux responds exponentially to nitrogen fertilizer in irrigated wheat in the yaqui valley, Mexico. *Agr. Ecosyst. Environ.* 261, 125–132. doi: 10.1016/j.agee.2018.04.003

Moll, R. H., Kamprath, E. J., and Jackson, W. A. (1982). Analysis and interpretation of factors which contribute to efficiency of nitrogen utilization. *Agron. J.* 74, 562–564. doi: 10.2134/agronj1982.00021962007400030037x

Pan, B., Xia, L., Lam, S. K., Wang, E., Zhang, Y., Mosier, A., et al. (2022). A global synthesis of soil denitrification: driving factors and mitigation strategies. *Agr. Ecosyst. Environ.* 327, 107850. doi: 10.1016/j.agee.2021.107850

Rahman, N., Richards, K. G., Harty, M. A., Watson, C. J., Carolan, R., Krol, D., et al. (2021). Differing effects of increasing calcium ammonium nitrate, urea and urea + NBPT fertiliser rates on nitrous oxide emission factors at six temperate grassland sites in Ireland. *Agr. Ecosyst. Environ.* 313, 107382. doi: 10.1016/j.agee.2021.107382

Recio, J., Alvarez, J. M., Rodriguez-Quijano, M., and Vallejo, A. (2019). Nitrification inhibitor DMPSA mitigated N_2O emission and promoted NO sink in rainfed wheat. *Environ. pollut.* 245, 199–207. doi: 10.1016/j.envpol.2018.10.135

Seth, C. S., and Misra, V. (2014). Changes in C–N metabolism under elevated CO_2 and temperature in Indian mustard (*Brassica juncea* L.): an adaptation strategy under climate change scenario. *J. Plant Res.* 127, 793–802. doi: 10.1007/s10265-014-0664-9

Shcherbak, I., Millar, N., and Robertson, G. P. (2014). Global metaanalysis of the nonlinear response of soil nitrous oxide (N_2O) emissions to fertilizer nitrogen. *P. Natl. Acad. Sci. U.S.A.* 111, 9199–9204. doi: 10.1073/pnas.1322434111

Shen, Y., and Zhu, B. (2022). Effects of nitrogen and phosphorus enrichment on soil N_2O emission from natural ecosystems: a global meta-analysis. *Environ. pollut.* 301, 118993. doi: 10.1016/j.envpol.2022.118993

Shi, Z., Li, D., Jing, Q., Cai, J., Jiang, D., Cao, W., et al. (2012). Effects of nitrogen applications on soil nitrogen balance and nitrogen utilization of winter wheat in a rice–wheat rotation. *Field Crop Res.* 127, 241–247. doi: 10.1016/j.fcr.2011.11.025

Shultana, R., Zuan, A. T. K., Naher, U. A., Islam, A. K. M. M., Rana, M. M., Rashid, M. H., et al. (2022). The PGPR mechanisms of salt stress adaptation and plant growth promotion. *Agronomy* 12, 2266. doi: 10.3390/agronomy12102266

Subbarao, G. V., Arango, J., Masahiro, K., Hooper, A. M., Yoshihashi, T., Ando, Y., et al. (2017). Genetic mitigation strategies to tackle agricultural GHG emissions: the case for biological nitrification inhibition technology. *Plant Sci.* 262, 165–168. doi: 10.1016/j.plantsci.2017.05.004

Takeda, N., Friedl, J., Rowlings, D., de Rosa, D., Scheer, C., and Grace, P. (2021). Exponential response of nitrous oxide (N_2O) emissions to increasing nitrogen fertiliser rates in a tropical sugarcane cropping system. *Agr. Ecosyst. Environ.* 313, 107376. doi: 10.1016/j.agee.2021.107376

vanDijk, M., Morley, T., Rau, M. L., and Saghai, Y. (2021). A meta-analysis of projected global food demand and population at risk of hunger for the period 2010-2050. *Nat. Food.* 2, 494–501. doi: 10.1038/s43016-021-00322-9

Wang, H., Ma, S., Shao, G., and Dittert, K. (2021). Use of urease and nitrification inhibitors to decrease yield-scaled N_2O emissions from winter wheat and oilseed rape fields: a two-year field experiment. *Agr. Ecosyst. Environ.* 319, 107552. doi: 10.1016/j.agee.2021.107552

Wang, Q., Noor, H., Sun, M., Ren, A., Feng, Y., Qiao, P., et al. (2022). Wide space sowing achieved high productivity and effective nitrogen use of irrigated wheat in south shanxi, China. *PeerJ.* 10, e13727. doi: 10.7717/peerj.13727

Xu, P., Jiang, M., Jiang, Y., Khan, I., Zhou, W., Wu, H., et al. (2022). Prior nitrogen fertilization stimulated N_2O emission from rice cultivation season under a rapeseed-rice production system. *Plant Soil.* 471, 685–696. doi: 10.1007/s11104-021-05162-x

Yan, G., Yao, Z., Zheng, X., and Liu, C. (2015). Characteristics of annual nitrous and nitric oxide emissions from major cereal crops in the north China plain under alternative fertilizer management. *Agr. Ecosyst. Environ.* 207, 67–78. doi: 10.1016/j.agee.2015.03.030

Ying, H., Yin, Y., Zheng, H., Wang, Y., Zhang, Q., Xue, Y., et al. (2019). Newer and select maize, wheat, and rice varieties can help mitigate n footprint while producing more grain. *Global Change Biol.* 25, 4273–4281. doi: 10.1111/gcb.14798

Yue, Q., Wu, H., Sun, J., Cheng, K., Smith, P., Hillier, J., et al. (2019). Deriving emission factors and estimating direct nitrous oxide emissions for crop cultivation in China. *Environ. Sci. Technol.* 53, 10246–10257. doi: 10.1021/acs.est.9b01285

Zhang, W., Liang, Z., He, X., Wang, X., Shi, X., Zou, C., et al. (2019). The effects of controlled release urea on maize productivity and reactive nitrogen losses: a meta-analysis. *Environ. pollut.* 246, 559–565. doi: 10.1016/j.envpol.2018.12.059

Zhang, G., Song, K., Miao, X., Huang, Q., Ma, J., Gong, H., et al. (2021). Nitrous oxide emissions, ammonia volatilization, and grain-heavy metal levels during the wheat season: effect of partial organic substitution for chemical fertilizer. *Agr. Ecosyst. Environ.* 311, 107340. doi: 10.1016/j.agee.2021.107340

Zheng, F., Qin, J., Hua, Y., Chu, J., Dai, X., and He, M. (2023). Nitrogen uptake of winter wheat from different soil depths under a modified sowing pattern. *Plant Soil.* doi: 10.1007/s11104-023-05952-5

Zhu, J. (2016). Abiotic stress signaling and responses in plants. *Cell.* 167, 313–324. doi: 10.1016/j.cell.2016.08.029

frontiers | Frontiers in Plant Science

TYPE Original Research
PUBLISHED 14 July 2023
DOI 10.3389/fpls.2023.1188077

OPEN ACCESS

EDITED BY
Ravi Gupta,
Kookmin University, Republic of Korea

REVIEWED BY
Muhammad Haroon,
Huazhong Agricultural University, China
Anshuman Singh,
Rani Lakshmi Bai Central Agricultural University, India

*CORRESPONDENCE
Aamir Raina
aamir854@gmail.com

†These authors have contributed equally to this work

RECEIVED 16 March 2023
ACCEPTED 01 June 2023
PUBLISHED 14 July 2023

CITATION
Raina A and Khan S (2023) Field assessment of yield and its contributing traits in cowpea treated with lower, intermediate, and higher doses of gamma rays and sodium azide.
Front. Plant Sci. 14:1188077.
doi: 10.3389/fpls.2023.1188077

Field assessment of yield and its contributing traits in cowpea treated with lower, intermediate, and higher doses of gamma rays and sodium azide

Aamir Raina[1,2*†] and Samiullah Khan[1†]

[1]Mutation Breeding Laboratory, Department of Botany, Aligarh Muslim University, Aligarh, India, [2]Botany Section, Women's College, Aligarh Muslim University, Aligarh, India

Across the globe, plant breeders of different organizations are working in collaboration to bring preferred traits to crops of economic importance. Among the traits, "high yielding potential" is the most important as it is directly associated with food security and nutrition, one of the sustainable development goals. The Food and Agriculture Organization acknowledges plant breeders' role and efforts in achieving local and global food security and nutrition. Recognizing the importance of pulses and increasing pressure on food security, the United Nations General Assembly declared 2016 the "International year of Pulses" owing to their preferred traits such as climate change resilience, wide adaptability, low agriculture input, and protein- and nutrient-rich crops. Keeping all these developments in consideration, we initiated an induced mutagenesis program by treating cowpea (*Vigna unguiculata* L. Walp.) with different doses of gamma rays and sodium azide aiming to enhance the yielding potential of an otherwise outstanding variety viz., Gomati VU-89 and Pusa-578. We noticed a substantial increase in mean values of agronomic traits in putative mutants raised from seeds treated with lower and intermediate doses of mutagens. Statistical analysis such as correlation, path, hierarchical clustering analysis (HCA), and principal component analysis (PCA) were used to assess the difference between mutagenized and control populations. A significant and positive correlation of yield with yield-attributing traits was recorded. However, among all the yield attributing traits, seeds per pod (SPP) depicted the maximum direct impact upon yield, and therefore, working on this trait may yield better results. A widely used PCA revealed 40.46% and 33.47% of the total variation for var. Gomati VU-89 and var. Pusa-578, respectively. Cluster analysis clustered treated and control populations into separate clusters with variable cluster sizes. Cluster V in the variety Gomati VU-89 and cluster V and VI in the variety Pusa 578 comprised of putative mutants were higher yielding and hence could be recommended for selection in future breeding programs. We expect to release such mutant lines for farmer cultivation in Northern parts of India depending on the performance of such high-yielding mutant lines at multilocations.

KEYWORDS

bio-physiological traits, quantitative traits, correlation analysis, path analysis, cluster analysis

Introduction

Cowpea, a self-fertilizing diploid with chromosome number 2n = 2x = 22, genome size 620 Mb, belongs to the Fabaceae family is a warm-season grain legume widely cultivated across a wide range of dry ecologies (Arumuganathan and Earle, 1991; Lo et al., 2020). Cowpea is an inexpensive plant-based protein resource, ranks second in diet value after cereals, and complements a protein-deficient cereal-based human diet. It is cultivated for its tender green leaves, unripe pods, and dry grains as a major source of dietary protein for millions of people across the globe (Uzogara and Ofuya, 1992). Its grains are rich in protein, carbohydrates, dietary fiber, vitamins, antioxidants, polyphenols, and polyunsaturated fatty acids (Ngoma et al., 2018; Ketema et al., 2020; Nkomo et al., 2021). Cowpeas are vital constituents of sustainable agriculture and are critical in enhancing human and livestock health. It offers vital ecological services through its capability to biologically fix nitrogen, recycle nutrients, improve soil carbon content, and diversify cropping systems (Nkomo et al., 2021). Cowpea is often referred to as climate-smart crop due to its dual resilience against heat and drought stress, low water footprint and agriculture input, and ability to thrive under diverse and adverse environmental conditions where other legumes cannot grow. Globally, 14.4 million hectares (ha) of land are devoted to its cultivation, and more than 8.9 million tonnes are produced annually. Africa contributes the maximum annual cowpea produce among the continents, followed by Asia and America (Figure 1). The main cowpea-producing countries are Nigeria, Niger, and Burkina Faso; however, the annual mean cowpea yield in Niger and Burkina Faso was 4,169 and 4,818 hectogram/hectare (hg/ha), respectively, which is less as compared to the world average of 6,163 hg/ha (FAOSTAT accessed on 06 Aug 2021). The unavailability of high-yielding cowpea varieties is the main obstacle to achieving higher production (Wamalwa et al., 2016; Raina et al., 2020). Therefore, cowpea breeders and geneticists have employed traditional and modern breeding strategies to improve yield, grain quality, and nutritional and nutraceutical properties. However, traditional breeding strategies are arduous, time-consuming, and inefficient in achieving the desired goals.

Among the breeding strategies, induced mutagenesis is a coherent tool for improving yield and yield-attributing traits. With wide public acceptance and no regulatory restrictions unlike transgenic plants, the mutation breeding approach has been most successful in developing thousands of elite mutant varieties in hundreds of plant species. Induced mutagenesis has successfully developed 3402 mutant varieties (https://mvd.iaea.org/ accessed on 08 July 2023). However, cowpea is the neglected crop in induced mutagenesis, and only 16 cowpea mutant varieties have been developed so far. Hence, it is imperative to develop mutants with a preferred set of traits through induced mutagenesis. Various cultivars were treated with a wide range of gamma (γ) ray doses in developing these cowpea mutant varieties. No information on the optimum doses of γ rays that could be used for the yield improvement of cowpea is available. Similarly, none of the workers have been successful in developing cowpea mutant varieties using optimum doses of sodium azide (SA). SA can induce AT→GC base pair transition and transversion (Supplementary Figure 1). Considering the need for optimization of γ rays and SA doses, an experimental study was undertaken by treating two cowpea varieties with single and combined doses of γ rays and SA. The γ rays are ionizing radiations with a short, high-energy wavelength and can interact and alter DNA base pairs. The γ rays cause hydrolysis of water that leads to the production of reactive free radicals that disturb DNA–DNA cross-links and eventually result in mutations (Reisz et al., 2014).

The yield is a complex trait governed by multiple genes that impart a small cumulative effect. In grain legumes, yield is total performance and the association of yield-contributing traits. The association between yield-contributing traits is achieved by assessing the correlation coefficients. Therefore, these traits are important and getting higher mean values is the ultimate aim of the breeding program. Even the success of the breeding program relies on the correlation direction and degree among yield-attributing traits (Ahmad and Saleem, 2003). This is why correlation analysis is important in formulating the breeding design and selection pressure (Sarawgi et al., 1997). Correlation analysis evaluates the degree and direction of the association between traits, enabling the breeders to exercise indirect selection much faster than traditional direct selection on the desired trait (Cruz et al., 2012).

Even though correlation analysis is widely used in analyzing the association between traits, it does not count the direct and indirect effects of these traits and provides zero information on cause and effect (Santos et al., 2014). Therefore, it can lead to errors in the selection strategy, and it not enough to assess the relationship between traits without including the direct and indirect effects. Hence, a breeder must have extensive knowledge of the direct and indirect relationship among yield-contributing traits in the selection of plants for breeding. To have an accurate picture of the association among traits, Wright (1921) formulated path analysis that quantifies the direct and indirect impact of the predictor variable upon its response variable. It also reveals the comparative significance of each trait contributing to the yield (Li, 1975; Cruz and Regazzi, 2006). It helps in the selection procedure and equips the breeders to isolate mutants simultaneously based on two or more traits (Salahuddin et al., 2010). Path analysis enables breeders to visualize direct and indirect effects, and hence, it has been widely used in crops such as *Passiflora edulis* (Araújo et al., 2007), *Brassica napus* (Coimbra et al., 2005), *Triticum aestivum* (Carvalho et al., 1999), *Theobroma cacao* (Almeida et al., 1994), and *Glycine max* (Bizeti et al., 2004). The overall aims of correlation and path analysis are to assess the role of yield-contributing traits in the determination of yield and to design selection criteria to isolate mutants with desirable traits for breeding programs.

Materials and methods

Plant material

The seeds of cowpea varieties viz., Gomati VU-89 and Pusa-578, were obtained from the National Bureau of Plant Genetic Resources and were irradiated at National Botanical Research Institute,

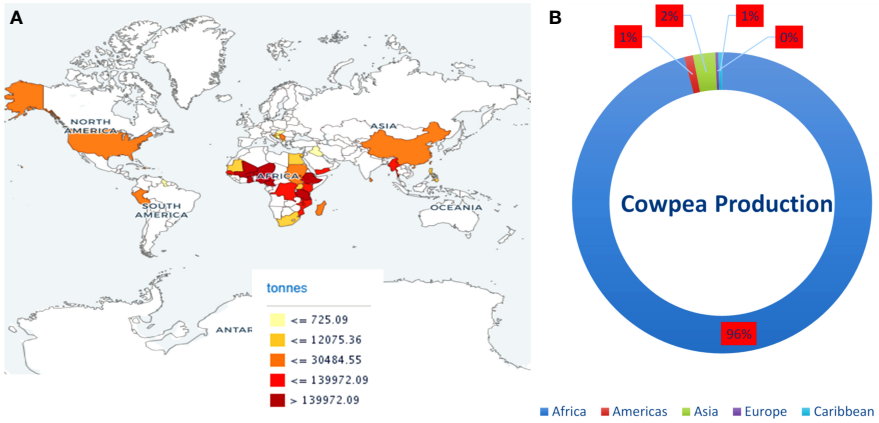

FIGURE 1
(A) Map showing cowpea producing countries and their production. **(B)** Average production of cowpea (dry) in continents from 2011-2021. Source: FAOSTAT https://www.fao.org/faostat (accessed on 20 June, 2023).

Lucknow, India, with 100, 200, 300, 400, 500, 600, 700, 800, 900, and 1,000 Gy doses of γ rays at a dose rate of 11.58 Gy/min. For chemical treatments, seeds were presoaked in double-distilled water for 6 h and then treated with several doses of SA such as 0.01%, 0.02%, 0.03%, 0.04%, 0.05%, 0.06%, 0.07%, 0.08%, 0.09%, and 0.1% of SA for 9 h at Mutation Breeding Laboratory, Botany Department, Aligarh Muslim University (AMU), Aligarh, India. For combined mutagen treatments, seeds were treated with 100 Gy γ rays + 0.01% SA, 200 Gy γ rays + 0.02% SA, 300 Gy γ rays + 0.03% SA and 400 Gy γ rays + 0.04% SA, 500 Gy γ rays + 0.05% SA, 600 Gy γ rays + 0.06% SA, 700 Gy γ rays + 0.07% SA, 800 Gy γ rays + 0.08% SA, 900 Gy γ rays + 0.09% SA, and 1,000 Gy γ rays + 0.1% SA. We found that doses beyond 400 Gy γ rays, 0.04% SA, and 400 Gy γ rays + 0.04% SA are detrimental and caused more than 50% reduction in seed germination and hence were discarded.

Field assessment

During mid-April 2014, 300 seeds/treatment/variety totaling 7,800 were sown in the agriculture field, AMU, Aligarh, in a randomized complete block design keeping 0.3-m seed-to-seed and 0.6-m row-to-row distance. The seeds were sown in 10 replications of 30 seeds. Each block (1.8 × 3 m) consisted of one replication from each treatment in the field (23.5 × 40 m) (Supplementary Figure 2). All the seeds from M_1 plants were harvested separately during mid-October 2014 and stored for raising subsequent generations.

Nitrate reductase activity

Secondary leaflets of M_1 seedlings were collected and washed thoroughly two to three times with running water after 10–15 days of sowing (DAS) to estimate nitrate reductase activities following the protocol of Jaworski (1971). The detailed methodology is given separately in Supplementary Files.

Chlorophyll and carotenoid contents

For estimation of chlorophyll and carotenoid contents, secondary leaflets of M_1 seedlings were collected and washed thoroughly two to three times with running water after 10–15 days after sowing (DAS) following the protocol of MacKinney (1941). The detailed methodology is given separately in Supplementary Files. The pigment contents were measured on a fresh weight basis (mg.g^{-1}FW) following the formula of Arnon (1949):

$$\text{Total chlorophyll} = \{20.2(OD_{645}) + 8.02(OD_{663})\} \times \frac{V}{1,000 \times W}$$

$$\text{Carotenoids} = \frac{7.6\,(OD_{480}) - 1.49\,(OD_{510})}{d \times 1,000 \times W} \times V$$

where OD_{645}, OD_{663}, OD_{480}, OD_{510} = optical densities at OD_{645}, OD_{663}, OD_{480}, and OD_{510}, respectively.

V= Volume of an extract
W = Mass of leaf tissues
d = Length of light path (d = 1.4 cm).

Quantitative traits

We chose 30 random mutagen dose-treated and untreated plants to generate the mean data of 10 quantitative traits. For plant height (PH), we measured the total length of plants from base to the apex. We recorded the days to flowering (DF), starting from seed sowing to the appearance of first floral buds. Similarly, total growth period or days to maturity (DM) was recorded by counting days from seed sowing to harvest. In cowpea, flowers develop at different times, which lead to a multiple pod set, and hence, pods

were harvested three to four times manually from September to October 2014. For pods per plant (PPP), we counted a total number of pods collected in a sequential harvests. Similarly, we randomly chose 60 pods from 30 plants to calculate the mean number of seeds per pod (SPP). The mean number of branches per plant was recorded by counting the branches during the flowering period. Mean seed weight (SW) was measured by taking the weight of 100 seeds. Pod length (PL) was recorded by measuring the length from the base to the pod tip. Plant yield (PY) was measured by taking the weight of total seeds harvested from 30 randomly selected plants. The harvest index (HI) was measured as a ratio of seed yield to biological yield or dry weight of aboveground parts subjected to 7 days of continuous sun drying.

Statistical analysis

To visualize the significance ($P \leq 0.05$) of the data (number of replications, n = 30), one-way analysis of variance and Duncan's multiple range test was conducted with the help of R software (R Core Team, 2019). Correlation and path coefficients were calculated from replicated data of 30 plants in control and mutagenized populations using SAS and IBM SPSS AMOS 26 software, respectively. Hierarchical Cluster Analysis (HCA) allowed us to visualize the heterogeneity produced among different mutagenized populations. The results were presented graphically in the form of dendrograms using SPSS version 16.0 (Team EQX). The biplot PCA graphs were constructed by taking the mean data of quantitative traits from control and treated populations using Past software version 3.26 (Hammer et al., 2001).

Results

Biophysiological traits

The results revealed a random and dose-independent decline in the biophysiological traits in the treated population of both varieties (Figures 2–4). A significantly higher Nitrate Reductase Activity (NRA) (531.12; 507.79 $nmol.h^{-1}.g^{-1}FW$), chlorophyll (2.07; 2.42 $mg.g^{-1}FW$), and carotenoid contents (0.49; 0.39 mg. $g^{-1}FW$) were recorded in a control population of the varieties Gomati VU-89 and Pusa-578, respectively. The combined mutagen doses induced a drastic reduction in biophysiological traits.

Quantitative traits

The results revealed that 200 Gy γ rays, 300 Gy γ rays, 400 Gy γ rays, 0.04% SA, 200 Gy γ rays + 0.02% SA, 300 Gy γ rays + 0.03% SA, and 400 Gy γ rays + 0.04% SA treatments induced a statistically significant decrease in mean PH in the var. Gomati VU-89 (Table 1). In the var. Pusa-578, all the mutagen doses except 400 Gy γ rays, 300 Gy γ rays + 0.03% SA, and 400 Gy γ rays + 0.04% SA treatments induced a statistically insignificant decrease in mean PH (Table 2). The highest reduction in mean PH was noted in 400 Gy γ rays + 0.04% SA treatment in Gomati VU-89 (174.13 cm) and Pusa-578 (173.05 cm). All the mutagen doses except 200 Gy γ rays, 300 Gy γ rays, and 100 Gy γ rays + 0.01% SA in the var. Gomati VU-89 and 100 Gy γ rays, 200 Gy γ rays, 300 Gy γ rays, 0.03% SA, and 0.04% SA in the var. Pusa-578 induced a decrease in the mean number of DF (Table 1). The highest reduction in the mean number of DF was recorded in the 400 Gy γ rays + 0.04% SA treatment in the var. Gomati VU-89 (77.93) and 0.02% SA and 300 Gy γ rays + 0.03% SA treatments in the var. Pusa-578 (86.43). The results revealed all the mutagen doses except 0.02% SA, 100 Gy + 0.01% SA in the var. Gomati VU-89 and 100 Gy, 0.01% SA, 0.02% SA, 100 Gy + 0.01% SA, and 200 Gy + 0.02% SA in the var. Pusa-578 induced a statistically insignificant decrease in the mean number of DM in both varieties (Tables 1, 2). The highest decrease in the mean number of DM was noted in 400 Gy γ rays + 0.04% SA treatment in the varieties Gomati VU-89 (148.83) and Pusa-578 (154.80). The results revealed 200 Gy γ rays, 0.02% SA, 100 Gy γ rays + 0.01% SA, 200 Gy γ rays + 0.02% SA, 300 Gy γ rays + 0.03% SA treatments in the var. Gomati VU-89 and 100 Gy γ rays and 100 Gy γ rays + 0.01% SA treatments in the var. Pusa-578 induced a statistically significant increase in the mean number of pods per plant (Tables 1, 2). The maximum increase in the mean number of pods per plant was noted with 100 Gy γ rays + 0.01% SA treatments in Gomati VU-89 (62.23) and Pusa-578 (42.63), respectively. The results revealed that only lower mutagen doses induced a statistically insignificant and significant decrease in the mean number of branches per plant in varieties Gomati VU-89 and Pusa-578, respectively (Tables 1, 2). The minimum decrease in the mean number of branches per plant was recorded with 400 Gy γ rays + 0.04% SA and 200 Gy γ rays treatments in Gomati VU-89 (8.20) and Pusa-578 (10.40), respectively. The results revealed that all the mutagen doses induced a statistically insignificant increase in seed per pod with the highest increase in 0.01% SA treatment in the var. Gomati VU-89 (12.70) (Table 1). Except for 100 Gy γ rays, 0.01% SA, 100 Gy γ rays + 0.01% SA, all the mutagen doses induced a statistically insignificant increase in the mean number of SPP with the highest increase in 0.01% SA treatment in the var. Pusa-578 (10.90) (Table 2). The results revealed all the mutagen treatments except 200 Gy γ rays + 0.02% SA in var. Gomati VU-89 and 200 Gy γ rays + 0.02% SA and 300 Gy γ rays+0.03% SA in the var. Pusa-578 significantly decreased the mean SW in both varieties (Tables 1, 2). The highest mean SW was noted in 200 Gy γ rays + 0.02% SA and 300 Gy γ rays + 0.03% SA treatments in the varieties Gomati VU-89 (14.80 g) and Pusa-578 (22.30 g), respectively. The highest increase in mean pod length was noted with 200 Gy γ rays + 0.02% SA and 200 Gy γ rays treatments in Gomati VU-89 (31.47 cm) and Pusa-578 (26.43 cm), respectively. The results revealed 100 Gy γ rays, 200 Gy γ rays, 300 Gy γ rays, 0.01% SA, 0.02% SA, 0.03% SA, 100 Gy γ rays + 0.01% SA, 200 Gy γ rays + 0.02% SA treatments in the var. Gomati VU-89 and 200 Gy γ rays, 0.01% SA, 0.02% SA, 100 Gy γ rays + 0.01% SA, 200 Gy γ rays + 0.02% treatments in the var. Pusa-578 induced a statistically significant increase in the mean pod length (Tables 1, 2). Except for 200 Gy γ rays + 0.02% SA in the var. Gomati VU-89, and 400 Gy γ rays + 0.04% SA treatments in the var. Pusa-578, all the mutagen doses induced a statistically significant increase in the mean plant yield with a maximum increase in 100

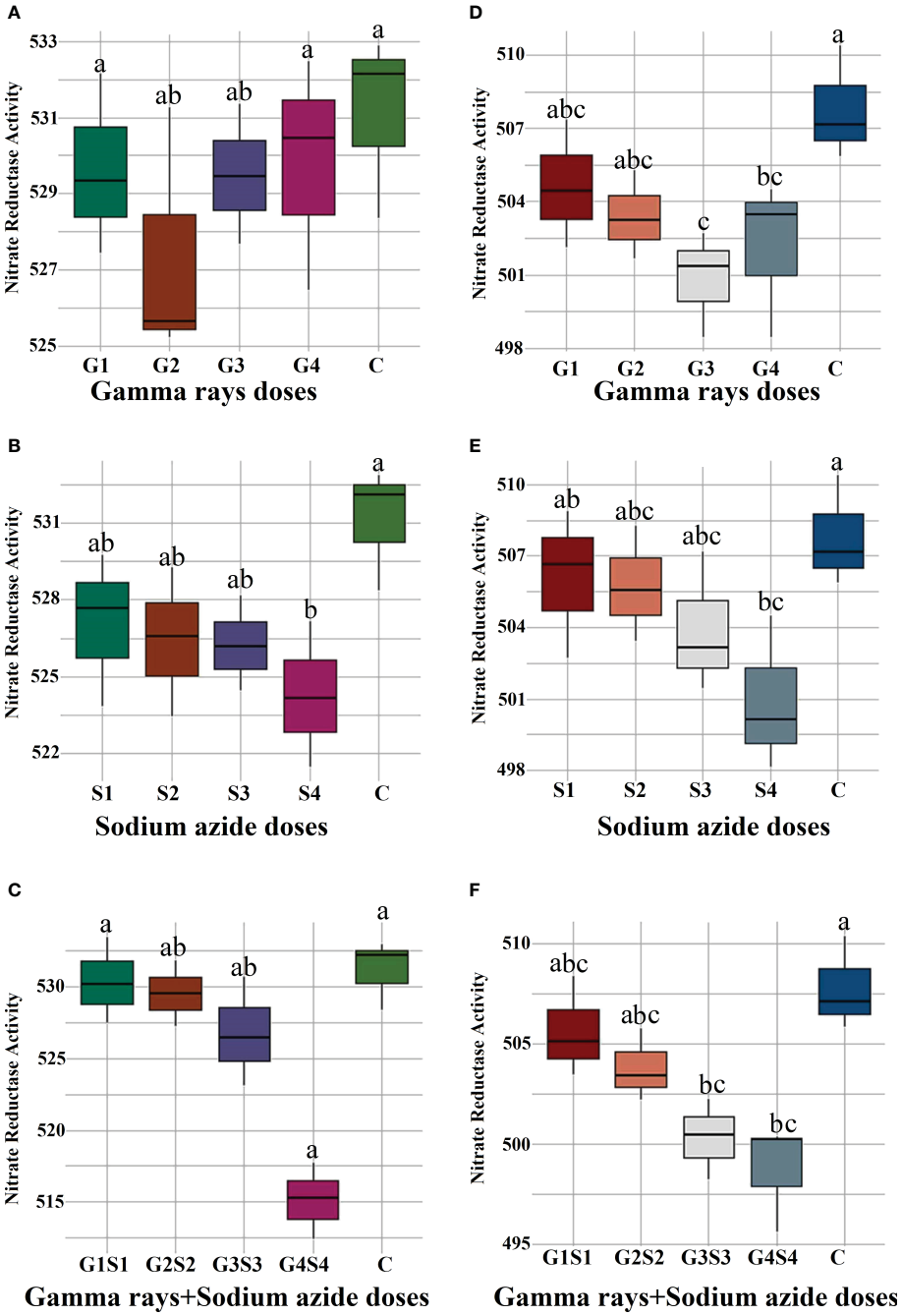

FIGURE 2
Effects of different doses of γ rays, SA, and γ rays + SA on nitrate reductase activity **(A–C)** in var. Gomati VU-89 and **(D–F)** in var. Pusa-578. The data are presented as mean and standard error (n = 30). #Means followed by the same letter is not different at 5% level of significance, based on the DMRT. C, Control; G1, 100 Gy γ rays; G2, 200 Gy γ rays; G3, 300 Gy γ rays; G4, 400 Gy γ rays; S1, 0.01% SA; S2, 0.02% SA; S3, 0.03% SA; S4, 0.04% SA; G1 +S1, 100 Gy γ rays+0.01% SA; G2+S2, 200 Gy γ rays+0.02% SA; G3+S3, 300 Gy γ rays+0.03% SA; G4+S4, 400 Gy γ rays+0.04% SA.

Gy γ rays and 0.01% SA treatment in the varieties Gomati VU-89 (113.02 g) and Pusa-578 (100.54 g), respectively (Tables 1, 2). All the lower and intermediate mutagen doses induced a statistically significant increase in the mean harvest index in both varieties, with the maximum increase in 100 Gy γ rays and 200 Gy γ rays treatment in the varieties Gomati VU-89 (40.53%) and Pusa-578 (37.42%), respectively (Tables 1, 2).

Correlation analysis

Pearson's correlation analysis revealed that PY is positively correlated with SW, SPP, PPP, and BPP ($P < 0.001$) and negatively correlated with DF ($P < 0.705$). In the var. Gomati VU-89, PY revealed a significant positive correlation with the HI (0.735), PPP (0.261), PL (0.362), PH (0.238), BPP (0.301), and

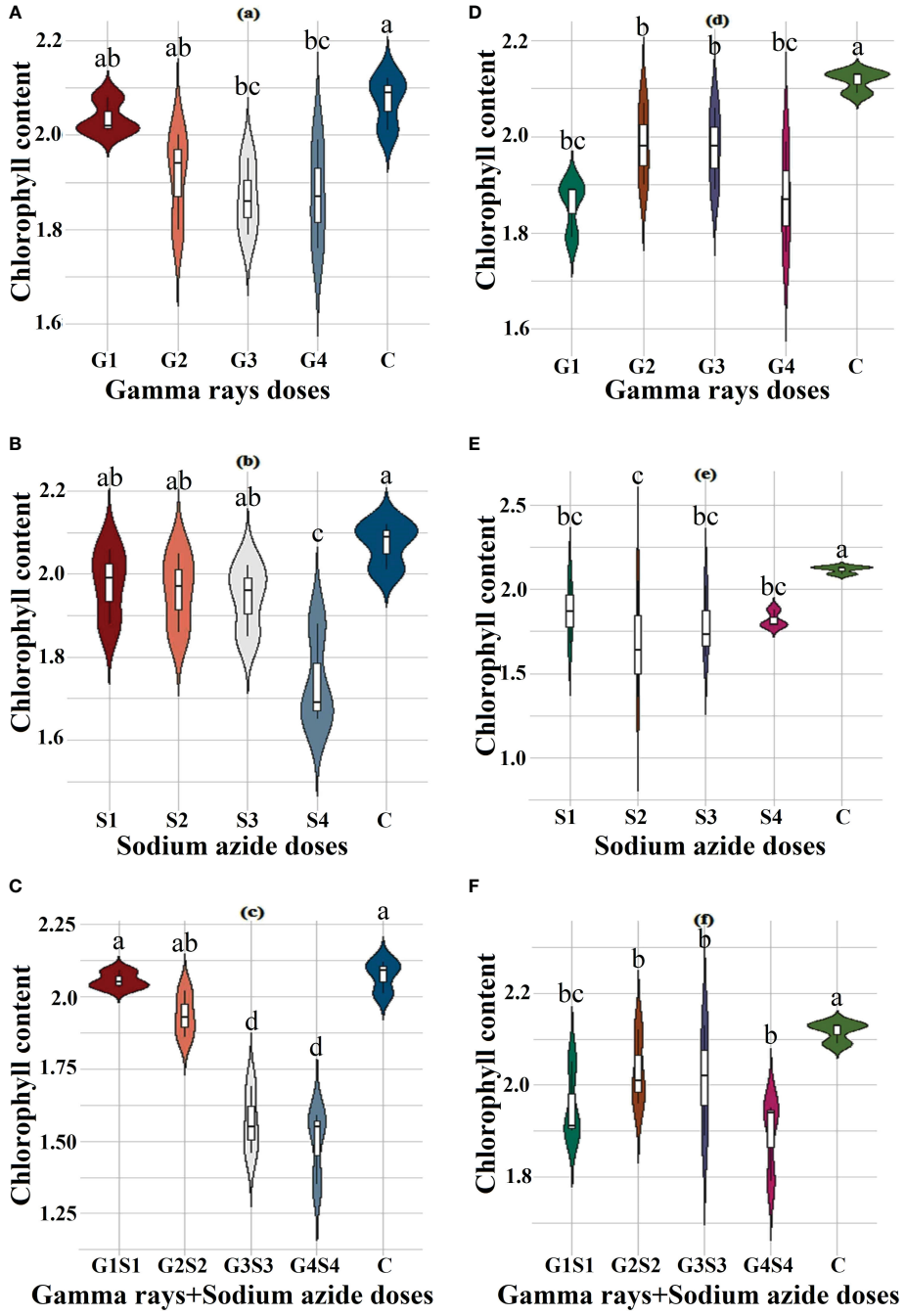

FIGURE 3
Effects of different doses of γ rays, SA, and γ rays + SA on chlorophyll contents **(A–C)** in var. Gomati VU-89 and **(D–F)** in var. Pusa-578. The data are presented as mean and standard error (n = 30). #Means followed by the same letter is not different at 5% level of significance, based on the DMRT. C, Control; G1, 100 Gy γ rays; G2, 200 Gy γ rays; G3, 300 Gy γ rays; G4, 400 Gy γ rays; S1, 0.01% SA; S2, 0.02% SA; S3, 0.03% SA; S4, 0.04% SA; G1 +S1, 100 Gy γ rays+0.01% SA; G2+S2, 200 Gy γ rays+0.02% SA; G3+S3, 300 Gy γ rays+0.03% SA; G4+S4, 400 Gy γ rays+0.04% SA.

SW (0.320) and an insignificant correlation with SPP (0.134), DF (-0.093), and DM (0.053). In the var. Pusa-578, PY showed a significant positive correlation with PPP (0.339), PL (0.331), SPP (0.240), SW (0.200), PL (0.331), and HI (0.475) and an insignificant correlation with PH (0.169), BPP (0.047), DF (-0.019), and DM (0.024) (Supplementary Table 1; Figure 5). Correlation analysis revealed that PL and PPP are the most important yield-attributing traits in Gomati VU-89 and Pusa-578, respectively. The contribution of these nine yield components in decreasing order was HI > PL > SW > BPP > PPP > PH > SPP > DF > DM in the var. Gomati VU-89 and HI > PPP > PL > SPP > SW > PH > PH > BPP > DM > DF in the var. Pusa-578.

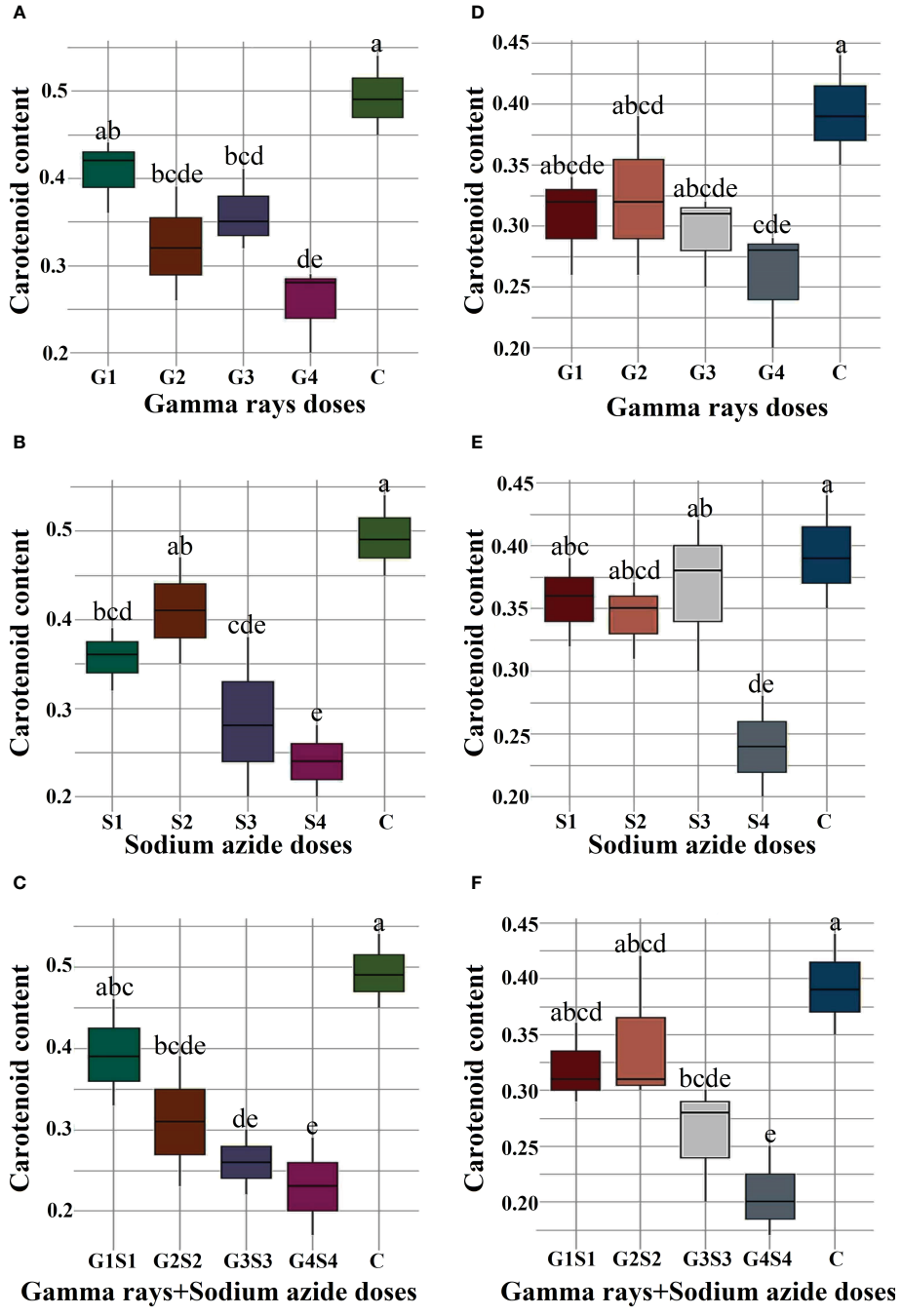

FIGURE 4
Effects of different doses of gamma (γ) rays, SA, γ rays + SA on carotenoid contents **(A–C)** in var. Gomati VU-89 and **(D–F)** in var. Pusa-578. The data are presented as mean and standard error (n = 30). #Means followed by the same letter is not different at 5% level of significance, based on the Duncan's Multiple Range Test (DMRT). C, Control; G1, 100 Gy γ rays; G2, 200 Gy γ rays; G3, 300 Gy γ rays; G4, 400 Gy γ rays; S1, 0.01% SA; S2, 0.02% SA; S3, 0.03% SA; S4, 0.04% SA; G1 +S1, 100 Gy γ rays+0.01% SA; G2+S2, 200 Gy γ rays+0.02% SA; G3+S3, 300 Gy γ rays+0.03% SA; G4+S4, 400 Gy γ rays+0.04% SA.

Path analysis

Path analysis revealed that SPP and SW had a maximum positive direct effect on the PY. However, PL and DM revealed a negative direct effect on yield. E1 in the diagram represents residual factors, unaccounted for and independent of the other variables. The contributions of trait toward yield showed an increasing trend, i.e., DM< DF< PH< PL< PL< HI< BPP< SW< SPP in the var. Gomati VU-89 and BPP< DM< PL< HI< DF< PH< PPP< SW< SPP in the var. Pusa-578 (Figure 6).

Plant yield vs. plant height

The direct effects of PH on PY was 0.02 and 0.6 in Gomati VU-89 and Pusa-578, respectively. It had positive indirect impact on PY

TABLE 1 Estimates of mean and standard error ($\bar{x} \pm SE$) (n = 30) for quantitative traits in M_1 generation of cowpea var. Gomati VU-89.

Treatments	PH	DF	DM	BPP	PL	PPP	SPP	SW	PY	HI
C	$182.25^{a} \pm 0.47$	$79.66^{ab} \pm 0.30$	$150.93^{a} \pm 0.29$	$10.73^{a} \pm 0.10$	$28.72^{f} \pm 0.15$	$59.20^{ef} \pm 0.20$	$11.90^{a} \pm 0.13$	$15.20^{a} \pm 0.42$	$93.69^{i} \pm 0.40$	$27.35^{j} \pm 0.13$
G1	$180.14^{abc} \pm 0.96$	$78.96^{abc} \pm 2.49$	$149.46^{a} \pm 0.61$	$9.46^{ab} \pm 0.16$	$29.85^{de} \pm 0.26$	$60.26^{cde} \pm 0.44$	$12.40^{a} \pm 0.20$	$14.10^{cd} \pm 0.35$	$113.02^{a} \pm 0.63$	$40.53^{a} \pm 0.37$
G2	$178.58^{bcde} \pm 1.19$	$79.96^{ab} \pm 0.49$	$150.03^{a} \pm 0.70$	$9.83^{ab} \pm 0.18$	$30.51^{bcd} \pm 0.28$	$62.20^{a} \pm 0.52$	$12.30^{a} \pm 0.24$	$14.20^{bcd} \pm 0.3$	$107.87^{cd} \pm 0.76$	$39.26^{bc} \pm 0.35$
G3	$177.43^{cdef} \pm 1.24$	$79.83^{ab} \pm 0.50$	$149.66^{a} \pm 0.98$	$9.03^{bcd} \pm 0.18$	$30.27^{cd} \pm 0.25$	$59.30^{ef} \pm 0.49$	$12.26^{a} \pm 0.24$	$14.30^{bcd} \pm 0.34$	$103.87^{f} \pm 0.58$	$38.10^{d} \pm 0.35$
G4	$175.67^{def} \pm 1.19$	$78.40^{bc} \pm 0.51$	$148.93^{a} \pm 1.03$	$8.53^{cdef} \pm 0.17$	$29.25^{ef} \pm 0.17$	$57.90^{g} \pm 0.51$	$12.00^{a} \pm 0.27$	$14.10^{cd} \pm 0.30$	$97.96^{g} \pm 0.49$	$35.58^{fg} \pm 0.29$
S1	$181.95^{ab} \pm 1.20$	$78.93^{abc} \pm 0.47$	$149.93^{a} \pm 0.71$	$9.23^{bcd} \pm 0.18$	$30.61^{bc} \pm 0.27$	$60.50^{bcde} \pm 0.35$	$12.70^{a} \pm 0.29$	$14.02^{cd} \pm 0.28$	$111.02^{b} \pm 0.79$	$39.73^{ab} \pm 0.44$
S2	$180.30^{abc} \pm 1.22$	$79.03^{abc} \pm 0.50$	$151.46^{a} \pm 0.81$	$8.90^{cde} \pm 0.18$	$31.20^{ab} \pm 0.26$	$60.70^{bcd} \pm 0.42$	$12.30^{a} \pm 0.26$	$14.50^{bcd} \pm 0.25$	$109.00^{c} \pm 0.65$	$38.73^{cd} \pm 0.38$
S3	$178.83^{abcd} \pm 1.22$	$79.46^{abc} \pm 0.56$	$149.50^{a} \pm 0.93$	$8.83^{cde} \pm 0.19$	$29.88^{de} \pm 0.21$	$59.70^{de} \pm 0.43$	$12.20^{a} \pm 0.23$	$14.62^{bcd} \pm 0.26$	$106.33^{de} \pm 0.66$	$36.22^{ef} \pm 0.25$
S4	$176.60d^{ef} \pm 1.24$	$78.80^{abc} \pm 0.57$	148.53a ± 0.98	$8.60^{cdef} \pm 0.19$	$28.88^{f} \pm 0.16$	$60.10^{cde} \pm 0.60$	$12.00^{a} \pm 0.26$	$13.71^{cd} \pm 0.37$	$98.80^{g} \pm 0.42$	$35.79^{ef} \pm 0.24$
G1+S1	$180.52^{abc} \pm 1.11$	$80.23^{a} \pm 0.54$	$150.83^{a} \pm 1.02$	$9.33^{ab} \pm 0.16$	$30.74^{bc} \pm 0.28$	$62.23^{a} \pm 0.32$	$12.10^{a} \pm 0.27$	$14.03^{cd} \pm 0.28$	$105.41^{ef} \pm 0.65$	$36.59^{e} \pm 0.38$
G2+S2	$177.30^{cdef} \pm 1.11$	$79.36^{abc} \pm 0.53$	$149.30^{a} \pm 1.02$	$9.13^{bcd} \pm 0.17$	$31.47^{a} \pm 0.27$	$61.43^{abc} \pm 0.34$	$12.00^{a} \pm 0.30$	$14.80^{a} \pm 0.27$	$107.62^{cd} \pm 0.71$	$34.78^{g} \pm 0.32$
G3+S3	$175.22^{ef} \pm 0.87$	$79.16^{abc} \pm 0.59$	$149.00^{a} \pm 1.13$	$8.40^{fgh} \pm 0.20$	$29.27^{ef} \pm 0.16$	$61.70^{ab} \pm 0.44$	$11.96^{a} \pm 0.29$	$13.45^{e} \pm 0.27$	$95.85^{h} \pm 0.57$	$31.54^{h} \pm 0.28$
G4+S4	$174.13^{f} \pm 0.77$	$77.93^{c} \pm 0.59$	$148.83^{a} \pm 1.18$	$8.20^{gh} \pm 0.18$	$28.96^{f} \pm 0.15$	$58.20^{fg} \pm 0.48$	$11.91^{a} \pm 0.26$	$13.60^{e} \pm 0.24$	$89.34^{j} \pm 0.53$	$29.91^{i} \pm 0.19$

PH, plant height; DF, days to flowering; DM, days to maturity; PPP, pods per plant; BPP, branches per plant; SPP, seeds per pod; SW, seed weight; PL, pod length; PY, plant yield; HI, harvest index. #Means having same letter is not different at 5% level of significance, based on the DMRT. C, Control; G1, 100 Gy γ rays; G2, 200 Gy γ rays; G3, 300 Gy γ rays; G4, 400 Gy γ rays; S1, 0.01% SA; S2, 0.02% SA; S3, 0.03% SA; S4, 0.04% SA; G1 +S1, 100 Gy γ rays+0.01% SA; G2+S2, 200 Gy γ rays+0.02% SA; G3+S3, 300 Gy γ rays+0.03% SA; G4+S4, 400 Gy γ rays+0.04% SA.

through DF (0.79 and 0.46), DM (1.65 and 0.92), PPP (0.97 and 1.87), BPP (0.58 and 0.43), SPP (0.31 and 0.51), SW (0.76 and 0.15), PL (0.75 and 0.97), and HI (2.76 and 2.71) in the var. Gomati VU-89 and var. Pusa-578, respectively (Figure 6).

Plant yield vs. days to flowering

The direct effect of DF on PY was -0.03 and 0.03 in the var. Gomati VU-89 and var. Pusa-578, respectively. It had a positive indirect impact on PY through DM (0.29 and 0.01), PPP (0.53 and 0.16), BPP (0.16 and 0.7), SPP (0.02 and 0.05), SW (0.09 and 0.15), PL (0.23 and 0.09), and HI (0.47 and 1.63) in the var. Gomati VU-89 and var. Pusa-578, respectively (Figure 6).

Plant yield vs. days to maturity

The direct effect of DM on PY was -0.36 and -0.07 in the var. Gomati VU-89 and var. Pusa-578, respectively. It had an indirect impact on PY through PPP (0.37 and 0.24), BPP (0.12 and 0.06), SPP (0.05 and 0.05), SW (0.15 and 0.01), PL (0.34 and 0.20), and HI (0.40 and 0.07) in the var. Gomati VU-89 and var. Pusa-578, respectively (Figure 6).

Plant yield vs. pods per plant

The direct effect of PPP on PY was 1.48 and 1.90 in the var. Gomati VU-89 and var. Pusa-578, respectively. It had a positive indirect impact on PY through BPP (0.37 and 0.45), SPP (0. 07 and 0.49), SW (0.17 and 0.32), PL (0.70 and 0.87), and HI (1.72 and 2.62) in the varieties Gomati VU-89 and Pusa-578, respectively (Figure 6).

Plant yield vs. branches per plant

The direct impact of BPP on PY was 1.26 and -0.11 in the var. Gomati VU-89 and var. Pusa-578, respectively. BPP also positively impacted PY through PL (0.22 and 0.08) in Gomati VU-89 and Pusa-578, respectively. A positive indirect impact on PY was shown by BPP through HI (1.16 and 0.50), SPP (0.06 and 0.04), and SW (0.16 and 0.02) in the var. Gomati VU-89 and var. Pusa-578, respectively (Figure 6).

Plant yield vs. seeds per pod

In the var. Gomati VU-89 and Pusa-578, the direct impact of SPP on PY was 8.66 and 9.23, respectively. It also had a positive indirect impact on PY through SW (0.10 and 0.11), PL (0.10 and

TABLE 2 Estimates of mean and standard error ($\bar{x} \pm SE$) (n = 30) for quantitative traits in M_1 generation of cowpea var. Pusa-578.

Treatments	PH	DF	DM	BPP	PL	PPP	SPP	SW	PY	HI
C	$180.46^{a} \pm 0.53$	$88.00^{abcd} \pm 0.21$	$156.00^{a} \pm 0.28$	$11.20^{a} \pm 0.16$	$23.53^{d} \pm 0.14$	$40.36^{bc} \pm 0.18$	$9.46^{de} \pm 0.14$	$22.97^{a} \pm 0.14$	$79.90^{f} \pm 0.32$	$28.79^{f} \pm 0.14$
G1	$178.90^{ab} \pm 1.00$	$88.53^{abc} \pm 0.67$	$155.53^{a} \pm 1.02$	$10.90^{b} \pm 0.25$	$23.72^{d} \pm 0.27$	$42.53^{a} \pm 0.63$	$10.56^{ab} \pm 0.22$	$21.70^{b} \pm 0.24$	$97.81^{b} \pm 1.01$	$34.28^{c} \pm 0.36$
G2	$178.25^{abc} \pm 1.12$	$89.43^{a} \pm 0.69$	$155.43^{a} \pm 1.12$	$10.40^{c} \pm 0.31$	$26.43^{a} \pm 0.37$	$41.73^{ab} \pm 0.56$	$10.10^{bcd} \pm 0.23$	$21.80^{bc} \pm 0.35$	$91.45^{c} \pm 0.84$	$37.42^{a} \pm 0.41$
G3	$177.54^{abc} \pm 0.91$	$88.43^{abc} \pm 0.57$	$156.46^{a} \pm 0.88$	$10.90^{b} \pm 0.20$	$23.56^{d} \pm 0.26$	$41.2^{abc} \pm 0.44$	$9.80^{cde} \pm 0.19$	$21.10^{bcd} \pm 0.26$	$86.07^{d} \pm 0.72$	$33.12^{d} \pm 0.31$
G4	$176.10^{bcd} \pm 0.83$	$87.8^{abcd} \pm 0.48$	$155.00^{a} \pm 0.79$	$10.80^{b} \pm 0.18$	$23.12^{d} \pm 0.23$	$40.53^{bc} \pm 0.64$	$9.90^{cde} \pm 0.19$	$20.96^{cd} \pm 0.18$	$83.21^{e} \pm 0.61$	$31.72^{e} \pm 0.21$
S1	$180.26^{a} \pm 1.14$	$87.53^{abcd} \pm 0.70$	$156.06^{a} \pm 1.13$	$10.70^{b} \pm 0.34$	$25.82^{ab} \pm 0.32$	$41.93^{ab} \pm 0.38$	$10.90^{a} \pm 0.23$	$21.04^{c} \pm 0.25$	$100.54^{a} \pm 1.02$	$36.42^{b} \pm 0.35$
S2	$179.24^{ab} \pm 1.18$	$86.43^{d} \pm 0.64$	$156.80^{a} \pm 1.16$	$11.1^{a} \pm 0.37$	$24.70^{c} \pm 0.29$	$41.26^{abc} \pm 0.49$	$10.00^{bcde} \pm 0.21$	$21.90^{b} \pm 0.29$	$90.35^{c} \pm 1.07$	$29.39^{g} \pm 0.25$
S3	$178.11^{abc} \pm 0.82$	$88.06^{abcd} \pm 0.51$	$155.03^{a} \pm 0.91$	$11.03^{a} \pm 0.22$	$23.60^{d} \pm 0.23$	$41.80^{ab} \pm 0.58$	$9.70^{cde} \pm 0.18$	$21.44^{bcd} \pm 0.24$	$86.97^{d} \pm 0.69$	$33.52^{cd} \pm 0.29$
S4	$177.76^{abc} \pm 1.22$	$89.00^{ab} \pm 0.50$	$155.90^{a} \pm 0.72$	$11.00^{a} \pm 0.22$	$23.22^{d} \pm 0.22$	$38.23^{d} \pm 0.60$	$9.90^{cde} \pm 0.18$	$20.89^{d} \pm 0.21$	$74.70^{g} \pm 0.54$	$32.85^{d} \pm 0.28$
G1+S1	$179.44^{ab} \pm 1.04$	$87.40^{bcd} \pm 0.71$	$156.03^{a} \pm 1.22$	$10.80^{b} \pm 0.31$	$25.55^{b} \pm 0.37$	$42.63^{a} \pm 0.43$	$10.20^{bc} \pm 0.24$	$22.10^{b} \pm 0.30$	$96.09^{b} \pm 0.96$	$34.38^{c} \pm 0.44$
G2+S2	$177.36^{abc} \pm 1.09$	$87.63^{abcd} \pm 0.75$	$156.30^{a} \pm 1.25$	$11.10^{a} \pm 0.30$	$25.24^{bc} \pm 0.35$	$41.00^{abc} \pm 0.54$	$9.56^{cde} \pm 0.20$	$22.20^{ab} \pm 0.25$	$85.74^{d} \pm 0.84$	$33.48^{cd} \pm 0.41$
G3+S3	$175.49^{cd} \pm 1.11$	$86.43^{d} \pm 0.47$	$155.00^{a} \pm 0.90$	$11.03^{a} \pm 0.20$	$23.62^{d} \pm 0.23$	$39.96^{c} \pm 0.68$	$9.46^{de} \pm 0.17$	$22.30^{a} \pm 0.21$	$82.32^{e} \pm 0.75$	$28.83^{g} \pm 0.28$
G4+S4	$173.05^{d} \pm 1.22$	$86.93^{cd} \pm 0.47$	$154.80^{a} \pm 0.86$	$11.0^{a} \pm 0.19$	$23.29^{d} \pm 0.21$	$37.83^{d} \pm 0.48$	$9.36^{e} \pm 0.15$	$22.0^{bc} \pm 0.20$	$76.10^{g} \pm 0.66$	$27.63^{g} \pm 0.24$

PH, plant height; DF, days to flowering; DM, days to maturity; PPP, pods per plant; BPP, branches per plant; SPP, seeds per pod; SW, seed weight; PL, pod length; PY, pant yield; HI, harvest index. #Means followed by the same letter is not different at 5% level of significance, based on the DMRT. C, Control; G1, 100 Gy γ rays; G2, 200 Gy γ rays; G3, 300 Gy γ rays; G4, 400 Gy γ rays; S1, 0.01% SA; S2, 0.02% SA; S3, 0.03% SA; S4, 0.04% SA; G1 +S1, 100 Gy γ rays+0.01% SA; G2+S2, 200 Gy γ rays+0.02% SA; G3+S3, 300 Gy γ rays+0.03% SA; G4+S4, 400 Gy γ rays+0.04% SA.

0.28), and HI (0.70 and 0.88) in the var. Gomati VU-89 and var. Pusa-578, respectively (Figure 6).

Plant yield vs. seed weight

The direct impact of SW on PY was 7.34 and 4.16 in the var. Gomati VU-89 and var. Pusa-578, respectively. SW also showed a considerable positive indirect impact on PY through PL (0.39 and 0.33) and a strong positive indirect impact on PY through HI (2.06 and 0.36) in the var. Gomati VU-89 and var. Pusa-578, respectively (Figure 6).

Plant yield vs. pod length

The direct impact of PL on PY was 0.03 and -0.05 in the varieties Gomati VU-89 and Pusa-578. PL also showed a strong positive indirect impact on PY through HI (2.06 and 2.08) in the var. Gomati VU-89 and var. Pusa-578, respectively (Figure 6).

Plant yield vs. harvest index

The direct impact of the HI on PY was -0.12 and 0.02 in the var. Gomati VU-89 and var. Pusa-578, respectively (Figure 6).

Multivariate analysis

Hierarchical cluster analysis

HCA categorized treated and control plants into separate clusters, each with cluster size ranging from 1 to 4 in both varieties. Each 12 treated and 1 untreated population were grouped into five and seven clusters in the varieties Gomati VU-89 Pusa-578, respectively (Figure 7). In the var. Gomati VU-89, group I included 400 Gy γ rays and 0.04% SA populations, group II comprised 300 Gy γ rays + 0.03% SA population, group III comprised control and 400 Gy γ rays + 0.04% SA populations, group IV comprised 0.03% SA, 200 Gy γ rays + 0.02% SA, 100 Gy γ rays + 0.01% SA, and 300 Gy γ rays populations, and group V constituted 100 Gy γ rays, 0.01% SA, 200 Gy γ rays, and 0.02% SA populations. In the var. Pusa-578, group I consisted of 300 Gy γ rays, 0.03% SA and 200 Gy γ rays + 0.02% SA populations; group II comprised 400 Gy γ rays and 300 Gy γ rays + 0.03% SA populations; group III consisted of 0.03% SA population; group IV included control, 0.04% SA, and 400 Gy γ rays + 0.04% SA populations; group V composed of 100 Gy γ rays and 100 Gy γ rays + 0.01% SA population; group VI consisted of 0.01% SA population; and group

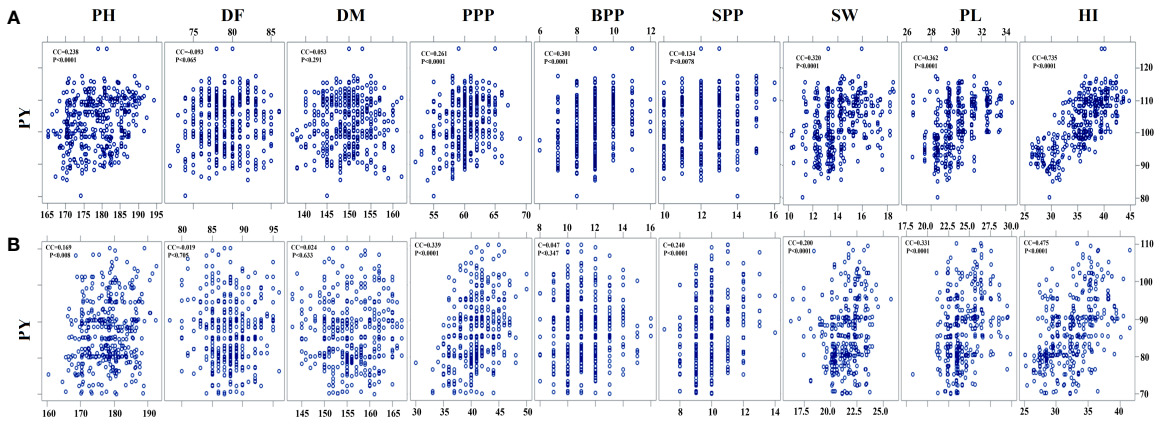

FIGURE 5
Estimates of Pearson's correlation coefficients between plant yield (PY) and yield- attributing traits **(A)** var. Gomati VU-89 and **(B)** var. Pusa-578 (n = 30 for each character). PH, plant height; DF, days to flowering; DM, days to maturity; PPP, pods per plant; BPP, branches per plant; SPP, seeds per pod; SW, seed weight; PL, pod length; PY, plant yield; HI, harvest index (n = 30 for each character).

VII consisted of 200 Gy γ rays population. Among mutagenized plants, 0.02% SA and 200 Gy γ rays populations were most diverged from untreated populations in Gomati VU-89 and Pusa-578, respectively.

Characteristic means of quantitative phenotypic traits of both treated and untreated populations were shown by three clusters I, II, and III (Supplementary Table 2). Among the clusters, cluster II showed maximum mean values for PPP (60.27 and 41.93), SPP (12.40 and 10.90), SW (15.10 and 22.04), PL (29.85 and 25.82), PY (113.02 and 100.54), and HI (40.54 and 36.42%) in the varieties Gomati VU-89 and Pusa-578, respectively. Therefore, the population that lies in cluster II could be used for isolating high-yielding mutant lines. The highest intercluster distance was noted between clusters I and II in the varieties Gomati VU-89 (19.28) and Pusa-578 (21.21), respectively (Supplementary Table 3).

The interpopulation dissimilarity matrix revealed the highest Euclidean distance between 400 Gy γ rays + 0.04% SA and 100 Gy γ rays populations in the var. Gomati VU-89 (26.88) and 400 Gy γ

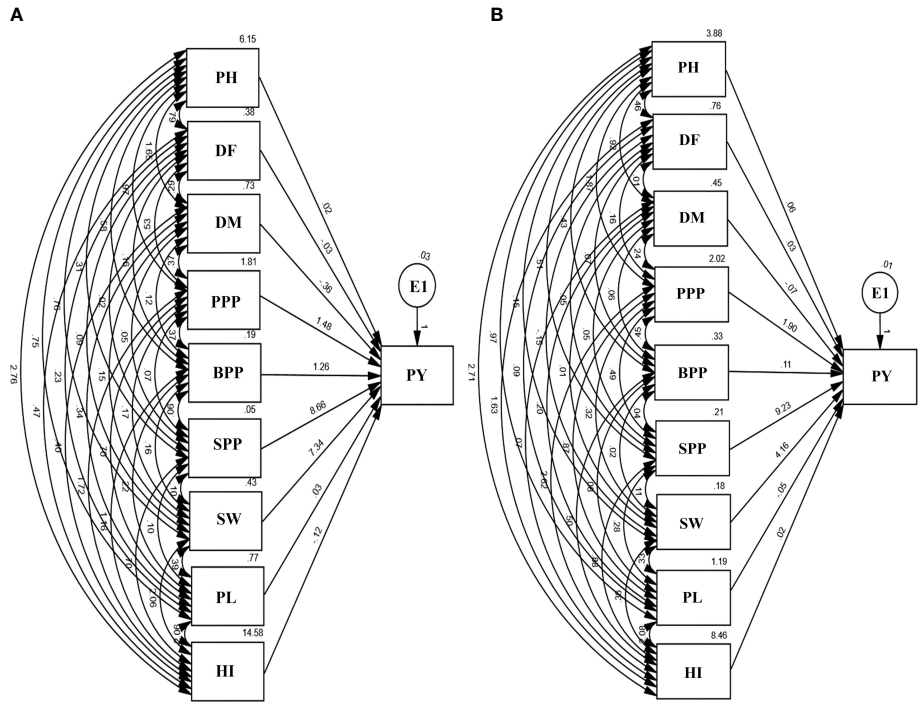

FIGURE 6
Path diagram **(A)** var. Gomati VU-89 and **(B)** var. Pusa-578 showing the interrelationship between PY and yield attributes viz., PH, plant height; DF, days to flowering; DM, days to maturity; PPP, pods per plant; BPP, branches per plant; SPP, seeds per pod; SW, seed weight; PL, pod length; PY, plant yield; HI, harvest index (n = 30 for each character) and E1: residual factors.

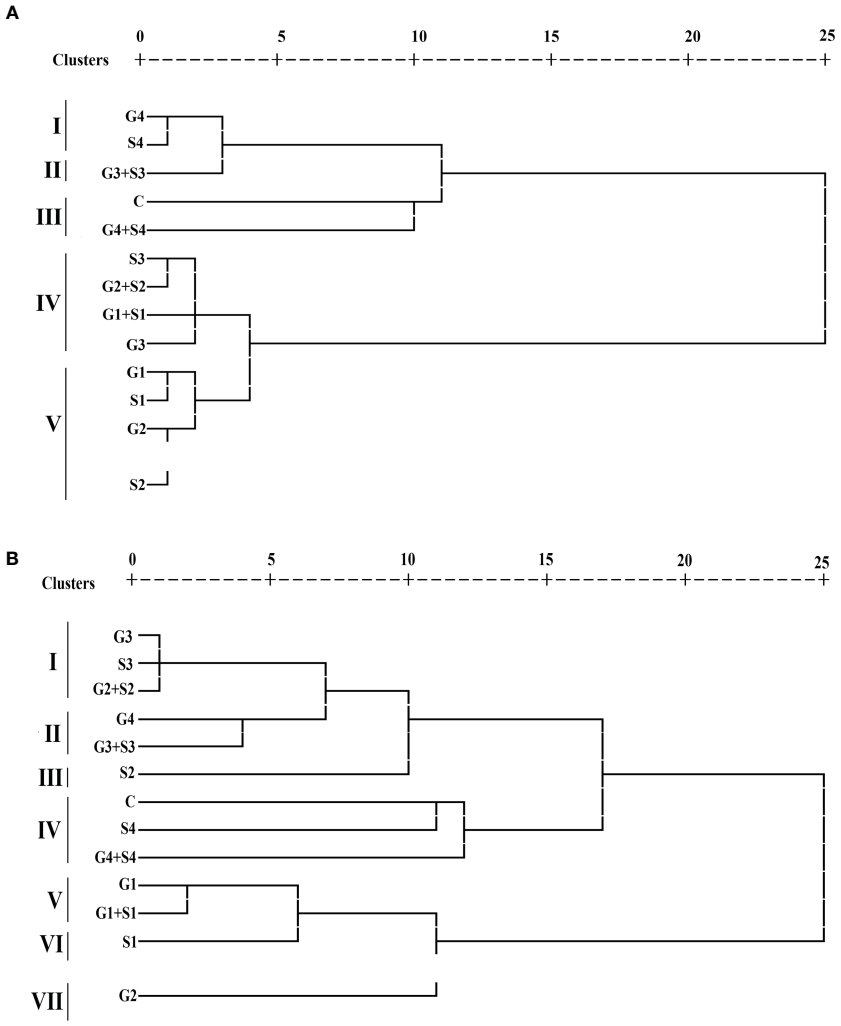

FIGURE 7
Dendrogram analysis **(A)** var. Gomati VU-89 and **(B)** var. Pusa-578 of control and mutagen-treated population based on 10 quantitative traits (n = 30). C, Control; G1, 100 Gy γ rays; G2, 200 Gy γ rays; G3, 300 Gy γ rays; G4, 400 Gy γ rays; S1, 0.01% SA; S2, 0.02% SA; S3, 0.03% SA; S4, 0.04% SA; G1 +S1, 100 Gy γ rays+0.01% SA; G2+S2, 200 Gy γ rays+0.02% SA; G3+S3, 300 Gy γ rays+0.03% SA; G4+S4, 400 Gy γ rays+0.04% SA.

rays + 0.04% SA and 0.01% SA populations in the var. Pusa-578 (27.47) indicate a dissimilar population. The minimum Euclidean distance was noted between 0.01% SA and 100 Gy γ rays populations in the var. Gomati VU-89 (3.03) and 0.03% SA and 300 Gy γ rays population in the var. Pusa-578 (2.09) indicates a similar population. The most distanced population from control was 100 Gy γ rays and 0.01% SA population in the varieties Gomati VU-89 (23.68) and Pusa-578 (22.27), respectively (Supplementary Table 4).

Principal component analysis

The PCA confirmed that lower and intermediate mutagen–treated populations viz., 100 Gy γ rays, 200 Gy γ rays; 0.01% SA, 0.02% SA; 100 Gy γ rays + 0.01% SA, 200 Gy γ rays + 0.02% SA and higher mutagen–treated population viz., 300 Gy γ rays, 400 Gy γ rays; 0.03% SA, 0.04% SA; 300 Gy γ rays + 0.03% SA formed their separate clusters as represented by different colored dots in a biplot (Figure 8). The PCA showed a total 40.47% (PC1 = 28.34%; PC2 = 12.12%) and 33.47% (PC1 = 21.92%; PC2 = 11.55%) variability of the data in the var. Gomati VU-89 and var. Pusa-578, respectively. PY (0.525 and 0.532) contributed more to the variation followed by HI (0.483 and 0.486), PH (0.436 and 0.197), PL (0.293 and 0.371), and BPP (0.269 and 0.166). SW (0.265 and 0.184) and PPP (0.199 and 0.375) had the highest loadings in PC1 in the varieties Gomati VU-89 and Pusa-578, respectively. Characters that contributed to the second component included PPP (0.554 and -0.181), DM (0.425 and -0.226), DF (0.344 and 0.666), SPP (0.331 and 0.161), and PL (0.243 and 0.212) in the varieties Gomati VU-89 and Pusa-578, respectively. PY and SW showed maximum positive and minimum negative loading on PC1 and PC2 in the var. Gomati VU-89 (0.525 and -0.345) and var. Pusa-578 (0.532 and -0.545), respectively (Supplementary Table 5). For PC2, DM revealed positive loading in var. Gomati VU-89 (0.425) and negative loading in the var. Pusa-578 (-0.226). Substantial positive correlations between PY and PPP, SPP, and BPP were recorded in both varieties. Based on the distribution pattern of mutagen-treated populations in the biplot, it can be concluded that mutagen doses

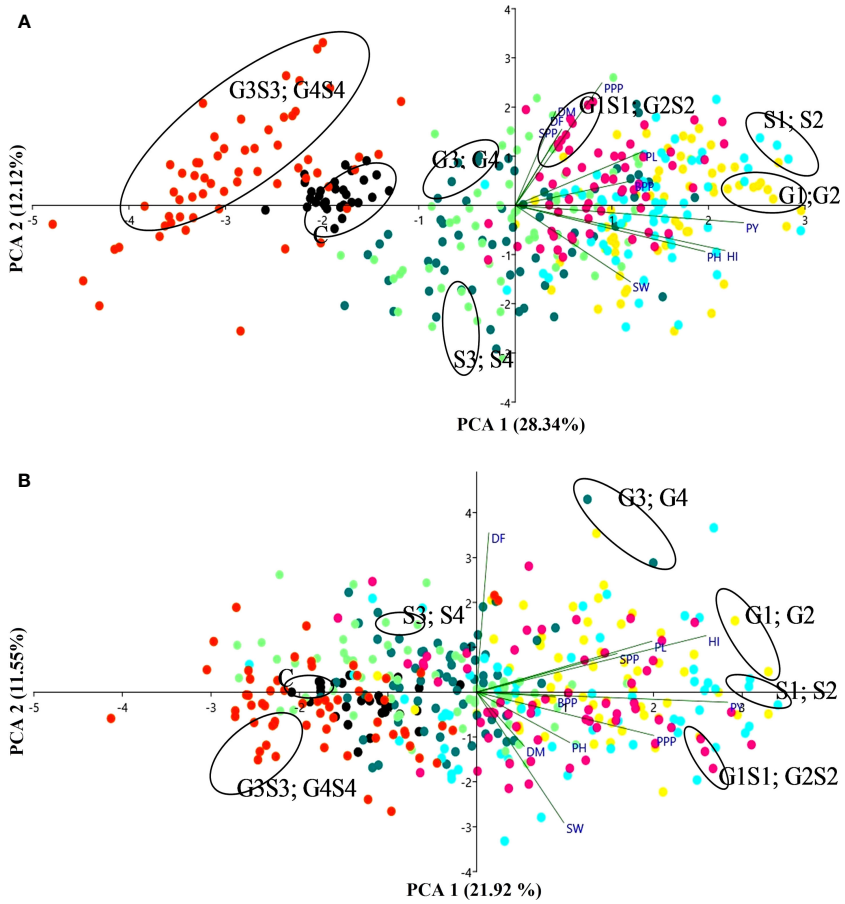

FIGURE 8
The biplots of principal component analysis **(A)** var. Gomati VU-89 and **(B)** var. Pusa-578 compare the effects of mutagens on mean yield and yield attributes (n = 30). PH, plant height; DF, days to flowering; DM, days to maturity; PPP, pods per plant; BPP, branches per plant; SPP, seeds per pod; SW, seed weight; PL, pod length; PY, plant yield; HI, harvest index. C, Control; G1, 100 Gy γ rays; G2, 200 Gy γ rays; G3, 300 Gy γ rays; G4, 400 Gy γ rays; S1, 0.01% SA; S2, 0.02% SA; S3, 0.03% SA; S4, 0.04% SA; G1 S1, 100 Gy γ rays+0.01% SA; G2S2, 200 Gy γ rays+0.02% SA; G3S3, 300 Gy γ rays +0.03% SA; G4S4, 400 Gy γ rays+0.04% SA.

induced substantial variation in the quantitative traits (Figure 8). PY was the most important trait contributing for the overall variability observed among the putative mutants. In the present study, PCA revealed that the first two principal components contributed maximum number of traits toward variability.

Discussion

Nitrate reductase activity, chlorophyll, and carotenoid contents assessment in control and treated plants

Nitrate reductase, a molybdoenzyme with a molybdenum atom linked to two sulfur atoms of molybdopterin, is involved in producing nitric oxide in plants. Nitric oxide is vital in germination, growth, apoptosis, stomatal regulation, and stress tolerance (Wendehenne, 2011; Sanz-Luque et al., 2015). In the present study, a linear decrease in Nitrate Reductase (NR) activity in the mutagen- treated seedlings was in propinquity with the results obtained by Laskar et al. (2015). However, the mechanism behind this inhibition is not fully understood, and several workers attributed mutagen-induced inhibition and metabolic dysfunctions of specific enzyme proteins to the decreased NR activity (Hopkins, 1995).

Chlorophyll plays a vital role in photosynthesis and influences key processes of plant growth and development (Li et al., 2018). Chlorophyll synthesis is a complex process involving several enzymes and steps like insertion of Mg^{2+} into protoporphyrin IX that affect chlorophyll biosynthesis (Tanaka and Tanaka, 2007). Any obstructive enzymatic reaction or step may lead to reduced chlorophyll content (Willows and Hansson, 2003). In the present study, a decrease in mean chlorophyll contents in mutagenized populations was in agreement with the findings of Borzouei et al. (2010) in *Triticum aestivum* and Verma et al. (2010) in *Euryale ferox*. The diminution in chlorophyll content may be due to mutagen-induced loss of function in genes related to chlorophyll synthesis. Moreover, reduction in chlorophyll content may be due to the gamma radiation–induced dephytolization and pheophytinization that eventually results in inhibition of chlorophyll synthesis (Saha et al., 2010). Mutagens, especially γ radiations, interact with the atoms and molecules and generate

highly reactive free radicals that destroy or modify photosynthetic pigments, thylakoid membranes, the antioxidative system, and essential constituents of a cell (Kovacs and Keresztes, 2002; Kulandaivelu and Noorudeen, 1983; Wi et al., 2007). Kim et al. (2004) reported that γ rays induced prominent structural changes in chloroplasts, such as inhibition of senescence and dedifferentiation into the agranal stage. Kiong et al. (2008) reported that the reduction in chlorophyll b is mainly due to selective degradation of chlorophyll b.

Carotenoids act as accessory pigments with vital roles in the light-harvesting process, quenching excess light energy, scavenging free radicals, and creating a plant defense system (Fukuzawa et al., 1998; Ramel et al., 2012; Hashimoto et al., 2016). The results revealed a substantial decrease in carotenoid contents in the treated population of both varieties. The results followed the findings of Amin et al. (2019) in mutagen-treated black cumin populations. The reduction in carotenoid contents may be attributed to mutagen-induced loss of function of carotenoid-synthesizing genes. The reduced carotenoids in treated seeds could reduce the light-harvesting and photosynthetic capacity. In general, alterations in the enzymes involved in the carotenoid synthesis could be considered one of the physiological effects caused by gamma rays and SA, which leads to decreased pigment contents in mutagenized populations.

Quantitative traits and their role in total plant yield

Small additive effects of multiple genes govern quantitative traits, and their expression is also influenced by environmental factors. Hence, statistical analysis of quantitative traits is required to visualize the data significance. In the present study, enhanced quantitative traits of lower and intermediate mutagen–treated plants could be attributed to the induction of desirable mutations. However, decreased quantitative traits in plants raised from seeds treated with higher combined mutagen doses might be ascribed to the synergistic effect of the combined mutagens. It is recommended to expose the plant material to individual mutagens to evade the deleterious effects of combined mutagens. Additionally, it will facilitate a chance for the second mutagen to target the DNA region left unaltered by the first mutagen, resulting in a high frequency of mutations.

In the present study, mutagen-induced reduction in plant height may be ascribed to a diminution of mitotic activity of meristematic tissues, cell length, cell number, and phytohormones (Austin et al., 1980; Cheng et al., 2019). The results were in propinquity with the findings obtained in lentil (Laskar et al., 2018), rapeseed and mustard (Zeng et al., 2011; Wei et al., 2018; Channaoui et al., 2019), and coriander (Kumar and Pandey, 2019). Mutagen-induced reduction in plant height is a crucial trait from the perspective of plant breeders. This is because short-statured plants have improved architecture, yield, harvest index, and lodging resistance and are less influenced by the fast-moving winds that are quite prevalent in the flowering season of cowpea. More and Malode (2016) also reported increased yield in dwarf mutants of canola treated with Ethyl methane sulphonate (EMS). Further, one could recall that the use of dwarfing genes was a crucial factor in accomplishing the green revolution (Khush, 2001). In the present study, mutagen doses positively affected flowering time and could lead to the isolation of early-flowering mutants in subsequent generations. The results followed the findings of Gnanamurthy and Dhanavel (2014), which reported a reduction in flowering time in the mutagenized cowpea population. Flowering time, the main modulator of plant growth, is influenced by environmental factors such as temperature, photoperiod, nutrient availability, light quality, and intensity (Pouteau et al., 2004). Therefore, it is difficult to assess the cause of reduction in flowering time in the plants raised from mutagen-treated seeds. Early flowering offers adequate time for pod filling, resulting in improved seed yield. Earliness is most commonly altered in mutagenesis programs, and many early maturing mutants have been developed (Malek and Monshi, 2009). In the present study, few early maturity mutants have been isolated in the treated population. These putative mutants mature earlier than the wild-type lines and can escape detrimental heat stress at the pod-filling stage usually encountered in cowpea-growing areas. Moreover, early-maturing putative mutants are also good at escaping insect damage and averting rise in the insect population due to the shorter reproductive phase duration (Jackai, 1982). Such early maturing putative mutants are also suitable for plantations in areas receiving short rainfall. The diversity in terms of genetic and physiological properties of the early-flowering and maturing putative mutants arising from common ancestry accentuates the importance of induced mutagenesis in broadening the genetic base of cowpea. Reduction in the maturity period has also been reported earlier in γ-irradiated cowpea (Adekola and Oluleye, 2007; Horn et al., 2016). These mutants were found to have a mutational variation in vernalization and/or photoperiodic response. Pods per plant are one of the most crucial yield attributes that meticulously correlate with plant yield. The number of pods per plant is considered one of the most reliable bases for predicting yield in grain legumes; an increase in pods per plant in lower and intermediate dose–treated populations may lead to the isolation of high-yielding mutants in subsequent generations. The stimulatory effects of the lower and intermediate mutagen doses may be attributed to an augmented pod per plant. The results followed the findings of Essel et al. (2015) that reported an increased number of pods in lower doses and a reduced number of pods at higher doses of colchicine in cowpea. Omosun et al. (2021) also reported increased pods per plant in the pigeon pea accessions treated with 0.03% and 0.04% EMS. The increased pods is an vital character from the perspective of plant breeders, and putative mutants with augmented pods are a vital genetic resource for future breeding programs. In the present study, all mutagen doses negatively impacted the number of branches. The decreased number of branches per plant might be due to cellular divisions at a low rate, reduced photosynthetic activities, and synthesis of growth regulators. Putative mutants with decreased branches were also found to have few pods, flowers, fodder, and seed yield. Contrary to the present study, mutagen doses caused a substantial increase in the number of branches reported earlier in mutagenized coriander (Kumar and Pandey, 2019) and tomato (Akhtar, 2014).

The number of seeds per pod plays an important role in developing high-yielding mutant lines, and working on the improvement of this trait could be an effective way to augment yield. Therefore, seeds per pod are a vital component of yield traits in grain legumes; mutants with more seeds per pod reflect higher yields than mutants with fewer seeds (Zhou et al., 2005). In the present study, we noted that lower treatments showed a substantial increase in the seeds per pod, indicating that γ rays and SA have a promoter effect on seed formation. This may be due to mutagen-altered gene expression that governs seed formation or increased activity of growth regulators that impact seed production (Omosun et al. (2021)). Mutagen-induced non-significant increase in seeds has been reported by Horn et al. (2016) in cowpea, Khursheed et al. (2018) in faba bean, and Laskar and Khan (2017) in lentil. In the rapidly increasing population era, there will be an ever-increasing pressure on food production, and more food will be needed to feed the burgeoning population. Hence, increasing food production is a major task for the 21st century. Since the world's food calories is obtained mostly from seed, one way to accomplish this task is to develop mutant lines with more and larger seeds. Furthermore, seed weight in grain crops is considered as one of the most important agronomic traits in plant breeding programs. During the domestication of crop plants, seed weight has been given a primary importance in selection (Linkies et al., 2010; Li and Li, 2014; Ge et al., 2016; Li and Li, 2016). In the present study, mutagen doses of γ rays and SA decreased the mean seed weight. Generally, seed weight is negatively correlated with pods per plant and seeds per plant. Therefore, it is not surprising to record a reduction in seed weight in a mutagen-treated population. The decrease in seed weight may be attributed to the inhibitory effects of mutagen doses. The results were in propinquity with the findings of Amin et al. (2015) in lentil. In the present study, the increased pod length may be attributed to the desirable mutations in the treated plants. Longer pods can accommodate more seeds, leading to enhanced yield (Omosun et al. (2021)). Mutagen induced increases in the mean length of pods have been reported in cowpea genotypes treated with lower doses of γ rays (Horn et al., 2016).

Yield is an essential agronomic trait, and its enhancement is the ultimate aim of plant breeders and farmers (Omosun et al. (2021)). To boost the crop yield and farmers' income, creating high- yielding cowpea varieties is necessary. In grain legumes, plant yield is determined by yield-attributing traits such as branches per plant, pods per plant, seeds per plant, and seed weight. The proportional increases and decreases in the plant yield, with increasing γ rays and SA doses reported in this study, were similar to the findings of Kumar et al. (2010) and Horn et al. (2016) in cowpea. Plant yield is a polygenic trait with a complex inheritance, making it difficult to determine its deviation from the control. Aside from random mutations, the influence of environmental flux on gene expression and the lack of whole genome sequencing data of cowpea are other obstacles in identifying the actual mutations that led to deviation from control plants. The ratio of seed yield to total dry weight defines the harvest index and signifies its capacity to allocate photosynthetic assimilates into grains (Donald and Hamblin, 1976; Sinclair, 1998; Wnuk et al., 2014). Plant yield is determined by two key components: biomass and harvest index. Biomass indicates the capability of producing an adequate amount of agricultural residue, while the harvest index indicates the capacity to allocate biomass to the desired harvestable product, such as grains in food legumes. Allocation of biomass or photosynthates toward desired harvestable product could play a vital role in obtaining a good yield and determines how plant biomass is converted to seed yield (Jack et al., 2014 (Chen et al., 2021). Allocation of photosynthates determines the overall seed yield and the commercial worth of grain crops. Hence, evaluation of the harvest index is imperative for harnessing the full genetic potential of legumes (Adeyanju, 2009). The harvest index also reveals the physiological efficiency in the conversion of dry matter into economic yield (Sharifi et al., 2009). An increase in the harvest index is associated with an increase in the economic portion of the crops (Sharma-Natu and Ghildiyal, 2005). In other words, a low harvest index may be attributed to low seed yield in food legumes. The harvest index plays a vital role in the augmentation of yield, which could help in accomplishing the feeding demands of the burgeoning population (Asefa, 2019). In the present study, the harvest index values indicated that only 30%–40% of the photosynthates were translocated to seeds in both varieties. The increased harvest index in the lower and intermediate treatments may be attributed to decreased branching, as secondary branches produce less seed than main stems. Laskar and Khan (2017) reported similar findings of an increased harvest index in lentil cultivars treated with lower doses of γ rays and hydrazine hydrates. Putative mutants showing a higher harvest index can be considered ideal genotypes for selection to improve yielding potential. Different putative mutants showed variation in the harvest index, which may be attributed to the physiological effects of γ rays and sodium azide. Increasing crop yield is required to supply sustained food and nutrition to the rapidly increasing world population. However, without increasing the harvest index, improvement in yield could not be accomplished. Therefore, the harvest index plays a critical role in enhancing crop productivity and may be considered selection criteria in crop improvement programs (Asefa, 2019).

Correlation analysis: association of yield with its component traits

Correlation analysis plays a pivotal role in determining the association between different yield- attributing traits (Sandhu and Gupta, 1996; Sinha et al., 2001; Rameeh, 2016). The role of mutagens in altering correlations between traits has also been reported earlier in several cultivars (Toker and Cagirgan, 2004; Shin et al., 2011). The apparent differences in the correlation coefficient for different traits may be due to the pleiotropic effects of mutated genes. Yield enhancement, a prime goal of the crop improvement programs, requires a broader understanding of the relationship between yield and yield-contributing traits. The yield was treated as a resultant variable in the present study, and other traits were estimated as causal variables. There were 8 of the 10 component characters studied that exhibited significant positive associations with plant yield. The significant and positive correlation observed between plant yield and yield-contributing

traits may be because these traits are vital determinants of plant yield. This showed that enhancement of these traits would result in better grain yield. Based on the strength of correlations, these six characters were ordered as the harvest index, followed by pod length, seed weigth, branches per plant, pods per plant, plant height, seeds per pod and days to maturity could be used as selection criteria in advanced generations for yield enhancement. However, plant yield correlated negatively with days to flowering in both varieties. Fewer days to flowering tend to have higher yields as early flowering helps the cowpeas evade detrimental heat stress during the reproductive phase. These findings also conformed to previous studies (Laskar and Khan, 2017) in which days to flowering were negatively associated with plant yield. Considerable positive phenotypic correlations for plant yield and pod length; plant yield and pods per per plant indicated that yield might be enhanced through the direct selection of these yield attributes.

Further direct selection for putative mutants bearing more pods and longer pods can provide better results for the improvement of yield in cowpea. Similar results have been reported by Aminu et al. (2016) while studying the correlation analysis in okra. Similarly, a strong positive correlation between plant yield and seed weight implies that plants with augmented seed weight would be more productive. Laskar and Khan (2017) also reported similar findings in lentils. The results revealed that the harvest index had a positive association with plant yield. Similar findings were reported by Marri et al. (2005), which also found a strong and positive correlation between yield and the harvest index. The present study revealed that there is scope for simultaneous improvement of these traits through selection. However, it is important to mention that correlation analysis produces fallacies about the trait association and is not enough to determine the direct and indirect impact of yield-attributing traits. Therefore, path analysis, a biometric technique, is important in assessing the exact picture of the relationship between different traits.

Path analysis: direction and degree of trait associations

Path analysis determines the cause-and-effect relationship between the yield and its component traits. It enables the breeders to visualize the association between traits by evaluating correlation coefficients into direct and indirect effects. It also identifies the traits that significantly affect yield for potential use as selection criteria. Teodoro et al. (2014) reported that path analysis provides a broader understanding of the direction and degree of trait associations. Path analysis revealed that all the yield-contributing traits except pod length and branches per plant positively impacted the plant yield in varieties Gomati VU-89 and Pusa-578, respectively. In the present study, the trait of maximum influence on plant yield was the seeds per pod, as it depicted the highest direct effect on plant yield and simultaneously caused a high indirect effect on the pod number. This trait had an indirect effect *via* the harvest index (that, in turn, depends on the dry matter) on plant yield since its coefficient (0.70 and 0.88) was superior to the residual effect (0.3 and 0.01). This reflects that mutants with high dry matter per plant could divert more assimilates to seeds and increase yield. Since biomass is a product of leaves, branches, and plant height, these traits could, directly and indirectly, contribute to higher seed yield. Seeds per pod can be considered a trait of interest in indirect selection in cowpea breeding programs. The results followed Magashi et al. (2017) findings that reported crops with more seeds per pod would be expected to have higher yield.

Similarly, Silva et al. (2014) reported seeds per plant were the main component having a direct effect, while pods per plant showed an indirect effect on soybean yield. In addition to the seeds per pod, seed weight and pods per plant showed a positive direct impact on the yield, and hence, plants with more pods yield higher than plants with fewer pods. Elliott et al. (2008) also found that heavier seeds show high germination and shoot weight and higher yield than lighter seeds. Salehi et al. (2010) also reported positive and significant correlations between the number of seeds per pod, the number of pods per plant, and pod length, with grain yield in common bean. The combined contributions of either pods per plant and seed weight or seeds per pod and seed weight indicated that improving these characters could enhance plant yield. Days to flowering and days to maturity were positively and significantly correlated with plant yield; however, their direct impact was negative, depicting that indirect impact would be the cause of the correlation. In this state, the indirect causal factors should be considered simultaneously for selection. Hence, it is recommended to consider the traits that show a high indirect impact on plant yield. The residual effect (0.3 and 0.01) depicted that traits, which are included in the path analysis, explained 70% and 99% of the total variation on the dependent variable, i.e., plant yield in the varieties Gomati VU-89 and Pusa-578, respectively (the rest, 30% and 1%, was the contribution of other factors, such as traits not studied).

Multivariate analysis: an effective tool in plant breeding programs

The multivariate analysis is useful for assessing the degree of divergence between mutagenized populations or putative mutants. Multivariate statistical techniques are also used to simultaneously analyze multiple measurements on each treated population. Irrespective of the data, whether morphological, biochemical, or molecular, multivariate statistical techniques are widely used in genetic diversity analysis. Among the multivariate techniques, PCA and HCA are useful in selection of mutants (Mohammadi and Prasanna, 2003). PCA and HCA are also considered the main tools for determining the relatedness and categorization of mutants based on quantitative data (Malek et al., 2014). In the present study, cluster analysis helped us in forming clusters for grouping putative mutants with similar features and vice versa. In any plant breeding experimentation, it is crucial to know plant traits that explain maximum variability. Therefore, PCA and HCA were conducted to run a classification analysis on the putative cowpea mutants using descriptive statistics and to understand the association of various characters. PCA and HCA, as described below, enabled us to categorize the putative mutants into distinct classes based on their genetic diversity.

Hierarchical cluster analysis: classifying putative mutants

In the present study, HCA was used to classify putative mutants into separate clusters based on genetic diversity among their quantitative traits. HCA categorized mutagenized populations into separate five clusters that significantly deviated from the respective controls in both varieties. HCA divided putative mutants into five and seven main clusters in Gomati VU-89 and Pusa-578 based on phenotypic traits. Clustering of putative mutants based on studied traits is presented in Figure 7. HCA grouped putative cowpea mutants into 12 clusters (5 clusters in the var. Gomati VU-89 and 7 clusters in the var. Pusa-578). In the var. Gomati VU-89, group I comprised of 400 Gy and 0.04% SA-treated populations and plants were short-statured, and low yielding as compared to all other genotypes of groups II, III, and V. Similarly, group II comprised of the 300 Gy + 0.03% SA population were having long pods, bold seeds, and higher yielding. Group III comprised of control, and the 400 Gy + 0.04% SA population were tall with a low pod set and total plant yield, while group IV comprised of 0.03% SA, 200 Gy + 0.02% SA, 100 Gy + 0.01% SA, and 300 Gy populations were with more number of pods and highest yield. Group V comprised 100 Gy, 0.01% SA, 200 Gy, and 0.02% SA populations were high yielding with desired traits. In the var. Pusa-578, a group I consisted of 300 Gy, 0.03% SA, and 200 Gy + 0.02% SA populations were tall, a low pod set, and low yielding, group II comprised of 400 Gy and 300 Gy + 0.03% SA populations were mostly plants with less number of seeds per pod that eventually resulted in low yield, group III consisted of the 0.03% SA population were low-yielding plants, group IV included control, 0.04% SA and 400 Gy + 0.04% SA populations were tall with fewer flowers that resulted into a low pod set and plant yield, group V composed of 100 Gy and the 100 Gy + 0.01% SA population were plants with more flowers per plant, more pod set, and high yield, group VI consisted of the 0.01% SA population were plants with bold-seeded pods, and group VII consisting of the 200 Gy population were plants with long pods. 0.02% SA and 200 Gy populations were most diverged from control populations in Gomati VU-89 and Pusa-578, respectively. The genetically similar and divergent mutagenized populations were distinctly separated and classified within the same and different clusters. The clustering of mutants based on their similarity/dissimilarity revealed that mutants grouped in different clusters are ideal for breeding programs aimed at broadening genetic variability. In induced mutagenesis, proper selection of mutant lines is achieved by selecting the most distinct cluster with respect to the control cluster. The intercluster distance determines the variability spectrum; the more distanced clusters indicate a broader spectrum of variability in the segregating generation and vice versa. In the present study, cluster II, the maximally contributing cluster, should be selected for further selection to broaden variability. The present study revealed that HCA allowed us to place the putative mutants and control plants in different clusters based on quantitative traits. Therefore, HCA can be considered an effective tool for sorting putative mutants and enables breeders to select the base material to design future breeding strategies in cowpea. In addition, it is imperative that while selecting base material, genetic barriers, and breeding methods must be given proper importance to achieve the desired goals of plant breeding.

Principal component analysis: assessing comparative contribution of traits toward variability

In cowpea, yield is the cumulative effect of many yield-contributing traits. Different characteristics such as pods per plant, seeds per pod, pod length, and seed weight assume vital importance and must be assessed for a contribution of variance in plant breeding programs aiming to develop high-yielding mutant varieties. PCA and HCA are recommended algorithms for this purpose (Sudre et al., 2007). PCA is commonly used to assess the comparative contribution of variance of different variables prior to cluster analysis (Jackson, 1991). PCA enables the breeders to visualize the traits that contribute maximally toward variability. This tool also equips the breeders in selecting the best mutants for breeding purposes. In the present study, the results of PCA revealed that the first two components contributed approximately 40.4% and 33.4% of the total variability in 13 populations in the varieties Gomati VU-89 and Pusa-578, respectively. In the var. Gomati VU-89, the PC1 alone explained 28.34% of the total variation, mainly due to plant yield, harvest index, and plant height. PC2 explained 12.12% of the total variation, mainly due to pods per plant, days to maturity and days to flowering. PC1 showed positive factor loadings for all the traits. However, plant height, seed weight, and harvest index contributed negative factor loadings toward PC2. Traits such as plant yield, plant height, and harvest index were those with the highest contribution to PC1, whereas pods per plant, seeds per pod, and days to maturity were the chief contributors to PC2. In the var. Pusa-578, PC1 alone explained 21.92% of the total variation, mainly due to variations in plant yield, harvest index, and pods per plant. PC2 explained 11.55% of the total variation, mainly due to variations in days to flowering and pod length. PC1 showed positive factor loadings for all the traits. However, except for days to flowering, seeds per pod, and harvest index contributed negative factor loadings toward PC2. It is obvious that traits such as plant yield, pods per plant, pod length, and harvest index were those with the highest contribution to PC1 whereas days to maturity were the chief contributors to PC2. These results clearly indicated that PCA highlighted a few traits for exercising selection. The findings were in good agreement with the results of Raina et al. (2022) that reported that the first two PCs explained 62.4% and 17.6% of the variance and were heavily weighted by measures of plant yield and harvest index in cowpea. Further, it also revealed that first principal components contributed the highest number of traits toward genetic diversity, which may prove crucial in crop improvement programs. Days to flowering, plant height, branches per plant, pod length, and plant yield contributed to the overall variability in treated population. In breeding populations, a high level of transgressive segregation could be attained by choosing characters with high variability. The PCA biplot also provided an overview of

the similarities and differences among the mutagenized populations and the interrelationships between the measured variables. The genetically similar populations, viz., 100 Gy + 0.01% SA, 200 Gy + 0.02% SA and 0.01% SA, 0.02% SA were concentrated around the origin of PC2. The genetically divergent populations, viz., 300 Gy + 0.03% SA, 400 Gy + 0.04%, and 100 Gy, 200 Gy, were placed at extreme origins in the PCA biplot. Therefore, it is important to include genetically divergent mutants in the breeding programs to broaden the genetic base.

Conclusions

The present study confirmed that lower doses of gamma rays and sodium azide increased the agronomic traits of both cowpea varieties. Hence, for agronomic improvement of the cowpea varieties, 100 Gy, 0.01% SA, and 100 Gy + 0.01% SA are suitable for beneficial mutation inducement. Potential high-yielding putative mutants were identified in M_1 populations that could greatly contribute to local food production and nutritional security. Based on the quantitative statistics, six higher-yielding mutagenized populations, viz., 100 Gy, 200 Gy, 0.01% SA, 0.02% SA, 100 Gy + 0.01% SA, and 200 Gy + 0.02% SA are recommended for further evaluation of high-yielding mutants. Pearson's correlation analysis revealed that association of plant yield and seed weight was positive and highly significant, depicting that these are yield-determinative traits. Moreover, path analysis depicted that the seeds per pod followed by seed weight had the highest positive direct effect. Strong correlation and the positive direct effect of seeds per pod with plant yield and strong correlation and the negative direct effect of days to maturity with plant yield revealed that mutants with more seeds per pod and early maturing should be emphasized in the selection of high-yielding cowpea mutants. Hence, selection of cowpea mutants with a high harvest index along with concurrent consideration of short days to maturity and more seeds per pod is a prerequisite for attaining improvement in cowpea yield. HCA grouped the genetically similar and divergent populations into different clusters and confirmed mutagen-induced heterogeneous populations in the two varieties. PCA scattered the mutagenized populations over the four quadrants, with genetically similar populations concentrated around the origin and genetically divergent populations placed at extreme positions from the origin in the PCA biplot. Therefore, it is essential to include genetically divergent mutants in the breeding programs for further improvement.

Data availability statement

The original contributions presented in the study are included in the article/Supplementary Material. Further inquiries can be directed to the corresponding author.

Author contributions

AR contributed to performing the experiments, assessing data, and drafting the manuscript. SK contributed to the supervision of overall experimentation. All authors contributed to the article and approved the submitted version.

Acknowledgments

The authors thank the Chairperson of the Botany department, Aligarh Muslim University, Aligarh, and the Director, National Botanical Research Institute, Lucknow, for providing basic research and gamma irradiation facilities.

Conflict of interest

The authors declare that the research was conducted in the absence of any commercial or financial relationships that could be construed as a potential conflict of interest.

Publisher's note

Supplementary material

The Supplementary Material for this article can be found online at: https://www.frontiersin.org/articles/10.3389/fpls.2023.1188077/full#supplementary-material

References

Adekola, O. F., and Oluleye, F. (2007). Induction of genetic variation in cowpea (*Vigna unguiculata* l. walp.) by gamma irradiation. *Asian J. Plant Sci.* 6.

Adeyanju, A. O. (2009). Genetics of harvest and leaf-yield indices in cowpea. *J. Crop Improvement* 23 (3), 266–274. doi: 10.1080/15427520902805555

Ahmad, A., and Saleem, M. (2003). Path coefficient analysis in zea mays l. *Int. J. Agric. Biol.* 5 (3), 245–248.

Akhtar, N. (2014). Effect of physical and chemical mutagens on morphological behavior of tomato (Solanum lycopersicum) CV. *Plant Breed. seed Sci.* 70, 69–79. doi: 10.1515/plass-2015-0014

Almeida, C. M. V. C., Vencovsky, R., Cruz, C. D., and Bartley, B. G. D. (1994). Path analysis of yield components of cacao hybrids (*Theobroma cacao* l.). *Braz. J. Genet.* 17, 181–186.

Amin, R., Laskar, R. A., and Khan, S. (2015). Assessment of genetic response and character association for yield and yield components in lentil (Lens culinaris l.) population developed through chemical mutagenesis. *Cogent Food Agric.* 1 (1), p.1000715.

Amin, R., Wani, M. R., Raina, A., Khursheed, S., and Khan, S. (2019). Induced morphological and chromosomal diversity in the mutagenized population of black

cumin (*Nigella sativa* l.) using single and combination treatments of gamma rays and ethyl methane sulfonate. *Jordan J. Biol. Sci.* 12 (1), 23–30.

Aminu, D., Bello, O. B., Gambo, B. A., Azeez, A. H., Agbolade, O. J., Iliyasu, A., et al. (2016). Varietal performance and correlation of okra pod yield and yield components. *Acta Universitatis Sapientiae Agric. Environ.* 8 (1), 112–125. doi: 10.1515/ausae-2016-0010

Araújo, E. C., Daher, R. F., Silva, R. F., and Viana, A. P. (2007). Path analysis for physiological traits that influence seed germination of *Passiflora edulis* f. flavicarpa deg. *Crop Breed. Appl. Biotechnol.* 7, 148–154. doi: 10.12702/1984-7033.v07n02a06

Arnon, D. I. (1949). Copper enzymes in isolated chloroplast polyphenoloxidase in *Beta vulgaris*. *Plant Physiol.* 24, 1–15. doi: 10.1104/pp.24.1.1

Arumuganathan, K., and Earle, E. D. (1991). Nuclear DNA content of some important plant species. *Plant Mol. Biol. Rep.* 9, 208–218. doi: 10.1007/BF02672069

Asefa, G. (2019). The role of harvest index in improving crop productivity: a review. *J. Natural Sci. Res.* 9, 1–5. doi: 10.7176/JNSR

Austin, R. B., Bingham, J., Blackwell, R. D., Evans, L. T., Ford, M. A., Morgan, C. L., et al. (1980). Genetic improvements in winter wheat yields since 1900 and associated physiological changes. *J. Agri Sci.* 94 (3), 675–689. doi: 10.1017/S0021859600028665

https://mvd.iaea.org/ [Accessed December 20, 2020].

Bizeti, H. S., Carvalho, C. G. P., Souza, J. R. P., and Destro, D. (2004). Path analysis under multicollinearity in soybean. *Braz. Arch. Biol. Technol.* 47 (5), 669–676. doi: 10.1590/S1516-89132004000500001

Borzouei, A., Kafi, M., Khazaei, H., Naseriyan, B., and Majdabadi, A. (2010). Effects of gamma radiation on germination and physiological aspects of wheat (*Triticum aestivum* l.) seedlings. *Pak. J. Bot.* 42 (4), 2281–2290.

Carvalho, S. P., Cruz, C. D., and Carvalho, C. G. P. (1999). Estimating gain by use of a classic selection under mulcollinearity in wheat (*Triticum aestivum*). *Genet. Mol. Biol.* 22, 109–113. doi: 10.1590/S1415-47571999000100021

Channaoui, S., Labhilili, M., Mouhib, M., Mazouz, H., El Fechtali, M., and Nabloussi, A. (2019). Development and evaluation of diverse promising rapeseed (*Brassica napus* l.) mutants using physical and chemical mutagens. *OCL* 26, 35. doi: 10.1051/ocl/2019031

Chen, J., Engbersen, N., Stefan, L., Schmid, B., Sun, H., and Schöb, C. (2021). Diversity increases yield but reduces harvest index in crop mixtures. *Nat. Plants* 7 (7), 893–898. doi: 10.1038/s41477-021-00948-4

Cheng, Q., Dong, L., Su, T., Li, T., Gan, Z., Nan, H., et al. (2019). CRISPR/Cas9-mediated targeted mutagenesis of GmLHY genes alters plant height and internode length in soybean. *BMC Plant Biol.* 19, 562. doi: 10.1186/s12870-019-2145-8

Coimbra, J. L. M., Benin, G., Vieira, E. A., Oliveira, A. C., Carvalho, F. I. F., Guidolin, A. F., et al. (2005). Consequências da multicolinearidade sobre a análise de trilha em canola. *Ciec. Rural* 35, 347–352. doi: 10.1590/S0103-84782005000200015

Cruz, C. D., and Regazzi, A. J. (2006). *Modelos biométricos aplicados ao melhoramento genético* (Viçosa: UFV), 585.

Cruz, C. D., Regazzi, A. J., and Carneiro, P. C. S. (2012). *Modelos biométricos aplicados ao melhoramento genético, 4th ed* (Viçosa: UFV), 514.

Donald, C. M., and Hamblin, J. (1976). The biological yield and harvest index of cereals as agronomic and plant breeding criteria. *Adv. Agron.* 28, 361–405. doi: 10.1016/S0065-2113(08)60559-3

Elliott, R. H., Franke, C., and Rakow, G. F. W. (2008). Effects of seed size and seed weight on seedling establishment, vigour and tolerance of Argentine canola (*Brassica napus*) to flea beetles, phyllotreta spp. *Can. J. Plant Sci.* 88, 207–217. doi: 10.4141/CJPS07059

Essel, E., Asante, I. K., and Laing, E. (2015). Effect of colchicine treatment on seed germination, plant growth and yield traits of cowpea (*Vigna unguiculata* (L.) walp). *Can. J. Pure Appl. Sci.* 9 (3), 3573–3576.

Fukuzawa, K., Inokami, Y., Terao, J., and Suzuki, A. (1998). Rate constants for quenching singlet oxygen and activities for inhibiting lipid peroxidation of carotenoids and α-tocopherol in liposomes. *Lipids* 3, 751–756. doi: 10.1007/s11745-998-0266-y

Ge, L., Yu, J., Wang, H., Luth, D., Bai, G., Wang, K., et al. (2016). Increasing seed size and quality by manipulating BIG SEEDS1 in legume species. *Proc. Natl. Acad. Sci.* 113 (44), 12414–12419. doi: 10.1073/pnas.1611763113

Gnanamurthy, S., and Dhanavel, D. (2014). Effect of EMS on induced morphological mutants and chromosomal variation in cowpea (*Vigna unguiculata* (L.) walp). *Int. Lett. Natural Sci.* 17, 33–43. doi: 10.56431/p-i0xny2

Hammer, Ø., Harper, D. A. T., and Ryan, P. D. (2001). PAST: paleontological statistics software package for education and data analysis. *Palaeontologia Electronica* 4, 9.

Hashimoto, H., Uragami, C., and Cogdell, R. J. (2016). Carotenoids and photosynthesis. *Carotenoids Nat.* 79, 111–139. doi: 10.1007/978-3-319-39126-7_4

Hopkins, W. J. (1995). *Introduction to plant physiology, 438* (New York: John Wily and Sons Inc.).

Horn, L. N., Ghebrehiwot, H. M., and Shimelis, H. A. (2016). Selection of novel cowpea genotypes derived through gamma irradiation. *Front. Plant science.* 7, 262. doi: 10.3389/fpls.2016.00262

Jack, B., Caligari, P. D. S., and Campos, H. A. (2014). *Second edition of introduction to plant breeding* (Hoboken, NJ, United States: John Wiley and Sons Ltd), 295.

Jackai, L. E. (1982). A field screening technique for resistance of cowpea (Vigna unguiculata) to the pod-borer maruca testulalis (Geyer)(Lepidoptera: pyralidae). *Bull. Entomological Res.* 72 (1), 145–156. doi: 10.1017/S0007485300050379

Jackson, J. E. (1991). *A user's guide to principal components* (New York: Wiley).

Jaworski, E. G. (1971). Nitrate reductase assay in intact plant tissues. *Biochem. Biophys. Res. Commun.* 43, 1274–1279. doi: 10.1016/S0006-291X(71)80010-4

Ketema, S., Tesfaye, B., Keneni, G., Amsalu Fenta, B., Assefa, E., Greliche, N., et al. (2020). DArTSeq SNP-based markers revealed high genetic diversity and structured population in Ethiopian cowpea [Vigna unguiculata (L.) walp] germplasms. *PloS One* 15 (10), e0239122. doi: 10.1371/journal.pone.0239122

Khursheed, S., Raina, A., Amin, R., Wani, M. R., and Khan, S. (2018). Quantitative analysis of genetic parameters in the mutagenized population of faba bean (*Vicia faba* l.). *Res. Crops* 19 (2), 276–284. doi: 10.5958/2348-7542.2018.00041.4

Khush, G. S. (2001). Green revolution: the way forward. *Nat. Rev. Genet.* 2, 815–822. doi: 10.1038/35093585

Kim, J. H., Baek, M. H., Chung, B. Y., Wi, S. G., and Kim, J. S. (2004). Alterations in the photosynthetic pigments and antioxidant machineries of red pepper (Capsicum annuum l.) seedlings from gamma-irradiated seeds. *J. Plant Biol.* 47 (4), 314–321. doi: 10.1007/BF03030546

Kiong, A. L. P., Lai, G. A., Hussein, S., and Harun, A. R. (2008). Physiological responses of orthosiphon stamineus plantles to gamma irradiation. *American-Eurasian J. Sustain. Agric.* 2 (2), 135–149.

Kovacs, E., and Keresztes, A. (2002). Effect of gamma and UV-B/C radiation on plant cells. *Micron* 33 (2), 199–210. doi: 10.1016/S0968-4328(01)00012-9

Kulandaivelu, G., and Noorudeen, A. M. (1983). Comparative study of the action of ultraviolet-c and ultraviolet-b radiation on photosynthetic electron transport [Amaranthus, chloroplast]. *Physiologia Plantarum (Denmark)* 58. doi: 10.1111/j.1399-3054.1983.tb04199.x

Kumar, G., and Pandey, A. (2019). Ethyl methane sulphonate induced changes in cyto-morphological and biochemical aspects of coriandrum sativum l. *J. Saudi Soc. Agric. Sci.* 18 (4), 469–475. doi: 10.1016/j.jssas.2018.03.003

Kumar, V. A., Vairam, N., and Amutha, R. (2010). Effect of physical mutagen on expression of characters in arid legume pulse cowpea (*Vigna unguiculata* (L.) walp.). *Electronic J. Plant Breed.* 1 (4), 908–914.

Laskar, R. A., and Khan, S. (2017). Assessment on induced genetic variability and divergence in the mutagenized lentil populations of microsperma and macrosperma cultivars developed using physical and chemical mutagenesis. *PloS One* 12 (9), e0184598. doi: 10.1371/journal.pone.0184598

Laskar, R. A., Khan, S., Khursheed, S., Raina, A., and Amin, R. (2015). Quantitative analysis of induced phenotypic diversity in chickpea using physical and chemical mutagenesis. *J. Agron.* 14 (3), 102–111. doi: 10.3923/ja.2015.102.111

Laskar, R. A., Laskar, A. A., Raina, A., Khan, S., and Younus, H. (2018). Induced mutation analysis with biochemical and molecular characterization of high yielding lentil mutant lines. *Int. J. Biol. Macromol.* 109, 167–179. doi: 10.1016/j.ijbiomac.2017.12.067

Li, C. C. (1975). *Path analysis: aprimer* (Pacific Grove: Boxwood), 346.

Li, Y., He, N., Hou, J., Xu, L., Liu, C., Zhang, J., et al. (2018). Factors influencing leaf chlorophyll content in natural forests at the biome scale. *Front. Ecol. Evol.* 6, 64. doi: 10.3389/fevo.2018.00064

Li, N., and Li, Y. (2014). Ubiquitin-mediated control of seed size in plants. *Front. Plant Sci.* 5, 332. doi: 10.3389/fpls.2014.00332

Li, N., and Li, Y. (2016). Signaling pathways of seed size control in plants. *Curr. Opin. Plant Biol.* 33, 23–32. doi: 10.1016/j.pbi.2016.05.008

Linkies, A., Graeber, K., Knight, C., and Leubner-Metzger, G. (2010). The evolution of seeds. *New Phytol.* 186 (4), 817–831. doi: 10.1111/j.1469-8137.2010.03249.x

Lo, S., Fatokun, C., Boukar, O., Gepts, P., Close, T. J., and Muñoz-Amatriaín, M. (2020). Identification of QTL for perenniality and floral scent in cowpea (Vigna unguiculata [L.] walp.). *PloS One* 15 (4), e0229167. doi: 10.1371/journal.pone.0229167

MacKinney, G. (1941). Absorption of light by chlorophyll solution. *J. Biol. Chem.* 140, 315–322. doi: 10.1016/S0021-9258(18)51320-X

Magashi, A. I., Gaya, A. G., Daraja, Y. B., Isah, S. D., Ado, M., Almu, H., et al. (2017). Assessment of cowpea (Vigna unguiculata (L.) walp) germplasm for agronomic traits in seed production. *Int. J. Adv. Agric. Environ. Eng.* 4, 111–115. doi: 10.15242/IJAAEE.C0417001

Malek, M. A., and Monshi, F. I. (2009). Performance evaluation of rapeseed mutants. *Bang J. Agric. Res.* 36, 81–84.

Malek, M. A., Rafii, M. Y., Afroz, M. S. S., Nath, U. K., and Mondal, M. M. A. (2014). Morphological characterization and assessment of genetic variability, character association, and divergence in soybean mutants. *Sci. World. J.* 1–12. doi: 10.1155/2014/968796

Marri, P. R., Sarla, N., Reddy, L. V., and Siddiq, E. A. (2005). Identification and mapping of yield and yield related QTLs from an Indian accession of. *BMC Genet.* 13, 33–39. doi: 10.1186/1471-2156-6-33

Mohammadi, S. A., and Prasanna, B. M. (2003). Analysis of genetic diversity in crop plants –salient statistical tools and considerations. *Crop Sci.* 43 (4), 1235–1248. doi: 10.2135/cropsci2003.1235

More, U. A., and Malode, S. N. (2016). Mutagenic effect of EMS on quantitative characters of *Brassica napus* l. cv. excel in M_1 generation. *J. Global Biosci.* 5, 4018–4025.

Ngoma, T. N., Chimimba, U. K., Mwangwela, A. M., Thakwalakwa, C., Maleta, K. M., Manary, M. J., et al. (2018). Effect of cowpea flour processing on the chemical properties and acceptability of a novel cowpea blended maize porridge. *PloS One* 13 (7), e0200418. doi: 10.1371/journal.pone.0200418

Nkomo, G. V., Sedibe, M. M., and Mofokeng, M. A. (2021). Production constraints and improvement strategies of cowpea (Vigna unguiculata l. walp.) genotypes for drought tolerance. *Int. J. Agron* 2021. doi: 10.1155/2021/5536417

Omosun, G., EberechiAkanwa, F., Ekundayo, E. O., Okoro, I. A., Ojimelukwe, P. C., and Egbucha, K. C. (2021). Effect of ethyl methane sulphonate (ems) on the agronomic performance of two pigeon pea (Cajanus cajan (L.) millspaugh) accessions. *J. Agric. Vet. Sci.* 14, 1–12.

Pouteau, S., Ferret, V., Gaudin, V., Lefebvre, D., Sabar, M., Zhao, G., et al. (2004). Extensive phenotypic variation in early flowering mutants of arabidopsis. *Plant Physiol.* 135 (1), 201–211. doi: 10.1104/pp.104.039453

Raina, A., Laskar, R. A., Tantray, Y. R., Khursheed, S., Wani, M. R., and Khan, S. (2020). Characterization of induced high yielding cowpea mutant lines using physiological, biochemical and molecular markers. *Sci. Rep* 10. doi: 10.1038/s41598-020-60601-6

Raina, A., Laskar, R. A., Wani, M. R., Jan, B. L., Ali, S., and Khan, S. (2022). Gamma rays and sodium azide induced genetic variability in high-yielding and biofortified mutant lines in cowpea [Vigna unguiculata (L.) walp.]. *Front. Plant Sci.* 13. doi: 10.3389%2Ffpls.2022.911049

Rameeh, V. (2016). Correlation and path analysis in advanced lines of rapeseed (Brassica napus) for yield components. *J. Oilseed Bras.* 1 (2), 56–60.

Ramel, F., Birtic, S., Ginies, C., Soubigou-Taconnat, L., Triantaphylidès, C., and Havaux, M. (2012). Carotenoid oxidation products are stress signals that mediate gene responses to singlet oxygen in plants. *Proc. Natl. Acad. Sci.* 109 (14), 5535–5540. doi: 10.1073/pnas.1115982109

R Core Team (2019). *R: a language and environment for statistical computing* (Vienna: R Foundation for Statistical Computing).

Reisz, J. A., Bansal, N., Qian, J., Zhao, W., and Furdui, C. M. (2014). Effects of ionizing radiation on biological molecules–mechanisms of damage and emerging methods of detection. *Antioxid. Redox Signal.* 21, 260–292. doi: 10.1089/ars.2013.5489

Saha, P., Raychaudhuri, S. S., Chakraborty, A., and Sudarshan, M. (2010). PIXE analysis of trace elements in relation to chlorophyll concentration in plantago ovata forsk. *Appl. Radiat. Isotopes* 68 (3), 444–449. doi: 10.1016/j.apradiso.2009.12.003

Salahuddin, S., Abro, S., Kandhro, M. M., Salahuddin, L., and Laghari, S. (2010). Correlation and path coefficient analysis of yield components of upland cotton (Gossypium hirsutum l.). *World Appl. Sci. J.* 8, 71–75.

Salehi, M., Faramarzi, A., and Mohebalipour, N. (2010). Evaluation of different effective traits on seed yield of common bean (Phaseolus vulgaris l.) with path analysis. *Am. Eurasian J. Agric. And Environmental Sci.* 9, 52–54.

Sandhu, S. K., and Gupta, V. P. (1996). Genetic divergence and correlation studies in brassica species. *Crop Improvement-India* 23, 253–256.

Santos, A., Ceccon, G., Davide, L. M. C., Correa, A. M., and Alves, V. B. (2014). Correlations and path analysis of yield components in cowpea. *Crop Breed. Appl. Biotechnol.* 14 (2), 82–87. doi: 10.1590/1984-70332014v14n2a15

Sanz-Luque, E., Chamizo-Ampudia, A., Llamas, A., Galvan, A., and Fernandez, E. (2015). Understanding nitrate assimilation and its regulation in microalgae. *Front. Plant Sci.* 6, 899. doi: 10.3389/fpls.2015.00899

Sarawgi, A. K., Rastogi, N. K., and Soni, D. K. (1997). Correlation and path analysis in rice accessions from Madhya pradesh. *Field Crops Res.* 52 (1-2), 161–167. doi: 10.1016/S0378-4290(96)01061-1

Sharifi, R. S., Sedghi, M., and Gholipouri, A. (2009). Effect of population density on yield and yield attributes of maize hybrids. *Res. J. Biol. Sci.* 4, 375–379.

Sharma-Natu, P., and Ghildiyal, M. C. (2005). Potential targets for improving photosynthesis and crop yield. *Curr. Sci.* 88, 1918–1928.

Shin, J.-M., Kim, B., Seo, S., Jeon, S. B., Kim, J., Jun, B., et al. (2011). Mutation breeding of sweet potato by gamma radiation. *Afr. J. Agric. Res.* 6 (6), 1447–1454.

Silva, A. F., Sediyama, T., Silva, F. C. S., Bezerra, A. R. G., Ferrerira, L. V., et al. (2014). Correlation and path analsysis of soyben componentes. *Int. J. Plant Anim. Environ. Sci.* 5, 177–179.

Sinclair, T. R. (1998). Historical changes in harvest index and crop nitrogen accumulation. *Crop Sci.* 38, 638–643. doi: 10.2135/cropsci1998.0011183X003800030002x

Sinha, P., Singh, S. P., and Pandey, I. D. (2001). Character association and path analysis in brassica species l. *Indian J. Agricult. Res.* 35 (1), 63–65.

Sudre, C. P., Leonardecz, E., Rodrigues, R., Junior, A. T. D. A., Moura, M. D. C. L., and Gonçalves, L. S. A. (2007). Geneticresources of vegetable crops: a survey in the braziliangermplasm collections pictured through papers published inthe journals of the Brazilian society for horticultural science. *Hortic. Bras.* 25, 496–503. doi: 10.1590/S0102-05362007000400002

Tanaka, R., and Tanaka, A. (2007). Tetrapyrrole biosynthesis in higher plants. *Annu. Rev. Plant Biol.* 58, 321–346. doi: 10.1146/annurev.arplant.57.032905.105448

Teodoro, P. E., Silva, C. A. J., Corrêa, C. C., Ribeiro, L. P., de Oliveira, E. P., and Lima, M. F., et al. (2014). Path analysis and correlation of two genetic classes of maize (Zea mays l.). *J. Agron.* 13, 23–28. doi: 10.3923/ja.2014.23.28

Toker, C., and Cagirgan, M. I. (2004). The use of phenotypic correlations and factor analysis in determining characters for grain yield selection in chickpea (*Cicer arietinum* l.). *Hereditas* 140, 226–228. doi: 10.1111/j.1601-5223.2004.01781.x

Uzogara, S., and Ofuya, Z. (1992). Processing and utilization of cowpeas in developing countries: a review. *J. Food Process. Preservation* 16, 105–147. doi: 10.1111/j.1745-4549.1992.tb00195.x

Verma, A. K., Banerji, B. K., Chakrabarty, D., and Datta, S. K. (2010). Studies on makhana (Euryale ferox Salisbury). *Curr. Sci.* 99, 795–800.

Wamalwa, E. N., Muoma, J., and Wekesa, C. (2016). Genetic diversity of cowpea (*Vigna unguiculata* (L.) walp.) accession in Kenya gene bank based on simple sequence repeat markers. *Int. J. Genomics*. doi: 10.1155/2016/8956412

Wei, C., Zhu, L., Wen, J., Yi, B., Ma, C., Tu, J., et al. (2018). Morphological, transcriptomics and biochemical characterization of new dwarf mutant of brassica napus. *Plant Sci.* 270, 97–113. doi: 10.1016/j.plantsci.2018.01.021

Wendehenne, D. (2011). New frontiers in nitric oxide biology in plant. *Plant Sci.* 181, 507–508. doi: 10.1016/j.plantsci.2011.07.010

Wi, S. G., Chung, B. Y., Kim, J. S., Kim, J. H., Baek, M. H., Lee, J. W., et al. (2007). Effects of gamma irradiation on morphological changes and biological responses in plants. *Micron* 38 (6), 553–564. doi: 10.1016/j.micron.2006.11.002

Willows, R. D., and Hansson, M. (2003). Mechanism, structure, and regulation of magnesium chelatase. *Porphyrin Handb. II* 13, 1–48. doi: 10.1016/B978-0-08-092387-1.50007-2

Wnuk, A., Gorny, A. G., Bocianowski, J., and Kozak, M. (2014). Visualizing harvest index in crops. *Commun. Biometry Crop Sci.* 8, 48–59.

Wright, S. (1921). Correlation and causation. *J. Agric. Res.* 20, 557–585.

Zeng, X., Zhu, L., Chen, Y., Qi, L., Pu, Y., Wen, J., et al. (2011). Identification, fine mapping and characterization of a dwarf mutant (bnaC. *dwf) Brassica napus. Theor. Appl. Genet.* 122 (2), 421–428. doi: 10.1007/s00122-010-1457-8

Zhou, X. A., Wang, X. Z., Cai, S. P., Jun, W. X., Sha, A. H., Qiu, D. Z., et al. (2005). Relation of three-seed and four-seed pods with yield of RIL in soybeans. *Chin. J. Oil Crop Sci.* 27, 22–25.

Frontiers in
Plant Science

Cultivates the science of plant biology and its applications

The most cited plant science journal, which advances our understanding of plant biology for sustainable food security, functional ecosystems and human health.

Discover the latest Research Topics

See more →

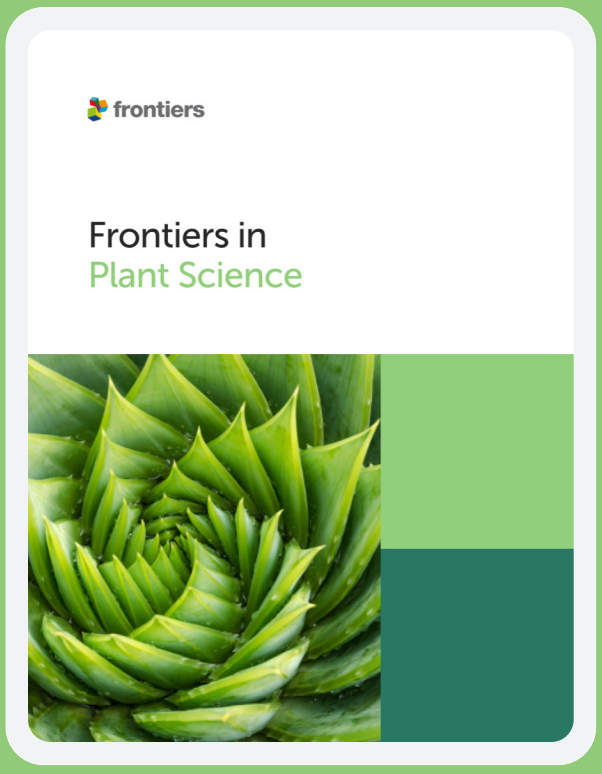

Frontiers

Avenue du Tribunal-Fédéral 34
1005 Lausanne, Switzerland
frontiersin.org

Contact us

+41 (0)21 510 17 00
frontiersin.org/about/contact